

Advances in Science, Technology & Innovation
IEREK Interdisciplinary Series for Sustainable Development

Domenico M. Doronzo · Emanuela Schingaro
John S. Armstrong-Altrin · Basem Zoheir *Editors*

Petrogenesis and Exploration of the Earth's Interior

Proceedings of the 1st Springer Conference of the
Arabian Journal of Geosciences (CAJG-1), Tunisia 2018

Advances in Science, Technology & Innovation

IEREK Interdisciplinary Series for Sustainable
Development

Editorial Board Members

Anna Laura Pisello
Dean Hawkes
Hocine Bougdah
Federica Rosso
Hassan Abdalla
Sofia-Natalia Boemi
Nabil Mohareb
Saleh Mesbah Elkaffas
Emmanuel Bozonnet
Gloria Pignatta
Yasser Mahgoub
Luciano De Bonis
Stella Kostopoulou
Biswajeet Pradhan
Md. Abdul Mannan
Chaham Alalouch
Iman O. Gawad

Series Editor

Mourad Amer

Advances in Science, Technology & Innovation (ASTI) is a series of peer-reviewed books based on the best studies on emerging research that redefines existing disciplinary boundaries in science, technology and innovation (STI) in order to develop integrated concepts for sustainable development. The series is mainly based on the best research papers from various IEREK and other international conferences, and is intended to promote the creation and development of viable solutions for a sustainable future and a positive societal transformation with the help of integrated and innovative science-based approaches. Offering interdisciplinary coverage, the series presents innovative approaches and highlights how they can best support both the economic and sustainable development for the welfare of all societies. In particular, the series includes conceptual and empirical contributions from different interrelated fields of science, technology and innovation that focus on providing practical solutions to ensure food, water and energy security. It also presents new case studies offering concrete examples of how to resolve sustainable urbanization and environmental issues. The series is addressed to professionals in research and teaching, consultancies and industry, and government and international organizations. Published in collaboration with IEREK, the ASTI series will acquaint readers with essential new studies in STI for sustainable development.

More information about this series at <http://www.springer.com/series/15883>

Domenico M. Doronzo
Emanuela Schingaro • John S. Armstrong-Altrin
Basem Zoheir
Editors

Petrogenesis and Exploration of the Earth's Interior

Proceedings of the 1st Springer Conference
of the Arabian Journal of Geosciences
(CAJG-1), Tunisia 2018



Editors

Domenico M. Doronzo
Consejo Superior de Investigaciones
Científicas
Barcelona, Spain

Basem Zoheir
Benha University
Benha, Egypt

and

Emanuela Schingaro
Università degli Studi di Bari Aldo Moro
Bari, Italy

University of Kiel
Kiel, Germany

John S. Armstrong-Altrin
Universidad Nacional Autónoma de México
Mexico City, Mexico

ISSN 2522-8714 ISSN 2522-8722 (electronic)
Advances in Science, Technology & Innovation
IEREK Interdisciplinary Series for Sustainable Development
ISBN 978-3-030-01574-9 ISBN 978-3-030-01575-6 (eBook)
<https://doi.org/10.1007/978-3-030-01575-6>

Library of Congress Control Number: 2018958954

© Springer Nature Switzerland AG 2019

This work is subject to copyright. All rights are reserved by the Publisher, whether the whole or part of the material is concerned, specifically the rights of translation, reprinting, reuse of illustrations, recitation, broadcasting, reproduction on microfilms or in any other physical way, and transmission or information storage and retrieval, electronic adaptation, computer software, or by similar or dissimilar methodology now known or hereafter developed.

The use of general descriptive names, registered names, trademarks, service marks, etc. in this publication does not imply, even in the absence of a specific statement, that such names are exempt from the relevant protective laws and regulations and therefore free for general use.

The publisher, the authors and the editors are safe to assume that the advice and information in this book are believed to be true and accurate at the date of publication. Neither the publisher nor the authors or the editors give a warranty, express or implied, with respect to the material contained herein or for any errors or omissions that may have been made. The publisher remains neutral with regard to jurisdictional claims in published maps and institutional affiliations.

This Springer imprint is published by the registered company Springer Nature Switzerland AG
The registered company address is: Gewerbestrasse 11, 6330 Cham, Switzerland

Preface

The Earth's interior is a source of heat, which attributes our planet a uniquely distinctive feature. It is actually the heat source that helps regulate the formation and evolution of rocks toward larger scales, while trending minerals and sediments toward minutely smaller scales. In this respect, the exploration of georesources (by-products) has to be closely related to petrogenesis (processes). Indeed, one of the major challenges encountered in quantitative geosciences lies in the eager attempt to retrieve the unknown causes of well-known effects, or inversely, predicting the unknown effects of well-known causes. It is actually in this junction that the beauty of science generally resides. More particularly, our planet is an ever-lasting stronghold of surprises worth of exhaustive studies, ranging from the inner thermodynamic processes affecting rocks evolution to the outer by-products characterizing exploration. Noteworthy, also, is that any geodynamic context proves to display peculiar geological, mineralogical, and petrological aspects, which help characterize the wide range of geographic areas lying on the surface.

These proceedings' volume is an outcome of the best-selected papers, accepted for presentation at the first Springer Conference of the Arabian Journal of Geosciences (CAJG-1), Tunisia 2018. The book exhibits a selection of the most recently conducted studies dealing with the area of rocks' petrogenesis and exploration of georesources, elaborated by experienced researchers from, but not limited to, well-established research institutes based in the Mediterranean and Mid-Eastern regions. The major raised themes and issues include, mainly, the composition and thermodynamics of rocks, mineralogy and mineral resources, geology and exploration of ore deposits, geochemistry, and provenance of sediments. This volume should provide new insights into the processes and products associated with the Earth's interior and the relating georesources. More specifically, the most recently drawn observations and proxy datasets, as figured in the book, should help fill some important gaps persisting in the existing mineralogical, geochemical, petrological, and volcano-logical records across, but not restricted to, the Mediterranean and Mid-Eastern regions.

Barcelona, Spain
Bari, Italy
Mexico City, Mexico
Benha, Egypt/Kiel, Germany
July 2018

Domenico M. Doronzo
Emanuela Schingaro
John S. Armstrong-Altrin
Basem Zoheir

Acknowledgements

Our appreciation is extended to the authors of the papers for their hard and diligent work in producing high-quality contributions. We would like to thank the reviewers of the papers for their in-depth reviews and great efforts in improving the quality of the papers. Also, thanks are extended to Amjad Kallel who supervised and handled the evaluation process, to Sahbi Moalla who handled the submission and evaluation system for the ten conference proceedings volumes, and to the publishing staff of Springer headed by Nabil Khélifi, Senior Editor for their efforts and contributions in completing this conference proceedings volume. All the above-mentioned efforts were very important in making this book a success.

About the 1st Springer Conference of the Arabian Journal of Geosciences (CAJG-1), Tunisia 2018



The *Arabian Journal of Geosciences (AJG)* is a Springer journal publishing original articles on the entire range of Earth sciences in partnership with the Saudi Society for Geosciences. The journal focuses on, but not limited to, research themes which have regional significance to the Middle East, the Euro-Mediterranean, Africa, and Asia. The journal receives on average 2000 submissions a year and accepts around 500 papers for publication in its 24 annual issues (acceptance rate 25%). It enjoys the participation of an editorial team of 100 international associate editors who generously help in evaluating and selecting the best papers.

In 2008, Prof. Abdullah Al-Amri, in close partnership with Springer, founded the Arabian Journal of Geosciences (AJGS). In this year, the journal celebrates its tenth anniversary. On this occasion and to mark this event, the Founder and Editor-in-Chief of the AJGS Prof. Al-Amri organized in close collaboration with Springer the 1st Conference of the Arabian Journal of Geosciences (1st CAJG) in Hammamet, Tunisia, from November 12 to 15, 2018 (www.cajg.org).

The conference was an occasion to endorse the journal's long-held reputation for bringing together leading authors from the Middle East, the Euro-Mediterranean, Africa, and Asia who work at the wide-ranging fields of Earth sciences. The conference covered all cross-cutting themes of Geosciences and focused principally on the following ten tracks:

- Track 1. Climate, paleoclimate and paleoenvironmental changes
- Track 2. Geoinformatics, remote sensing, geodesy
- Track 3. Geoenvironmental engineering, geomechanics and geotechnics, geohazards
- Track 4. Geography, geoecology, geoarcheology, geotourism
- Track 5. Geophysics, seismology
- Track 6. Hydrology, hydrogeology, hydrochemistry
- Track 7. Mineralogy, geochemistry, petrology and volcanology
- Track 8. Petroleum engineering and petroleum geochemistry
- Track 9. Sedimentology, stratigraphy, palaeontology, geomorphology, pedology
- Track 10. Structural/petroleum/mining geology, geodynamics, marine geology

The dynamic four-day conference provided more than 450 attendees with opportunities to share their latest unpublished findings and learn the newest geoscience studies. The event also allowed attendees to meet and discuss with the journal's editors and reviewers.

More than 950 short contributing papers to the conference were submitted by authors from more than 70 countries. After a pre-conference peer review process by more than 500 reviewers, 700 papers were accepted. These papers were published as chapters in the conference proceedings by Springer.

The conference proceedings consist of ten edited volumes, each edited by the following group of *Arabian Journal of Geosciences* (AJGS) editors and other guest editors:

Volume 1. Patterns and Mechanisms of Climate, Paleoclimate, and Paleoenvironmental Changes from Low-Latitude Regions

Zhihua Zhang (AJGS Editor): Beijing Normal University, Beijing, China
 Nabil Khélifi (AJGS Editor): Earth Sciences Editorial Department, Springer, Heidelberg, Germany
 Abdelkader Mezghani (Guest Editor): Norwegian Meteorological Institute, Norway
 Essam Heggy (Guest Editor): University of Southern California and Jet Propulsion Laboratory, Caltech, USA

Volume 2. Advances in Remote Sensing and Geo Informatics Applications

Hesham M. El-Askary (Guest Editor): Schmid College of Science and Technology at Chapman University, USA
 Saro Lee (AJGS Editor): Korea Institute of Geoscience and Mineral Resources, Daejeon, South Korea
 Essam Heggy (Guest Editor): University of Southern California and Jet Propulsion Laboratory, Caltech, USA
 Biswajeet Pradhan (AJGS Editor): University of Technology Sydney, Sydney, Australia

Volume 3. Recent Advances in Geo-Environmental Engineering, Geomechanics and Geotechnics, and Geohazards

Amjad Kallel (AJGS Editor): ENIS, University of Sfax, Tunisia
 Zeynal Abiddin Erguler (AJGS Editor): Dumlupinar University, Kutahya, Turkey
 Zhen-Dong Cui (AJGS Editor): China University of Mining and Technology, Xuzhou, Jiangsu, China
 Ali Karrech (AJGS Editor): The University of Western Australia, Australia
 Murat Karakus (AJGS Editor): University of Adelaide, Australia

Pinnaduwa Kulatilake (AJGS Editor): Department of Materials Science and Engineering, The University of Arizona, USA

Sanjay Kumar Shukla (AJGS Editor): School of Engineering, Edith Cowan University, Perth, Australia

Volume 4. Exploring the Nexus of Geoecology, Geography, Geoarcheology and Geotourism: Advances and Applications for Sustainable Development in Environmental Sciences and Agroforestry Research

Haroun Chenchouni (AJGS Editor): University of Tebessa, Algeria

Ezzoura Errami (Guest Editor): Chouaib Doukkali University, El Jadida, Morocco

Fernando Rocha (Guest Editor): University of Aveiro, Portugal

Luisa Sabato (AJGS Editor): Università degli Studi di Bari “Aldo Moro”, Bari, Italy

Volume 5. On Significant Applications of Geophysical Methods

Narasimman Sundararajan (AJGS Editor): Sultan Qaboos University, Muscat, Oman

Mehdi Eshagh (AJGS Editor): University West, Trollhättan, Sweden

Hakim Saibi (AJGS Editor): United Arab Emirates University, Al-Ain, Abu Dhabi, UAE

Mustapha Meghraoui (AJGS Editor): Université de Strasbourg, Strasbourg, France

Mansour Al-Garni (AJGS Editor): King Abdulaziz University, Jeddah, Saudi Arabia

Bernard Giroux (AJGS Editor): Centre Eau Terre Environnement, Québec, Canada

Volume 6. Advances in Sustainable and Environmental Hydrology, Hydrogeology, Hydrochemistry and Water Resources

Helder I. Chaminé (AJGS Editor): School of Engineering (ISEP), Polytechnic of Porto, Portugal

Maurizio Barbieri (AJGS Editor): University of Rome La Sapienza, Italy

Ozgur Kisi (AJGS Editor): Ilia State University, Tbilisi, Georgia

Mingjie Chen (AJGS Editor): Sultan Qaboos University, Muscat, Oman

Broder J. Merkel (AJGS Editor): TU Bergakademie Freiberg, Freiberg, Germany

Volume 7. Petrogenesis and Exploration of the Earth’s Interior

Domenico Doronzo (AJGS Editor): Consejo Superior de Investigaciones Cientificas, Spain

Emanuela Schingaro (AJGS Editor): Università degli Studi di Bari Aldo Moro–UniBa, Italy

John S. Armstrong-Altrin (AJGS Editor): The National Autonomous University of Mexico, Mexico

Basem Zoheir (Guest Editor): Benha University, Egypt and University of Kiel, Germany

Volume 8. Advances in Petroleum Engineering and Petroleum Geochemistry

Santanu Banerjee (AJGS Editor): Indian Institute of Technology Bombay, Mumbai, India

Reza Barati (AJGS Editor): The University of Kansas, Lawrence, KS, USA

Shirish Patil (Guest Editor): Saudi Aramco and King Fahd University of Petroleum and Minerals, Dhahran, Saudi Arabia

Volume 9. Paleobiodiversity and Tectono-Sedimentary Records in the Mediterranean Tethys and Related Eastern Areas

Mabrouk Boughdiri (AJGS Editor): University of Carthage, Amilcar, Tunisia

Beatriz Bádenas (AJGS Editor): University of Zaragoza, Zaragoza, Spain

Paul Selden (AJGS Editor): University of Kansas, Lawrence, KS, USA

Etienne Jaillard (Guest Editor): University of Grenoble Alpes, France

Peter Bengtson (AJGS Editor): University of Heidelberg, Heidelberg, Germany

Bruno R. C. Granier (AJGS Editor): University of Bretagne Occidentale, Brest, France

**Volume 10. The Structural Geology Contribution to the Africa-Eurasia Geology:
Basement and Reservoir Structure, Ore Mineralisation and Tectonic Modelling**

Federico Rossetti (Guest Editor): Università Roma Tre, Roma, Italy

Ana Crespo Blanc (Guest Editor): University of Granada, Spain

Federica Riguzzi (Guest Editor): National Institute of Geophysics and Volcanology, Roma, Italy

Estelle Leroux (Guest Editor): IFREMER, Unité Géosciences Marines, Plouzané, France

Kosmas Pavlopoulos (Guest Editor): Sorbonne University Abu Dhabi, Abu Dhabi, UAE

Olivier Bellier (Guest Editor): CEREGE, Aix-en-Provence, France

Vasilios Kapsimalis (Guest Editor): Institute of Oceanography, Hellenic Centre for Marine Research, Anavyssos, Greece

About the Conference Steering Committee

General Chair



Abdullah Al-Amri: Founder and Editor-in-Chief of AJGS, King Saud University, Saudi Arabia

Conference Supervisor



Nabil Khélifi: Senior Publishing Editor, Springer Middle East and North African Program Springer, a part of Springer Nature, Heidelberg, Germany

Scientific Committee Chair

François Roure: Guest of Editorial Board of AJGS, IFP—
Energies Nouvelles, France



Walter D. Mooney: Guest of Editorial Board of AJGS, US
Geological Survey Western Region, USA

Local Organization Chair

Mabrouk Boughdiri: Associate Editor of AJGS, University of
Carthage, Amilcar, Tunisia

Evaluation Chair



Amjad Kallel: Assistant Editor of AJGS, ENIS, University of Sfax, Tunisia

Publication Chair



Biswajeet Pradhan: Associate Editor of AJGS, University of Technology Sydney, Sydney, Australia



Essam Heggy: Guest of Editorial Board of AJGS, University of Southern California and Jet Propulsion Laboratory, Caltech, USA

Program Chair

Hakim Saibi: Associate Editor/Assistant Editor of AJGS, United Arab Emirates University, Al-Ain, Abu Dhabi, UAE



Domenico Doronzo: Associate Editor/Assistant Editor of AJGS, Consejo Superior de Investigaciones Cientificas, Spain

Communication Chair

Mohamed Ksibi: Guest of Editorial Board of AJGS, ISBS, University of Sfax, Tunisia

English Language Advisory Committee

Abdelmajid Dammak: ENIS, University of Sfax, Tunisia

Chokri Khalaf: FMS, University of Sfax, Tunisia

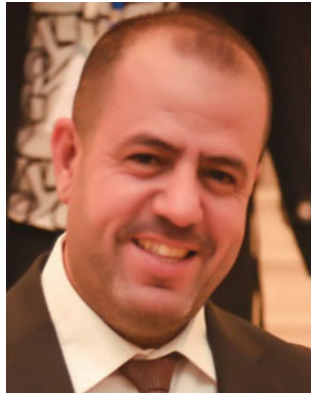
Dhouha Mabrouk: FLSHS, University of Sfax, Tunisia

Mohamed Elbahi: ENIS, University of Sfax, Tunisia

Sami Shami: ENIS, University of Sfax, Tunisia

Yasmine Basha: FLSHS, University of Sfax, Tunisia

Conference Manager



Mohamed Sahbi Moalla: Coordinator of AJGS, ISET,
University of Sfax, Tunisia

Contents

Part I Keynote

- Biogeochemical Mapping: A New Tool to Assess the Soil Quality and Health** 3
Pablo Higuera, Juan Antonio Campos, José María Esbrí, Eva M. García-Noguero, and Intissar Elmayel

Part II Petrogenetic Processes: Geochemistry, Geochronology and Geophysical Approaches

- Geochemical and Geophysical Evolution of Regional Mantle Flow Beneath Volcanic Harrats in the West Arabian Shield (Saudi Arabia)** 9
Abdullah Alamri, Robert Duncan, Adam Kent, and Fouzan Alfouzan
- Petrology, Geochemistry and Petrogenesis of the Sidi El Hemissi Triassic ‘Ophites’ (Souk Ahras, NE Algeria)** 13
Rabah Laouar, Halima Saadia Zanouda, Sihem Salmi-Laouar, Amar Sebai, Chrystèle Verati, Salah Bouhlel, and Adrian J. Boyce
- Geochronology, Petrogenesis and Tectonic Implication of A-Type Granite from Zaranda (North-Central Nigeria)** 17
Hafizullah Abba Ahmed, Lian-Xun Wang, Chang-Qian Ma, Ibrahim Garba, Musa Bala Girei, and Victor Ikechukwu Vincent
- New Model of Wadati-Benioff Zone in Java-Sumatra Subduction System and Its Tectonic Implication** 21
Mirzam Abdurrachman, Sri Widiyantoro, and Muhammad Zaky Abdul Alim
- Geothermal and Volcanic Evaluation of Harrat Rahat, Northwestern Arabian Peninsula (Saudi Arabia)** 25
Abdullah Al-Amri, Robert Mellors, David Harris, Vector Camp, and Kamal Abdelrahman
- The South West Atakor Volcanic District (Hoggar-Algeria): Petrography and Mineralogy from the Taessa Lavas** 29
Amel-Zoulikha Benhallou, Yasmine Megueni, Faouzi Boussisse, Faiza Ikhlef-Debabha, Youcef Babkar, Zakaria Boukhalifa, Khaled Aghanbilou, Abla Azzouni-Sekkal, Jean-Marie Dautria, and Jean-Louis Bodinier
- Primary Studies of Taessa-Torak Granitic Massif: Petrography and Mineralogy (Central Hoggar, Algeria)** 33
Faiza Ikhlef-Debabha, Abla Azzouni-Sekkal, Amel-Zoulikha Benhallou, Delphine Bosch, and Carlos J. Garrido

Tracing the Missing Argoland Beneath Java: Evidence from Geochemical Signature and Seismic Tomogram	37
Mirzam Abdurrachman, Sri Widiyantoro, Asep Saepuloh, and Idham Andri Kurniawan	
Rb-Sr and Oxygen Isotope Study of the Swat Granite Gneisses (Pakistan): Implications for the Magmatic Source and Tectonic Setup	41
Tahseenullah Khan, Abid Ahmad, Hafiz Ur Rehman, Muhammad Nawaz Chaudhry, Mamoru Murata, and Muhammad Zafar	
Textural and Mineral Chemistry Data Related to the Karapinar-Karacadag Volcanic Complex (Konya-Central Anatolia)	45
Huseyin Kurt, Gulin Gencoglu Korkmaz, and Kursad Asan	
Characteristic Magnetic Behavior of Southwest Nigerian Granitoids	49
Cyril Okpoli, Michael Oladunjoye, and Emilio Herrero-Bervera	
Petrographical and Geochemical Characteristics of the Mauritanides Belts' Birbirites	55
Didi Ould Moctar, Ali Moukadiri, Abdellah Boushaba, Sid'Ahmed Ould Mohamed Lemine, and Michel Dubois	
Petrography, Origin and Geochemical Characters of the Granitoids of the Southern Part of the Nellore Schist Belt, Andhra Pradesh, India	59
Sumit Kr. Mitra and Tushar Meshram	
Petrography, Mineralogy and Thermodynamic Modeling of Eclogites from the Serkout Area, Central Hoggar, Algeria	63
Doukkari Sidali, Godard Gaston, Ouzegane Khadidja, Arab Amar, and Bendaoud Abderrahmane	
The First Example of Kyanite-Staurolite-Garnet-Bearing Metapelites from the Hoggar (Eg�r� Terrane, South Algeria)	67
Amar Arab, Khadidja Ouzegane, Abderrahmane Bendaoud, Sidali Doukkari, and Gaston Godard	
Petrographic, Mineralogical and Geothermometric Study of Garnet Hornfels from the Region of Iddeleh Silet Hoggar Occidental Algeria	71
Khedoudja Nedjraoui, Abla Azzouni-Sekkal, Rekia Kheloui, Mohamed Hamoudi, and Riad Ben El Khazndji	
Physical Characteristics of the Massive Meteorite of Saudi Empty Quarter	75
V. Masilamani, Nasser Alarif, W. Aslam Farooq, Muhammad Atif, Shahid Ramay, Hayat Saeed Althobaiti, Saqib Anwar, Ibrahim Elkhedr, M. S. AlSalhi, and Bassam A. Abuamarah	
Study of the Compositional, Mechanical and Magnetic Properties of Saudi Meteorite	79
Muhammad Atif, Saqib Anwar, W. A. Farooq, M. Ali, V. Masilaimani, M. S. AlSalhi, and Bassam A. Abuamarah	
Part III Surficial Processes: Sedimentation and Facies Analysis	
Microfacies Analysis and Geochemical Evaluation of Campanian-Maastrichtian Limestone Along the Benin Flank, Southwestern Nigeria	85
Oladotun Oluwajana, Olugbenga Ehinola, Collins Ofiwe, Evidence Akhayere, Kehinde Egunjobi, Joseph Asanbe, and Oluwafemi Akinjo	

Heavy Metal Concentration of Sediments from the Eastern Niger Delta Basin, South-East Nigeria	89
Azubuike Ekwere	
Distribution of Major and Trace Elements in Soil and Sediments Along the Nile River and Delta—(Egypt): A Case Study	93
Wael Badawy, Octavian G. Dului, Marina V. Frontasyeva, and Hussien El-Samman	
Enigma of Ferruginous Inclusions in Evaporites	97
Rail Kadyrov, Mikhail Glukhov, Evgeny Statsenko, and Bulat Galiullin	
Grain Size Distribution and Enrichment Evaluation of Trace Metals in the Mediterranean Harbor Lagoon (Kalaât Andalous, Tunisia)	101
Samia Khsiba, Oula Amrouni, Chrystelle Bancon-Montigny, Karim Ben Mustapha, Lassaad Chouba, Nadia Gaâloul, and Gil Mahé	
Trace Metal Concentrations in Surface Water in Ichkeul Lake Basin: a Case Study	105
Nesrine Ouchir, Lassaad Ben Aissa, and Mabrouk Boughdiri	
Geochemistry and Mineralogy of the Miocene and Pliocenesediments of the Northern Margin of the Lower Chelif Basin (Western Tellian Domain, North Algeria)	109
Fatiha Hadji, Abbas Marok, and Ali Mokhtar Samet	
Mineralogical and Geochemical Characterization of the Northern Phosphatic Series of the Sra-Ouertane Basin (Tunisia)	113
Naima Ahmadi, Ali Enneili, Mongi Felhi, Khaoula Kaissi, Fathi Ben Mabrouk, and Ali Tlili	
Stable Isotope Geochemistry of the Pleistocene Lacustrine-Palustrine Carbonates (Borj Edouane Unit, NW Tunisia)	117
Naoufel Ghannem, Clemente Recio, Ildefonso Armenteros, and Kamel Regaya	
Geochemistry and Mineralogy of Paleocene-Eocene Depositional Sequences in Oued Thelja Section, SW Gafsa, Tunisia	121
Ali Enneili, Hadj Ahmed Amel, Mongi Felhi, Kamel Zayani, Nabil Fattah, and Ali Tlili	
Mineralogical and Geochemical Characterization of the Tamerza Area Upper Lutetian-Preabonian Successions (Southwest Tunisia)	125
Samiha Euch, Mongi Felhi, Nabil Fattah, and Ali Tlili	
Potential Heavy Mineral-Enriched Black Sand Deposits South Ras Banas Red Sea Coast (Egypt)	129
Tarek Ibrahim, Gouda Dabour, Minghua Ren, Gad El-Qady, Philip Goodell, Ibrahim Gaafar, Luis Sandoval, and Munazzam Ali	
Geochemistry of Urban Soil in the Fast-Growing Kuito City (Angola)	133
Maria Manuela Vinha G. Silva, Marina Cabral Pinto, Pedro Alexandre Dinis, and Lucas Mandavela	
Phosphorus Speciation and Trace Metals in Core Sediment of Kuwait Bay	137
Eqbal Al-Enezi and Fatema Al-Shammari	
New Insights on the Ermioni VMS Ore Based on Ore Texture and Host Rock Lithology and Geochemistry (SE Argolis Peninsula, Peloponnese, Greece)	141
Stavros Triantafyllidis and Nikolaos Diamantakis	

Elemental Geochemistry of Subsurface Sediments of Lower Baitarani Basin, East Coast of India: Implications for Paleoredox Condition	145
Uzma Parveen and S. Sreekesh	
Mineralogical and Chemical Comparison of Carbonate From Sites Selected for Artisanal Cement Production With Limestone Used in Commercial Operations	149
Freeman E. D, Senzani and Antoine F. Mulaba-Bafubiandi	
Stratigraphic and Mineralogical Study of Chouabine Formation in the Meknassy Basin (Central Tunisia)	153
Sinda Sassi, Karima Horchani-Naifer, Nabil Fattah, and Mokhtar Ferid	
What Factors Determine the Geometries of Fault-Associated Dolomitization Geometries in Shallow-Marine Carbonates?	157
Shuqing Yao, Enrique Gomez-Rivas, Juan Diego Martín-Martín, David Gomez-Gras, Anna Travé, Albert Griera, and John Howell	
Part IV Applied Mineralogy and Tectonics	
Fracture-Related Dolomitization Affecting Late Jurassic—Lowermost Cretaceous Syn-rift Deposits (Maestrat Basin, Southern Iberian Chain, Eastern Spain)	163
Anna Travé, Judit Nadal, Elisabet Playà, Ramon Salas, Juan Diego Martín-Martín, and Enrique Gomez-Rivas	
First Report of Cryptomelane in Altered Rhyolite from Tazrouk Volcanic District, Latea, Hoggar, Algeria	167
Riad Ben El Khaznadji, Abderrahmane Bendaoud, and Abderaouf Seffari	
Mineralogy Recognition from In-Situ Elemental Concentration Log Data Using Factor Analysis	171
Ahmed Amara Konaté, Heping Pan, Nasir Khan, Oumar Keita, Mamady Cissé, Mory Kourouma, and Daouda Keita	
Fluid Inclusions, Solid-Solid Transitions in Salt, Ceramics and Minerals to Calibrate the Microthermometric Stage	175
Mouna El Mekki-Azouzi and Claire Ramboz	
Palygorskite Versus Tetra (N-Methylpyridyl) Porphyrin: Characterization and Interaction	179
Amira Lajmi, Emmanuel Joussein, Stéphanie Leroy-Lhez, Marilyne Soubrand, Valentin Robin, and Mounir Medhioub	
Mg-Exchanged Montmorillonite Undergoing External Environmental Solicitation: Crystalline Swelling Process Investigation	183
Marwa Ammar, Walid Oueslati, and Abdesslem Ben Haj Amara	
Potassium Fixation in Beidellite Through Wetting and Drying	187
Hachemi Zaidi, Abdellah Bakhti, and Mohamed Larid	
Geochemistry of Hydrothermal Chlorite in the OB48 Borehole (Nefza, Northern Tunisia)	191
Randa Ben Abdallah, Mounir Medhioub, and Jean Marc Baele	
Elaboration and Characterization of New Ceramic Ultrafiltration Membranes from Natural Clay: Application of Treatment of Textile Wastewater	195
Saida Bousbih, Emna Errais, Raja Ben Amar, Joelle Duplay, Malika Trabelsi-Ayadi, and Fadila Darragi	

Characterization at High Temperature of the Porcelanite Mineral Phases from the Gafsa-Metlaoui Basin and Valuation in the Ceramic Domain	199
Rahma Bourawi, Ali Tlili, Jalila Essid, Raja Saidi, and Nabil Fattah	
Mineralogy and Geochemistry of Supergene Alteration of Neogene Hawaiites of Moktaa el Hadid (Nefza, Northern Tunisia)	203
Sonia Lazaar, Randa Ben Abdallah, Marilyne Soubrand, Emmanuel Joussein, and Mounir Medhioub	
Structural Properties of Phosphate-Washing Waste Based Geopolymeric Mortars	207
Rawia Dabbebi, José Barroso de Aguiar, and Samir Baklouti	
The Montagut Fault System: Geometry and Fluid Flow Analysis (Southern Pyrennes, Spain)	211
Luis Fernando Martinez Casas, Anna Travé, David Cruset, and Daniel Muñoz-López	
From Rock-Buffered to Open Fluid System During Emplacement of the Lower Pedraforca Thrust Sheet (South Pyrenees)	215
David Cruset, Jaume Vergés, Irene Cantarero, and Anna Travé	
Evolution of the Fluid System During the Formation of the Fault-Related Bóixols Anticline (Southern Pyrenees)	219
Nicholas Nardini, Daniel Muñoz-López, David Cruset, Irene Cantarero, Juan Diego Martín-Martín, and Anna Travé	
Controls on Convective Fluid Flow Systems Resulting in the Formation of Massive Diagenetic Alterations	223
Enrique Gomez-Rivas, Juan Diego Martín-Martín, Paul D. Bons, Albert Griera, Shuqing Yao, Maria-Gema Llorens, and Anna Travé	
Biogenic Methane Production from Various Coal Rank and Its Controlling Factors Using Ruminant Waste as a Microorganism-Consortium Source	225
Ahmad Helman Hamdani, Ellin Harlia, and Winantris Sanusi	
Part V Geological Research Applied to Mineral Deposits	
Sn-W Mineralization Associated with the DJILOUET Complex, Eastern Hoggar (Algeria)	231
Fatiha Oulebsir, Mokrane Kesraoui, and Dalila Nemmour-Zekiri	
Mineralogic Data and Geochemical Characteristics of the Berrahal Banded Iron Formations (Edough Massif. NE of Algeria)	235
Bachir Henni	
Contribution to the Study of Bauxites' Formation in the Fongo-Tongo (Western Cameroon) Sites	241
Franck Wilfried Nguimatsia Dongmo, Rose Fouateu Yongue, Anthony Temidayo Bolarinwa, Ralain Bryan Ngatcha, Christopher Fuanya, and Marc Anselme Kamga	
Mapping Geochemical Anomalies Through Principal Components Analysis in BIF Mines: An Approach Referring to the Bonito Mine, Northeastern Brazil	245
Helano Fonteles, Henrique Pereira, Carla Rocha, and César Veríssimo	
The Mineral Exploration of the Iron Ores in the Eastern Aswan, by Using Geophysical Techniques	249
Mahmoud Mekkawi, Sultan Arafa, Ayman Ismail, and Mohamed Abbas	

Unique PGE-Cu-Ni Oktyabr'skoe Deposit (Noril'sk Area, Siberia, Russia): New Data on Its Structure and Mineralization	253
Nadezhda Krivolutskaya, Maria Nesterenko, Bronislav Gongalsky, Dmitry Korshunov, Yana Bychkova, and Natalia Svirskaya	
Micro-Geochemical Research in Mineral Exploration, Case Study of the Massive Sulfides of the Bathurst Mining Camp, Canada	257
Azam Soltani Dehnavi	
Gold Metallogeny of the Egyptian South Eastern Desert	261
Basem Zoheir, Ashraf Emam, Nehal Soliman, and Astrid Holzheid	
Geology, Petrography, and Mineral Chemistry of the Zn Pb-Cu-Sulfide Deposits of the Filfila Massif (East Algeria)	265
Touati Lyes, Kolli Omar, and Boutaleb Abdelhak	
Reef Cenomanian Carbonate Hosted Fluorite Ore Deposits at Jebel Mokta, Northeastern Tunisia	269
Bejaoui Jaloul	
Geomagnetic Assessment of the Igbeti Marble Deposit (Nigeria)	273
Saminu Olatunji and Warith Adebisi	
Mineralogical and Sulfur Isotopes in Ghar Roubane Barite Lead-Zinc Deposit, (Western Algeria)	277
Nacera Hadj Mohamed, Abdelhak Boutaleb, Maria Boni, and Djamel Eddine Aissa	
Cr-Ni-PGE Mineralization and Serpentinization of Peridotites in Beni Bousera Massif (Internal Rif, Morocco)	281
Zaineb Hajjar, Fernando Gervilla, and Amina Wafik	
The Use of Rare Earth Elements Patterns in the Exploration of Massive Sulphide Ores, Ariab Area, Red Sea Hills, NE Sudan	285
Samia Ibrahim, Elshiek Mohammed, and Murad Ali	
Classification of Composite Pegmatite via Staining and Digital Image Processing in the Bulfat Complex, Qala Deza, NE (Iraq)	291
Shareef Th. Al-Hamed, Khalid J. Aswad, and Nabaz R. Aziz	

About the Editors



Dr. Domenico M. Doronzo is a holder of a B.Sc., an M.Sc., and a Ph.D. degree (in 2011) in Earth Sciences from Università degli Studi di Bari Aldo Moro, Italy. Theses and specialties related to the degrees include physical volcanology, experimental and computational fluid dynamics, petrology, and natural hazards. Since then he has worked in volcanology and sedimentology, fluid dynamics and combustion, environmental sciences, and rock physics in the United States, Italy, and Mexico. He is currently a contract Researcher at the Consejo Superior de Investigaciones Científicas, Spain. Particularly, he has received the Rittmann Medal (in 2014) from the Associazione Italiana di Vulcanologia, usually assigned to the best young Italian volcanologist. His research interests were focused on integrating theory, field, numerical modeling, experiments, and laboratory experiments aimed to study the geological processes and products in volcanic areas as based on fluid dynamics and natural hazard perspectives. More specifically, he engages in studying pyroclastic energy currents, sand and dust storms, turbidity currents, man-made environmental phenomena, and georesources. He has recently coordinated the Topical Collection on Dust for the Arabian Journal of Geosciences. He is an Associate Editor of the Arabian Journal of Geosciences, responsible for evaluating submissions associated with the areas of Petrology, Volcanology, and Georesources, as an Assistant Editor supporting the Editor-in-Chief.



Dr. Emanuela Schingaro holds a B.Sc. in Physics (1990) and a Ph.D. in Earth Sciences (1994) from the Università degli Studi di Bari (Italy). Presently, she is an Associate Professor of Mineralogy at the Department of Earth and Environmental Sciences of the Università degli Studi di Bari ALDO MORO (Italy). The scientific activity is focused mainly on the area of mineralogical crystallography (single crystal and powder X-ray diffraction). Research interests include mainly the subjects of crystal chemical characterization of complex silicate minerals, relationships between crystal chemistry and geologic environments/petrogenetic conditions, clay minerals characterization, structure and disorder in rare mineral phases, along with the thermal behavior of minerals and their solid-state transformations. Collaboration with scientific societies, in 2002–2004, she is the Counselor at the Italian Society of Mineralogy and Petrology (SIMP); in 2007–2012, she is the Counselor at the Gruppo Nazionale di Mineralogia (GNM); and in 2015–2017, she is a member of the Teaching Committee of the Associazione Italiana di Cristallografia (AIC)—Italian Association of Crystallography. From December 1, 2015 to November 1, 2018, she was elected as a Representative of the Scientific Area 04 (Earth Sciences) in the Academic Senate. From October 31, 2014 to the present, she is a member of the Task Force of University of Bari Research. In 2018, she joined the AJGS as an Associate Editor, responsible for evaluating submissions relevant to the Mineralogy area.



Dr. John S. Armstrong-Altrin holds an M.Sc. in Geology (1993) from Madurai Kamaraj University (V.O. Chidambaram College, Tuticorin, Tamil Nadu, India) and a Ph.D. in Geology specialized in Sedimentology (1999) from University of Madras (India). He has completed his postdoctoral research (2003) at the Renewable Energy Institute (IER), Temixco, Mexico. He is currently a Senior Researcher at the Institute of Marine Sciences and Limnology of the National Autonomous University of Mexico, Mexico City. His research interests are focused on sediment provenance, geochemistry, tectonic environments, and U-Pb geochronology of zircon grains. He has conducted a noticeable number of research projects dealing with coastal and deep-sea sediments of the Mexico Gulf. He has published more than 60 research papers in indexed referenced Journals. He is one of the Associate Editors in the AJGS, and responsible for evaluating submissions in the fields of geochemistry, sediment provenance, sedimentology, and tectonics.



Dr. Basem Zoheir is a Full Professor of Mineralogy and Economic Geology at the Benha University (Egypt), and now an AvH fellow at Kiel Univ. (Germany). He was a DAAD doctorate at the University of Munich (Germany), a Visiting Researcher at the Universities of Tübingen, TU Clausthal, Geneva, Stockholm, Graz, TU Lulea, and a Fulbrighter at the USGS DFC-Denver. He has published no less than 42 articles in international peer-reviewed ISI journals. He served as a reviewer and guest editor for a number of Geoscience journals, and as an examiner for several research funding institutions. Aside the academic work, he has provided consultations to national and international mining companies exploring for gold in the Nubian Shield.

Part I
Keynote



Biogeochemical Mapping: A New Tool to Assess the Soil Quality and Health

Pablo Higuera, Juan Antonio Campos, José María Esbrí, Eva M. García-Noguero, and Intissar Elmayel

Abstract

Soil health is a recently established soil-biogeochemistry related concept. It has been defined as “the continued capacity of the soil to function as a vital living ecosystem that sustains plants, animals and humans”. As such, it can be considered as an approach to the consideration of soil as a living being. The parameters used to assess soil health are multiple, some of which are easy and cheap to measure, while others prove to be economically costly and time-consuming, as it is the case with the genetic identification and characterization of the microbiological communities, living in a certain soil, which represent the soil biodiversity and vitality. Other parameters can be considered as approximations to this concept. In this introduction to the concept, we consider to put forward three case studies. Two of them correspond to real “case studies”, carried out in heavily polluted soils in relation with mining activity. As for the third study case, it corresponds to a recently funded project aimed to get a global view of the soil health relevant to the entirety of the South-Central Spain region.

Keywords

Biogeochemistry • Soil • Environment • Assessment • Case studies

P. Higuera (✉) · J. A. Campos · J. M. Esbrí · E. M. García-Noguero · I. Elmayel
Instituto de Geología Aplicada, Universidad de Castilla-La Mancha, 13071 Ciudad Real, Spain
e-mail: pablo.higuera@uclm.es

P. Higuera · E. M. García-Noguero
Escuela de Ingeniería Minera e Industrial de Almadén, 13400 Almadén (Ciudad Real), Spain

J. A. Campos · J. M. Esbrí
Escuela Técnica Superior de Ingenieros Agrónomos de Ciudad Real, Universidad de Castilla-La Mancha, 13071 Ciudad Real, Spain

I. Elmayel
Sfax University, 3029 Sfax, Tunisia

1 Introduction—Concepts of Soil Quality and Health

Soil has for long been intensively affected with human activities ever since the initiation of agricultural practices. In particular, modern agriculture, highly dependent on the use of phytosanitary products for the production of intensive crops, has deeply modified the biogeochemistry of soil. Such products prove to depend highly on both of the soil’s inorganic composition, and on the biochemical activity developing on this substrate. On these bases, the soil quality concept turns out to be quite recognizable, implying the soil’s characteristics which influence its agronomic productivity. Accordingly, a modern consensus definition should be: “the capacity of a soil to function, within ecosystem and land use boundaries, to sustain productivity, maintain environmental quality, and promote plant and animal health” [1]. Actually, the soil health concept is rather modern, most often defined as “the continued capacity of the soil to function as a vital living ecosystem that sustains plants, animals and humans” [2, 3]. This implies well identifying and quantifying the temporal evolution of quality, i.e., the productivity trends, based on the generalized supposition of a decay in productivity occurring in several soils exploited for extremely long-time spans, applying soil complements, but without any heed being paid to the soil-management related effects on the soil associated microbiota.

Soil quality has been traditionally assessed by means of classical edaphological parameters, including, the soil reactivity (pH), its soluble salt contents (electric conductivity, EC), its content in organic matter (SOM), texture, structure, among several other well-known concepts and via normalized analytical procedures.

Besides, soil geochemistry, which involves the implementation of chemical analysis of major and trace elements through different analytical techniques, helps provide valuable information as to the possibilities of soil use potentials. It also provides the possibility of detecting anomalous

(excessively high or excessively low) concentrations of the so-called “potentially toxic elements”, including the alternative denominations of “heavy metals and metalloids” or similar, conditioning, via the “contaminated soil” concept, the agronomic possibilities of such soils.

Soil biochemistry has traditionally included the application of only a few basic parameters such as the SOM and/or other related parameters, including the total or available C, N and P contents. As for modern biochemistry, however, it includes a wider range of parameters, whose initial analyses have proved to demonstrate the importance of the related systematic monitoring, whereby soil quality and health could be effectively assessed, as basically supported by the biomass biodiversity.

On this basis, soil health assessment turns out to be rather focused on integrating and optimizing the soil’s chemical, physical, and biological characters, very critical for sustained productivity and environmental quality to take place.

2 Assessment of Soil Quality and Health

As already stated, the parameters constituting the soil’s classical “Edaphological parameters” are very well known, and the related measurement protocols are included in a wide range of general publications, with no important novelties being put forward over the last decades.

Geochemistry, on the other hand, has been marked with a drastic change in respect of the classical analytical-chemistry based primitive methods. Indeed, the newly advanced instrumental methods, displaying lower cost and analysis time consumption benefits, including the possibility of drawing reliable results directly from the solid samples, without the need for digesting the soil and, subsequently, diluting or handling the representative samples associated contamination risks, or getting errors in the analytical process. More particularly, the application of portable X Ray Fluorescence spectrometry has provided the possibility of reaching analytical results in real time, which could, in some cases, stand as an important tool, at least in respect of the previously implemented assessment methodology, whereby soil quality could be measured in terms of major-element contents, and possible soil contaminations detected in real time.

Biogeochemistry implies the determination of new parameters involving new technologies, whose economic cost has recently been marked with a remarkable decrease, such as the PCR technology (Polymerase Chain Reaction), or other even more recent approaches useful for identifying the soil persisting microbiological communities. Yet, other technologies, of simpler application, and/or lower cost, could still be applied in the preliminary assessment

procedures. Worth citing among these includes are the soil respirometry, enzymatic activity, microbial biomass, to cite but a few.

3 Case Studies

Three case studies, corresponding to the region of Castilla-La Mancha (South-Central Spain), were selected to constitute our research study set, as specified below.

3.1 Geochemical Map of the Castilla-La Mancha Agricultural Soils

Castilla-La Mancha is an extensive region sited in South-Central Spain, characterized with a low degree of industrial development, with an economy primarily based on agricultural practices, predominantly based on oil and wine production. Bravo et al. present the results of a geochemical study based on the analysis of topsoil samples, as collected from 200 soil profiles, relevant to the region based agricultural areas [4]. More specifically, it consists in a model of geochemical maps, closely similar to the general atlas [5, 6]. This study has been subject of a research project funding provided by CLM Regional government, entitled “Soil biogeochemistry of Castilla-La Mancha region—Elaboration of thematic maps and setting of background- and reference levels”. Accordingly, a total of 1000 additional samples of regional soils has been selected and will be analyzed using XRF, and sequential extraction tests. The analyses will serve to stand as a recently updated geochemical data base, including the characterization of baseline and anomalous levels, along with reference values for risk assessment studies.

Besides, the project will include the recollection of 200 samples for biogeochemical analysis, including microbial biomass, soil respirometry, microbial metabolic coefficient (qCO_2) and enzymatic activity.

3.2 Mercury Contamination and Dehydrogenase Activity

Almadén is a town located SW the CLM region, globally known as the source origin of almost third of total mankind produced mercury. The mining production of cinnabar (HgS), the main and almost-ore bearing elements (together with sphalerite, ZnS, usually rich in this element) had been taking place for more than 2000 years, ever since the Roman times up until 2008. The ore had been processed through pyrometallurgy to obtain the liquid metal from a number of precincts, always enclosed to avoid robbery, due to the

element's high price. One of these precincts is that sited in Almadenejos, a village within some 15 km East of Almadén, and with minor Hg ore deposits. The precinct related activity started in 1750 and ceased in 1890, and has remained closed since then. Millán et al. analyzed soil respirometry in the area lying soils, while Campos et al. studied the distribution of dehydrogenase activity in the same area [7, 8]. Both of the studies reached results proved to demonstrate that the presence of highly elevated levels of total mercury, along with its most toxic species, methylmercury, did not appear to affect the measured parameters. Notworthy, however, is that the sites with higher Hg and MeHg contents inside the precinct proved to display a practical absence of vegetal cover, highlighting the possible effect of these toxics on vegetation and, probably, on certain bacterial communities. In this respect, we consider conducting a thorough investigation of the of these toxics presence on the soil quality and health.

3.3 Decommissioned San Quintín Pb–Ag Mining Area

San Quintín constituted to act as a relatively important mine, active during the late 19th Century and the early 20th Century, for the extraction of Ag-rich galena (PbS). Together with galena, the presence of other sulphides, including pyrite and sphalerite, as well as the lack of reclamation measures after the mine and froth flotation plant, has produced an intense environmental affection in the area [9]. Zamorano et al. analyzed diverse enzymatic activities on the different scenarios actually present in the affected area, including soils with different degree of PTEs' based contamination, old residua piles and dumps, etc. [10]. The analyses included DHA as well as the activities of β -galactosidase, acid- and alkaline phosphomonoesterase and urease. The attained results proved to reveal that the different scenarios have had null activity for certain enzymes, but normal activities for others, evidencing the presence of different bacterial communities, each living, most probably, in media supporting their specific nutrition requirements.

A similar study is being carried out by I. Mayel, from the University of Sfax, in the Trozza mine (the Kairouan region, central Tunisia), with DHA variability comparable to this found in San Quintín mine area.

4 Conclusions

The major conclusions to be retained following the conduction of this communication are mainly:

- Biogeochemistry stands presently as an important tool whereby soil health could be effectively assessed, commonly recognized as the soil-to-a-living-being approach.
- Biogeochemical parameters are still underway. Still, some of them can be interpreted properly in terms of microbiological health, i.e., in terms of appropriate biodiversity and vitality of the corresponding-soil persisting microbiological communities.
- The soil-health related assessment processes are having, and would continue to have, an increasingly greater importance with respect to the environmental oriented studies.

References

1. Doran, J.W., Coleman, D.C., Bezdicek, D.F., Stewart, B.A.: Defining Soil Quality for a Sustainable Environment. SSSA Special Publication No. 35. Soil Science Society of America, Madison, WI, USA (1994)
2. Magdoff, F.R., van Es, H.M.: Building Soils for Better Crops: Sustainable Soil Management. Handbook Series Book 10. Sustainable Agric. Research and Education, Waldorf, MD, USA (2009)
3. USDA: Agricultural research service northern great plains research laboratory cover crop chart (<http://www.ars.usda.gov/Main/docs.htm?docid=20323>) (2014)
4. Bravo, S., García-Ordiales, E., García-Navarro, F.J., Amorós, J.A., Pérez-de-los-Reyes, C., Jiménez-Ballesta, R., Esbrí, J.M., García-Noguero, E.M., Higuera, P.: Geochemical distribution of major and trace elements in agricultural soils of Castilla-La Mancha (Central Spain). Finding criteria for baselines and delimiting regional anomalies. *Environ. Sci. Pollut. Res* (in press). <https://doi.org/10.1007/s11356-017-0010-6>
5. Salminen, R., Batista, M.J., Bidovec, M., Demetriades, A., De Vivo, B., Lima, A.: Foregs—Geochemical atlas of Europe. Part 1. Background information, methodology, and maps (2005)
6. IGME: Geochemical atlas of Spain (Atlas Geoquímico de España). Instituto Geológico y Minero de España, Madrid. In Spanish (2012)
7. Millán, R., Schmid, Th, Sierra, M.J., Carrasco-Gil, S., Villadóniga, M., Rico, C., Ledesma, D.M.S., Puente, F.J.D.: Spatial variation of biological and pedological properties in an area affected by a metallurgical mercury plant: Almadenejos (Spain). *Appl. Geochem.* **26**(2), 174–181 (2011)
8. Campos, J.A., Esbrí, J.M., Madrid, M.M., Naharro, R., Peco, J., García-Noguero, E.M., Amorós, J.A., Moreno, M.M., Higuera, P.: Does mercury presence in soils promote their microbial activity? The Almadenejos case (Almadén mercury mining district, Spain). *Chemosphere* **201**, 799–806 (2018)
9. Rodríguez, L., Ruiz, E., Alonso-Azcárate, J., Rincón, J.: Heavy metal distribution and chemical speciation in tailings and soils around a Pb–Zn mine in Spain. *J. Environ. Manag.* **90**(2), 1106–1116 (2009)
10. Zamorano, P., Campos, J.A., Moreno, M.M., González-Mora, S., Peco, J.D., Higuera, P.: Mapping biological activity in soils disturbed by mining processes. In: 22nd International Conference on Environmental Indicators (ICEI2017). Helsinki, Finland (2017)

Part II

**Petrogenetic Processes: Geochemistry,
Geochronology and Geophysical Approaches**



Geochemical and Geophysical Evolution of Regional Mantle Flow Beneath Volcanic Harrats in the West Arabian Shield (Saudi Arabia)

Abdullah Alamri, Robert Duncan, Adam Kent, and Fouzan Alfouzan

Abstract

In this study, three field programs have been conducted to determine the distribution and structure of volcanic landforms (lava flows, cinder cones, eruptive centers), and collect samples for analytical studies (age determination, mineral and whole composition, isotope geochemistry). The first expedition was to Harrat Lunayyir, where recent seismic activity has indicated the possibility for developing new volcanic systems. The second expedition targeted Harrat Hutaymah, as a remarkable area for providing an extraordinary range of mantle and crustal xenoliths, which are rock fragments carried up from great depths (40–70 km) by magmas that fed lava flows and cinder cones.

Keywords

Geochemical • Geophysical evolution • Regional mantle • Harrats • Western Arabian shield

1 Introduction

The Arabian Peninsula is composed of the western Arabian Shield and the eastern 45 Arabian Platform. The Shield is composed of Proterozoic island arc terranes, of a number 46, accreting together 600–900 Ma, and the basement rocks predominating the region have little to no sediment 3 47

A. Alamri (✉)
Department of Geology and Geophysics, King Saud University,
Riyadh, Saudi Arabia
e-mail: amsamri@ksu.edu.sa

R. Duncan · A. Kent
College of Earth, Ocean and Atmospheric Sciences,
Oregon State University, Corvallis, USA

F. Alfouzan
KACST, National Center for Oil and Gas Technology,
Riyadh, 11442 Saudi Arabia

cover. However, the Platform prevailing Proterozoic basement rocks are covered with up to 10 km of 48 Phanerozoic sediments. Several studies have shown that the upper mantle lying beneath the Arabian Shield and the Red Sea is anomalously slow, with 50 most likely associated with a shallow lithosphere-asthenosphere boundary (LAB), and 51 velocities increase towards the interior continent.

2 Materials and Methods

We reviewed previously set mapping and geologic data concerning the large Harrat Khaybar volcanic area, including the Kura, Khaybar and Ithnayn volcanic fields. The field operations were based at the Khaybar city, wherein mapping and sample collection were conducted. The suitability for future analytical work has also been assessed (age determinations, major and trace element compositions). All the existing seismic data, as provided by SGS and temporary seismic stations, have been analyzed through; (1) thin section preparation for petrographic examination of 36 samples, (2) samples' selection for age determination purposes by means of ^{40}Ar - ^{39}Ar incremental heating method and for the He isotope and melt inclusion studies, and (3) analysis of the major and trace element compositions through X-ray fluorescence and ICP-MS analyses. We derived new ^{40}Ar - ^{39}Ar incremental heating-age determinants, major and trace element concentrations, and He-isotopic compositions of lava flows out of selected harrats for a better understanding of the temporal distribution of the volcanism, contribution of distinct mantle sources, along with the variable depth and melting degree across the region. We also applied the ambient noise tomography technique using data drawn from twelve seismic stations relevant to the Saudi Geological Survey, as well as from deployed portable seismic stations.

3 Results

3.1 Evaluation and Integration of Entire Datasets

The most significantly striking results achieved are the following: Volcanic activity in the transect area started with the eruption of the Kura unit alkali basalt magmas as early as 8.4 Ma. A major break in the activity occurred between 5.9 and 1.7 Ma, followed by a more or less continuous activity up to the present. The Lunayyir harrat has been active ever since 600 ka till the present, and the Hutaymah harrat from 850 ka to the present. All centers have exhibited a recent geological activity (i.e., Holocene, younger than 10 ka). However, rocks younger than about 20 ka cannot be precisely dated by the ^{40}Ar - ^{39}Ar incremental heating method, and further resolution of age relationships among the youngest eruptions entail implementation of other methods, such as ^{14}C . A significant outcome of our dating determination studies was the recognition of errors occurring in the previously reported K-Ar age determinations, due to mantle-derived (“excess”) ^{40}Ar predominantly characterized with xenolithic material. Hence, the activity prevailing in Lunayyir and Hutaymah is considerably younger than previously reported.

The lava flows and cinder cones predominating the Harrats transect are predominantly of alkali basalt composition, and quite distinct from the tholeiitic basalt compositions characterizing the Red Sea floor and margins. This finding is the result of differing melting conditions (shallow and extensive under the Red Sea, deeper and less melting under the Arabian shield), and probably differing mantle source compositions (a depleted asthenosphere vs a somewhat enriched one). The rocks prevailing at Lunayyir and Hutaymah fall entirely within the alkali basalt and basanite fields, indicating little modification of magmas arising from the mantle to eruption sites occurring at the surface. At Harrat Khaybar, however, evolved compositions such as trachytes and phonolites occur, indicating that magmas have accumulated in shallow level crustal chambers, and have been fractionated due to the removal of minerals such as olivine, clinopyroxene and plagioclase. Evidence for the importance of crustal magma chambers lying at this Harrat site is also noticeable in the development of large central volcanoes.

Hence, it follows that the Harrat volcanic provinces could well be the result of a passive response to lithospheric faulting and thinning taking place around the plate edges. Active geodynamic models [1, 2] involve flow of the upper mantle into the region, emanating either from below or laterally, anomalously providing hot material for melting, lithospheric thinning by thermal erosion, and uplift due to

buoyancy. As for the vertical flow, taking the form of several small mantle plumes, it is located beneath the largest volcanic systems. Northward lateral flow may well originate from the Afar region, a well-known mantle plume that burst into activity at about 32 Ma [3]. Considerable support for these asthenospheric flow models is drawn from the relevant seismic imaging [4, 5].

4 Conclusions and Recommendations

Measurements of He-isotopic compositions predominant in Harrat Khybar turn out to be remarkably homogeneous at $8.2 \pm 0.1 R_A$ (2 s, n = 3). Major, trace and rare earth element compositions are similar to the southern neighboring Harrat Rahat, indicating that primitive magmas have been formed starting from 10 to 18% partial melting of depleted peridotite at 15–40 km depth. Additionally, an intriguing trend of increased melting degrees is noticed at shallowing depths, with time (Zr/Nb and La/Yb trends), which we interpret as being an evidence for the lithosphere thinning process. Inversely, the magmas lying at the Harrat Lunayyir (100 km east of the Red Sea) appear to be formed at 65–80 km depth from 8 to 12% upper mantle partial melting. The tholeiitic magmas erupted at the level of the Red Sea spreading axis prove to derive from $\sim 25\%$ partial melting of upwelling depleted upper mantle, occurring within depths of 0–10 km. This regional variability characterizing mantle melting can have its explanation in the modest lithospheric extension and mantle decompression melting coupled with northward asthenospheric flow from the Afar hot spot (Fig. 1).

Seismic tomographic inversion showed low shear wave velocity within the range of 2.0–3.2 km/s. The study area is clearly resolved with the lowest westward group velocity. It is worth mentioning that the study area is located towards the northeast of the May 19, 2009 epicenter (ML = 5.4), where the area is presumably enriched with magmatic intrusions. The crust surrounding the fast intrusion is slower in process than that suggested by the broader Arabian-Shield associated scale models. The largest magnitude events, as occurring early in the swarm, are concentrated at shallow depths (~ 2 to 8 km) beneath northern Harrat Lunayyir, and these events are associated with the dyke intrusion. Geologically, these Harrats may host between 150 and 300 °C geothermal systems, hence its importance as a potential energy production source. The reached results imply a possibility for the existence of magmatic materials, of low shear-wave velocity beneath Harrat Khaybar, as a result of magma upwelling in the region. Overall, the competing geodynamic models prove to fall into two broad categories: passive and active. Such novel results also support the

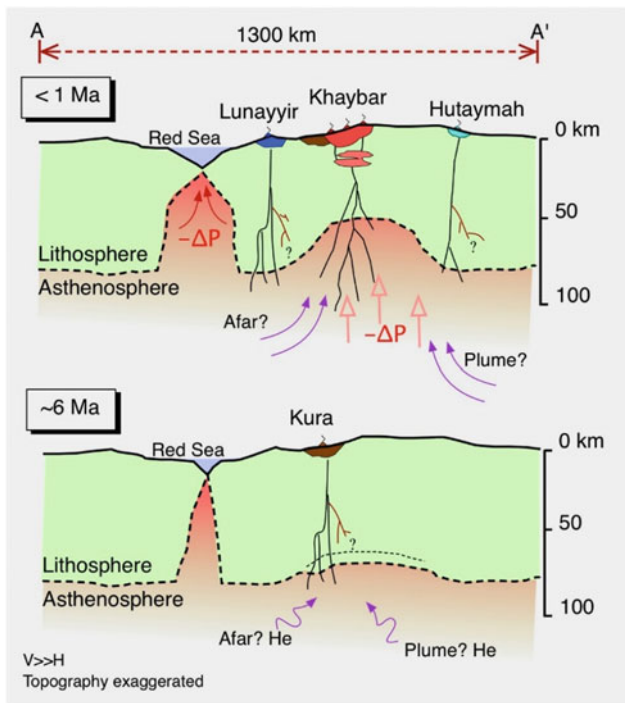


Fig. 1 Cartoon cross-section going from the Red Sea to Harrat Hutaymah for two time frames, (<1 Ma and ~6 Ma). The scale is schematic to show features. The boundary layer below the base of the lithosphere contains convective stirring of enriched, delaminated lithosphere with asthenosphere beneath the Makkah-Madinah-Nafud (MMN) lineament and eastward transport in an enriched sub-lithosphere layer to the lithosphere-asthenosphere boundary (LAB) beneath Hutaymah. Geochemical data support geophysical imaging of the LAB, which shows greater thinning under the MMN-line compared with marginal harrats such as Lunayyir and Hutaymah

presumption of active geodynamic models. The He-isotopic compositions of some of the Khaybar and Rahat lavas (with values >10 R_A) prove to indicate the implication and involvement of mantle plume material. Still, flow cannot be directly distinguished from beneath these lateral flow systems, lying north from the Afar region.

References

1. Camp, V.E., Roobol, J.: Upwelling asthenosphere beneath Western Arabia and its regional implications. *J. Geophys. Res. Solid Earth* **97**(B11), 15255–15271 (1992)
2. Krienitz, M.-S., et al.: Tectonic events, continental intraplate volcanism, and mantle plume activity in Northern Arabia: constraints from geochemistry and Ar–Ar dating of Syrian Lavas. *Geochem. Geophys. Geosyst.* **10**(4) (2009)
3. Chang, S.-J., Van der Lee, S.: Mantle plumes and associated flow beneath Arabia and East Africa. *Earth Planet. Sci. Lett.* **302**, 448–454 (2011). <https://doi.org/10.1016/j.epsl.2010.12.050>
4. Hansen, J., Sato, M., Ruedy, R., Lo, K., Lea, D., Medina Elizade, M.: Global temperature change. *Proc. Natl. Acad. Sci.* **103**, 14288–14293 (2006). <https://doi.org/10.1073/pnas.0606291103>
5. Hansen, J., Sato, M., Ruedy, R., Kharecha, P., Lacis, A., Miller, R., Nazarenko, L., Lo, K., Schmidt, G. A., Russell, G., Aleinov, I., Bauer, S., Baum, E., Cairns, B., Canuto, V., Chandler, M., Cheng, Y., Cohen, A., Del Genio, A., Faluvegi, G., Fleming, E., Friend, A., Hall, T., Jackman, C., Jonas, J., Kelley, M., Kiang, N.Y., Koch, D., Labow, G., Lerner, J., Menon, S., Novakov, T., Oinas, V., Perlwitz, J., Perlwitz, J., Rind, D., Romanou, A., Schmunk, R., Shindell, D., Stone, P., Sun, S., Streets, D., Tausnev, N., Thresher, D., Unger, N., Yao, M., Zhang, S.: Climate simulations for 1880–2003 with GISS modelE. *Clim. Dyn.* (2007). <https://doi.org/10.1007/s00382-007-0255-8>



Petrology, Geochemistry and Petrogenesis of the Sidi El Hemissi Triassic ‘Ophites’ (Souk Ahras, NE Algeria)

Rabah Laouar, Halima Saadia Zanouda, Sihem Salmi-Laouar, Amar Sebai, Chrystèle Verati, Salah Bouhlel, and Adrian J. Boyce

Abstract

Sited in Souk-Ahras, the Sidi El Hemissi region stands as part of the Tellian Atlas, where the Triassic formation tectonically outcrops under the Tellian nappes of the Maghrebide chain. Dubbed ‘ophites’, mafic rocks, mainly gabbros and dolerites are interbedded in $\sim 200 \times 30$ m lenticular body within the Triassic gypsum-rich formation. These rocks are composed of plagioclase, amphibole, pyroxene and scarce olivine crystals. Albitization represents the major alteration process, though chloritization, calcitization and epidotization of ferromagnesian minerals are also perceived. The geochemical observations prove to reveal that these mafic rocks exhibit medium- to low-Ti continental tholeiitic basalt affinity. They are enriched in LILE and LREE, as compared to HFSE and HREE, and display enriched-mid-ocean ridge basalt (E-MORB)-like incompatible element patterns in primitive mantle-normalized multi-element pattern. The weak Nb anomaly, along with the medium- to low-Ti contents, suggests

possible interaction between an enriched mantle source-derived magma and lower crustal rocks. These chemical features display high similarities with those sited in the central Atlantic magmatic province (CAMP) of upper Triassic–lower Jurassic age. Hence, they turn out to be considered as highly linked to the western branch of the Alpine Tethys system, geologically and tectonically associated with the Central Atlantic Ocean opening.

Keywords

Ophites • Geochemistry • Tholeiites • Continental flood basalts • Souk-Ahras

R. Laouar (✉) · H. S. Zanouda · S. Salmi-Laouar
Département de géologie, Université Badji Mokhtar Annaba,
B.P. 12, 23000 Annaba, Algeria
e-mail: rabahlaouar@yahoo.fr

R. Laouar
Laboratoire de Géodynamique, Géologie de l'Ingénieur et
Planétologie, F.S.T.G.A.T., USTHB, BP. 32, Bab Ezzouar,
16111, Algiers, Algeria

A. Sebai
Département de Génie Minier, E.N.P., B.P. 182, El Harrach,
Algiers, Algeria

C. Verati
Laboratoire GéoAzur, Université Nice-Sophia Antipolis,
Nice, France

S. Bouhlel
Mineral Resources Team, LRM2E, Geology Department,
Faculty of Sciences of Tunis, University Tunis El Manar,
Tunis, 2092, Tunisia

A. J. Boyce
Isotope Geosciences Unit, SUERC, East Kilbride, Glasgow,
G75 0QU, UK

1 Introduction

The Triassic formation that crops out in both the Algerian Saharan and Tellian Atlas appear to display blocks and sills of exotic mafic rocks. Often labelled ‘green rocks’ or ‘ophites’, these rocks are thought to be emplaced in an extensional setting during the Triassic period [1].

A number of Triassic tholeiitic magmatic products, resembling those observed in this region, are exposed in south-western Europe and north-western Africa. This magmatic activity is believed to be related to the continental rifting, as associated with the early stages of the Pangea breakup. As a novel contribution provided by the present study, an initial attempt is made to highlight the petrological and geochemical features characterizing the Triassic ophites of the Tellian Atlas, as modeled in the Sidi El Hemissi outcrops. The results to be achieved, we reckon, would help, to our mind, elucidate the magma sources and the geodynamic context attached to their placement siting.

The Sidi El Hemissi region is part of the Medjerda chain, pertaining to the Tellian Atlas. This area is characterized with large outcrops of the Triassic formation, brought up to the surface under the effects of the Atlasic and Alpine tectonic events. Overlaid with the Tellian and Numidian nappes

as well as the alloctonous Sellaoua units, such a formation is composed of chaotic evaporitic rocks of middle Muschelkalk to upper Keuper age [2].

The ophitic body is inter-bedded within a thick gypsum-bearing clay layer, displaying a lenticular form of about 200 m in length and up to 30 m in width. Overall, the rock is more or less altered and fractured, though massive lithologies with little alteration appear to be easily observable. In certain places, lava flows and brecciated rocks can also be identified. Based on local and detailed in situ field observations, granular, microgranular and microlithic textures turn out to be distinguishable. Mineral phases consist of large plagioclase laths of about 1 to 4 mm long, prismatic amphibole, orthopyroxene and clinopyroxene. Olivine is sporadically persistent along with the likely presence of rare biotite flakes. Accessory minerals are mainly opaques (oligiste), while the alteration products are sericite, saussurite, serpentine, uralite, epidote and chlorite.

2 Methods

Twenty samples were selected among the least altered lithologies for geochemical analyses. These samples were trimmed to remove regolith crust, trimmed to centimeter-size grains then sent to the ALS Minerals, in Spain, for major, trace and rare earth elements' (REE) analysis. The entirety of the samples were crushed using a jaw crusher and pulverised by means of a low-chrome steel mill at the ALS. The major oxides were analyzed using lithium metaborate fusion digestion and inductively coupled plasma atomic emission spectroscopy (ICP-AES). Trace elements, including rare-earth elements, were determined using lithium metabo-

rate fusion digestion and inductively coupled plasma mass spectrometry (ICP-MS). Based on the standards and replicates relating analyses, the analytical precision turned to be generally greater than 5% for most of the major and trace elements.

3 Results

According to the different relevant discrimination diagrams, the studied ophites fall within the field of tholeiitic basalts (Fig. 1a) and liable to be classified as medium- to low-Ti tholeiites, displaying continental tholeiitic basalt affinity (Fig. 1b). The chondrite-normalized REE diagram (Fig. 2) displays a negative slope with enrichment in light REE, as compared to the heavy REE. A weak negative Eu anomaly is observed in the highly depleted samples, whereas the enriched samples show weak positive anomaly. The REE pattern also exhibits weak Pr negative and weak Nd positive anomalies.

4 Discussion

The Sidi El Hemissi ophites appear to reveal a relatively low Zr/Nb and high Zr/Y as well as Nb/Y ratios, indicating that the source region of these rocks proves to be predominantly of enriched mantle (EM) type [8]. Similarly, the $(La/Ce)_N$ values are greater than 1, further confirming the enriched mantle origin presumption of such rocks. In the Ta/Yb versus Th/Yb diagram, the analyzed samples plot in a shifted position in respect of the mantle array (Fig. 3), clearly highlighting the possible interaction between an enriched mantle source-derived magma and a lower crustal rock

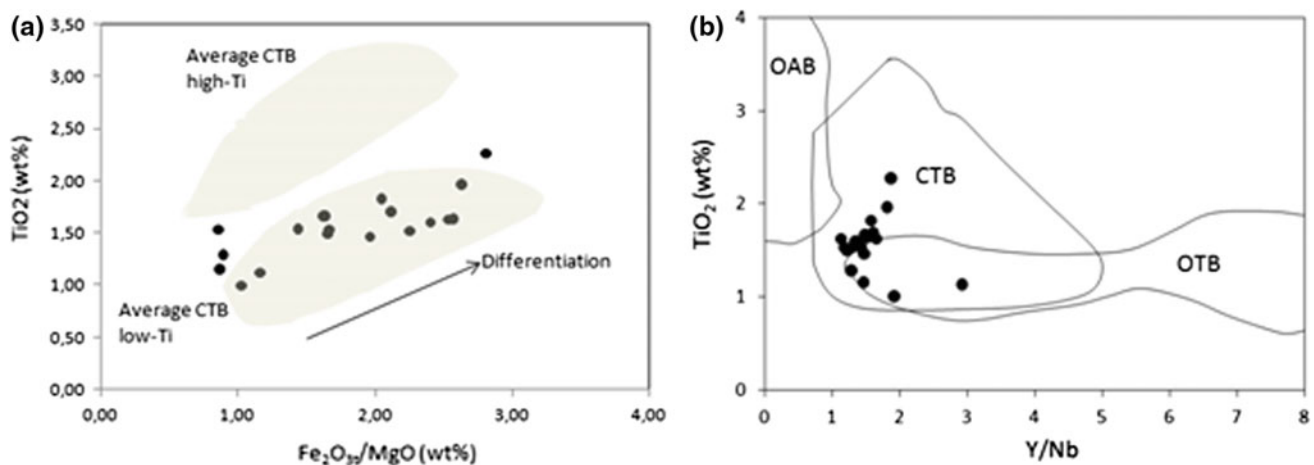


Fig. 1 a TiO_2 versus Fe_2O_3/MgO diagram of [3], and b Y/Nb versus TiO_2 discrimination diagram of [4], both of them highlighting the continental tholeiitic basalt affinity (CTB) of the Sidi El Hemissi ophites

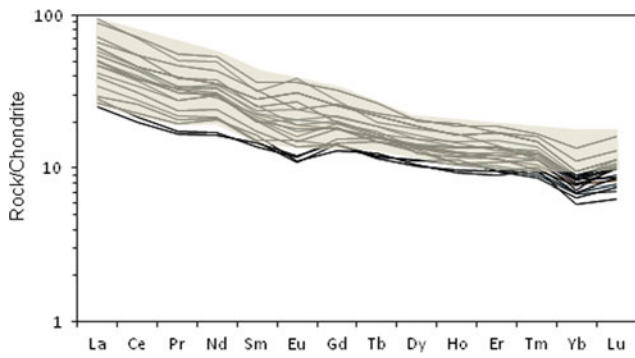


Fig. 2 Chondrite-normalized [5] REE patterns of the Sidi El Hemissi ophites. Shaded field is for low-Ti CAMP tholeiites in West Africa [6, 7]

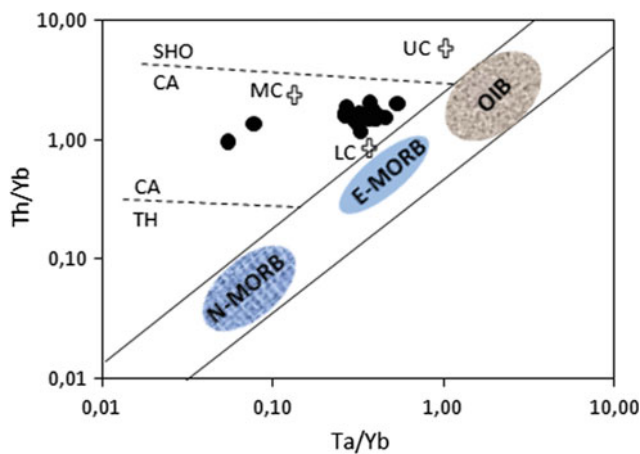


Fig. 3 Ta/Yb versus Th/Yb diagram indicating the position of Sidi El Hemissi ophites

source. Figure 4 highlights well that the studied samples clearly pertain to the field of enriched-mid ocean ridge basalts (E-MORB) and within-plate tholeiites.

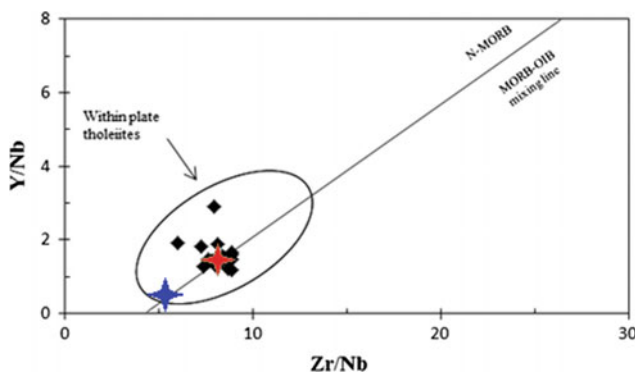


Fig. 4 Y/Nb versus Zr/Nb plot indicating the position of the Sidi El Hemissi ophites

The chemical composition of the investigated ophites proves to match well with those relating to the other late Triassic lava flows, especially those associated with the Central Atlantic Magmatic Province (CAMP). These similarities could be summed up as follows: (a) they highlight well the ophites’ tholeiitic character; (b) on the Fe_2O_3/MgO versus TiO_2 diagram of [3], they plot within the field of low-Ti continental flood basalts; (c) they reveal similar REE patterns with enriched LREE and LILE, as compared to HREE and HSFE; (d) they exhibit similar multi-element, primitive mantle-normalized patterns, often displaying an Nb anomaly; and (e) their geochemical features prove to confirm the persistence of a within-plate, anorogenic, tectonic type of setting. Accordingly, the Sidi El Hemissi ophites appear to reflect well a possible affinity with the CAMP. This igneous activity is commonly related to the Early Mesozoic fragmentation of the Pangea supercontinent and the subsequent opening of the Central Atlantic Ocean. Noteworthy, however, the origin of the Sidi El Hemissi ophites may well be considered to have a high association with the western branch of the Alpine Tethys system, as geologically and tectonically linked with the break-up of the Pangea and Central Atlantic Ocean opening.

5 Conclusions

The petrology and geochemistry study, as conducted in regard of the Sidi El Hemissi ophites, turn out to highlight persistent similarities with the findings documented concerning the CAMP of late Triassic–early Jurassic age, as actually cropping out on north-western Africa, south-western Europe, north-eastern and south-eastern America. Both magmas comprise low-Ti, LILE- and LREE-rich tholeiitic basalts, associated with the Early Mesozoic fragmentation of the Pangea supercontinent and, subsequently, the opening of the Central Atlantic Ocean.

References

1. Kurtz, J.: Geochemistry of early mesozoic basalts from Tunisia. *J. Afr. Earth Sci* **1**(2), 113–125 (1983)
2. David, L.: Etude géologique de la haute Medjerda. *Bulletin Service de la Carte Géologique de l’Algérie*, 11, Algérie (1956)
3. Albarede, F.: How deep do common basaltic magmas form and differentiate? *J. Geophys. Res.* **97**, 10997–11009 (1992)
4. Floyd, P.A., Winchester, J.A.: Magma type and tectonic setting, discrimination using immobile elements. *Earth Planet. Sci. Lett.* **27**, 211–218 (1975)
5. Sun, S.S., McDonough, W.F.: Chemical and isotopic systematics of oceanic basalts: implications for mantle composition and processes. In: Saunders, A.D., Norry, M.J. (eds.) *Magmatism in Ocean Basins*,

- vol. 42, pp. 313–345. Geological Society of London, Special Publication (1989)
6. Deckart, K., Bertrand, T.H., Liégeois, J.P.: Geochemistry and Sr, Nd, Pb isotopic composition of the Central Atlantic Magmatic Province (CAMP) in Guyana and Guinea. *Lithos* **82**, 289–314 (2005)
 7. Meddah, A., Bertrand, H., Elmi, S.: La province magmatique de l'Atlantique central dans le bassin des Ksour (Atlas saharien, Algérie). *C.R. Geosci.* **339**, 24–30 (2007)
 8. Workman, R.K., Hart, S.R.: Major and trace element composition of the depleted MORB mantle (DMM). *Earth Planet. Sci. Lett.* **231**, 53–72 (2005)

Geochronology, Petrogenesis and Tectonic Implication of A-Type Granite from Zaranda (North-Central Nigeria)

Hafizullah Abba Ahmed, Lian-Xun Wang, Chang-Qian Ma, Ibrahim Garba, Musa Bala Girei, and Victor Ikechukwu Vincent

Abstract

A-type granites were emplaced in Zaranda at 203 ± 1 Ma corresponding to Late Triassic. Petrologically, the A-type granite association includes syenite, quartz syenite and alkali granite of ferroan-alkalic composition. In Yb/Ta versus Y/Nb binary plots, they display certain characteristics typical of OIB derived A-type granites. The depletion in Ba, Sr, Ti and Eu indicates fractionation of feldspars, biotite, amphiboles and augite. The isotopic analysis of Zaranda, as drawn from a previously conducted study yielded lower $^{87}\text{Rb}/^{86}\text{Sr}$ values of 0.7048 and positive $\epsilon\text{Nd}_{(t)} + 0.9$. Overall, the above data proved to reveal that the Zaranda A-type granites were formed from assimilation fractional crystallization of OIB-like magmas, as derived from lithospheric mantle. Late Triassic crustal extension, preceding the opening of the Atlantic Ocean in Early Jurassic, was most probably the main trigger for the emplacement of such A-type granite suites, which ranks them within plate A-type granite *sensu stricto*.

Keywords

Zaranda • OIB derived A-type granites • Alkaline granites • Nigerian younger granite • Petrogenesis

1 Introduction

The Nigerian younger granite (NYG) province is widely acknowledged as a classical example of anorogenic A-type granites worldwide. This province is made up of some 52 intrusive complexes. Among them is the Zaranda complex, a high-level syenite-granite complex of about 6 km in diameter, that intruded a low-lying Pan-African basement consisting of gneisses and granitoids in north central Nigeria (Fig. 1a).

While the recently made advances in analytical techniques, relevant to the petrological, geochemical and isotopic studies, have significantly improved our understanding of A-type granites elsewhere in the world, there still remains a paucity of data in regard of the NYG. Our current understanding of the NYG is limited to few petrological and whole-rock geochemical studies carried out over the last few decades. Hence, through this modest contribution, an initial novel presentation attempt of the zircon U–Pb geochronology is provided, in addition to new geological and geochemical data concerning the Mesozoic A-type granites relating to the Zaranda complex in north-central Nigeria. The new data are used to discuss the petrogenesis associated with this Mesozoic alkaline granitoids and the relevant tectonic implications.

2 Geological Background and Sampling

North-central Nigeria is characterized with the predominance of underlining Precambrian Schists and gneisses, which were later intruded by Pan-African granitoids also referred to as Older granites. The Mesozoic younger granite province intruded the Precambrian-Paleozoic basement rocks episodically from north to south, extending from the Republic of Niger covering an area of about 200 km wide and 1600 km long [8]. In a previously conducted study using Rb–Sr isochron, it was revealed that the Zaranda

H. A. Ahmed · L.-X. Wang (✉) · C.-Q. Ma · M. B. Girei
Faculty of Earth Sciences, China University of Geosciences,
Wuhan, 430074, China
e-mail: lianxunwang@cug.edu.cn

H. A. Ahmed · V. I. Vincent
Department of Geology, Modibbo Adama University of
Technology, Yola, Nigeria

I. Garba
Department of Geology, Ahmadu Bello University, Zaria, Nigeria

M. B. Girei
Department of Geology, Bayero University, Kano, Nigeria

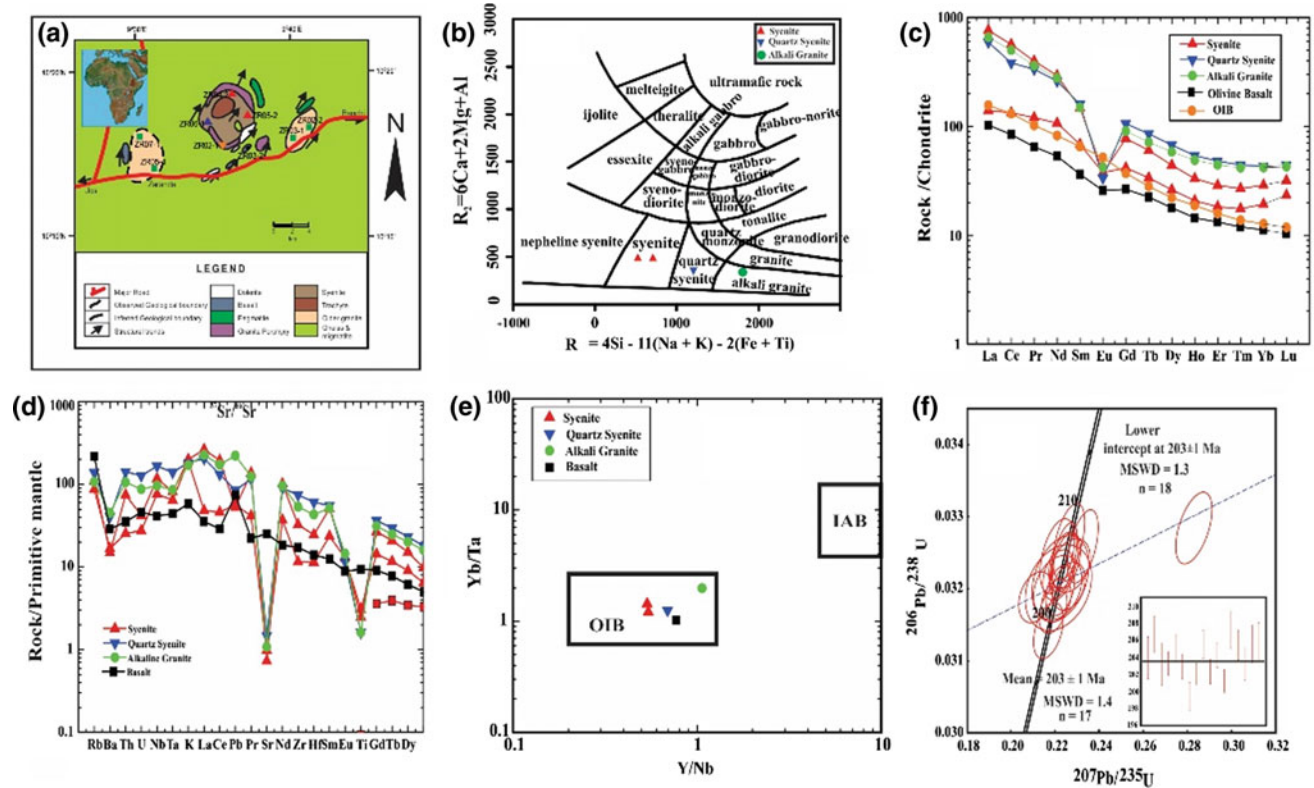


Fig. 1 a Geological Map of Zaranda, b R1–R2 Plot [2], c chondrite-normalized REE patterns, d primitive-mantle normalized trace element spider diagrams, e Yb/Ta versus Y/Nb [5], f LA-ICP-MS

zircon U–Pb concordia plots of Zaranda. The normalization values for Fig. 1c, d are from Sun and McDonough [9]

complex was emplaced around 190 ± 15 Ma [10]. The above set age, however, rests on the accuracy of Rb–Sr isotope technique.

Regarding the present study, however, five samples of syenites, quartz syenite, alkali granite were collected for whole-rock geochemistry and U/Pb isotopic dating study purposes. In addition, samples of olivine basalt associated with syenite and granites, pertaining to the area, were also taken for comparison ends. Generally, the rocks appear to range from fine to coarse grains in texture, with varying mineralogical compositions.

3 Results

3.1 Whole Rock Geochemistry

A classification diagram relevant to the Zaranda intrusive rocks is presented in (Fig. 1b). They prove to belong to the peralkaline series, and are characterized with a fairly high $\text{Na}_2\text{O} + \text{K}_2\text{O}$ content, along with (9.44–11.76 wt%), SiO_2 (62.94–70.07), MgO (0.07–0.11), CaO (1.0–1.59 wt%), Fe_2O_3 (4.0–6.1 wt%) and P_2O_5 (0.03–0.06) contents.

3.2 Sr–Nd Isotopes

The Sr–Nd isotopes, as used in this study, were the same as those reported by Dickin et al. [3]. An average of $^{87}\text{Sr}/^{86}\text{Sr}$ from two syenite samples was reported of a rate of 0.7049, while the average $\epsilon\text{Nd}(t)$ rate was + 0.9.

3.3 Geochronology

The results of LA-ICP-MS zircon U–Pb isotopic analyses yielded a weighted mean $^{206}\text{Pb}/^{238}\text{U}$ age of 203 ± 1 Ma (Syenite sample, 17 spots) (Fig. 1f). The zircons are mostly subhedral to euhedral, revealing a weak oscillatory zoning in cathodoluminescence (CL) images.

4 Discussion

4.1 Petrogenesis

The origin of A-type granitoids has been a highly debated issue for decades. To date, there remains a lack of consensus

regarding the origin/source of these rocks (e.g. [6]). Models advanced over the years, with the aim of setting up the origin of A-type granite, include fractional crystallization of mantle derived mafic magmas, with or without crustal contamination [7].

The low silica content in the less fractionated samples such as syenite and quartz syenite suggests that, model involving granitoid derivation from wholly crustal sources is not suitable for the Zaranda A-type suites. This leaves open the possibility that the granitoids were derived from fractional crystallization of mantle-derived magmas (e.g. [1]). More importantly, a consistent trend from olivine basalt to syenite and quartz syenite is apparent on both of the chondrite REE diagram and primitive mantle normalized multi-element plots (Fig. 1c, d), suggesting a common mantle source at least for the less fractionated rocks. Additionally, in the Yb/Ta versus Y/Nb plot [5], all the analyzed samples turn out to be plotted within the OIB field (Fig. 1e). However, the systematic increase in SiO₂ content from syenites-quartz syenite-alkali granite (62.94, 67.77, and 70.07 wt% respectively), appears to indicate increasing trend of crustal contamination. Likewise, the low ⁸⁷Rb/⁸⁶Sr value 0.7049 and positive εNd_(t) + 0.9 [3], indicate a largely mantle source with little input from crustal contribution, largely responsible for the formation of the Zaranda A-type granite suites. Therefore, it could well be inferred that the A-type granite of the Zaranda site appear to be most probably originated from a largely enriched (OIB-type) mantle source through assimilation fractional crystallization (AFC). Such a model proves to be consistent with both of the trace element and isotope data as presented in this work, and may well be applicable to some A-type granite elsewhere in the world.

4.2 Geochronology

The new LA-ICP-MS zircon U–Pb isotopic dating yielded 203 ± 1 Ma relevant to the Zaranda A-type granites, suggesting their emplacement during the Late Triassic. Although younger ages were obtained in regard of the complex by means of Rb–Sr and K–Ar dating techniques [10], the U/Pb isotope of zircon remains the most robust and reliable dating technique fit for the felsic igneous rock case. Consequently, the study reported age turns out to be rather more accurate.

4.3 Tectonic Setting

The geochemical results turn out to highlight that Zaranda granitoids appear to prevail within plate A-type granites *sensu stricto*. Similarly, on Nb–Y–3*Ga and Nb–Y–Zr/4 geochemical discrimination plot of [5], all samples plotted within a field typical of A₁ type granite, as derived from deep crust or upper mantle [4, 5]. Tectonic episodes, preceding the opening of the Atlantic Ocean during the Early Jurassic, were most likely dominated by crustal extension, rifting and magmatism. Extension during the Late Triassic probably caused the upsurge of small volume of metasomatized lithospheric OIB-like magmas. The Zaranda syenite and A-type granites could well have been formed from the evolved fraction of these magmas through assimilation fractional crystallization.

5 Conclusions

1. In this study, we present combined LA-ICP-MS U–Pb zircon isotope dating, Sr–Nd isotope and whole-rock geochemistry data in a bid to constrain the origin and age of the A-type granite-syenite association in Zaranda, north-central Nigeria.
2. The LA-ICP-MS U–Pb geochronology result appears to indicate that the A-type granite suites were emplaced at 203 ± 1 Ma, corresponding to Late Triassic.
3. The combined petrological Sr–Nd isotope and trace element data, such as Yb/Ta versus Y/Nb, prove to suggest that the A-type granite suites formed from assimilation fractional crystallization of enriched OIB-type mantle derived magmas. This finding is supported by the consistent variation noticeable in incompatible elements and the increase in silica stemming from olivine basalt-syenite-granite.
4. Late Triassic crustal extension that preceded the opening of Atlantic Ocean in Early Jurassic were most probably the main trigger for the emplacement of such A-type granites suites.
5. The role of enriched OIB-like mantle in the formation of A-type granites therefore merits further investigation especially as it can adequately account for the mixed crust-mantle isotopic signatures commonly observed in most A-type granite suites.

Acknowledgements We acknowledge the National Natural Science Foundation of China (Grant: 41530211, 41502046) and the Fundamental Research Funds for the Central Universities, China University of Geosciences (Wuhan) (CUGCJ1711) for the financial support rendered for this work. The Society of Economic Geologists Inc. USA is sincerely acknowledged for fully funding the fieldwork for this study.

References

1. Bonin, B.: A-type granites and related rocks: evolution of a concept, problems and prospects. *Lithos* **97**(1), 1–29 (2007)
2. De La Roche, H., Leterrier, J., Grandclaude, P., Marchal, M.A.: Classification of volcanic and plutonic rocks using R1R2-diagram and major-element analyses: its relationships with current nomenclature. *Chem. Geol.* **29**, 183–210 (1980)
3. Dickin, A.P., Halliday, A.N. and Bowden, P. A.: Pb, Sr and Nd isotope study of the basement and Mesozoic ring complexes of the Jos Plateau, Nigeria. *Chem. Geol. (Isot. Geosci. Sect.)*, **94**, 23–32 (1991)
4. Eby, G.N.: The A-type granitoids: a review of their occurrence and chemical characteristics and speculations on their petrogenesis. *Lithos* **26**(1), 115–134 (1990)
5. Eby, G.N.: Chemical subdivision of the A-type granitoids: petrogenetic and tectonic implications. *Geology* **20**(7), 641–644 (1992)
6. Huang, X.L., Xu, Y.G., Li, X.H., Li, W.X., Lan, J.B., Zhang, H. H., Liu, Y.S., Wang, Y.B., Li, H.Y., Luo, Z.Y., Yang, Q.J.: Petrogenesis and tectonic implications of Neoproterozoic, highly fractionated A-type granites from Mianning, South China. *Precamb. Res.* **165**, 190–204 (2008)
7. Litvinovsky, B.A., Jahn, B.-M., Zandvilevich, A.N., Saunders, A., Poulain, S.: Petrogenesis of syenite–granite suites from the Bryansky Complex (Transbaikalia, Russia): implications for the origin of A-type granitoid magmas. *Chem. Geol.* **189**, 105–133 (2002)
8. Rahaman, M.A., Van Breemen, O., Bowden, P., Bennett, J.N.: Age migrations of anorogenic ring complexes in Northern Nigeria. *J. Geol.* **92**, 173–184 (1984)
9. Sun, S., McDonough, W.F.: Chemical and isotopic systematics of oceanic basalts: implications for mantle compositions and processes. In: Saunders, A.D., Norry, M.J. (eds.), *Magmatism in the Ocean Basalts*, vol. 42. Geological Society of London, Special Publication, pp. 313–345 (1989)
10. Van Breemen, O., Hutchinson, J., Bowden, P.: Age and origin of the Nigerian Mesozoic granites—a Rb–Sr isotope study. *Contrib. Mineral. Petrol.* **50**, 157–172 (1975)

New Model of Wadati-Benioff Zone in Java-Sumatra Subduction System and Its Tectonic Implication

Mirzam Abdurrachman, Sri Widiyantoro,
and Muhammad Zaky Abdul Alim

Abstract

The previously Wadati-Benioff Zone (WBZ) proposed models, relevant to the Java and Sumatra region, turn out to be unable to provide thorough explanations as to the variation noticeable in the volcanic positions associated with both islands. Some volcanic positions are not aligned and prove to have different distances from the trench. For the purpose of providing a reliable explanation concerning the volcanic position related irregularity relevant to this particular area, 2977 relocated earthquakes concerning the interval 1964–2007 were implemented, and 2580 earthquake hypocenters were selected and applied to design a novel WBZ model. Our study reached results prove to indicate that the newly established WBZ model can be divided into four zones, namely, the Sumatra, West Java, Central Java, and East Java zones. These zones can help explain the volcanic position relating irregularity as formed in Sumatra and Java. The attained results are also confirmed through the phenocryst appearances and K_2O_{55} distribution persistent in the Java zone. In this meeting our newly established WBZ model relevant to the Sumatra and Java areas will be presented.

Keywords

WBZ • Sumatra • Java • Tectonic

1 Introduction

Several WBZ related models relevant to the Java-Sumatra area have already been proposed by several researchers. The models proposed by [1, 2], for instance, are deemed rather too simple and lacking in thorough explanation of the geological phenomena within the area, especially the non-linearity of the volcanic arc lying in the Java-Sumatra region. This research has been conducted in a bid to construct a detailed WBZ model, whereby the geological phenomena occurring in Java and Sumatra could be well explained.

2 Data and Method

Earthquake hypocenters relevant to the period 1964–2007 were derived from [3, 4]. A set of 2580 hypocenters were selected from a total number of 2977 points, and more than 300 hypocenters were excluded, as their related data are based on the overriding plate.

The earthquake data consist of time, coordinate, depth, and magnitude scale. In this context, we undertake to combine the entirety of these data to set up several maps, such as: coordinate vs depth map, depth contour of WBZ with vertical cross-sections, and a 3D model with wireframe using several software systems, i.e., Global Mapper, Surfer, and Micromine.

Supporting data from [5], e.g., the distance of the volcanoes to the trench, the distribution of mafic mineral phenocryst, in addition to K_2O_{55} are used to strengthen the interpretation of our new WBZ model. Our results are presented as follows.

M. Abdurrachman (✉) · M. Z. A. Alim
Department of Geology, Bandung Institute of Technology,
40132 Bandung, Indonesia
e-mail: mirzam@ge.itb.ac.id

S. Widiyantoro
Global Geophysics Research Group, Bandung Institute
of Technology, 40132 Bandung, Indonesia

3 Results

3.1 Hypocenter Distribution

Three dominant hypocenter-depth intervals have been distinguished, i.e., 0–49, 50–99, and 100–149 km. It is worth noting that below the Java Island, the hypocenters were recorded till depths >500 km, while in Sumatra, the hypocenters associated depths are <300 km.

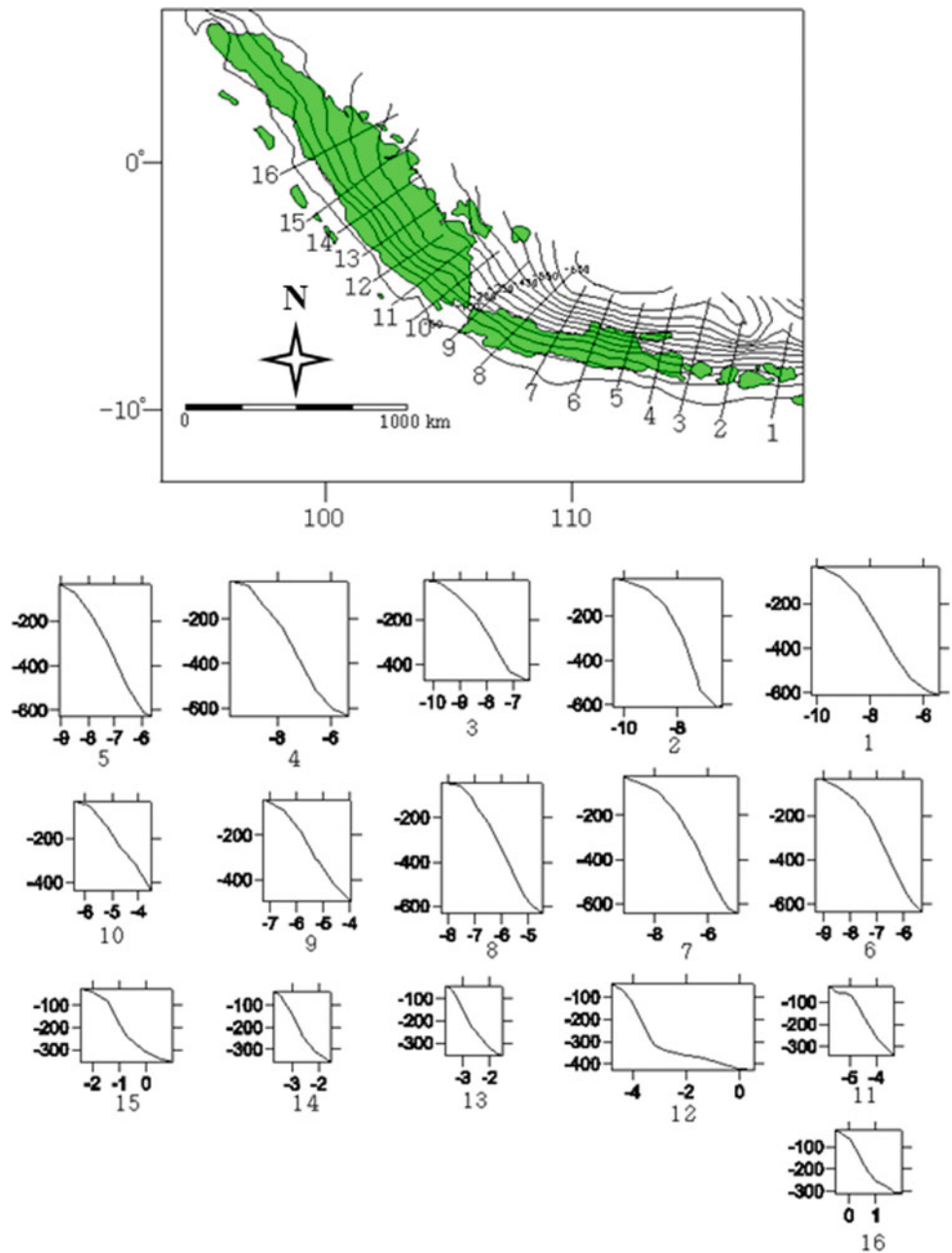
In the central and east Java areas, a seismic zone was discovered lying at the depth interval of 300–500 km. This

situation is interpreted as the tear zone in the subducted plate, as explained by [6].

3.2 WBZ Depth Contour Map and Cross-Sections

The Java relating contour pattern looks tighter in respect of the Sumatra contour, with neither straight nor linear contour lines (Fig. 1). This is interpreted as the outcome of noticeable changes perceived in subduction style and angle within each segment.

Fig. 1 WBZ depth contour map and cross sections



4 Discussion

A number of geological parameters have been applied to confirm our new WBZ model effectiveness, mainly, volcano density and distribution, mafic mineral phenocryst appearance (Fig. 2), and K_2O_{55} distribution (Fig. 3). A noticeable difference between the volcano density ratios in Sumatra and Java has been perceived (3: 3.5, respectively), indicating that

Java proves to be more dense as compared to Sumatra. We may argue that perpendicular subduction system controls volcano density. On the other hand, the volcanoes' distribution on each island (Figs. 2 and 3) is non-linear, as a result of the subduction angle (Fig. 1).

The appearance of mineral mafic phenocryst is strongly related to partial melting temperature and H_2O content [7]. Figure 2 illustrates the non-linear distribution of mafic

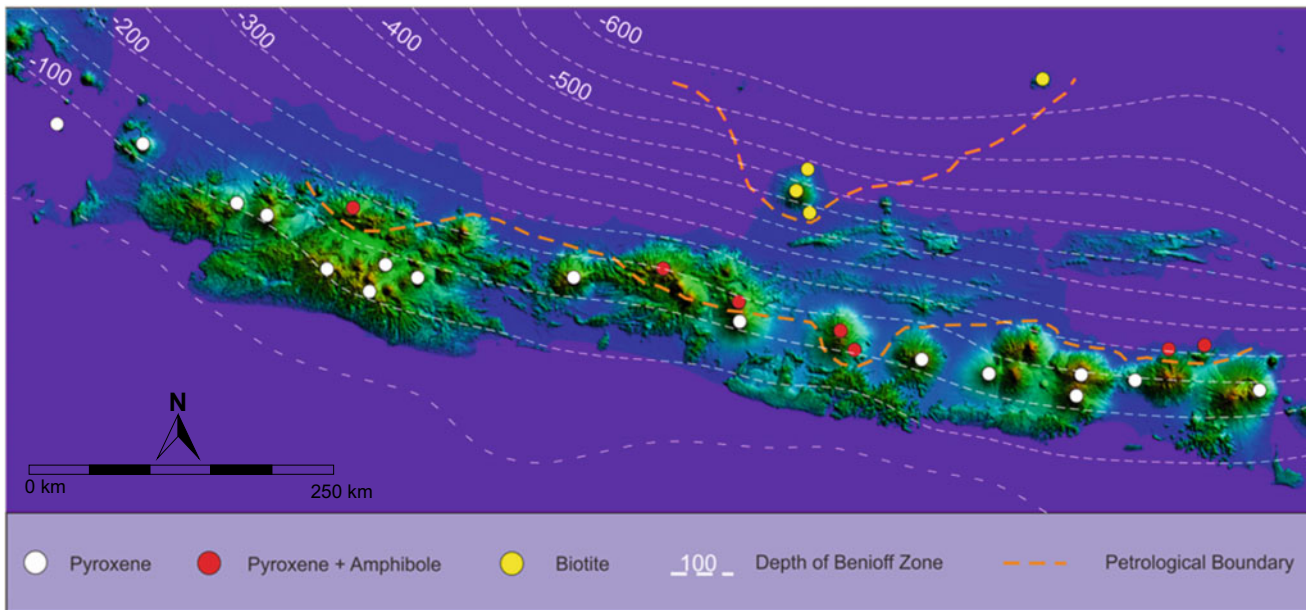


Fig. 2 Map of mineral mafic phenocryst zone of Java Island

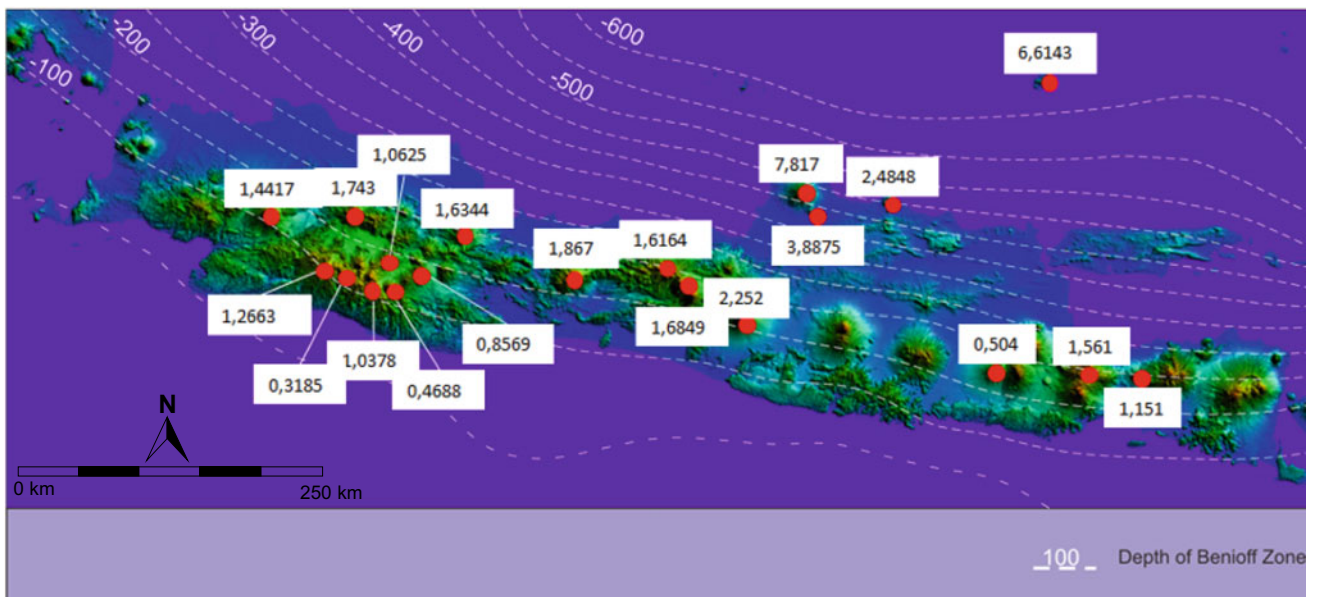


Fig. 3 Map of K_2O_{55} distribution for Quaternary volcanoes in Java

mineral phenocryst in Java, which may well be explained by the effect of subduction angle variation lying beneath Java, as depicted in Fig. 1 (segment 1–7).

Figure 3 shows a non-linear pattern of K_2O_{55} of Javan volcanic rocks. In West Java, for instance, low K_2O_{55} of Cikuray (0.46) is contiguous with medium value of Papan-dayan (1.03) [5]. The K_2O distribution generally increases with increasing distance from the trench. The irregularity noticeable in the K_2O_{55} distribution pattern in Java can be easily explained via the newly advanced WBZ model, as being a consequence of different subduction angle variations, as perceived in each segment, as shown in Fig. 1.

5 Concluding Remarks

Our newly put forward WBZ model helps depict a non-linear contour pattern as a result of subduction angle variation in Java and Sumatra. This new model, we consider, is likely to help in providing a certain explanation of some of the associated geological phenomena, such as the volcanoes' distribution and density, and the appearance of phenocryst as well as the K_2O distribution.

References

1. USGS Homepage: <https://pubs.usgs.gov/pp/1078/report.pdf>. Last accessed 21 Apr 2018
2. Hall, R.: Indonesia, geology. In: Gillespie, R., Clague, D. (eds.) *Encyclopedia of Islands*, pp. 454–460. University of California Press, Berkeley, California (2009)
3. Engdahl, E.R., van der Hilst, R.D., Buland, R.: Global teleseismic earthquake relocation with improved travel times and procedures for depth determination. *Bull. Seismol. Soc. Am.* **88**, 722–743 (1998)
4. Engdahl, E.R., Villasenor, A., DeShon, H.R., Thurber, C.H.: Teleseismic relocation and assessment of seismicity (1918–2005) in the region of the 2004 Mw 9.0 Sumatra-Andaman and 2005 Mw 8.6 Nias Island great earthquakes. *Bull. Seismol. Soc. Am.* **97**, S43–S61 (2007)
5. Abdurrachman, M., Pratama, F.Y.: Petrology and geochemistry of Java volcanoes, Indonesia: a key for understanding the lithospheric interior beneath Western Sunda Arc. IAVCEI Poster Presentation July 24th 2013, Kagoshima, Japan (2013)
6. Widiyantoro, S., Pesicek, J.D., Thurber, C.H.: Geological society, London. *Spec. Publ.* **355**, 139–155 (2011)
7. Sakuyama, M.: Lateral variation of H_2O contents in Quaternary magmas of Northeastern Japan. *Earth Planet. Sci. Lett.* **43**, 103–111 (1979)

Geothermal and Volcanic Evaluation of Harrat Rahat, Northwestern Arabian Peninsula (Saudi Arabia)

Abdullah Al-Amri, Robert Mellors, David Harris, Vector Camp, and Kamal Abdelrahman

Abstract

Saudi Arabia offers a strong potential for geothermal energy, but only a limited amount of exploration efforts has taken place. We conducted a preliminary, low-cost, reconnaissance level evaluation of the western volcanic areas (harrats) based on mapped geology and existing seismic data. The emphasis is on the Harrat Rahat volcanic area in western Saudi Arabia although a survey of other major harrats is conducted using geologic data. The goal is to test the procedure and identify areas for future, more intensive study.

Keywords

Geothermal • Volcanic • Harrat rahat • Evaluation Arabian peninsula

1 Introduction

Saudi Arabia has approximately 80,000 km² of lava fields, known as Harrats. They are represented by volcanic eruptions, mainly basaltic in composition, that extend along the coastal part of the Red Sea at the western of Saudi Arabia. Harrats of Khaybar and Rahat are believed to be the best in terms of high heat flow and enthalpy. The volcanic areas of the Arabian Peninsula show promise as hosts of geothermal and mineral resources. Modern systematic geothermal exploration strategies integrate a fundamental understanding

A. Al-Amri (✉) · K. Abdelrahman
Department of Geology and Geophysics, King Saud University,
Riyadh, Saudi Arabia
e-mail: amsamri@ksu.edu.sa

R. Mellors
Lawrence Livermore National Laboratory, Livermore, CA, USA

D. Harris
Deschutes Signal Processing, Maupin, OR, USA

V. Camp
San Diego State University, San Diego, CA, USA

of geology and tectonics with geophysical measurements to map areas of high geothermal and volcanic potential. The western third of the Arabian Peninsula is composed of the Precambrian Arabian Shield, overlain to the east by younger Phanerozoic rocks of the Arabian Platform. The Arabian Shield is composed of at least five geologically distinct terranes that were sutured together 715–630 million years ago and created the Najd fault zone, a major, 2000-km-long, left-lateral wrench fault that displaced the northern part of the craton ~250 km to the northwest.

2 Materials and Methods

The geologic survey of the harrats focused on evaluating potential sources of subsurface heat and groundwater. Sub-surface heat is based on age of erupted volcanics and expected volume of subsurface magma chambers. An analogy with an existing geothermal field in a similar setting in Mexico suggests that the faults and coincident seismicity may be associated with higher permeability. We have processed data from four seismic stations within the Harrat Rahat for detection of microseismic events and processed ambient noise for construction of a velocity model. Low velocities are observed within Harrat Rahat and two areas with coincident basements faults and possible enhanced subsurface temperatures are identified. The harrats are ranked in terms of geothermal potential, with Harrat Rahat, Lunayir, and Khaybar selected as highest potential. During the course of this work, two extended abstracts and presentations were made at the 2015 and 2016 Geothermal Resources Council annual meeting and this provided useful input.

3 Results and Discussion

The main zone of mantle upwelling beneath the harrats appears to be reflected in the Makkah-Madinah-Nafud volcanic line, a linear system of vents that extends in a northerly

direction over a distance of ~ 600 km [1]. This volcanic line marks the main eruption sites for Harrats Rahat, Khaybar and Ithnayn. Petrologic data suggest that this feature delineates the axis of mantle upwelling with lavas along its length generated by higher degrees of partial melting when compared to the harrat lavas lying farther to the west and east [1]. This main axis of upwelling is consistent with seismic tomography that has resolved a large north-south prong of hot mantle with an axis coincident with the Makkah-Madinah-Nafud volcanic line [2]. All of these harrats contain common Quaternary lava flows, many of which are Holocene in age. Two of these harrats (Khaybar and Hutaymah) are notable in containing abundant, young phreatomagmatic tuff rings, indicating the availability of water from sub-surface sources. There is no indication that such sources lie beneath Harrats Lunayyir or Ithnayn; however, both of these harrats show evidence of very young Holocene activity. In fact, the entire volcanic history at Harrat Lunayyir may be less than 600 ka [3], with the most recent event being a near eruption between April and June, 2009. Extensive geological mapping and historic eruptions in Harrat Rahat indicate active volcanic activity. The youngest unit (Qm7) is historic in age and includes the only two historic eruptions in Saudi Arabia for which eyewitness accounts exist: the 1256 AD eruption southeast of Al Madinah [4], and a small eruption in 641 AD expressed as four small pyroclastic cones located in the southwest corner of Al-Madinah City.

Subunit Qm6 is considered post-Neolithic in age because the lavas lack abundant Neolithic burial mounds that characterize the upper surface of other flows. These burial mounds appear to have a ^{14}C ages between 7000 and 4500 years B.P. We therefore believe that all of the units of Qm6 are at least as young as 6000 years B.P., and possibly younger than 4500 years B.P. Since this time, there have been 13 post-Neolithic and historic eruptions on northern Harrat Rahat. If we assume that all are younger than 4500 years, the average eruption rate since that time has been one per 346 years. Eroded vents older than Qm4 are spread across a wide region of northern Harrat Rahat. However, all of the young non-eroded vents (Qm4–Qm7) lie within a distinct northwest-trending linear axis in the central part of the harrat, the only exception being the 641 A.D eruption SW of Al-Madinah. The geologic data suggest that this central area should be the focus of geothermal exploration.

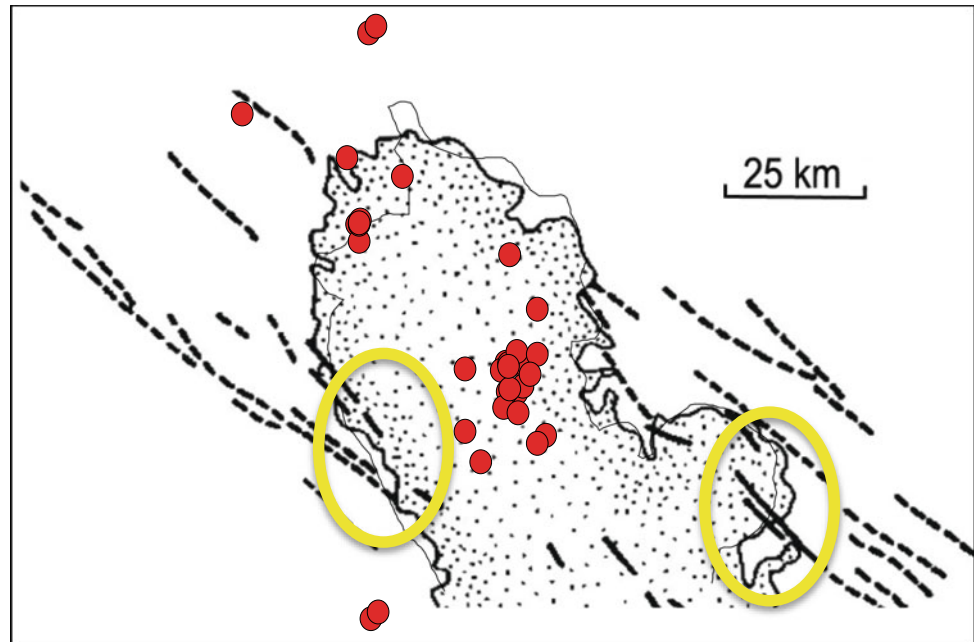
4 Conclusions

A preliminary evaluation of a selection of harrats suggest that several, based on likely subsurface heat, groundwater, and possible permeability are reasonable prospects for future evaluation. It should be noted that proximity to major metropolitan areas is a significant consideration in developing geothermal resources for power production, as this ensures a nearby market without the need for extensive power lines, as these lines add to the cost. Proximity to a city also reduces the cost and effort required for construction although locations near the coast may be useful in terms of providing energy for desalination. Harrats Rahat, Lunayir, and Khaybar appear to be the most promising. A major uncertainty is the distribution of permeability, which is essential. In general, the harrats are comparable in setting to the Tres Virgines geothermal plant in Baja California, Mexico. This plant currently produces 10 MW but is estimated to overlie a resource capable of 40 MW (Table 1).

As the Harrats cover a much larger area, the associated resources may be much larger. A preliminary investigation based on available seismic data at Harrat Rahat showed that advanced detection algorithms could increase the number of detected events although the increase was not sufficient to improve geothermal exploration. Ambient noise tomography is effective at estimating crustal velocities on a regional scale. It was not possible to evaluate attenuation due to sparse data. Geology indicates that the volcanism and seismicity roughly correlates with the northerly trending faults, which may be associated with higher permeability, as is the case in Mexico. Work in other areas suggests that intersecting fault are often productive and especially at a high angle. Ideally, areas with dense northerly trending faults intersecting with northeast trending faults would be the preferred areas to investigate further. The flow of groundwater in the region is unknown but it is possible that it flows outward from the slightly higher volcanic. Therefore, areas at the edge may be preferable as well as easier logistically for drilling equipment and power lines. This investigation could be based on detailed remote sensing combined with spectral analysis to detect zones of surface alteration, which are frequently associated with geothermal fluids. A high density deployment of seismometers on the Harrat would be useful to improve resolution of potential resources (Fig. 1).

Table 1 Summary of results and geothermal promise

Location	Subsurface heat source	Permeability	Water	Proximity to major areas of use	Overall assessment
Lunayir	Good	Perhaps good	Yes	Fair	Good
Khaybar	Good	Uncertain	Yes	Good	Good
Ithnayn	Poor	Uncertain	Unclear	Fair	Poor
Hutaymah	Poor	Uncertain	Yes	Fair	Fair
Rahat	Good	Possibly good	Yes	Good	Good

Fig. 1 Possible areas for further investigation (in yellow)

References

1. Camp, V.E., Roobol, J.: Upwelling asthenosphere beneath Western Arabia and its regional implications. *J. Geophys. Res. Solid Earth* **97**(B11), 15255–15271 (1992)
2. Chang, S.J., Van der Lee, S.: Mantle plumes and associated flow beneath Arabia and East Africa. *Earth Planet. Sci. Lett.* **302**(3–4), 448–454 (2011). <https://doi.org/10.1016/j.epsl.2010.12.050>
3. Duncan, R.A., Al-Amri, A.M.: Timing and composition of volcanic activity at Harrat Lunayyir, western Saudi Arabia. *J. Volcanol. Geoth. Res.* **260**, 103–116 (2013)
4. Camp, V.E., Hooper, P.R., John, R.M., White, D.L.: The Madinah eruption, Saudi Arabia: magma mixing and simultaneous extrusion of three basaltic chemical types. *Bull. Volcanol.* **49**(2), 489–508 (1987)

The South West Atakor Volcanic District (Hoggar-Algeria): Petrography and Mineralogy from the Taessa Lavas

Amel-Zoulikha Benhallou, Yasmine Megueni, Faouzi Boussisse, Faiza Ikhlef-Debabha, Youcef Babkar, Zakaria Boukhalfa, Khaled Aghanbilou, Abla Azzouni-Sekkal, Jean-Marie Dautria, and Jean-Louis Bodinier

Abstract

The Taessa lavas are located in the Atakor volcanic domain, (Hoggar Algeria). The Atakor district has undergone a significant magmatic activity during the Mio-plio-quadernary, which lead to the outpouring of massive amounts of alkaline lava. This magmatic activity resulted in the reactivation of the Pan-african orogenesis accidents that occurred during the collision between the African and European continents (Liégeois in *Plates, Plumes and Paradigms: Geological society of America Special Paper*, pp. 379–400, [10]). The petrographic and mineralogical studies relating to the Taessa's alkali basalts highlighted the persistence of two basaltic groups: olivine-pyroxene basalt and olivine-green-pyroxene basalt. They are mainly represented by magnesian olivines, whose crystallization process ended by 693 °C, according to the Fabriès geothermometer (Contr Mineral Petrol 69:329–336, [6]) olivine-spinel, pyroxenes (diopside, augite and hedenbergite) which crystallized by 500–1300 °C (phenocrysts), and by 1100–1300 °C (micro-lites), according to Lindsley geothermometer (Pyroxene thermometry. *American Mineralogist* 68:477–493, [11]), plagioclases (andesine –labrador) and sanidine, Oxides (titano-magnetites and spinel).

Keywords

Atakor • Central hoggar • Mio-plio-quadernary alkaline volcanism • Alkali basalts

1 Introduction

Several volcanic provinces were developed in the African plate during the Cenozoic. The Hoggar Volcanic Province (HVP) is located within the African plate ~1200 km south of the Mediterranean coast (Fig. 1). It is composed of several massifs of contrasting ages and eruptive styles. It covers a total area of approximately 11,700 km² with an estimated total volume of solids of 1650 km³. The magmatic activity began at around 34 Ma [1], and continued throughout the mio-plio-quadernary, leading to the outpouring of lavas overlying a Precambrian basement or its Tassili sandstone cover. It is associated with a crustal swell, whose significance remains controversial [10, 12]. The volcanic formations of the Atakor massif are made up of phonolite and trachyte domes, associated with scoria cones and necks. Mafic magma produced extensive lava flows that formed large dissected plateaus.

2 Geological Setting

The Atakor massif stands as a section of the Hoggar volcanic province, laying on top of a basement swell initiated during the Cretaceous. Its formations cover an area of 2150 km² for a total volume of rocks estimated roughly at 250 km³, corresponding to 10–15% of the entire Hoggar volcanic province. The Taessa lavas are situated, in the southern parts of Atakor, at the limit of the three terranes: Azou N'Fad, Laouni and Tefedest (Fig. 1a). It is bounded by 5 ° 17' to 5 ° 40' E longitudes, and by 22 ° 55' to 23 ° 25' N latitudes. The investigated lava flows [5] were mainly effused on the basement, consisting mainly of Eburnean migmatitic

A.-Z. Benhallou (✉) · F. Ikhlef-Debabha · Y. Babkar
Z. Boukhalfa · K. Aghanbilou
CRAAG, Route de L'observatoire, BP63, Bouzaréah,
Alger, Algérie
e-mail: zoulema@yahoo.com

A.-Z. Benhallou · Y. Megueni · F. Boussisse · F. Ikhlef-Debabha ·
A. Azzouni-Sekkal
Laboratoire de Métallogénie et Magmatisme de L'Algérie
(LMMA) USTHB, FSTGAT, BP 32, El Alia, 16111 Bab Ezzouar,
Alger, Algérie

A. Azzouni-Sekkal
SNV-STU, Université Abou Bekr Belkaïd, BP 119, 13000
Tlemcen, Algérie

J.-M. Dautria · J.-L. Bodinier
Géosciences Montpellier, Université de Montpellier,
Montpellier, France

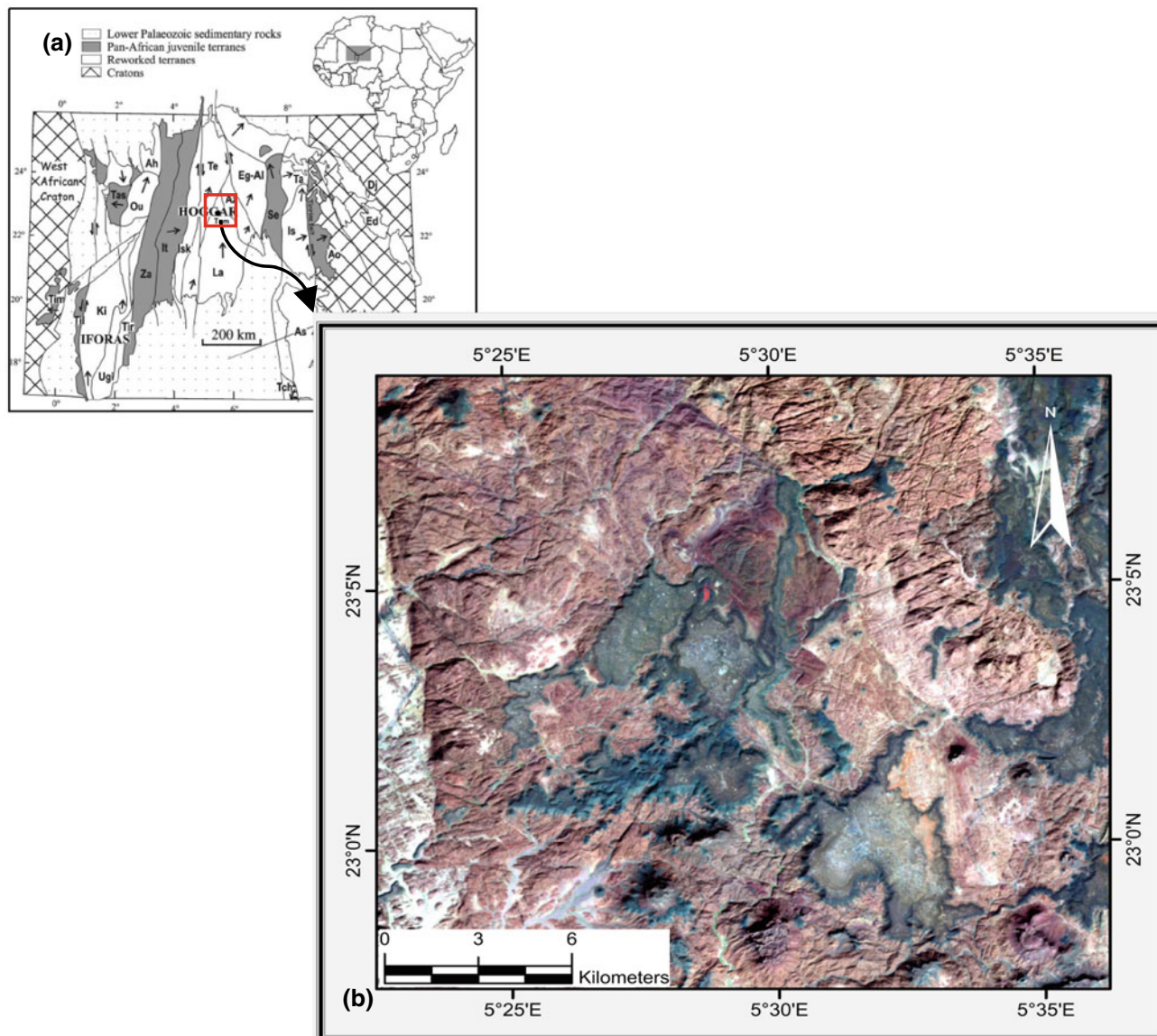


Fig. 1 a Tuareg shield terrane map (from [4]); b Landsat 7ETM + image. The Taessa lavas appear in dark blue

gneisses, Taessa granites and ultramafic Edikel massif (Fig. 1b) [8]. Representative samples were collected and examined under the optical microscope. Unaltered samples were carefully selected for electron microprobe analyses, available at the University of Montpellier.

3 Petrography

Morphologically, the rocks prove to be homogeneous. The Outcrops show a brown patina, a gray black fracture and, often, a porphyritic appearance with phenocrysts of olivine and pyroxene. The prevailing porphyritic texture is micro-litic, with phenocrysts of olivine, pyroxene, and plagioclase. The groundmass consists of plagioclase microlites, molded

without preferential orientation, associated with pyroxene, olivine and opaque mineral grains. Clinopyroxene phenocrysts, often skeletal, have a green core texture comparable to the described Hoggar relating phenocrysts (Atakor [7, 13]; Tazrouk [3]; and Manzaz [2]).

4 Mineralogy and Geothermometry

The macroscopic and microscopic observations of the different samples was accomplished by means of mineral-phase analysis, implemented with the electronic microprobe of a type CAMECA SX 100, available at the Geosciences laboratory, Montpellier University. The analytical conditions' specifications were: current intensity of a range 12 nA, 10 s

counting time, an acceleration voltage of 15 kV, and joint synthetic and natural standards. The major minerals' structural formulas were calculated on the following bases: 3 cations and 4 anions oxygen for olivine, 4 cations and 6 anions oxygen for pyroxenes, 5 cations and 8 oxygen anions for feldspars. The chemical compositions of olivine displays a continuum of contents of forsterite (Fo) molecules that range from Fo85 to Fo57, including crystals with mantle-derived compositions from Fo80 to 85, illustrating evolution during the crystallization to more iron-rich terms. Pyroxenes phenocrysts and microlites are diopside, rarely hedenbergite in green core pyroxene. The Mg# ratio varies continuously from 0.85 to 0.57 with respect to olivine, and from 0.47 to 0.80 regarding the pyroxene. Plagioclases (La_{An69} to And_{An31}) are associated with sodi-potassic crystals (Or_{51} - Or_{16}). Opaque minerals belonging to ulvöspinel—magnetite solid solution. Chromite spinel in the form of olivine inclusion was also analyzed in the Taessa basanite. Temperatures ranging between 1300 and 500 °C have been computed, using a Pyroxene thermometer [11]. Temperatures are estimated at 693° for the olivine-spinelle type of thermometer [6].

5 Comparison and Conclusions

The Taessa basalts turn out to exhibit certain similarities and differences with respect to the neighboring basalts of Tamanrasset, [9] and other volcanic districts as Tazrouk [3].

In effect, both of the Taessa and Tamanrasset based clinopyroxenes appear to have a homogeneous composition and low Ti (0.005–0.12), while the Tazrouk related ones prove to be richer in Ti (0.15).

The Taessa olivines (Fo₅₇–Fo₈₅) are less magnesian compared to those based in Tazrouk and Tamanrasset (Fo₈₀–Fo₉₀).

The plagioclases turn out to be similar with respect to the three regions (andesine-labrador). The presence of anorthoclase is specific to Tamanrasset and Taessa. The Taessa region is distinguished from the other regions by the presence of sanidine.

The titanomagnetite of the Tazrouk and Tamanrasset sites are similar to those sited in Taessa.

The mineralogical and geothermometric study of the minerals reveals that the first crystals of cpx and probably olivine are formed around 1300 °C. Their crystallization ends up at 693 °C for the olivines and 500 °C concerning the cpx.

The geochemical study is in progress, this preliminary results show that the fractional crystallization model does actually persist. The high magnesium content of pyroxenes and olivines, along with the presence of mantle olivine suggest a mantle origin without crustal contamination. A field study of the Taessa lavas helped highlight three main directions: NNE–SSW, NE–SW and N–S. They prove to follow the general orientations of Pan-African (N–S) and Mesozoic fractures (NE–SW), resulting in the establishment of Hoggar volcanism in response to the Africa-Europe convergence [10].

Acknowledgements NB. This research has received funds from the project IRSES-MEDYNA a FP7-Marie Curie Action funded under Grant Agreement PIRSES-GA- 2013-612572.

References

1. Ait-Hamou, F.: Nouvelles données géochronologiques et isotopiques sur le volcanisme Cénozoïque de l'Ahaggar (Sahara Algérien): Des arguments en faveur d'un panache. Comptes Rendus de l'Académie des Sciences de Paris **330**(12), 829–836 (2000)
2. Benhallou, A.Z.: Le district volcanique du Manzaz (Hoggar, Sahara algérien): géologie, pétrographie et minéralogie. Bulletin du Service Géologique de l'Algérie (2016)
3. Ben El Khaznadj, R.: Etude pétrologique des laves alcalines et hyperalcalines de la région de Tazrouk (Blocs Azrou N-Fad, Egéré Aleksod-Hoggar Central): Thèse de Magister, 165p, USTHB-FSTGAT. Alger, Algérie (2008)
4. Black, R.: Pan-African displaced terranes in the Tuareg shield (Central Sahara). *Geology* **22**, 641–644 (1994)
5. Boussisse, I.F., Megueni, Y.: Etude pétrographique et minéralogique des basaltes alcalins de la région de Taessa, Hoggar, 120p. Master, USTHB-FSTGAT, Alger, Algérie (2017)
6. Fabriès, J.: Spinel-olivine geothermometry in peridotites from ultramafic complex. *Contr. Mineral. Petrol.* **69**, 329–336 (1979)
7. Girod, M.: Le massif volcanique de l'Atakor (Hoggar, Sahara Algérien). *Mem. CRZA, Ser. Geol.*, 12, 155 p. CNRS, Paris (1971)
8. Ikhlef-Debabha, F.: Premières données cartographiques sur l'association acide-basique (massif granitique de Taessa complexe mafique ultramafique d'Edikel), terrane de Laouni (LATEA, Hoggar central, Algérie). Colloque national sur la géologie et les ressources minérales du Hoggar, pp. 75–76, Alger (2014)
9. Khedimi, O.K.: Etude pétrographique et minéralogique de quelques édifices volcaniques Cénozoïque de la région de Tamanrasset (Hoggar central, Algérie). Mémoire d'ingénieur d'état, 103p, Faculté des Sciences de la vie, de la terre et de l'Univers, Université Abou Bekr Belkaid, BP 119, 13000, Tlemcen, Algérie (2013)
10. Liégeois, J.P.: The Hoggar swell and volcanism: reactivation of the precambrien Tuareg shield during Alpine convergence and West

- African Cenozoic volcanism. In: Foulger, G.R., Natland, J.H., Presnall, D.C., Anderson, D.L., (eds.) *Plates, Plumes and Paradigms*: Geological Society of America Special Paper 388, pp. 379–400 (2005)
11. Lindsley, D.H.: Pyroxene thermometry. *Am. Miner.* **68**, 477–493 (1983)
 12. Rougier, S.: Eocene exhumation of the Tuareg shield (Sahara Desert, Africa). *Geology* **41**(5), 615–618 (2013)
 13. Yahiaoui, R.: Etude du volcanisme alcalin de la région de l'Assekrem (Hoggar central). Etude pétrographique, minéralogique, géochimique et géothermobarométrique, 164 p. thèse Magister, USTHB-FSTGAT, Alger, Algérie (2003)

Primary Studies of Taessa-Torak Granitic Massif: Petrography and Mineralogy (Central Hoggar, Algeria)

Faiza Ikhlef-Debabha, Abla Azzouni-Sekkal, Amel-Zoulikha Benhallou, Delphine Bosch, and Carlos J. Garrido

Abstract

The Taessa massif, located in the Laouni Terrane (LATEA, Hoggar), belongs to the Tamanrasset Taourirt group. The region was the seat of an important post-orogenic magmatic activity during which large volumes of granite were set up. The petrographic and mineralogical study implemented on the Torak unit granitoids revealed the persistence of three types of granites: two-mica granite, biotite granite and alaskite, characterized with the following mineralogical features:

- Essential minerals, namely: quartz, plagioclase (albite-oligoclase), alkaline feldspar (orthose and microcline), micas (protolithionite to Sidérophyllite group, phengite to Li-phengite group).
- The accessory minerals, specifically: zircon, monazite, allanite and opaque oxides (magnetite and rutile).
- Secondary minerals, mainly: chlorite (brunsvigites, diabanites), fluorite and secondary muscovite.

The trioctahedral micas (biotites), as perceived in the samples, appear to have been crystallized in three different stages: $521\text{ °C} < T < 657\text{ °C}$ for primary micas, $426\text{ °C} < T < 372\text{ °C}$ for rebalanced micas, and $T < 372\text{ °C}$ for the neoformed ones. These micas belong to the range of hyperaluminous granitoids, which display close similarities to the protolithionites of the albite-topaz granite pertaining or belonging to the Tamanrasset region. In this massif, they initiate the alumino-potassic line represented by the lithic micas, noticeably persisten in the highly evolved facies of the “Taourirts” complexes.

Keywords

Granite taourirt • Post-orogenic • LATEA • Hoggar • Lithium micas

F. Ikhlef-Debabha (✉) · A.-Z. Benhallou
CRAAG, Route de L’Observatoire, BP 63, Bouzaréah,
Alger, Algérie
e-mail: debabhaf@yahoo.fr

F. Ikhlef-Debabha · A. Azzouni-Sekkal · A.-Z. Benhallou
Laboratoire de Métallogénie et Magmatisme de L’Algérie
(LMMA) USTHB, FSTGAT, BP 32, El Alia,
16111 Bab Ezzouar, Alger, Algérie

A. Azzouni-Sekkal
Faculté Des Sciences de La Vie, de La Terre et de L’Univers,
Université Abou Bekr Belkaïd, BP 119, 13000 Tlemcen, Algérie

D. Bosch
Géosciences Montpellier, Université de Montpellier,
Montpellier, France

C. J. Garrido
Instituto Andaluz de Ciencias de La Tierra (IACT),
CSIC and Universidad de Granada, Avenida de Las Palmeras 4,
18100 Armilla, Granada, Spain

1 Introduction

The LATEA metacraton is one of the best-represented polycyclic Precambrian regions of the Tuareg Shield. At the end of Murzukian orogeny [5, 9], post-collisional stage was dominated by the emplacement of calc-alkaline batholiths along the intra-terrane shear zones. Later, and up to the Cambrian, strike movements along the inter-terrane shear zones resulted in the current LATEA configuration. They constituted the preferential sites for the emplacement of sub-circular alkali-calcic and alkaline granitic complexes, defining the “Taourirt” suite [2]. In the Laouni terrane, these provinces are represented by several plutons as occurring in Tounine 552 Ma [6], Aheleheg, and the Taessa massif subject of the present study. Some are granites mineralized with albite-topaz [4, 8], which constitute the most evolved terms of the Taourirt suite, set up on the boundary between the block of Laouni and Azrou-N’Fad.

2 Geological Setting

Taessa is a 37 km long granitic massif, oriented NNW-SSE, alike the late pan-African granites characterizing the region (In Tounine, Aheleheg, etc.), and constitutes a striking regional structural feature. It belongs to the Tamanrasset Taourirts group [2], and outcrops in the Laouni terrane, at the limit of three LATEA terranes (Laouni, AzrouN'Fad and Tefedest).

In the west, Taessa outcrops in Eburnean migmatitic gneisses and granites, adjoining the ultramafic Edikel massif [7]. To the east, it crosscuts the early syntectonic Atakor granites. It is composed of coarse porphyritic granites, often displaying planar fluidity, medium to fine-grained alkaline granites, and an uncommon granitic facies, with a rapakivi texture lying on its northwestern border (Fig. 1). Most of the collected samples are derived from the Torak unit south Taessa.

3 Petrography

The detailed petrographic study revealed the presence of three granitic facies, characterized with a fairly simple and homogeneous mineralogy, including two micas granite, alaskite and biotite granite. One could also note the presence of greisen pockets and micas schlieren.

Essential minerals are represented by quartz, plagioclase, alkaline feldspar (microcline, orthoclase and/or perthitic orthoclase), biotite and Lithium micas. Secondary minerals are represented by chlorites, muscovite and fluorite. Accessory minerals are numerous, represented mainly by apatite, zircon, monazite, allanite, magnetite and rutile.

4 Mineralogy and Geothermometry

The implemented mineralogical studies proved to reveal the following features:

- **Feldspars**

In the Or-Ab-An diagram, the orthoclase reaches 97% in biotite granite and 72–98% in alaskite. In biotite granite,

the plagioclase is mainly albite-oligoclase (An_{2-16}), and albite for the rest of the facies.

- **Micas**

The related micas are of two groups: **Trioctaedric micas**, which define evolution trend ($0.34 < Li < 0.69$) from siderophyllite (Fe micas) to protolithionite compositions (Li-Fe micas), and **the dioctahedral micas** projecting into the phengite and Li-phengite fields.

- **Geothermometry of micas**

Protolithionite-siderophyllite group of micas (biotite), belonging to biotite granite group, crystallized over three intervals: $521\text{ °C} < T < 657\text{ °C}$, $426\text{ °C} < T < 372\text{ °C}$ and $T < 372\text{ °C}$. Micas from the two micas granite group prove to have been crystallized at 366 °C .

5 Discussion and Conclusions

The mineralogical comparison of Taessa-Torak granites with those of the Tamanrasset region (In Tounine [4]; Hanana and Tin-Amzi cupola [8]), and Ideles [3], yields the following results.

Taessa siderophyllites and protolithionites have similar Al^{Tot} contents with those pertaining to the Tounine site. These micas display higher contents of Al^{Tot} compared to those the Ideles based ones. They initiate the alumino-potassium character represented by the lithium micas, well known in the GIIB group of the Silet group [1], while the granites of the Hanana and Tin-amzi domes and the albite-topaz leuco-granites prove to display Al^{Tot} contents above 4, and Mg contents ranging between 0.0 and 0.15. They are, therefore, alumino-potassic (Fig. 2).

These results are consistent with the data derived from a conducted regional structural study. Indeed, the NNW-SSE Taessa orientation follows the same trend as that of the late Pan-African granites (In Tounine, Aheleheg, etc.), and constitutes a regional structural feature. This alignment suggests a close relationship with these granites in terms of setting up, origin and probably ages.

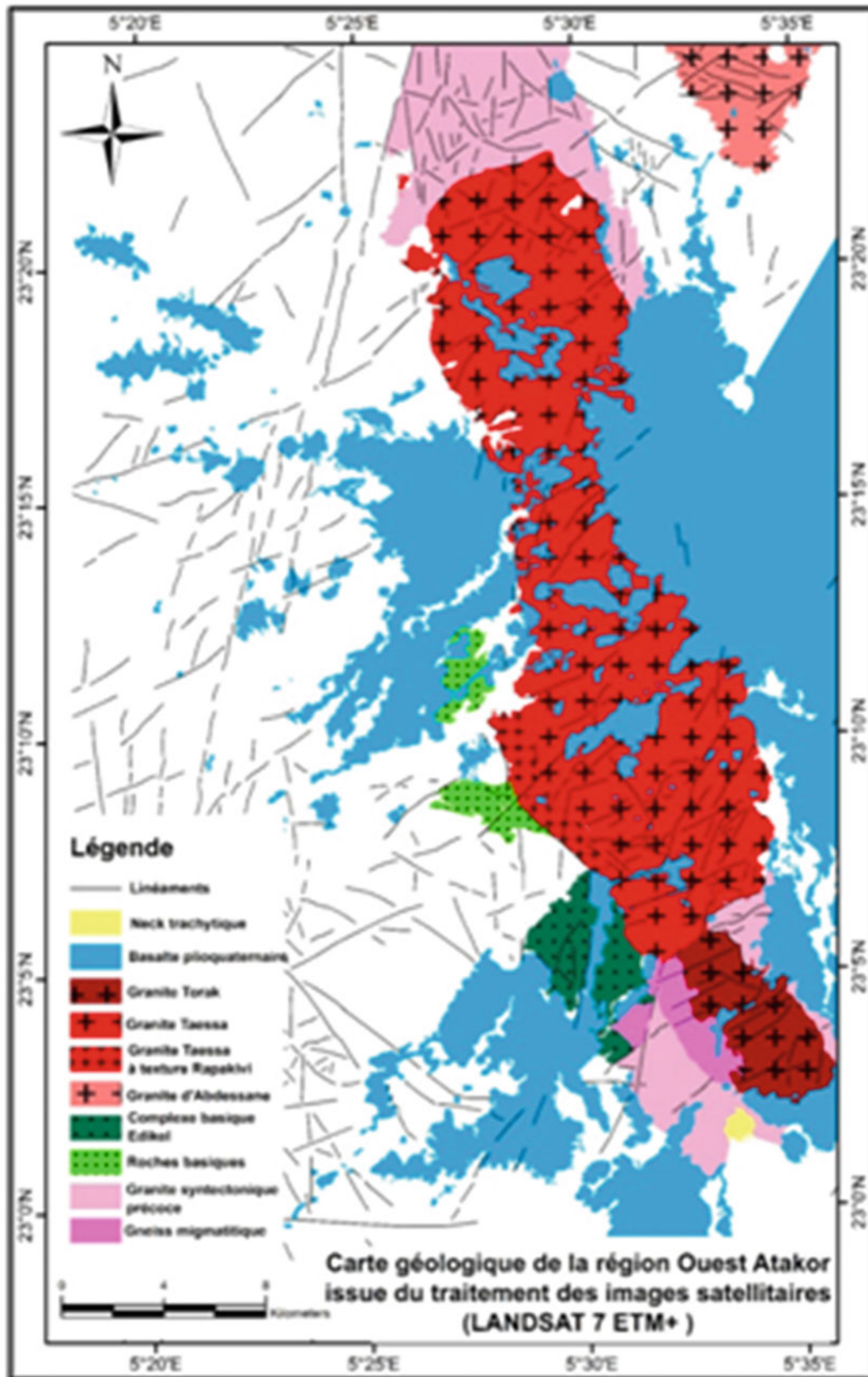


Fig. 1 Geological map of Taessa-Torak massif and surrounding rocks

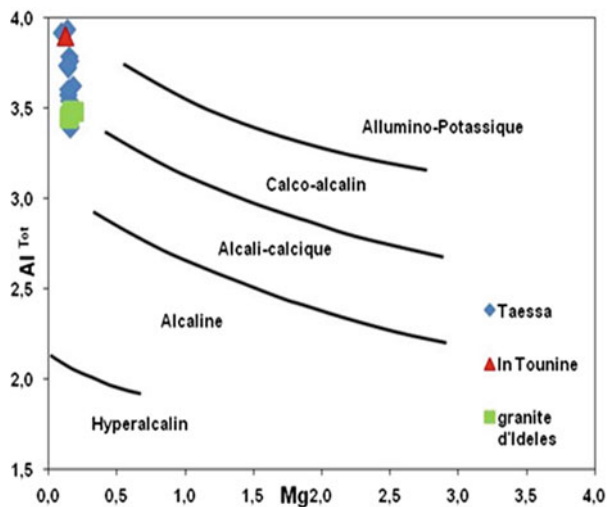


Fig. 2 Al^{Tot} —Mg diagram [10]

For this reason, a detailed study, based on geochemistry and geochronology, is underway to complete the present one.

Acknowledgements NB. This research has received funds from the project IRSES-MEDYNA a FP7-Marie Curie Action funded under Grant Agreement PIRSES-GA- 2013-612572.

References

1. Azzouni-Sekkal, A.: Une province magmatique de transition du calco-alcalin à l'alcalin: les granitoïdes panafricains à structure annulaire de la chaîne pharusienne du Hoggar (Algérie). Bulletin Société Géologique France **164**, 597–608 (1993)

2. Azzouni-Sekkal, A.: The “Taourirt” magmatic province, a marker of the closing stage of the Pan-African orogeny in the Tuareg Shield: review of available data and Sr-Nd isotope evidence. J. Afr. Earth Sc. **37**, 331–350 (2003)
3. Azzouni-Sekkal, A.: Le magmatisme bimodal post-panafricain au Hoggar (Algérie). Colloque national sur la géologie et les ressources minérales du Hoggar, pp 9–10, Algérie (2014)
4. Cheilletz, A.: Géochimie et géochronologie Rb/Sr, $^{40}Ar/^{39}Ar$ des complexes granitiques pan-africains de la région de Tamanrasset (Algérie): Relation avec les minéralisations Sn-W associées et l'évolution tectonique du Hoggar central. Bull. Soc. Géol. **163**, 733–750 (1992)
5. Fezaa, N.: Late Ediacaran geological evolution (575–55 Ma) of the Djanet Terrane, Estren Hoggar, Algeria, evidence. For a Murzukian intracontinental episode. Precamb. Res. **80**, 299–327 (2010)
6. Idir, T.: Géochimie et géochronologie du massif tardif d'In Tounine (Terrane de Laouini Hoggar central, Algérie) 3MA Magmatisme, Métamorphose et Minéralisations Associées, pp. 136–141. Maroc (2015)
7. Ikhlef-Debabha, F.: Premières données cartographiques sur l'association acide-basique (massif granitique de Taessa, complexe mafique ultramafique d'Edikel), terrane de Laouini (LATEA, Hoggar central, Algérie). Colloque national sur la géologie et les ressources minérales du Hoggar, pp 75–76. Algérie (2014)
8. Kesraoui, M.: Nature et évolution comparées de granites à métaux rares dans le Hoggar central (Algérie) à travers la pétrographie, la cristalochimie des micas et des minéraux à Ta, Nb, Sn, W et la géochimie. Thèse de doctorat, 237 p. IST/ USTHB (2005)
9. Liégeois, J.P.: Metacraton: Nature, genesis and behavior. Gondwana Research **23**, pp. 220–237. Elsevier (2013)
10. Nachit, H.: Compositions chimiques des biotites et typologie magmatique des granitoïdes. Comptes Rendus de l'Académie des Sciences, Paris **301**, 813–818 (1985)

Tracing the Missing Argoland Beneath Java: Evidence from Geochemical Signature and Seismic Tomogram

Mirzam Abdurrachman, Sri Widiyantoro, Asep Saepuloh, and Idham Andri Kurniawan

Abstract

Argoland is a piece of Gondwana that collided to the southeastern margin of Sundaland during Late Cretaceous to Early Tertiary. Recently, the existence and continuation of the missing Argoland beneath southern Java have become a hot topic related to geological exploration. The involvement of crustal assimilation of Argoland plays an important role in magma genesis. It controls eruption style, magma composition and also mineral deposit type. Although some studies have indicated the presence of micro continent beneath the southern part of West and East Java, they still could not explain its existence precisely and there are some difficulties to connect one to another. Petrological and geochemical studies of twenty active volcanoes from west to east were combined with tomographic study result to elucidate the problem and give better understanding of crust architecture and interior in Java. Our study shows that some of these magmas derived from Active Continental Margin represent those produced by partial melting of mantle wedge induced by natural fluid in subduction system due to interaction of continental and oceanic crusts. In agreement with geochemical data, high velocity zone from tomographic data are clearly shown in the southern part of Late Cretaceous to Early Tertiary Melange. If that is so, the extension of Argoland in East Java seems to continue to the Central and West Java. A new map of Argoland distribution, crust architecture and interior of Java is proposed.

Keywords

Argoland • Java • Geochemistry • Seismic tomogram

M. Abdurrachman (✉) · A. Saepuloh · I. A. Kurniawan
Department of Geology, Bandung Institute of Technology,
Bandung, 40132, Indonesia
e-mail: mirzam@gc.itb.ac.id

S. Widiyantoro
Global Geophysics Research Group, Bandung Institute of
Technology, Bandung, 40132, Indonesia

1 Introduction

Indonesia is situated at the boundaries of three major plates lying on the southern margin of the Eurasian Plate, i.e., Eurasian, Indian-Australian and Pacific-Philippine Plates [1] (Fig. 1). The Indian-Australian Plate moves northward and is being subducted beneath the Eurasian Plate at a convergent rate of about 7 cm/year [2]. The southeastern part of the Eurasian Plate is widely recognized as Sundaland, a heterogeneous continental crust formed ever since Mesozoic through the amalgamation of continental blocks [1, 3].

In the early Cretaceous, a micro-continental fragment was detached from Gondwana and drifted northwestward, approaching the subduction zone [4]. Further study mentioned that this micro continent has been originated from Western Australia and known as Argoland [3]. This study is conducted in a bid to trace the extension of Argoland, as lying beneath the Java Island.

2 Data and Method

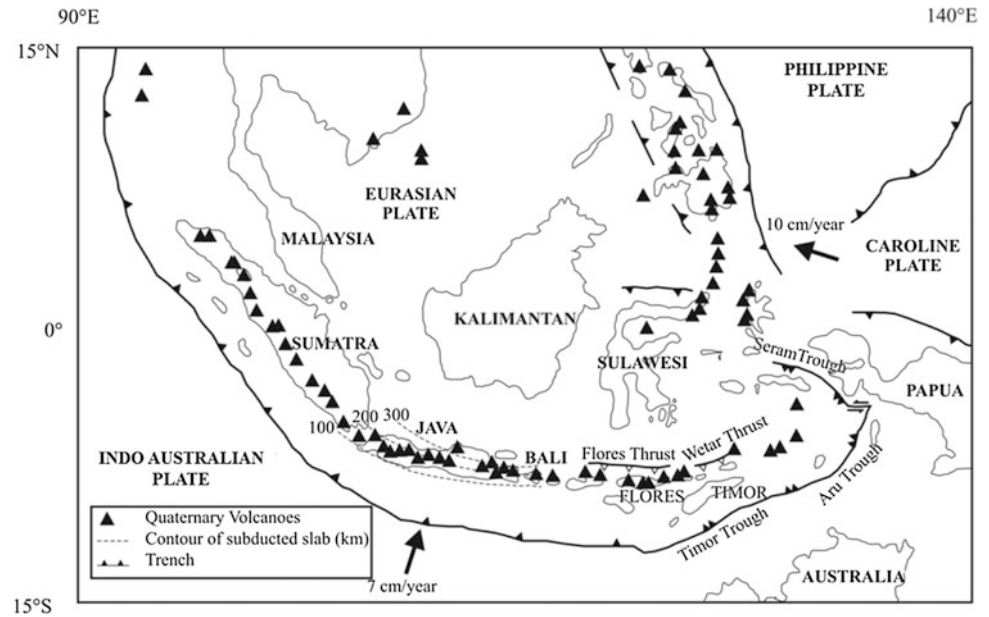
In this study, we used representative whole-rock geochemical data (major, trace and rare earth elements, as well as the Sr-Nd isotopes) from several Javan Quaternary volcanoes combined with published data. We also used S-wave tomographic model in order to enrich and strengthen our interpretation.

3 Results

3.1 Whole Rocks Geochemistry

The Harker diagram analyses have indicated that the magma genesis lying beneath Java is controlled by several processes, e.g., magma mixing and assimilation along with crystal fractionation. These diagrams also reveal that the

Fig. 1 Tectonic map of Indonesia showing the interaction of 3 major plates Modified from [1]



magmatic series persisting in Java are mostly calc-alkaline, resulting from the subduction of ocean crust beneath continental crust, as a typical feature of active continental margin.

In agreement with whole rocks geochemistry, Sr-Nd mixing model shows that the magma genesis lying beneath Java is strongly affected by the contamination of Australian granites (Argoland), as explained by [5].

3.2 Seismic Tomogram

S-wave tomographic model clearly depicts a high velocity zone lying in the southern part of the Late Cretaceous to Early Tertiary Melange (cf. Figs. 2 and 3), implying the existence of continental crust.

4 Discussion

The noticeable shifts marking the geochemical variety in Java coincides with the Late Cretaceous to the Early Tertiary Melange boundary line. Volcanic rocks lying in the southern

part of this line are typically derived from magma related to the partial melting of the mantle wedge induced by the traditional fluids in an active continental margin system that are strongly related to northern area based volcanoes. This condition proves to be in agreement with the model proposed by [5] (Fig. 2), and also with the S-wave velocity model (Fig. 3).

5 Concluding Remarks

Whole-rock geochemistry data, which are in agreement with Sr-Nd isotopic data, have provided new insights into the magma genesis lying beneath the Javan Volcano. It has been discovered that volcanic rocks from the southern part of the Late Cretaceous to the Early Tertiary Melange represent volcanic rocks derived from partial melting of the mantle wedge in the active continental margin that is contaminated by Australian granites as mirrored by the Sr-Nd isotopes. The presence of Australian granites in the southern part of the Late Cretaceous to Early Tertiary Melange is highlighted via the S-wave tomogram (Fig. 3).

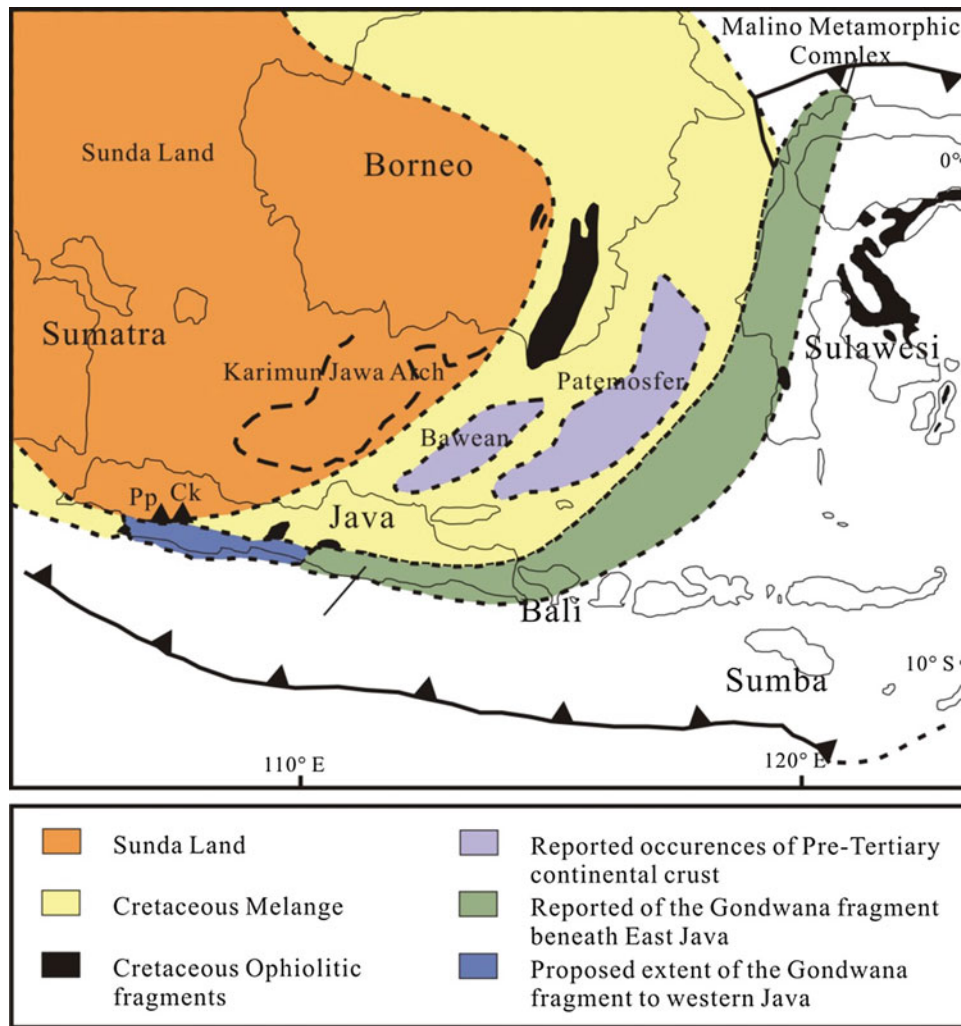


Fig. 2 A new map showing the proposed extent of the East Java fragment to the West Java Modified from [4, 5]

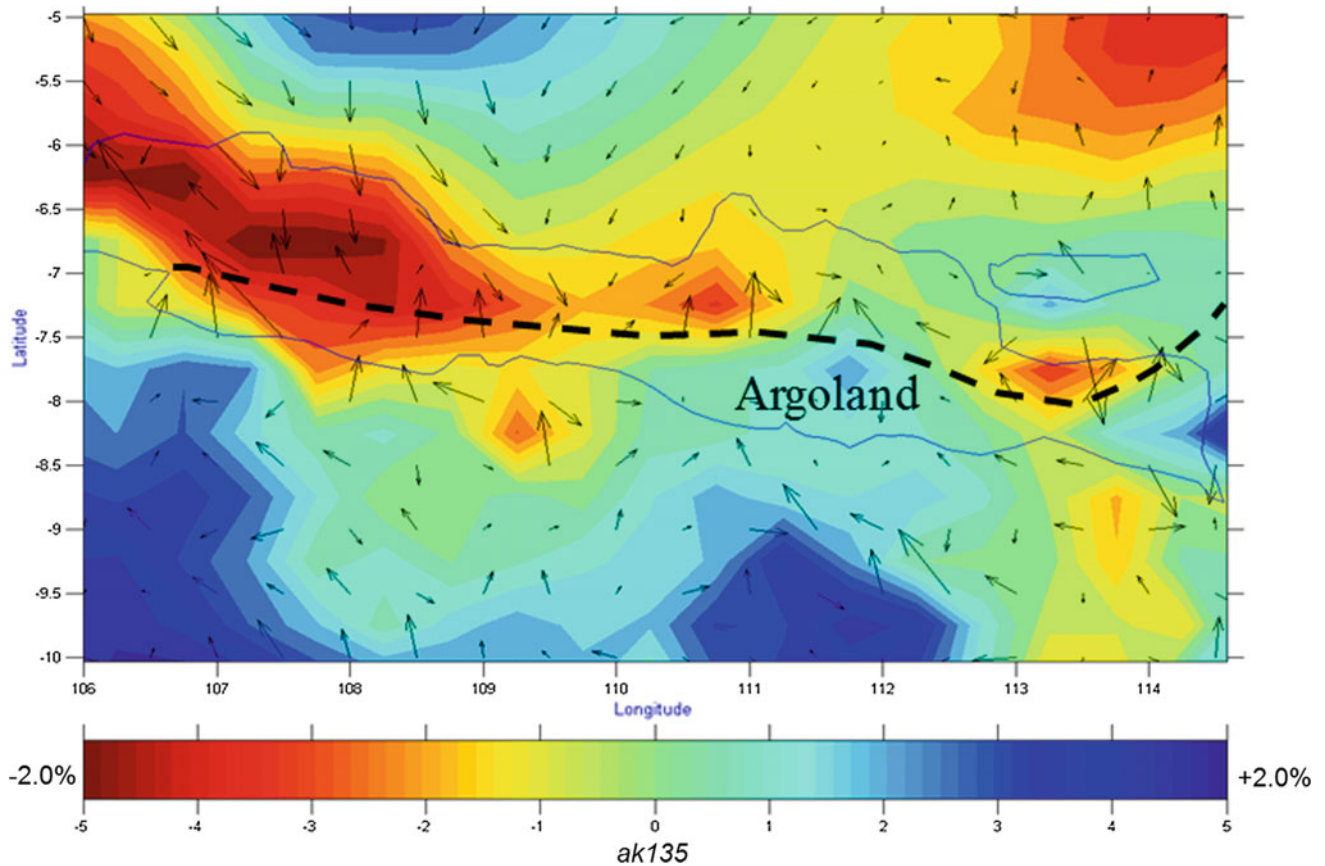


Fig. 3 S-wave layer anomaly map (depth interval 35–70 km) depicting the boundary of Late Cretaceous to early tertiary Melange

References

1. USGS Homepage. <https://pubs.usgs.gov/pp/1078/report.pdf>. Last accessed 21 Apr 2018
2. Hall, R.: Indonesia, geology. In: Gillespie, R., Clague, D. (eds.) *Encyclopedia of Islands*, pp. 454–460. University of California Press, Berkeley, California (2009)
3. Metcalfe, I.: Tectonic framework and Phanerozoic evolution of Sundaland. *Gondwana Res.* **106**, 97–122 (2011)
4. Smyth, H.R., Hamilton, P.J., Hall, R., Kinny, P.D.: The deep crust beneath island arcs: inherited zircons reveal a Gondwana continental fragment beneath East Java, Indonesia. *Earth Planet. Sci. Lett.* **258**, 269–282 (2007)
5. Abdurrachman, M., Yamamoto, M.: Geochemical variation of quaternary volcanic rocks in Papandayan area, West Java, Indonesia: a role of crustal component. *J. Geol. Soci. Thai.* 40–57 (2013)

Rb-Sr and Oxygen Isotope Study of the Swat Granite Gneisses (Pakistan): Implications for the Magmatic Source and Tectonic Setup

Tahseenullah Khan, Abid Ahmad, Hafiz Ur Rehman,
Muhammad Nawaz Chaudhry, Mamoru Murata,
and Muhammad Zafar

Abstract

A wide range of granite bodies are lying in the Pakistani Himalaya along the northern leading edge of the Indian plate in the Swat area of Pakistan. Several such bodies are collectively designated here as Swat granite gneisses. The latter are exposed mainly across the Chakdarra, Ilam-Karakar and Saidu-Parona areas. Lens-shaped K-feldspar augens in a groundmass of quartz, feldspar and biotite characterize these bodies. Garnet, epidote, titanite, zircon and opaque minerals are also noticed to persist in minor amounts in the form of prevailing accessories. Both quartz and feldspar appear to display extreme stretching parallel to the predominant foliation due to shearing. On the basis of Rb-Sr geochronology and oxygen isotope composition, the granite gneiss at Chakdarra yields Rb-Sr whole-rock isochron age of 213 ± 24 Ma. As for the Ilam-Karakar and Saidu-Parona areas, the granite gneisses respectively display age ranges of 260 ± 52 Ma and 285 ± 8 Ma. The $\delta^{18}\text{O}$ values determined in the Chakdarra, Ilam-Karakar and Saidu-Parona based granite gneisses range from +8.8 to +9.2‰, and +8.6 to +9.4‰ and +9.0 to +9.5‰, respectively. On the basis of mineral

assemblages, these granites seem to be of an S-type. Noteworthy, however, is that the Swat granite gneisses, which contain less than 10% of $\delta^{18}\text{O}$ values, prove to be of the I-type granites. Their peraluminous signatures seem to be due to fractional crystallization process. Our newly obtained age data indicate Permian magmatic activity that belongs to the early rifting of the Cimmerian microcontinent from Gondwana.

Keywords

Granite gneisses • Swat • Geochronology • Petrogenesis • Tectonic setting

1 Introduction

A series of granitic bodies are exposed along the northern leading edge of the Indian plate across the Swat area of Pakistan [1]. Several plutons, collectively designated as Swat granites, mainly granite gneisses, are exposed immediately south of the Main Mantle Thrust (MMT; see Fig. 1). These granite gneisses are characterized with prevailing lens-shaped K-feldspar augens in a groundmass of quartz, feldspar and biotite. Garnet, epidote, titanite, zircon and opaque minerals persist in minor amounts and as accessories. Both quartz and feldspar display extreme stretching parallel to the predominant foliation as a result of frequent shearing. These granites were correlated with the 516 ± 16 Ma Mansehra granites lying across the Higher Himalayan Crystalline (HHC) region [2–6]. Recent petrological, geochemical, and geochronological studies dealing with the metamorphosed mafic volcanic rocks lying across the Kaghan Valley of Pakistan (Panjal Trap volcanic) represent within-plate-basaltic activity during Permian (267 ± 2 Ma U-Pb data from magmatic zircon) [7]. Since most of the basement rocks exposed in the Kaghan Valley also belong to the HHC, they could well be correlated with the Swat area relating granite gneisses. To examine their

T. Khan (✉) · M. Zafar

Department of Earth and Environmental Sciences,
Bahria University, Islamabad, Pakistan
e-mail: tkhan.buic@bahria.edu.pk

A. Ahmad

Pakistan Institute of Engineering and Applied Sciences,
Atomic Energy Commission, Nilore, Islamabad, Pakistan

H. U. Rehman

Department of Earth and Environmental Science,
Faculty of Science, Kagoshima University, Kagoshima,
890-0065, Japan

M. N. Chaudhry

Department of Environmental Science and Policy, Faculty of
Basic Sciences, Lahore School of Economics, Barki Road, Lahore,
Pakistan

M. Murata

Department of Geosciences, Faculty of Science, Naruto University
of Education, Tokushima, 772-8502, Japan

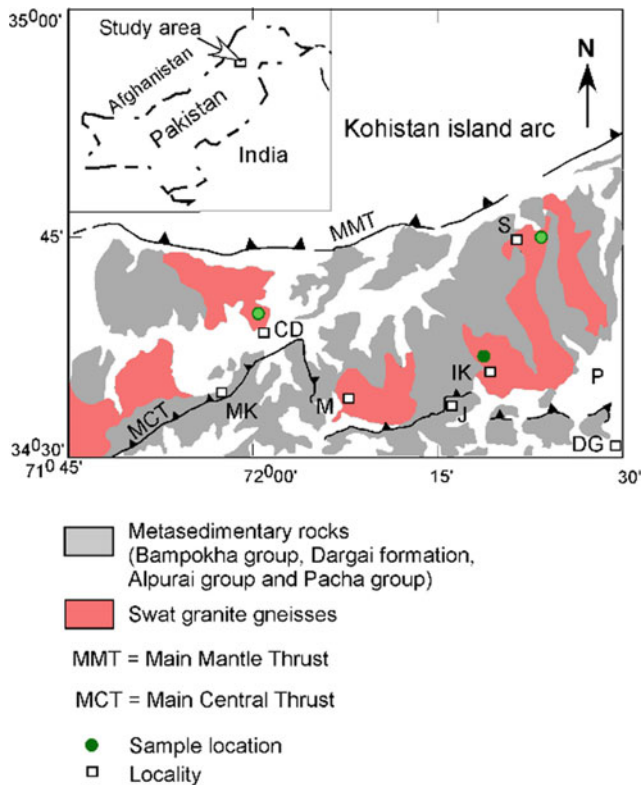


Fig. 1 A simplified geological map of the Swat area. The highlighted localities are: MK, Malakand; CD, Chakdarra; IK, Ilam-Karakar; S, Saidu Parona; P, Pacha; DG, Dagar; J, Jowar; M, Mura

magmatic origins and tectonic evolution, we conducted Rb-Sr and oxygen isotope studies on the representative rock samples, as collected from three granite gneisses bodies belonging to the Swat area (see Fig. 1).

2 Methodology

Sixteen rock samples collected from the Swat granite gneisses were analyzed for geochronological and isotope chemistry studies. In these samples, Sr and Rb concentrations were determined via the isotope dilution method, using thermal ionization mass spectrometer and XRF. The applied computational decay constant of ^{87}Rb is $\lambda = 1.42 \times 10^{-11}/\text{yr}$.

The oxygen isotopes were determined on the basis of a modified version of VG-SIRA12 mass spectrometer, using the laser fluorination technique. The analyses were carried out in duplicate with analytical accuracy of $\pm 0.1\%$. The reached results ($\delta^{18}\text{O} \text{‰}$) were calculated according to the following equation:

$$\delta^{18}\text{O} \text{‰} = \left[\frac{R_{\text{sample}}}{R_{\text{standard}}} - 1 \right] \times 10^3, \text{ where } R = \frac{^{18}\text{O}}{^{16}\text{O}}$$

3 Results

Six rock samples extracted from the Chakdarra granite gneiss and five samples collected from Ilam-Karakar and Saidu-Parona granite gneisses were analyzed. The Chakdarra granite gneiss appears to contain Rb (195–412 ppm) and Sr (9–392 ppm). It yields 213 ± 24 Ma age with an initial $^{87}\text{Sr}/^{86}\text{Sr}$ ratio of 0.704 ± 0.0051 . The related $\delta^{18}\text{O}$ values amount to $+8.8$ and $+9.2\%$. The Rb and Sr concentrations prove to vary from 260 to 404 ppm and 58 to 363 ppm, respectively, with respect to the Ilam-Karakar granite gneiss. It displays an age range of 260 ± 52 Ma with $^{87}\text{Sr}/^{86}\text{Sr}$ initial ratio of 0.709 ± 0.01 . The $\delta^{18}\text{O}$ values amount to $+8.6$ and $+9.4\%$. The Rb and Sr concentrations associated with the Saidu-Parona granite gneiss appear to vary from 125–360 ppm to 85–340 ppm, respectively. It exhibits an age of 285 ± 7.5 Ma with an initial $^{87}\text{Sr}/^{86}\text{Sr}$ ratio of 0.709 ± 0.0002 . The $\delta^{18}\text{O}$ values amount to $+9.0$ and $+9.5\%$.

4 Discussion

Permian granites have previously been reported to persist in the Swat area [8, 9]. The entire Rb-Sr rock isochron age of the Chakdarra granite gneiss is poorly constrained in this study. The U-Pb zircon data relating to the Swat granite gneisses belonging to the northern part of the Loe Sar dome in Mingora prove to yield an age of 267 ± 2 and 265 ± 3 Ma, nearly the same age range as that of Saidu-Parona granite gneiss (285 ± 7.5 Ma) [9]. The Saidu-Parona granite gneiss appears to stand as a southward continuation of the Loe Sar dome of the Swat granite gneisses. The Ilam-Karakar granite gneiss age data appear to fall closely with the 265 Ma age range [9], and with the Saidu-Parona granite gneiss age range, displaying a co-magmatic character. The initial $^{87}\text{Sr}/^{86}\text{Sr}$ ratios relevant to the Ilam-Karakar and Saidu-Parona granite gneisses amount to ~ 0.709 . In normal rates, the range in initial $^{87}\text{Sr}/^{86}\text{Sr}$ ratios of the I-type granites usually range between 0.704 and 0.712, and in the S-type of granites, the corresponding values normally range between 0.708 and 0.717 [10]. The initial $^{87}\text{Sr}/^{86}\text{Sr}$ data corresponding to the Swat granite gneisses prove to categorize them within the I-type of

granites. In terms of oxygen isotope, the $\delta^{18}\text{O}$ values of the S-type granites are usually higher than 10‰. As for the $\delta^{18}\text{O}$ values relevant to the Swat granite gneisses, they appear to amount to less than 10‰, confirming their pertinence to the I-type affinity of these granites. Generally, the I-type granites are sub- and metaluminous, while the Chakdarra, Ilam-Karakar and Saidu-Parona granite gneisses turn out to display a peraluminous mineralogy. Based on the initial $^{87}\text{Sr}/^{86}\text{Sr}$ ratio and oxygen isotopes, these granites owe an I-type of affinity, and their peraluminous signatures seem to be due to fractional crystallization [11]. Actually, our newly discovered age data prove to indicate the existence of a magmatic activity in Permian similar, for instance to the alkaline magmatism (315 ± 15 – 297 ± 4 Ma) of the Ambela area Pakistan, and the mafic Panjal volcanism (284 ± 4 – 262 ± 1 Ma), as occurred during the early rifting of the Cimmerian micro-continent from Gondwana [12].

5 Conclusion

The Swat granite gneisses with less than 10‰ $\delta^{18}\text{O}$ values turn out to be granites of the I-type. The relevant peraluminous affinity proves to have its origins in fractional crystallization. These granites appear to be due to Permian magmatic event, correlated with the early rifting affecting the Cimmerian micro-continent from Gondwana.

References

- Ahmad, I., Jan, M.Q., DiPietro, J.A.: Age and tectonic implications of granitoid rocks from the Indian plate of Northern Pakistan. *J. Virt. Explorer, Electronic Edition* 11(2) (2003)
- Le Fort, P., Debon, F., Sonet, J.: The ‘Lesser Himalayan’ cordierite granite belt. Typology and age of the pluton of Mansehra (Pakistan). In: Tahirkheli, R.A.K., Jan, M.Q., Majid, M. (eds.) *Proceedings of the International Committee on Geodynamics, Group 6 Meeting at Peshawar 1980, Special issue vol. 13*, pp. 51–61, Geol. Bull. Univ. Peshawar (1980)
- Le Fort, P., Debon, F., Sonet, J.: The lower Paleozoic “Lesser Himalayan” granitic belt: emphasis on the Simchar pluton of Central Nepal. In: Shams, F.A. (ed.) *Granites of Himalayas, Karakoram and Hindukush*, pp. 235–255. Institute of Geology, University of the Punjab, Lahore, Pakistan (1983)
- Jan, M.Q., Asif, M., Tazeem, T., Kamal, M.: Tectonic subdivision of granitic rocks of north Pakistan. *Geol. Bull. Univ. Peshawar* **14**, 159–182 (1981)
- Shams, F.A.: *Granites of Himalayas Karakorum and Hindu Kush*. Institute of Geology, University of the Punjab, Lahore, Pakistan (1983)
- Chaudhry, M.N., Hussain, S.S., Dawood, H.: The lithostratigraphic framework of northwest Himalaya, south of the main mantle thrust along the Mingora-Doggar section, Swat Zone, Pakistan. *Pakistan J. Geology* **1**, 29–40 (1992)
- Rehman, H., Lee, H.Y., Chung, S.L., Khan, T., O’Brien, P.J., Yamamoto, H.: Source and mode of the Permian Panjal Trap magmatism: evidence from zircon U–Pb and Hf isotopes and trace element data from the Himalayan ultrahigh-pressure rocks. *Lithos* **260**, 286–299 (2016)
- DiPietro, J.A., Isachsen, C.E.: U–Pb zircon ages from the Indian plate in northwest Pakistan and their significance to Himalayan and pre-Himalayan geologic history. *Tectonics* **20**, 510–525 (2001)
- Anczkiewicz, R., Oberli, F., Burg, J.P., Villa, I.M., Gunther, D., Meier, M.: Timing of normal faulting along the Indus Suture in Pakistan Himalaya and a case of major $^{231}\text{Pa}/^{235}\text{U}$ initial disequilibrium in zircon. *Earth Planet. Sci. Lett.* **191**, 101–114 (2001)
- Chappell, B.W., White, A.J.R.: Two contrasting granite types. *Pac. Geol.* **8**, 173–174 (1974)
- Murata, M., Yoshida, T.: Trace elements behavior in Miocene I-type and S-type granitic rocks in the Ohmine district, central Kii peninsula. *J. Assoc. Mineral. Petrolo. Econ. Geol.* **80**, 227–246 (1985)
- Le Bas, M.J., Mian, I., Rex, D.C.: Age and nature of carbonatite emplacement in north Pakistan. *Geol. Rundsch.* **76**(2), 317–323 (1987)

Textural and Mineral Chemistry Data Related to the Karapınar-Karacadağ Volcanic Complex (Konya-Central Anatolia)

Huseyin Kurt, Gulin Gencoglu Korkmaz, and Kursad Asan

Abstract

The Plio-Quaternary associated with the Karapınar-Karacadağ Volcanic Complex (Konya-Central Anatolia) involves dacitic-andesitic domes/flows and basaltic lava flows, and their pyroclastic equivalents (e.g., base surges, ash-block flows, scoria and ash falls). The present study deals with examining the new mineral chemistry and textural investigations concerning the Karapınar mildly alkaline to calc-alkaline basalts and Karacadağ calc-alkaline intermediate rocks predominant in Central Anatolia. Application of amphibole thermobarometry and clinopyroxene-liquid thermobarometry to the Karacadağ andesites has yielded temperature estimates in the range of 855–1198 °C and pressure estimates of a range of 1.34–5.95 kbar, indicating the presence of a magma chamber lying at the middle-upper crust for intermediate unit. Temperature and pressure estimate's as drawn from pyroxene, related to the Karapınar basalts are in the range of 1173–1251 °C and 8.9–12.2 kbar, highlighting persistence of crystallization at the crust base level. Some of the andesites, particularly the enclave bearing andesites, enclose spongy cellular, fine-coarse sieved, oscillatory and inverse zoned plagioclase, standing as the evidence of open system process. Besides, the Karapınar basalts include abundant quartz and biotite xenocrysts. There is no physical contact between the Karacadağ andesites and the Karapınar basalts surrounding the area, but the relating geochemical and textural properties appear to indicate that the Quaternary Karapınar basalts prove to be evidently assimilated from Pliocene associated with the Karacadağ andesites.

Keywords

Assimilation • Pressure • Temperature • Textural • Open system

1 Introduction

The Mio-Pliocene volcanic rocks outcropping Central Anatolia are mainly calc-alkaline, dominantly andesitic-dacitic in composition, with a distinctive subduction component inherited from a previous subduction related to the convergence between the Afro-Arabian and Eurasian plates (Fig. 1). Quaternary volcanics cropping out around the Karapınar area are mildly alkaline and considered as maar craters, basaltic scoria cones, andesitic lava domes and lava flows [2]. In the Karacadağ stratovolcano, the volcanic rocks involve pyroclastics and dacite, andesites and rarely basalts. The conducted geochemical and petrological studies suggest that these rocks are predominantly calc-alkaline, associated with previous subduction of the Afro-Arabian plate under the Anatolian block. In this project, we undertake to investigate the Karapınar-Karacadağ Volcanic Complex, highlighting the new mineralogical and chemical examinations regarding the Karapınar mildly alkaline-calc-alkaline basalts and Karacadağ calc-alkaline intermediate rocks, as prevailing in Central Anatolia.

2 Materials and Methods

The volcanic rock samples were collected from the Karapınar-Karacadağ area of Konya, Central Anatolia. According to the petrographical and geochemical observations, the freshest and most representative samples were selected for electron microprobe analyses, as performed at the Laboratory of Geoscience Application and Research Center (YEBIM) of the Ankara University.

H. Kurt (✉) · G. G. Korkmaz · K. Asan
Department of Geological Engineering, Selçuk University,
Konya, Turkey
e-mail: hkurt@selcuk.edu.tr

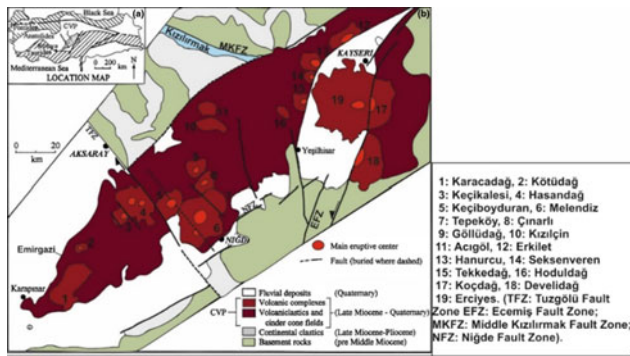


Fig. 1 a The map of Turkey highlighting the main tectonic units (modified from [1, 5]), b A simplified geological map of Central Anatolia Volcanic Province (CAVP) (modified from [6])

3 Results

3.1 Petrography

The Karacadağ andesites prove to display a hypocrySTALLINE porphyritic texture and generally contain phenocrysts of plagioclase, amphibole, clinopyroxene \pm orthopyroxene \pm olivine xenocryst \pm trace amounts of biotite \pm quartz. Two types of enclaves appear to prevail in some of the Karacadağ andesites, namely, cumulate enclaves (gabbroic) (Fig. 2a) and mafic magmatic enclaves (andesitic-dioritic and basaltic) (Fig. 2b). On the other hand, the Karapınar basalts appear to exhibit a hypocrySTALLINE porphyritic texture, including olivine, plagioclase and rare clinopyroxene phenocrysts, quartz and to a less extent biotite xenocrysts, with a groundmass being composed of plagioclase, clinopyroxene, olivine and Fe–Ti oxide. Some basalts contain cumulate enclaves (as is the case with dunite and basalt composition) (Fig. 2c) and/or include frequently embayed-ocelli quartz xenocrysts and rare biotite xenocrysts (Fig. 2d).

3.2 Mineral Chemistry and Geothermobarometry

Based on the electron-microprobe data, Karapınar basalts appear to include olivine (Fo: 0.74–0.89), diopside (in mildly alkaline basalts) and augite (with diopside in calc-alkaline basalts) as clinopyroxene phases. As for the mildly-alkaline basalts, they include bytownite, and some of the Karapınar calc-alkaline basalts contain two different types of plagioclase, namely, a microlitic phase involving bytownite-anorthite composition, and a phenocryst phase which encloses an oligoclase, andesine and rare labrador composition. These phenocryst phases may be xenocrysts

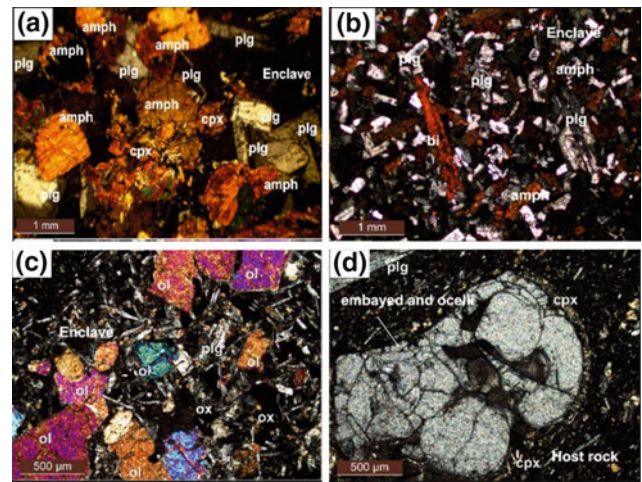


Fig. 2 a Cognate xenolith; b magma mixing enclave in andesites; c cognate xenolith and d embayed and ocelli quartz xenocryst in basaltic host rock

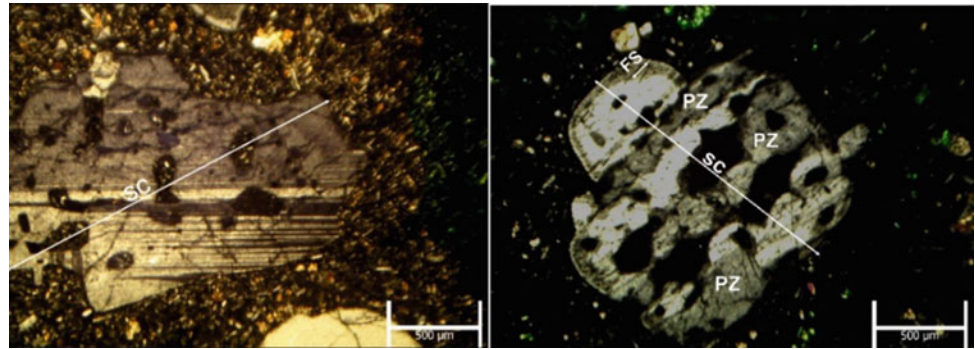
plucked from the Karacadağ volcanites, including quartz and biotite xenocrysts. Basalts also contain trace amount of anorthoclase and sanidine. Concerning the Karacadağ andesites, they include olivine (Fo: 0.80–0.88) diopside and augite as clinopyroxene phases, andesine-labrador-bytownite as well as rare anorthoclase and sanidine as feldspar phases. The amphibole phases are magnesiohastingsite and magnesiohornblende in andesites.

The EPMA data derived from both amphibole and clinopyroxene phenocrysts from the Karacadağ andesites and clinopyroxene phenocrysts from the Karapınar basalts were used to estimate the crystallization pressure and temperature. The amphibole thermobarometer, as implemented by Ridolfi et al. [4], and the clinopyroxene-liquid thermobarometer, as administered by Putirka [3], were used for the calculations to be administered. The temperature estimates related to the amphibole and clinopyroxene phenocrysts concerning the Karacadağ andesites appear to range between 855–1023 °C and 1114–1198 °C, respectively. In addition, the pressure estimates relevant to the amphibole and clinopyroxene phenocrysts range between 1.46–5.95 kbar and 1.34–4.56 kbar, respectively. The application of clinopyroxene thermobarometer to Karapınar basalts indicates that the clinopyroxene phenocrysts were crystallized, at the lower crust level, by means of temperature range of 1173–1251 °C and pressure range of 8.9–12.2 kbar.

4 Discussion and Conclusions

In general, the reached results, as drawn from the amphibole thermobarometer, appear to be consistent with those obtained from pyroxene thermobarometer. Noteworthy,

Fig. 3 Fine sieve (FS), patch zoning (PZ) and spongy cellular (SC) textures in plagioclase phenocrysts as drawn from the Karapınar calc-alkaline basalts



however, some amphibole phenocrysts may prove to be in disequilibrium with the melt due to the higher pressure values they display in respect of the pyroxenes. According to the EPMA data, relevant to the middle-upper crust, the amphibole and clinopyroxene phenocrysts appear to have been crystallized from the andesitic magma. As for the clinopyroxenes, they turn out to have been crystallized at the lower crust level as a result of the basaltic magma.

The open-system associated magmatic processes (i.e., magma mixing/recharging/contamination/assimilation) seem to play an important role in the evolution of the investigated volcanic rocks. Fine sieve textures, patch zoning and spongy cellular textures may well reveal pervasive dissolution as open system process for the plagioclase phenocrysts associated with the Karapınar calc-alkaline basalts (Fig. 3).

Although no real crustal xenolith has been extracted from basement rocks, the quartz and rare biotite xenocrysts, as plucked from the Karacadağ volcanites, were observed in the Karapınar volcanites. The reached EPMA and petrographical findings prove to indicate that the Quaternary Karapınar basalts are significantly contaminated from the Neogene Karacadağ volcanics. Such observations turn out to be

noticeably important in that they help in highlighting the open-system nature of the subduction related volcanic system.

References

1. Guezou, J.C., Temiz, H., Poisson, A., Gu'rsoy, H.: Tectonics of the Sivas Basin: Neogene record of the Anatolian accretion along the inner Tauric suture. *Int. Geol. Rev.* **38**(10), 901–925 (1996)
2. Keller, J.: Quaternary maar volcanism near Karapınar in Central Anatolia (1974)
3. Putirka, K.: Thermometers and barometers for volcanic systems. In: Putirka, K., Tepley, F. (eds.) *Minerals, Inclusions and Volcanic Processes. Reviews in Mineralogy and Geochemistry*, vol. 69. Mineralogical Society of America, pp. 61e120 (2008)
4. Ridolfi, F., Renzulli, A., Puerini, M.: Stability and chemical equilibrium of amphibole in calcalkaline magmas: an overview, new thermobarometric formulations and application to subduction-related volcanoes. *Contr. Mineral. Petrol.* **160**(1), 45–66 (2010)
5. Şengör, A.M.C.: Türkiye'nin tektonik tarihinin yapısal sınıflaması, *Ketin Sempozyumu*, pp. 37–62. Ankara (1984)
6. Toprak, V.: Vent distribution and its relation to regional tectonics, Cappadocian Volcanics, Turkey. *J. Volcanol. Geoth. Res.* **85**, 55–67 (1998)

Characteristic Magnetic Behavior of Southwest Nigerian Granitoids

Cyril Okpoli, Michael Oladunjoye, and Emilio Herrero-Bervera

Abstract

The present work constitutes a primary initiative whereby the initially achieved results are released, following a detailed regional thermomagnetic study of granitoids from the Precambrian basement rocks of southwestern Nigeria. In this respect, a selection of multifunctional kappabridge (MFK1-FA), Scanning electron microscope, alternating field demagnetizer, spinner magnetometer, vibrating sample magnetometer have been applied to characterize the basement rocks relating magnetic behavior. Standard samples have been prepared using 2.5 cm by 2.1 cm, in the form of cylindrical cores, to depict the relevant paleomagnetic character, while polished samples and grains/powder have been applied for mineralogical characterization purposes. The reached results prove to reveal the stability attached to the representative samples, along with the dominance of PSD/MD magnetic domain state with regard to the magnetite polymorphs.

Keywords

Thermomagnetic • Granitoids • Maghemites • Precambrian • Nigeria

1 Introduction

Most of the studies dealing with the rocks' magnetic character appear to be predominantly focused on the granitoids relating procurement and data processing dimensions. Noteworthy, however, is that little attention is often paid to the minerals' sources and the combined paragenetic sequences leading to the rocks associated magnetic anomalies [1]. Indeed, single domain magnetite, maghemite, titanohematite, titanomagnetite, and pyrrhotite of varying magnetization prove to display a magnetic behavior characteristic [1]. The continental lithosphere has a contribution to the reorganization of the strike-slip faults [2]. Actually, hydrothermal fluids appear to participate remarkably in the appreciable variations associated with the rocks' components [3]. In effect, the crystallization and temperature cooling rates appear to have evidence of magnetic characteristic variations, particularly in granitoids [4], basaltic pillow lava [5] or submarine basaltic glasses [6]. In this study, the Precambrian granitoids related magnetic behavior will be thoroughly characterized.

2 Materials and Methods

In this context, the MFK1-FA, VSM, AF Demagnetizer, JR5 Spinner magnetometer and Jeol JSM-5900LV scanning electronic microscope are used to characterize the magnetic behavior associated with the southwestern Nigeria granitoids.

3 Results

See Figs. 1, 2, 3, 4 and 5.

C. Okpoli (✉)

Department of Earth Sciences, Faculty of Science,
Adekunle Ajasin University, PMB 1, Akungba-Akoko,
Ondo State, Nigeria
e-mail: cyril.okpoli@aaau.edu.ng

M. Oladunjoye

Department of Geology, University of Ibadan, Ibadan, Nigeria

E. Herrero-Bervera

Paleomagnetism and Petrofabrics Laboratory, School of Ocean & Earth Science & Technology (SOEST), Hawaii Institute of Geophysics and Planetology (HIGP), 1680 East West Road, Honolulu, HI 96822, USA

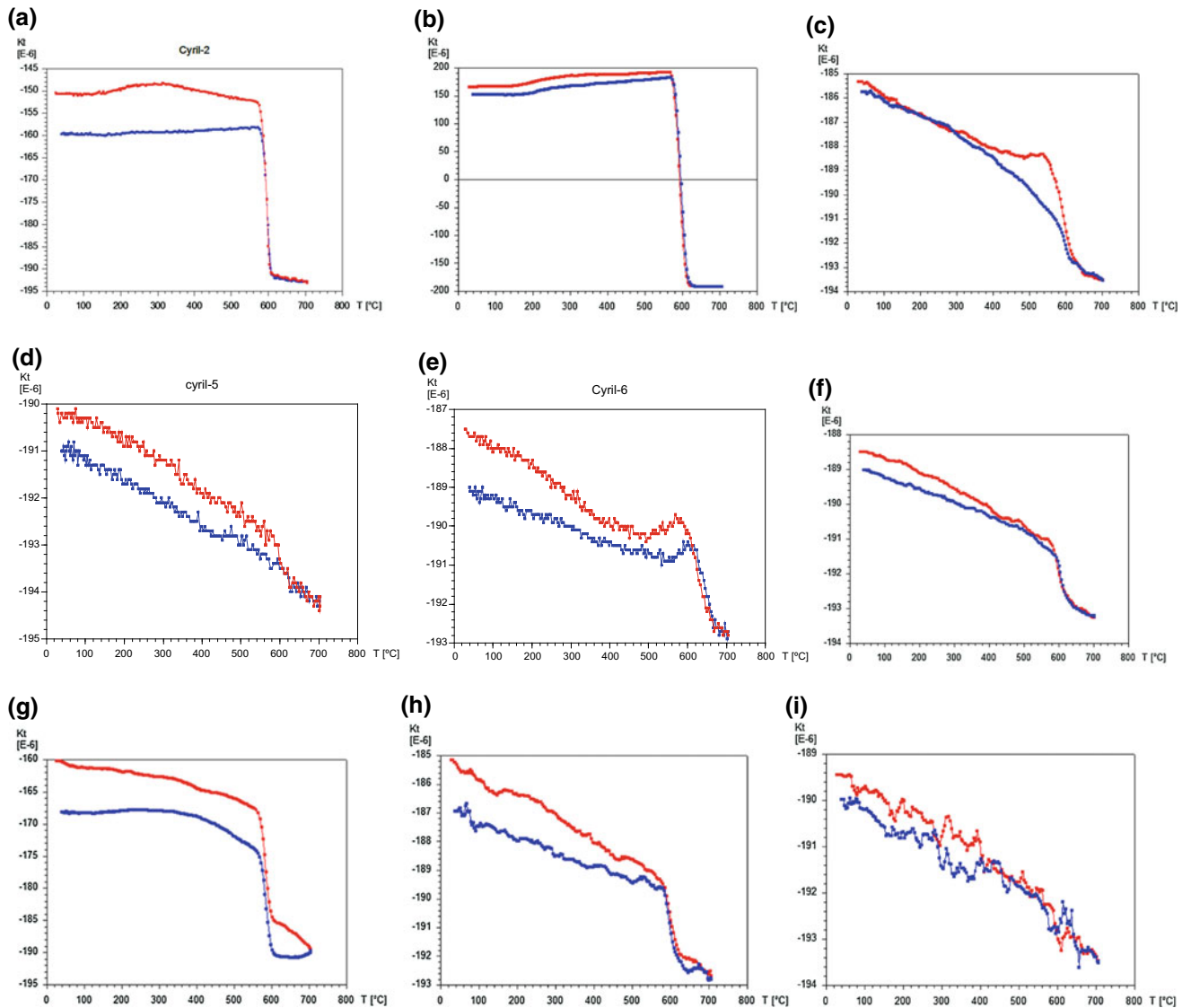


Fig. 1 Depicts the thermomagnetic and paramagnetic properties as verified through the magnetization curve, measured by Agico MFK1-FA kappabridge for **a** granite **b** biotite granite gneiss and **c** charnockite **d** quartzite **e** BIF **f** Porphyritic granite **g** Augen Gneiss **h** Banded Gneiss **i** Granite gneiss

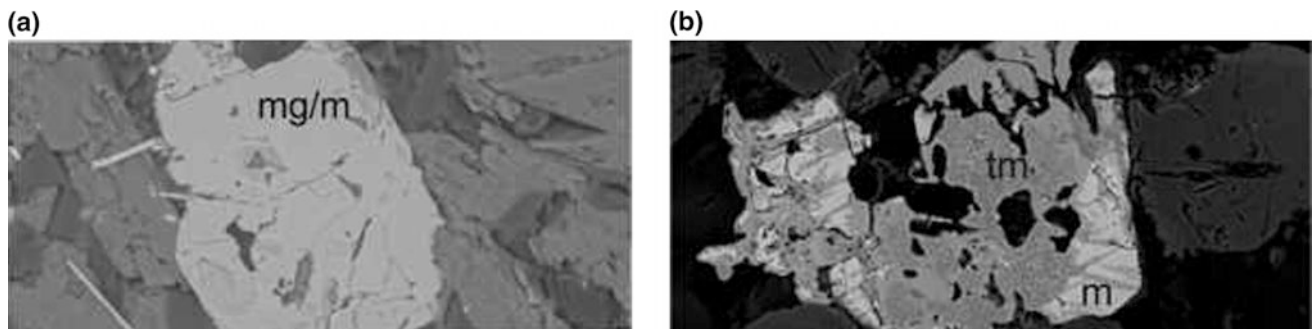


Fig. 2 Illustration of the SEM relevant result, as achieved via JEOL JSM-5900LV. **a** Maghemite and magnetite of southwestern Nigeria granitoids (scale:10 pm), **b** titanomagnetite and magnetite of southwestern Nigeria granitoids (scale:10 pm).

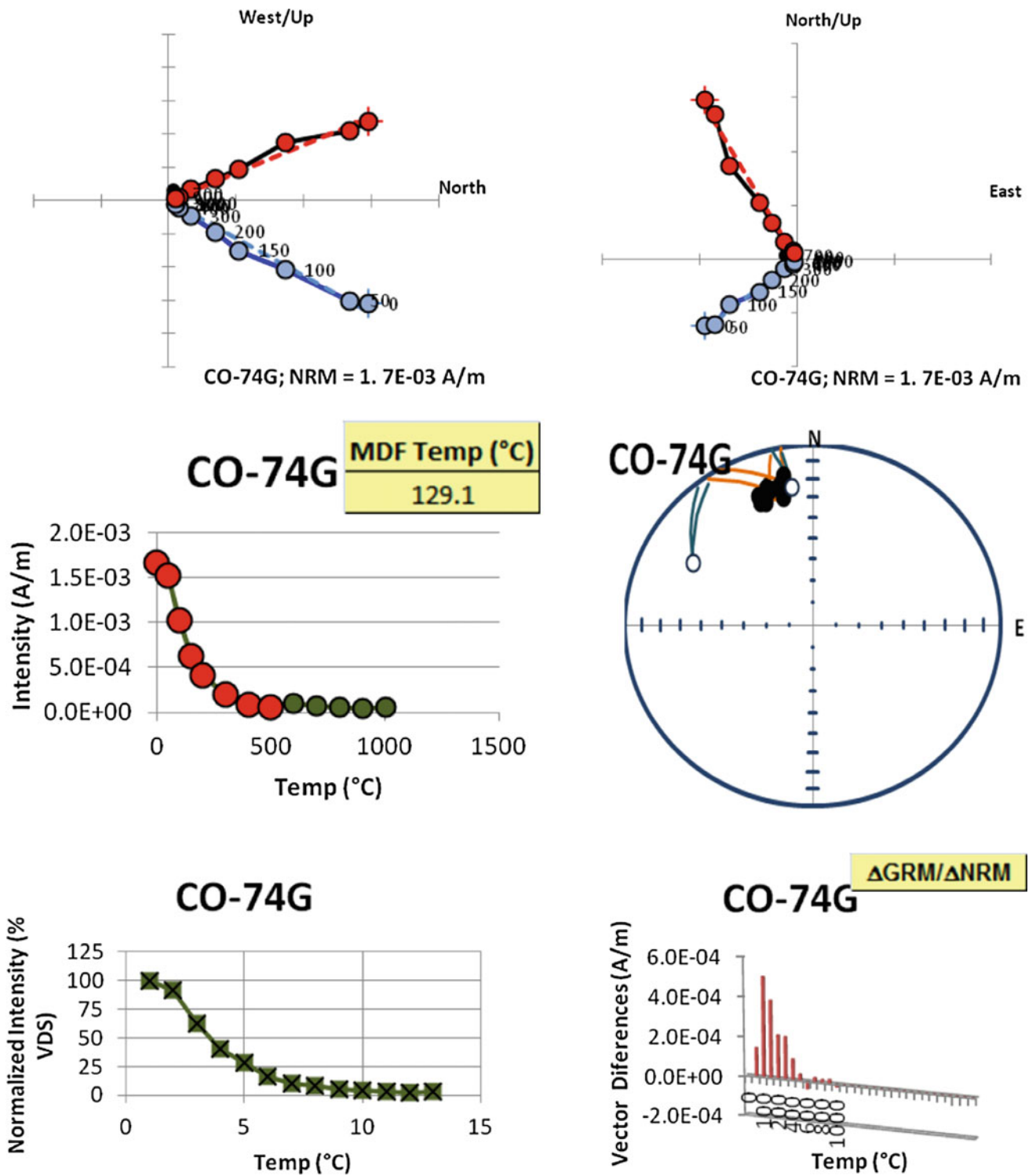


Fig. 3 AF demagnetization highlighting zijderveld orthogonal vectorization, using the DAIE software of Sagnotti, 2013.

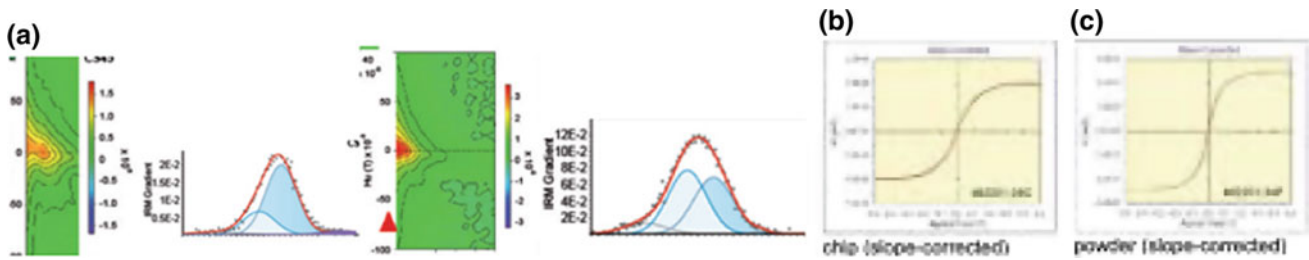


Fig. 4 a FORC diagrams showing PSD behavior, linear and Gaussian cumulative treatment, respectively depicting the dominance of Maghemite and hematite and decreasing magnetic grain size, b and c hysteresis loop of granite

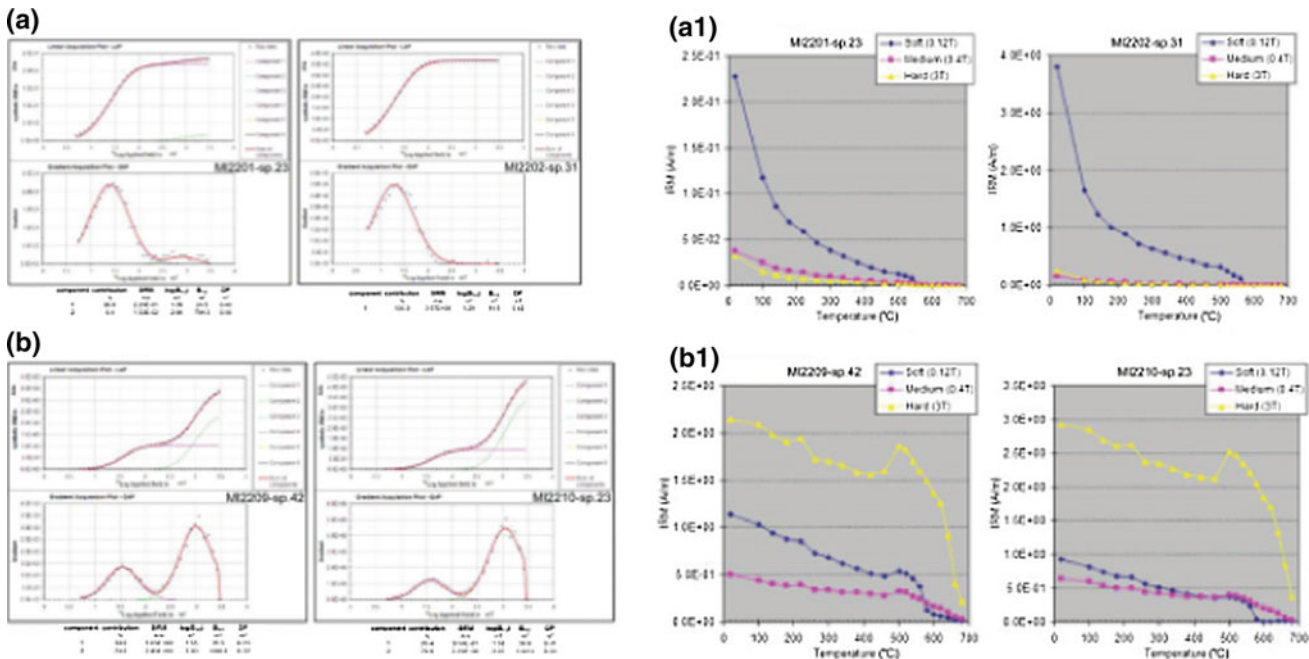


Fig. 5 Linear acquisition plot (LAP), gradient of acquisition plot (GAP) and thermal demagnetization of isothermal remanent magnetization (IRM), as acquired in direct magnetic fields of up to 3 T for a,a1

granite and b,b1 aplite intrusive rock Specimens were processed after alternating field demagnetization at 100 mT

4 Discussion

Representative thermomagnetic data for the western craton of the Nigerian shield are shown in Fig. 1, with the bulk of the southwestern Nigeria granitoids are demonstrated with reversible heating and cooling curves, with an approximate rate of about 585 °C Curie temperature, signifying a PSD/MD magnetic domain state of magnetite [7]. The SEM (Fig. 2) shows evidence of Maghemite, titanomagnetite and magnetite, corroborating Curie thermomagnetic results. The demagnetization (Fig. 3) of specimen shows stability results, while FORCs, GAP, LAP (Fig. 4) and hysteresis loop (Fig. 5) typify the magnetic behavior characteristic associated with the Precambrian rocks.

5 Conclusions

The multifunctional kappabridge (MFK1-FA) thermomagnetic curves appear to reveal the dominance of maghemite magnetite in the Precambrian basement terrain of southwestern Nigeria as mainly associated with the Pan African episode. Linear and Gaussian cumulative treatment corresponds to the polymorph of magnetite. The first-order reversal curves (FORCs), along with the hysteresis loop diagrams prove to corroborate the dominance of PSD/MD magnetic domain state. A paleomagnetic investigation prove to highlight the stability related to syenite, granite gneiss and biotite granite, despite the tectonometamorphic phases associated with the Precambrian rocks. Thus, the studied

area turns out to display very high magnetic susceptibilities resulting in the contribution and distribution of regional magnetic anomalies, as noticed to prevail in the western craton of the Nigerian shield.

References

1. Clark, D.A.: Magnetic petrophysics and magnetic petrography: aids to geological interpretation of magnetic surveys. *J. Aust. Geol. Geophys.* **17**, 83–103 (1997)
2. Daly, M.C., Lawrence, S.R., Diemu-Tshiband, K., Matouana, B.: Tectonic evolution of the Cuvette Centrale, Zaire. *J. Geol. Soc.* **149** (4), 539–546 (1992)
3. Pariso, J.E., Stokking, L., Allerton, S.: Rock magnetism and magnetic mineralogy of a 1-km section of sheeted dikes, hole 504B, Proc. Ocean Drill. Program Sci. Results, **137/140**, 253–262 (1995)
4. Miller, C.F., Wooden, J.L.: Anatexis, hybridization and the modification of ancient crust: Mesozoic plutonism in the old woman mountain area, California. *Lithos* **32**, 111–133 (1994)
5. Zhou, W., Van der Voo, R., Peacor, D.R., Zhang, Y.: Variable Ti-content and grain size of titanomagnetite as a function of cooling rate in very young MORB. *Earth Planet. Sci. Lett.* **179**, 9–20 (2000)
6. Pick, T., Tauxe, L.: Characteristics of magnetite in submarine basaltic glass. *Geophys. J. Int.* **119**, 116–128 (1994)
7. Dunlop, D.J., Özdemir, Ö.: *Rock magnetism: fundamentals and frontiers*. Cambridge University Press, New York/London/Cambridge, 573 pp (1997)

Petrographical and Geochemical Characteristics of the Mauritanides Belts' Birbirites

Didi Ould Moctar, Ali Moukadiri, Abdellah Boushaba, Sid'Ahmed Ould Mohamed Lemine, and Michel Dubois

Abstract

The Gouéarate region represents the most important area of birbirites' outcrops, sited in the Mauritanides Belts. In this paper, the petrological description of such facies is highlighted. The Gouéarate Birbirites are mainly composed of silica (chalcedony and microquartz) and talc, geochemically characterized with high SiO₂ level (up to 80%). They are derived from a highly refractory peridotite and serpentinite, which correspond to former dunite, harzburgite and serpentinite. The birbirites are mainly formed of ultramafic rocks' weathering, which has resulted in the concentration of SiO₂ and the transformation of olivine, pyroxene and serpentines into chalcedony, quartz and talc.

Keywords

Mauritanides belts • Birbirites • Peridotites
Serpentinites • Weathering

1 Introduction

Birbirites are scarce rocks emanating from the alteration of mantellic-serpentinized formations. In general, the term birbirite refers to cherty aspect rocks commonly associated with gold, platinum and mercury deposits, which culminate in the silicification of listvenites or serpentinized ultramafic rocks [1]. Birbirites provide an opportunity for the study of the

different mineralogical transformation stages associated with peridotites. This present work's contribution consists in investigating the birbirites' relating petrographical and geochemical description, along with the associated protoliths, as sited in the Gouéarate region of the Mauritanides Belts. The best birbirites outcrops, as located across the Mauritanides Belts, are discovered to lie over the region of Gouéarate, and are characterized with two major lithological units: (i) birbirites, and (ii) rocks with medium to high grade of metamorphism. To note, the Gouéarate region encloses, mainly: birbirites, amphibolites, pyroxenites, eclogited pyroxenites, kyanites black rocks and laterite formations [2, 3].

2 Materials and Methods

The selected samples have predominantly been analyzed via XRD, for the nature of constitutive phases to be determined. An XRD was performed on powder. Using a PRO X'PERT of company PANalytical, the obtained spectra were identified by means of the "PDF-2" database of *The International Center for diffraction Data*.

More specifically, a selection of six samples were collected from the different birbirites' outcrops for geochemical analysis purposes. The major associated elements were determined by means of X-ray fluorescence spectrometry (PANalytical Axios XRF 3KW). Sample disks were obtained at 1150 °C by mixing 1 g of the sample already dried at 105 °C with 9 g of lithium tetraborate. The spectrometer relating calibration has been performed by means of certified referential material.

Trace elements were determined via inductively coupled plasma-atomic emission spectrometry (HORIBA Jobin Yvon Activa); the solution is nebulized in an argon plasma at 8000 °C, which provides highly efficient atom excitation. The samples were digested on a hotplate involving three phases: firstly, using HF + HCl, then HCl + HNO₃ and finally HCl.

D. O. Moctar (✉)
Ecole Supérieure Polytechnique, Nouakchott, Mauritanie
e-mail: ouldmoctar.didi@esp.mr

A. Moukadiri · A. Boushaba
Université Sidi Mohamed Ben Abdellah, Fès, Maroc

M. Dubois
Université de Lille, 1/LGCgE, Lille, France

S. O. M. Lemine
Aura Energy Mauritania, Nouakchott, Mauritania

3 The Attained Results

3.1 The Petrographical Results

The Birbirites appear to be affected with an intense silicification, as testified by the development of silica crust surrounding the relevant samples (Fig. 1a). The matrix is predominantly composed of silica with small amounts of talc. The silica associated phases are mainly composed of chalcedony, despite the prevalence of a great deal of microquartz, as figuring in the matrix (Fig. 1b, c).

3.2 The Geochemical Results

The major as well as the trace element contents of the entirety of the birbirites extracted rocks, as pertaining to the

Gou erarate region are respectively depicted on Tables 1 and 2. The birbirites prove to display high SiO_2 contents (80.02–92.87 wt%) along with medium $\text{Fe}_2\text{O}_3\text{T}$ and MgO concentrations (respectively ranging from 4.05 to 6.74 wt% and 1.03 to 5.09). The examined samples prove to reveal low levels of Al_2O_3 , CaO , Na_2O , K_2O and TiO_2 (less than 2.3 wt%).

With regard to trace elements, the birbirites particular composition turns out to be enriched in Ni, Cr, Co and depleted in Cu, Ce, V, Zn.

4 Discussion

The absence of olivine, pyroxenes or serpentine in the matrix of birbirites suggests a complete transformation of their protoliths. Besides, this complete transformation was attested

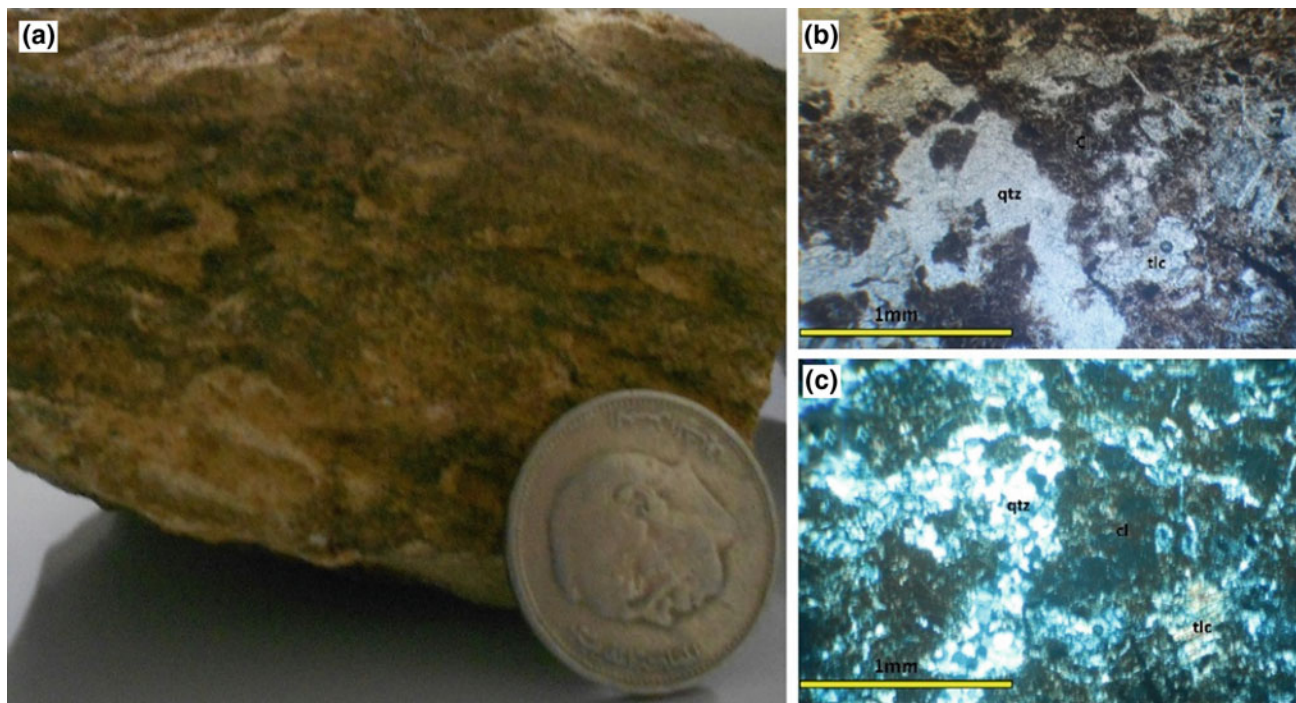


Fig. 1 Photo and photomicrographs of the Gou erarate region extracted birbirites: **a** a birbirite sample showing the development of silica crust. **b** and **c** Matrix of birbirites dominated chalcedony (cl), microquartz (qtz) and talc (tlc)

Table 1 The major element related data relevant to the Gou erarate region associated birbirites

Samples	SiO_2 (%)	TiO_2 (%)	Al_2O_3 (%)	$\text{Fe}_2\text{O}_3\text{T}$ (%)	MnO (%)	MgO (%)	CaO (%)	Na_2O (%)	K_2O (%)	P_2O_5 (%)	LOI (%)	Total (%)
GS1-1	91.62	<0.05	0.56	4.34	0.11	1.56	0.20	<0.05	<0.05	0.03	1.66	100.08
GS1-2	92.87	<0.05	0.61	4.34	0.11	1.59	0.22	<0.05	<0.05	0.03	1.65	101.41
GS2-1	89.35	<0.02	0.59	4.85	0.08	1.95	1.01	0.68	0.04	<0.02	1.56	99.39
GS2-2	91.09	<0.02	0.72	4.05	0.08	1.03	1.00	0.73	0.04	<0.02	1.66	99.63
GS6	80.06	<0.05	0.59	6.68	0.07	5.49	2.28	0.05	<0.05	0.04	4.82	100.03
GS6-1	80.02	<0.02	0.51	6.74	0.05	5.33	2.75	0.71	0.04	0.01	4.81	100.22

Table 2 Trace element data concerning the Gou erarate area relating birbirites

Samples	Ce ppm	Co ppm	Cr ppm	Cu ppm	Ni ppm	Pb ppm	Sb ppm	V ppm	Y ppm	Zn ppm	Sb ppm
GS1-1	6	88	329	13	2378	<5	<5	10	<5	36	<5
GS1-2	6	85	328	6	2340	<5	<5	10	<5	32	<5
GS2-1	<5	146.15	338.06	12.66	1932	<5	<5	8.83	<5	17.43	<5
GS2-2	<5	148.24	332.06	4.35	2054.7	<5	<5	8.83	<5	17.35	<5
GS6	8	94	607	9	2248	<5	<5	37	<5	44	<5
GS6-1	<5	189	685	7	2181	<5	<5	36	<5	40	<5

by the dominance of chalcedony, quartz and talc in one side and by the silica crust surrounding the rock on the other side.

Birbirites show high SiO₂ which can be related to the intense weathering that affected their protoliths. These birbirites are depleted in MgO due to its high mobility during weathering. In contrast, Al₂O₃ is normally immobile, but these birbirites show low levels of Al₂O₃ which indicate the refractory character of their protoliths.

Birbirites of Gou erarate are rich in Cr and Ni which involve that neither the serpentinization nor the silicification of the serpentinites has reset the mantle signature of the ultramafic protoliths.

In conclusion, birbirites of the region of Gou erarate result from transformation of the mantle rocks (dunites and/or serpentinites) that form the complex ophiolitic of Mauritanides belts. Field observations show that birbirites are always overlaid by laterite. Such an evidence leads us to conclude that the birbirites are in phase to transformation into laterites.

5 Conclusions

The implemented petrography, DRX and geochemical analyses, as undertaken in this study, prove to yield three major concluding remarks, mainly that: (a) the Gou erarate

relating birbirites are but the result of intense silicification affecting refractory peridotites or serpentinites; (b) these birbirites are geochemically characterized with the persistence of high SiO₂ levels, and (c) the field observations prove to indicate well that the examined birbirites are always overlaid with laterite and are undergoing a stage of transformation into laterites.

References

1. Esteban, J., Cuevas, J., Jos , M., Tub , J.M., Velasco, F., Vegas, N.: Petrographical and mineralogical characteristics of birbirites from the Ronda peridotites (Betic Cordilleras). *Geogaceta* **50-1**, 39–42 (2011)
2. Ould Moctar, D.: Serpentinisation des ophiolites des zones de suture : exemple des r gions d'Agane et de Gou erarate (Zone axiale des Mauritanides, Mauritanie). Th se Doctorat, Universit  Sidi Mohamed Ben Abdellah, Maroc, 158p. (2013)
3. Ould Moctar, D., Boushaba, A., Dubois, M.: Serpentinization of mantle formations in the Mauritanides Belt: regions of Agane and Gou erarate (middle-western Mauritania). *Arab. J. Geosci.* **7**, 1985–1992 (2014)

Petrography, Origin and Geochemical Characters of the Granitoids of the Southern Part of the Nellore Schist Belt, Andhra Pradesh, India

Sumit Kr. Mitra and Tushar Meshram

Abstract

The Archaean to Paleoproterozoic migmatitic gneisses and granitoids, surrounding Rapur, in the southern part of Nellore Schist Belt, Andhra Pradesh, include low-K Tonalite-Trondhjemite-Granodiorite Suite (TTG), Tonalite-Granodiorite-Monzogranite Suite (TGM) and Monzogranite-Syenogranite Suite (MS). The TTG suite shows calcic to calc-alkaline nature and compositionally straddle the boundaries between metaluminous and peraluminous as well as ferroan and magnesian characters. They display highly fractionated REE pattern in chondrite-normalized diagram along with a low HREE content, with moderate to small positive Eu anomalies. The TGM suite's composition is transitional between the TTG and MS suites. The latter are comparable with continental margin calc-alkaline rocks, characterized with higher alkali content and lower CaO than the TTG suite, with a rather fractionated REE pattern highlighting a typically increased LREE rate, with slightly negative and positive Eu anomalies and flat to depleting HREE. The MS granites display a chemical homogeneity (especially in major elements), characterized with a K-rich nature bearing pink and grey feldspar and trace element percentage. The MS suite of granites exhibit increased LREE rates, with negative Eu anomaly, and flat HREE with a predominant proportion of LREE over HREE. The relating chemical compositions suggest well that the TGM rocky suites have been recycled through crustal re-melting processes, culminating in the MS suite associated granites. The mineralogical and geochemical shifts characterizing the granitoids composition are related to changes in magma source. The TGM and MS suites' transition from TTG to more potassic granitoids proves to

be gradual, with the more recently formed granitoids having evolved over a substantial period of time, ranging from the Archaean to the late Archaean age. The MME, as occurring within TGM suite, are fine grained, slightly dark and enriched in mafic minerals compared to the host granitoids, displaying a wide variation in REE contents, as judged by their compositional heterogeneity, but generally characterized with high LREE ($\Sigma\text{LREE} = 315.27$) and low HREE ($\Sigma\text{HREE} = 29.77$) contents. The MME display fractionated LREE and flat HREE patterns, along with slightly negative ($\text{Eu}/\text{Eu}^* = 0.83$), or even no Eu-anomalies. Most MMEs prove to demonstrate noticeable enrichment in Sr, Th, Zr, Hf, and REE relative to the mantle values.

Keywords

TTG • TGM • MS • LREE • HREE

1 Introduction

The late Archaean granite green stone terrain of Andhra Pradesh involves vast stretches of granitoids along with high strain equivalent gneisses that enclose linear green stone belts. The Granitoids surrounding Rapur, southern part of Nellore Schist Belt, Andhra Pradesh, can be divided and classified into four major types with respect to their corresponding mineral assemblages, field association and petrographical features, as well as the relating chemical characteristics. These types are: (1) Tonalite-Trondhjemite-Granodiorite (TTG) suite (2) Tonalite-Granodiorite-Monzogranite (TGM) Suite and (3) the underlying latent Mafic Microgranular Enclaves (MME), along with the (4) Monzogranite-Syenogranite (MS) Suite. Concerning the present work, only the petrology, geochemistry and petrogenesis characters of these granitoids are described (Fig. 1).

S. Kr. Mitra (✉)

Geological Survey of India, 284/1A, NSC, Bose Road,
700047 Kolkata, India
e-mail: sumit0224@rediffmail.com

T. Meshram

Geological Survey of India, Nagpur, India

© Springer Nature Switzerland AG 2019

D. M. Doronzo et al. (eds.), *Petrogenesis and Exploration of the Earth's Interior*,

Advances in Science, Technology & Innovation, https://doi.org/10.1007/978-3-030-01575-6_14

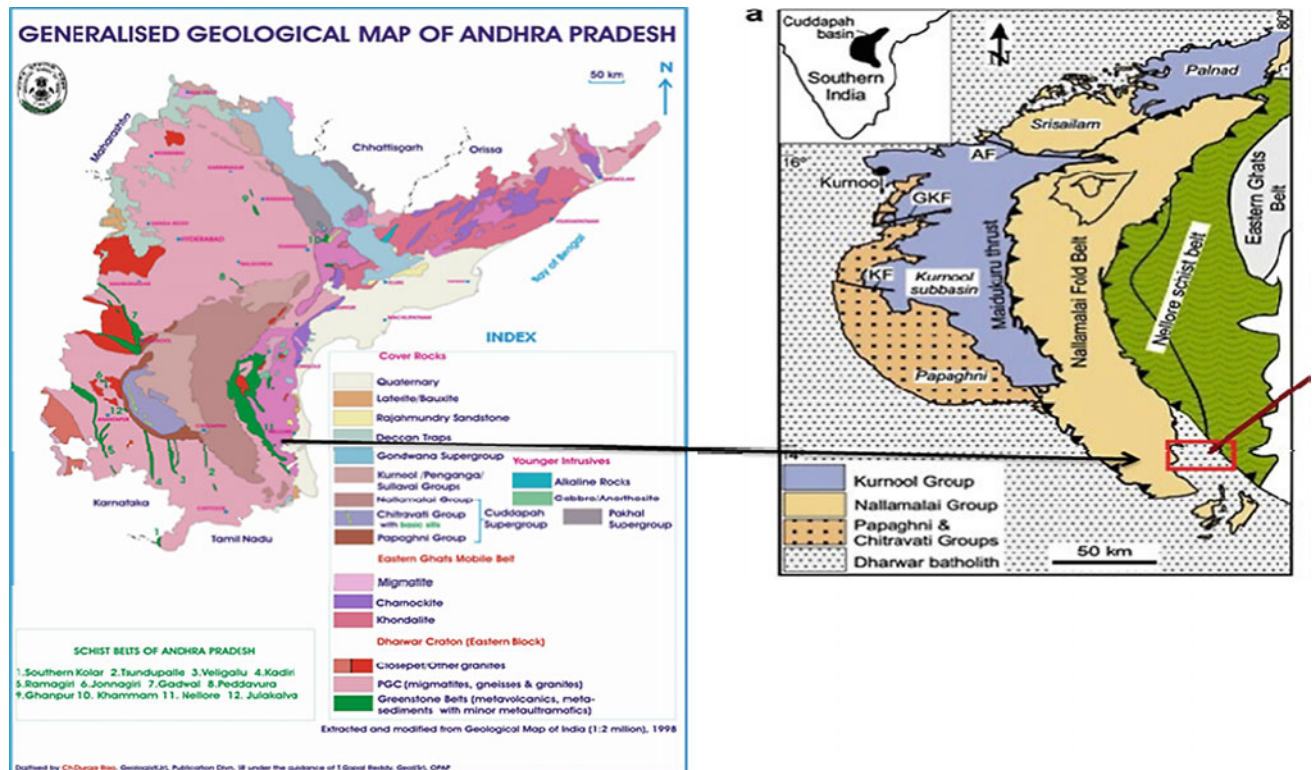


Fig. 1 The area subject of study, as shown in the generalized geological map of Andhra Pradesh

2 Methodology

The present work was carried out through extensive field-work of geological mapping, structural detailing, geochemistry, petrological along with EPMA studies.

3 Results and Discussions

Detailed field and petrographic studies of unclassified Archaean crystalline complex (PGC), as depicted across the Rapur surrounding area, in the southern part of the Nellore Schist Belt (NSB), Andhra Pradesh, helped to identify the suites of granites, as per IUGS scheme, namely, the TTG suite (the oldest), the TGM and MME suites, along with the youngest MS suite.

The D1 deformation has produced the regional gneissosity within granite gneiss and tight isoclinals to rootless F1 folds, with the development of pervasive axial planer schistosity in the rocks of NSB (metabasalt with patches of quartzite and schist). The D2 deformation has produced upright fold with axial plane trending NE-SW, along with the development of crenulation cleavage in the NSB, and large scale folding, as testified through the map pattern, north of Rapur. The D3 deformation has produced open

folds in three sets of vertical axial planes (viz., N330°, N75° and N285°). Type-3 interference pattern, resulting from the superposition of F2 folds on F1 isoclinal folds, and Type-1 interference pattern, resulting from the superposition of upright F3 folds on upright F2 folds, have been observed.

All these Granitoids display a remarkable chemical similarity, highlighting their formation from similar source. The magmatic evolution has resulted in decreased compatible trace elements, Ti, Zr, CaO, FeO, MgO, and increasing Sr and Ba concentrations starting from the TTG through the TGM to the MS suites. (Fig. 2).

The low-moderate Rb and high Sr contents prove to suggest that the mafic TTG gneisses have evolved from the partial melt of the greenstones' amphibolites.

The TGM granitoids are mostly either syntectonic or post-to late tectonic in nature. These granites are rich in SiO₂ and poor in CaO, MgO, FeO, predominantly displaying a cordilleran type of affinity, while bearing higher Sr and Ba but lower Rb values. The calc-alkaline feature characterizing the TGM suite points out to magma mingling and mixing, and to fractional crystallization differentiation.

Most of the MS granitoids, however, have high SiO₂, alkalis, CaO, MgO, Sr, Ba and low Rb. These granites fall in the field of within-plate granites [2]. These granites are characterized with enrichment of Zr, REE, Fe and fairly uniform trace and REE abundance, along with the persistent

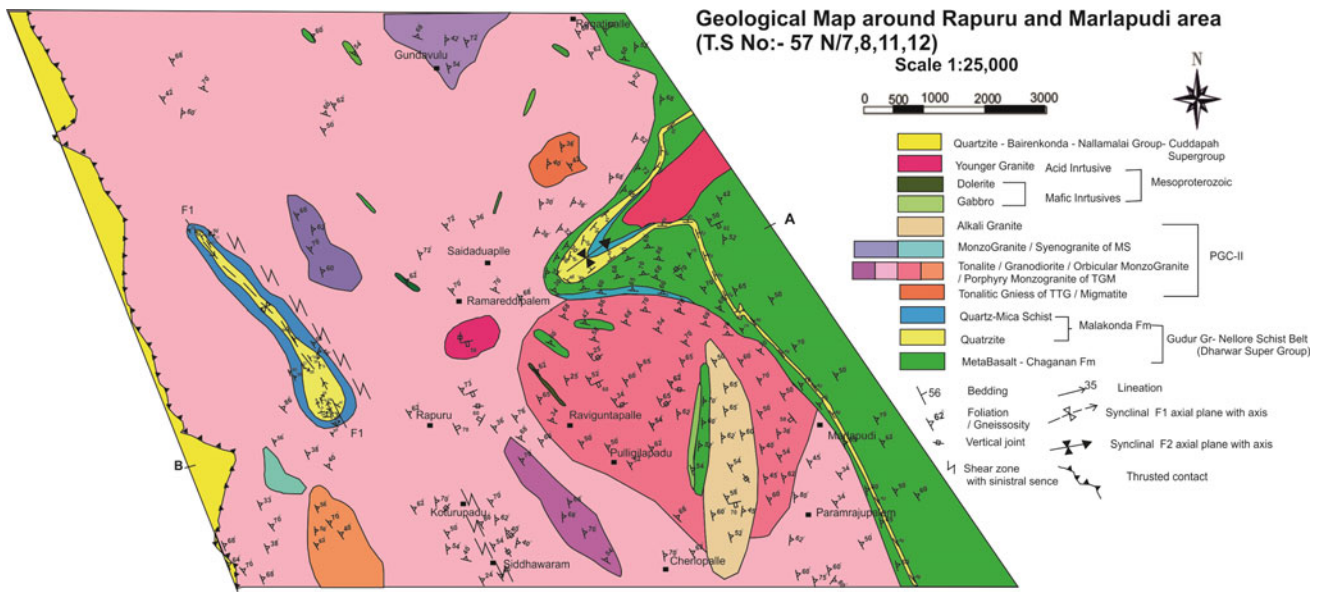


Fig. 2 Geological map of the area surrounding Rapuru and Marlapudi

variation of CaO, MgO, Fe₂O₃ (T), Rb, Sr and Ba, indicating their formation from both crustal and mantle sources [1] for their genesis, unlike the anorogenic granitoids of late-Archaean age. The detailed EPMA studies conducted have brought out, for the first time, the occurrence of uraninite, REE minerals along with thorite and sulphide minerals within younger granite (the MS Suite). Sporadically, disseminated grains of pyrite and chalcopyrite have been observed at places within the metabasalts associated with the NSB (Figs. 3 and 4).

4 Conclusion

From a geochemical perspective, all the granitoid suites of Rapur area, Nellore Schist Belt, Andhra Pradesh, appear to exhibit calc-alkaline trend, and in an A/NK-A/CNK plot, they are positioned at the juncture of peraluminous-metaluminous-peralkaline field. These granites are calc-alkaline in nature. The REE studies prove to reveal a general enrichment of LREE, pronounced negative Eu-anomaly and

Fig. 3 IUGS classification of granitoids of the present study

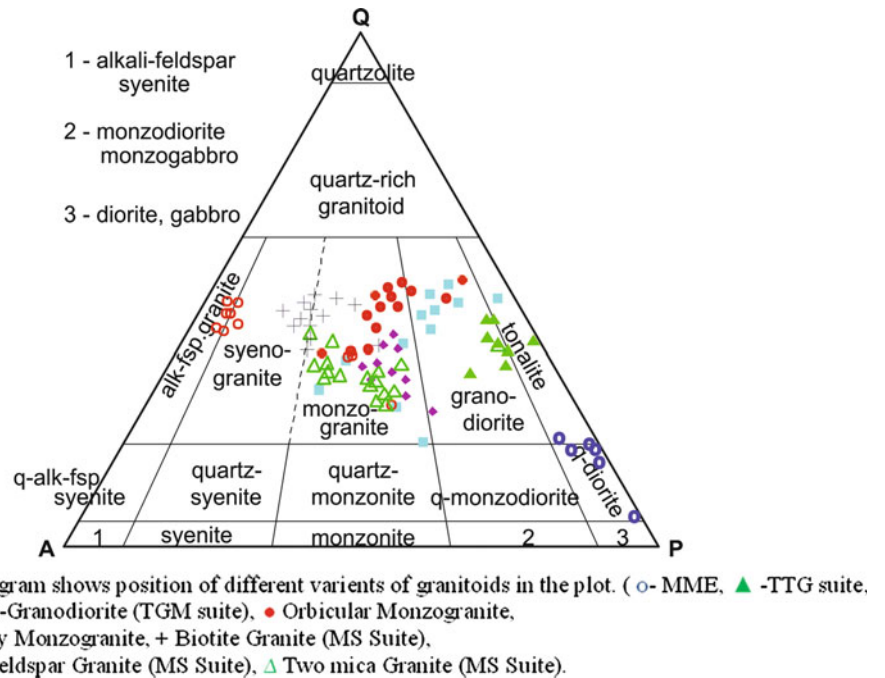
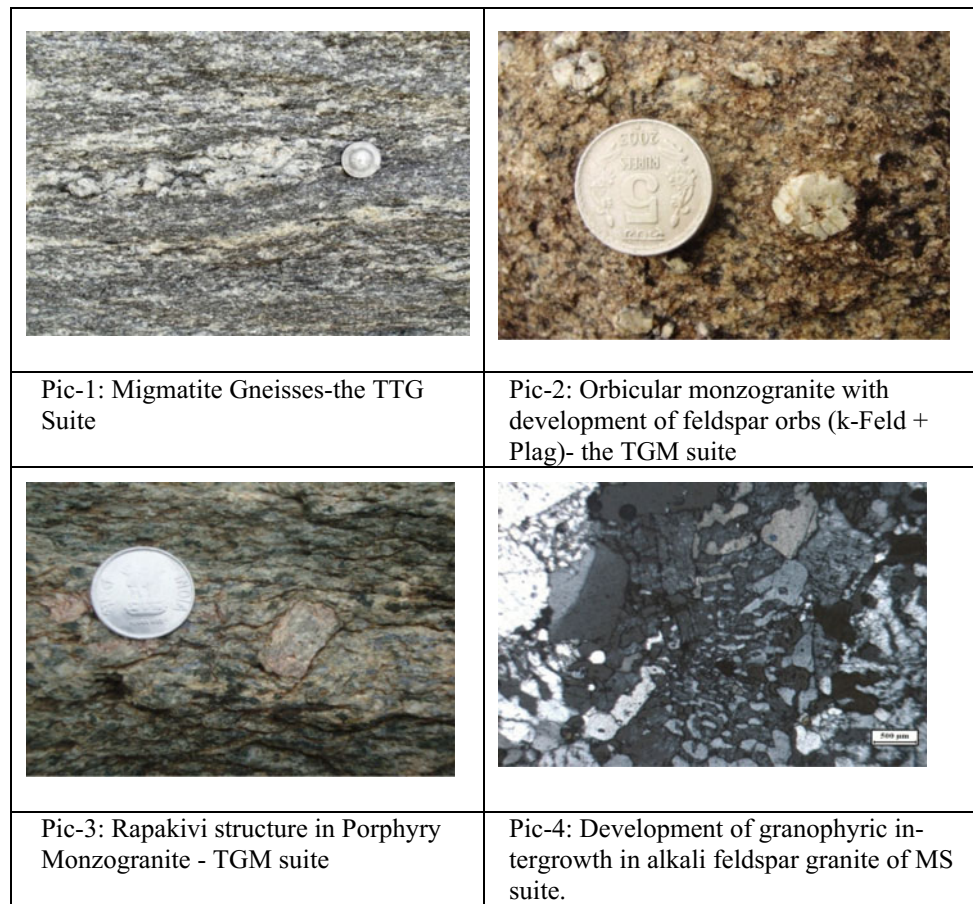


Fig. 4 Characteristic textures of the different type of granitoids of the present study area



flat HREE patterns. The TTG suite is considered to be formed by the partial melting of a pre-existing amphibolite, possibly part of an older simatic crust. The calc alkaline TGM suite is metaluminous with mafic microgranular enclaves indicating mingling and mixing of mantle-derived and crustally derived melt, followed by fractional crystallization differentiation for their genesis in a continental arc environment. The intrusive MS suite is younger to TTG and TGM suites. The origin of this suite is related to the melts' mixing due to crustal anatexis and also, partly, from the mantle derived melts.

References

1. Divakara Rao, V., SubbaRao, M.V., Murthy, N.N.: Proterozoic alkali rich granites of South India: Evidence for crust-mantle interaction. In: Proceedings of ICU 29th Annual Convention, 1–11 (1993)
2. Pearce, J.A., Harris, N.B., Tindle, A.G.: Trace element discrimination diagrams for the tectonic interpretation of granitic rocks. *J. Petrol.* **25**(4), 956–983 (1984)

Petrography, Mineralogy and Thermodynamic Modeling of Eclogites from the Serkout Area, Central Hoggar, Algeria

Doukkari Sidali, Godard Gaston, Ouzegane Khadidja, Arab Amar, and Bendaoud Abderrahmane

Abstract

The Aleksod terrane Eclogites, sited in the Central Hoggar, preserve a selection of eclogite-facies assemblage (coarse garnet, omphacite, quartz, clinozoisite and amphibole). During retrogression, these minerals were partially substituted with coronas and symplectites of diopside-plagioclase and amphibole-plagioclase. The almandine-dominated garnet proves to enclose heterogeneous compositions (X_{Alm} 0.30–0.56). The omphacite displays a high X_{Jd} of 0.31. The eclogite-facies coarse amphibole is magnesio-hornblende with $Na_{M4} = 0.31–0.47$. The plagioclase is usually secondary exhibiting a range of composition from oligoclase to anorthite ($X_{An} = 0.20–0.99$), where albite-rich and anorthite-rich compositions prove to correspond, respectively, to symplectite after omphacite and coronas around epidote. The relevant P - T pseudosections using THERMOCALC-340 are calculated to estimate peak conditions and trace the P - T evolution. At H_2O -saturated conditions, inclusions of amphibole in garnet core with garnet composition from core to inner rim are used to trace pre-peak P - T path from 14 kbar–610 °C to 18 kbar–700 °C. At H_2O -undersaturated conditions, the retrograde path has been traced using secondary phases as plagioclase, diopside and amphibole at 10 kbar–720 °C.

Keywords

Eclogite • Serkout • Hoggar • Thermodynamic modeling • P-T path

D. Sidali (✉) · O. Khadidja · A. Amar · B. Abderrahmane
LGGIP, FSTGAT, U.S.T.H.B., B.P. 32 El Alia, Dar El Beida,
16111 Algiers, Algeria
e-mail: Sidali.doukkari@gmail.com

G. Gaston
IPGP, 1, rue Jussieu, 75238 Paris Cedex 05, France

1 Introduction

The Aleksod terrane (Fig. 1b) is situated in the central part of the Hoggar Shield, also dubbed LATEA (acronym of Laouni, Azrou-n-fad, Tefedest, and Egere-Aleksod) [1].

Most of the HP eclogite provinces sited in the Hoggar are included in the LATEA (Fig. 1a), and the best preserved among them are described in the Egere-Aleksod terrane [2]. The Serkout area (Fig. 1c) includes four districts, the first (I) is characterized with an Arechchoum basement. The second (II) contains metasedimentary rocks (quartzite, Marble) known as the Aleksod unit. The third district and the fourth districts are underlain by very deformed rocks with eclogite lenses along shear zones in the northern parts [3].

2 Materials and Methods

Petrography and mineral identification were carried out using reflected microscopy and the SEM techniques. The mineral chemistry of metamorphic mineral phases' index was determined by means of a Cameca SX100EPMA, made available at the University of Paris VI, with operating conditions of 15 kV, and 10 nA. The pseudo-sections were calculated after the (NCKFMASHTO) chemical system, using THERMOCALC v3.40 [4] and an updated version of the data set [5] (file tc-ds62.txt). The mineral compositions, as used in the pseudo-section (isopleths), are aimed to determine the P-T path of the investigated eclogites.

3 Results

3.1 Petrography

The peak metamorphic stage (M2) is preserved in the studied samples and highlighted through the eclogite-facies paragenesis of coarse garnet, omphacite, quartz, clinozoisite and

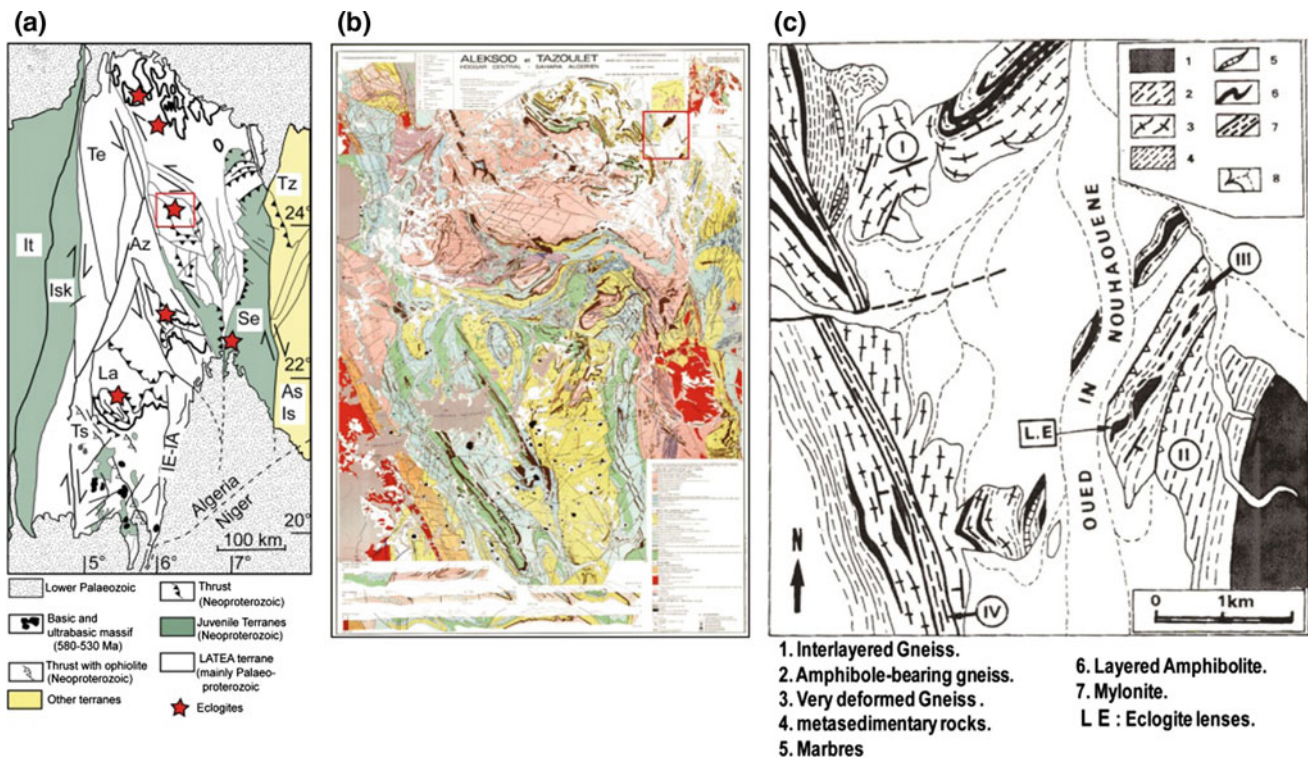


Fig. 1 a A sketch map of the LATEA pertaining terranes [1]. b Aleksod and Tazoulet geological map, [3]. c Geological map of Serkout area [3]

amphibole. However, these minerals are partially substituted with retrograde stage M3 coronas and symplectites of diopside + plagioclase and amphibole + plagioclase. The backscattered electron micro-images prove to display the persistence of coarse-grained garnet crystals with abundant amphibole, quartz, epidote and rutile inclusions, assumed to be formed in a pre-eclogite stage (M1). Omphacite is usually destabilized into fine-grained diopside + plagioclase symplectites. Coronas of plagioclase + amphibole are observed lying between garnet and omphacite, suggesting the reaction $\text{Grt} + \text{Omp} + \text{H}_2\text{O} \rightarrow \text{Amp} + \text{Pl}$. The epidote, on the other hand, shows coronas of zoned plagioclase, where it stands in contact with amphibole and diopside + plagioclase symplectites.

3.2 Mineralogy

Garnet profiles show a flat core profile of almandine-rich and grossular poor, with the inner rim exhibiting an increase in almandine and grossular contents. The outer rim is rich in pyrope and poor in grossular-almandine components (Fig. 2a). Clinopyroxenes are bearing cores rich in Na and Al^{VI} , and Ca, Fe and Mg-enriched rims (Fig. 2b). Plagioclase shows compositional variations associated with the

different textural varieties, where the albite-rich compositions correspond to symplectite after omphacite, and the anorthite-rich ones correspond to coronas around epidote (Fig. 2c). Amphibole occurs under a variety of textural forms, with compositions comparable to the Sanbagawa, Franciscan, Dalradian and Abukuma terranes (Fig. 2d).

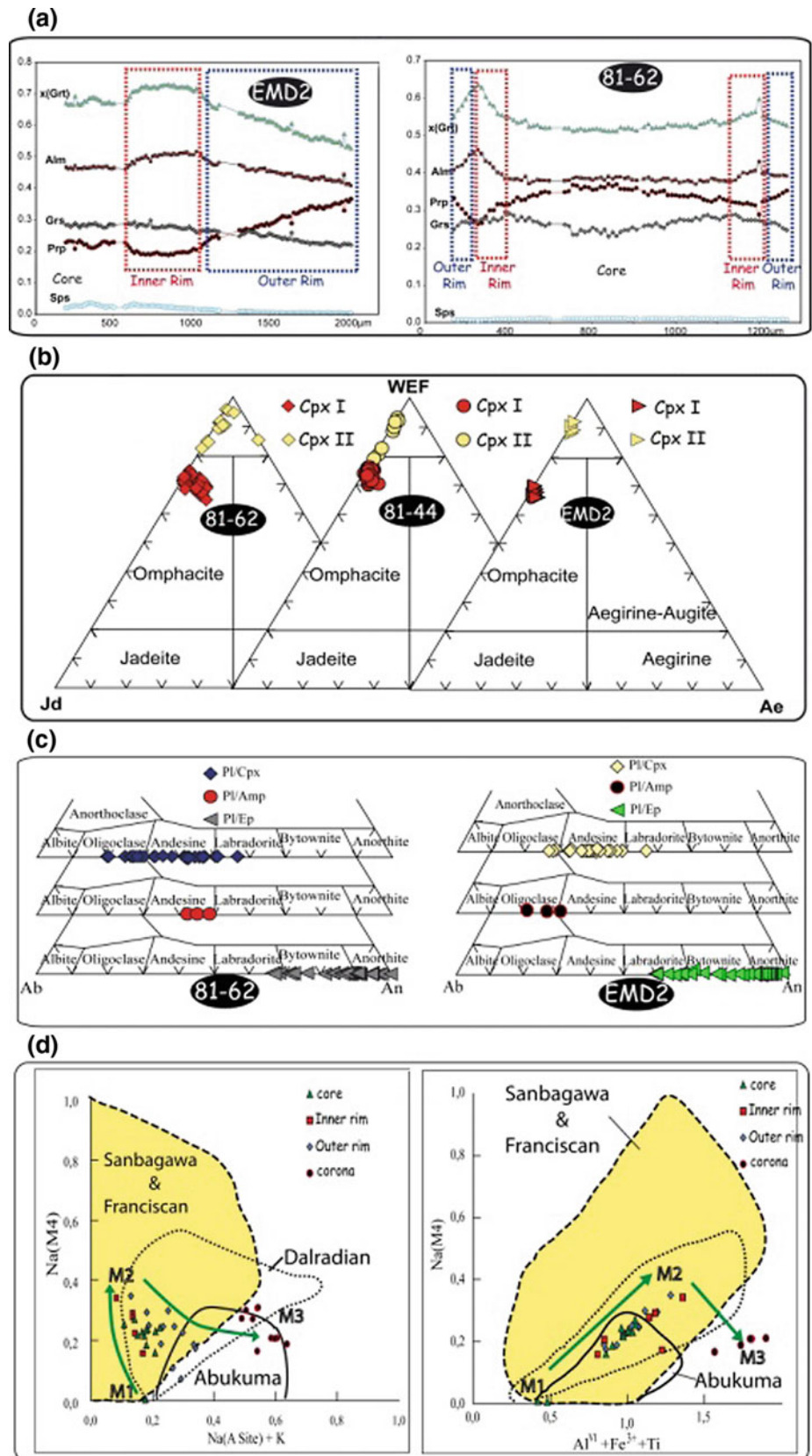
3.3 Thermodynamic Modeling

See Fig. 3.

3.4 Discussion

Three distinct metamorphic stages were proposed in the Study area, namely, the pre-peak stage (M1: garnet core, amphibole, epidote, quartz, rutile), the peak eclogitic stage (M2: omphacite, garnet rim, amphibole, epidote, quartz, rutile), and the retrograde stage (M3), with initial decompression resulting in the formation of plagioclase. The prograde path from M1 (17–18 kbar, 580 °C) to M2 (21 kbar, 650–670 °C) at H_2O -saturated conditions, can be attained during subduction tectonics. The M3 stage took place at lower pressure conditions (8–9 kbar, 730–750 °C) in H_2O -undersaturated conditions.

Fig. 2 Diagrams illustrating compositions of garnet, clinopyroxene, plagioclase and amphibole



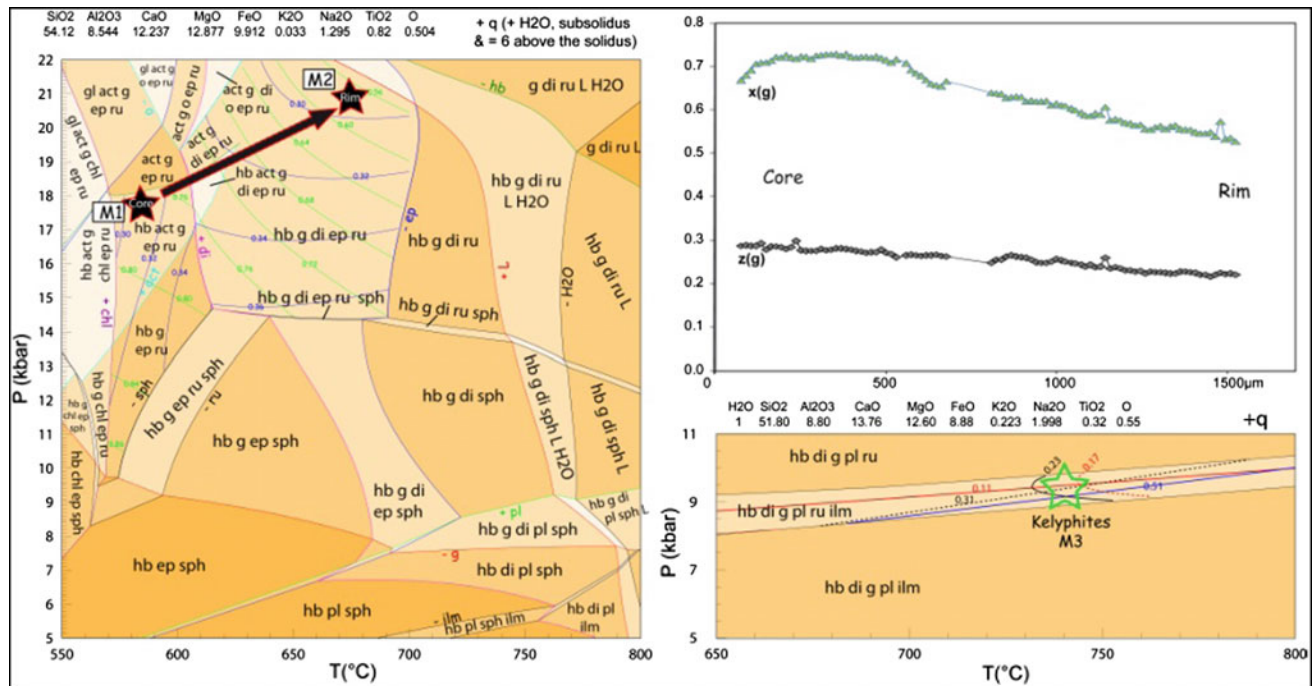


Fig. 3 P-T path for Serkouteclogites as traced from pseudo-sections

4 Conclusions

The pseudo-section modeling turns out to reveal the presence of a clockwise P-T path with peak conditions at $P = 19$ kbar and $T = 720$ °C. The subduction of a light continental passive margin highlights that it is pulled down by a dense oceanic lithosphere. The subduction of the oceanic lithosphere led to the formation of a subduction arc systems in the Iskel area. The subducting slab was, therefore, west-dipping. The P-T conditions near peak metamorphism (19 kbar–720 °C) proved to operate under a mildly gentle temperature-depth gradient (10 °C/km), typical of a cold passive margin subduction during the closure of the Neoproterozoic oceanic basin.

References

- Liégeois, J.P., Latouche, L., Boughrara, M., Navez, J., Guiraud, M.: The LATEA metacraton (Central Hoggar, Tuareg shield, Algeria): behavior of an old passive margin during the pan-African orogeny. *J. Afr. Earth Sci.* **37**, 161–190 (2003)
- Doukkari, S., Ouzegane, K., Godard, G., Diener, J.F.A., Kienast, J. R., Liégeois, J.P., Arab, A., Drareni, A.: Prograde and retrograde evolution of eclogite from Adrar Izzilatène (Egéré-Aleksod terrane, Hoggar, Algeria) determined from chemical zoning and pseudosections, with geodynamic implications. *Lithos* **226**, 217–232 (2015)
- Bertrand, J.M.L.: Evolution polycyclique des gneiss précambriens de l'Aleksod (Hoggar central, Sahara Algérien). Thèse d'Etat, In: C.N. R.S. (C.R.Z.A) (ed.), aspects structuraux, pétrologiques, géochimiques et géochronologiques. Série Géologique 19, p. 350 (1974)
- Powell, R., Holland, T.J.B.: An internally consistent thermodynamic dataset with uncertainties and correlations: 3. Applications to geobarometry, worked examples and a computer program. *J. Metamorph. Geol.* **6**, 173–204 (1988)
- Holland, T.J.B., Powell, R.: An improved and extended internally consistent thermodynamic dataset for phases of petrological interest, involving a new equation of state for solids. *J. Metamorph. Geol.* **29**, 333–383 (2011)
- Liégeois, J.P., Latouche, L., Boughrara, M., Navez, J., Guiraud, M.: The LATEA metacraton (Central Hoggar, Tuareg shield, Algeria):

The First Example of Kyanite-Staurolite-Garnet-Bearing Metapelites from the Hoggar (Egéré Terrane, South Algeria)

Amar Arab, Khadidja Ouzegane, Abderrahmane Bendaoud,
Sidali Doukkari, and Gaston Godard

Abstract

Metapelites containing kyanite, garnet, staurolite, biotite cordierite, and spinel are relatively rare. However, they have been reported from a numerous metamorphic terranes around the world. kyanite-garnet-staurolite-bearing metapelites have been identified among the various lithologies featuring the Egéré area (Central Hoggar). These rocks contain mineral assemblages consisting of garnet, kyanite, quartz, staurolite, spinel, cordierite, biotite, \pm plagioclase and muscovite. These rocks display complex symplectites and coronas reaction textures comprises spinel and cordierite resulted from the breakdown of the peak paragenesis formed by garnet, kyanite and staurolite. Garnets porphyroblasts with inclusions of quartz, biotite, plagioclase, and rutile reveal an obvious compositional core-rim-outer-rim zonation, particularly in grossular, and pyrope, which is related to the metamorphic evolution of their host metapelitic rocks. Phengitic white micas display high-Si content that indicates crystallization under relatively high pressure conditions. The textural observations and mineral chemical compositions described in this contribution are interpreted via the application of P-T pseudosections, which were calculated in the system MnO-Na₂O-CaO-K₂O-FeO-MgO-Al₂O₃-SiO₂-H₂O-TiO₂ (MnNCKFMA SHT). The obtained results indicate that the metamorphic evolution recorded in these rocks started at pic conditions

of 12 kbar and 700 °C from amphibolitic facies and pursued via retrograde path toward granulitic facies conditions around 5 kbar and 850 °C. The combination of the observed mineral paragenesis, microstructural relationships and mineral chemistries, coupled with thermodynamic modeling of representative metapelitic samples, provide evidences that the Egéré kyanite-staurolite-bearing metapelites experienced relatively high pressure conditions, followed by exhumation to the earth's surface through a clockwise P-T path during the Pan-African orogeny.

Keywords

Hoggar • Egéré • Residual Metapelites • Equilibrium phase diagram • P-T path

1 Introduction

Metapelitic mineral assemblages containing garnet, kyanite, biotite, staurolite, spinel and cordierite stand as some of the most problematic issues in metamorphic petrology and are very scarce in metamorphic settings.

Representative samples of the studied metapelites have been collected from different sites within the Egéré area that represents the northern part of Egéré-Aleksod terrane (Central Hoggar, South Algeria, Fig. 1).

The Egéré region is composed of two superimposed tectonic units differing in lithology and metamorphic grade: (i) the Arechchoum basement, which consists of migmatitic orthogneiss; and (ii) the Egéré meta-sedimentary cover, made up mainly of kyanite-staurolite-bearing metapelites, marble and quartzite and numerous mafic rocks.

This contribution has an object of describing the petrological investigations, mineral chemistries, microtextures phase relations; and clarify the P-T path of the kyanite, staurolite, spinel-bearing metapelites from the Egéré.

A. Arab (✉) · K. Ouzegane · A. Bendaoud · S. Doukkari
Faculté des Sciences de la Nature et de la Vie et des Sciences de la
Terre, Université de Bouira (UAMOB), Bouira, Algeria
e-mail: a.arab@univ-bouira.dz; amarab@usthb.dz

A. Arab · G. Godard
Laboratoire de Géodynamique, Géologie de l'Ingénieur et de
Planétologie, FSTGAT-U.S.T.H.B, B.P. 32 El Alia, Dar el Beida,
16111 Alger, Algeria

A. Arab · K. Ouzegane · A. Bendaoud · S. Doukkari · G. Godard
Institut de Physique du Globe de Paris, Sorbonne Paris Cité,
Université Paris-Diderot, UMR 7154, CNRS, 1 rue Jussieu, Paris,
75238, France

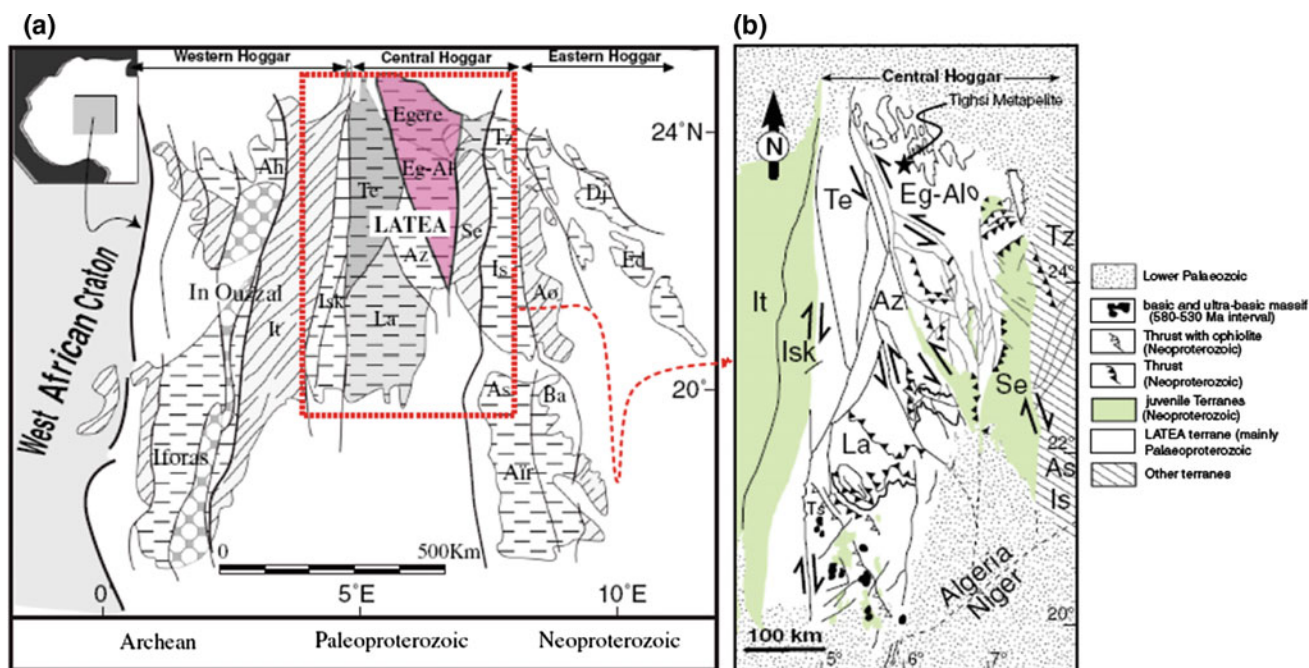


Fig. 1 **a** Geological sketch of the Touareg shield with terrane boundaries [1]. **b** Geological map of the LATEA metacraton [2] showing location of the studied metapelites from Tighsi area. Ah, Ahnet; Aïr, is the full name; Ao, Aouzegueur; As, Assodé; Az,

Azrou-n-Fad; Ba, Barghot; Dj, Djanet; Ed, Edembo; Eg-Al, Egéré-Aleksod; Is, Issalane; Isk, Iskel; It, In Teidini; La, Laoni; Se, Serouenout; Te, Tefedest; Tz, Tazat

2 Results

2.1 Petrology and Mineral Chemistries

The investigated metapelites are migmatitic and dominantly restitic, they are mainly composed of garnet (Grt), kyanite (Ky), quartz (Qtz), biotite (Bt), staurolite (St), cordierite (Crd), spinel (Spl) along with minor amount of accessory minerals such as rutile (Rt), ilmenite (Ilm) and zircon (Zr). Two distinct metamorphic parageneses have been recognized, (i) the primary coarse-grained centimeter-scale (M1) paragenesis at higher-medium pressure consisted of large garnets (Grt1) in equilibrium with kyanite, large staurolite crystals (St1), biotite, quartz and rutile. (ii) the secondary paragenesis (M2) at lower pressure composed of small staurolite (St2) and garnet (Grt2) grains, spinel, cordierite and ilmenite. The petrographic observations show that that minerals forming the primary assemblage are constantly separated by either coronas or symplectites microtextures.

Garnets represent the major phase within these metapelites (Fig. 2), two generations have been recognized, the first generation (Grt1) is large crystals (1–2.2 mm) rich of inclusions of quartz, biotite, plagioclase, rutile and ilmenite; these garnets display a perfect zoning pattern, with core rich in almandine (61–70%) and poor in pyrope (21–28%) and grossular (7–12%), where the rim is relatively poor in

almandin (60–63%) and rich pyrope (24–29%) and grossular (8–12%). On the other hand, an outer-rim is perceptible and displays a noticeable decrease in grossular and pyrope contents (Pyr0.26, Grs0.08), related mainly to the retrograde evolution of these rocks towards lower pressure.

The second generation of garnets is observed as small grains (0.05–0.3 mm) associated to staurolite and cordierite. They reveals an elevated X_{Fe} (0.73–0.81) and are characterized by (Alm0.65–0.72, Pyr0.17–0.24, Grs0.07–0.11, Sps0.01–0.02).

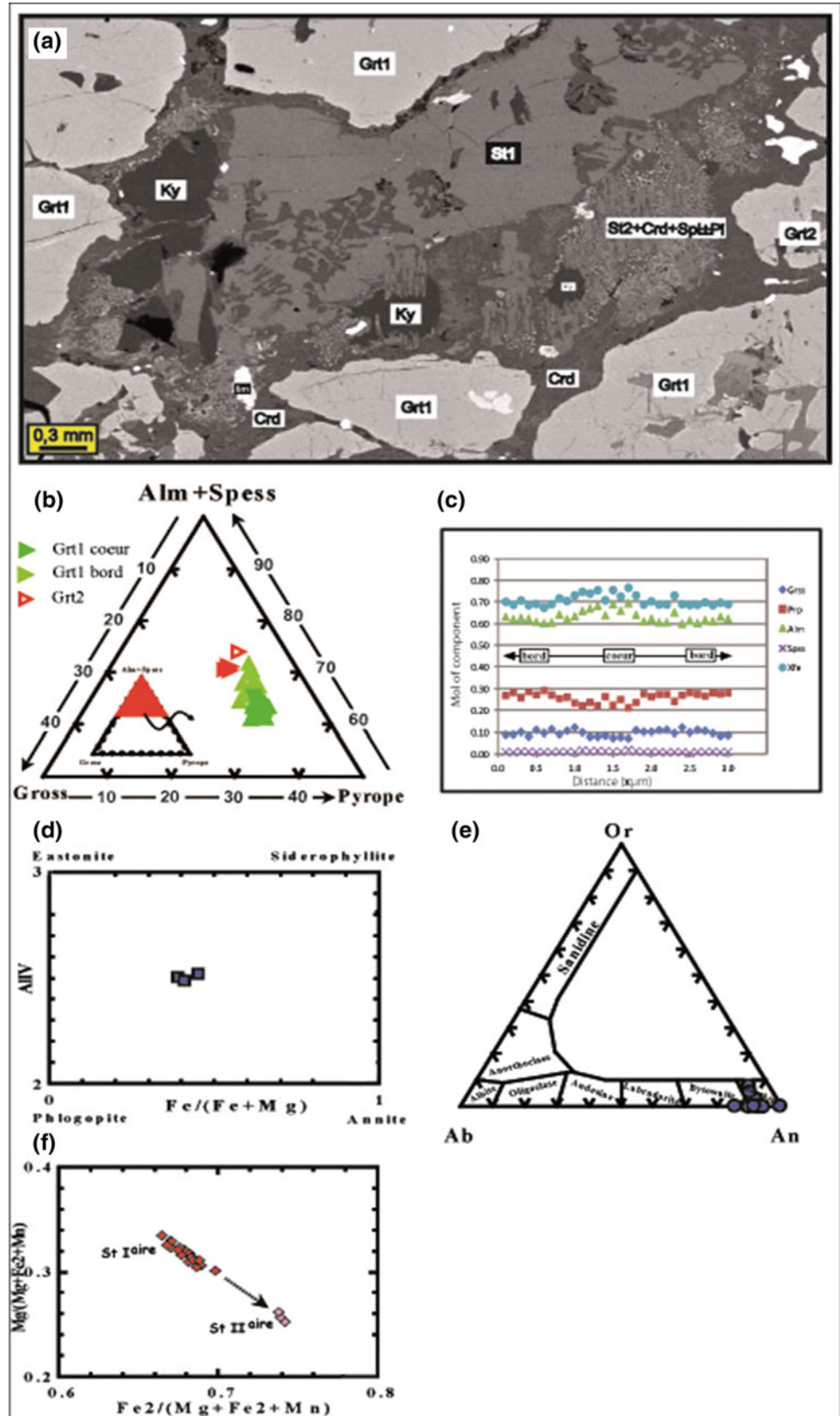
Biotite is considered in the primary state, often in small crystals enclosed within garnet but also elongated flakes scattered among the garnet porphyroblasts and associated to staurolite (Fig. 2). It is characterized with an X_{Mg} ranging from 0.55 to 0.61 and Al^{IV} values varying between 2.49 and 2.52 a.p.f.u.

White micas appear as large flakes that expose relatively high si contents (5.93–6.43 a.p.f.u). The X_{Fe} varies in a wide range [0.38–0.93].

Kyanite features the high-grade paragenesis. It is observed as large elongated crystals, separated from garnets either by a cordierite corona or by spinel-cordierite ± staurolite symplectites microtexture (Fig. 2).

The staurolite belongs to two distinct parageneses. The primary one (St1) is recognized as large crystals (1.2 mm) associated to porphyroblastic garnets-kyanite-biotite. The secondary staurolite (St2) is in the form of small grains integrown with cordierite-spinel (Fig. 2). The St1 is characterized by a high X_{Mg} ratio (0.25–0.33) and displays

Fig. 2 **a** Back-scattered electron (BSE) images showing a various textural relationship. **b** Garnet compositions plotted in the (almandine + spessartine)–grossular–pyrope diagram. **c** Garnet zoning profiles. **d** Projection of biotite composition in Guidotti diagram (1984). **e** Plagioclase compositions plotted in the albite–anorthite–orthoclase diagram. **f** Diagram $[Mg/(Mg + Fe + Mn)]$ versus $[Fe/(Mg + Fe + Mn)]$ shows the staurolite nature



Si values ranging from 7.20 to 7.93 a.p.f.u. whereas, the St2 is featured by an average ratio of X_{Mg} (0.20–0.23) and Si contents of 7.19–7.59 a.p.f.u.

Plagioclase is included in primary garnets (Fig. 2), or associated to the secondary paragenesis of cordierite-spinel. The last one displays an anorthite composition (An85-99) (Fig. 2).

Symplectites of spinel-cordierite-plagioclase developed systematically in contact of kyanite. With advance stage of metamorphism kyanite is completely replaced by these symplectite microtextures (Fig. 2).

2.2 Thermodynamic Modeling

In a bid to explain the petrographic observations and provide further details in regard of the micro-textural paragenesis development in the investigated metapelites, while illustrating their overall pressure-temperature evolution and the extent to which the P–T history has been preserved, the application of thermodynamic modeling stands as a powerful tool [3, 4].

Metapelitic rocks are sensitive recorders of the pressure–temperature variations in high-grade terranes. For this reason, and in order to elucidate and give details of the metamorphic and textural evolution of the Egéré metapelites, pseudo-sections of the representative samples were calculated with respect to the MnO–Na₂O–CaO–K₂O–FeO–MgO–Al₂O₃–SiO₂–H₂O–TiO₂ (MnNCKFMASHT) system. To this end, the thermodynamic software THERMOCALC v3.40 [5] and an updated version of the Holland and Powell [6] data set (file tc-ds62.txt) were used. The activity–composition models used are those set by White et al. [7]. The kyanite-staurolite-bearing metapelites followed a clockwise P–T path, where the presumed retrograde trajectory is well investigated, starting from the peak conditions about 12 kbar and 700 °C along decompression, till reaching the threshold of about 5 kbar and 850 °C.

3 Discussion

The studied metapelites appear to reveal the development of two main parageneses, the primary paragenesis consists of Grt1-ky-St1-Bt-Qz and RT. The secondary paragenesis encloses the Grt2-St2-Crd-Sp-and Ilm. The evolution order

of the different mineral assemblages turns out to be the following:

The appearance of garnet: $Qtz + Bt1 + Ms + Chl + Pl \rightarrow Grt1 + Rt + H_2O \dots (R1)$.

The appearance of kyanite: $Grt1 + Ms \rightarrow Ky + Bt2 + Qtz \dots (R2)$.

The appearance of staurolite 1: $Grt1 + Ky + H_2O + Rt \rightarrow St1 + Qtz + Ilm \dots (R3)$.

The appearance of staurolite 2-spinel-cordierite.

$Grt1 + Ky + St1 + Ru \pm Qz \rightarrow St2 + Crd + Spl + Ilm + Grt2 + Pl \dots (R4)$.

4 Conclusions

The textural observations and mineral compositional constraints jointly combined with the pseudosection construction are considered as a powerful tool whereby our understanding of the metamorphic evolution of the Egéré area could be further improved.

References

- Black, R., Latouche, L., Liégeois, J.P., Caby, R., Bertrand, J.M.: Pan-African displaced terranes in the Tuareg shield (central Sahara). *Geol.* **22**(7), 641–644 (1994)
- Liégeois, J.P., Latouche, L., Boughrara, M., Navez, J., Guiraud, M.: The LATEA metacraton (Central Hoggar, Tuareg shield, Algeria): behaviour of an old passive margin during the Pan-African orogeny. *J Afr. Earth. Sci.* **37**(3), 161–190 (2003)
- Powell, R., Holland, T.J.B., Worley, B.: Calculating phase diagrams involving solid solutions via non-linear equations, with examples using THERMOCALC. *J. Metamorph. Geol.* **16**, 577–588 (1998)
- White, R.W., Powell, R.: On the interpretation of retrograde reaction textures in granulite facies rocks. *J. Metamorph. Geol.* **29**, 131–149 (2011)
- Powell, R., Holland, T.J.B.: An internally consistent dataset with uncertainties and correlations: 3. Applications to geobarometry, worked examples and a computer program. *J. Metamorph. Geol.* **6** (2), 173–204 (1988)
- Holland, T.I.M., Powell, R. Calculation of phase relations involving haplogranitic melts using an internally consistent Thermodynamic dataset. *J. Petrol.* **42**(4), 673–683 (2001)
- White, R.W., Powell, R., Holland, T.J.B., Johnson, T.E., Green, E. C.R.: New mineral activity–composition relations for thermodynamic calculations in metapelitic systems. *J. Metamorph. Geol.* **31**, 261–286 (2014)

Petrographic, Mineralogical and Geothermometric Study of Garnet Hornfels from the Region of Iddeleh Silet Hoggar Occidental Algeria

Khedoudja Nedjraoui, Abla Azzouni-Sekkal, Rekia Kheloui, Mohamed Hamoudi, and Riad Ben El Khazndji

Abstract

The emplacement of Neoproterozoic mafic-ultramafic complexes in the Iddeleh area, Silet Block (Western Hoggar) was associated with garnet hornfels facies contact metamorphism of the Pharusian I metapelites. EPMA data of garnet reveal formation temperatures as high as 900 °C. A later metamorphic event is manifested in the persistence of chlorite schist, in which the chlorite composition (Al^{iv} contents) indicates a temperature range of 300–400 °C. It is, therefore, suggested that juxtaposition of the Silet terrane and the microcontinent LATEA was not the outcome of a collisional regime.

Keywords

Iddeleh • Iskel • Pharusien I • Garnet hornfels • EPMA

1 Introduction

The Touareg shield is part of the Pan-African range and was formed by the amalgamation of twenty terranes [1], of which some are juvenile and others are Archaean or Paleoproterozoic in age.

In this contribution, we study the juvenile terrane of Silet, which is considered to be an insular arc accrued to the microcontinent of LATEA [2] (Laouni, Azrou N'Fad, Tefedest, Egere-Aleksod and Assodé-Issalane, acronym of LATEA).

K. Nedjraoui (✉) · M. Hamoudi
Laboratoire de Géophysique, FSTGAT – USTHB, Babezzouar,
Algiers, Algeria
e-mail: nedjraoui.khedoudja@gmail.com

A. Azzouni-Sekkal · R. B. E. Khazndji
Laboratoire de métallogénie et du magmatisme,
FSTGAT – USTHB, Babezzouar, Algiers, Algeria

R. Kheloui
Ecole Normale Supérieure, Vieux-Kouba, Algiers, Algeria

The purpose of this paper is to unearth the metamorphic history of this terrane, particularly within the context of the aureoles contact with mafic-ultramafic complexes in Iddeleh.

2 Materials and Methods

Polished thin sections were petrographically studied and used for mineral-chemistry analysis ends.

The analysis was carried out using an SX 50 electron microprobe (CAMPARIS), available at the University of Jussieu (Paris VI).

3 Results

3.1 Petrographical Results

Two sub-facies have been identified in the metapelites from the Iddeleh's metamorphic aureole, namely:

1. Almandin + Quartz + Feldspar + Muscovite- Phengite + Chlorite which, corresponding to the first sub-facies as shown in Fig. 1.
2. Biotite + Quartz + Feldspar + Muscovite + Chlorite, which correspond to the second subfacies, as shown in Fig. 2.

3.2 Mineral Chemistry Results

The EPMA data of garnet metapelites prove to reveal that the variation perceived in the index minerals' chemical composition helps provide more insights into the metamorphic grade, allowing the discrimination between regional and contact metamorphic events. In what follows, the mineral chemistry associated results, related to the minerals characterizing each subfacies or metamorphism, are displayed.

Fig. 1 Heterogranular granoblastic oriented texture of garnet metapelites, (right PLA, left PL Gr $\times 10$) (gt: garnet, qz: quartz, op: opaque mineral, pl: plagioclase)

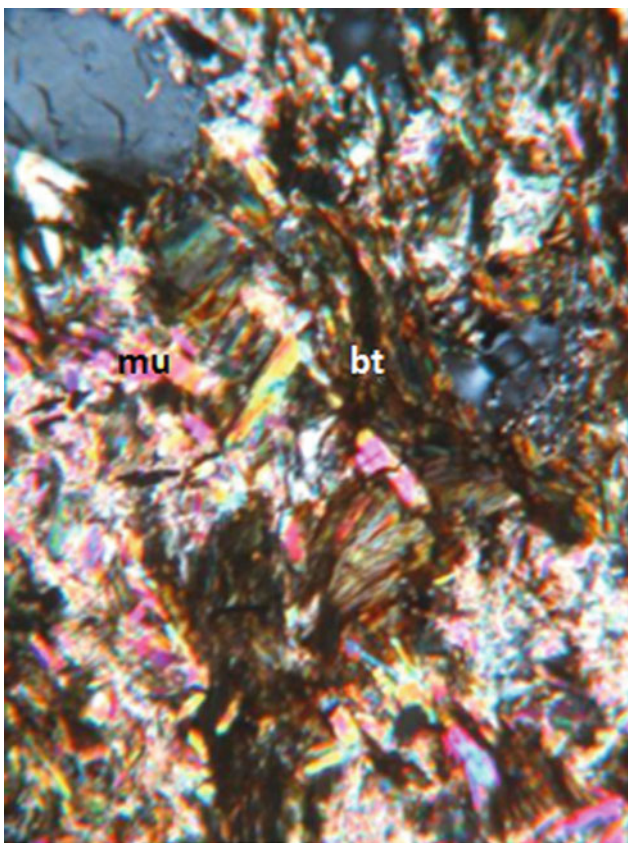
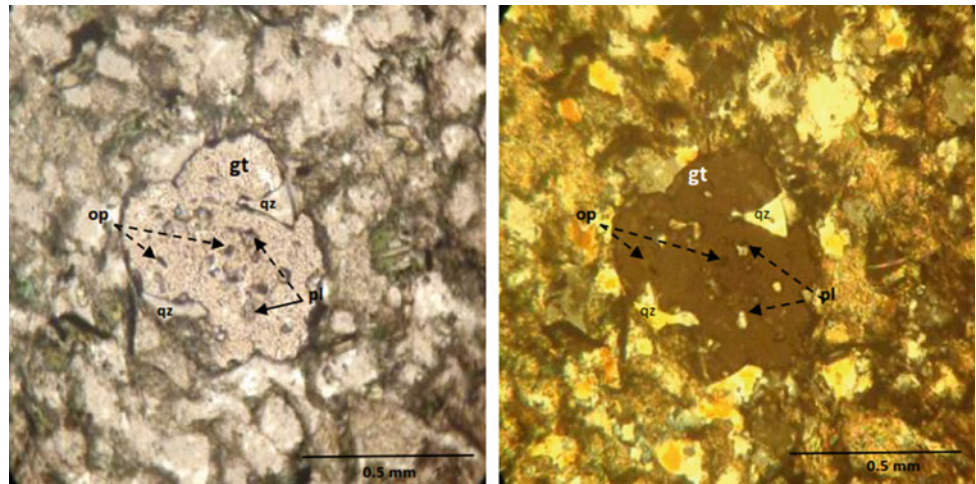


Fig. 2 Slightly oriented granoblastic grained texture of biotite metapelites, sample ID40' (In PLA, Gr 10×30) (bt: biotite, mu: muscovite) [3]

3.2.1 Regional Metamorphism

Most of the metapelite chlorites persistent in the Iddeleh's aureole turn out to be of the ripidolites type, according to Hey's classification (1954). In general, ripidolites occur in

metapelitic rocks of low metamorphic grade restricted to greenschist facies.

- Plagioclase

The analyses show well that these plagioclases appear to have an oligoclase composition with anorthite contents comprised between (An_{20} – An_{30}).

According to Smith [4], oligoclase can constitute the isograd limiting the two facies' amphibolite and greenschist, which is the case in the present study.

3.2.2 Contact Metamorphism

It is highlighted through the study of garnet and white micas

- White Mica

The triangular Ti–Mg–Na diagram [5] of the Iddeleh aureole muscovites is distributed among the fields of primary muscovites and secondary muscovites. The low TiO_2 levels of some muscovites help reflect their late characters, as they might well be derived from a hydrothermal activity caused by the circulation of fluids due to conductive heat transfer, which started immediately when the intrusion was put in place. Such a phenomenon provides an explanation as to the destruction of ferromagnesian minerals (as judged by the absence of biotite in the garnet zone). The alteration results in a significant loss of Fe, Mn, Mg and Ti along with a significant increase in Al.

- Garnet

The garnets of the Iddeleh metamorphic aureole are rich in Fe and Mn, as represented by: the pole Almandin + Spessartine with $X_{alm} = (50-70\%)$ and $X_{sps} = (15-24\%)$.

3.3 Results of Geothermometry

The geothermometric study is implemented to highlight the temperature conditions responsible for the minerals' genesis.

1. Geothermometry of garnets

The geothermometry of garnets allowed us to highlight the contact associated metamorphism. To calculate the temperature range leading to the formation of garnet, we used the muscovite garnet geothermometer, as defined by Wu and Zhao [6], based on the empirical calibration, and using the metapelites that were metamorphosed to physical conditions of 238–1306 MPa and 490–700 °C, whose formula looks as follows:

$$T(K)\{1 + 0.1663 \ln[(\text{Fe}/\text{Mg})^{\text{grt}}/(\text{Fe}/\text{Mg})^{\text{mus}} + 0.1255X_{\text{gros}}(1 - X_{\text{sps}})]\} = 1080.68 - 0.012P(\text{MPa}) - 228.1(X_{\text{Fe}}^{\text{mus}} - X_{\text{Mg}}^{\text{mus}}) - 41.6X_{\text{pyr}}^2 + 127X_{\text{alm}}^2 + 276.14X_{\text{gros}}(1 - X_{\text{sps}}) - 170.8X_{\text{alm}}X_{\text{pyr}}(1 - X_{\text{sps}}) - 84.3X_{\text{gros}}(X_{\text{pyr}} - X_{\text{alm}}).$$

The temperatures obtained appear to vary between 637 and 916 °C.

2. Geothermometry of chlorites

The chlorites' relating geothermometry has been used to confirm the regional metamorphism. The temperature estimation results, reached by means of the Al IV diagram, as a function of temperature correlated with the empirical geothermometer of Hillier and Velde [7], prove to yield three types of chlorites: metamorphic chlorites, with temperatures ranging between 300 and 480 °C, diagenetic chlorites with low temperatures less than 80 °C, and hydrothermal chlorites' with temperature ranges comprised between 150 and 250 °C.

4 Conclusions

The petrographic, mineral chemistry and geothermometric data concerning the contact metamorphic aureole enabled to highlight two types of metamorphisms, a contact metamorphism, and a regional metamorphism posterior to the first one. The geothermometric associated results appear to indicate that contact metamorphism has been able to induce temperatures as high as 900 °C. This contact metamorphism has been followed by a regional metamorphism, in which the temperature ranges do not exceed the rate of 480 °C. This finding suggests well that the union between the Silet terrane and the microcontinent of LATEA was relatively soft and was not the result of frontal collision.

References

1. Black, R., Latouche, L., Liégeois, J.P., Caby, R., et al.: Pan-African displaced terranes in the Tuareg shield (central Sahara). *Geology* **22**(7), 641–644 (1994)
2. Liégeois, J.P., Latouche, L., Boughrara, M., et al.: The LATEA métacraton (central Hoggar, Tuaregsheild, Algeria): behaviour of an old passive margin during the Pan-African orogeny. *J. Afr. Earth Sci.* **37**(3–4), 161–190 (2003)
3. Kheloui, R.: Étude pétrographique, mineralogique, et géochimique du massif mafique a ultramafique d'Iddeleh (silet, bloc d'Iskel, Hoggar, Algérie). Magisterial Thesis. USTHB, ALGERIA (2008)
4. Smith, J.V.: Feldspar minerals. Crystal structure and physical properties, vol. 1. Springer, Berlin, Heidelberg, New York (1974)
5. Miller, C.F., Stoddard, E.F., Bradfish, L.J., et al.: Composition of plutonic muscovite: genetic implications. *Can. Mineral.* **19**(1), 25–34 (1981)
6. Wu C., Zhao., Y.: Precise revision of the garnet-muscovite geothermometer. *Springer*, **45**(3), 270–279 (2002)
7. Hillier, S., Velde, B.: Octahedral occupancy and the chemical composition of diagenetic (low-temperature) chlorites. *Clay Miner. Soc.* **26**(2), 149–168 (1991)

Physical Characteristics of the Massive Meteorite of Saudi Empty Quarter

V. Masilamani, Nasser Alarif, W. Aslam Farooq, Muhammad Atif, Shahid Ramay, Hayat Saeed Althobaiti, Saqib Anwar, Ibrahim Elkhedr, M. S. AlSalhi, and Bassam A. Abuamarah

Abstract

The meteorite found in the Empty Quarter of the KSA is the largest meteorite and has the shape of an irregular ellipsoid of semi axes ($0.65 \times 0.38 \times 0.27$) and density of 6400 kg/m^3 and mass of 2550 kg. It is a massive piece belonging to the category of iron–nickel meteorites with an occurrence (or fall) of only 5% of total showers. The present report was on the physical characteristics (elemental composition and structural) of this piece using laser break down spectroscopy (LIBS), X-ray fluorescence (XRF) and Energy dispersive X-ray spectrophotometer (EDX), Scanning Electron microscope (SEM) Xray diffraction (XRD) etc. Our investigation indicated that this piece consists of 91% iron, 5% Ni, 1.51% P, 0.3% Co, and a host of others; most of them exist as oxides. Since the measured density is only 6400 kg/m^3 the meteorite is porous (approximately about 19%) which is confirmed by the micro hardness. Based on these physical measurements, it is very likely that this meteorite would have “escaped” from the belt around Mars and Jupiter and unlikely from the moon or elsewhere. This could be the first investigation, employing the above sophisticated instruments, on that massive Saudi meteorite.

Keywords

Physical characteristics • Massive meteorite • Saudi empty quarter • Modern analytical methods

1 Introduction

The last two decades have seen a very powerful research activity for the development, advancement and achievement of laser-induced break-down spectroscopy (LIBS) as a practicable and effective analytical tool that can be used for the study of air, water, and solid materials [1–4] plus geo-materials [5–7].

In the current study, the physical characteristics of meteorite samples were studied using laser break down spectroscopy (LIBS), X-ray fluorescence (XRF) and Energy dispersive X-ray spectrophotometer (EDX), Scanning Electron microscope (SEM) and Xray diffraction (XRD) etc.

2 Materials and Methods

The following instruments were used LIBS (Applied Spectra, USA), XRF (S8 Tiger, Bruker), EDX, SEM (JSM-6380 LA, JEOL) to study the meteorite samples (Fig. 1).

3 Results and Discussion

3.1 LIBS Analysis

We have recorded the meteorite sample LIBS spectra at different points and with altered laser energy, delay time and gate width in air atmosphere. The experimental results show highest abundance in the sample with Ni and P etc. in different proportions as shown in Fig. 2. In order to estimate the different elements concentrations, the revealed elements

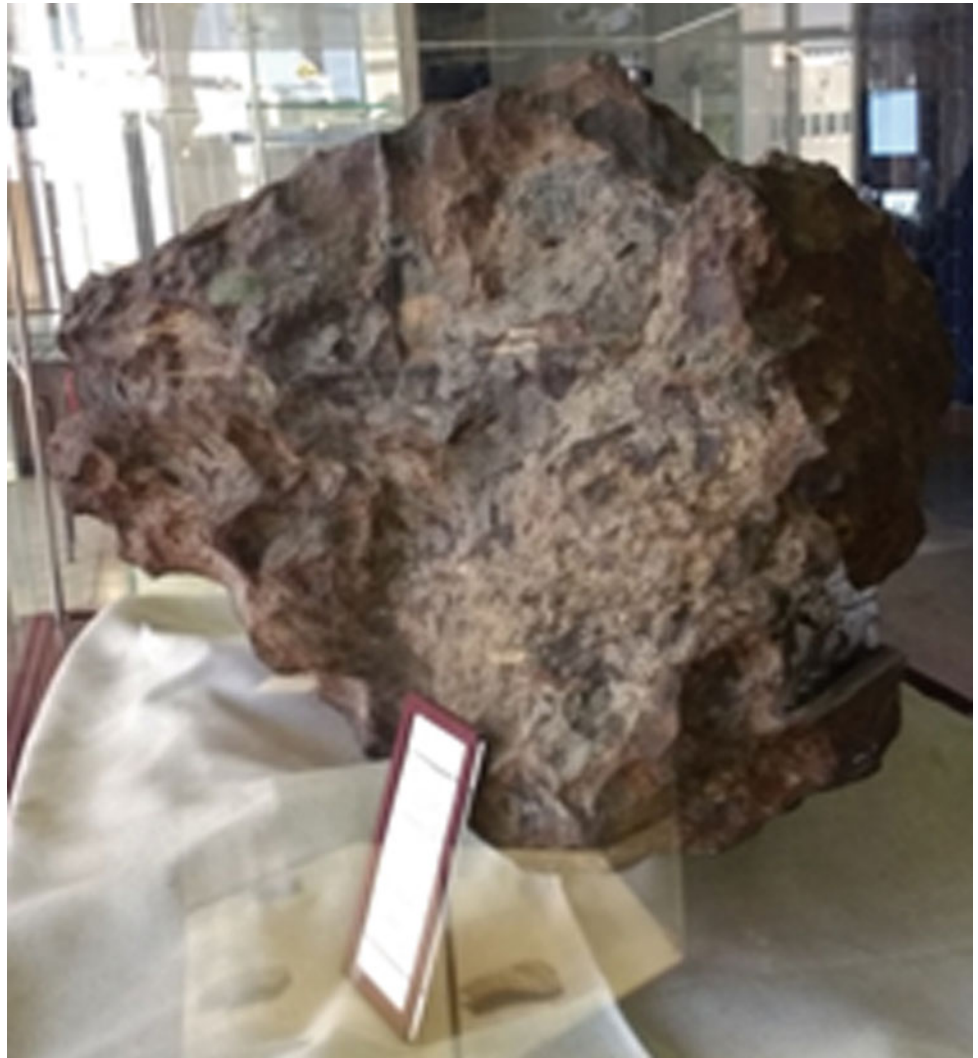
V. Masilamani · W. A. Farooq · M. Atif (✉) · S. Ramay
H. S. Althobaiti · M. S. AlSalhi
Physics and Astronomy Department, College of Science,
King Saud University, Riyadh, Saudi Arabia
e-mail: atifhull@gmail.com

V. Masilamani · M. Atif · M. S. AlSalhi
Research Chair for Laser Diagnosis of Cancer, King Saud
University, Riyadh, Saudi Arabia

N. Alarif · I. Elkhedr · B. A. Abuamarah
Department of Geology and Geophysics, College of Science,
King Saud University, Riyadh, Saudi Arabia

S. Anwar
Industrial Engineering Department, College of Engineering,
King Saud University, P.O. Box 800 Riyadh, 11421, Saudi Arabia

Fig. 1 A photograph of the massive meteorite



were compared to those found in the LIBS from calibration curves drawn for the corresponding elements [8].

3.2 X Ray Fluorescence Analysis

Figure 3 presents the characteristic X-ray lines of dissimilar elements present in the sample. Note that the sharp lines of different elements arise to different levels of excitation like Fe (91%) to Gallium (Ga).

4 Conclusion

This paper presents some of the preliminary results from the biggest meteorite of the KSA. It is found that the meteorite samples consist of Fe, Ni, P and Co.

Comparing the XRF with the LIBS technique revealed good qualitative analysis in shorter time without any special preparations of the sample.

Fig. 2 Laser (266 nm YAG laser) induced breakdown spectra of the sample

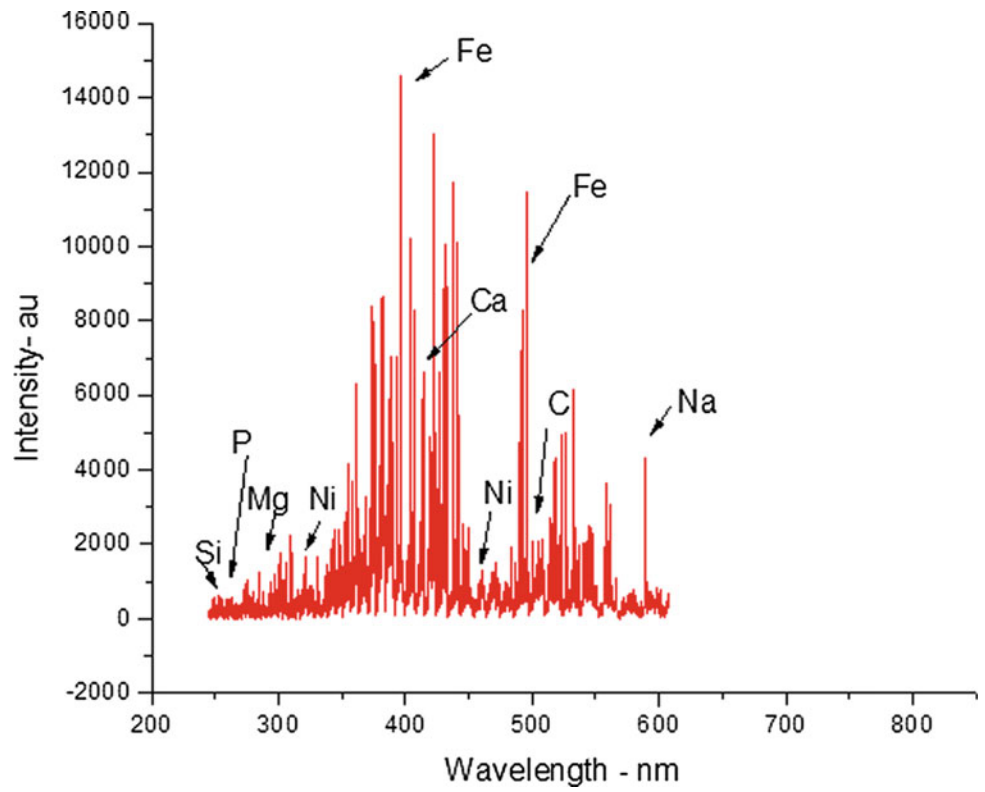
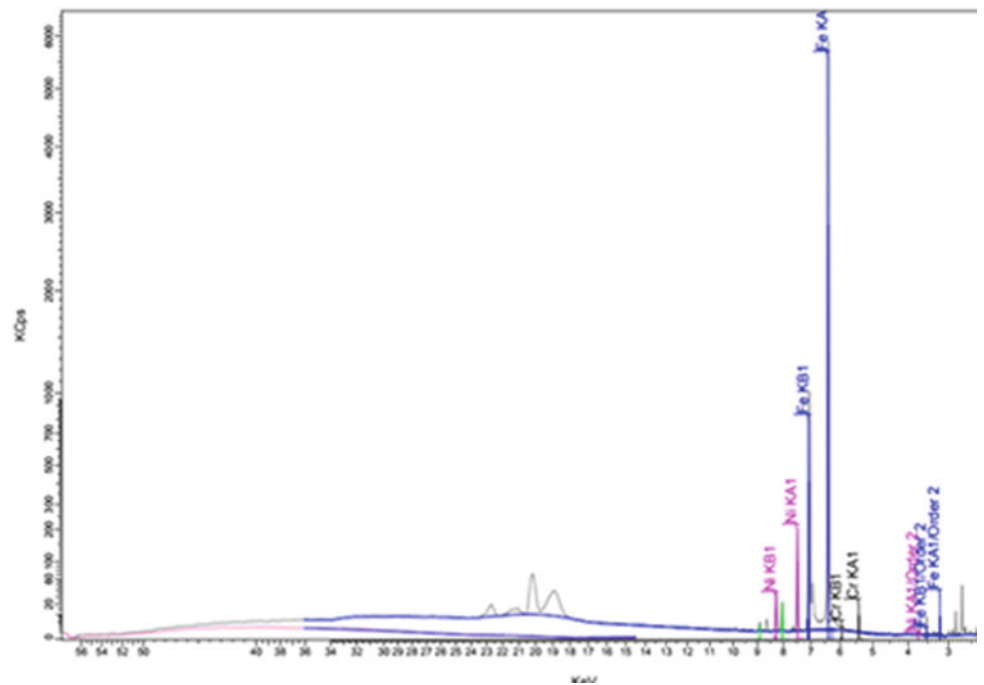


Fig. 3 XRF spectra of the above sample for elemental composition



Acknowledgements The authors are grateful to the Deanship of Scientific Research, King Saud University for funding through Vice Deanship of Scientific Research Chairs.

References

1. Corrigan, C.M., Chabot, N.L., McCoy, T.J., McDonough, W.F., Watson, H.C., Saslow, S.A., Ash, R.D.: The iron–nickel–phosphorus system: effects on the distribution of trace elements during the evolution of iron meteorites. *Geochim. Cosmochim. Acta* **73**, 2674–2691 (2009)
2. Hahn, D.W., Omenetto, N.: Laser-induced breakdown spectroscopy (LIBS), part II: review of instrumental and methodological approaches to material analysis and applications to different fields. *Appl. Spectrosc.* **66**, 347–419 (2012)
3. Cremers, D.E., Radziemski, L.J.: *Handbook of Laser-Induced Breakdown Spectroscopy*, pp. 99–168. John Wiley & Sons, New York, USA (2006)
4. Clegg, S.M., Sklute, E., Dyar, M.D., Barefield, J.E., Wiens, R.C.: Multivariate analysis of remote laser-induced breakdown spectroscopy spectra using partial least squares, principal component analysis, and related techniques. *Spectrochim. Acta B* **64**, 79–88 (2009)
5. Harmon, R.S., Russo, R.E., Hark, R.R.: Applications of laser-induced breakdown spectroscopy for geochemical and environmental analysis: a comprehensive review. *Spectrochim. Acta, Part B* **87**, 11–26 (2013)
6. Senesi, G.S.: Laser-induced breakdown spectroscopy (LIBS) applied to terrestrial and extraterrestrial analogue geomaterials with emphasis to minerals and rocks. *Earth Sci. Rev.* **139**, 231–267 (2014)
7. Tempesta, G., Agrosi, G.: Standardless, minimally destructive chemical analysis of red beryls by means of laser induced breakdown spectroscopy. *Eur. J. Miner.* **28**(3), 571–580 (2016). <https://doi.org/10.1127/ejm/2016/0028-252>
8. Senesi, G.S., Tempesta, G., Manzari, P., Agrosi, G.: An innovative approach to meteorite analysis by laser-induced breakdown spectroscopy. *Geostand. Geoanal. Res.* **40**(4), 533–541 (2016)



Study of the Compositional, Mechanical and Magnetic Properties of Saudi Meteorite

Muhammad Atif, Saqib Anwar, W. A. Farooq, M. Ali, V. Masilaimani, M. S. AlSalhi, and Bassam A. Abuamarah

Abstract

In the current study, the experimental results of the investigation on the compositional, mechanical and magnetic properties of Saudi meteorite were presented. Meteorite specimen was examined using techniques like scanning electron microscopy, EDAX, Backscattered electron imaging, XRD, hardness testing (Rockwell, Vicker, Brinell) and magnetic properties measurements. The composition analysis results of the meteorite reveal that it is essentially composed of an iron-Ni alloy with iron playing a dominant role. The hardness testing shows that the meteorite is formed of soft material with a Rockwell hardness of 22.5 HRC. Furthermore the magnetic measurement also supports the fact that the meteorite specimen is a soft ferromagnetic material. The saturation magnetization (M_s) of 0.701 emu/g was found for the saturation field of (H_s) = 5025 Oe. No trace of radioactivity is revealed when using a sensitive GM counter.

Keywords

EDAX • Backscattered electron imaging • XRD • Hardness testing (Rockwell, Vicker, Brinell) • Magnetic properties measurements

1 Introduction

The ancient specimens of meteorite are called remnants that were formed some 4.6 billion years ago in the solar system due to geologic processes. Most Meteorites come from the outer space to the Earth and provide information on the solar system relevant to the creation, growth and structure of the Earth. A lot of information about their celestial history can be unveiled from iron-bearing minerals which are classified as an important component of meteorites. These mainly consist of iron-nickel alloys commonly known as iron meteorites [1–5] which represent 5% of the total discovered meteorites. In this study the compositional, mechanical and magnetic properties of Saudi meteorite were investigated.

2 Materials and Methods

Field emission scanning electron microscope (SEM) JSM-7600F Jeol Japan was used to carry out the microscopic studies. The SEM equipped with energy dispersive X-ray (EDX) system for morphological and elemental compositional analysis. In order to characterize the specimen for its mechanical properties, its hardness was measured by the Zwick/Roel ZHU hardness tester capable of performing various types of hardness tests. The EZ7 Vibrating Sample Magnetometer (VSM) was used to measure the magnetic properties of the meteorite.

M. Atif (✉) · W. A. Farooq · V. Masilaimani · M. S. AlSalhi
Physics and Astronomy Department, College of Science,
King Saud University, Riyadh, Saudi Arabia
e-mail: atifhull@gmail.com

M. Atif · V. Masilaimani · M. S. AlSalhi
Research Chair for Laser Diagnosis of Cancer, King Saud
University, Riyadh, Saudi Arabia

S. Anwar
Industrial Engineering Department, College of Engineering,
King Saud University, P.O. Box 800 Riyadh, 11421, Saudi Arabia

M. Ali
King Abdullah Institute of Nanotechnology (Kain), King Saud
University, Riyadh, Saudi Arabia

B. A. Abuamarah
Department of Geology and Geophysics, College of Science,
King Saud University, Riyadh, Saudi Arabia

3 Results and Discussion

A scanning electron microscope (SEM) JSM-7600F Jeol Japan was used as one of the tools to characterize the Saudi meteoroid specimen. The specimen was scanned in its initial form—i.e., as it reached the Earth—and also after being ground with silicon carbide papers of a grit size of 180, 300 and 600. The energy dispersive X-ray spectrum results of the ground region show that only iron and nickel are the major constituting elements of the Saudi meteoroid specimen as shown in Fig. 1.

The specimen was cut into small pieces and kept embedded firmly into a bakelite base in order to measure the surface hardness by three types of standard instruments

(Rockwell, Vicker and Brunell). Table 1 summarizes the hardness test values from different tests.

With the major composition of the Fe, Ni and CO, the piece has shown good magnetic properties with a magnetic field strength of 3 gauss as measured by a Hall probe.

It was subjected to a magnetization and demagnetization cycle with a Lab VSM E27 to obtain a hysteresis loop as shown in Fig. 2 which gives a coercive field value of 152 oersted and the saturation magnetization (M_s) of 45.4 emu/g, remnant magnetization 154 emu/g and coercivity (H_c) is 9.66, all as determined from the hysteresis loop. All these values are indicative of ferromagnetic soft iron. The magnetic properties of stony achondrites are identical with FeNi alloys, usually by low Ni kamacite [6, 7].

Fig. 1 Shows the energy dispersive X-ray spectrum results of the ground region

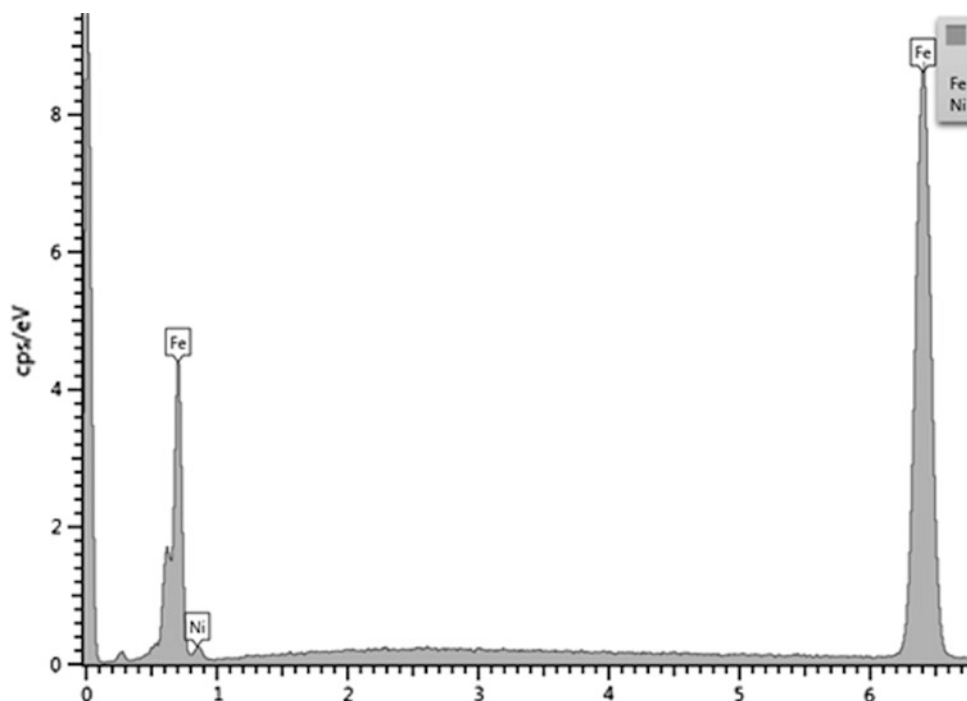
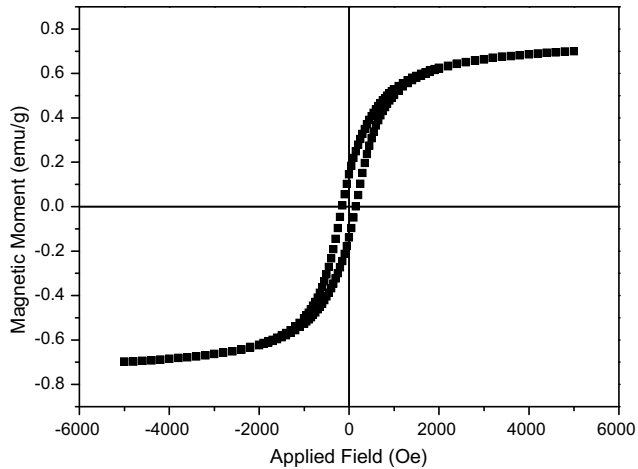


Table 1 Hardness tests results

Test#	Test type	Load used (KG)	Hardness value
1	Rockwell hardness (HRA)	60	60.5
2	Rockwell hardness (HRC)	150	22.5
3	Vicker hardness (HV)	30	181.7
4	Brinell hardness (HB)	62.5	184.15

**Fig. 2** Hysteresis loops; applied-field dependences of magnetization recorded at room temperature

4 Conclusion

This paper gave new insights of the biggest meteorite of the Kingdom of Saudi Arabia. The meteorite composition analysis disclosed that it is iron nickel alloy and iron-Ni alloy with iron playing a dominant role. The experimental results of hardness show that it is a soft material.

Furthermore the magnetic properties of the meteorite specimen confirmed that it was a soft ferromagnetic material.

Acknowledgements The authors are grateful to the Deanship of Scientific Research, King Saud University for funding through Vice Deanship of Scientific Research Chairs.

References

1. Corrigan, C.M., Chabot, N.L., McCoy, T.J., McDonough, W.F., Watson, H.C., Saslow, S.A., Ash, R.D.: The iron–nickel–phosphorus system: effects on the distribution of trace elements during the evolution of iron meteorites. *Geochim. Cosmochim. Acta* **73**, 2674–2691 (2009)
2. Garcia-Guinea, J., Tormo, L., Ordoñez, A.R., Garcia-Moreno, O.: Non-destructive analyses on a meteorite fragment that fell in the Madrid city centre in 1896. *Talanta* **114**, 152–159 (2013)
3. Goldstein, J.I., Scott, E.R.D., Chabot, N.L.: Iron meteorites: crystallization, thermal history, parent bodies, and origin. *Chem. Erde* **69**, 293–325 (2009)
4. Hafner, S., Kalvius, M.: The Mössbauer resonance of Fe⁵⁷ in troilite (FeS) and pyrrhotite (Fe_{0.88}S). *Z. Kristal.* **123**, 443–458 (1966)
5. Kruse, O., Ericsson, T.: A Mössbauer investigation of natural troilite from the Agpalilik meteorite. *Phys. Chem. Miner.* **15**, 509–513 (1988)
6. Nagata, T.: Meteorite magnetism and the early solar system magnetic fields. *Phys. Earth Planet. Inter.* **20**, 324–341 (1979)
7. Sugiura, N., Strangway, D.W.: Magnetic studies of meteorites. In: Kerridge, J.F., Matthews, M.S. (eds.) *Meteorites and the Early solar system*, pp. 595–615. University of Arizona Press, Tucson, USA, 1269 pp (1988)

Part III

**Surficial Processes: Sedimentation
and Facies Analysis**

Microfacies Analysis and Geochemical Evaluation of Campanian-Maastrichtian Limestone Along the Benin Flank, Southwestern Nigeria

Oladotun Oluwajana, Olugbenga Ehinola, Collins Ofiwe, Evidence Akhayere, Kehinde Egunjobi, Joseph Asanbe, and Oluwafemi Akinjo

Abstract

Outcrops of the Campanian-Maastrichtian limestone unit exposed along the Benin Flank in southwestern Nigeria, were sampled and analyzed in order to characterize the carbonate microfacies, determine chemical composition, mineralogy and depositional environment of the limestone unit. The investigation was undertaken by means of thin-section petrography, Scanning Electron Microscopy with Energy Dispersive Spectroscopy (SEM/EDS), Energy Dispersive X-ray Fluorescence (ED-XRF) analysis and X-ray diffraction analysis. Three (3) carbonate microfacies were characterized, namely; wackestone, bioclastic wackestone-packstone and arenaceous proto-dolomite. The microfacies association characterizes sedimentation within shallow carbonate (lagoonal) marine setting. The results of major oxide geochemistry showed that the analyzed limestone samples are calcitic. The study findings highlighted the deposition of calcite limestone and arenaceous proto-dolomite of Campanian-Maastrichtian age along the Benin Flank within a shallow carbonate (lagoonal) marine environment.

Keywords

Campanian-Maastrichtian • Limestone • Microfacies • Benin flank

O. Oluwajana (✉) · K. Egunjobi · J. Asanbe · O. Akinjo
Department of Earth Sciences, Adekunle Ajasin University,
Akungba-Akoko, Nigeria
e-mail: oladotun.oluwajana@aau.edu.ng

O. Ehinola
Energy and Environmental Research Group (EERG),
Department of Geology, University of Ibadan, Ibadan, Nigeria

C. Ofiwe
National Agency for Science and Engineering Infrastructure
(NASENI), Akure, Nigeria

E. Akhayere
Environmental Research Centre, Cyprus International University,
Nicosia, Cyprus

1 Introduction

The Campanian-Maastrichtian limestone units exposed along Benin Flank of southwestern Nigeria play a crucial role in the economic and industrial growth of Nigeria. Yet, little attention has been paid to detailed chemical composition, microfacies, mineralogy and depositional setting of the carbonate rocks because outcrops of Late Cretaceous limestone of significant thickness are poorly exposed along the Benin Flank.

The limestone sections are exposed along Omi-Alayo (in Okeluse), Forest Reserves (in Okeluse), River Eleja (in Ayadi) and Ore-Ode Irele road (Fig. 1), southwestern part of Nigeria. This present study attempts an integrated study incorporating field studies and advanced analytical programs aimed at characterizing the microfacies, determine chemical composition, mineralogy and depositional framework of the Late Cretaceous limestone beds exposed along the Flank.

2 Geology of the Study Area

The deposition and sedimentation processes characterizing the Benin Flank of the eastern Dahomey Basin started in the Lower Cretaceous (Hauterivian-Barremian), when a succession of non-fossiliferous well-rounded quartz pebbly conglomerate and sands of Ise Formation were deposited across the Pre-Cambrian Basement Complex.

Overlying the basal conglomerate are the Campanian-Maastrichtian Afowo Formation and Araromi Formation. The Afowo Formation is typically composed of massive medium-to-coarse grained sandstone. The Araromi Formation consists of highly fossiliferous shale and limestone [1]. The Paleogene-Neogene sediments characterizing the Benin Flank comprise the Ewekoro, Akinbo, Oshosun, Ilaro and Benin Formations.

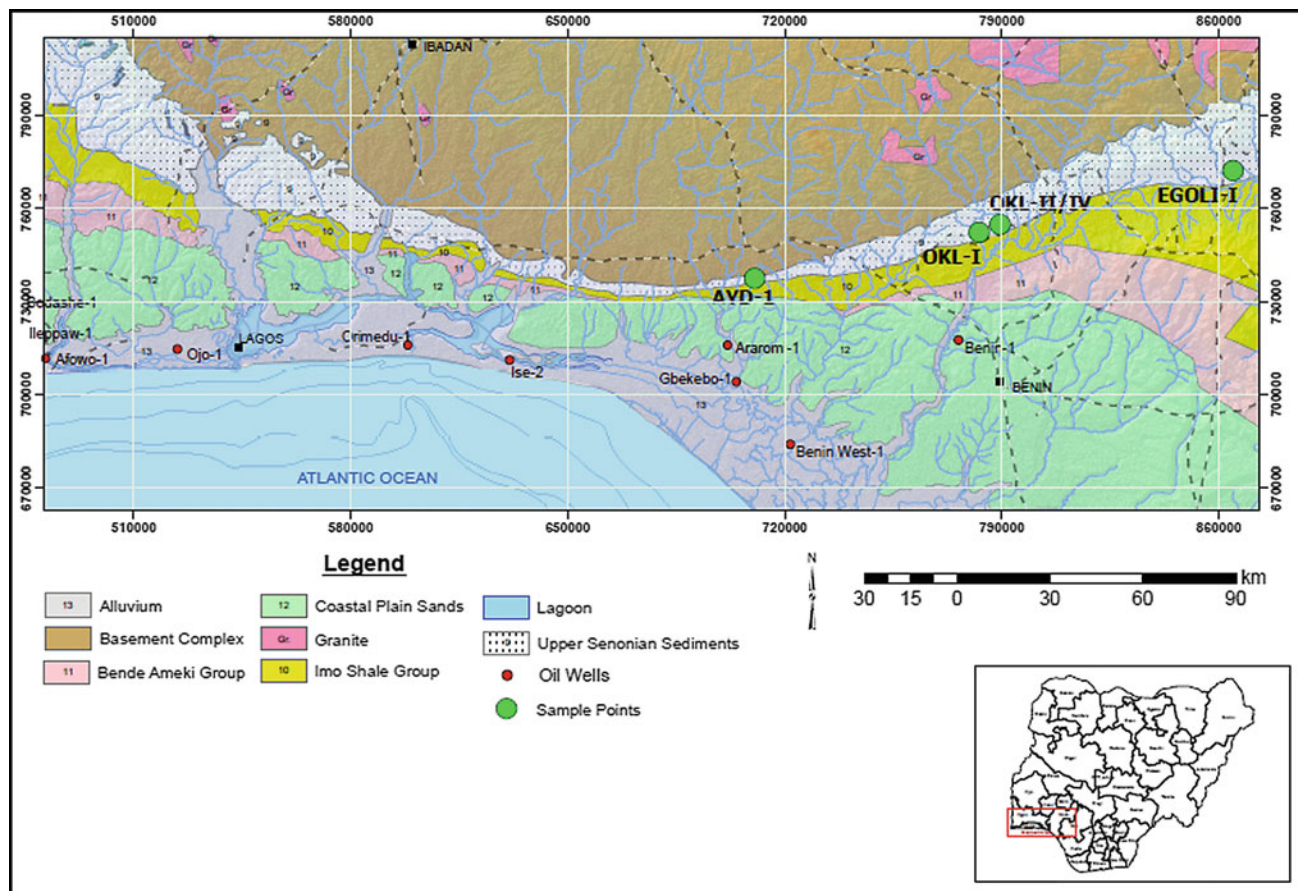


Fig. 1 The study area (in green colored circles) in simplified regional geographical/geological map, showing Cretaceous to Quaternary sediments of the Nigerian sector of the Dahomey Basin (Benin Basin)

3 Materials and Methods

Field mapping was carried out along the Benin Flank of the Dahomey (Benin) Basin. The limestone outcrops were examined to identify the relevant megascopic attributes, mainly the color, macrofossils and macro-textural features. Samples were recovered from eight (8) outcrop sections. The laboratory analysis involves thin-section petrographic analysis, X-ray Diffraction (XRD) analysis, Energy Dispersive X-ray Fluorescence (ED-XRF) analysis and Scanning Electron Microscopy with Energy Dispersive Spectroscopy (SEM/EDS).

4 Results

4.1 Microfacies

The observed limestone sections around Ayadi (River Eleja and along Ore-Ode Irele road) are grey and

fossiliferous. Petrographically, this microfacies is named bioclastic wackestone-packstone. Thin section petrographic analysis of limestone samples recovered from outcrop sections at Okeluse (Omi-Alayo and Forest Reserves) indicated that the limestone samples are mud-supported. Microfacies of this type is regarded as wackestone [2]. Arenaceous proto-dolomite was observed within the wackestone at Okeluse (Omi-Alayo). The dolomite is fine-grained and fractured. Quartz grains lined the observed fractures.

4.2 Chemical Composition

The results of geochemical (major oxides) analyses of the limestone samples showed that the SiO_2 and CaO concentrations range between 0.37–15.13 wt.% and 39.84–50.92 wt.% respectively (Table 1). The mean values associated with the Al_2O_3 and Fe_2O_3 contents (1.29 and 2.60 wt.%, respectively) are generally low.

Table 1 Table showing major oxides of selected limestone samples

Sample_ID	Microfacies texture	wt%							
		CaO	SiO ₂	Al ₂ O ₃	MgO	K ₂ O	Na ₂ O	SO ₃	Fe ₂ O ₃
OKL_1a	Wackestone	50.92	1.52	0.87	0.56	0.04	0.06	1.48	1.79
OKL_2	Wackestone	49.47	2.48	1.24	1.04	0.03	0.03	0.13	1.52
OKL_3	Wackestone	48.77	1.55	0.90	1.73	0.03	0.00	0.49	2.26
OKL_4	Wackestone	49.51	0.37	0.48	0.26	0.02	0.04	0.12	1.20
OKL_5	Wackestone	45.78	4.42	1.65	0.70	0.05	0.63	0.17	5.16
ODR_6	Bioclastic wackestone-packstone	39.84	15.13	2.57	0.22	0.09	0.31	0.25	3.67
Mean values		47.38	4.25	1.29	0.75	0.04	0.18	0.44	2.60

4.3 Mineralogy

The results of X-ray diffraction (XRD) analysis revealed that the selected limestone samples with wackestone and wackestone-packstone fabrics are composed of mainly calcite, while XRD result of arenaceous proto-dolomite sample indicate dolomite as the predominant mineral. SEM images of limestone samples with wackestone and wackestone-packstone showed mottled shapes, while SEM image of arenaceous proto-dolomite revealed tightly bounded structures of dolomite grains.

5 Discussion

The three (3) observed microfacies are identified on the basis of field and laboratory studies, namely: Wackestone, bioclastic wackestone-packstone and arenaceous protodolomite.

The ratio of matrix to grain of the carbonate types and the occurrence of certain faunal constituents assisted in interpreting the depositional environment. The deposition of wackestone and wackestone-packstone occurred in a lagoonal environment [3]. The observed arenaceous protodolomite at Okeluse suggests early diagenetic replacement with dolomite and a break in organic matter accumulation [3].

The average percentage mean value of magnesium oxide (MgO), as observed on the results of major oxide analysis, is low (0.75 wt%), indicating that the limestone samples are non-dolomitic [4]. Mineralogical analyses of limestone samples recovered along the Benin Flank indicated that the analyzed samples could be regarded as calcite limestone.

The arenaceous protodolomite is composed mainly of dolomite.

6 Conclusions

Three microfacies have been identified, namely, wackestone, bioclastic wackestone-packstone and arenaceous proto-dolomite. The geochemical and mineralogical analyses of selected Campanian-Maastrichtian limestone samples reflect calcitic nature of the limestone exposed along the Flank. The limestone samples appear to characterize quiet-water sedimentation within shallow marine (lagoonal) environment. This study highlights the occurrence of three different carbonate microfacies of Campanian-Maastrichtian age deposited along the Benin Flank within the shallow carbonate marine setting.

References

1. Ehinola, O.A., Oluwajana, O.A., Nwabueze, E.: Depositional environment, geophysical mapping and reserve estimation of limestone deposit in Arimogija-Okeluse Area, Southwestern Nigeria. *Res. J. Eng. Appl. Sci.* **1**(1), 7–11 (2012)
2. Dunham, R.J.: Classification of carbonate rocks according to depositional texture. In: Ham, W.E. (eds.) *Classification of Carbonate Rocks*, American Association of Petroleum Geologists Mem., AAPG, vol. 1, pp. 108–121 (1964)
3. Nichols, G.: *Sedimentology and Stratigraphy*. Blackwell Science Ltd., London, p. 335 (2009)
4. Armstrong-Altrin, J.S., Verma, S.P., Madhavaraju, J., Lee, Y.I., Ramasamy, S.: Geochemistry of upper miocene kudankulam limestones, southern India. *Int. Geol. Rev.* **45**, 16–26 (2003)

Heavy Metal Concentration of Sediments from the Eastern Niger Delta Basin, South-East Nigeria

Azubuikwe Ekwere

Abstract

This study documents the baseline geochemistry of sediments in portions of the Eastern Niger Delta, focusing on the distribution of selected heavy metals (Pb, Zn, Cd, Cr, As and Ni). Concentration level of metals was determined through Atomic Absorption Spectrophotometry (AAS) and results interpreted with statistical techniques. Interrelations between elements reveal a control by three dominant geogenic factors. The result of this study shows that heavy metal geochemistry of sediments is related to regional and local geology with minor imprints of anthropogenic activities.

Keywords

Trace metals • Sediments • Factor analysis • Geogenic • Niger Delta • Nigeria

1 Introduction

Levels of heavy metals within geo-environments have received tremendous attention in recent times, predicated on a variety of interest including but not limited to the following; (a) their insidious contributions as related to public health concerns (b) their effects on biota growth and diversity and (c) academic interest in establishing baseline data and decipher the fate and dynamics of metal transport within geo-systems.

Coastal sediments are particularly important traps for trace elements and as observed, marine sediments in coastal regions near large industrial and urban areas contain heavy metals sometimes in amounts higher than their natural background.

An estimated 90% of transport of most heavy metals in river systems is shown to be as a solid phase in sediments. Mobilization of these sediments into the major rivers and eventually into reservoirs may concentrate metals at non-background levels, existing as chemical species or fractions that exhibit different bioavailability and potential risk to human beings.

This study attempts to document the heavy metal chemical trend and species availability of sediments in parts of the Eastern Niger Delta basin, south-eastern Nigeria. The geochemistry of sediments in the study area is believed to be controlled by lithology through which rivers and streams within the catchment flow. Concentrations of heavy metals may be derived from mineral deposits and rocks through weathering processes that may concentrate metals from rocks not containing large amounts of these metals. Similarly, the anthropogenic activities may also be imprinted on the geochemical data of the sediments.

The objective of this study is to determine the concentration levels of selected heavy metals in sediments of the study area and establish their possible sources.

2 Materials and Methods

The Eastern Niger Delta extends eastwards from the shoreline fringe of Ikot Abasi area to the coastal plain physiographic provinces of Calabar area of south-eastern Nigeria, delimited by longitudes $7^{\circ} 30' - 8^{\circ} 15' E$ and latitudes $4^{\circ} 30' - 4^{\circ} 40' N$.

Geologically the area is composed of Tertiary and Quaternary sediments referred to as Coastal Plain Sands, consisting of alternating sequence of gravel, sand, silt, clay and alluvium, sourced from three major geologic units on the hinterlands: (1) Precambrian Oban Massif (migmatites-gneisses, granites, schists, para-schists, pegmatites and a host of other ultra-mafic rock suites), (2) Cretaceous sedimentary fill known as the Calabar Flank, composed of limestones, sandstones, shales and marls and (3) The lower

A. Ekwere (✉)
Department of Geology, University of Calabar, Calabar, Nigeria
e-mail: zerratta77@yahoo.com

Benue Trough of post-Cretaceous sediments with lodes of sulphide deposits. Another source of sediments into the study area is the Cross River Delta (Rio Del Rey Basin).

Three major rivers (Imo, Qua-Iboe and Cross River) drain the geologic units of the hinterlands, with a morphology that lies within the flat and low-lying terrain of the coastal lowland Niger Delta region with elevations ranging from less than 10 m at the coastal fringe to about 80 m northwards. Selected metals for analysis includes: Zn, Pb, Ni, As, Cd and Cr.

Fifty two (52) stream sediment samples were collected from the three major rivers and their tributaries within the study area at shallow depths of 0–30 cm. Concentration levels of metals were determined through Atomic Absorption Spectrophotometry (AAS) and results interpreted with statistical techniques (Fig. 1).

3 Results and Discussions

Table 1 shows a statistical summary of the trace element concentrations of stream sediments sampled from the study area. The table also shows global averages as well as data of studied sediments of similar provenance as a means of comparison.

The trend of dominance of the trace elements for the Cross River and Qua Iboe River sediments was $Zn > Pb >$

$Ni > As > Cd > Cr$ while for Imo River the trend was $Zn > Cr > Pb > Ni > As > Cd$.

Lead (Pb), zinc (Zn) and cadmium (Cd) showed highest mean values from the Cross River, followed by Qua-Iboe and least values in Imo River sediments. On the other hand chromium (Cr), arsenic (As) and nickel (Ni) had highest mean values on the Imo River sediments and lesser in the other two rivers.

Mean variances of data from the three rivers were assessed using t-test. At 95% confidence level values are: CRS/QIR (0.012), CRS/IMR (0.036) and QIR/IMR (0.047). These indicate no significance of variance of data between the rivers. Higher values of Pb, Zn and Cd in the Cross River can be attributed to the catchment of the river. This is mainly the Precambrian basement dominated by ultra-mafic and mafic rock suites that are hosts to most trace and rare metals species as revealed from hydrogeochemical modeling. Ni, Cr and Co are also from mafic rocks.

Economic activities of mining and quarrying within the basement complex are also responsible for disaggregation and mobilization of sediments with species of these metals. Cross River and Qua Iboe rivers drain most of the urbanized and industrial settlements within the study area. These areas have the presence of large and small scale processing and production outfits, automobile repair and service shops and wide variety of artisanal industries, which may serve as

Fig. 1 Map of Niger Delta Basin showing sampled rivers; inset index map of Nigeria (modified from [2])

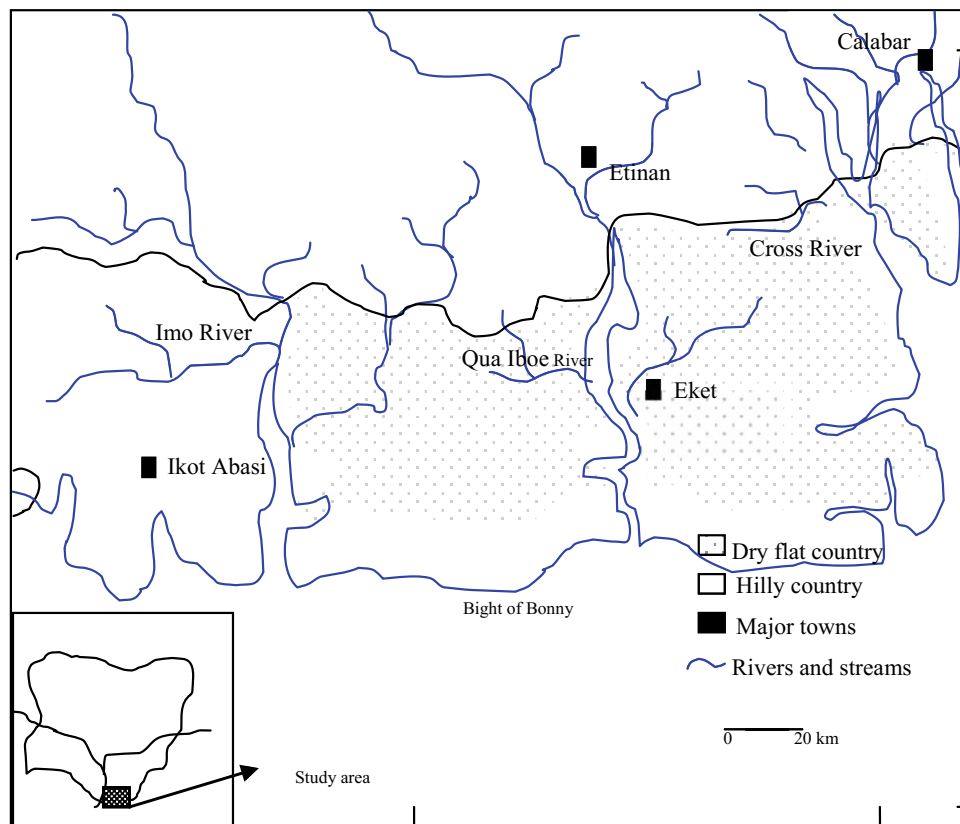


Table 1 Statistical summary of trace metal concentrations in sediments

River/element	Pb (mg/kg)	Zn (mg/kg)	Cd (mg/kg)	Cr (mg/kg)	As (mg/kg)	Ni (mg/kg)
<i>CRS (n = 20)</i>						
Range	27.40–86.40	88.30–117.85	1.20–2.60	0.10–1.70	1.60–2.20	1.20–14.60
Mean	56.51	108.77	1.85	0.97	2.05	7.03
S.D	22.81	12.90	0.44	0.47	0.93	4.50
<i>QIR (n = 16)</i>						
Range	38.20–68.35	74.20–108.30	1.00–3.20	0.50–1.20	1.30–3.80	1.20–8.40
Mean	53.12	90.55	1.78	0.82	2.56	5.44
S.D	10.11	11.87	0.72	0.22	0.85	2.15
<i>IMR (n = 16)</i>						
Range	9.00–29.00	31.00–306.00	1.00–1.80	10.00–67.00	30.02–22.00	6.00–28.00
Mean	18.81	65.90	1.40	40.06	6.88	15.73
S.D	14.14	194.45	0.57	40.31	5.66	15.56
Bight of Bonny	16.41 (7.20–45.5)	647.6 (180–1410)	0.71 (0.30–1.60)	16.71 (6.40–46.10)	–	–
Calabar River	(0.60–30.0)	(0.80–27.0)	–	(0.60–3.30)	–	(1.20–22.50)
Gulf of California	17	88	3	44	7	38
Average shale	20	95	1	90	10	68

CRS Cross River sediments; *QIR* Qua Iboe River sediments values in parentheses indicate ranges; *IMR* Imo River sediments; *S.D* Standard deviation

sources of trace metal release from their effluents into the environment.

Agriculture is the main occupation of the inhabitants of the study area and possibly past practice resulting in erosion and deposition of sediments within stream channels have affected and may continue to influence stream sediment geochemistry.

Higher Cr, As and Ni concentrations in the Imo River are attributable to the shale dominated sedimentary geology of the lower Benue trough.

Mean values of heavy metals for sediments from the entire study area were; Pb (34.30 ppm), Zn (80.00 ppm), Cd (1.55 ppm), Cr (23.10 ppm), As (3.90 ppm) and Ni (11.60 ppm).

Observation reveals the heavy metals to be within ranges and in proximity to levels of sediments of similar provenance and global averages. The values are close to background and below levels that can affect the quality of life of marine biota.

Correlation and factor analyses were executed on the heavy metal concentration of sediments in order to identify important and significant inter-relations. The extraction method for factor analysis was based on the maximum likelihood factors. Correlation matrix shows that there exists a strong positive correlation between Cr and Ni (0.86). A moderate negative correlation is seen between Cr and Pb (–0.66). Correlations among all other elements are generally weak (<±0.50). Variations in geochemical mobilities of the

metals result in a non-uniform distribution pattern with a cumulative distribution function of 0.006.

The data was subjected to factor analysis and this extracted three factors accounting for over 82% of total data variance. Cluster of loadings shows that Pb (0.59), Cr (0.93) and Ni (0.93) for factor 1 and Zn (0.67), Cd (0.67) and As (0.72) for factor 2 determines the oblique factors for hierarchical analysis. Only factor loadings with scores greater than ±0.60 were considered significant.

Factor 1 (Pb, Zn and Cd) extracted about 49% of total data variance. The loadings reflect signatures of sediments derived from the weathering of sulphide lode deposits found within the lower Benue trough. There is a reported occurrence of galena (PbS) and sphalerite (ZnS) in the Abakaliki area of the lower Benue trough and this area forms part of the drainage basin of the eastern Niger Delta [2].

Factor 2 (Cr and Ni) accounts for about 20% of total data variance and represents inputs of sediments of ultra-mafic origin. This loading can be associated with lineament zones (faults and joints) which may contain sheared ultra-mafic rocks. Cr and Ni coincidence suggest association with meta-basaltic rocks (amphibolites), and these are common within the adjoining basement complex. Effects of acidic rain water leaching altered rocks of the basement complex and Cretaceous rocks of the Calabar Flank can also be adjudged. Sandstone has been shown to be a major source of trace elements, thus supporting the role of the Cretaceous Awi sandstones of the Calabar Flank.

Factor 3 (As) accounts for about 12.5% of total data variance. This factor suggests litho-geochemical input representative of weathering and mobility of sediments from arsenic related mineralization. Cretaceous sediments as well as the poly-metallic sulphide lodes of the lower Benue trough have been reported of Mo–As associations [1].

4 Conclusions

This study has provided an important baseline geochemical data for the eastern sector of the Niger Delta basin. The heavy metals are generally at levels within or in proximity to global background levels and sediments of similar provenance. The data indicates that regional and local geology are

the most important factors controlling heavy metal geochemistry with minimal anthropogenic inputs. Statistical analysis reveals interrelations between metals as indicated by factor loadings to be controlled by three dominant factors of geogenic origin.

References

1. Ekwere, A.S., Elueze, A.A.: Trace element assessment of stream sediments around the Aluminium Smelting Company in Ikot Abasi, south-eastern Nigeria. *Res. J. Appl. Sci. Eng. Tech.* **4**(4), 256–261 (2012)
2. Elueze, A.A., Ekwere, A.S., Nton, M.E.: Geoenvironmental assessment of the environs of the Aluminium Smelting Company in Ikot Abasi, south-eastern Nigeria. *J. Geol. Min.* **45**(2), 115–128 (2009)

Distribution of Major and Trace Elements in Soil and Sediments Along the Nile River and Delta—(Egypt): A Case Study

Wael Badawy, Octavian G. Dului[✉], Marina V. Frontasyeva, and Hussien El-Samman

Abstract

The objective of the present work consists in gathering and examining the maximum amount of data concerning the geochemistry of the Nile solid load. To this end, the distributions of 28 major and trace elements in 176 soil and sediment samples collected from the Egyptian section of the Nile River and Nile Delta were determined via epithermal neutron activation analysis. Compared with the Upper Continental Crust corresponding data, the reached results appear to indicate the presence of detrital material of igneous origin, most probably resulting from weathering on Ethiopian highlands as transported by the Blue Nile, the Nile main tributary. The Ni, Zn and As concentrations perceived in the investigated areas appear to be in line with UCC corresponding data. The Na geographical distributions along with the principal component analysis achieved results prove to suggest a possible atmospheric supply from the neighboring Mediterranean and Red Seas.

Keywords

Nile river • Nile delta • Soil • Sediment • Major elements • Trace elements

W. Badawy

Nuclear Research Center, Radiation Protection & Civil Defense Department, Egyptian Atomic Energy Authority (EAEA), Abu Zaabal, 13759, Egypt

O. G. Dului (✉)

Faculty of Physics, Department of Atomic and Nuclear Physics, University of Bucharest, 405, Atomistilor str., 077125 Magurele, Romania
e-mail: o.dului@fizica.unibuc.ro

W. Badawy · O. G. Dului · M. V. Frontasyeva

Frank Neutron Physics Laboratory, Joint Institute for Nuclear Research, 6, Joliot Curie str., 141980 Dubna, Russian Federation

H. El-Samman

Faculty of Science, Department of Physics, Menoufia University, Shibin El-koom, Egypt

1 Introduction

As one of the largest rivers on Earth (6853 km), the Nile River has two major tributaries: Table 1. Mean \pm St.Dev. of the content (in mg/kg) of the elements investigated in 176 samples of sediments (43 samples) and soil (133 samples). The latter relate to the Egyptian sector of the Nile River, together with the corresponding UCC values of the Blue Nile, originating from the Ethiopian High Plateau, and the White Nile, which flows from the Great Lakes and transports the remaining 20% of water supply. Yet, due to the nature of local geomorphology, about 95% of the total sediment load originates from the Ethiopian Plateau through the Blue Nile and Atbara River, the Nile's third major tributary [1]. Consequently, the soil lying along the Nile Valley and Nile Delta turns out to consist mainly of the materials carried away and deposited by the river, with a certain amount of detrital components rich in carbonates, and transported by wind emanating from the Egyptian Desert.

At the same time, due to the presence of the Aswan Dam, about 90% of the sediment load turns out to be accumulated behind the Dam, thus influencing both of the sediments and soils associated geochemistry downstream the Dam. Hence, a rather thorough investigation of the sediments and soils underlying the Nile Valley and Delta, starting from the Dam, could well prove to bring new data regarding the above cited factors' influence on both of the Nile River associated sediments and soils.

2 Materials and Methods

A total of 176 soil and sediment soil samples were collected along the Egyptian sector of the Nile River and Delta. The samples, collected in conformity with the IAEA protocol [2], were cleaned of plant debris and other extraneous materials, air-dried at room temperature to a constant weight, ground and homogenized using an agate ball mill [3]. Further, the

Table 1 The elemental content (in mg/kg) of investigated elements

Element	Mean \pm St.Dev	UCC	Element	Mean \pm St.Dev	UCC	Element	Mean \pm St.Dev	UCC
Na	7630 \pm 4010	24,260	Co	20 \pm 9	17.3	Ba	386 \pm 143	628
Mg	10,610 \pm 6045	14,950	Ni	45 \pm 21	47	La	20 \pm 8	31
Al	47,240 \pm 20,290	81,510	Zn	73 \pm 35	67	Ce	39 \pm 18	63
Ca	28,160 \pm 14,490	25,660	As	3.2 \pm 7.2	4.8	Sm	3.8 \pm 2.7	4.7
Sc	13.4 \pm 5.7	14	Br	43 \pm 90	1.6	Tb	0.6 \pm 0.2	0.7
Ti	8580 \pm 5850	3840	Rb	27 \pm 10	84	Hf	6.8 \pm 4.3	5.3
V	130 \pm 65	97	Sr	260 \pm 130	320	Th	3.8 \pm 2	10.5
Cr	130 \pm 70	92	Zr	290 \pm 200	193	U	1.5 \pm 2.8	2.5
Mn	780 \pm 460	775	Sb	0.3 \pm 0.2	0.4			
Fe	40,900 \pm 16,800	39,200	Cs	0.7 \pm 0.4	4.9			

For comparison, the content of the same elements in the Upper Continental Crust (UCC) [5] is reproduced too

contents of 28 major and trace elements (Na, Mg, Al, Ca, Sc, Ti, V, Cr, Mn, Fe, Co, Ni, Zn, As, Br, Rb, Sr, Zr, Sb, Cs, Ba, La, Ce, Sm, Tb, Hf, Th, and U) were determined with respect to all samples. The investigation was executed by means of epithermal neutron activation analyses (ENAA), performed at the Frank Laboratory of Neutron Physics sited in the Joint Institute of Nuclear Research, Dubna, the Russian Federation, at the IBR 2 pulsed reactor, in conformity with the analytical procedure detailed in [3, 4].

3 Results

The measurements' experimental results, relevant to the 28 considered elements' contents, are reproduced on Table 1, together with the corresponding values concerning the Upper Continental Crust (UCC) [5].

4 Discussion

On investigating the geochemistry relating to the Egyptian sector of the Nile Valley, including the Nile Delta, we have tried to elucidate three main aspects: (i) the origin of sedimentary materials, while accounting for the Nile River's three major tributaries (the Blue and White Niles as well as the Atbara tributaries); (ii) the relationship between the sediments and the soil; (iii) the anthropological influence of more than four millennia, as confined in a thin strip of fertile land along the Nile banks, as depicted on Table 1.

Regarding the first aspect, the Na content appeared to be lower than the UCC content, due probably to an increasing Na^+ mobility during the weathering and water transport processes. The same peculiarity has been noticed to prevail in regard of Al, whose content in both of the sediments and soil was discovered to lower than the UCC case, particularly concerning that related to the basaltic Ethiopian plateau,

source of the Blue Nile tributary. Inversely, however, the Ca appeared to display an increased content, due probably to the persistence of limestone deposits, with the exception of the Nile Delta, with respect to almost the entirety of the Egyptian section.

As for the remaining two major elements, Ti and Fe, they proved to display either a higher content or a greater variability. To our mind, these facts could well relate to the existence of a large number of steel, cement and ceramic factories, which intensely use steel alloys containing titanium or high-quality clay minerals rich in Ti.

More detailed information has been obtained by investigating the distribution of trace elements, mainly the incompatible ones, such as Sc, Zr, Hf, REE, Th or U. Indeed, a ternary Sc–La–Th discriminatory diagram (Fig. 1a) proved that in addition to a significant fraction of continental material, both of the sediments and soil proved to contain a specific quantity of mafic detritus, emanating most probably from the High Ethiopian Plateaus, and consisting mainly of basal with a small amount of felsic material. This observation has been confirmed mainly by the La/Th ratio of 5.1 ± 1.5 concerning the sediments, and 5.5 ± 1.5 concerning soil, significantly different from the UCC relating value of 2.73 (Fig. 1b).

The answer to the second question is given by the numerical value of the Spearman's ρ correlation coefficient, whose value of 0.997 proves to testify a good correlation persisting between the entirety of the 28 elements' content in both of the sediments and soils.

As regard the third aspect concerning any anthropogenic influence on the geochemistry of the Nile valley relating sediments and soil, the average contents of the possible contaminants (heavy elements V, Cr, Co, Ni, Zn and As) were discovered to be relatively close to those associated with the UCC, suggesting the persistence of a minor anthropogenic influence in some local points.

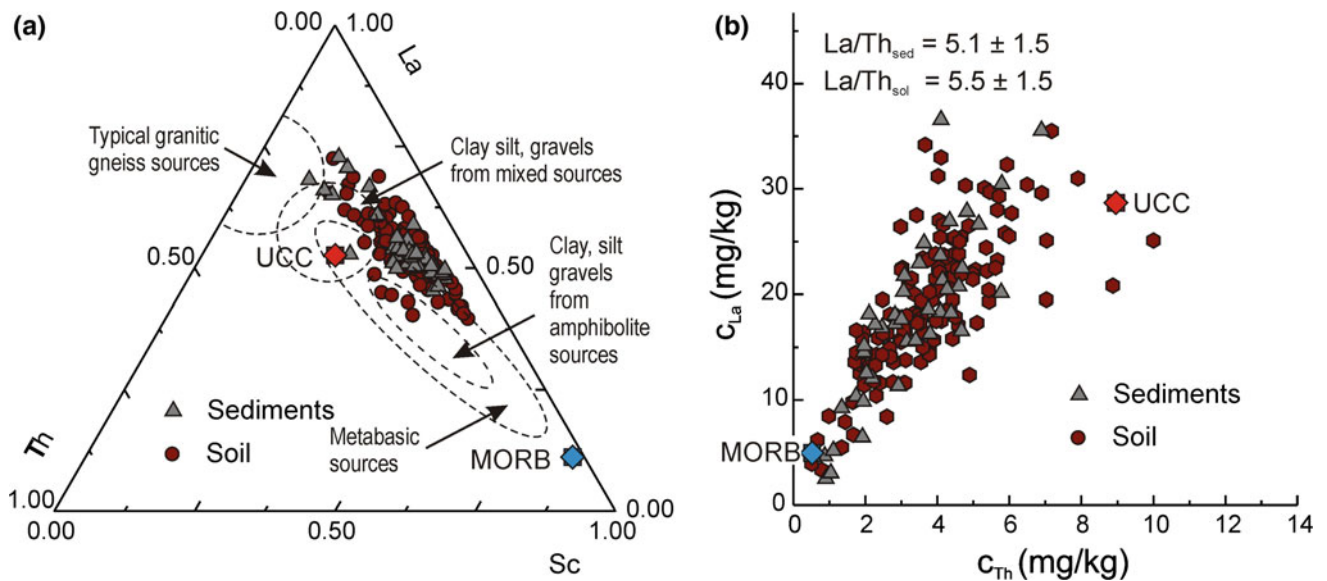


Fig. 1 The Sc–La–Th ternary discriminating diagram (a) and La versus Th bi-plot illustrating the presence of a certain amount of mafic material in both of the investigated materials' sediments and soil. The

points, corresponding to the Upper Continental Crust (UCC) and Mid-ocean Ridge Basalt (MORB), are figured for a better comparison

5 Conclusions

The distribution of 28 major and trace elements persistent in 176 sediments and soil samples turns out to be almost uniformly distributed along the Egyptian sector of the Nile River and Delta. It highlighted that, within experimental uncertainties, and except for some isolated locations, the sediments and soils appeared to display almost the same composition. This fact proves to point out that the Nile sediments stand as the main source of the Nile River soil. In the meantime, it was discovered that the geochemistry of sedimentary material turns out to be too close to those relating to the Upper Continental Crust. Finally, the noticeable influence of some mafic materials appears to originate, most probably, from the Ethiopian high plateau.

References

1. Zaid, B.A., Koll, K.A., Wiesemann, J.U., et al.: Analysis of suspended sediment transport data in the River Nile. In: Schleiss et al. (eds.) *River Flow*, Taylor & Francis (2014)
2. Soil Sampling for Environmental Contaminants, IAEA-TECDOC-1415, IAEA, Vienna (2004)
3. Arafa, W.M., Badawy, W.M., Fahmi, N.M., et al.: Geochemistry of sediments and surface soils from the Nile Delta and lower Nile valley studied by epithermal neutron activation analysis. *J. Afr. Earth Sci.* **107**, 57–64 (2015)
4. Badawy, W.M., Ghanim, E.H., Dului, O.G., El Samman, H., Frontasyeva, M.V.: Major and trace element distribution in soil and sediments from the Egyptian central Nile Valley. *J. Afr. Earth Sci.* **131**, 53–61 (2017)
5. Rudnick, R.L., Gao, S.: Composition of the continental crust. In: Holland, H.D., Turekian, K.K. (eds.) *Treatise Geochem*, vol. 4, 2nd edn, pp. 1–51. Elsevier, Oxford (2014)

Enigma of Ferruginous Inclusions in Evaporites

Rail Kadyrov, Mikhail Glukhov, Evgeny Statsenko, and Bulat Galiullin

Abstract

The ferruginous inclusions were discovered to persist in the evaporite sample, as extracted from the Upper Roadian gypsum deposits of the Kamsko-Ustyinskoe field (Russia). The particles have different forms, from tabular to spherical, with various surface textures. The chemical compositions include Fe, C, O, less Al, Si, Mn, but Ni is absent. The inclusions are assumed to have a terrestrial origin.

Keywords

Evaporites • Gypsum • Ferruginous • Particles
Iron

1 Introduction

The Kamsko-Ustyinskoe gypsum field is located 100 km to the south of the Kazan city, sited in the right bank of the Volga river. The deposit includes 2 layers of gypsum from upper Roadian of Permian system [1]. Several samples from the lowest layer were examined by means of the X-Ray computed tomography method. It has been discovered that one of the samples, enclosing a mixture of gypsum, anhydrite and dolomite, appears to contain some strange inclusions with high attenuation coefficients (Fig. 1). The major goal of this conducted research consists in understanding the origin of the dense particles incorporated in the evaporite sample. In this paper, the reached preliminary results are depicted.

2 Methods

The sample associated microtomography was performed by means of a micro- and nanofocus research X-ray system for computed tomography General Electric V | tome | X S 240 (Germany). A digital model of the sample was created in the Avizo Fire software on the basis of the grayscale distribution, highly relying on the x-ray attenuation. In a next stage, the sample part was analyzed via SEM FEI XL-30 ESEM. The survey was conducted in a low-vacuum mode with an accelerating voltage of 25 keV. The qualitative quantitative chemical analysis was performed by means of an EDAX energy dispersive spectrometer built into the SEM. Another part of the sample was powdered and magnetic inclusions were separated through neodymium magnet. The separated particles were then examined via SEM.

3 Results

Based on the SEM displayed results, and on implementing an electron dispersive spectral analysis (EDS), all inclusions turn out to exhibit different forms and contain a significant amount of iron (Figs. 2 and 3). Their morphology proves to vary from scaly (Fig. 2a), tabular (Fig. 2b) to spherical (Fig. 2c–f). The spherical particles' texture also differs: some of them bear holes on the surface (Fig. 2c), others are filiform (Fig. 2d), some others are relatively smooth (Fig. 2e) and others have a squared surface (Fig. 2f). The particles' chemical composition includes plenty of Fe, C, O, less Al, Si and rarely Ti and Mn.

4 Discussion

Despite the fact that some of them have spherical forms close to micrometeorites [2, 3], the presence of other forms (scaly and tabular) and absence of Ni in the chemical

R. Kadyrov (✉) · M. Glukhov · E. Statsenko · B. Galiullin
Kazan Federal University, Kazan, 420008, Russia
e-mail: Rail7777@gmail.com

Fig. 1 A 3D model of the researched evaporite sample: translucent—gypsum, yellow—dolomite, blue—anhydrite, red—dense inclusions with high attenuation coefficients

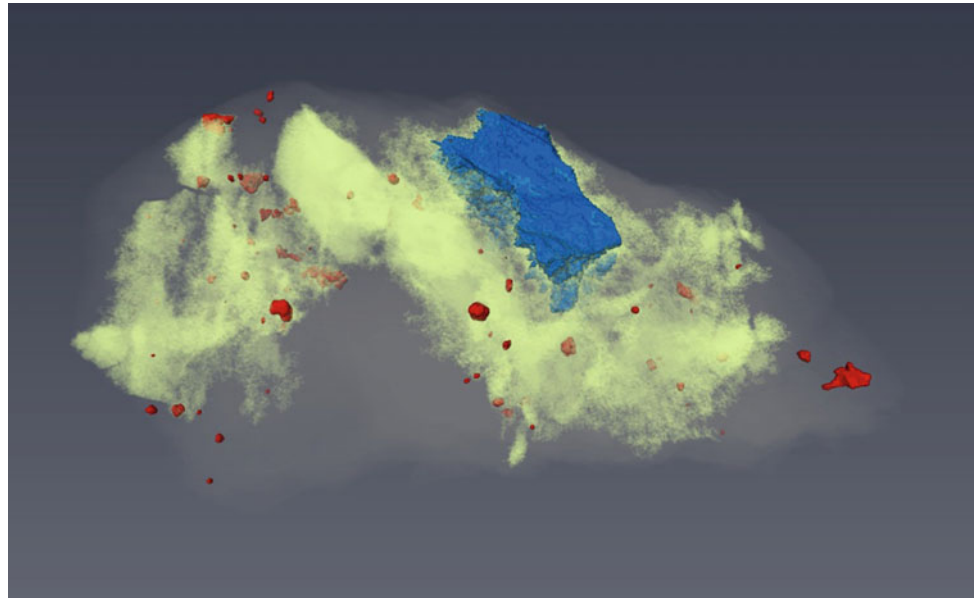


Fig. 2 Different forms of ferruginous inclusions as contained in the evaporite sample: **a**—scaly, **b**—tabular, **c**—spherical with holes on the surface, **d**—spherical filiform, **e**—spherical relatively smooth, **f**—spherical with squared surface

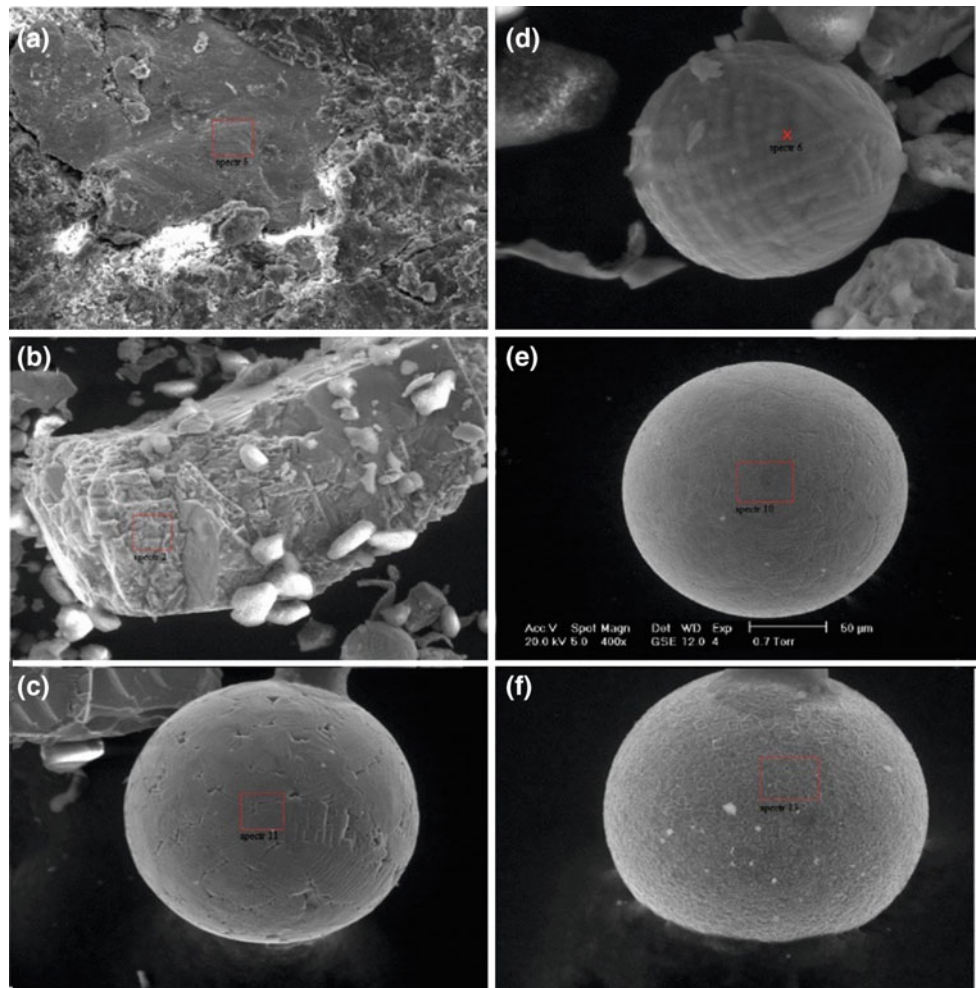
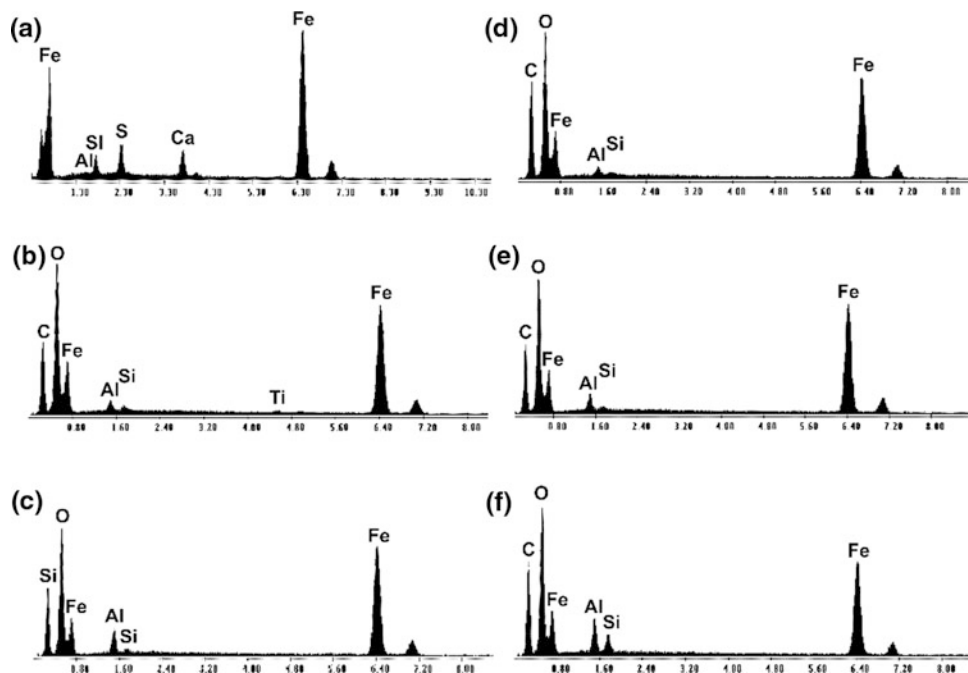


Fig. 3 Spectra of energy dispersive analysis of the Fig. 2 particles: **a**—includes spectrum of background material, **b–f**—separated from rock matrix



composition casts doubt on this. The **particles'** composition appears to include a minor amount of Mn, as confirmed by XRF. It is also worth noting that a significant amount of carbon persisting in the samples does not seem to be associated with their graphitization for SEM. To sum it up, the terrestrial origin of ferruginous inclusions turns out to be well assumed. For more thorough conclusions to be achieved, an additional study of the mineral composition and impurities of the elements seems imposed. In particular, the Mn and Al should be further investigated for the cosmogenic isotopes ^{53}Mn and ^{26}Al to be convincingly distinguished as being they extraterrestrial or not [4, 5].

5 Conclusions

The ferruginous inclusions were found in upper Roadian evaporite sample from Kamsko-Ustyinskoe gypsum deposit on the bank of Volga river, near the Kazan city in Russia. Particles have different forms: from tabular to spherical with various texture on the surface. Their chemical composition includes in addition to Fe, C, O, less Si, Al, Mn and absence of Ni. The terrestrial origin of inclusions is assumed.

Acknowledgements The work is performed according to the Russian Government Program of Competitive Growth of Kazan Federal University.

References

1. Sungatullin, R.K., Kuleshov, V.N., Kadyrov, R.I.: Isotope ($\delta^{13}\text{C}$ and $\delta^{18}\text{O}$) compositions of dolomites from the Permian evaporitic sequences of the Eastern Russian Plate: evidence from the Syukeevo gypsum deposit. *Lithol. Min. Resour.* **49**(5), 406–415 (2014)
2. Taylor, S., Lever, J.H., Harvey, R.P.: Numbers, types and compositions of an unbiased collection of cosmic spherules. *Meteorit. Planet. Sci.* **35**(4), 651–666 (2000)
3. Genge, M.J., Engrand, C., Gounelle, M., Taylor, S.: The classification of micrometeorites. *Meteorit. Planet. Sci.* **43**(3), 497–515 (2008)
4. Nishiizumi, K., Arnold, J.R., Brownlee, D.E., Finkel, R.C., Harvey, R.P., et al.: ^{10}Be and ^{26}Al in individual cosmic spherules from Antarctica. *Meteoritics* **30**(6), 728–732 (1995)
5. Ganapathy, R., Brownlee, D.E., Hodge, T.E., Hodge, P.W.: Silicate spherules from deep-sea sediments: confirmation of extraterrestrial origin. *Science* **201**(4361), 1119–1121 (1978)

Grain Size Distribution and Enrichment Evaluation of Trace Metals in the Mediterranean Harbor Lagoon (Kalaât Andalous, Tunisia)

Samia Khsiba, Oula Amrouni, Chrystelle Bancon-Montigny, Karim Ben Mustapha, Lassaad Chouba, Nadia Gaâloul, and Gil Mahé

Abstract

Sediments are important carriers of pollutants and they help greatly in describing the aquatic ecosystem relating state. The aim of this study is to characterize the Kalaât Andalous harbor lagoon sediments' grain size, their spatial distribution as well as their relating quality. To this end, a study of their trace elements content has been conducted to highlight the associated natural and anthropogenic contribution. Hence, twelve subsurface lagoon sediment samples were extracted at the level of six radials and subjected to a granulometric analysis. The calculation of such indexes as the average mean size (MZ), sorting index (σ) and asymmetry index (SKI) helped greatly in defining the grain size-distribution character. Samples underwent different analyses in a bid to evaluate seven trace metals relevant rates (As, Cd, Cr, Cu, Ni, Pb, Zn). The obtained metal concentrations were compared to the American Oceanic and Atmospheric Administration (NOAA) guidelines, ERL and ERM. The enrichment factor (EF) analysis is used to assess the contamination level, and distinguish both of the relating natural and anthropogenic origin sources. The reached results proved to display that the sediments turn out to be predominantly sandy, with fine sand dominating the area, while medium sand is being located at the channel and the south-western section of the quay. The latter is characterized with a

muddy facies. The majority of trace elements' concentrations are discovered to be lower than the ERL values. The implemented enrichment factors proved to indicate that the lagoon is mainly enriched in As and Cd.

Keywords

Kalaât Andalous lagoon • Grain size distribution • Trace metals • Enrichment factor

1 Introduction

The Mediterranean coastal areas are often threatened with the predominance of metallic contamination [1]. Trace metals prove to penetrate into the aquatic ecosystems from natural sources including pedogeochemical background [2], weathering processes and erosions [3] as well as anthropogenic sources originating from the increase of human activity [1]. In fact, the port relating activities are associated with a particular contamination of aquatic areas and bottom sediments [4]. The accumulation of trace metal in sediments participate noticeably in engendering different changes in the environmental conditions, due mainly to potential remobilization and bioaccumulation in biocenosis [5]. Several researchers have used sediments as environmental indicators whereby trace metal contamination assessed [1, 6, 7]. The purpose of this study is threefold. In a first place, it is designed to characterize the Kalaât Andalous lagoon sediments' related grain size and spatial distribution. In a second place, it is aimed to evaluate the pollution status affecting the study area with respect to the sediment quality guidelines. Finally, It is focused on evaluating the contamination level and differentiating between both of the associated natural and anthropogenic sources by means of the Enrichment Factor (EF) analysis.

S. Khsiba (✉) · O. Amrouni · K. B. Mustapha · L. Chouba
National Institute of Marine Science and Technologies,
2025 Salammbô, Tunisia
e-mail: khsibas@gmail.com

C. Bancon-Montigny
University of Montpellier, 34090 Montpellier, France

N. Gaâloul
Unity of Paleoenvironnements, Geomateriaux et Risques
sismiques, Faculty of science, University of Tunis El-Manar,
Tunis, Tunisia
e-mail: ngaaloul1@yahoo.fr

G. Mahé
UMR HydroSciences Montpellier/IRD, 34090 Montpellier, France

2 Materials and Methods

A sampling campaign was performed in March 2017 for twelve subsurface lagoon sediments to be collected at the level of six radials (2 stations per radial) surrounding the lagoon. The latter is characterized with the predominance of northern and north-western winds. Tidal heights were estimated at about 0.5, 0.2, 0.4 m during the current campaign. The sediment samples were initially subjected to a granulometric analysis by means of an AFNOR column sieving process. The grain size distribution was determined through calculation of the different relating indices (average mean size (MZ), sorting index (σ), and asymmetric index (SKI)) in conformity with Folk and Ward [8]. The $\leq 63\text{-}\mu\text{m}$ -sized fraction (silt and clay fractions) underwent a microgranulometric analysis via a sedigrapher type Mastersizer 2000, and the facies' curves were interpreted according to Barousseau [9]. In a second place, and for the inorganic-metal concentrations to be evaluated, 50 mg aliquots of sediments were digested through an acid mixture. The digestion process was carried out in a microwave oven (Thermo Scientific Ultra-wave Microwave). The trace-element concentrations' rates (As, Cd, Cr, Cu, Ni, Pb, Zn) were measured using ICP-MS-Q, iCAP-Q (Thermo Scientific). The obtained metal concentrations were compared to the American Oceanic and Atmospheric Administration (NOAA) guidelines: the effect range low ERL, the concentration below which adverse effects rarely occur, and the effect range median ERM, the concentration above which adverse effects frequently occur [10, 11]. The Enrichment Factor (EF) is used to determine the natural as well as the anthropogenic trace elements' origins [1, 12, 13]. It is calculated by means of the following equation: $EF = (M/AI)_{\text{sample}} / (M/AI)_{\text{background}}$, where the (M/AI) sample and (M/AI) background are the concentration ratio of the trace element being tested (M) to the concentration of (AI) in the sample and the background value. AI is used as a normalizer to correct the differences noticeable in the sediments' grain size and mineralogy [12]. EF&s are interpreted as follows [14]: $EF < 1$ indicates no enrichment; $EF < 3$ denotes a minor enrichment; $3 < EF < 5$ implies a moderate enrichment; $5 < EF < 10$ highlights a moderately severe enrichment; $10 < EF < 25$ signifies a severe enrichment; $25 < EF < 50$ indicates a very severe enrichment and $EF > 50$ refers to an extremely severe enrichment.

3 Results

The preliminary outcomes appear to display that the sediments turn out to be predominantly sandy (60%). The sandy sediments are (100%) unimodal, with modals ranging from

0.125 to 0.25 mm. The sandy distribution is characterized with the prevalence of a fine sand with: Mz varying from 2Φ to 3Φ , which is predominantly well sorted, and σ ranging from 0.35Φ to 0.5Φ . The SKI index proves to indicate that the sand is mainly asymmetric towards fine sands (positively skewed). 30% of the sediments are silty with a mean grain size D50 ranges from 3.99ϕ to 7.97ϕ . The lagoon sediment relating spatial distribution reveals that the study area is dominated by fine sand. Channel zone, the upper part of the south-western quay area and the north-western part of the lagoon are characterized with the predominance of medium sand. The $\leq 63\text{-}\mu\text{m}$ -sized sediments (clay sediments) are both located at the quay and the lagoon areas' north-western parts.

The geochemical study proved to reveal that the mean trace metal contents in the sediment samples followed the order: $Zn > Pb > Cr > Ni > Cu > As > Cd$, with mean concentrations of respectively 124.88, 53.46, 47.94, 23.31, 14.56, 10.64 and 0.51 mg/kg. Station 1 from radial 3 (R3S1), located close to the channel, is characterized with the lowest Cd, Cr, Cu, Ni, Pb, Zn concentrations. As is lower at radial 2 of station 1. R2S1, as sited on the harbor quay, appeared to exhibit the highest concentration rates for Ni (29.3 mg/kg), Pb (70.58 mg/kg) and Zn (155.94 mg/kg). Sediments pertaining to the lagoon northern part (R1S10) contained the highest Cr and Cu concentrations. The Cd revealed a higher concentration in the south of the lagoon. Station 1 to the lagoon north western part is characterized with the highest As concentration level (14.96 mg/kg). This particular study yielded concentrations of Cd, Cr, Cu and Zn turn out to be inferior to the entirety of the stations related ERL. The As, Ni and Pb concentrations are mainly comprised between ERL and ERM, except for the first station sited at the quay channel level and the north western part of the lagoon, which displayed lower ERL values.

The EF values and mean values are depicted on Table 1.

4 Discussion

The study area related sediments are mostly composed of a very fine sand. Muddy sediments are mainly characterized by a parabolic facies indicating either channel deposits or turbidity deposits deposited by charge excess [15]. Medium sand at the level of the channel might be carried in by both the north to south longshore drift generated by a northeastern wind [16] and by the storm wave action and high level tidal daily oscillations into the lagoon system. The lagoon ecosystem is recently generated by the dynamic sandy spit (i.e. Foug El Oued) migration following the NE-SW longshore drift since 1972 [17].

The latter exhibited the lowest Cd, Cr, Cu, Ni, Pb, Zn concentrations which must be due to both the sandy texture

Table 1 The EF values for trace elements in Kalaât Andalous harbor lagoon, Gulf of Tunis; mean EF values

		EF (As)	EF (Cd)	EF (Cr)	EF (Cu)	EF (Ni)	EF (Pb)	EF (Zn)
R1	R1S1	15.71	10.96	3	1.16	2.57	7.05	4.34
	R1S10	8	8.85	2.69	1.82	1.94	6.15	2.79
R2	R2S1	8.52	11.08	2.60	0.92	1.97	6.95	2.85
	R2S10	13.24	9.09	2.54	1.00	2.22	7.13	3.33
R3	R3S1	81.92	22.20	6.04	2.21	6.63	13.16	7.91
	R3S10	14.5	11.09	2.91	1.11	2.52	7.6	4.28
R4	R4S1	17.59	10.67	2.95	1.24	2.48	7.61	3.69
	R4S10	15.98	10.11	2.77	1.11	2.49	7.97	4.30
R5	R5S1	17.04	12.49	2.89	1.28	2.53	8.05	3.83
	R5S10	23.92	19.15	3.70	1.75	4.23	12.59	5.83
R6	R6S1	16.71	9.23	2.93	0.96	2.14	6.26	2.87
	R6S10	11.73	9.68	2.81	0.99	2.25	7.17	3.38
	Mean value	20.40	12.05	3.15	1.30	2.83	8.14	4.12
	Ecart type	10.84	2.95	0.57	0.32	0.87	1.58	1.01

of this station and to the regular explosion of this area to marine exchanges due to coastal current responsible for mixing lagoon sediments. High concentration of Pb and Zn in the second radial (harbor quay) might be due to lead fishing nets. Trace elements concentrations are mainly less than the ERL, they are below which adverse effects frequently, which can be explained by the harbor recent implantation age (since 1995). Mean Enrichment factor values, mainly indicate a minor enrichment in both Cu (1.30 ± 0.31) and Ni (2.83 ± 0.86), a moderate enrichment in Cr (3.15 ± 0.57) and Zn (4.11 ± 1.01), a moderate severe enrichment for Pb (8.14 ± 1.57), a severe enrichment in both Cd (12.04 ± 2.94) and As (20.40 ± 10.83). Station R3S1, at the level of the channel, demonstrated the highest enrichment factor values with respect to the entirety of trace elements with (EF As = 81), highlighting that it displays the most anthropogenic inputs compared to the rest of the station. The EFs approaching unity point out to the crustal origin, while those exceeding 10 are refer to a non-crustal source origin [18]. This highlights well that all the examined trace elements are of a natural source, such as mining sources driven by the Medjerda river, except for the As and Cd with EF > 10, which point out to an anthropogenic origin.

5 Conclusions

Grain size distribution analyses of the Kalaât Analous Harbor lagoon surface sediments revealed that sediments are discovered to be mainly constituted of fine sand. Medium sand, with a low proportion of silt and clay in the channel, are caused by a lack of dispositional process due to the wave

and current ebb-flow actions. Whereas the silty to clay facies are located at both of the harbor quay and the north western lagoon areas. The latter correspond to an area that is well protected from hydrodynamic factors.

The geochemical evaluation appeared to indicate that Zn and Pb display the highest mean concentrations. The sediment quality guidelines showed that most of this ecosystem associated trace elements prove to be lower than that the ERL relating ones, with As, Ni and Pb ranging between ERL and ERM. The EF related values proved to indicate that the lagoon sediments are severely enriched in both Cd and As. These two elements are of an anthropogenic source (EF > 10). The lagoon sediments are mostly enriched in the rest of the examined trace elements, which turn out to be of a natural origin.

References

1. Brik, B., Ayadi, A., Riahi, C., Sdiri, A., Regaya, K.: Contamination levels and vertical distribution of trace metals with application of geochemical indices in the sediment cores of the Bizerte lagoon-Ichkeul lake complex in Northeastern Tunisia (2017)
2. Bryan, G.W.: Heavy metal contamination in the sea. In: Johnston, R. (ed.) Marine Pollution, pp. 185–302. Academic Press, London (1976)
3. Shang, Z., Ren, J., Tao, L., Wang, K.: Assessment of heavy metals in surface sediments from Gansu section of yellow rivers, China. Environ. Monit. Assess. **187**(79), 10 (2015)
4. Denton, G.R.W., Concepcion, L.P., Wood, H.R., Morrison, R.J.: Trace metals in sediments of four harbours in Guam. Mar. Pollut. Bull. **50**, 1121 (2005)
5. Nemati, K., Bakar, N.K.a, Abas, M.R., Sobhanzadeh, E.: Speciation of heavy metals by modified BCR sequential extraction procedure in different depths of sediments from Sungai Buloh, Selangor, Malaysia. J. Hazard. Mater. **192**, 402–410 (2011)

6. Christophidis, A., Stamitis, N., Orfanidis, S.: Sediment heavy metals of Mediterranean Coastal lagoon: Agisma, Nestos Delta, Eastern Macedonia (Greece) (2007)
7. Chouba, L., Mzoughi, N.: Assessment of heavy metals in sediments and in suspended particles affected by multiple anthropogenic contribution in harbors (2012)
8. Folk, R. L., Ward, W. C.: Brazos River bar, a study in the significance of grain size parameters. *Jour. Sed. Petr.* **27**, 514 (1957)
9. Barusseau, J. P.: Evolution du plateau continental rochelais (golfe de Gascogne) au cours du Pléistocène terminal et de l'Holocène. Les processus actuels de la sédimentation. Thèse d'Etat, Bordeaux I (1973)
10. Long, E.R., MacDonald, D.D., Smith, S.L., Calder, F.D.: Incidence of adverse biological effects within ranges of chemical concentrations in marine and estuarine sediments. *Environ. Manag.* **19**(1), 81–97 (1995)
11. Buchman, M.F.: NOAA screening quick reference tables, NOAA OR&R Report 08–1. Off. Response Restor. Div. Nat. Oceanic Atmos. Adm. Seattle, p. 34 (2008)
12. Alexander, C.R., Smith, R.G., Calder, F.D., Schropp, S.J., Windom, H.L.: The historical record of metal enrichments in two Florida estuaries. *Estuaries* **16**, 627–637 (1993)
13. Valdés, J., Vargas, G., Sifeddine, A., Ortlieb, L., Guinez, M.: Distribution and enrichment evaluation of heavy metals in Mejillones Bay (23°S), Northern Chile: geochemical and statistical approach. *Mar Pollut. Bull.* **50**(12), 1558–1568 (2005)
14. Birch, G.: A scheme for assessing human impacts on coastal aquatic environments using sediments. In: Woodcoffe, C.D., Furness, R.A. (eds.) *Coastal GIS 2003*. Wollongong University Papers in Center for Maritime Policy, Australia (2003)
15. Barusseau, J.P.: Evolution du plateau continental rochelais (golfe de Gascogne) au cours du Pléistocène terminal et de l'Holocène. Les processus actuels de la sédimentation. Thèse d'Etat, Bordeaux I (1973)
16. Amrouni, O., Hermassi, T., Abdeljaouad, S., Messaoudi, S.: Contribution of grain size trend to sediment of microtidal beach. Case of the Gulf of Tunis bay (Cape Ferina- Cape Gammarth, Tunisia). *Res. J. Environ. Sci.* **8**, 161–177 (2014)
17. Oueslati, A.: Les côtes de la Tunisie. Géomorphologie et environnement et aptitudes à l'aménagement. Université de Tunis, 387 p (1993)
18. Nolting, R.F., Ramkema, A., Everaats, J.M.: The geochemistry of Cu, Cd, Zn, Ni and Pb in sediment cores from the continental slope of the Banc d'Arguin (1999)
19. Guelorget, O., Perthuisot, J. P.: Le domaine paraliq. Expressions géologiques, biologiques et économiques du confinement. Travaux de laboratoires de géologie, Presses de l' Ecole Normale Supérieure, Paris, 136 p (1983)

Trace Metal Concentrations in Surface Water in Ichkeul Lake Basin: a Case Study

Nesrine Ouchir, Lassaad Ben Aissa, and Mabrouk Boughdiri

Abstract

This study presents informations about the water quality and design of monitoring network for effective management of water resources. The Ichkeul lake basin is situated in the North of Tunisia. Exposed to domestic sewages along with industrial, municipal, recreational discharges and the old (Pb–Zn) Jalta mine, the lake receives metal concentrations that risk provoking harmful and irreversible disruptions on the fauna and flora. The assessment of trace metals in surface water showed that the maximum values of Fe, Mn, Pb, Zn, Cu and Ni were all below the national and international standard, except for Fe in Hammam Ben Abbes thermal spring and Pb in Wadi Tinja as a result of the solid mining accumulation wastes after the processing of the Pb–Zn and the mineral paragenesis associated with hydrothermal metalliferous conditions of Jebel Ichkeul, added to these the uncontrolled releases of domestic, industrial and agricultural waste water. These factors contribute to the environmentally degradation of the lake water quality.

Keywords

Ichkeul lake • Thermal springs • Geochemistry Mine • Trace metals

1 Introduction

The Ichkeul ecosystem is considered one of the four major wetland areas in the western Mediterranean, together with Donana, Spain, the Camargue, France and the El Kala region, Algeria, and is classified as a UNESCO World

Heritage site. The study area is surrounded by an accumulation of solid mining wastes from the old Jalta mine after the processing of Pb–Zn, we focused on the assessment of metal contamination in the lake's tributaries [1]. Surface water chemistry depends on several natural factors such as variations in precipitation, erosion, alteration of crustal materials, and anthro-pogenic factors, such as the discharge of domestic, industrial wastewater, which presents a serious problem since it led to the disturbance and degradation of aquatic ecosystems [2], [3]. In addition, the pollution of surface waters by metallic trace elements such as Zn, Pb and Cd has a particular attention. These elements can pose a serious threat to aquatic ecosystems and human health [4]. The purpose of this study was to evaluate the concentrations of Pb, Zn, Cu, Fe, Mn, and Ni in surface waters.

2 Materials and Methods

2.1 Water Sampling

Water samples were collected in August 2014 from 15 sites in the Ichkeul Lake basin Fig. 1. The sampling sites were selected at the mouths of the main rivers flowing into the lake: Morra (S1), Hammam Ben Abbes (S2), Sejnane (S3), Hammam Echfa (S4), Joumine (S5), Douimis (S6), Tinja (S7), Melah (8), Ain Attrous (S9), Malah (S10), Ain Negrez (S11), Hammam Abdelkader (S12), Mine (S13), Khloufi (S14), Ghezala (S15).

In order to determine the concentrations of trace elements (Fe, Mn, Sb, Zn, Cu and Pb), 1-litre water samples were collected in pre-cleaned, washed polyethylene bottles and immediately filtered through Whatman filter paper No. 42 (2.4 μm pore size) before being acidified with 0.1 N HNO_3 to avoid precipitation of metals [4]. They were then returned to the laboratory and stored at 4 °C until analysis on an Atomic Absorption Spectrophotometer (AAS). Maps concentrations of metallic trace elements (mg L^{-1}) in waters of the Ichkeul have been done with ArcGis software.

N. Ouchir (✉) · L. B. Aissa · M. Boughdiri
Department of Earth Sciences, Faculty of Sciences of Bizerte,
University of Carthage, 7021 Jarzouna, Tunisia
e-mail: nesrine.ouchir@gmail.com

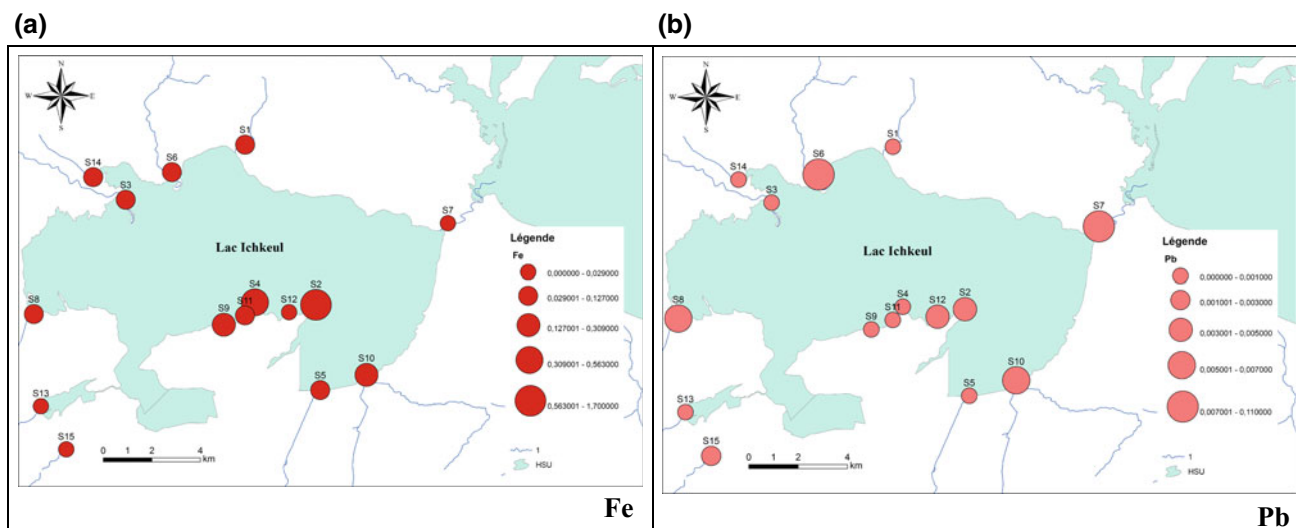


Fig. 1 Maps concentrations of trace metals (mgL^{-1}) in waters of the Ichkeul

3 Results

3.1 Geochemistry of Metallic Trace Elements

The results of the studied surface waters concentrations in summer period are classified as follows: $\text{Fe}(0.23) > \text{Ni}(0.09) > \text{Mn}(0.056) > \text{Zn}(0.05) > \text{Cd}(0.02) > \text{Pb}(0.018) > \text{Sb}(0.017) > \text{Cu}(0.005)$. These results show that during wet seasons the metal concentrations are diluted and therefore they are low. On the other hand in dry period they increase due to the effect of the evaporation. The maximum concentrations of Fe in the studied waters are recorded at the thermal springs, especially site S2 (Hammam ben Abbes). They are in the order of 1.7 mg L^{-1} which is higher than the water potability standards set at 1 mg L^{-1} as well as Tunisian standards of rejection in the public hydraulic areas. This enrichment in Fe is due to the fact that this element characterizes the mineral paragenesis associated with the hydrothermal metalliferous indices of Jebel Ichkeul.

The average concentrations of Mn shows that the thermal springs S2 (Hammam Ben Abbes), S4 (Hammam Echfa), S12 (Hammam Sidi Abdelkader), S9 (Ain attrous) and S11 (Ain Negrez) are enriched in Mn which confirms that Fe and Mn are often found together in nature, Mn is an element which characterizes the mineral paragenesis associated with the hydrothermal metalliferous indices of Jebel Ichkeul.

The analysis of Pb shows that the highest levels 0.06 mg L^{-1} are recorded at the S6 site (mouth of the wadi Douimis), this concentration is related to the agricultural practices of Douar Douimis.

The studied waters in Zn concentrations shows that the highest ones are recorded at the downstream of the Ghezini wadi (S13) which drains the old Pb–Zn mine from Jalta. The increase in levels at this site is easily related to the leaching of Zinc and Lead mineral deposits and the mine dumps effect which hugely influence the lake Ichkeul.

The low concentrations of Cd in the study sites with the exception of the S7 site, leads us to conclude that the abundance of carbonate and salt formations in the Ichkeul region, and their affinity towards certain metals, controls the distribution of these elements, especially in the flood period where the dissolution of these formations is important.

4 Discussion

The low concentrations of Fe in the others studied sites can be explained by the fact that Triassic carbonate deposits act as substrates, which also contribute, in the behavior of iron and manganese, and the rest of the metals by acting on the pH that causes their precipitation. The main form of iron (oxyhydroxide) is a prime scavenger for metals.

Lead accumulates easily in soils where it interacts with organic molecules. It is sensitive to erosion phenomena that can remobilize lead and store it in the soil. Normally, high concentrations of Pb in the S13 site of Wadi Ghezini, which drains the Pb–Zn dumps from Jalta and leads into the lake and marshes, should have been high. The low levels (below the limit of detection) can be explained by the phenomenon of metal retention, in fact, the work of Mlayah and Jallali in 2014 showed that the CaCO_3 tested was very effective in

removing lead in several experimental situations. Lead was fully eliminated by a 20 gL^{-1} test of marble waste [5]. The elimination of lead seems to be controlled by the following two reactions:

Simultaneous precipitation in the form of cerussite (PbCO_3) and hydrocerussite ($\text{Pb}_3(\text{CO}_3)_2(\text{OH})_2$) followed by adsorption on surface particles by cation exchange and complexation. The Jalta mine site is characterized by mineralization hosted in two stratigraphic levels; the Triassic contact fault and the Mio-Pliocene. The mineralization replaces the carbonate cement in breaches of Triassic formations and conglomeratic deposits. The lithological nature of the Ichkeul lands are at the origin of the low Pb contents, which can be complexed and/or adsorbed on the different lithological components of the geological outcrops.

5 Conclusions

The enrichment in Fe in the hydrothermal source (S2) is due to the fact that this element characterizes the mineral paragenesis associated with the hydrothermal metalliferous indices of Jebel Ichkeul. As for the low concentrations found in the other sites, they can be explained by the buffering capacity of the geological outcrops which act on the rise of the pH in this hydric system which causes the adsorption, the complexation and the precipitation of the dissolved metals. Thus the waters studied do not present a risk of pollution by metals. However, they remain vulnerable to contaminant

inputs from industrial and domestic discharges on tributaries that feed the lake, as well as the impact of Pb–Zn mine dumps left in the wild without any protection. The abundance of carbonate soils “salt complex” of Jebel Ichkeul participates in the control of the distribution of Zn, Cd and Pb, in particular at the period of the floods where the dissolution is important, from where their affinity towards certain metals.

References

1. Ouchir, N., Morin, S., Ben Aissa, L., Boughdiri, M., Aydi, A.: Periphytic diatom communities in tributaries around Lake Ichkeul, northern Tunisia: a preliminary assessment. *Afr. J. Aquat. Sci.* **42**(1), 65–73 (2017)
2. Mishra, A.K., Arya, M., Mathur, R.: Assessment of pre-monsoon and post monsoon ground water quality with special reference to fluoride concentration in Narwar, Shivpuri, Madhya pradhesh, India. *J. Env. Res. Dev.* **6**(1), 77–81 (2011)
3. Varol, M., Gokot, B., Bekleyen, A.: Dissolved heavy metals in the Tigris River (Turkey): spatial and temporal variations. *Env. Sci. Pollut. Res.* **20**(9), 6096–6108 (2013)
4. Wilken, R.D., Hintelmann, H.: Mercury and methylmercury in sediments and suspended particles from the river Elbe, North Germany. *J. Water Air Soil Pollut.* **56**(1), 427–437 (1991)
5. Mlayah, A., Jellali, S.: Study of continuous lead removal from aqueous solutions by marble wastes: efficiencies and mechanisms. *Int. J. Environ. Sci. Technol.* **12**(9), 2965–2978 (2014)

Geochemistry and Mineralogy of the Miocene and Pliocenesediments of the Northern Margin of the Lower Chelif Basin (Western Tellian Domain, North Algeria)

Fatiha Hadji, Abbas Marok, and Ali Mokhtar Samet

Abstract

The Chelif basin is one of the basins in the Mediterranean that preserve sedimentary deposits that span the Miocene including evaporites from the Messinian Salinity Crisis (MSC). Mineralogical and geochemical analyses were integrated in this study and conducted on a set of fifteen samples, collected from a selected section (Amarna). The lithostratigraphic succession of this section is represented by three formations, which are, from bottom to top: the Tortonian Blue marls formation, the Messinian marls, including gypsy-calcareous beds, and the Zanclean Trubi marls formation. The integration of relating mineralogical and geochemical data allowed us to better constrain the noticeable transition in this region. The onset of the lower Pliocene is marked with a sudden appearance of an important content of a smectite mineral, the occurrence of an abnormal positive peak of a celestine mineral (30%), reflected in the important shift of SrO in the layer A₉, along with an important sulphur content (10%) and reduced environmental conditions.

Keywords

Amarna • Chelif basin • Miocene • Pliocene • Mineralogy • Geochemistry • Paleoclimate

1 Introduction

The study area is a part of the Northern margin of the Chelif basin, an elongated basin lying 350 km in an ENE-WSW direction, filled with Miocene and Pliocene sediments (Fig. 1).

This margin and its Miocene-Pliocene transition remain unrecognized on mineralogical and geochemical planes. In this context, a representative geological section (Amarna) was examined. This section is located east of Djebel Diss, sited at the southwestern end of the Dahra Mounts, on the northern margin of the Chelif Basin. Its lithostratigraphic succession is represented by three formations, which are from bottom to top: the Tortonian blue marls formation, the Messinian marls, including gypsy-calcareous beds, and the Zanclean Trubi marls formation (Fig. 2).

In this paper, we depict the results of mineralogical and geochemical studies, carried out on upper Miocene and lower Pliocene of the Amarna section of the Chelif basin. The attained results allow us to discuss the noticeable variations in the mineral and geochemical contents through the transition.

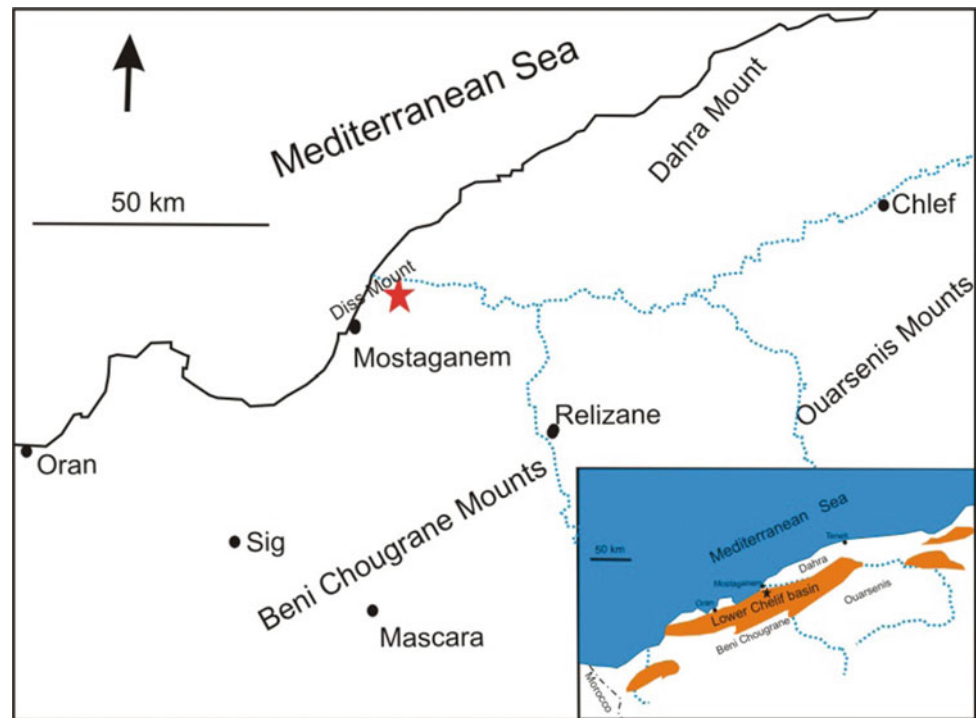
2 Materials and Methods

This study is based on the processing and analysis of fifteen samples (Fig. 2) collected from the marl layers. A semi-quantitative X-ray identification of the crystalline phases was applied on the whole rock and clay fraction, by means of a PANanalytical: XPERT-PRO. Total element contents were determined via an XRF spectrometer (Brucker-Axs: SRS 3400) in homogenized powdered bulk samples, after drying, to determine the loss of ignition (LOI). The analyzed oxides were: SiO₂, Al₂O₃, Fe₂O₃, CaO, MgO, Na₂O, K₂O, P₂O₅, SO₃, MnO, TiO₂, Cr₂O₃, ZrO₂, SrO, Rb₂O, ZnO, PbO, CuO, NiO, BaO.

F. Hadji (✉) · A. Marok
Department of Earth and Universe Sciences,
University of Tlemcen, P.O. Box 119 Tlemcen, Algeria
e-mail: fm_hachemi@yahoo.fr

A. M. Samet
Department of Hydraulic, University of Chlef,
P.O. Box 151 Chlef, Algeria

Fig. 1 Section and lower Chelif basin locations



3 Results and Discussion

The clay fraction, of the studied section, is composed of smectite mineral (0–70%) (including random illite/smectite: 15–25%), chlorite (0–15%), illite (tr–50%) and kaolinite (0–50%). Non-clay minerals are, in the descending order, quartz, calcite, dolomite, feldspar (plagioclase and orthoclase). An important content of celestine (30%) was depicted at the transition in layer A₉, while all the other layers are completely bereft of this species.

During the upper Miocene, smectite mineral proves to exist in small quantities (5%), but only in two layers (A₄ and A₅), while during the lower Pliocene, the content appears to vary between 15 and 70%, decreasing from the bottom to the top. Inversely, kaolinite is persistent in small quantities in the upper Miocene layers (10–50%), and reaches lower contents during the lower Pliocene (0–10%). In parallel, the distribution of chlorite persists as discontinuous trends during the study stratigraphical range, varying between 0 and 10%.

The smectite mineral is virtually absent during the upper Miocene. It makes a sudden appearance in the lower Pliocene at the level of the A₉ layer with 70% and, subsequently, records a significant reduction at the section's top level (Layer A₁₄). Chlorite is persistent at the top of the upper Miocene layers with low rates, and disappears at the A₈ and A₉ samples, to reappear with a small percentage (10%) in

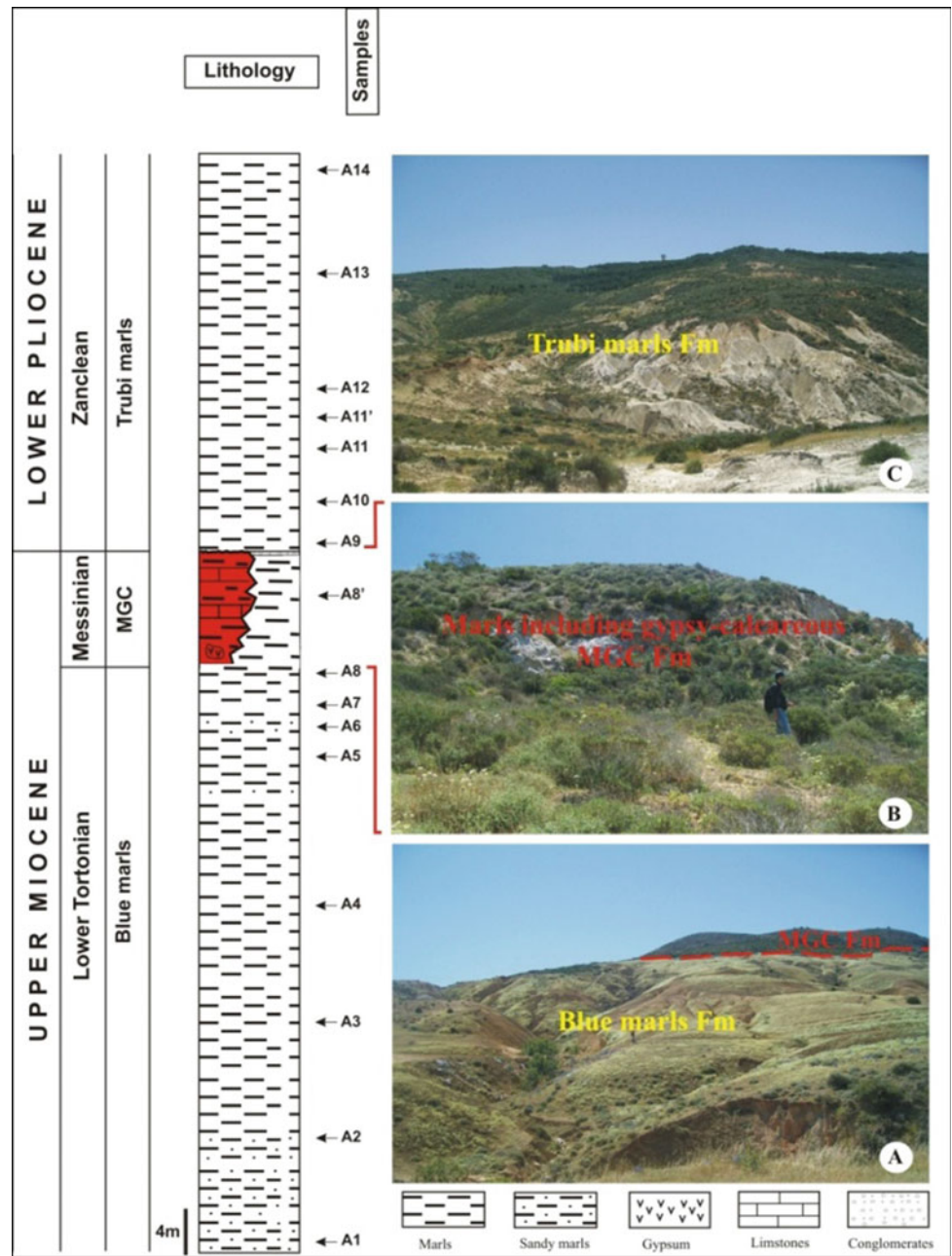
A₁₁ (in the lower Pliocene). It is worth noting that layer A₈ is bereft of all mineral clays (0 to trace).

The clay mineral ratios, lying at the Amarna section, are kaolinite/illite (0–1.67), smectite/illite (0–2.33), kaolinite/(illite + chlorite) (0.09–1.67) and smectite/(illite + chlorite) (0–0.3), towards the section base in the upper Miocene, and higher values (0.3–2.33 and 0.25–2.33, respectively) during the lower Pliocene. Kaolinite/(illite) and Kaolinite/(illite + chlorite) appear to exhibit a coherent pattern increasing up-section, with the highest values (2.33) being attained at the level of layer A₉.

Concerning the non-clay minerals, quartz exists in large quantities in the upper Miocene (34–69%), and ranges from 11 to 33% in the lower Pliocene. This indicates that the upper Miocene deposits are materialized with silicoclastic sediments, indicating the persistence of a significant erosion, along with a shallow depositional environment. The calcite mineral exhibits lower contents down section, somewhat higher concentrations up section, suggesting a basin deepening during the lower Pliocene. The plagioclase and orthoclase exhibit small contents (0–3%). The quartz content proves to vary inversely in respect of that of the calcite lying in the upper part of Amarna section.

In the Amarna samples, SiO₂, Fe₂O₃, and Al₂O₃ are, respectively, the three most abundant elements (as oxides),

Fig. 2 Stratigraphic column and sampling point locations



and together make up, by rock mass, 24.4–69.2%, in the upper Miocene and 12.6–42.8% in the Lower Pliocene.

The SiO₂, Al₂O₃, Fe₂O₃, MgO, P₂O₅, TiO₂, Cr₂O₃, ZrO₂, Rb₂O, ZnO and BaO contents prove to display a decrease in the lower Pliocene, compared to the upper Miocene, and the CaO appears to vary inversely to the above cited oxides and MgO.

The C-values [2] prove to range from 0.04 to 0.41, reflect a generally arid to semi-arid paleoclimate and Cu/Zn ratios [1, 3]. They also reflect oxygenated depositional conditions, except in samples A₈ and A₉, where the relevant values are indicative of suboxic and anoxic environments.

4 Conclusions

The following conclusions can be reached from this study.

- (1) The transition between Miocene and Pliocene sediments of the Amarna section is marked with a sudden appearance of an important content of smectite mineral (70%).
- (2) Unlike the upper Miocene, increased calcite, decreased kaolinite and quartz characterize the Trubi marls layers of the lower Pliocene, and suggest deepening during this interval.
- (3) The transition between the Miocene and Pliocene formations was marked with the occurrence of an abnormal content of celestine mineral, reflected by the important shift of SrO in the layer A₉ and an important content of sulphur in the same layer, along with a negative shift of Rb₂O.

References

1. Hallberg, R.O.: A geochemical method for investigation of palaeoredox conditions in sediments: Ambio, - *Special. Report* **4**, 139–147 (1976)
2. Jian, C., Ming, W., Yan, C., Kai, H., Lizeng, B., Longgang, W., Ying, Z.: Trace and rare earth element geochemistry of Jurassic mudstones in the northern Qaidam Basin, northwest China. -*Chemie der Erde* **72**, 245–252 (2012)
3. Mortazavi, M., Moussavi-Harami, R., Mahboubi, A., Nadjafi, M.: Geochemistry of the Late Jurassic-Early Cretaceous shales (Shurijeh Formation) in the intracontinental Kopet-Dagh Basin, northeastern Iran: implication for provenance, source weathering, and paleoenvironments. *Arab. J. Geosci.* **7**(12), 5353–5366 (2014)

Mineralogical and Geochemical Characterization of the Northern Phosphatic Series of the Sra-Ouertane Basin (Tunisia)

Naima Ahmadi, Ali Enneili, Mongi Felhi, Khaoula Kaissi, Fathi Ben Mabrouk, and Ali Tlili

Abstract

The phosphates lying across the Sra Ouertane area are generally classified as phosphates poor in P_2O_5 , in respect of those available in the central and eastern basins. Still, the setting up of an appropriate enrichment method could well help in enhancing the effective exploitation of such deposits. Among the enrichment associated methods, the flotation technique seems worth applying as a potentially yield enhancing strategy. The present work is aimed to characterize the phosphatic series, available across the Northern basin, by means of geochemistry and mineralogy, while considering a suitable treatment protocol fit for optimizing the yield's commercial and marketing potentials. Mineralogical studies of specimens sampled from geological sections of the phosphatic series and trenches, as implemented via X-ray diffraction, prove to reveal that these samples are predominantly composed of hydroxylapatite, calcite, quartz and feldspars. The geochemistry of major and trace elements, administered by means of X-ray fluorescence analyses, appear to indicate three remarkable enrichment in SiO_2 , Cr, U, Zn and CaO.

Keywords

Paleocene • Eocene • Northern Basin • Sra Ouertane
Mineralogy • Geochemistry • Phosphorites
Flotation

1 Introduction

Tunisia is one of the world's largest phosphates' producers, ranked fifth among the world's natural phosphate producers [2]. In the last seven years, the production of natural phosphates has decreased, reaching 3.5 million tons in 2016, which stands as a major enticement for the Tunisian and foreign companies to invest in mining and enrichment activities with low yield, mainly those associated with the Sra Ouertane mine. The phosphorites attached to this basin are concentrated mainly in the formation of Chouabine (Thanetian-Ypresian), [1, 3 and 4]. Several studies have been conducted to investigate this basin relating characteristics, through the examination of the relevant stratigraphy, mineralogy and geochemistry. In this context, the present study is devoted to investigate the Sra Ouertane basin associated phosphate series. It is focused on conducting a mineralogical (XRD) and geochemical (XRF) study of phosphorites, as observed through samples collected from a section and a trench of the Jebel Ayata site, in a bid to valorize the underlying ore and to recognize the Paleocene-Eocene paleoenvironment.

2 Materials and Methods

As part of this work, nine unweathered samples were collected from a trench made by the phosphate company of Sra Ouertane, at the Jebel Ayata site. After 48 h of oven drying and grinding, X-ray diffraction (XRD) was applied to identify each sample related mineral association. The relevant chemical analysis was performed by means of X-ray fluorescence (XRF).

N. Ahmadi (✉) · A. Enneili · M. Felhi · A. Tlili
Research Laboratory: GEOGLOB (LR12ES23), Faculty
of Sciences of Sfax, University of Sfax, Sfax, Tunisia
e-mail: naimaahmadi38@gmail.com

K. Kaissi · F. B. Mabrouk
Phosphates Company of Sra Ouertane, Sra Ouertane, Tunisia

© Springer Nature Switzerland AG 2019

D. M. Doronzo et al. (eds.), *Petrogenesis and Exploration of the Earth's Interior*,
Advances in Science, Technology & Innovation, https://doi.org/10.1007/978-3-030-01575-6_27

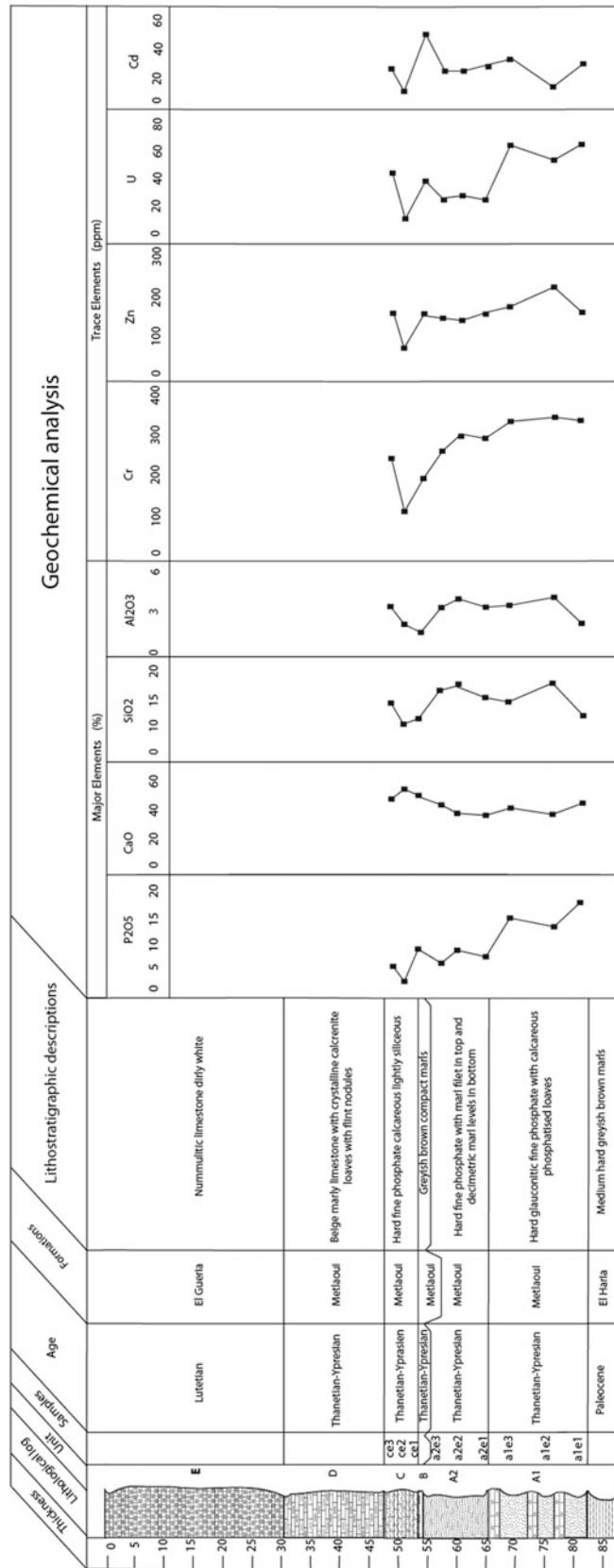


Fig. 1 Lithostratigraphic section of the Jebel Ayata phosphate series in the Sra Ouertane basin, highlighting the major and trace elements' related trends

3 Results

The X-ray fluorescence analysis, as applied on fractions of less than 2 μm (Fig. 1), proves to indicate that the P_2O_5 content appears to decrease starting from the base to the top of the series, reaching the highest content (18%) at the level of layer A1, with a relatively high content of carbonates (CaO) reaching the rate of (55%).

The couple ($\text{SiO}_2/\text{Al}_2\text{O}_3$) turns out to display the same tendency across the entirety of the series, displaying relatively low contents. The variation noticeable in trace elements proves to highlight that the phosphate series is rich in Cr. The maximum content of Zinc (Zn) is recorded at the level of layer A1. As for Cd and U, they prove to exhibit almost the same trend along the entire phosphate series.

The X-ray diffraction mineralogical analysis indicates well that the phosphate series is essentially composed of hydroxylapatite, calcite, quartz, feldspar and some clay minerals, in consistence with the geochemical-composition reached results, as determined via (XRF).

4 Conclusions

The present work is designed for the purpose of retracing the geochemical and mineralogical variations, as persisting in the Paleocene-Eocene series of the Sra Ouertane basin.

The conducted geochemical study relevant to the four units of phosphatic series, namely, A1, A2, B and C, proves to reveal that P_2O_5 appears to vary from a layer to another, reaching the maximum value (18%) at the level of layer A1. The variation noticeable in P_2O_5 is positively correlated with CaO, while no significant correlation has been noticed to persist with SiO_2 and Al_2O_3 . Noteworthy, Also, is that the analyzed phosphate series turns out to be rich in Cr and Zn. The mineralogical characterization, as implemented via XRD, has identified hydroxylapatite, quartz, feldspar, and calcite to stand as the main mineral constituents of the phosphate series.

References

1. Felhi, M., Tlili, A., Montacer, M.: Geochemistry, petrography and spectroscopy of organic matter of clay-associated kerogen of Ypresian series: Gafsa-Metlaoui phosphatic basin, Tunisia. *Resour. Geol.* **58**, 428–436 (2008)
2. Jasinski, S.M.: Phosphate rock, mineral commodity summary, January 2011. U.S. Department of the Interior, U.S. Geological Survey (2011)
3. Ounis, A.: Contribution of geochemistry of rare earths and isotopes for understanding the mechanisms of phosphatogenesis: example of the western part of the Gafsa-Métlaoui basin. Ph.D. thesis, Faculty of Sciences of Tunis, University of Tunis El Manar, Tunis, p. 198 (2011)
4. Zaïer, A.: Tectono-sedimentary evolution of the west-central Tunisian phosphate basin mineralogy, petrography, geochemistry and phosphorite genesis. Ph.D. thesis, University of Tunis II (1999)

Stable Isotope Geochemistry of the Pleistocene Lacustrine-Palustrine Carbonates (Borj Edouane Unit, NW Tunisia)

Naoufel Ghannem, Clemente Recio, Ildefonso Armenteros, and Kamel Regaya

Abstract

The Pleistocene carbonates of the Borj Edouane unit are made up of two principal facies associations: (1) calcrete-palustrine-laminar crust and (2) microbialites. The former represents the deposition in shallow lakes, as subjected to periodic exposure, while the second represents a steadier lacustrine environment. The isotopic analyses show singular high $\delta^{13}\text{C}$ values (up to 11.7‰) with respect to both associations, while most $\delta^{18}\text{O}$ values are constrained within the range comprised between -4.5 and -6.5 ‰. High $\delta^{13}\text{C}$ values are mainly affected by the predominance of carbon emanating from the dissolution of the underlying and surrounding Cretaceous rocks. Additional influences of photosynthetic activity of plant, especially associated with the microbialite association, and evaporation degassing could increase the heavier carbon isotope. The $\delta^{18}\text{O}$ related values prove to reflect a strong meteoric imprint.

Keywords

Isotopes • Microbialites • Palustrine • Calcrete • Pleistocene

1 Introduction

Stable isotopes in fluvial and lacustrine carbonates are used as paleoclimate proxies [1] carrying other paleoenvironmental indications. High $\delta^{13}\text{C}$ values are infrequent in fluvial and lacustrine carbonates [2], as only the lacustrine carbonate facies linked to sulphate-poor waters may produce diagenetic carbonates in a methanogenic environment and/or

in a highly-productive lake, resulting in positive $\delta^{13}\text{C}$ values [3]. In continental carbonates, the $\delta^{18}\text{O}$ values are mainly imposed by the meteoric water isotopic value and its related temperature, while the $\delta^{13}\text{C}$ values reflect the DIC origin in the fluids. They are also largely determined by the relative proportion of isotopically light CO_2 stemming from soil organic matter, and the heavier carbon originating from the dissolution of aquifer limestones [4]. A poor correlation of the $\delta^{13}\text{C}$ with the $\delta^{18}\text{O}$ values ($r < 0.5$) is a characteristic of open lacustrine systems: small variations of $\delta^{18}\text{O}$ and large changes in $\delta^{13}\text{C}$ have been observed in some open lakes.

2 Geological Setting

The continental carbonate unit of Borj Edouana (BEU, Mid-Late Pleistocene) crops out in the El Gara basin, northwest Tunisia (Lat. $35^\circ 57' - 35^\circ 55' \text{ N}$ and Long. $8^\circ 23' - 8^\circ 24' \text{ E}$) [5]. The El Gara basin forms an elliptical-shaped low high plain, lying between Sarrath, Mellegue and the Ezarga River, with a surface area of approximately 8 km^2 . Geologically, it is located at the transition between the central and northern Tunisian paleogeographic domains. The BEU occupies the central circular area of the Quaternary Gara basin, where it lies unconformably on Cretaceous rocks.

Several samples were collected along the stratigraphic succession for isotopic analysis purposes, selected to represent the different identified facies as well as the regional Cretaceous carbonates hosting the BEU.

The $\delta^{13}\text{C}$ and $\delta^{18}\text{O}$ isotopic ratios were determined with regard to some 10 mg samples, initially roasted on a plasma asher (to eliminate any organic content) on CO_2 liberated by acid attack (103% H_3PO_4) under vacuum, at 25°C [6]. The analyses were implemented on a dual-inlet SIRA-II mass spectrometer. Accuracy and average precision (± 0.02 ‰ for $\delta^{13}\text{C}$; ± 0.12 ‰ for $\delta^{18}\text{O}$) were monitored through repeated analyses of internal and international (NBS-19) reference materials. Results are reported in “delta” notation relative to PDB, as figuring on Table 1 and Fig. 1.

N. Ghannem (✉) · K. Regaya

Faculty of Science of Bizerte, University of Carthage, 7021 Zarzouna, Tunisia

e-mail: ghannemnaoufel@gmail.com

C. Recio · I. Armenteros

Salamanca University, 37071 Salamanca, Spain

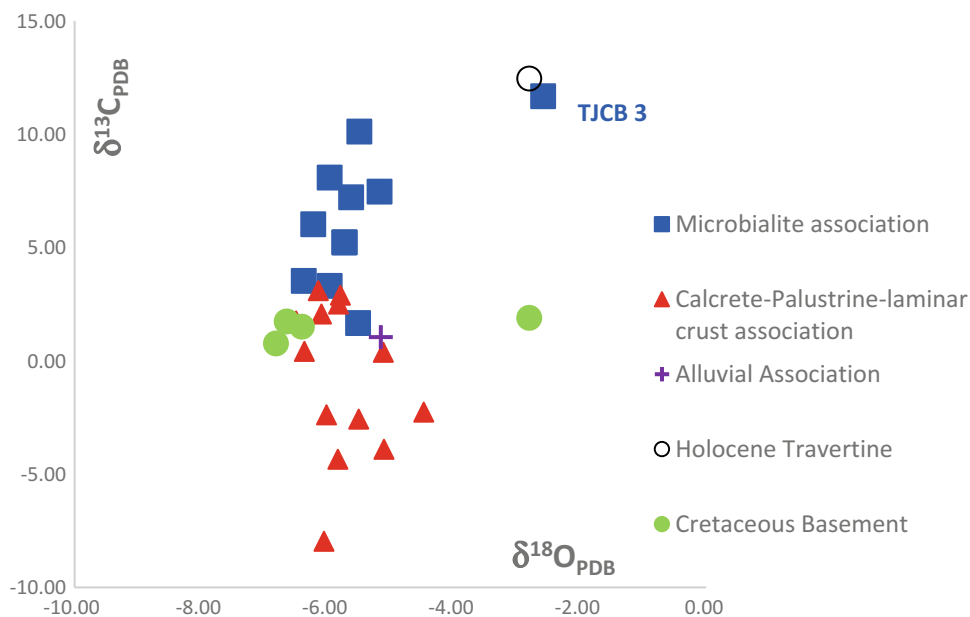
© Springer Nature Switzerland AG 2019

D. M. Doronzo et al. (eds.), *Petrogenesis and Exploration of the Earth's Interior*,

Advances in Science, Technology & Innovation, https://doi.org/10.1007/978-3-030-01575-6_28

Table 1 Mean isotopic values relevant to the studied sample groups

	$\delta^{13}\text{C}_{\text{PDB}}$	$\delta^{18}\text{O}_{\text{PDB}}$		$\delta^{13}\text{C}_{\text{PDB}}$	$\delta^{18}\text{O}_{\text{PDB}}$
	Microbialite association			Calcrete-palustrine-laminar crust association	
Av.	6.3	-5.5	Av.	-0.8	-5.8
$\pm 1\sigma$	3.0	1.0	$\pm 1\sigma$	3.4	0.6
Max	11.7	-2.6	Max	3.1	-4.5
Min	1.7	-6.4	Min	-8.0	-6.5
n	11	11	n	13	13
	Cretaceous basement			Alluvial association	
Av.	1.5	-5.7		1.05	-5.15
$\pm 1\sigma$	0.5	1.9			
Max	1.9	-2.8			
Min	0.8	-6.8		Holocene travertine	
n	4	4		12.46	-2.80

Fig. 1 $\delta^{13}\text{C}_{\text{PDB}}$ and $\delta^{18}\text{O}_{\text{PDB}}$ plot of lacustrine-palustrine carbonates from BEU, together with a Holocene Travertine and Cretaceous basement samples in the Gara Basin

3 Results

3.1 Facies

The BEU has a maximum thickness of 4 m. In the central-western area, the unit consists mostly of tabular beds of massive calcretes, palustrine limestones and laminar crusts, whereas in the unit's eastern part, lacustrine microbialite facies are dominant. The BEU carbonate facies are surrounded by alluvial facies, especially in the western and north-eastern margins. The alluvial association (sandstone and conglomerate facies, rich in Cretaceous carbonate clasts)

represents sedimentation in medial-distal alluvial fans. The BEU consists of two main facies groupings: (1) calcrete-palustrine-laminar crust association, and (2) microbialite association [7]. The former is mainly developed along the western and southern margins, associated with distal alluvial facies; it is also associated with microbialite facies (south margin). The calcrete facies reflect carbonate precipitation in surficial soils within shallow vadose-phreatic conditions; palustrine facies were typically deposited in shallow, low-slope and energy-carbonate lakes, subjected to drastic level changes. As for the laminar crusts, they represent a restricted sedimentation occurring in marginal puddles during severe dry conditions. The microbialite association

consists of oncolite facies, characterized with spherical laminated stromatolites and planar stromatolites. The oncolite facies are either massive, extending throughout the basin's central areas, or organized facies that extend along the eastern and south-eastern margins, associated with the planar stromatolites. Travertine-like facies occur in the southernmost corner in the form of transition facies towards planar stromatolites. Organized oncolite facies display transitional fluvial-lacustrine and marginal lacustrine areas, while the massive (oncomicrite texture) facies reflect calmer lacustrine conditions in the central areas. Planar stromatolites as occurring in the marginal lacustrine areas were probably nourished from springs. Abundant water supply and steady lacustrine conditions favored microbialite development.

3.2 Isotopes

The measured $\delta^{13}\text{C}$ and $\delta^{18}\text{O}$ values are those figuring on Table 1, and have been plotted on Fig. 1. The $\delta^{18}\text{O}$ values related to the microbialite association are quite similar to each other ($\delta^{18}\text{O}_{\text{PDB}} = -5.5 \pm 0.3\text{‰}$; $n = 11$; $\text{Max} = -2.6\text{‰}$, $\text{Min} = -6.4\text{‰}$), contrary to the $\delta^{13}\text{C}$ values ($\delta^{13}\text{C}_{\text{PDB}} = +6.3 \pm 5.0\text{‰}$; $n = 11$; $\text{Max} = +11.7\text{‰}$, $\text{Min} = -1.7\text{‰}$), which are very variable. An obvious outlier, corresponding to a reworked oncolite, has $\delta^{13}\text{C}_{\text{PDB}} = +11.7\text{‰}$, $\delta^{18}\text{O}_{\text{PDB}} = -2.6\text{‰}$, which is remarkably similar to that measured on a Holocene travertine ($\delta^{18}\text{O}_{\text{PDB}} = -2.8\text{‰}$; $\delta^{13}\text{C}_{\text{PDB}} = +12.5\text{‰}$). Samples attributed to the calcrete-lacustrine-laminar crust association behave in a similar way as the microbialite ones, with very close $\delta^{18}\text{O}$ values ($\delta^{18}\text{O}_{\text{PDB}} = -5.8 \pm 0.7\text{‰}$; $n = 13$; $\text{Max} = -4.5\text{‰}$, $\text{Min} = -6.5\text{‰}$) and noticeably variable $\delta^{13}\text{C}$ values ($\delta^{13}\text{C}_{\text{PDB}} = -0.8 \pm 2.5\text{‰}$; $n = 13$; $\text{Max} = +3.1\text{‰}$, $\text{Min} = -8.0\text{‰}$). Inversely, the Cretaceous basement displays similar C ($\delta^{13}\text{C}_{\text{PDB}} = +1.5 \pm 0.5\text{‰}$; $n = 4$) but bimodal $\delta^{18}\text{O}$ distribution, with three values within $\delta^{18}\text{O}_{\text{PDB}} = -6.6 \pm 0.2\text{‰}$ and a single value at $\delta^{18}\text{O}_{\text{PDB}} = -2.8\text{‰}$. The alluvial association's conglomerate exhibits a similar $\delta^{18}\text{O}_{\text{PDB}}$ (-5.15‰) and a slightly positive $\delta^{13}\text{C}_{\text{PDB}}$ value ($+1.05\text{‰}$), very close to that relating to the majority of basement samples. No obvious correlations are suggested by the plot of Fig. 1. Above all, there is a hint of an increasing trend of $\delta^{13}\text{C}$ with increasing $\delta^{18}\text{O}$ relevant to the microbialite association relating samples, while the opposite (decreasing $\delta^{13}\text{C}$ with increasing $\delta^{18}\text{O}$) is true in regard of the calcrete-palustrine-laminar crust association, though none of them seems to be statistically significant.

4 Discussion

Based on Table 1 and Fig. 1, it appears that most samples prove to display a large dispersion of $\delta^{13}\text{C}$ values, while the $\delta^{18}\text{O}$ related values seem to be constrained within a range of 2‰. It is obvious and intriguing that $\delta^{13}\text{C}$ relating values (positive) relevant to the microbialite association turn out to be high, and the values related to the calcrete-palustrine-laminar crust association (negative to slightly positive values) appear to be relatively high. On the other hand, the $\delta^{13}\text{C}$ values related to the area based Cretaceous limestones prove to be quite similar to each other within the range of $\pm 1.5\text{‰}$, while the $\delta^{18}\text{O}$ values prove to vary between ~ -3 and $\sim -6.5\text{‰}$. The measured values concerning the alluvial conglomerates, involving Cretaceous carbonate clasts, appear to bear similar $\delta^{13}\text{C}$ and intermediate $\delta^{18}\text{O}$ values (Fig. 1). The Uppermost Cretaceous carbonates pertaining to the Tethys realm are characterized with slightly positive $\delta^{13}\text{C}$ ($\sim +1/+3\text{‰}$) and slightly negative $\delta^{18}\text{O}$ ($\sim -1.5/-3.5\text{‰}$) data in [4] and [8], highlighting that the CRT 3 sample ($\delta^{13}\text{C} = +1.9\text{‰}$; $\delta^{18}\text{O} = -2.8\text{‰}$) represents primary sedimentary carbonate, while the other Cretaceous samples display the weathering effects. The current precipitation average values (IAEA's Cartago Station) are of a rate of $\delta^{18}\text{O} = -3.6\text{‰}$, but can be as low as -8.5‰ , and karstic groundwater in the nearby Teboursouk area displays an average $\delta^{18}\text{O}$ value of $-6.1 \pm 0.5\text{‰}$ [9], consistent with the oxygen values as measured on the weathered Cretaceous basement. It is highly likely, therefore, that the TDIC values persisting in the waters draining into the Gara Basin display isotopic values quite similar to $\delta^{13}\text{C} = +1.5\text{‰}$; $\delta^{18}\text{O} = -6.5\text{‰}$. Evaporation of the standing water mass, likely coupled with a rise in temperature, favored CO_2 degassing and the precipitation of lacustrine carbonates. Originally, available HCO_3^- reflected the predominance of a regional Cretaceous carbon source produced by carbonate weathering. Once within the basin, however, this matter was modified by in situ processes. Indeed, in Pleistocene stromatolites of the African Rift lakes, high $\delta^{13}\text{C}$ values of up to 5‰ have been attributed to the preferential use of light carbon by microbes during the photosynthesis, likely to engender a relative ^{13}C -enrichment of the surrounding TDIC and subsequent precipitation of ^{13}C -enriched calcite [10]. The high value of $\delta^{13}\text{C}$ for TJCB 3, together with a similar trend in the $\delta^{18}\text{O}$ are consistent with an intense degassing process. Some samples (calcrete-palustrine-laminar crust) with $\delta^{13}\text{C}$ lower than the postulated water TDIC, but similar to $\delta^{18}\text{O}$ (i.e., OT3, C1) are likely to record an increased contribution of respired CO_2 . In the calcrete-palustrine

setting, however, the relative importance of regional runoff, as compared to in situ processes, turns out to be lower. Evaporation is also a factor that results in a progressively higher $\delta^{18}\text{O}$ value. Still, TDIC is no longer dominated by carbonate dissolution, and an important contribution of isotopically light respired CO_2 becomes evident, driving $\delta^{13}\text{C}$ towards lighter values. Obviously, the less the water proportion is (higher evaporation and higher $\delta^{18}\text{O}$ value), the larger the proportional contribution of respired CO_2 is, and therefore, the lower the $\delta^{13}\text{C}$ value turn out to be.

5 Conclusions

The Pleistocene carbonate BEU consists of calcrite-palustrine-laminar crust and microbialite associations representing, respectively, shallow lakes with intermittent level falls and permanent lakes. Singular high $\delta^{13}\text{C}$ values have been recorded (up to 11.7‰), and most of the $\delta^{18}\text{O}$ associated values are constrained to the range between -4.5 and -6.5 ‰. High $\delta^{13}\text{C}$ values are attributed to the predominance of carbon derived from the dissolution of the regional Cretaceous rocks, with additional effects resulting from photosynthetic activity, especially in the case of the microbialite association, and degassing by evaporation. The $\delta^{18}\text{O}$ associated values are consistent with a meteoric imprint set averages.

References

- Leng, M.J., Marshall, J.: Palaeoclimate interpretation of stable isotope data from lake sediment archives. *Quaternary Sci. Rev.* **23** (7–8), 811–831 (2004)
- Utrilla, R., Vázquez, A., Anadón, P.: Paleohydrology of the Upper Miocene Bicorn Lake (eastern Spain) as inferred from stable isotopic data from inorganic carbonates. *Sed. Geol.* **121**(3–4), 191–206 (1998)
- Talbot, M.R., Kelts, K.: Paleolimnological Signatures from Carbon and Oxygen Isotopic Ratios in Carbonates, from Organic Carbon-Rich Lacustrine Sediments: Chapter 6. In: Katz, B.J., Rosendahl, B.R. (eds.), *Lacustrine Exploration: Case Studies And Modern Analogues*. Mem. Am. Ass. petrol. Geol., **50**, 99–112 (1991)
- Andrews, J.E.: Palaeoclimatic records from stable isotopes in riverine tufas: Synthesis and review. *Earth Sci. Rev.* **75**(1–4), 85–104 (2006)
- Ben Haj Ali, M., Jédoui, Y., Dali, T., Bensalem, H., Memmi, L.: *Carte géologique de la Tunisie au 1/500 000*. Service des Mines, de l'Industrie et de l'Énergie, Tunis, Tunisie (1985)
- Craig, H.: Isotopic standards for carbon and oxygen and correlation factors for mass spectrometric analysis of carbon dioxide. *Geochim. Cosmochim. Acta.* **12**, 133–149 (1957)
- Ghannem, N., Armenteros, I., Riahi, C., Regaya, K.: The lacustrine carbonate in the El Gara basin (Mid-Late Pleistocene, NW Tunisia). *Sociedad Geologica de España, Geo-Temas* **16**(2), 621–624 (2016)
- Elkhazri, A., Abdallah, H., Razgallah, S., Moullade, M., Kuhnt, W.: Carbon-isotope and microfaunal stratigraphy bounding the Lower Aptian Oceanic Anoxic Event in northeastern Tunisia. *Cretac. Res.* **39**, 133–148 (2013)
- Ayadi, Y., Mokadem, N., Besser, H., Khelifi, F., Harabi, S., Hamad, A., Hamed, Y.: Hydrochemistry and stable isotopes ($\delta^{18}\text{O}$ and $\delta^2\text{H}$) tools applied to the study of karst aquifers in southern Mediterranean basin (Teboursouk area, NW Tunisia). *J. Afr. Earth Sc.* **137**, 208–217 (2018)
- Casanova, J., Hillaire-Marcel, C.: Late Holocene hydrological history of Lake Tanganyika, East Africa, from isotopic data on fossil stromatolites. *Palaeogeogr. Palaeoclimatol. Palaeoecol.* **91**(1–2), 35–48 (1992)



Geochemistry and Mineralogy of Paleocene-Eocene Depositional Sequences in Oued Thelja Section, SW Gafsa, Tunisia

Ali Enneili, Hadj Ahmed Amel, Mongi Felhi, Kamel Zayani, Nabil Fattah, and Ali Tlili

Abstract

The Paleocene-Eocene series associated with the Oued Thelja area is characterized with the diversity of depositional environment, evolving from sebkha to deep marine environment. This evolution is related to the occurrence of various rock types during the Paleocene-Eocene interval such as evaporates, carbonates, clays and phosphates. The mineralogical results reached by means of X-ray diffraction appear to reveal that marine transgression characterizing the El Haria and Chouabine Formations turns out to be dominated with clay minerals, carbonate-fluorapatite and calcite, which require the availability of a deep marine environment to precipitate. As for marine regression, it is represented essentially by gypsum and dolomite, indicating the existence of a shallow marine environment marking out the Thelja Formation. The geochemical results, as provided through X-ray fluorescence, appear to highlight an enrichment of SiO₂, P₂O₅ and CaO during marine transgression, and high amounts of SO₃, CaO and MgO during decreasing sea level. The stratigraphic framework

relevant to the studied section helps determine eleven third-order depositional sequences, each containing a set of sedimentary system tract. The geochemistry and mineralogy should explain the occurrence of depositional sequences and eustatic variations relevant to each sedimentary basin.

Keywords

Paleocene-Eocene series • Mineralogy • Geochemistry • Depositional sequences • Sedimentary systems tract • Eustatic variation

1 Introduction

In the Gafsa-Metlaoui basin, the Paleocene-Eocene interval is essentially characterized with the predominance of evaporates, phosphates, carbonates, clay deposits and some other silicate phases. Several studies appear to be interested in investigating the Paleocene-Eocene series, such as stratigraphy, sedimentology, geochemistry and mineralogy [5, 6]. The stratigraphic framework accomplished by El Ayachi et al. [3] reveals the occurrence of a wide range of depositional sequences and depositional environment. In the Gafsa basin, the related mineralogy and geochemistry are thoroughly studied, but without any association being made with sequence stratigraphy. The present work is focused on highlighting the Paleocene-Eocene series persistent in the Oued Thelja section (SW Gafsa), in a bid to investigate the predominant mineralogical and geochemical variations prevailing during sea level fluctuations and depositional sequences.

A. Enneili (✉) · H. A. Amel · M. Felhi (✉) · A. Tlili
Laboratory GEOGLOB, Department of Earth Sciences,
Faculty of Sciences, Sfax University, 3029 Sfax, Tunisia
e-mail: enneiliali@gmail.com

M. Felhi
e-mail: mongi_felhi@yahoo.fr

H. A. Amel
e-mail: hadjahmed_amel@yahoo.fr

A. Tlili
e-mail: alitlili@yahoo.fr

K. Zayani · N. Fattah
Metlaoui Research Center, Gafsa Phosphates Company,
2130 Metlaoui, Tunisia
e-mail: zayanikamel@yahoo.fr

N. Fattah
e-mail: nabil.fattah@cpg.com.tn

© Springer Nature Switzerland AG 2019

D. M. Doronzo et al. (eds.), *Petrogenesis and Exploration of the Earth's Interior*,
Advances in Science, Technology & Innovation, https://doi.org/10.1007/978-3-030-01575-6_29

2 Materials and Methods

Some sixty-seven samples were collected across the Oued Thelja section. They are distributed as follows: 4 samples from the El Haria Formation, 37 from the Thelja Formation, and 26 samples belong to the Chouabine Formation. These samples involve clay, carbonate, evaporate and phosphate facies. The various rock types are studied to understand the evolution noticeable in both sea level and depositional sequences. A geochemical study was implemented by means of X-rays fluorescence XRF with Thermo scientific device of a type Niton FXL FM-XRF Analyzer, available in the Earth Sciences Department at the Faculty of Sciences in Sfax. This method has been applied in order to determine the chemical elements constituting the bulk rock. The mineralogical analyses were performed via a P-Analytical (X'Pert PRO X-ray) diffractometer sited at the Metlaoui research center of the Gafsa Phosphate Company and operable at 40 kV/40 Ma, using a $\text{CuK}\alpha$ radiation source.

3 Results

3.1 Mineralogy

The XRD patterns of the bulk-rock samples, as collected from the Oued Thelja section, have displayed a composition predominantly involving different rates of carbonate-fluorapatite, clay minerals (smectite, sepiolite, palygorskite, illite and kaolinite), calcite, dolomite, clinoptilolite, gypsum, celestite, quartz and opal CT (Cristobalite/Tridymite) (Fig. 1). This mineral assemblage corroborates that documented in a number of previously conducted studies [4, 5]. The strongest manifestation reflections of these minerals appear at the rates of 2.79, 4.46, 3.03, 2.89, 7.56, 2.97, 3.34, and 4.09 Å, respectively.

3.2 Geochemistry

The SiO_2 appears to display a positive correlation with Al_2O_3 (Fig. 1). Its highest amount is detected in both of the El Haria and Chouabine Formation. The highest amounts of MgO and CaO are essentially recorded with regard to the Thelja Formation. The noticeable MgO variation proves to reveal a positive correlation with CaO (Fig. 1). Within the Chouabine Formation, the geochemical study reveals a high percentage of P_2O_5 exceeding 20%. The P_2O_5 variation exhibits a positive correlation with CaO. The most important SO_3 contents are recorded in the Thelja Formation,

indicating a high occurrence rate of gypsum. As for trace elements, the set of Paleocene-Eocene series is marked by significant richness in Zn, Cr, Cl, Cd, Zn and U, whose contents prove to exceed the average rates documented by Altschuler [1].

3.3 Depositional Environment

The paleocene-Eocene relevant to the Oued Thelja series is characterized with multiple depositional environments, which are related to facies variety. The facies analysis indicates that El Haria and Chouabine Formation correspond to deep marine environment. Thelja Formation represents an evolution from lagoon environment to sebkha.

3.4 Sequence Stratigraphy

In Oued Thelja section, the stratigraphic framework appears to display a relative similarity with a previous study conducted by El Ayachi et al. [3], that helped define eleven third-order depositional sequences. The El Haria Formation corresponds to one sequence occurring during marine transgression. The Thelja Formation is subdivided into four sequences. These depositional sequences prove to reveal a decrease in sea level. As for the Chouabine Formation, it consists of six depositional sequences displaying a transgressive trend.

4 Discussion

The dynamic depositional model and the stratigraphic framework relevant to the Oued Thelja section is mainly represented by evolution from a shallow to a deep marine environment, in addition to a set of depositional sequences [3]. This observation is confirmed by the relating mineralogical and geochemical data (Fig. 1). The clay minerals, as observed in El Haria Formation, are recognized by the positive correlation between SiO_2 and Al_2O_3 ($r = 0.79$). They suggest marine transgression, where high amounts of SiO_2 prove to persist. The abundance of gypsum and dolomite in the Thelja Formation characterize the marine regression. The decrease in sea level, corresponding to a high system tract, is manifested by an increase in the SO_3 , CaO and MgO contents. The high amounts of MgO help indicate the occurrence of dolomite, and the positive correlation between CaO and MgO ($r = 0.87$) highlights that both elements proved to predominantly pertain to dolomite [5]. The gypsum precipitation proved to occur

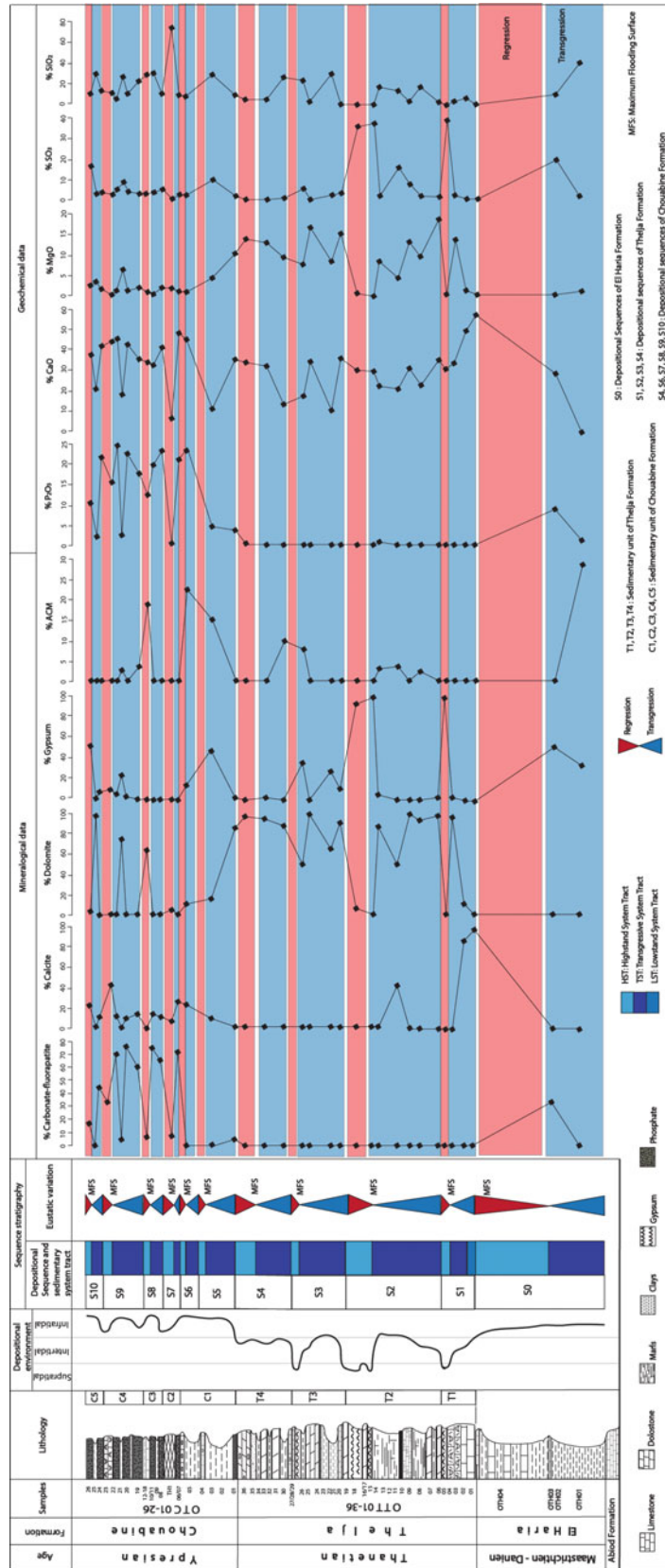


Fig. 1 Mineralogical and geochemical variations according to eustatic fluctuations

under an arid climate, when water became hypersaline [2], in restricted lagoon [6]. Concerning the Chouabine Formation, the depositional environment is essentially characterized with the predominance of carbonate-fluorapatite, calcite, clay minerals and opal C/T. Such mineral phases appear to prevail essentially across transgressive intervals. Transgressive system tracts are recognized through high P_2O_5 , CaO and SiO_2 rates.

5 Conclusions

The geochemistry and mineralogy of the depositional sequences (Paleocene-Eocene) persistent in Oued Thelja has its explanation in the stratigraphic framework and the evolution of eustatic cycles. The increasing of sea level, which occurs in transgressive system tract (TST), is represented by the abundance of calcite, carbonate-fluorapatite and clay mineral. They are associated to high amounts of CaO, P_2O_5 and SiO_2 . The amounts of P_2O_5 and SiO_2 are very weak during marine regression. The decrease of sea level period is marked by occurrence of CaO, MgO and SO_3 characterizing the dolomite and gypsum minerals phases. These minerals represent the highstand system tract (HST) in depositional sequence.

References

1. Altschuler, Z.S.: The geochemistry of trace elements in marine phosphorites; part I. Characteristic abundance and enrichment. *SEPM Special. Publication* **29**, 19–30 (1980)
2. Daraei, M., Amini, A., Ansari, M.: Facies analysis and depositional environment study of the mixed carbonate-evaporate Asmari Formation (Oligo-Miocene) in the sequence stratigraphic framework, NW Zagros. Iran. *Carbonates Evaporates* **30**, 253–272 (2015)
3. El Ayachi, M.S., Zagarni, M.F., Snoussi, A., Bahrouni, N., Gzam, M., Ben Assi, I., Hammami, K., Abdelli, H., Ben Rhaiem, H.: The paleocene-lower eocene series of the Gafsa basin (South-Central Tunisia): integrated stratigraphy and paleoenvironments. *Arab. J. Geosci.* **9**, 395 (2016)
4. Felhi, M., Saidi, R., Fattah, N., Tlili, A.: Textural evidences for dissolution of silica-rich rocks of the Ypresian phosphatic series, Gafsa-Metlaoui basin, southwestern Tunisia: implication of biogenic silica supply on genesis of fibrous clays. *Arab. J. Geosci.* **9**, 695 (2016)
5. Garnit, H., Bouhlel, S., Jarvis, I.: Geochemistry and depositional environments of Paleocene-Eocene phosphorites: Metlaoui Group, Tunisia. *J. Afr. Earth Sci.* **134**, 704–736 (2017)
6. Jomaa Salmouna, D., Chaabani, F., Dhahri, F., Mzoughi, M., Salmouna, A., Bessaies Zijlstra, H.: Lithostratigraphic analysis of the Turonian–Coniacian Bireno and Douleb carbonate Members in Jebels Berda and Chemsî, Gafsa basin, central-southern Atlas of Tunisia. *J. Afr. Earth Sci.* **100**, 733–754 (2014)

Mineralogical and Geochemical Characterization of the Tamerza Area Upper Lutetian-Priabonian Successions (Southwest Tunisia)

Samiha Euch, Mongi Felhi, Nabil Fattah, and Ali Tlili

Abstract

The Upper Lutetian-Priabonian series (Seugd Formation), lying in the Tamerza area (southwestern Tunisia) is commonly represented by two facies, composed mainly of dolomite and gypsum. In this context, the present work is aimed to determine the mineralogy and geochemistry relating to two sampled sections, characterized with distinguished lithology and thickness, in a bid to follow the facies featuring distribution. The systematic specimen of Great Cluse (GC) and Little Cluse (LC) sections were investigated by means of X-ray diffraction (XRD), and Fluorescence X (XRF). The obtained data prove to indicate that the samples pertaining to the Little Cluse (LC) section are mostly made up of dolomite with an obvious prevalence of palygorskite minerals lying on the top. As for the Great Cluse (GC) section associated samples, they turn out to be predominantly composed of dolomite persisting at the lower part, and gypsum predominating the upper part. These mineralogical constituents are confirmed through geochemical analyses, whereby, both of the Little Cluse (LC) as well as the Great Cluse (GC) sections respective samples appear to display remarkable amounts of CaO and MgO. The upper part of the Great Cluse (GC) section related samples proved to reveal that they are characterized with the persistence of high SO₃ amounts. Both of the sections, under review, are separated with the N120 fault, which seems to contribute remarkably in the facies' noticeable thickening and distinguishable distribution.

Keywords

Upper Lutetian-Priabonian series • Facies variation • Dolomite • Gypsum • Palygorskite

S. Euch · M. Felhi (✉) · A. Tlili
Sfax University, 3029 Sfax, Tunisia
e-mail: mongi_felhi@yahoo.fr

N. Fattah
Gafsa Phosphates Company, 2130 Metlaoui, Tunisia

1 Introduction

The Tunisia lying upper Lutetian-Priabonian successions are distinctive for their attached litho-facies' variations, stretching northward from the south. They are marked with a shift that transcend laterally, from a facies of an evaporitic type in the south, to a deep type of facies lying northwards. In the northern section, the series are characterized with the predominance of thick clay and limestone sequences, dubbed Souar Formation [1, 2]. In central Tunisia, such series are predominantly made up of limestone-marl alternations, as identified by [3] persisting, mainly, within the Jabel Cherahil mount and the Cherahil Formation. Noteworthy, however, is that even though the upper Lutetian-Priabonian successions are mainly of an evaporitic character in the Gafsa-Metlaoui basin, they turn out to be characterized with prevailing litho-facies variation, locally in the Tamerza area, where a completely dolomitic sequence outcrops remarkably. In this context, the present work is focused on identifying and monitoring the laterally trending shift, in terms of litho-facies of upper Lutetian-Priabonian succession, by relying on mineralogical and geochemical studies.

2 Geological Setting Lithological Description

The Tamerza area is located in the southwestern part of Tunisia, at the joint crossing of the 34° 3'N latitude and 7° 9'E longitude. The local outcropping deposits marking the area are almost closely similar to those observed across the Gafsa Metlaoui basin, corresponding mainly to anticlines [4, 5]. These deposits originally stem from the top Campanian-Maastrichtian successions, to end up in the Mio-plio-quadernary deposits [2, 4]. For the purpose of examining the vertical/lateral litho-facies' variation characterizing the upper Lutetian-Priabonian deposits, as lying across the Tamerza area, a meticulous investigation has been

implemented. Actually, it concerns two sections (the Little Cluse (LC) section, and the Great Cluse (GC) one), limited at the bottom with the massive limestones of the Kef Eddour Formation, and at the top with the Beglia sandstone Formation, as often widely defined by several authors [2, 4]. The 70 m thick (LC) section is alternatively composed of massive dolomite as well as fractured and rich silica nodules of flint silica. As for the (GC) section, it is rather thick (100 m), as explained by the bottom lying dolomite, overlain by thick evaporitic series at the top. As an outcome of such an exploration, the mapping turns out to display vertical and lateral types of facies' marking variations.

3 Materials and Methods

Detailed in situ field works were executed in the Tamerza and Midess areas. The systematic sampling and mapping were predominantly centered on the key lithologic outcrop sections. This lithology includes dolomite, gypsum, dolomitic limestones and clays. Actually, 43 samples, covering the upper Lutetian-Priabonian series, were collected, then, analyzed by means of X-ray diffraction measurement [3]. The chemical analyses were carried out via the X-ray fluorescence method, where only 28 specimen were selected from two sections based on mineralogical analysis. The samples related ignition loss was measured in terms of calcinations at 1000 °C.

4 Results and Discussion

4.1 Mineralogical Analysis

The XRD drawn data proved to indicate that the Little Cluse (LC) section sampled specimen are mainly composed of

dolomite, calcite, quartz, mineral clay (palygorskite), feldspars, opal CT (Cristobalite-Tridymite) and halite. Their highest reflexion rates appear at the levels of 2.88; 3.03; 3.34; 4.49; 3.18; 4.11 and 2.82 Å, respectively. As for the XRD data regarding 20 Great Cluse (GC) section collected samples, they appeared to reveal that the area predominant bulk rock is essentially made up of dolomite, gypsum, calcite, quartz, clay minerals, opal CT, feldspars, halite and anhydrite. Their characterizing reflexions is more conspicuously apparent at the levels of 2.88; 7.59; 3.03; 3.34; 4.49; 4.11; 3.20; 2.82 and 3.49 Å respectively (Fig. 1).

4.2 Chemical Composition

The chemical analysis, as implemented on the (LC) samples, turn out to exhibit high CaO and MgO rates. These oxides correspond to the main constituent of dolomite, although the two samples' displayed levels appear to highlight the dominance of calcite (LC15 and LC17 samples), which coincides with the lithological description of the (LC) section. The main trace elements detected to persist at the (LC) section level turn out to be: strontium, the content of which appears to vary from 74.07 to 249.47 ppm, and manganese, the highest content of which is of the rate of 205.68 ppm, detected to prevail at the bottom of the section. In the (GC) section related sample, however, the CaO contents proved to fluctuate between 15 and 33%, while the maximum MgO content rate recorded is approaching 17%, particularly noticeable at the very bottom part of the studied section. Contrary to the LC samples, the upper part relating samples proved to reveal the persistence of a high amount of SO₃. Such findings turn out to be congruent with the lithological facies subject of analysis, in which gypsum levels prove to predominate the upper part. The trace elements' Chemical analysis, concerning the (GC) associated samples,

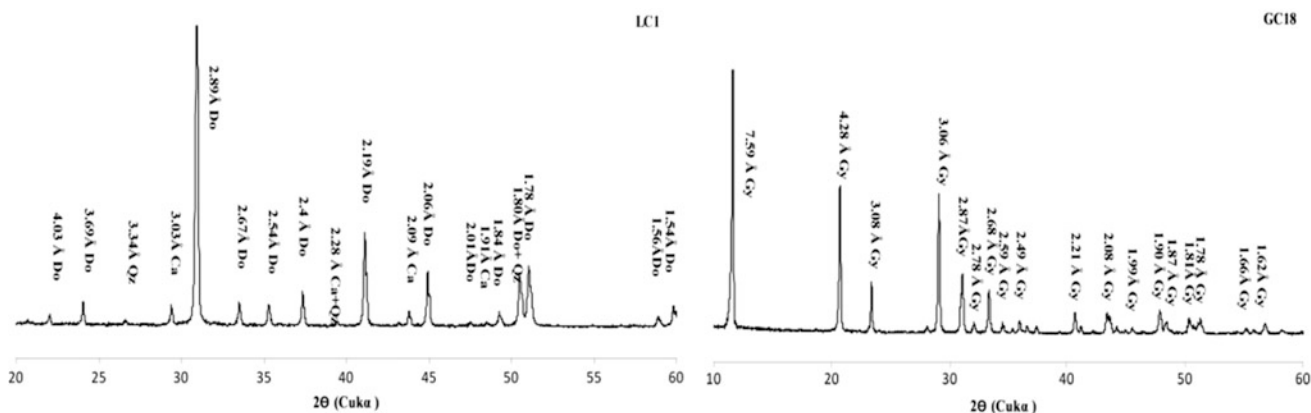


Fig. 1 X ray diffraction (Cu α radiation) of the Little Cluse section bulk rock samples (LC1); (Do: dolomite; OCT: opal CT; Qz: quartz), and sample (GC18) of the Great Cluse section (Gy: gypsum)

Table 1 Geochemistry of bulk rock specimen (relevant to the LC1 sample of the Little Cluse section, and to sample GC18 of the Great Cluse section)

Samples	SiO ₂	Al ₂ O ₃	Fe ₂ O ₃	SO ₃	P ₂ O ₅	TiO ₂	CaO	MgO	K ₂ O	Cl ₂	LOI	Total
LC1	1.40	0.18	0.05	0.84	ND	0.02	34.71	15.26	0.06	0.02	46.05	98.59
GC18	3.15	0.89	0.23	57.36	ND	0.04	29.58	5.12	0.18	0.01	23.9	90.21

proved to record high strontium values, ranging between 112.1 and 19147.25 ppm. Such finding may well have its explanation in the geode of celesto barite, as noticed to prevail at the bottom level of the section (Table 1).

The analyzed samples associated chemical composition proves to agree, congruently, with the relating mineral composition. Indeed, the examined samples proved to display rather high amounts of CaO and MgO, highlighting that the section under review turns out to be predominantly composed of dolomite. Inversely, however, the Great Cluse (GC) section turns out to be characterized with a prevailing vertical facies' variation. Principally, the relating samples appear to enclose dolomite at the bottom base level, and gypsum at the top level.

5 Conclusions

The reached findings prove to indicate that the upper Lutetian-Priabonian, as lying in the Tamerza area, appears to be characterized with the predominance of lateral and vertical variations marking the underlying facies, noticeable even at local levels. Such a locally persistent change is confirmed and justified by the administered mineralogical and geochemical analyses relevant to both of the studied

sections. The persistence of gypsum, immediately following the westward trending N-120, seems to indicate well that this fault could certainly be controlled locally in the Tamerza area, highlighting that the thickening and litho-facies marking variation appears to be of Seugdal Formation.

References

1. Arnould, M.: Explanatory note of the geological map at the scale of 1/50 000 Tunisia, sheet N° 22, Menzel bouzelfa. *Ann. Geolo. Tunis*, 31p (1950)
2. Burolet, P.F.: Contribution to the stratigraphic study of Central Tunisia. Thesis Doct. Es-Sciences Paris. *Annales of Mines and Geology, Tunis*, No. 18, 350p (1956)
3. Comte, D., Dufaure, P.: Some precisions on tertiary stratigraphy and palaeo-geography in central and central southeastern Tunisia from Cape Bon to Mezzouna. *Deliv. Jub. M. Solignac Ann. Min. Geol. Tunisia* **26**, 241–256 (1973)
4. Ahmadi, R. Utilisation des marqueurs morphologiques, sédimentologiques et microstructuraux pour la validation des modèles cinématiques de plissement. Application à l'Atlas méridional tunisien. Université de Nantes, 215p (2006)
5. Felhi, M., Saidi, R., Fattah, N., Tlili, A.: Textural evidences for dissolution of silica-rich rocks of the Ypresian phosphatic series, Gafsa-Metlaoui basin, southwestern Tunisia: implication of biogenic silica supply on genesis of fibrous clays. *Arab. J. Geosci.* **9**, 695 (2016)

Potential Heavy Mineral-Enriched Black Sand Deposits South Ras Banas Red Sea Coast (Egypt)

Tarek Ibrahim, Gouda Dabour, Minghua Ren, Gad El-Qady, Philip Goodell, Ibrahim Gaafar, Luis Sandoval, and Munazzam Ali

Abstract

The Red Sea Coast in the southernmost part of Egypt is characterized with an early geological history of erosion and sediment transportation through a remarkably long and wide paleo-channel. Several alluvial deposits rich in economic heavy minerals have been identified along the coastal strip lying between Ras Banas and the Sudanese border. Accumulations of heavy minerals have been observed along the Red Sea beaches sited at Ras Manazel, Khudaa, Shalateen and Wadi Diit. These deposits have been formed not only by transport processes related to the Red Sea offshore currents, but also by the drainage networks operating in the Eastern Desert of Egypt. Satellite imagery of the drainage networks indicates that the granites of the Sudanese highlands are the source origin of these minerals, with minor input from granites in the southern Egyptian highlands. Inland deposits emanating from the Red Sea current coastline have been formed before the opening of the Red Sea, and subsequent erosion and reworking through flash flooding and other catastrophic transport mechanisms has created more recent deposits along the current coastline. The deposits lying across the study area prove to contain ilmenite, magnetite, rutile, garnet, zircon and monazite, along with some radioactive minerals such as thorite with traces of gold. These mineral compositions are of high quality and match with those related to the granites persisting in Sudan and southern Egypt, as observed through the satellite imagery. The mineral concentrations and

compositions appear to reflect the ilmenite granite series of Sudan and the magnetite granite series of the Egyptian Eastern Desert as derivative resources.

Keywords

Red sea fans • Flash flooding • Weathering
Transportation • Black sand • Economic mineral resources

1 Introduction

Although the delineation of new heavy-mineral deposits available in Egypt displays high potential objectives, the Red Sea coastline remains unexplored in regard of such deposits. The Egyptian black sand deposits are present in the form of either beach sediments, or coastal sand dunes lying along the Mediterranean Sea coast. Not until recently that some exploration activities have been carried out on the beach placers lying along the Red Sea coast, from Ras Banas in Egypt to the Sudanese border [1, 2]. These activities were intended to assess the available reserves of ilmenite, rutile and zircon. Many of these deposits, mainly the alluvial fans of wadi Keraf & Diit (Fig. 1), are lying on the Red Sea Coast about 70 km south of the Shalateen City. These deposits originated with the successive sediments transported during flood days, through W. Keraf and its extensions in the Sudanese high land.

The delta, subject of investigation, displays a triangular shape, with its apex trending nearly in the southwest direction at the mouth of W. Keraf & Diit, while its base represents the Red Sea Shoreline. It is extending over about 38 km, trending nearly NW–SE, while, with an average height of about 25 km, covering an area of about 275 km² of sediments. The objective of this study consists in evaluating these sediments' mineralogical potential and identifying their economic aspects.

T. Ibrahim (✉) · G. Dabour · I. Gaafar
Nuclear Materials Authority, Cairo, Egypt
e-mail: elsahabi@yahoo.com

M. Ren
University of Nevada-Las Vegas, Las Vegas, USA

G. El-Qady
National Research Institute of Astronomy and Geophysics,
Cairo, Egypt

P. Goodell · L. Sandoval · M. Ali
University of Texas at El Paso, El Paso, USA

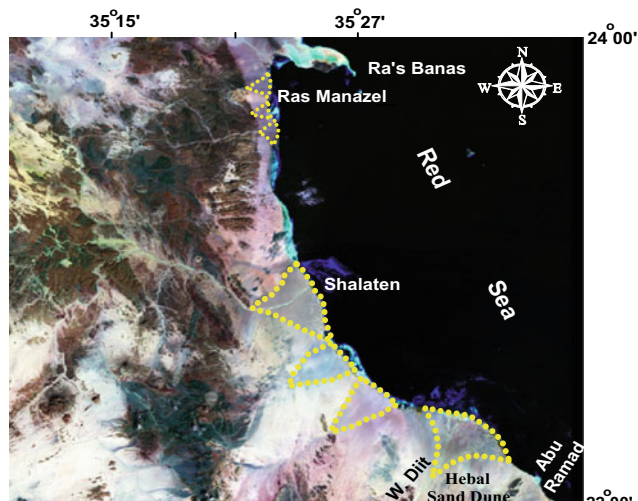


Fig. 1 Google Earth map shows the location of W. Keraf & Diit Delta. (Coastal alluvial fans along the foot-slopes of the mountains of the Red Sea, Egypt)

2 Materials and Methods

Thirty soil samples were collected along six profiles covering the entire delta (lying between $36^{\circ} 00' 26''$ – $36^{\circ} 17' 30''$ E and $22^{\circ} 29' 00''$ – $22^{\circ} 40' 55''$ N), using an auger sampler to a depth of about one meter. The collected samples were dried and weighed about 10 kg. They were, then, subjected to preparation in order to be ready for the different investigations. Sand grains and finer sizes represent the main constituents in these sediments (up to 95%).

A representative sample weighing about 400 mg of sand and finer sizes, drawn from each sample, is prepared to be ready for the different analyses. Each sample is divided into two halves, one for a grain-size analysis, and the other for mineralogical investigation, starting from magnetite separation, followed by heavy liquids separation using both Bromoform (2.8) and then Methylene Iodid (3.3). The obtained fractions, enclosing all the heavy economic minerals, will be subjected to microscopic examination to identify their relating economic potential.

3 Results

The frequency of the different sand fractions was computed with respect to each single sample, and the reached results are depicted on Table 1. For the mineralogical investigation

to be implemented, the medium, fine and very fine sized sand fractions were subjected to heavy liquid separation. The study was initiated with magnetite separation, followed by heavy liquids separation, using Bromoform (2.8) and then Methylene Iodid (3.3) as figuring on Table 2. The ilmenite represents the main constituent persisting in the heavy mineral fractions belonging to the delta of Wadi Keraf & Diit, in which it represents up to 50% of the total economic minerals.

4 Discussion

The presence of zircon and some other high valuable rare metals made it necessary to check the chemical analyses of these minerals. Some diagnostic polished thin sections, representing the different fractions of the economic separates from Delta W. Keraf & Diit, were prepared for the micro-analysis. More than 1000 spot analyses among the ilmenite and other valuable mineral crystals were analyzed in the microprobe-lab, made available at the Geological Science Department, University of Nevada, Las Vegas (UNLV), USA.

The micro-analysis data are grouped and processed statistically for each single mineral to obtain its related potential marketing specifications. The processed microprobe analyses prove to show that 66.17% of the ilmenite contains from 50 to 52% TiO_2 while 10.41% from the ilmenite contains from 52 to 54% TiO_2 . Generally, the average TiO_2 content persistent in the ilmenite is up to 50.5%, while the major percentage of FeO content in the ilmenite proves to range from 44 to 47%. On the other hand both of the Chromium and Niobium contents are less than 0.05%, highlighting that the studied ilmenite is of high quality and conveniently fit for marketing purposes, particularly for use in the white-painting industry and other industrial applications.

Zircon represents an average of 0.02% among the economic separates of the studied area. The Zircon associated analysis reveals that the majority of the zircon crystals contain about 65% zirconium, while the most of them contain about 34% SiO_2 which testifies the availability of high-quality zircon. The analyzed ilmenites (349 separate grains) reveal that the ilmenites contain numerous exsolution lamellae of magnetite. The analyzed magnetite samples (170 separate grains) prove to reveal significant rates of carbonate and titanite inclusions. In addition, the rutile analyses (78 separate grains) turn out to be extremely pure.

Table 1 Frequencies of the particle have grain sizes coarser than 2.0 mm, the sand sizes and the finer sizes in W. Kiraf Delt alluvial sediments

S. No.	>2.0 m (%)	Sand (%)	Mud (%)	S. No.	>2.0 mm (%)	Sand (%)	Mud (%)
1	0.70	93.39	5.91	16	8.37	82.34	9.29
2	5.73	93.03	2.24	17	10.26	81.81	7.93
3	10.70	70.54	8.76	18	4.96	92.61	2.43
4	9.85	80.55	9.60	19	2.74	91.84	5.42
5	8.72	81.75	9.53	20	8.07	84.46	7.47
6	4.81	82.42	12.77	21	4.82	92.30	2.88
7	6.27	87.09	6.64	22	4.91	95.09	L
8	3.40	92.46	4.14	23	10.00	83.80	6.20
9	2.01	91.23	6.76	24	0.22	97.59	2.19
10	0.38	92.08	7.54	25	8.00	85.90	6.10
11	0.45	98.32	6.73	26	5.96	94.04	4.18
12	5.29	86.89	7.82	27	12.80	77.20	14.64
13	3.29	90.59	5.12	28	14.93	78.63	6.44
14	0.22	95.74	4.04	29	4.80	83.87	11.33
15	1.41	98.59	4.95	30	23.94	62.18	13.88

Table 2 Percentages of magnetite, total heavy content, sink and float fractions in Methylene Iodide separation of the total heavy minerals fraction in the studied alluvial sediments

S. No.	Magnetite	Heavy (2.8)	H2.8–L3.3	Heavy (3.3)	S. No.	Magnetite	Heavy (2.8)	H2.8–L3.3	Heavy (3.3)
1	0.45	10.87	9.26	1.61	16	0.67	13.42	11.07	2.35
2	0.70	10.62	8.61	2.01	17	0.64	9.69	8.08	1.61
3	0.55	9.34	8.30	1.04	18	0.49	9.14	7.61	1.53
4	0.39	11.18	9.57	1.61	19	0.63	13.33	11.64	1.69
5	0.51	11.49	9.96	1.53	20	0.49	10.10	8.37	1.73
6	0.60	13.46	11.38	2.08	21	0.62	11.61	9.64	1.97
7	0.71	12.36	10.11	2.25	22	0.55	10.81	8.62	2.19
8	0.80	12.71	10.36	2.35	23	0.57	10.46	7.80	2.66
9	0.51	11.64	9.94	1.70	24	0.59	10.22	8.26	1.96
10	0.46	10.45	8.85	1.60	25	0.49	11.51	9.43	2.08
11	0.56	13.37	11.40	1.97	26	1.00	16.66	12.62	4.04
12	0.68	13.79	11.90	1.89	27	1.50	18.97	13.71	5.26
13	0.72	13.26	11.01	2.25	28	0.69	17.14	13.48	3.66
14	0.62	13.38	11.38	2.00	29	0.52	12.08	9.67	2.41
15	0.67	14.35	11.83	2.52	30	0.39	10.34	8.25	2.09

5 Conclusions

Overall, the Delta of W. Keraf & Diit turns out to display minerals of high economic potential, relevant mainly to the Sudanese derived samples, with little contribution from the Egyptian samples as drawn from the flood pathways.

The presence of magnetite in the ilmenite component appears to constitute a significant problem, as the ilmenite is not pure enough to fit efficiently for the TiO₂ market. At the same time, the inclusions in magnetite will contribute to a

high proportion of magnetite remaining in any non-magnetic portion, as separated by magnetic means.

In sum, the sands of the studied area are sorted, the very fine sand fractions (0.50–0.125 mm.) constitute of about 85% of the samples and are rich in heavy minerals.

The economic minerals include ilmenite, garnet, zircon, rutile, leucosene, titanite and monazite. Other economic minerals, such as gold, were also detected. Ilmenite represents the main constituent in the heavy minerals' fraction, and is characterized with a relatively high rate of TiO₂ (51.3%).

Rutile is the only product that proves to be currently suitable for extraction, but high proportions of rutile will be required before the deposit can be economically mined. Despite the numerous inclusions, after applying the complete flowsheet, gravity, magnetic (low and high intensity) and electrostatic separations turn out to be attainable. A final high-grade ilmenite concentrate should be free of magnetite, ferriilmenite, titanhematite, chromite, calcite, Fe–Mg silicates. The high-grade ilmenite concentrate will be relatively high in its titanium content (more than 51%) and low in its iron, chromium and Ca contents. This would in turn improve its chemical specifications to be marketable.

References

1. Ibrahim, T.M., Abu Halawa, A., Ali, K.G., Gaafar, I.M.: Occurrence of black sand deposits on the Red Sea coastal plain of Wadi Diib, south Eastern Desert, Egypt: a preliminary study. *Sed. Egypt* **17**, 107–116 (2009)
2. Abu Halawa, Masoud, S.M., Shahin, H.A.A., Embaby, A.A.: Economic and radioactive heavy minerals of El Hebal sand dunes, southern Eastern Desert, Egypt. *Ann. Geol. Surv. Egypt* **XXXI**, 449–465 (2009)



Geochemistry of Urban Soil in the Fast-Growing Kuito City (Angola)

Maria Manuela Vinha G. Silva, Marina Cabral Pinto,
Pedro Alexandre Dinis, and Lucas Mandavela

Abstract

The city of Kuito is located in the Central Plateau of Angola, with elevations above 1500 m high. The soils are classified as ferralsols and arenosols, developed over laterites and clastic recent sediments of the Kalahari Group, respectively. The soils have very low clay contents, less than 3.9%, and loamy sand to sandy loam texture. The urban soil has higher pH (7.4) and electrical conductivity (267 $\mu\text{S}/\text{cm}$) levels than natural soils. To note, the latter usually have an average pH value of 5.8 and an average value of 7.2 $\mu\text{S}/\text{cm}$ of electrical conductivity. There is no distinction in the organic matter content in both types of soils. Urban soil has 0.69% and the natural soil has 0.71%, of organic carbon. The urban soils also display higher concentrations of Na, P, Cu, Zn, Sn, Sb, Cd and Pb than the natural ones, and the contaminating elements in the urban soils are Cu, Zn, Sn, Sb, Cd and Pb. These elements are added to the soils by anthropic activities, such as the uncontrolled deposition of domestic and industrial effluents and car traffic. It is actually the type of soil and the modification of its pH which control these elements' fixation in the urban soils.

Keywords

Geochemistry • Soils • Contamination •
Urbanization • Angola

1 Introduction

Urbanization and automobile traffic are rapidly increasing in the developing countries, along with industrialization. The related environmental contamination may pose a serious risk for the urban residents and may adversely affect the soil ecosystem services [1–3].

Differences among cities, mainly in population density and industrial activities, as well as traffic density could have some impacts on the results of individual studies. Comprehensive investigations and assessments of urban soils are needed, but information is often missing in regard of some recently and rapidly developing regions [2]. In this context, the example of an expanding city with growing population, but where the industrial activities are incipient (Kuito city in Central Angola) has been selected as subject of the present study. In this region many farmers moved to the city and started to dedicate themselves to the construction and small food industries, locksmiths, metal workshop, car workshops etc. These new activities are potentially dangerous to the surrounding environment and even to human health, especially children, because the city has very deficient systems for collecting domestic and industrial wastes, which are often freely disposed of in the soil. Similarly, the liquid effluents emanating from domestic activities (baths, dishes, clothes and car washings) are freely disposed in the soil.

2 Materials and Methods

The city of Kuito is located in the Bié province, in the middle of the Central Plateau of Angola. The climate is usually hot and humid, with dry winters. The mean monthly average temperatures for the period 1901–2015 ranged from 15.5 to 20.4 °C, and the mean annual rainfall was around 1319 mm [4]. The municipality of Kuito is the most populous (424,169 inhabitants) of the Bié province, which encompasses 1,338,923 inhabitants [5]. Since the civil war,

M. M. Vinha G. Silva (✉)
CEMMPRE—Earth Sciences Department, Coimbra University,
Coimbra, Portugal
e-mail: mmvsilva@ci.uc.pt

M. Cabral Pinto
Geobiotec, Aveiro University, Aveiro, Portugal

P. A. Dinis
MARE—Earth Sciences Department, Coimbra University,
Coimbra, Portugal

L. Mandavela
Kuito, Angola

the city has grown in an uncontrolled way, without sewage and domestic wastes collection systems, urban planning and water distribution systems. Hence, serious basic sanitation related problems started to emerge. The Kuito region is mostly covered with laterites and clastic sedimentary deposits which are part of the Kalahari Group [6]. Soils in the Kuito region are ferralsols and arenosols. The arenosols have developed over the clastic sediments and are very susceptible to erosion. Ferralsols are heavily leached, but developed on laterites. They consist essentially of Al and Fe oxides, which agglomerate quartz particles giving them a sandy texture. They also have a kaolinite and a yellow to reddish colour. The urban soil samples were collected in the interior of the cities, where access was allowed and the superficial part of the profile was sampled. Natural soils were sampled where little anthropic influence was detected. Composite samples, resulting from 5 sub-samples collected in an area of about 1 m² were collected. They were dried outdoors (while covered with paper), desegregated, sieved to <2 mm, homogenized and quartered to determine the pH, electrical conductivity (EC) and texture levels by means of laser diffraction. Organic carbon was reduced by dry combustion and analyzed through infra-red detection. Another fraction was sieved at <180 µm and analyzed via ICP-OES and ICP-MS, after digestion with *aqua regia* in Actlabs laboratories, with an analytical error of less than 10%.

3 Results

The urban soil proves to display significantly higher pH, CE, silt and sand contents and lower clay contents than the natural soil, with is no significant difference being noticed in regard of organic carbon values (Table 1). The pH sample/mean pH values relevant to the Kuito natural samples appeared to range from 0.98 to 1.44, the greatest amounts of which were greater than 1.2 (Fig. 1d). As for CE, the ratio values proved to range from 6.4 to 59.5 (Fig. 1e). The urban soil is richer in Mg, Ca, Na, K, P, Mn, Ba, Cu, Zn, Sn, Sb, Cd, Pb and is poorer in Al and Zr than the natural soil (Fig. 1c). The differences between the elementary

contents of both soil types are more explicit by calculating the ratio between the elements' concentration in each sample by the mean value of the element in the natural soil (Fig. 1f).

Concerning the urban soils of Kuito, values higher than 2 for this ratio were discovered with respect to Mg, Ca, Na, K, Mn, Sr, Ba, Ni, Bi, Cu, Zn, Sn, Sb, Cd, and Hg (Fig. 1f). The heavy metals, which stand as major contaminants of the urban soils in the city of Kuito turn out to be: Cu, Zn, Sn, Sb, Cd, Pb and Hg.

4 Discussion

Both soils are classified to stand as loamy sand to sandy loam, and the natural soil turns out to be acid, while the urban soil is discovered to be neutral. The fact that the natural soils prove to be acid is mainly due to their derivation from sands rich in quartz and iron oxides. Besides, the precipitation rate and altitude are high and the leaching is intense. The Kuito's natural soil proves to display lower EC values which might well be due to lower pH values, which promotes more intense salt leaching. Increases in Na and P contents have their explanation in the introduction of organic wastes and detergents, while the other elements (Cu, Zn, Sn, Sb, Cd and Pb) recorded increases can be justified by the expansion of industrial activity (locksmiths, car workshops etc.), and also by the increase in traffic.

The higher values of electrical conductivity noticeable in the samples collected in the urban zone can have its justification in the contribution of salts derived from domestic effluents and small industries, both liquid and solid, which are freely discharged in the soils. The water discharged freely by washing clothes, dishes and motor vehicles add a lot of salts to the soil. The city has a small industrial structure, but in expansion due to the continuous growth in urban population, including the transformation of food, sawmills, car workshops industries, etc., that do not have effluent collection systems. Considering the Canadian Legislation [7] for soil standards, some urban soil samples turn out to be highly polluted in Cr, Zn, Sn, Sb and Pb.

Table 1 Some physical-chemical characteristics of the analyzed soils

	Natural soil		Urban soil	
	Average	s	Average	s
% Clay	2.40	0.90	1.45	0.49
% Silt	25.90	12.00	16.66	4.84
% Sand	71.70	12.90	81.89	5.26
% Organic carbon	0.69	0.25	0.68	0.41
Electrical conductivity	7.30	3.10	266	154
pH	5.8	0.2	7.4	0.7

Average Average values; s Standard deviation; Electrical conductivity in µS/cm

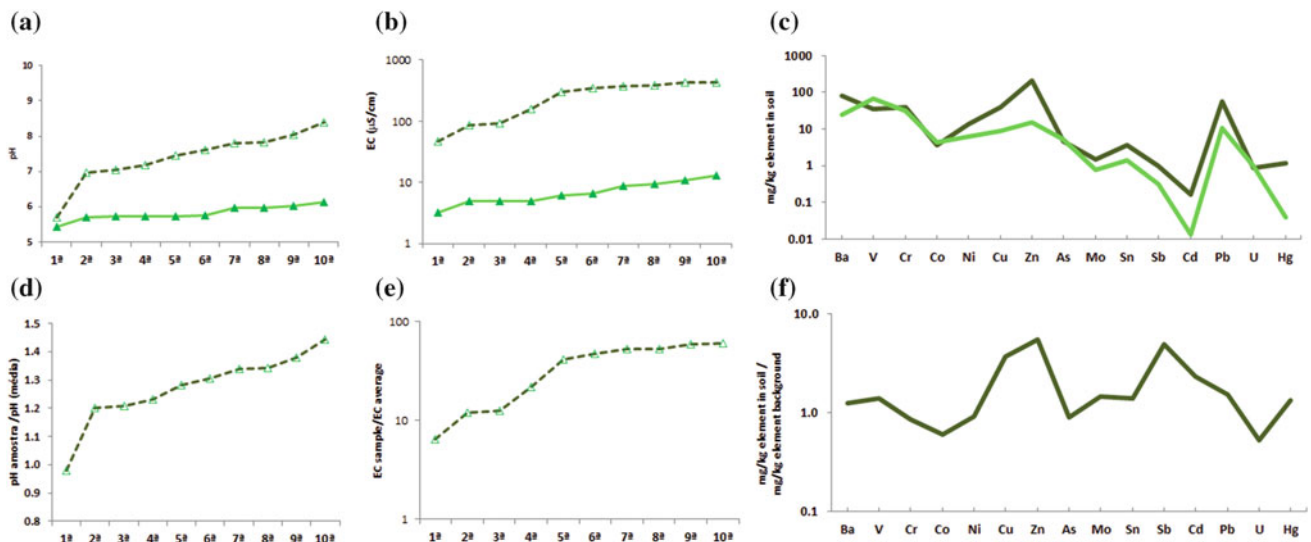


Fig. 1 Values of pH **a** electrical conductivity, **b** trace elements, **c** of the soil samples collected from Kuito, and ratios of urban soil sample values/average of natural samples. Symbols filled: natural soil samples;

open symbols: urban soil samples. In **c** and **f**—light green line: natural soil samples; dark green line: urban soil samples

5 Conclusions

The Kuito lying urban soils are discovered to display higher pH and EC values than the natural soils. Urbanization has remarkably led to their enrichment in Na, P, Cu, Zn, Sn, Sb, Cd and Pb contents. The urban soil is polluted in Cr, Zn, Sn, Sb and Pb. These elements are predominantly added to the soils by the effect of anthropic activities, such as the uncontrolled deposition of domestic and industrial effluents and car traffic.

References

1. Khorshid, M.S.H., Thiele-Bruhn, S.: Contamination status and assessment of urban and non-urban soils in the region of Sulaimani City, Kurdistan, Iraq. *Environ. Earth Sci.* **75**, 1171 (2016)
2. Luo, X.S., Yu, S., Zhu, Y.G., Li, X.D.: Trace metal contamination in urban soils of China. *Sci. Total Environ.* **421–422**, 17–30 (2012)
3. Islam, S., Ahmed, K., Al-Mamun, H.: Distribution of trace elements in different soils and risk assessment: a case study for the urbanized area in Bangladesh. *J. Geochem. Explor.* **158**, 212–222 (2015)
4. CCKP.: Climate Change Knowledge Portal. http://sdwebx.worldbank.org/climateportal/index.cfm?page=country_historical_climate&ThisRegion=Africa&ThisCCCode=AGO. Accessed in December 2017 (2017)
5. CENSO.: Resultados Preliminares do Recenseamento Geral da População e da Habitação de Angola 2014. INE, Angola. <http://censo.ine.gov.ao/xportal/xmain?xpid=censo2014&xpgid=relatorioscenso2014&actualmenu=8377701>. Accessed in December 2017 (2014). (In Portuguese)
6. Araújo, A.G., Guimarães, F., Perevalov, O.V., Voinovsky, A.S., Tselikovosky, A.F., Agueev, Y.L., Polskoi, F.R., Khodirev, V.L., Kondratiev, A.I.: Geologia de Angola—Notícia Explicativa da Carta Geológica de Angola à escala de 1:1000 000. Serviço Geológico de Angola, 136 p (1992). (in Portuguese)
7. Ministry of the Environment: Soil, Ground Water and Sediment Standards for Use Under Part XV.1 of the Environmental Protection Act (2011)

Phosphorus Speciation and Trace Metals in Core Sediment of Kuwait Bay

Eqbal Al-Enezi and Fatema Al-Shammari

Abstract

Kuwait Bay constitutes a unique ecosystem and a significant nursery ground for many fishes and shrimps. The nutrient, phosphorus, is essential for the growth of marine organisms. Yet, at high concentrations, this nutrient could stimulate excessive algal blooms, and deplete oxygen, causing eutrophication. This study is designed to study the concentrations of different phosphates species and trace metals with high affinity to phosphate in samples of sediment cores. Sediment cores collected from Kuwait Bay were sliced into surface, middle and bottom layers. In all of the samples of sediment cores, the dominant phosphate fraction was $\text{CaCO}_3\text{-P}$, while the dominant metal was Ca. Pearson correlation shows a positive and negative correlation between phosphate species and metals e.g., organic P and Mn, and $\text{CaCO}_3\text{-P}$ and Fe, respectively. This study is important as it provides an overview of the different phosphate species and their high-affinity trace metals levels from the present time back.

Keywords

Kuwait Bay • Phosphate • Sediment • Speciation • Trace metals

1 Introduction

Kuwait Bay is an elliptically shaped embayment that protrudes from the Arabian Gulf in the westward direction at its northwestern corner. The Bay is characterized by relatively shallow water throughout where the tidal currents are the major source of water movement. Kuwait Bay presents a unique ecosystem and a significant nursery ground for many fishes and shrimps, as its water is nutrient-rich. It could be polluted naturally from the discharges derived from the Shatt Al Arab river or from the fallout of dust storms. The Bay hosts numerous industrial activities, such as Shuwaikh Port, three major power-generating stations (Doha East, Doha West and Subiya), and four desalination plants (Doha East, Doha West, Subiya, and Shuwaikh). In addition, many types of commercial and metropolitan activities have been developed along the southern coast of the Bay. Discharges from these activities could also be a source of pollution to the marine environment. High-nutrient concentrations stimulate excessive algal blooms, which then deplete oxygen as they decompose in a phenomenon called eutrophication. Phosphorus is critical for metabolic processes and plays a predominant role in cellular energetics as adenosine triphosphate (ATP) and as an important part of many structural and biochemically functional components in cell growth of plants including algae [1]. Phosphorus can be found in the sediment matrix as complex calcium, iron or aluminum salts and organic species, or adsorbed onto the surface of minerals. Phosphorus also exists in the water in several forms: organic phosphate, orthophosphate total phosphorus. Reference [1] noted that the positive correlation between active iron, aluminum, and the amount of phosphorus adsorption. Also, it has been found out that oxygenated sediments retain phosphorus by fixation to iron (III), while reduced sediments release phosphorus by reduction of iron and subsequent dissolution of iron-phosphorus complexes [2–4]. In Kuwait Bay, the trace metal pollution may be derived from discharges from the power and desalination

E. Al-Enezi (✉)

Environmental and Life Sciences Research Center, Kuwait
Institute for Scientific Research, P.O. Box 24885 13109 Safat,
Kuwait
e-mail: enezi@kisir.edu.kw

F. Al-Shammari

College of Health Sciences, The Public Authority for Applied
Education and Training, P.O. Box 24885 13109 Safat, Kuwait

plants, solid waste disposal and municipal drains. A few studies have been carried out on nutrient concentrations, sources and biogeochemical cycle in seawater and/or sediment. The objective of this study is to determine the concentration of phosphorus fractions and trace metals that have strong affinities to phosphorus (Fe, Al, Mn, Mg and Ca) in different sediment layers.

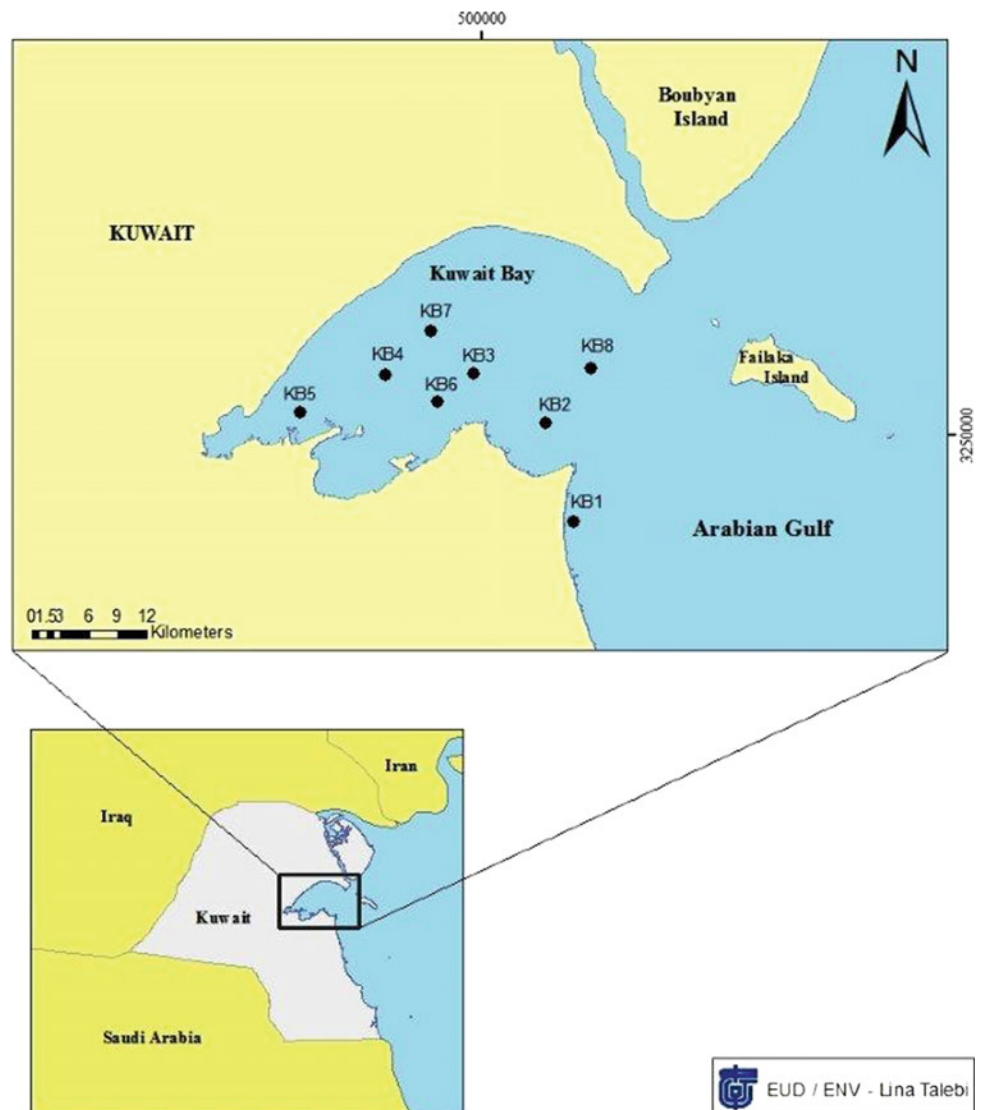
2 Materials and Methods

A total of eight core sediment samples (30 cm in depth) were collected from the bottom of Kuwait Bay (Fig. 1). The sediment cores were transferred to the laboratory in an icebox and stored at $-20\text{ }^{\circ}\text{C}$ until processing. Each sediment core was then sliced into three layers using a plastic

spatula: surface (1–2 cm), middle (12–13 cm) and bottom (29–30 cm).

The sedimentary phosphate was separated using the sequential extraction (SEDEX) procedure that is described by [3], with minor modifications in the incubation time. The SEDEX method consists of five steps that separate the major reservoirs of phosphate into five fractions, such as: loosely sorbed phosphate (LSP), Fe-bound phosphate (Fe-P), authigenic apatite plus CaCO_3 -bound phosphate plus biogenic apatite (CaCO_3 -P, detrital apatite plus other inorganic phosphate (inorganic P) and organic phosphate (organic P). The trace metals were extracted using the method described in the [4]. The concentration of trace metals was determined using an inductively coupled plasma-optical emission spectrophotometer (ICP-OES). Manganese (Mn), aluminum (Al), calcium (Ca), iron (Fe), magnesium (Mg).

Fig. 1 Location map of the sampling stations



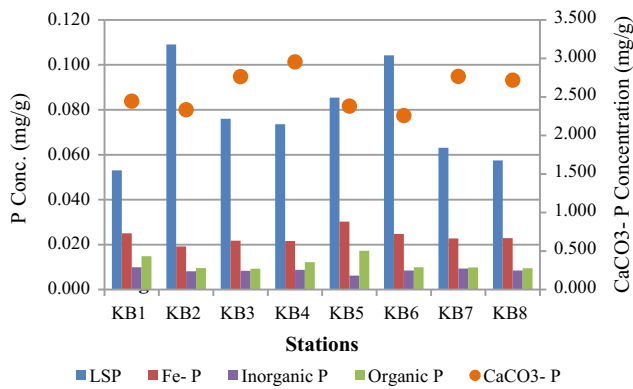


Fig. 2 Five phosphorus fractions

3 Results

Based on an average sedimentation rate of 0.96 ± 0.13 cm/yr [5], the upper layer of the sediment core could be used to trace pollution history of the present day to the past 2–2.5 yrs; the middle layer could be used to trace pollution history for the period from around 11–15 yrs, and the lower layer was used to trace pollution for the period from around 26–36 yrs ago.

The identification of phosphorus species in sediments is a useful approach for the assessment of potential sources or

sinks of phosphorus, and helps to understand the biogeochemical processes that control the availability of phosphorus. Among the five phosphate fractions in the surface layer (Fig. 2), the $\text{CaCO}_3\text{-P}$ was the dominant fraction. The sedimentary phosphate fractions were on the rank order: $\text{CaCO}_3\text{-P} > \text{LSP} > \text{Fe-P} > \text{organic P} > \text{inorganic-P}$ as shown in Table 1.

Of the trace metals that have strong affinity to phosphorus, calcium had the highest concentrations (Fig. 3). The high Ca concentration in the samples of sediment core indicates an urban pollution source to the marine environment.

4 Discussion

Overall, the sedimentary phosphate fractions were on the rank order: $\text{CaCO}_3\text{-P} > \text{LSP} > \text{Fe-P} > \text{organic P} > \text{inorganic-P}$ (Table 1). The results show that the concentration of phosphate forms are reduced as the sediment depth increased except the $\text{CaCO}_3\text{-P}$ fraction that increase with depth, that might be because the high content of organic matter in sediment. In all the sediment layers the trace metals concentrations were on the rank order: $\text{Ca} > \text{Mg} > \text{Al} > \text{Fe} > \text{Mn}$. The studied sediment samples indicate the pollution history from the present day to approximately around

Table 1 Mean concentration of phosphate fractions and trace metals in the three sediment core layers, Kuwait Bay

Phosphate fraction	Surface	Middle	Bottom
LSP	0.078 0.021	0.075 0.021	0.076 0.01
Fe-P	0.024 0.003	0.021 0.003	0.019 0.002
$\text{CaCO}_3\text{-P}$	2.577 0.254	2.599 0.234	2.927 0.487
Inorganic P	0.008 0.001	0.007 0.002	0.007 0.001
Organic P	0.012 0.003	0.01 0.003	0.008 0.002
Mn	276 13	284 8	280 13
Al	42,013 2247	43,352 1909	45,053 6252
Ca	166,747 19,570	168,241 10,724	172,727 17,492
Fe	28,521 1364	28,990 13,450	29,887 3837
Mg	76,019 6958	75,019 2750	76,860 6738

Standard deviation expressed in bold

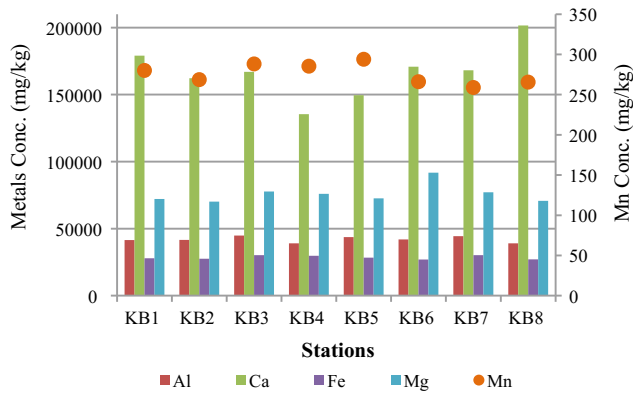


Fig. 3 Trace metals concentration

36 years ago. The high Fe concentrations indicate chronic pollution of Kuwait Bay with Fe, possibly as a result of discharge from the Tigris, Euphrates and Shatt Al-Arab rivers coupled with industrial activities along the coast of Kuwait Bay. The Pearson correlation coefficient shows a negative correlation between the LSP and the $\text{CaCO}_3\text{-P}$, Fe-P and inorganic P, and Mn and Ca. A positive correlation found between the Fe-P and organic P, $\text{CaCO}_3\text{-P}$ and Fe. There was a negative correlation between Fe-P and Mn, and Mg. This means that as the concentration of the metals Mn and Mg increases, the sediment tends to adsorb less phosphate in the iron bound form. These strong correlations indicate that phosphate in the inorganic form is attached to these trace metals. The Fe-P fraction in the bottom sediment layer, had positive correlation with metals Al, Fe and Mg which could be explained as those metals trigger the deposition of phosphate in the form of Fe-P in the sediment.

5 Conclusions

This study has found out that the dominant phosphate fraction was $\text{CaCO}_3\text{-P}$. The sedimentary phosphate fractions were on the rank order: $\text{CaCO}_3\text{-P} > \text{LSP} > \text{Fe-P} > \text{organic P} > \text{inorganic-P}$, while the trace metals concentrations were on the rank order: $\text{Ca} > \text{Mg} > \text{Al} > \text{Fe} > \text{Mn}$. A negative and positive correlation has been found between some phosphate species i.e., inorganic P and organic P fraction with Fe-P and with trace metals elements i.e., Fe and Al. These findings will add to the knowledge base of phosphate and trace metals dynamics in Kuwait territorial water and will help in the update of the baseline data on sediment quality parameters that is often sought for making comprehensive Marine Environment Impact Assessments.

Acknowledgement The authors would like to thank the Kuwait Foundation for the Advancement of Sciences (KFAS) for supporting the participation of the first author at CAJG - Tunisia 2018.

References

1. Zhou, A., Tang, H., Wang, D.: Phosphorus adsorption on natural sediments: modeling and effects of pH and sediment composition. *Water Res.* **39**, 1245–1254 (2005)
2. Al-Enezi, E.: Modelling of phosphorus adsorption processes in estuarine and coastal water. Ph. D. Thesis, Cardiff University (2011)
3. Al-Enezi, E., Al-Dousari, A., Al-Shammari, F.: Modeling adsorption of inorganic phosphorus on dust fallout in Kuwait Bay. *J Eng. Res.* **2**(1). ISSN 2307-1877 (2014)
4. Al-Enezi, E., Bockelmann-Evans, B., Falconer, R.: Phosphorus adsorption/desorption processes of estuarine-sediment: a case study—Loughor Estuary, UK. *Arab. J. Geosci.* **9**, 200 (2016)
5. Ruttenberg, K. C.: Development of a sequential extraction method for different forms of phosphorus in marine sediments. *Limnol. Oceanography* **37**(7), 1460–1482 (1992)

New Insights on the Ermioni VMS Ore Based on Ore Texture and Host Rock Lithology and Geochemistry (SE Argolis Peninsula, Peloponnese, Greece)

Stavros Triantafyllidis and Nikolaos Diamantakis

Abstract

The formerly described as Cyprus-type Ermioni Volcanogenic Massive Sulfide (VMS) mineralization was investigated in a bid to provide new insights on the ore type, and the corresponding geotectonic setting of ore formation. Pyrite is the major ore phase, with minor chalcopyrite and sphalerite. The identified ore textures include massive, stringer and depleted ore types, and the geochemical investigation of the massive ore revealed that the Co content and the Cu/(Cu + Zn) ratio fall within the value ranges associated with the Besshi-type of deposits. The ore is hosted in reworked mafic volcanics and Tertiary terrigenous sediments, including shales, arkoses and sandstones. The texture of the host volcanics is remarkably different from the typical host pillow lava texture of Cyprus-type mineralizations. Additionally, the typical Cyprus-type rock succession, including mafic pillow lavas attached to both of the footwall and the hanging wall, is absent. The trace elements' geochemistry revealed that the Ermioni host volcanics range from calc-alkaline to island arc tholeiites, indicating a supra-subduction zone setting in close proximity to the continental margin, as identified by the host turbidites high silica content.

Keywords

Volcanogenic massive sulfides • Besshi-type • Massive and stringer ore • Calc-alkaline mafic volcanics • Turbidites

1 Introduction

The volcanogenic massive sulfide (VMS) deposits have always been regarded as an important source of Cu, Zn, Pb, precious and strategic metals, ever since the early stages of human history [1]. The Ermioni (Argolis) massive sulfide mineralization has made subject of extensive research since the 1950s. Starting from early studies, the hydrothermal character of the mineralization genetically, as related to mafic volcanism, was established. Subsequent studies further described the Ermioni ore as Cyprus-type, which was mainly attributed to the extent of Vardar-Axios Ocean Jurassic ophiolites, and ophiolitic fragments in the Argolis peninsula.

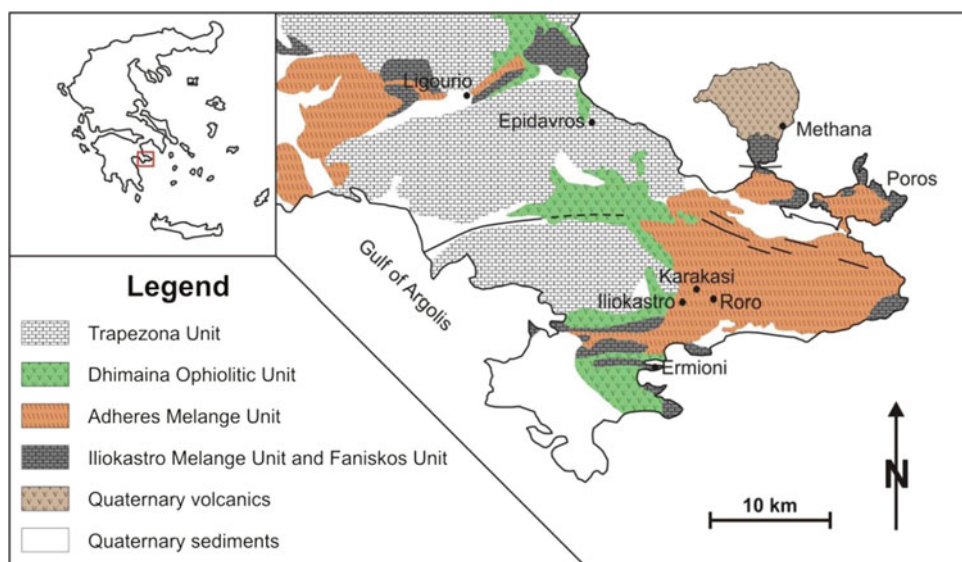
The purpose of the present work consists in providing a detailed textural, mineralogical and geochemical description of the ore and the host rocks, in order to provide new insights on the formation of the Ermioni massive sulfide mineralization.

2 Sampling-Analytical Methods

Host rock and ore samples were collected from the mine sites of Karakasi and Roro (Fig. 1). Metal sulfide concentrates were commercially analyzed by means of fire assay and ICP-AES for Au grade, and X-ray Fluorescence for As, Bi, Co, Cr, Cu, Fe, Mn, Mo, Ni, Pb, S, Sb, Sn, Ta, V and Zn. Screened host rock samples were crushed, pulverized, homogenized and analyzed for major (ICP-AES), minor and trace elements (ICP-MS and ICP-AES). Both of the ore and host rock mineralogy were determined by means of transmitted and reflected light optical microscopy, Raman Spectroscopy, X-ray Diffractometry, and Scanning Electron Microscopy, available at both of the laboratories of the School of Mining and Metallurgical Engineering, and the National Technical University of Athens.

S. Triantafyllidis (✉) · N. Diamantakis
School of Mining and Metallurgical Engineering, National
Technical University of Athens, Iroon Polytechniou 9, 157 80
Zografou, Athens, Greece
e-mail: striantafyllidis@metal.ntua.gr

Fig. 1 Simplified geological map of the Argolis Peninsula including the major mine sites of Karakasi and Roro



3 Results

3.1 Ore Texture, Mineralogy and Geochemistry

Optical and Scanning Electron Microscopy revealed three major ore textures including “Massive Sulfide”, “Quartz-Pyrite” (stringer), and “Depleted” ore types. Pyrite predominates in all ore types, with minor chalcopyrite and sphalerite. The Fe content of sphalerite ranges between 5 and 20 wt% (as moles wt% FeS), which is typical for sea-floor VMS mineralizations. The stringer ore texture bears the characteristics of the lower silicification and stringer zones of VMS deposits [2].

The Cu content of the Ermioni massive sulfide ore ranges between 2.64 and 4.18 wt%, whereas the Zn and Pb contents range between 0.09 and 0.15 wt% and below 0.01 wt% respectively. The As content is below the detection limit (0.01 wt%), and the Sb content is higher and ranges between 0.01 and 0.03 wt%. Bismuth and Sn show average content 0.03 and 0.02 wt% respectively, and the Co content ranges between 0.07 and 0.11 wt%. The Au content of the Ermioni massive ore is low ranging between 0.43 and 0.55 ppm.

3.2 Host-Rock Lithology and Geochemistry

The Ermioni ore is hosted in mafic volcanics and turbidites with high silica content ranging between 50.7 and 69.3 wt%. The footwall mafic volcanics are reworked, massive and propylitized with albite clasts and a groundmass dominated by chlorite, epidote, prehnite–pumpellyite and minor quartz. Angular to subangular clasts of mafic volcanics with ophitic

to sub-ophitic texture are also observed within the host volcanics, indicating limited transportation of pillow lava clasts. The propylitized volcanics are cut by prehnite–pumpellyite \pm quartz, and quartz–epidote veins and veinlets, which are cross-cut by late stage coarse-grained quartz and quartz–calcite veins. Footwall rock types include sheared volcanics and black to black-green shales. The hanging wall lithology comprises red shales with mafic volcanic olistoliths, unconformably overlain by argillic shales and immature, unsorted sandstones.

4 Discussion

As stated by [2], Besshi-type ores usually lie among terrigenous formations with high silica content ranging between 50 and 60 wt%, with predominant black shales and arkoses, interbedded with subordinate basic volcanic rocks, and similar facies are identified at Ermioni. Major and trace element geochemistry of the Ermioni host volcanics revealed the calc-alkaline to tholeiitic, subduction related character of the host volcanics (Fig. 2a). This observation is also supported by Chondrite normalized spider diagram that shows similar trend of the Ermioni host volcanics to island arc volcanic rocks, with moderate LREE and relatively constant HREE values (Fig. 2b).

The Ermioni mineralization is characterized by similar geochemistry to Besshi-type deposits of the Rudny-Altai region in Siberia, with low Zn content (below 1.0 wt%), and low Au grades (below 1.0 ppm). According to [5], the Co content and the Cu/(Cu + Zn) ratio are key features in distinguishing between Cyprus and Besshi-type deposits, and the Ermioni ore is characterized by Co content ranging between

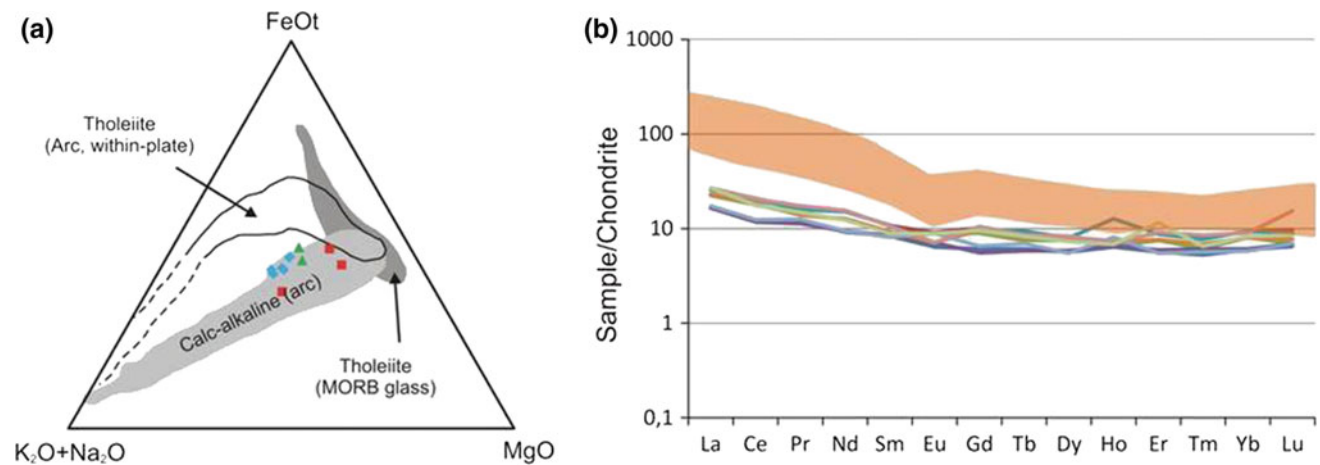


Fig. 2 **a** AFM ternary diagram of the Ermioni host mafic volcanics. Rhombs this study, squares and triangles are data from [3] and [4] respectively. **b** Chondrite normalized spider diagram of the Ermioni ore

host mafic volcanics. Shaded area corresponds to the Ermioni host terrigenous sediments (turbidites)

0.07 and of 0.11 wt% (average 0.09 wt%), and Cu/(Cu + Zn) ratio ranging between 0.8410 and 0.9721, that both fall within the range of values for Besshi-type massive ores.

Concluding, there are strong arguments that support the Besshi-type character of the Ermioni VMS ore including ore mineralogy and geochemistry, host rock lithology, texture and geochemistry. Geochronological data on both the host mafic volcanics and the massive ore is required in order to provide definitive results on the age of mafic volcanism, as well as the type and age of formation of the Ermioni sulfide mineralization.

5 Conclusions

The Ermioni VMS ore bears several characteristics that could correlate it to Besshi-type mineralizations, including:

- The consistent transition from footwall mafic volcanics to terrigenous sediments (turbidites) at the hanging wall,
- The texture of the reworked footwall mafic volcanics, which is markedly different than the typical host pillow lavas texture of Cyprus-type mineralizations,
- The absence of mafic pillow lavas at the footwall and the hanging wall, typical for Cyprus-type mineralizations,
- The calc-alkaline to island arc tholeiitic character of the host mafic volcanics, indicating a supra-subduction zone

setting in close proximity to the continental margin, as identified by the high silica content of the host turbidites,

- The Co content and the Cu/(Cu + Zn) ratio of the Ermioni massive ore that fall within the range of values typical for Besshi-type deposits.

References

1. Galley, A.G., Hannington, M.D., Jonasson, I.R.: Volcanogenic massive sulphide deposits. In: Goodfellow, W.D. (ed.). Mineral Deposits of Canada: A Synthesis of Major Deposit-Types, District Metallogeny, the Evolution of Geological Provinces, and Exploration Methods, vol. 5. Geological Association of Canada, Mineral Deposits Division, Special Publication, pp. 141–161 (2007)
2. Dergatchev, A.L., Eremin, N.I., Sergeeva, N.E.: Volcanic-Associated Besshi-type copper sulfide deposits. Mosc. Univ. Geol. Bull. **66**(4), 274–281 (2011)
3. Tombros, S., Seymour, K.: Hermione, evolution of a Te-bearing epithermal mineralization, Argolis. Hellas. Bull. Geol. Soc. Greece **40**, 996–1008 (2007)
4. Sideris, C., Skounakis, S.: Metallogeny in the basic rocks of a paleosubduction area—the case of Ermioni Cu-bearing Pyrite Mines (East Peloponnesos, Greece). Chem. Erde **47**, 93–96 (1987)
5. Lobanov, K.V., Gaskov, I.V.: The Karchiga copper massive sulfide deposit in the high-grade metamorphosed rocks of the Kurchum block: geologic structure, formation, and metamorphism (Rudny Altai). Russ. Geol. Geophys. **53**, 77–91 (2012)

Elemental Geochemistry of Subsurface Sediments of Lower Baitarani Basin, East Coast of India: Implications for Paleoredox Condition

Uzma Parveen and S. Sreekesh

Abstract

The distribution of redox sensitive trace elements and rare earth elements (REEs) has provided the opportunity to interpret conditions observable during the deposition time. The trace and rare earth elements are sensitive to redox changes and highly enriched in reducing sediments, potentially making them robust proxies to study paleoredox conditions. The variability and concentration of the redox sensitive metals have been widely studied as a paleo-redox proxy both in marine and fluvial environments. The present study is an attempt to analyze the paleo-redox condition in the lower reaches of the Baitarani Basin, Odisha, East Coast of India.

Keywords

Redox • Crustal average • Trace elements • Rare earth elements • Variability • Concentration

1 Introduction

Understanding the systematic variation in the distribution and concentration of redox sensitive elements (major, trace and rare earth elements (REEs)) has provided us with the opportunity to analyze and interpret the environmental conditions as occurring at the time of sedimentation. The trace and rare earth elements are sensitive to redox changes and highly enriched in reducing condition, making them stand as potentially robust proxies, useful for studying the paleoredox conditions [8].

The Eastern Coast of India is an amalgam of the distinctly segmented Bengali, Mahanadi, Krishna-Godavari, Palar and Cauvery Basins. These blocks are developed into exclusive basins throughout the Mesozoic-Cenozoic age, upon

inherent subcrustal discrepancy along the East Coast [4]. The processes carving out lower the Baitarani basin area are different from those actively operating along the other coasts [9].

The most extensively studied redox sensitive elements include V, Cr, Mo, Fe, Ce, Co, Ni, Cu, Re, U and Zn [1, 3, 5, 8]. In this paper, we undertake to analyze the redox sensitive trace and REEs underlying the subsurface sediments, and determine their response under a range of redox conditions. We also consider investigating the utility of trace and rare earth elements, as means whereby the paleo-redox condition related to a marginal marine environment, along the Baitarani River, Odisha, East coast of India could be recognized.

2 Materials and Methods

The subsurface sediment sample is collected from up to 10 m depth, using borehole drilling from Jhumpuri, Odisha ($20^{\circ} 49' 52.5''/86^{\circ} 26' 40.5''$). Facies are identified based on color and textural variation lying at different depths. Each of these sub-samples is analyzed for geochemical and total organic carbon (TOC).

The samples are oven-dried and finely ground using agate mortar. Approximately 2 g of powder was combined with boric acid and pressed to get powder pellets. Boric acid is used to provide a homogenous layer to the sample to ensure that X-ray has penetrated to a homogenous depth, and that no refraction has taken place. The Energy Dispersive X-Ray Spectrometry (EDXRF) is performed at the AIRF of the Jawaharlal Nehru University, New Delhi, India. TOC is determined by means of Walkley-Black method. In the present paper, the following elements Fe, Al, Ti, V, Cr, Ba, La, Ce and Nd have been selected to provide better proxies, as widely applied in different paleoredox-analysis based studies.

U. Parveen (✉) · S. Sreekesh
Jawaharlal Nehru University, New Delhi, 110067, India
e-mail: parveen.uzma5@gmail.com

3 Results

3.1 Aluminum, Titanium and Iron

The Al concentration is discovered to lie between 11.69 and 13.74% (Table 1), as compared to the crustal average of 15.4 [7]. Ti proves to vary from 0.24 to 0.92%. In comparison to crustal average, the Ti concentration is discovered to be higher in content in L1, L2, L3, L5, L6, L7, L8 and L11, while in L4 and L10 the content is lower than the crustal average of 0.64 [7]. The Fe concentration is considerably higher than the crustal average of 5.04 [7]. It appears to fluctuate from 5.82 to 17.36.

The Al/Ti ratio proves to vary between 12.54 and 46.63. In comparison with the crustal mean of 21.24, the L4, L7 and L10 appear to display the highest Al/Ti ratio, while in the other layers this ratio is noticeably lower. Fe/Al is discovered to lie between 0.47 and 1.46, as compared to the crustal average of 0.48 [7]. Only in L11 does the ratio turns out to be lower than the crustal mean.

3.2 Vanadium and Chromium

V is recorded to prevail in rates ranging between 43 and 76, with an average concentration of 61.27 as compared to the crustal mean of 97. Cr is discovered to vary between 153 and 233, much higher than the crustal average of 92 [7] (Fig. 1).

Three ratios, V/Ti, V/Al and V/Cr are calculated for V and for Cr, Cr/Ti, and Cr/Al is examined as well. V/Ti is found to lie between 68.48 and 179.17, much lower than the crustal average of 252.80. V/Al is recorded to persist between 3.73 and 6.55, which is, once again, below the crustal mean of 11.90 [7]. The V/Cr ratio proves to vary in

range from 0.18 to 0.44. The Cr/Ti is calculated to range between 192.71 and 970.71, while Cr/Al is discovered to lie between 12.30 and 18.29, much higher than the crustal average of 11.29 [7].

4 Discussion

The concentration of major, trace and rare earth elements (REEs) proves to display a significant variation at the study site. Variability of V has been examined in comparison to Ti, Al and Cr, in order to illustrate the influence of selected detrital tracers on its concentration. The ratios are discovered to lie below the crustal mean. Cr is also studied in respect of Ti and Al. the Cr/Al turns out to exhibit higher values than the crustal mean. The Fe contribution in the detrital flux is also analyzed by means of Fe/Al ratio, often used as an indicator of reducing environment. As for the Al/Ti, it is generally used to trace the provenance.

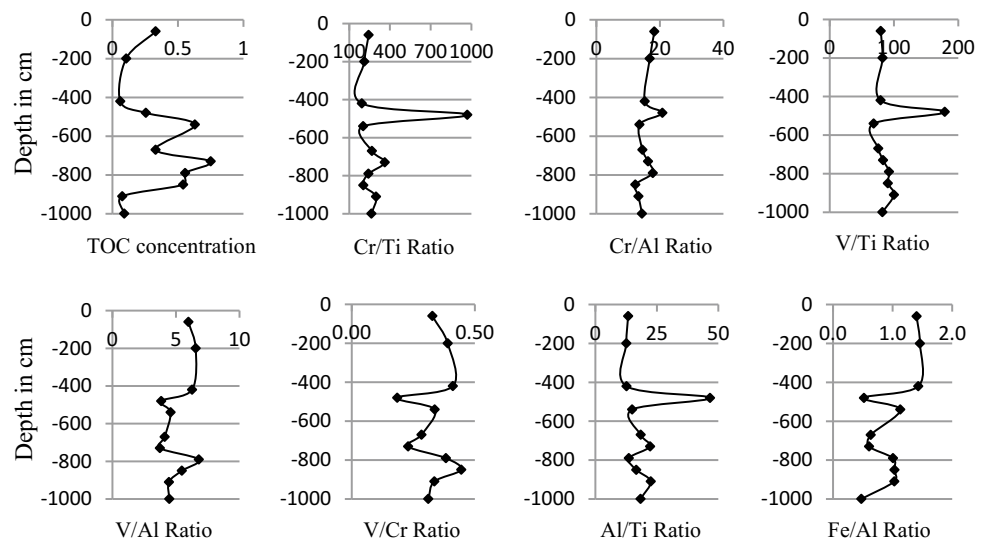
5 Conclusions

The selected major, trace and rare earth elements, subject of the present study, have been discovered to vary significantly in respect of the crustal average. The findings appear to reveal that the area has experienced oxic and anoxic conditions at different time intervals, which have already been reported to persist in various regions of the Indian subcontinent. The higher ravalues of Cr/Ti, Cr/Al, V/Ti and Al/Ti between 400 and 500 m depth suggest increased surface runoff conditions in the lower reaches of Baitarani Basin. Such events have been reported in different parts of Indian subcontinent by Yadav et al. [10] and Prasad et al. [6].

Table 1 Variability and concentration of elements in different layers at Jhumpuri

Layers	L1	L2	L3	L4	L5	L6	L7	L8	L9	L10	L11	Average	SD
Depth (cm)	0–60	60–200	200–420	420–480	480–540	540–670	670–730	730–790	790–850	850–910	910–1000		
Al ₂ O ₃	11.70	11.29	12.13	11.19	13.74	13.62	11.79	10.74	12.44	11.69	12.30	12.06	0.90
TiO ₂	0.88	0.90	0.96	0.24	0.92	0.74	0.53	0.79	0.75	0.52	0.67	0.72	0.21
Fe ₂ O ₃	16.40	16.47	17.36	5.82	15.49	8.63	7.13	10.81	12.82	12.03	5.83	11.71	4.19
V	70	74	76	43	63	56	44	73	68	52	55	61.27	11.39
Cr	214	190	185	233	187	198	192	191	153	155	177	188.64	21.89
Ba	466	496	497	385	393	384	324	520	479	385	386	428.64	61.30
La	50	53	49	10	45	52	38	24	35	25	20	36.45	14.11
Ce	84	108	101	25	84	91	64	60	60	48	47	70.18	24.33
Nd	31	38	39	10	30	30	19	17	22	13	15	24.00	9.62

Fig. 1 Variability of total organic carbon (TOC), Cr/Ti, Cr/Al, V/Ti, V/Al, V/Cr, Al/Ti and Fe/Al in the different layers of the Jhumpuri location, Odisha



Consequently, further supplementary analyses seem imposed. However, this preliminary work turns out to be significant in that it helps remarkably in bridging the gap between geochemistry and paleo-climatic studies relevant to the study area.

References

1. Cole, D.B., Zhang, S., Planavsky, N.J.: A new estimate of detrital redox-sensitive metal concentration and variability in fluxes to marine sediments. *Geochemical et Cosmochimica Acta* **215**, 337–353 (2017)
2. Khandelwal, A., et al.: Vegetation history and sea level variations during the last 13,500 years inferred from a pollen record at Chilika Lake, Orissa, India. *Veg. History Archaeobot* **17**, 335–344 (2008)
3. Kumar, M.: Remote sensing and GIS based SLR inundation assessment of Bhitarkanika forest and adjacent eco-fragile area, Odisha. *Int. J. Geomatics Geosci.* **5**(4), 684–696 (2015)
4. Lal, N.K., Siwal, A., Kaul, A.K.: Evolution of East Coast of India —a plate tectonic reconstruction. *J. Geol. Soc. India* **73**, 249–260 (2009)
5. Pi, D.H., Liu, C., Zhou, G.A.S., Jiang, S.Y.: Trace and rare earth element geochemistry of black shale and Kerogen in the early Cambrian Niutitang Formation in Guizhou province, South China: constraints for redox environment and origin of metal enrichment. *Precambr. Res.* **225**, 218–229 (2013)
6. Prasad, V., et al.: Mid-Late Holocene monsoonal variations from mainland Gujarat, India: A multi proxy study for evaluating climate culture relationship. *Palaeogeogr. Palaeoclimatol. Palaeoecol.* **397**, 38–51 (2014)
7. Rudnick, R., Gao, S.: Composition of the continental crust. In: Holland, H.D., Turekian, K. K. (eds.) *Treaties on Geochemistry*, 2nd edn. Elsevier, Oxford, pp. 1–51 (2014)
8. Tribouillard, N., Algeo, T.J., Lyons, T., Riboulleau, A.: Trace metals as paleoredox and paleoproductivity proxies: an update. *Chem. Geol.* **232**, 12–32 (2006)
9. Vaidyanadhan, R., Ghosh, R.N.: Quaternary of the east coast of India. *Curr. Sci.* **64**, 804–816 (1993)
10. Yadav, A., et al.: Mid-Late Holocene climate variability in the Indian monsoon: evidence from continental shelf sediments adjacent to Rushikulya river, Eastern India. *Quater. Int.* **443**, 155–163 (2017)

Mineralogical and Chemical Comparison of Carbonate From Sites Selected for Artisanal Cement Production With Limestone Used in Commercial Operations

Freeman E. D, Senzani and Antoine F. Mulaba-Bafubiandi

Abstract

The present mineralogical and chemical related study, as based on a selection of carbonate-rock-deposit samples extracted from South African sites, is aimed to test these materials' suitability for producing cement, necessary for the achievement of local infrastructure projects. The sites are located on the Rietfontein, Rooikop and Wiedouw farms. The study has been implemented via petrographic, X-Ray Diffraction and X-Ray Fluorescence techniques. The reached results reveal that the Rietfontein material to be composed of calccrete, while that extracted from the Rooikop site is composed of recycled micrite. At Wiedouw, the carbonate turns out to be a low metamorphic grade marble with classic metamorphic polygonal grains and grain boundaries. The undertaken experiments prove that, thanks to their purity, the selected sites' available carbonate material is suitable not only for cement manufacture, but also for the production of calcium oxide for use in various industrial processes requiring high-grade lime or limestone. Future development should, therefore, consider exploitation of these deposits as raw material sources fit for cement as well as limestone and lime production. Noteworthy, however, is that while the Wiedouw marble and the Rooikop limestone prove to constitute compact and tough rocks, requiring higher costs for blasting, crushing and grinding for the small quarry, the Rietfontein calccrete turns out to be softer and, therefore, highly preferred in respect of the former two materials.

Keywords

Cement • Clinker • Limestone • Reconnaissance • Site selection

1 Introduction

This work is conducted for the sake of providing some kind of support for an initiative aimed at contributing in maintaining infrastructure development projects in non-urban areas. It is undertaken to investigate the mineralogical and chemical characteristics of carbonate as based on specific samples extracted from some South African selected sites. The sites have been identified as having a remarkable cement production potential.

2 Materials and Methods

The study samples have been extracted from three different sites, as determined in an earlier conducted study, namely, from the Rietfontein, Rooikop and Wiedouw farms [1]. The farms fall, respectively, in the provinces of Limpopo, Free State and Western [2, 3]. The investigation has been executed by means of petrographic, X-Ray Diffraction and X-Ray Fluorescence techniques. The XRD determination was conducted using a Rigaku, Ultima IV, at 40 kV, with a 30 Ma copper source and a K-beta filter, along with a scintillation counter detector. The scan axis was $2\theta/\theta$, while the scan range was 5000° to $900,000^\circ$.

As for the XRF analysis, it has been implemented via a Rigaku ZXS Primus II with SQX Analysis in conformity with the scatter FP method. The wave has been generated using an X-ray tube set with an end window and Rh-anode, respectively running at a power and voltage of 3 kW and 60 kV. The wavelength was dispersive and sequential, while the sample was rotated at a speed of 30 rpm. The instrumentation also involved a primary filter (Al, Ti, Cu and Zr),

F. E. D. Senzani (✉) · A. F. Mulaba-Bafubiandi
Department of Metallurgy, Faculty of Engineering and the Built Environment, School of Mining Metallurgy and Chemical Engineering, Mineral Processing Technology Research Centre, University of Johannesburg, P. O. Box 17911 Doornfontein, 2028, South Africa
e-mail: fsenzani@uj.ac.za

a beam collimator and a crystal charger with 10 crystals. Temperature was stabilized at $36.5 \pm .1$ °C. The results reached were then compared to the actual carbonate material characteristics as utilized at a selection of Portland cement producing plants.

3 The Reached Results

Carbonate material, as extracted from Rietfontein consists of light-brown to cream calcrite englobing three main categories of very fine grains, namely, micrite grains held in micrite cement. Both of the grains and cement contain small sparite grains. Multiple carbonate-precipitation cycles are indicated by the presence of earlier micrite grains inside the subsequent ones. Calcite micro-veins postdating the rock's precipitation have also been perceived (Fig. 1).

Regarding the Rooikop resource, it involves a compact limestone, and is also composed of grey micrite with sparite spots and micro-veining. The veins are composed of an outer (earlier), ferruginous phase, along with an inner (later) phase of calcite micro crystals. There is also a persistence of cryptic zones of lighter and darker grey, which appear twisted, expectedly indicating that parts of the carbonate sections look as if they had gone through a plastic flow stage (Fig. 2). As for the Wiedouw based carbonate, it actually consists of a low grade marble with classic polygonal grains,

uniformly 1 mm across, forming high-angle contact, thus giving evidence for a low-grade metamorphism. It also contains zones where shear movement appear to have flattened or ground the grains. Still, no development of new metamorphic minerals has been detected (Fig. 3).

4 Discussion

On being compared to the carbonate oxides chemical content fit for Portland cement production as extracted from various sites worldwide, the target sites available materials appear to lie within a noticeably satisfactory range (Table 1). Still, the high average of MgO content characterizing the Wiedouw samples, noticeably exceeding the required range, proves to indicate well the persistence of local low-magnesia carbonate likely to be blended with the high-magnesia material.

Concerning the Rietfontein carbonate, it turns out to be fine-grained and friable, making it easy to grind during preparation. As for the Rooikop limestone, it is also fine-grained, though hard, compact and well-cemented, therefore, requiring greater energy for comminution. Among the three investigated sites, the Wiedouw marble turns out to entail the greatest energy requirement to crush and mill, due mainly to the low-grade metamorphism. Besides, the calcite-crystal constituents have the largest grain sizes of the three sites.

Fig. 1 Plane-polarized microphotograph of the Rietfontein based calcrite—composed of fine micritic calcite lumps (light brown) surrounding quartz grains (white), in turn surrounded by more micritic calcite mixed with fine iron-hydroxide (dark brown). The latter is cut by calcite veins (white). Field of view = 3 mm

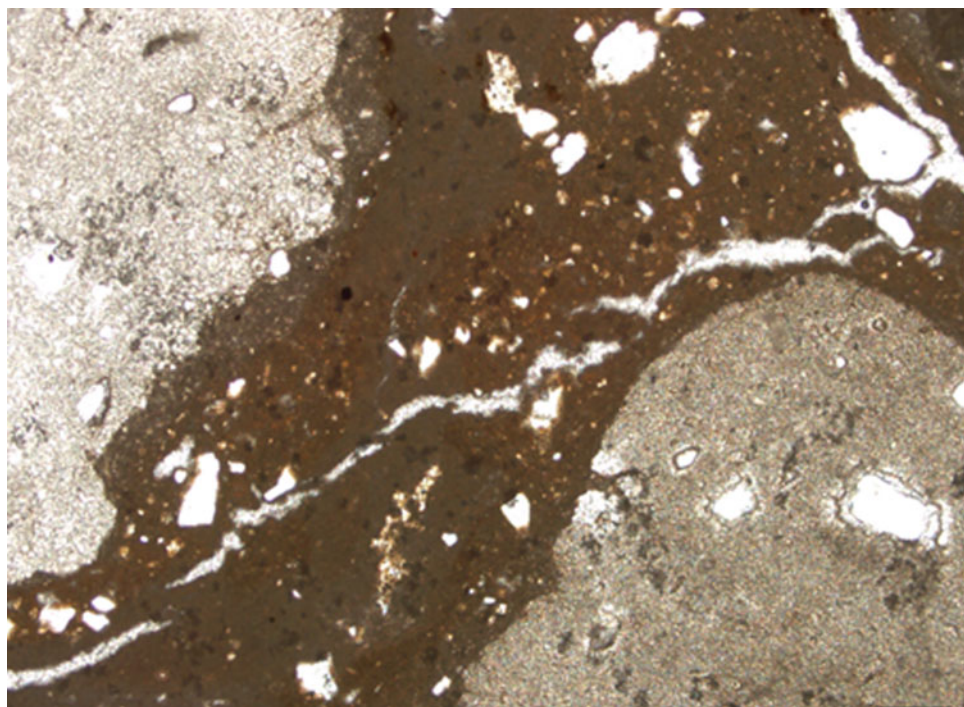


Fig. 2 Plane-polarised microphotograph of indurated limestone from Rooikop— composed of micrite (dark brown) with spar spots and networks (lighter colours). It also includes an iron-hydroxide vein later infilled by fine calcite. Field of view = 3 mm

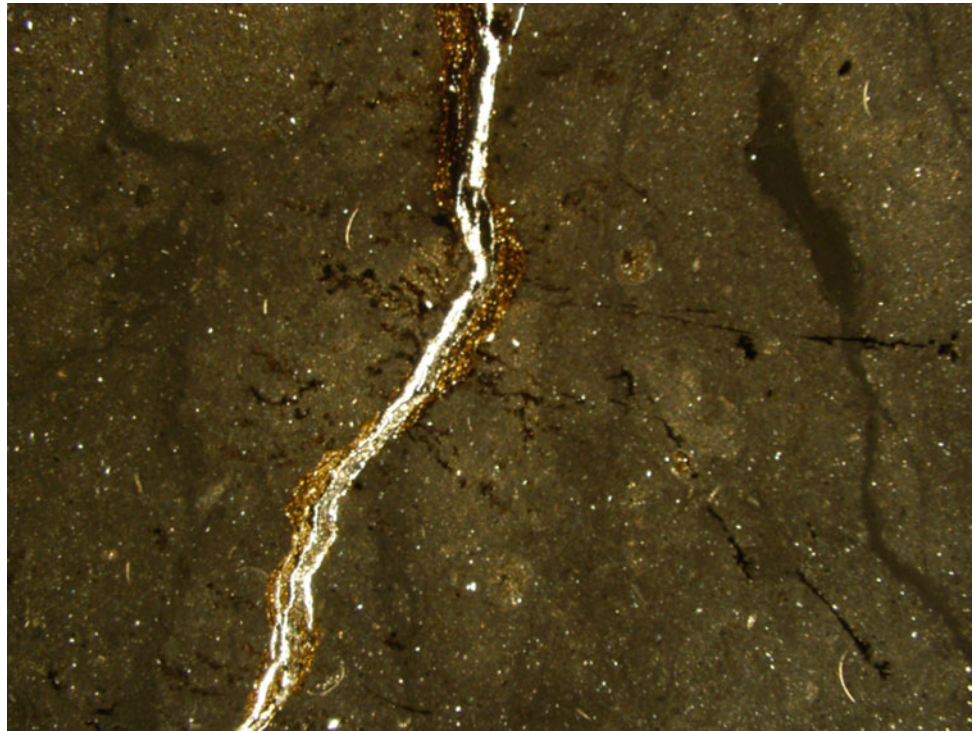


Fig. 3 Plane-polarized photomicrograph of calcitic Wiedouw marble, as characterized with low-grade metamorphic angular grain contacts. Field of view = 12 mm

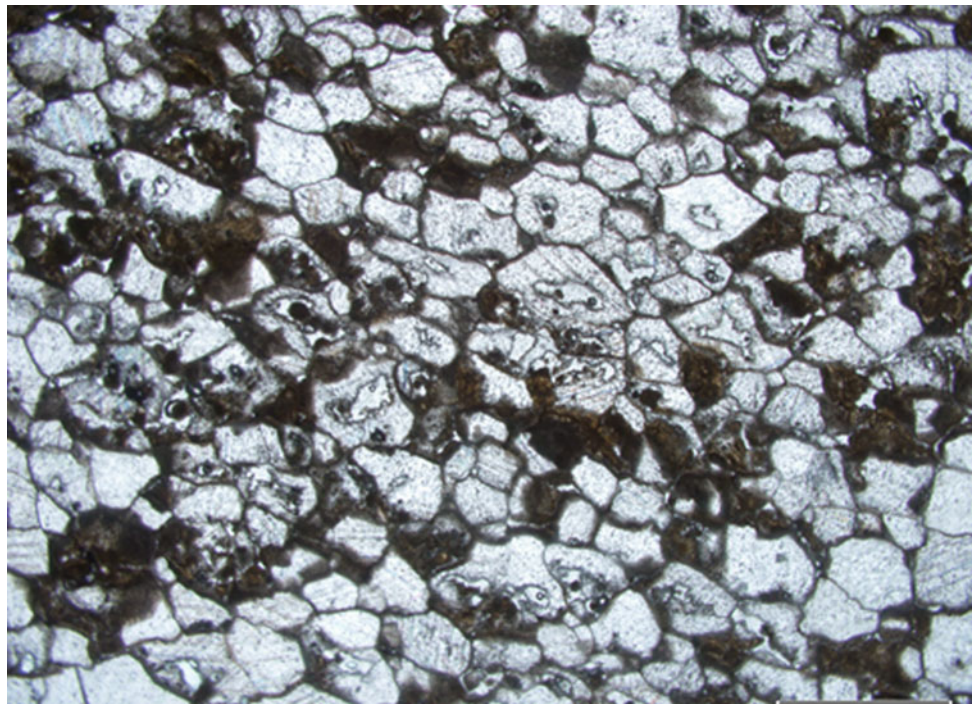


Table 1 Average chemical analyses of the major rock carbonate components

Oxide wt%	Rietfontein	Rooikop	Wiedouw	Acceptable ranges ^a
Al ₂ O ₃ plus Fe ₂ O ₃	2	8	1	<16
Na ₂ O plus K ₂ O	6	1	0	<0.6
CaO	47	43	52	>42
MgO	1	1	10	<4
Silica ratio (SiO ₂ /Al ₂ O ₃ + Fe ₂ O ₃)	4	2	2	1–4
SiO ₂	7	15	1	<16

^aASTM (American Standards Test Methods) [4] and BGS (British Geological Survey) [5]

5 Conclusions

The conducted microscopic petrographic study, along with the X-Ray Diffraction and X-Ray Fluorescence analyses, as administered on a selection of carbonate samples extracted from the South African Rietfontein, Rooikop and Wiedouw farm sites, prove to highlight well that the related minerals appear to be characterized with a high calcite content. The investigation also reveals that the materials, subject of study, have acceptable levels of MgO, Fe₂O₃, Al₂O₃, SiO₂, Na₂O, K₂O and silica ratios that fall within the tolerated range necessary for the cement production, as well as the various industrial processes requiring high-purity lime or limestone (Table 1). To sum it up, the Rietfontein site related material is discovered to display the most optimally convenient potential as a remarkably fine-grained and friable fit substance.

References

1. Senzani, F.E.D., Mulaba-Bafubiandi, A.F.: Semi-quantitative Site Determination of Sites for Artisanal Rock Carbonate Processing Using Qualitative Multifactor Analysis: case Studies—Malawi and South Africa. In press (2018)
2. Martini, J.E.J.: Limestone and Dolomite Resources of the Republics of South Africa, Bophuthatswana, Ciskei, Transkei and Venda. Geological Survey, Department of Mineral and Energy Affairs, Handbook 9. Government Printer, Pretoria, 112p (1987)
3. Vorster, C.J.: Limestone and Dolomite Deposits of South Africa, Lesotho and Swaziland. SAMINDABA. Council for Geoscience, Pretoria (2003)
4. ASTM (American Standards Test Methods): Annual Book of ASTM Standards, vol. 04.01 (Cement, Lime, Gypsum) ASTM. Pasadena, USA (1998)
5. BGS (British Geological Survey): Mineral profile: cement raw materials. Natural Environment Research Council. Office of the Deputy Prime Minister, London, 20p (2005)

Stratigraphic and Mineralogical Study of Chouabine Formation in the Mknassy Basin (Central Tunisia)

Sinda Sassi, Karima Horchani-Naifer, Nabil Fattah, and Mokhtar Ferid

Abstract

A 39-m thick phosphate rock was subdivided into 8 layers based on facies changes. The mineralogical composition of these layers was investigated using XRD and binocular loupe. The result appeared to reveal that the layers prove to contain carbonate-fluorapatite, quartz, calcite, gypsum and dolomite, in proportions that vary from a layer to another. This variation is also persistent in the implemented chemical analyses. A simple washing was carried out to obtain a commercial phosphate. The phosphorus pentoxide content (29.41%) in the layer CIII₄ turns out to be high enough that it does not require further treatment. Noteworthy, however, is that it appears economically interesting to mix layer CI₁ (26.58% P₂O₅) with layer CIII₄ for a 28.77% phosphorus pentoxide content to be attained.

Keywords

Facies change • Stratigraphy • Washing
Commercial phosphate • XRD

1 Introduction

Sited in central Tunisia, the Mknassy Basin is characterized with the persistence of outcrops dating back from the Triassic to the Quaternary period [1–3]. Phosphatic sedimentation is observed in several localities of the Mknassy basin, particularly in the Djebel Bouzer (Fig. 1), which corresponds to a middle to upper Eocene heart, surrounded by Triassic gypsum. In this work, the Chouabine formation series will be subjected to a stratigraphic study and the phosphatic layers will be treated in such a way as to meet the required commercial standard category.

2 Materials and Methods

A lithostratigraphic section was logged 40 km north of Mknassy. An investigation of the Paleocene-Eocene sedimentary series has been undertaken during a work field. The sampling was carried out at the level of each change in facies. Laboratory analyses were carried out for the chemical and mineralogical characteristics to be identified. A series of scrubbing and wet screening operations were carried out. The mineralogical composition was determined by means of XRD and binocular loop analysis. Chemical analyses were used to determine the content of phosphorus pentoxide, calcium oxide, cadmium, magnesium oxide and silica oxide, before and after the washing process.

S. Sassi (✉) · K. Horchani-Naifer · M. Ferid
Laboratory of Physical Chemistry of Mineral Materials and Their Applications, National Research Center in Materials Sciences, Technopole Borj Cedria, B.P. 73, 8027 Soliman, Tunisia
e-mail: sindassii@gmail.com

N. Fattah
Phosphate Company of Gafsa, Research Center, 2134 Metlaoui, Tunisia

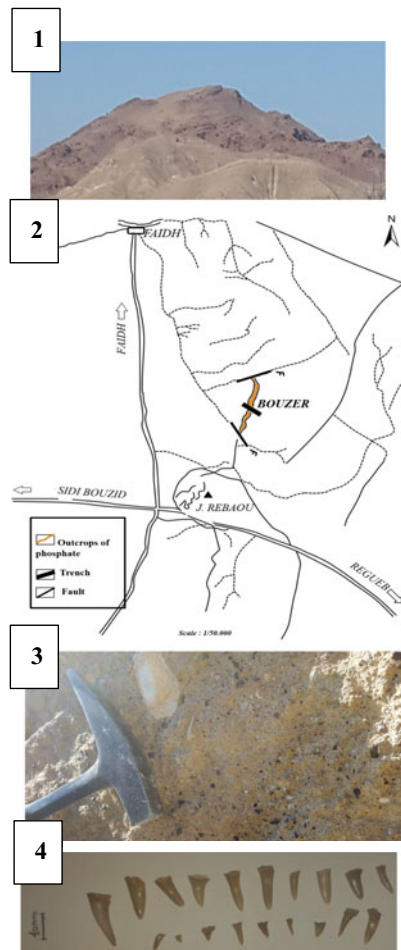


Fig. 1 Stratigraphic section of Djbel Bouzer, 1: Picture of Djbel Bouzer, 2: Localization of the phosphate outcrops, 3 + 4: Shark teeth

3 Results

3.1 Lithostratigraphy

Fieldwork and sampling were carried out for the phosphatic facies lying across the Djbel Bouzer, Mknassy Basin.

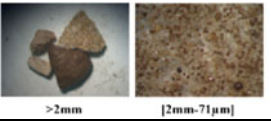
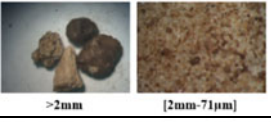



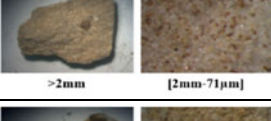


	Log	Description
CHOUABINE formation (Ypresian)		2.35 m phosphatic limestone; 1.15 m of coprolitic phosphate; 0.65 m phosphate with limestone nodule; 5.65 m siliceous phosphate; 1 m limestone with marl passage 3.5 m phosphatic limestone; 0.95 m marl 1.6 m greyish phosphate 0.6 m alternation marl-gypsum-phosphate 2.2 m yellowish phosphate 0.5 m limestone 0.6 m yellowish phosphate 1 m alternation marl-limestone 3.9 m phosphate with limestone nodule 0.3 m limestone 0.7 m phosphate 3.7 m green marl 0.7 m limestone with gypseous passage 1.4 m green marl 0.3 m limestone 0.25 m coprolitic phosphate 1.5 m limestone 0.4 m chert 4.1 m phosphate (shark teeth)

3.2 Chemical Analysis

Raw phosphorites, along with the commercial phosphate and wastes, were chemically investigated. The reached findings are depicted on Table 1.

A mixture of Cl_1 and Cl_{II_4} proved to yield a phosphate ore with 28.77% P_2O_5 content.

Table 1 Chemical composition (oxide wt%, ppm) of each layer before and after washing

	Sample	P ₂ O ₅ (wt %)	CaO (wt %)	SiO ₂ (wt %)	Cd (ppm)	MgO (wt %)	Binocular loop observation
C ₀	Raw	18.61	38.67	19.79	29	1.92	
	+2000	17.32	36.27	14.11	23	3.55	
	+71	19.61	38.03	19.28	23	5.33	
	-71	18.56	34.63	22.13	31	4.18	
CI ₁	Raw	23.90	43.17	12.46	30	1.02	
	+2000	23.95	42.73	16.36	24	1.06	
	+71	26.58	43.41	12.18	17	0.51	
	-71	19.20	37.10	19.85	67	0.74	
CI ₂	Raw	10.39	30.41	35.11	27	1.27	
	+2000	7.13	26.44	37.55	24	1.18	
	+71	11.77	19.94	49.63	16	1.94	
	-71	10.76	34.01	25.04	40	1.20	
CII	Raw	4.84	31.81	3.17	13	2.45	
	+2000	6.64	35.48	1.85	14	0.51	
	+71	7.54	26.56	2.40	12	0.64	
	-71	12.38	35.31	2.63	17	0.53	
CIII ₁	Raw	11.55	24.08	3.77	39	2.84	
	+2000	11.86	25.02	3.15	26	0.69	
	+71	10.44	23.43	3.27	29	0.51	
	-71	16.04	31.36	2.44	34	0.64	
CIII ₂	Raw	9.91	22.06	3.11	34	3.08	
	+2000	9.81	22.83	1.83	41	0.55	
	+71	9.19	21.36	3.29	26	0.51	
	-71	14.75	31.18	3.79	64	0.52	
CIII ₃	Raw	8.18	22.06	4.05	47	1.91	
	+2000	8.82	23.88	2.63	52	0.61	
	+71	7.63	20.89	1.94	48	0.72	
	-71	10.87	27.35	1.97	59	0.69	
CIII ₄	Raw	24.42	42.81	3.68	36	1.40	
	+2000	20.10	43.00	2.13	78	0.56	
	+71	29.41	47.82	1.22	35	0.64	
	-71	16.10	43.00	1.17	71	0.51	

The values written with bold character represent the highest content of P₂O₅

3.3 Mineralogical Analyses

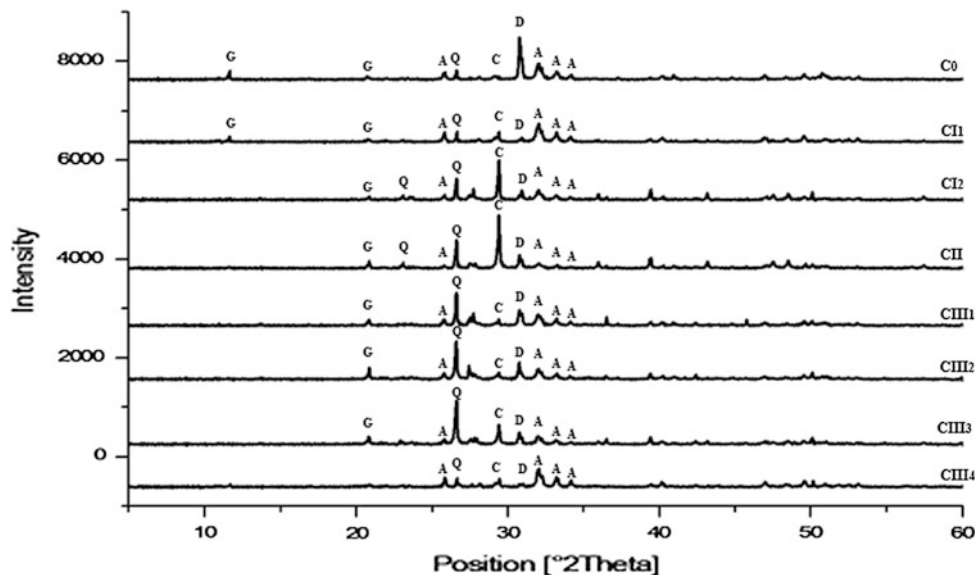
The XRD patterns shows that the main minerals in this raw phosphorites are carbonate-fluorapatite, calcite, dolomite, quartz and gypsum (Fig. 2).

4 Discussion

The examined samples appear to display noticeable variation. The major gangue minerals prevalent in this phosphate rock are calcite, silica and gypsum in lower amount;

dolomite is also persistent. It was also discovered that the P₂O₅ content varies from 4.84 to 24.42%, while the CaO content displays an average of 37%. After simple washing, the P₂O₅ content can reach a 5% higher rate; the same applies to the layer CIII₄ case. The latter proves to contain a 29.41% rate of P₂O₅. Owing to this high P₂O₅ content and the corresponding high CaO component, the ratio CaO/P₂O₅ proves to yield a result of 1.7, which is considered normal in respect of the rocks used for industrial purposes. The layer CI₁ displays a P₂O₅ rate of 26.58% following washing and mixing with layer CIII₄ providing a mixture enclosing a 28.77% pentoxide content.

Fig. 2 XRD of the raw phosphorites, A: Carbonate-fluorapatite; C: Calcite; Q: Quartz; D: Dolomite and G: Gypsum



5 Conclusions

The reached findings prove to help noticeably in identifying the phosphatic outcrops. The sediment particles, as discovered to persist in the Djbel Bouzer deposit turn out to be of diagenetic and biogenic origins. Potentially, the spatial heterogeneities in sedimentation could well account for a thickness variation distinguishing the relevant layers as well as for the layers relating mineralogical-characteristic variation. Notably, the administered chemical study proves to reveal that some of the phosphatic layers are not liable to exploitation, while others could be selected for

commercialization, such as the layer CIII₄. Indeed, a mixture of this layer and CI₁ turns out to culminate in a solution for a remarkably more effective productivity.

References

1. Burolet, F.: Contribution à l'étude stratigraphique de la Tunisie Centrale (1956)
2. Castany, G.: Geological study of the Eastern Tunisian Atlas (1951)
3. Mrabet, A.: Stratigraphy, Sedimentation and Carbonate Diagenesis of the Lower Series of central Tunisia (1987)



What Factors Determine the Geometries of Fault-Associated Dolomitization Geometries in Shallow-Marine Carbonates?

Shuqing Yao, Enrique Gomez-Rivas, Juan Diego Martín-Martín, David Gomez-Gras, Anna Travé, Albert Griera, and John Howell

Abstract

The present study investigates the controls on fault-associated dolostone geometries based on the Benicàssim outcrop analogue (Maestrat Basin, E Spain). It is also aimed to provide new insights into the prediction of fault-associated dolomitized hydrocarbon reservoirs. To this end, mapping, logging and log correlation were carried out in the Benicàssim area, where a >1600 m-thick succession of Aptian-Albian carbonate ramp sediments of the Benassal Fm are partly replaced by fault-associated dolostones. The results reveal that km-wide massive dolostone patches form near large-scale faults, indicating that they acted as entry points for dolomitizing fluids. These dolostones laterally pass to large stratabound bodies extending for at least 7 km away from feeding faults. The presence of a siliciclastic low-permeability unit (Escucha Fm) on top of the Benassal Fm constrained the dolomitizing fluids to a window whose top and bottom boundaries are about 100 m and 550 m below the base of the sealing unit, respectively. Thus, only the limestones comprised within this interval were dolomitized, indicating a clear relationship between the stratigraphic framework and the preferred replaced beds. Dolomitization mostly affected mid-ramp sediments (wackestones and packstones). Such facies are mostly abundant in the eastern part of the study area around the maximum flooding zone of the top sequence, which is preferentially dolomitized.

Keywords

Fault-Associated dolomitization • Outcrop analogue • Aptian-Albian • Maestrat Basin • Stratigraphic sequence • Diagenesis

1 Introduction

Fault-associated dolomitization is one of the most important diagenetic processes that modifies the petrophysical properties of carbonate rocks, and can result in the formation of reservoir rocks [1]. The resulting dolostone bodies typically present a variety of geometries, ranging from patches close to faults to stratabound bodies that can extend for long distances away from them [2, 3]. Their distribution and response to fluid flow are very difficult to predict using limited subsurface data. Despite recent advances based on outcrop analogues [1–4], understanding the controls on the different replacement geometries and providing tools for predicting them in the subsurface are still key issues in academic and hydrocarbon-industry research.

The overarching aim of this contribution is to provide an improved framework for the prediction of fault-associated dolomitization geometries in shallow-marine carbonates, based on the understanding of dolostone occurrence in relation to sedimentary facies, stratigraphic sequences and position with respect to feeding faults. We utilize the world-class Benicàssim outcrop analogue (Maestrat Basin, E Spain). This succession hosts large-scale fault-associated dolostones with various geometries and associated Mississippi-Valley-Type (MVT) ore deposits. The Benicàssim limestones were deposited in a carbonate ramp during the Aptian-Albian, and present a variety of lithofacies similar to age-equivalent major carbonate reservoirs within the Tethyan realm, such as those in the Middle East [5, 6]. The excellent exposures make this outcrop analogue a unique case study for improving our understanding of controls on fault-associated dolostones.

S. Yao · E. Gomez-Rivas (✉) · J. Howell
School of Geosciences, University of Aberdeen, Aberdeen, AB24 3UE, UK
e-mail: e.gomez-rivas@ub.edu

E. Gomez-Rivas · J. D. Martín-Martín · A. Travé
Departament de Mineralogia, Petrologia i Geologia Aplicada,
Universitat de Barcelona, 08028 Barcelona, Spain

D. Gomez-Gras · A. Griera
Departament de Geologia, Universitat Autònoma de Barcelona,
08193 Barcelona, Spain

© Springer Nature Switzerland AG 2019

D. M. Doronzo et al. (eds.), *Petrogenesis and Exploration of the Earth's Interior*,
Advances in Science, Technology & Innovation, https://doi.org/10.1007/978-3-030-01575-6_38

2 Methodology

This work is based on detailed mapping, systematic logging and correlation in the field area. 19 stratigraphic logs distributed across the studied area were built and correlated based on key stratigraphic units and marker facies. The areal extent of the dolostone bodies was estimated using conventional field mapping and Virtual Outcrop models (VOs), focusing on the transition between different geometries and their potential relationship with depositional facies, transgressive-regressive sequences, fault systems and fracture networks. The geometries of dolostone bodies are recognised based on their dimensions and spatial association with faults and bedding [2, 3].

3 Results

3.1 Structural and Sedimentary Framework

Correlation of the exposed Benassal Fm in the Benicàssim area shows significant variations in sediment thickness across the three main blocks defined by the Campello and Benicàssim faults, indicating that the most important structure at the time of deposition was the W-E-trending Campello Fault (Fig. 1). It forms an N-S structural framework that is consistent with a half-graben basin. The east-to-west structure of the study area was influenced by the N-S-trending Benicàssim Fault.

The Benassal Fm is stacked in three transgressive-regressive sequences. They generally reflect an evolution from basinal to inner ramp depositional settings, with significant variations of lithofacies distributions between the footwall and hangingwall blocks of the Campello Fault (Fig. 1). The distribution of lithofacies throughout the hangingwall of the Campello Fault is relatively homogeneous, with minor differences if we look at the north-south trend (Orpesa Range) compared to the east-west trend (Orpesa Range to Ferradura). By contrast, the lithofacies associations of the footwall block of the Campello Fault (Cingle del Morral) generally represent shallower environments than the stratigraphically equivalent rocks of the hangingwall.

3.2 Dolostone Geometry and Distribution

Two types of dolostone end-member geometries have been recognized, showing a clear spatial association between them: (i) fault-associated massive patches that laterally

evolve to (ii) stratabound bodies, forming a continuum as classical Christmas tree patterns (Fig. 1). The distribution of Benicàssim dolostones shows a close relationship with faults of different scales, the stratigraphic framework and the depositional settings, and the likely top seal for dolomitizing fluids (Fig. 1). The main controls are:

- i. Faults: The vast majority of dolostones are associated with the Campello Fault. Km-scale patches close to this fault in the north pass to stratabound dolostones with an extension of at least 7 km to the south.
- ii. Top seal: Dolostones in this area only occur in the Benassal Fm and are vertically restricted to a zone below the base of the overlying Escucha Fm (about 70–130 m at the top and 400–650 m at the bottom below the base of the Escucha Fm).
- iii. Stratigraphic framework: Dolostones only replace limestones in sequence III in the north of the Orpesa Range and sequence II in Cingle del Morral, but replace both the two sequences in the south of the Orpesa Range and Ferradura.
- iv. Depositional settings and lithofacies distribution: Most dolomitized sediments were deposited in middle ramp settings with wackestone-packstone textures.

4 Discussion: Controls on Fault-Associated Dolostone Geometries

In this study, the master feeding fault (Campello) defined a lateral dolomitization window along its hangingwall. This probably implies a predictable relative size of fault-associated dolostone geobodies associated with extensional faults (Fig. 1). A non-dolomitized zone occurring at 70–130 m beneath the base of the Escucha Fm (Fig. 1) is likely associated with a clastic top seal (Escucha Fm) in this study. This differs from the frequently reported shale seals in other fault-associated dolomitization systems, where limestones just below the sealing shale unit normally appear extensively dolomitized [1]. Moreover, this study demonstrates how the distribution of dolostone geobodies can be predicted by combining information on (i) sediment position with respect to feeding faults and (ii) the existence of a vertical dolomitization window defined by the stratigraphic framework in a way that only certain beds, systems tracts and sequences can potentially be replaced (Fig. 1). This concept can be applied to analogous subsurface cases. The depositional setting and distribution of lithofacies normally determine the units that are can be preferentially dolomitized and the extent of dolomitization [2–4], which is also the case here.

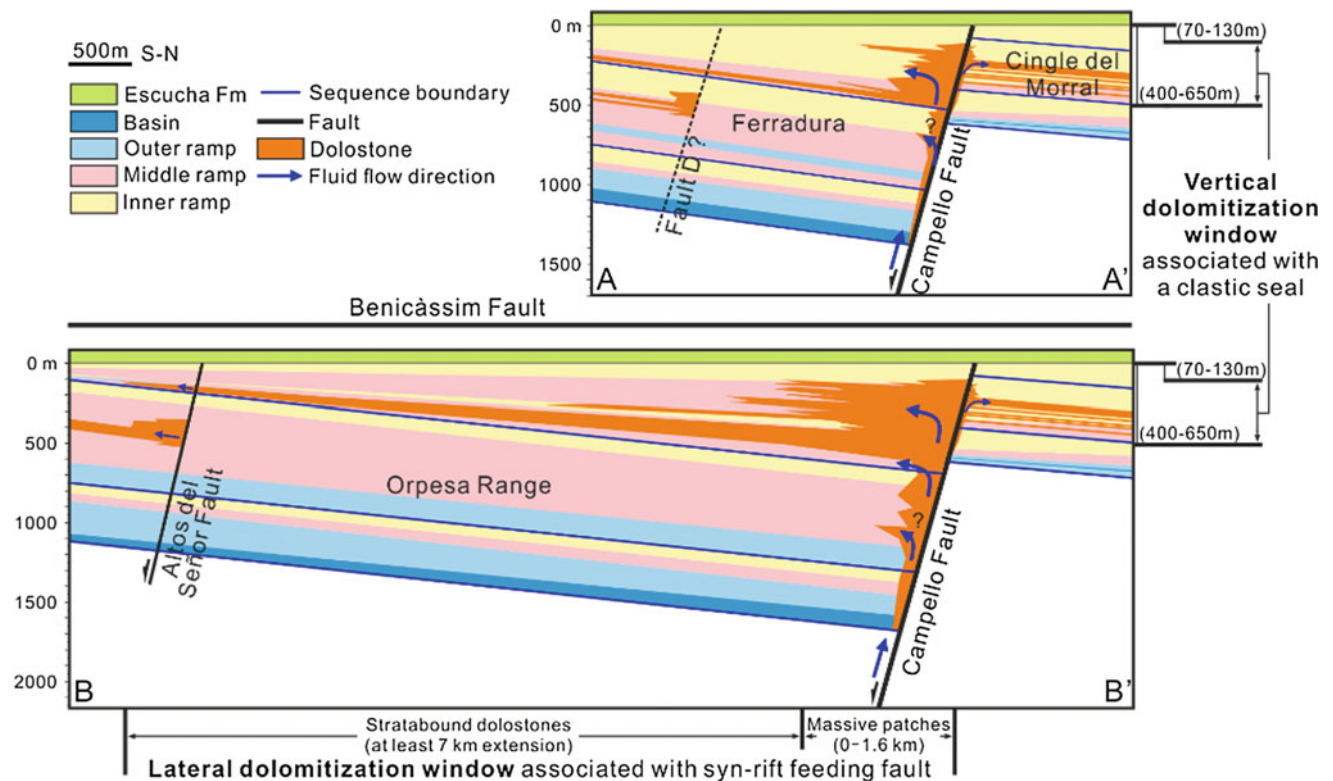


Fig. 1 Sketches of the half-graben structure showing the main depositional environments (inner, middle and outer ramp) and the distribution of dolostones across the study area

5 Conclusions

This contribution shows how the geometry and distribution of fault-associated dolostone geobodies can be controlled by the presence of large-scale faults, a regional top seal, the depositional settings and the stratigraphic architecture of the basin infill. The results of this study provide new insights into the prediction of fault-associated dolostones in the subsurface, and are therefore useful for hydrocarbon exploration, development and production activities.

References

1. Davies, G.R., Smith Jr., L.B.: Structurally controlled hydrothermal dolomite reservoir facies: an overview. *AAPG Bull.* **90**(11), 1641–1690 (2006)
2. Wilson, M.E., Evans, M.J., Oxtoby, N.H., Nas, D.S., Donnelly, T., Thirlwall, M.: Reservoir quality, textural evolution, and origin of fault-associated dolomites. *AAPG Bull.* **91**(9), 1247–1272 (2007)
3. Sharp, I., Gillespie, P., Morsalnezhad, D., Taberner, C., Karpuz, R., Vergés, J., Horbury, A., Pickard, N., Garland, J., Hunt, D.: Stratigraphic architecture and fracture-controlled dolomitization of the Cretaceous Khami and Bangestan groups: an outcrop case study, Zagros Mountains, Iran. *Geol. Soc. London Spec. Publ.* **329**(1), 343–396 (2010)
4. Hollis, C., Bastesen, E., Boyce, A., Corlett, H., Gawthorpe, R., Hirani, J., Rotevatn, A., Whitaker, F.F.: Fault-controlled dolomitization in a rift basin. *Geology* **45**(3), 219–222 (2017)
5. Gomez-Rivas, E., Corbella, M., Martín-Martín, J.D., Stafford, S.L., Teixell, A., Bons, P.D., Griera, A., Cardellach, E.: Reactivity of dolomitizing fluids and Mg source evaluation of fault-controlled dolomitization at the Benicassim outcrop analogue (Maestrat basin, E Spain). *Mar. Petrol. Geol.* **55**, 26–42 (2014)
6. Martín-Martín, J.D., Travé, A., Gomez-Rivas, E., Salas, R., Sizun, J.P., Vergés, J., Corbella, M., Stafford, S.L., Alfonso, P.: Fault-controlled and stratabound dolostones in the Late Aptian–earliest Albian Benassal Formation (Maestrat Basin, E Spain): petrology and geochemistry constrains. *Mar. Petrol. Geol.* **65**, 83–102 (2015)

Part IV
Applied Mineralogy and Tectonics

Fracture-Related Dolomitization Affecting Late Jurassic—Lowermost Cretaceous Syn-rift Deposits (Maestrat Basin, Southern Iberian Chain, Eastern Spain)

Anna Travé, Judit Nadal, Elisabet Playà, Ramon Salas, Juan Diego Martín-Martín, and Enrique Gomez-Rivas

Abstract

Late Jurassic-lowermost Cretaceous limestones and dolomites are oil reservoirs in the offshore Mediterranean field. Because the same dolomitization process exists in the neighboring onshore Maestrat basin, a thorough understanding of the dolomitization model will help greatly in understanding the reservoir properties. The studied dolomites are Ca-rich, Mn, Sr and Na-poor, with a variable content of Fe, and are attributed to multiple dolomitization events at various temperatures and/or from fluids with variable $\delta^{18}\text{O}_{\text{SMOW}}$ values. The fluid inclusions indicate the contribution of deep basin brines. Mg was provided by partial dissolution of Triassic and Liassic carbonates and evaporites, together with the expulsion of crystallization water from clay minerals. Dolomitization occurred in still porous and poorly compacted limestones, simultaneous with the earliest Cretaceous syn-rift re-structuration, giving rise to a significant subaerial exposure of the uplifted blocks, with the development of a well developed erosive surface on top of the Berriasian succession.

Keywords

Fracture-related dolomitization • Maestrat Basin

1 Introduction

Dolomite reservoirs associated to structural lineaments form many fields, among which there are the world's largest oil and gas field. Dolomitization is a common process that highly

affects the reservoir quality. The Maestrat basin (onshore), together with the adjacent Mediterranean offshore areas, have been explored for hydrocarbons. The late Jurassic Mas d'Ascla Fm is a well-known source rock [1] of the adjacent Amposta oil field [2, 3]. Late Jurassic-Cretaceous limestones and dolomites constitute the reservoir rocks. A thorough understanding of the dolomitized formations and fluid circulation patterns in the Maestrat basin can be of great economical interest.

The present study discusses the dolomite bodies contained in the Upper Jurassic–lowermost Cretaceous carbonate units of the Maestrat Basin (southern Iberian Chain) in order to establish a conceptual model for fluid circulation in the basin. Hosting limestones and dolomites were systematically sampled at each outcrop for petrological and geochemical study purposes. Other fault-related dolomites from Aptian-Albian age as persisting in the neighboring areas differ noticeably, and were formed at later events [4].

2 Geological Setting

The Maestrat Basin is located Southeast the Iberian Chain, and was developed by the inversion of Mesozoic rifts during the Paleogene. The late Jurassic-early Cretaceous syn-rift deposits are characterized with the predominance of shallow marine carbonates. The onset of rifting coincided with a significant rise in sea-level. Rapid subsidence of an array of tilted blocks resulted in the rapid drowning of shallow-water Oxfordian carbonate and the accumulation of Kimmeridgian deeper carbonate sediments. Thin bedded lime-mudstones and sponge build-ups capped the crests of fault blocks and these facies turned, vertically, into anoxic basinal marls (Ascla Fm.) in the evolving hanging-wall basins. The Tithonian to Berriasian sequence is composed of platform carbonates which graded basin-wards into hemipelagic Calpionella limestones. The Valanginian to Barremian succession, lying along the basin margins, is characterized with estuarine shallow-water carbonate platforms that represents

A. Travé (✉) · E. Playà · R. Salas · J. D. Martín-Martín
E. Gomez-Rivas
Departament de Mineralogia, Petrologia i Geologia Aplicada,
Facultat de Ciències de la Terra, Universitat de Barcelona (UB),
Martí i Franquès s/n, 08028 Barcelona, Spain
e-mail: atrave@ub.edu

J. Nadal
Pasturabosc, Gaüses, Vilopriu (Baix Empordà), Spain

a lost of subsidence. The late Barremian consists of a tidally-dominated delta complex. During the Aptian, marine conditions prevailed again and very expansive, rapidly prograding shallow-water carbonate platforms developed. The early-to-middle Albian sequence consists of a very extensive tidally-influenced delta system (Escucha Fm).

3 Results

The dolomitization process appears to affect four different limestone formations: Polpís Fm, Ascla Fm, Bovalar Fm and Pleta Fm. Dolomite occurs either as replacive or as cement filling vug and fracture porosity.

The late Jurassic-lowermost Cretaceous host-limestones lying in the Maestrat basin appear to display $\delta^{18}\text{O}$ values ranging from -8.1 to -0.1‰ V-PDB, and $\delta^{13}\text{C}$ values ranging between -6.6 and $+2.3\text{‰}$ V-PDB. The $\delta^{18}\text{O}$ values of the replacive dolomite and dolomite cement prove to range from -9.8 to -1.3‰ , while the $\delta^{13}\text{C}$ values range from -3.9 to $+2.4\text{‰}$ V-PDB. The dolomites affecting the Kimmeridgian limestones display isotopic compositions similar to those affecting the Tithonian-Berriasian limestones, suggesting a widespread dolomitization process. In the Salzedella sub-basin, the oxygen isotopic compositions of replacive dolomite are about $2\text{--}3\text{‰}$ lighter than the $\delta^{18}\text{O}$ values of the precursor limestones. On comparing samples extracted from different palaeogeographic sites, the dolomites located in the depocenter prove to reveal the largest range of $\delta^{18}\text{O}$ compositions, while the depositional high sited dolomites appear to display a dispersion of $\delta^{18}\text{O}$ values of up to $2\text{--}4\text{‰}$. In the Aliaga and Morella sub-basins, the precursor limestones and dolomites prove to display similar ranges.

The $^{87}\text{Sr}/^{86}\text{Sr}$ ratios of the replacive dolomites turn out to be more radiogenic than the limestones related ones, ranging from 0.70740 to 0.70798 . Homogenization temperatures (Th) prove to range from 70 to 120 °C, and salinity from 16 to 23 wt% NaCl equivalent.

4 Discussion

Dolomitization in the late Jurassic-lowermost Cretaceous limestones in the Maestrat Basin was controlled not only by fractures, but also by unconformities, precursor limestone texture, stratification planes and heterogeneities. The dolomitized bodies are decimetric to kilometric in length, of up to 150 m thick, displaying a wedge morphology associated with the faults.

The youngest limestone unit affected by dolomitization (Bovalar Fm) was deposited between 148 and 142 My (Middle Tithonian-Lower Berriasian [5]). In the Tossal d'Orenga outcrop, the dolomitized section proves to be

affected with an erosive surface, above which were deposited the freshwater non-dolomitized limestones with charophytes of Valanginian-early Hauterivian age. The Upper Hauterivian marine deposits lying on top of these freshwater limestones are dated as early as 134 My. The presence of dolomite cobbles within the non-dolomitised freshwater limestones indicates that the time constrained for the dolomitizing process proved to occur between 142 and 134 My ago.

Dolomitization occurred simultaneously with the main structuration of the horsts and grabens of the late Jurassic-early Cretaceous rifting stage and during subaerial exposure of the uplifted blocks, creating a fini-Berriasian erosive surface in these threshold zones. Dolomitization occurred soon after limestone deposition, affecting the still porous and poorly compacted limestones. This phenomenon occurred at different burial depths, from relatively buried sediments in the more subsident areas to more surficial levels in the threshold zones.

Exposure of the uplifted and titled blocks, during the rifting, favored for the topographically-driven meteoric waters to penetrate the basin downwards, towards a good permeable horizon, 3200 meters below, as manifested by the highly karstified Lower Muschelkalk carbonates. This fluid became enriched in Mg when passing through Triassic and Jurassic carbonates and evaporated, producing partial dissolution—and the incorporation of their minor remaining connate waters—and it probably mixed with Mg-rich fluids derived from the expulsion of crystallisation waters during clay transformation and dewatering. The deduced isotopic composition of the fluid (-5 to $+10\text{‰}$ SMOW), together with fluid temperatures ranging between 70 and 120 °C, and salinities ranging from 16 to 23‰ NaCl equivalent, support the contribution from deep basin brines.

In this extensional setting, high convective cells were probably originated at depth, related to a regional thermal anomaly, heating and driving the infiltrated meteoric fluids (converted into hot brines) upwards, towards shallower settings along the fractures. They migrated along the fractures till reaching a more surficial and permeable limestone horizon ready to be dolomitized. The dolomitization potential diminished away from the fracture.

These dolomites, Ca-rich with low Mn, Sr and Na contents and variable Fe content, are all attributed to a single and continuous dolomitization event. Accumulation of ascending fluids in a fault zone at pressures and temperatures greater than the surrounding pore-fluids produced a replacement of the host limestone, preferentially in the hanging wall. The petrographic and geochemical similarities noticeable between all the studied dolomites point out to a single dolomitization event. The most consistent hypothesis for the Mg origin seems to be a combination of partial

dissolution of the underlying carbonate and sulphate levels, along with the expulsion of crystallisation waters during clay transformation.

5 Conclusions

Dolomitization occurred between 142 and 134 My, soon after limestone deposition, affecting still porous and poorly compacted limestones.

Exposure of the uplifted and tilted blocks, during the rifting, favoured topographically-driven meteoric waters to enter the basin towards a good permeable horizon, 3200 m below and represented by the highly karstified Lower Muschelkalk carbonates. This fluid became enriched in Mg when passing through Triassic and Jurassic carbonates and evaporites, producing partial dissolution, and probably mixed with Mg-rich fluids derived from the expulsion of crystallisation waters during clay transformation and dewatering. The deduced composition of the fluid (−5 to +10‰ SMOW), together with fluid temperatures (70–120 °C) and salinities (16–23% NaCl equivalent) support contribution from deep basin brines.

In this extensional setting, high convective cells were probably originated at depth, heating and driving the infiltrated meteoric fluids upwards towards shallower settings along fractures. They migrated along fractures until they reached a more surficial and permeable limestone horizon ready to be dolomitized. The potential of dolomitization diminished away from the fracture.

These dolomites, Ca-rich with low Mn, Sr and Na contents and variable Fe content, are attributed to multiple

dolomitization events at various temperatures and/or from fluids with variable $\delta^{18}\text{O}_{\text{SMOW}}$ values. Accumulation of ascending fluids in a fault zone at pressures and temperatures greater than the surrounding pore-fluids produced replacement of the host limestone.

Acknowledgements This work was funded by the Spanish Government Project CGL2015-66335-C2-1-R and the “Sedimentary Geology Catalan Research Group” 2017SGR-824.

References

1. Rossi, C., Goldstein, R.H., Marfil, R., Salas, R., Benito, M.I., Permanyer, A., de la Peña, J.A., Caja, M.A.: Diagenetic and oil migration history of the Kimmeridgian Ascla formation, Maestrat Basin, Spain. *Mar. Petrol. Geol.* **18**, 287–306 (2001)
2. Salas, R., Permanyer, A.: Evidencias de generación de hidrocarburos en la formación de margas del Mas d’Ascla (Jurásico superior, Cadena Ibérica oriental) y su relación con el campo de Amposta de la Cuenca de Tarragona. *Boletín Geológico y Minero* **114**, 75–86 (2003)
3. Permanyer, A., Salas, R.: Integrated thermal model, diagenetic history and oil correlation in Western Mediterranean, Spain. IV ALAGO Workshop-Basin Modeling, Buenos Aires, Argentina (2005)
4. Martín-Martín, J.D., Travé, A., Gomez-Rivas, E., Salas, R., Sizun, J.-P., Vergés, J., Corbella, M., Stafford, S.L., Alfonso, P.: Fault-controlled and stratabound dolostones in the Late Aptian-earliest Albian Benassal Formation (Maestrat Basin, E Spain): petrology and geochemistry constrains. *Mar. Pet. Geol.* **65**, 83–102 (2015)
5. Bádenas, B., Salas, R., Aurell, M.: Three orders of regional sea-level changes control facies and stacking patterns of shallow platform carbonates in the Maestrat Basin (Tithonian-Berriasian, NE Spain). *Int. J. Earth Sci. (Geol Rundsch)* **93**, 144–162 (2004)

First Report of Cryptomelane in Altered Rhyolite from Tazrouk Volcanic District, Latea, Hoggar, Algeria

Riad Ben El Khaznadj, Abderrahmane Bendaoud, and Abderaouf Seffari

Abstract

X-ray diffraction, ore microscopy, and electron microprobe studies have been implemented on ore samples obtained from rhyolitic rock collected at the Tazrouk volcanic district, Hoggar. The identified manganese ore minerals include Alkali-felspar, Magnesio-arfevdsonite and cryptomelane. All these minerals are poorly crystalline. The minerals' chemical compositions indicate little contamination with other elements. Modes of occurrence are principally taking place through replacements, cavity or fracture fills, leaching and precipitation. Mineral associations seem rather complex, which makes definite paragenetic relations impossible to establish. Supergene formation of the manganese oxide ore is highlighted by the abundance of manganese minerals in solution channels, such as fractures and cavities within silicate gangue. Much of the ore, however, appears to have been enriched by leaching of gangue minerals and the subsequent addition of manganese. Noteworthy, also, is that this large field occurrence of cryptomelane has initially been described with respect to the Hoggar shield.

Keywords

Cryptomelane • Manganese ore • Rhyolite • Tazrouk • Mineralisation • Hoggar

1 Introduction

The Tazrouk Volcanic Region (RVT) is located a hundred kilometers NE of Tamanrasset, perched at over 1900 m altitude [1]. In the study area (lying between N23° 10, E6° 20 and N23° 35, E6° 20), there lies, essentially, a bedrock of Eburnean age (quartzo-feldspathic gneiss, plagioclastic gneiss with garnet, leptynites and amphibolites), along occasional dioritic intrusions and granite, occasionally covered with Cenozoic volcanic formations on lacustrine environment [2–5]). The occurrence of the cryptomelane ore is described as occurring on a very large field in combination with Cenozoic felsic lavas, lying across an area of about 50 Km². Cryptomelane is a potassium manganese oxide mineral of the formula $K(Mn^{4+}, Mn^{2+})_8O_{16}$ [6]. The region is highly deformed and many N030 faults are observed to display, mainly, senestre deformation (Fig. 1) [7, 8].

The present work's major contribution consists in an initial attempt made to report the occurrence of an important deposit of cryptomelane, as identified to occur in the investigated Eocene felsic rocks of the Tazrouk area.

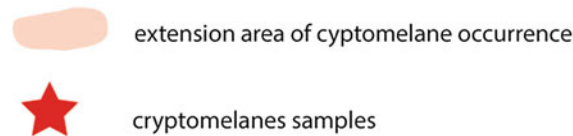
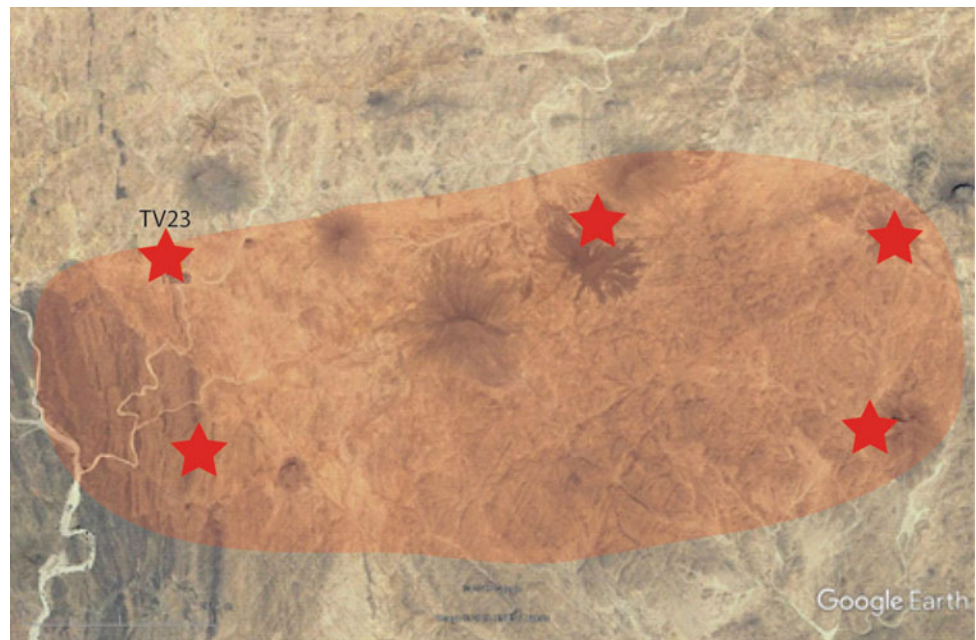
2 Methods

The minerals relating optical properties were studied by means of the Leitz polarizing microscope. The cryptomelane associated chemical composition was determined via the CAMECA SX100 electron microprobe, made available at the Montpellier University (France). The rock samples were crushed to a powder size of less than 30 μm. An X-ray diffraction analysis was performed by means of the PW 1729 diffractor. The Xpovder software was used to identify the relevant mineral phases.

R. Ben El Khaznadj (✉)
Laboratoire de Métallogénie et Magmatisme de l'Algérie,
USTHB, Bab Ezzouar, Algeria
e-mail: rbenelkhaznadj@usthb.dz

A. Bendaoud · A. Seffari
Laboratoire de Géodynamique, Géologie de l'Ingénieur et
Planétologie, USTHB, Bab Ezzouar, Algeria

Fig. 1 Google Earth satellite picture showing the extend of the cryptomelane outcrop



3 Results

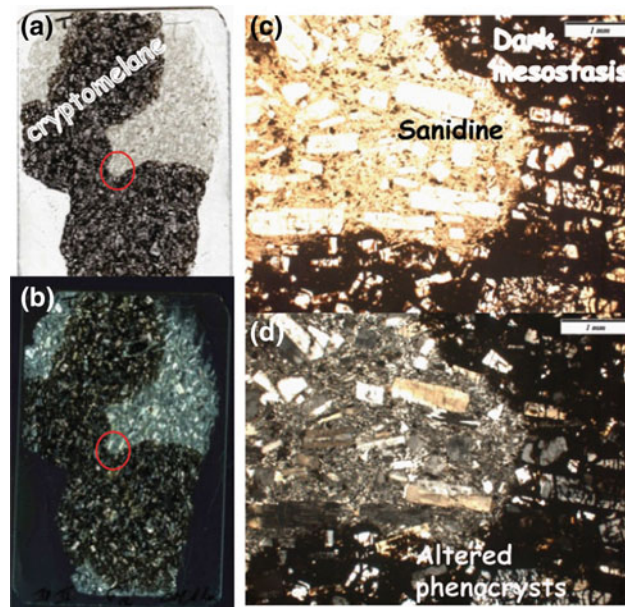
The cryptomelane related chemical composition study (Table 1) has revealed the predominance of potassium (1.506 apfu) over sodium (0.107 apfu). It has also been discovered that traces of Ca (up to 0.069 apfu) and P (0.059 apfu) persist. The petrographic study reveals clearly that the cryptomelane is mainly represented through the glass phase, interpenetrating the rhyolite mesostase, as illustrated through Fig. 2. The texture undergone replacement has made it hard to distinguish any relationship between the original felsic texture and the contaminated one.

4 Conclusions

An initially drawn report has been elaborated concerning the widely abundant occurrence of cryptomelane across the Hoggar shield, particularly their concentration along a remarkably large extension of the Tazrouk area. Their nature has been confirmed by means of electron probe microanalyses and the X-Ray diffraction method. The deposit formation might well be closely related to the hot springs persisting in such a lacustrine environment. The deposits appear to be located along draining corridors, often corresponding to fault zones, and could probably provide certain

Table 1 Chemical composition (oxide wt%-top-and atoms per formula units (a.p.f.u.)-bottom-of the Tazrouk area based cryptomelane

Sample	TV23	TV23	TV23	TV23
	95/1	96/1	97/1	99/1
SiO ₂	0.23	0.30	0.44	0.26
TiO ₂	0.00	0.00	0.01	0.00
Al ₂ O ₃	0.32	0.34	0.79	0.20
FeO _T	0.00	0.00	0.00	0.00
MnO	93.89	93.87	91.34	94.40
MgO	0.00	0.00	0.06	0.02
CaO	0.07	0.07	0.34	0.09
Na ₂ O	0.22	0.26	0.29	0.17
K ₂ O	6.25	6.14	4.53	6.20
Cr ₂ O ₃	0.00	0.03	0.03	0.00
P ₂ O ₅	0.00	0.04	0.37	0.09
Cl	0.01	0.00	0.01	0.00
Total	100.8	101.0	98.11	101.3
Si	0.043	0.056	0.084	0.048
Ti	0.000	0.000	0.002	0.000
Al	0.071	0.076	0.177	0.043
Fe ²⁺ all ferrous	0.000	0.000	0.000	0.000
Mn	15.02	14.96	14.73	15.01
Mg	0.000	0.000	0.017	0.006
Ca	0.014	0.014	0.069	0.018
Na	0.081	0.095	0.107	0.063
K	1.506	1.473	1.101	1.485
Cr	0.000	0.004	0.004	0.001
P	0.000	0.006	0.059	0.014
Cl	0.002	0.000	0.002	0.001
Total	16.72	16.67	16.34	16.68



- (a) and (b) scanned thin section
- (c) Thin polarized section showing the dark mesostasis rich on cryptomelane
- (d) Thin polarized and analysed section of the same rhyolitic host rock
- zoom area of the thin section

Fig. 2 Cryptomelane (dark) in association with rhyolite from RVT area

explanation as to the supragene post-generation of the cryptomelane veins, as associated with the latest felsic magmas rich in potassium [9, 10].

References

1. Ben El Khaznadji, R.: Etude pétrologique des laves alcalines et hyperalcalines de la région de Tazrouk (Blocs Azrou N-Fad, EgéréAleksod-Hoggar Central). Thèse de Magister, USTHB-FSTGAT, Alger, Algérie, 165 p (2008)
2. Liégeois, J. P., et al.: Early and late Pan-African orogenies in the Air assembly of terranes (Tuareg Shield, Niger). *Precamb. Res.* **67**, 59–88 (1994)
3. Girod, M.: Le massif volcanique de l'Atakor (Hoggar, Sahara algérien). *Mém. CRZA, Sér. Géol.* **12**, 155. ed. CNRS, Paris, (1971)
4. Ait-Hammou, F., et al.: Le magmatisme Cénozoïque du Hoggar: une synthèse des données disponibles. Mise au point sur l'hypothèse d'un point chaud. *Bulletin, Service géologique d'Algérie*, **5**(1), 49–68 (1994)
5. Ben El Khaznadji, R., et al.: Neogene felsic volcanic rocks in the Hoggar province: volcanology, geochemistry and age of the Azrou trachyte-phonolite association (Algerian Sahara). *J. Afr. Earth Sci.* (2017). <https://doi.org/10.1016/j.jafrearsci.2016.07.013>
6. Richmond, W.E., Fleischer, M.: Cryptomelane, a new name for the commonest of the "psilomelane" minerals. *Am. Mineral.* **27**, 607–610 (1942)
7. Ben El khaznadji, R., et al.: Interpretation géodynamique des données morphostructurales du volcanisme du hoggar. 1st Arabgu International Conference (AIC-1) February 17–18th, 2016. FSTGAT-USTHB, Algiers, Algeria (2016)
8. Ben El Khaznadji, R., et al.: Contexte géodynamique de mise en place du volcanisme intraplaque Eocènequaternaire du LATEA: Une métacratonisation du Hoggar central. CAG24—Addis Abeba—Ethiopie (2013)
9. Hewett, D.F., Fleischer, M.: Deposits of the manganese oxides. *Econ. Geol.* **55**, 1–55. Society of Economic Geologists (1960)
10. Dill, H.G., Gerdes, A., Weber, B.: Age and mineralogy of supergene uranium minerals—tools to unravel geomorphological and palaeohydrological processes in granitic terrains (Bohemian Massif, SE Germany). *Geomorphology* **117**, 44–65 (2010)

Mineralogy Recognition from In-Situ Elemental Concentration Log Data Using Factor Analysis

Ahmed Amara Konaté, Heping Pan, Nasir Khan, Oumar Keita, Mamady Cissé, Mory Kourouma, and Daouda Keita

Abstract

Understanding log response in crystalline rocks is one of the major challenges encountered by geoscientists in general, and well-log analysts in particular. Owing to the persistence of metamorphism process, log interpretation in crystalline rocks appears to be a challenging task. In this context, the present study is focused on reporting the results drawn from the interpretation of elemental concentration log data. For an effective elemental concentration interpretation to take place, an appeal is made to the factor analysis method. Hence, constructing a model whereby elemental concentrations could be associated with mineral abundances is investigated and discussed. The reached results appear to reveal that the elemental concentration logs turn out to provide enough information useful for an accurate lithological description of crystalline rocks to take place, especially with regard to UHPM rocks.

Keywords

Crystalline rocks • Log interpretation • Factor analysis • Geochemical log

1 Introduction

The well logs relating applications are noticeably advanced in the petroleum industry. Consequently, log signatures in sedimentary rocks turn out to be widely known. Yet, this is not always the case for crystalline rocks [2]. Compared with sedimentary rocks, crystalline rocks are more diverse,

bearing rather complex compositions, textures, and structures, ensuing in various challenges in their lithological identification [3]. Noteworthy, also, is that no systematically formulated interpretation method, dealing with the crystalline-rock cases, has so far been made available [4] in geophysics. As a result, understanding log response in crystalline rocks remains a major challenge the geoscientists face, particularly the well-log analysts.

The CCSD project, subject of the present study, stands as one of the major geoscientific projects ever executed in China. The project has received financial and technical support from the part of the International Continental Drilling Program. The CCSD-Main Hole (CCSD-MH) is located too close to the Maobei Donghai County, at the Sulu Ultrahigh pressure metamorphic (UHPM) belt of Eastern China.

Despite the existing research works, the CCSD-MH geochemical log database has not yet been thoroughly and fully exploited. Hence, it offers a unique opportunity to investigate the elemental concentration log responses associated with the Sulu UHPM belt.

In this respect, the study intent lies in analyzing the CCSD-MH related elemental concentration log responses. To this end, a factor analysis approach is applied to construct a model whereby elemental concentration logs could be closely linked to the mineral abundances, while discussing the lithological-identification explanatory potentials and capacities. This study will contribute to the understanding of the log responses in regard of the CCSD-MH, as lying in the UHPM belt of Eastern China.

2 Data and Methodology

The obtained in situ geochemical logs were: Aluminum (Al) [wt%], Calcium (Ca) [wt%], Iron (Fe) [wt%], Gadolinium (Gd) [ppm], hydrogen (H) [wt%], silicon (Si) [wt%], Sulfur (S) [wt%], Titanium (Ti) [wt%], Potassium (K) [%], Thorium (Th) [ppm], and Uranium (U) [ppm].

A. A. Konaté (✉) · O. Keita · M. Cissé · M. Kourouma · D. Keita
 Institut Supérieur des Mines et Géologie de Boké,
 BP: 84, Boké, Guinea
 e-mail: konateahmed@hotmail.com

H. Pan · N. Khan
 Institute of Geophysics and Geomatics, China University of
 Geosciences (Wuhan), Wuhan, 430074, China

The entirety of these logs would serve to measure the chemical properties likely to help in partly diagnosing lithology. Actually, a combined analysis of these logs may well provide, through a statistical approach, a remarkably enhanced diagnostic strength for an effective lithological understanding of the study area.

Factor Analysis (FA) is a statistical approach aimed to detect the underlying variables (factors) that contribute in providing valuable explanation relevant to the correlation patterns underlying a set of observed variables. FA is frequently applied for data reduction purposes, in a bid to detect a certain number of factors that help explain most of the variance extent, noticeable within the scope of a great deal of manifest variables. The major advantages associated with the FA framework lie in the facts that it is quick, reliable and provides objective evaluation. The present research maintains that the FA emanating factors could well display close connections with the minerals making up the CCSD-MH predominant rock.

3 Results and Discussions

The FA approach was implemented on the standardized values of the elemental concentration logs via a correlation matrix bearing a zero mean and a variance of 1. The retained input log turns out to enclose Al, Si, Fe, Ti, K and Th. It is worth noting that Ca, Gd, H, S and U were discovered to prevail with low communality ranges (of less than 0.4). Consequently, the factor model would not fit adequately well on including them. On this Basis, they were discarded from the model. In this regard, the Kaiser criterion was applied to decide on the number of factors necessary to be extracted. Accordingly, the original set of six logs turned out to be reduced to a small set englobing just two factors, accounting for 76.261% of the initial set relating variance. Table 1, depicts the relevant factor loadings, as attained via Varimax and the communality estimates. The factor loadings help correlate the factors and the variables, while the

communality can be interpreted as the estimate of the variables' reliability. Based on Table 1, factor1 appears to help in explaining 57.515% of the total variance through strong absolute loadings of Al, Si, Fe, and Ti. This finding indicates well that these logs prove to display an effective congruence with factor 1. Amphibole minerals have been noticeably observed in several of the CCSD-MH gneiss samples [6]. The amphibole mineral related chemical composition (Hornblende) proves to contain the chemical elements predominantly abundant in the Earth's crust, mainly: Al, Fe, Si, and Ti. Therefore, Factor1 could well serve to reflect the amphibole mineral. Factor2 enabled to explain 18.746% of variance with high loading of K and Th. Still, K proves to display the highest load value with factor2. Such a remarkable correlation can also be viewed graphically through Fig. 1. The metamorphic rocks' potassium content is mainly related to feldspar \pm quartz. The Donghai area, lying across the southern Sulu UHPM belt is predominantly underlain with large K-feldspar associated gneiss [5]. K-feldspar is commonly potassium rich, with abundance of Th < 0.01 ppm [1], Table 13.15). Hence, factor2 may well be referred to as K-feldspar mineral.

After retaining and interpreting both factors on the consideration of the CCSD-MH attached mineral abundance, they were cross-plotted in a bid to observe their capacity to separate the metamorphic rock types from the CCSD-MH. Figure 2 depicts the cross plot of mineral logs as drawn from FA. An examination of Fig. 2 highlights well the amphibolites' visualization displaying the most scattered log data, with no severe overlaps being noticed to persist among the investigated rocks. However, the pertaining orthogneisses, amphibolites and paragneisses appear to be well distinguished. Still with Fig. 2, metamorphic rocks are witnessed to bear the following characteristics. The orthogneisses appear to display intermediate-high K-feldspar and intermediate-high amphibole mineral, while the paragneisses prove to reveal moderate K-feldspar and moderate amphibole mineral. As for the amphibolites, they turned out to exhibit a low K-feldspar and an intermediate amphibole

Table 1 Proportion of variance using varimax rotation and communality estimates

Log curve	Rotated solution		Communality estimates
	Factor 1	Factor 2	
Al	0.963	-0.114	0.940
Fe	0.974	-0.107	0.960
Si	-0.852	0.106	0.737
Ti	-0.843	-0.087	0.719
K	-0.048	0.798	0.639
Th	-0.130	0.751	0.581
% Variance	57.515	18.746	

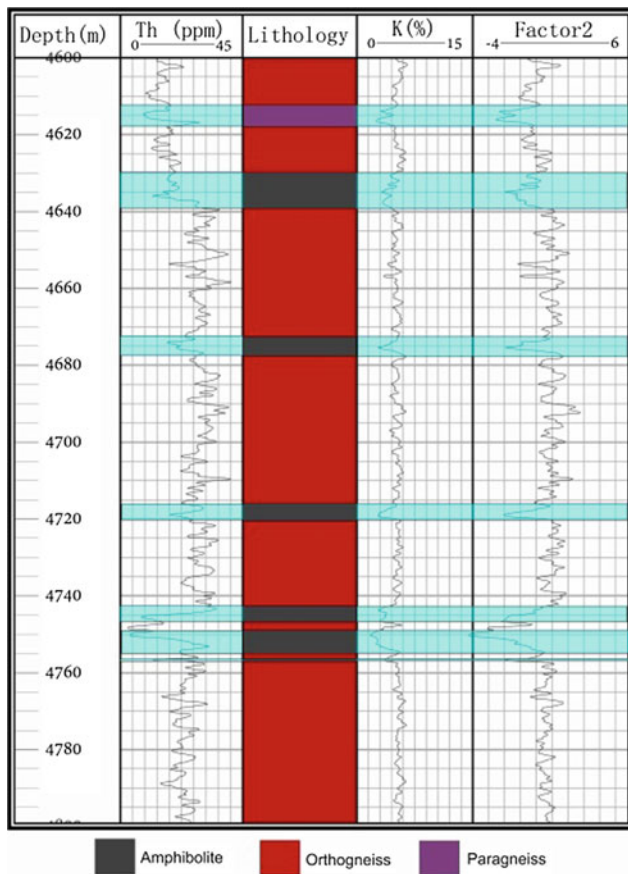


Fig. 1 The factor2 log with detail interpretation. Factor2 log as responding mainly to the K and Th related changes

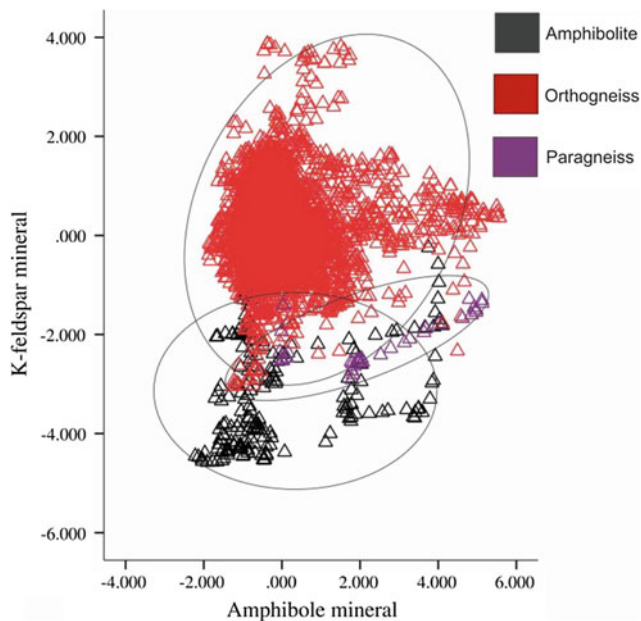


Fig. 2 Cross-plot relevant to mineral logs

mineral. This finding turns out to be consistent with the core analysis results as drawn from the study area, highlighting that the K-feldspar and amphibole minerals have been discovered to persist in gneisses [5].

4 Conclusions

FA proves to stand as an effective means whereby geochemical logging data could be efficiently condensed and interpreted. The reached findings prove to reveal that the implemented two-factor model (where factor1 (amphibole mineral) included Al, Fe, Si, and Ti, while factor2 (K-feldspar mineral) enclosed K and Th) proved to help in explaining 76.261% of the log-response variations. The model served to describe the constituent minerals making up the CCSD-MH rock, and contributed significantly in characterizing the predominant rocks persistent within the UHPM environment. Noteworthy, however, is that this research was conducted within the context of a single deep well. It would sound rather interesting, therefore, to extend the FA scheme application to other geologically complex zones of interest.

References

1. Bigelow, E.L.: Introduction to Wireline Log Analysis. Western Atlas International, Houston, Texas (1992)
2. Bartetzko, A., Delius, H., Pechnig, R.: Effect of compositional and structural variations on log responses of igneous and metamorphic rocks. I: mafic rocks. In: Harvey, P.K., Brewer, T.S., Pezard, P.A., Petrov, V.A. (eds.) *Petrophysical Properties of Crystalline Rocks*. Geological Society, London, Special Publications, pp. 255–278 (2005)
3. Maiti, S., Tiwari, R.K.: A hybrid Monte Carlo method based artificial neural networks approach for rock boundaries identification: a case study from KTB Borehole. *Pure. Appl. Geophys.* **166**, 2059–2090 (2009)
4. Pechnig, R., Delius, H., Bartetzko, A.: Effect of compositional variations on log responses of igneous and metamorphic rocks. II: acid and intermediate rocks. In: Harvey, P.K., Brewer, T.S., Pezard, P.A., Petrov, V.A. (eds.) *Petrophysical Properties of Crystalline Rocks*. Geological Society, London, Special Publications, pp. 279–300 (2005)
5. Zhang, Z., Xu, Z., Xu, Z.: Petrology of the non-mafic UHP metamorphic rocks from a drillhole in the southern Sulu orogenic belt, eastern central China. *Acta Geol. Sin.* **77**(2), 173–186 (2003)
6. Zhang, Z., Xiao, Y., Hoefs, J., Liou, J.G., Simon, K.: Ultrahigh pressure metamorphic rocks from the Chinese continental scientific drilling project: I. petrology and geochemistry of the main hole (0–2,050 m). *Contrib. Mineral Petrol.* **152**, 421–441 (2006)

Fluid Inclusions, Solid-Solid Transitions in Salt, Ceramics and Minerals to Calibrate the Microthermometric Stage

Mouna El Mekki-Azouzi and Claire Ramboz

Abstract

The Linkam THMS 600 microthermometric stage use the fluid inclusions to deliver quantitative paleo-temperatures of subsurface past environments that are critical not only for understanding past climate evolution but also to validate the outcome of predictive models of future climates. In this case, the calibration of the microthermometric stage is the primordial condition to have the most precise temperatures. Thus the calibration of the microthermometric stage is performed from -56 to $+573$ °C using reversible fusions or solid-solid transitions in standards as salts, ceramics, minerals or synthetic fluid inclusions. The nine transitions measured define a linear calibration curve with negative slope, showing a correction ranging from 1.6 to 16 °C between -60 and 600 °C. The vertical and lateral gradients (temperature bias) are estimated and discussed.

Keywords

Calibration • Microthermometric stage • Temperature • Fluid inclusion • Phase transitions • Gradients

1 Introduction

To calibrate a temperature microthermometry stage with an accuracy $\leq 5\%$, standards have ideally to be unalterable products in laboratory conditions, display one or more reversible phase transitions observable on sample thickness of some 100 to 1000 μm , i.e. the same magnitude order of

the fluid inclusions (FI) studied by microscopy [1]. Jehl [2] has extensively calibrated the Chaixmeca conduction stage between 0 and 3 °C using natural FI and a set of inorganic standards proposed by Merck. Macdonald and Spooner [3] used the same standards, and in addition employed solid compounds and metals to calibrate a Linkam TH 600 stage. The inorganic Merck standards are small crystals or powder. It is therefore difficult with this type of product to perform an accurate calibration point: due to the important mass effects, melting occurs in the lateral and vertical gradients of temperature even more important when the temperature is high. The measurements are difficult to observe, the fusion begin and finish often outside the scope of the objective. The precisions obtained with these products are bad, about 5 at 330 °C [2]. About the melting of metals, it is difficult to see under a microscope without reflected light. The use of natural or synthetic FI to calibrate the microthermometric stage constitutes a real progress. FI are not sensitive to the laboratory conditions and do not change during the measurement. Finally, synthetic FI provide absolute standard temperatures, by allowing the measurement of temperature transitions on assemblies of invariant phases under microscope, also easily repeatable to infinity. The use of synthetic FI as standard temperature under microscope presents some limitations. The highest temperature invariant points which are measurable with synthetic FI are the critical points. On one hand, the critical points of salt solutions do not exceed 450 °C. On the other hand, the critical transition is essentially a continuous transition and not an abrupt change. FI synthesized with aqueous fluids of critical density are small. All these arguments justify that the critical temperature measurements are imprecise and difficult to realize with FI.

In this work we present a calibration curve of the microthermometric stage Linkam THMS 600 made with 9 temperatures references distributed between -56 and 573 °C. Several new types of standards are used, including ceramic, quartz containing micro-solids and salts. The objective of this work is multiple: (i) to provide an experimental confirmation of the linearity of the calibration curve

M. El Mekki-Azouzi (✉)
Bizerte School, Carthage University, 7021 Jarzouna, Tunisia
e-mail: mouna.elmekki-azouzi@laposte.net

C. Ramboz
Institut des Sciences de la Terre d'Orléans, UMR 6113,
CNRS/Universités d'Orléans et Tours, 1A rue de la Férellerie,
45071 Orléans Cedex, France

between -56 and 573 °C. (ii) to present new standards, especially one which is reliable and easy to measure providing a highly accurate calibration point close to the temperature limit of the device. This point plays on the slope precision of the straight correction, and so on the accuracy of the measurement itself. Moreover, the vertical and horizontal bias on temperature, especially for small samples, are evaluated and discussed.

2 Experimental Setup

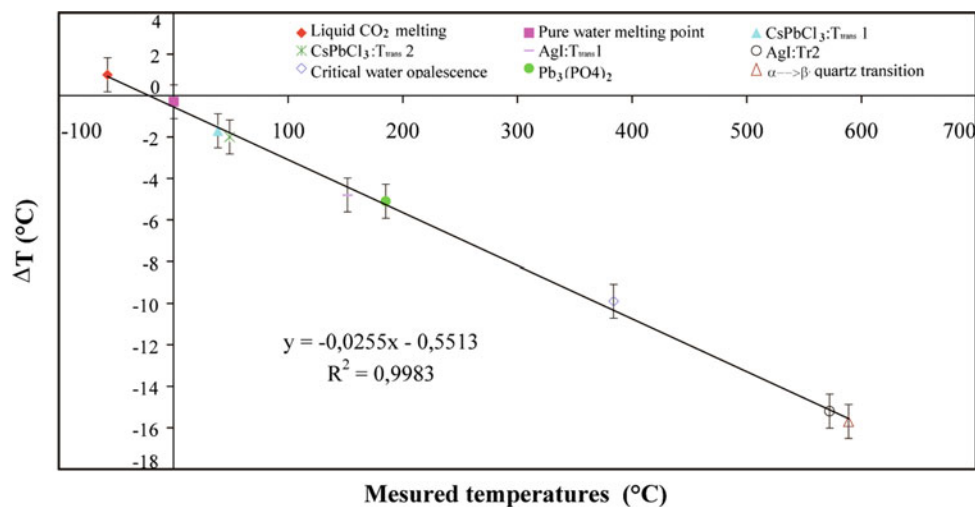
A Linkam THMS 600 microthermometric stage mounted on an Olympus BH2 microscope equipped with long frontal distance objectives. The microthermometric stage is driven by computer with software written in Labview.

Standards used at negative temperature: The pure water synthetic FI was used to calibrate the melting point at 0 °C. The natural FI in quartz Camperio with three phases, water and CO_2 liquid and CO_2 vapor were used to calibrate the melting temperature of solid CO_2 at -56.6 °C.

Standards used at positive temperature: We used a synthetic solid standards showing phase transitions at known temperatures between 32 and 574 °C.

- The AgI salt: a phase transition β/γ AgI \rightarrow α AgI at 147 °C and a melting at 557 °C.
- Superconductor Ceramics with solid-solid transition: CsPbCl_3 and $\text{Pb}_3(\text{PO}_4)_2$.
- The α - β transition in quartz from Soufriere volcano. All measurements were made with a rate gradient from 0.2 to 1 °C/min.

Fig. 1 Calibration curve of the microthermometric stage linkam THMS 600



3 Results

3.1 Calibration Curve

The measurements are summarized in Fig. 1. The error of the confidence interval 95% on the measure is estimated at about ± 1 °C.

3.2 Temperature Bias

Figure 2 shows horizontal and vertical temperature gradients evaluated by Infra-Red versus the conduction. All experiments involving a very low absolute error on temperature ($\leq \pm 0.3$ °C).

4 Discussion

In this study, the quality of the standards, the centred, the reproducible and the reversible measurements have confirmed the linearity of the calibration curve for the microthermometric stage Linkam THMS 600. Macdonald and Spooner (1981) have worked on the repeatability of measurements, but because of the poor quality of their standards, the statistical dispersion is low but the bias is strong. They have made their measurements with a single speeds of ramp at 0.4 °C/min. They choose this speed after few ten measurements on melting point on the same standard, but they have not taken into account all the dynamics of temperature, surface properties and structure of each individual standard. The majority of the standards used in

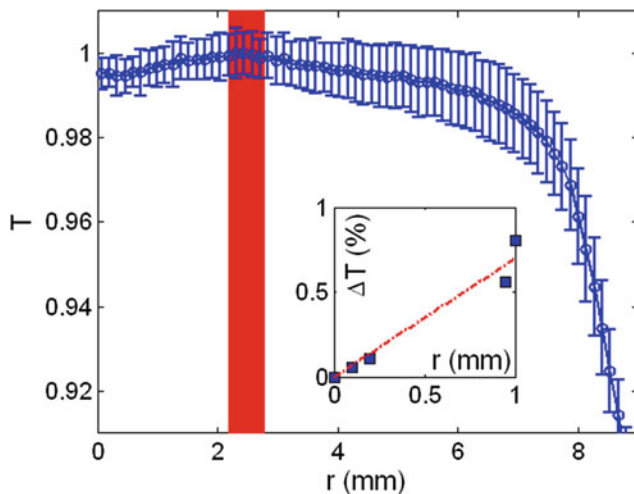


Fig. 2 Average normalized temperature $T(r)$ measured by infra-red along all the angular coordinate as a function of r from the center ($r = 0$) to the edge stage ($r = R$). The resistor position is enlightened in red.—Inset: Relative temperature errors obtained on fluid inclusion of quartz as a function of the radial coordinate in percent

last studies are organic and inorganic chemical products. On the one hand, these standards have heterogeneous microstructures; consequently, the fusion does not occur at a fixed temperature but over a range up to several degrees. On the other hand, measurements were difficult to observe because the phase transition is outside the scope of the microscope lens due to important mass effect of standards.

5 Conclusions

The microthermometric stage Linkam THMS 600 was calibrated with 8 selected standards (9 temperature transitions) which do not change in the laboratory and result appear

reversible, reproducible and easy to observe. These standards are: natural and synthetic fluid inclusions, ceramics, salt and liquids. Due to the use of many standards covering a wide temperature range, we obtained a linear calibration curve. These results validate our measurement protocol: always keep the sample centered on the Linkam stage and move all the system to bring it under the optical axis, heat slowly at a controlled speed of ramp from 0.2 to 1 °C/min near phase transitions and the observation zone of the standard has to be placed as close as possible to the heating silver block of the stage. We show that the horizontal and vertical biases are lower or equal to the uncertainty of the temperature measurements (± 0.3 °C). Another interesting point is that to calibrate the Linkam THMS 600, due to the linearity of the calibration curve, only two standards are necessary.

References

1. El Mekki Azouzi, M., Pallares, G., Tripathi, C., Gardien, V., Caupin, F.: Brillouin spectroscopy of fluid inclusions as a paleothermometer for subsurface rocks. *Sci. Rep.* **28**(5), 13168 (2015)
2. Jehl, V.: Le métamorphisme et les fluides associés des roches océaniques de l'atlantique nord. Recherche sur les équilibres entre fluides et minéraux. Thèse ing. Doc., Univ. Nancy I, p. 242 (1974)
3. Macdonald, A.J., Spooner, E.T.C.: Calibration of a Linkam TH-600 programmable heating-cooling stage or microthermometric examination of fluid inclusions. *Econ. Geol.* **76**, 1248–1258 (1981)

Palygorskite Versus Tetra (N-Methylpyridyl) Porphyrin: Characterization and Interaction

Amira Lajmi, Emmanuel Joussein, Stéphanie Leroy-Lhez, Marilyne Soubrand, Valentin Robin, and Mounir Medhioub

Abstract

Palygorskite is a natural clay mineral that has many potentially important uses in different industrial fields as it is an effective support for guests loading and controlled-release. The photofunctional properties of organic molecules, such as porphyrins, are described to stand as promising properties for various applications. In this context, our primary goal consists in understanding the palygorskite interactions with porphyrins. Hybrids clay/porphyrin were studied by means of XRD, FTIR, UV-Visible and fluorescence spectroscopy in order to evidence the porphyrins interactions (surface or inter-layer) relative to the clay associated properties.

Keywords

Palygorskite • Clay • Cationic porphyrin • Interaction • Morphology • Photofunctionality

1 Introduction

Clay minerals are widely applied thanks to their organic molecules' attached absorption capabilities, making it an interesting host that helps induce the formation of dye molecular assemblies. Palygorskite is a clay mineral that frequently displays a peculiar fibrous morphology and has a structure characterized with zeolite-like channels running parallel to the c direction. Such features make such clay minerals prove to be highly suitable for environmental and health applications (e.g., pollutants, i.e., by acting as an absorbent and remover, drugs carrier, excipients, etc.) [1, 2].

A. Lajmi · E. Joussein (✉) · S. Leroy-Lhez · M. Soubrand
V. Robin
Université de Limoges, PEREINE EA 7500 GRESE, 87100
Limoges, France
e-mail: emmanuel.joussein@unilim.fr

A. Lajmi · M. Medhioub
Faculté des Sciences, Université de Sfax, 3029 Sfax, Tunisia

The porphyrins and related photofunctional compounds offer a wide range of extremely versatile applications due to their specific and unique spectral and luminescent photoactive properties [3] such as bio-mimic membranes or in non-linear optics. The interactions between clay minerals and porphyrins may induce interesting photo-functional properties, among which are the most promising properties of photo-functional systems [4]. Porphyrins are known as heterocyclic macrocycle organic compounds with four pyrroles ring. Additionally, clay minerals are abundant and low-cost materials presenting the main property as high cation exchange capacity (CEC). Accordingly, the development of novel functional organic/inorganic hybrid materials [5], along with knowledge of the specifically involved interactions are some of the remarkable up-to-date and major concerns. The present work is aimed to help in understanding the palygorskite associated interactions with the tetra (N-methylpyridyl) porphyrin. To this end, the relevant samples were characterized via XRD, FTIR, UV-Visible and confocal microscopy in order to observe the dye-guest interaction types, the relationship associated with the clay relating properties, and to localize the porphyrin as absorbed onto the clay particles.

2 Materials and Methods

The sample of palygorskite clay minerals is directly provided by the Clay Mineral Society source under the label palygorskite PFI-1. The applied cationic porphyrin sample is a tetra (N-methylpyridyl) porphyrin (i) with the metalloporphyrin one, or (ii) without Zn^{2+} cation, namely Cp-Zn and Cp, respectively, and synthesized with Scientific Frontier. Several characterization techniques have been implemented to determine the materials associated physicochemical properties, i.e., CEC, specific surface area (SS), zeta-potential and chemical composition. The interaction between porphyrins and clay host were examined by means of FTIR,

Table 1 The chemical composition (wt%) and physicochemical parameters of palygorskite

Sample	SiO ₂	Al ₂ O ₃	Fe ₂ O ₃	TiO ₂	CaO	MgO	Na ₂ O	K ₂ O	CEC (cmol/kg)	SS (m ² /g)	Zeta
Palygorskite	60.9	10.4	2.98	0.49	1.98	10.2	0.058	0.8	19.5	136.35	-10.3

UV-visible, fluorescence spectroscopy, and finally confocal microscopy.

In this paper the focus is done on two types of cationic porphyrin, one free base and the other metallated with zinc. For the free-base porphyrin, the percentages of carbon, hydrogen and nitrate are respectively 64.4, 4.67 and 13.65% whereas for the metalloporphyrin are, respectively, 59.78, 4.10 and 12.68% whereas the percentage of zinc is 7.40%.

Table 1 reports chemical composition and main physicochemical parameters of untreated palygorskite.

3 Results

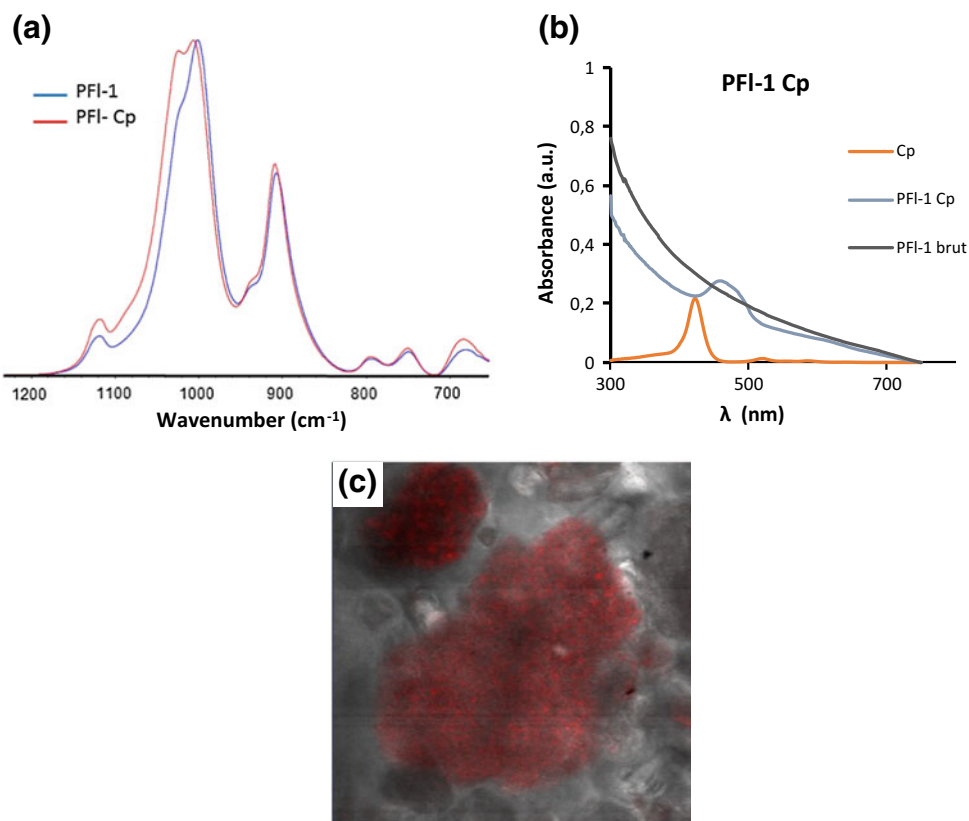
Details of the experimental results relating to the clay-porphyrin hybrids are reported below. The raw samples (palygorskite and porphyrin) have been characterized

according to various techniques. In so far as the present paper is concerned, only the clay-porphyrin relating hybrids are highlighted.

The relevant results are depicted in Fig. 1. The FTIR spectra of the mixtures appear to reveal a shift associated with the Si–O–M band following porphyrin interaction, engendered by the influence of the porphyrin absorption onto tetrahedral sheet. Noteworthy, however, is that the Si–O associated shift seems to be quite lower on using the Cp–Zn, due mainly to the difference noticeable in the porphyrins relating charge (⁴⁺ instead of ⁶⁺ for Cp–Zn and Cp, respectively).

The electronic absorption spectrum emanating from UV spectroscopy of porphyrin consists in a transition to the second excited state ($S_0 \rightarrow S_2$), i.e., the Soret band (Fig. 1a). Concerning the hybrid samples' case, this band turns out to be clearly shifted. The complex applied Confocal image

Fig. 1 **a** Infrared spectrum of raw palygorskite (PFI-1) and palygorskite-porphyrin hybrid (PFI-Cp). **b** Superposition of the UV-visible spectrum of porphyrin (in red), the palygorskite-porphyrin hybrid (in blue), and raw palygorskite (in black). **c** Confocal image of the palygorskite-porphyrin hybrid



proves to reveal the persistence of aggregates corresponding to the porphyrins and palygorskite complex.

4 Discussion

The shifting of the Soret band might well be due to various factors. The most prominent is linked to the aggregation of dye molecules upon absorption onto clay platelets. This suggests well that the interaction of porphyrins with clay minerals occurs mainly at the edge and surface levels of the clay particles. This fact has also its explanation in the fluorescence spectroscopy, as the emission bands turn out to be shifted. Moreover, a noticeable a modification in the Si–O–M band from the infrared spectroscopy has also been observed, following the interaction of palygorskite with the porphyrins molecules. This shift in infrared signal may well be related to the presence of molecules onto the clay surface, inducing distortion of the tetrahedral layer. Finally, it seems that a relevant role of the porphyrin charge impacts appears to be effective. The captured confocal image clearly evidenced the localization of porphyrins onto the palygorskite. However, due to the large size of porphyrins, their presence in the palygorskite channels is discovered to be impossible.

5 Conclusions

Palygorskite versus porphyrins molecules were investigated through various characterization techniques. From the above cited results, reached by means of a number of spectroscopic investigations, the porphyrins interaction is evidenced, but it may be dependent on the clay relating charge densities (as already shown for other type of clay minerals), their morphology as well the porphyrins' charge onto host clay (data not shown).

References

1. Bin, M.: Adsorption of dyes onto palygorskite and its composites: a review. *J. Environ. Chem. Eng.* **4**, 1274–1294 (2016)
2. Ran, Y.: Properties and mechanisms of palygorskite for removal of various ionic dyes from water. *Appl. Clay Sci.* **151**, 20–28 (2018)
3. Alexander, Ć.: Spectral properties of porphyrins in the systems with layered silicates (2009)
4. Guilherme, S.M.: Cationic and anionic metalloporphyrins simultaneously immobilized onto raw halloysite nanoscrolls catalyze oxidation reactions. *Appl. Catal. A: General* **460–461**, 124–131 (2013)
5. Kosiur, D.R.: Porphyrin adsorption by clay minerals. *Clays Clay Miner.* **25**, 365–371 (1977)

Mg-Exchanged Montmorillonite Undergoing External Environmental Solicitation: Crystalline Swelling Process Investigation

Marwa Ammar, Walid Oueslati, and Abdesslem Ben Haj Amara

Abstract

This work reports a characterization of the possible effects that might affect the hydration properties of Mg-exchanged low-charge montmorillonite (SWy-2-Mg) when undergoes an external environmental solicitation. The latter was created by an alteration of relative humidity rates (i.e. RH%) over two hydration-dehydration cycles with different sequence. The study was mainly based on the X-ray diffraction profile modeling approach. Obtained results show strong hydration dependence as a function of the RH sequence. The interlayer configuration presents a heterogeneous hydration behavior which was systematically observed at different stages of both cycles. The interlayer water uptake process presents similar hysteresis characterized by fluctuations of interlayer water molecule abundances.

Keywords

Clay mineral • Ion exchange process • Environmental solicitation • XRD profile modeling approach

1 Introduction

Smectites are swelling clay minerals that belong to the group of the 2:1 phyllosilicates naturally occurring in both terrestrial and marine environments where they often represent the most effective components. Smectite play important role in many geological processes, in petroleum migration phenomena, greenhouse gas sequestration, in oilfield and engineering. Over the last decades, the smectites were widely used as a crucial component for the design of natural barriers to isolate the hazardous wastes, and for the removal of heavy

metal cations from wastewater [1–4]. They were also proposed as geotechnical barrier for nuclear waste disposal [5, 6]. The hydration behavior of these minerals is very sensitive to the change of environmental surroundings conditions (e.g., temperature, pressure, RH) which may influence the stability of the clay microstructure therefore the stability of the geotechnical barrier. Hence, an understanding of the swelling smectites properties (the hydration and the dehydration mechanism), is of paramount importance for many natural processes and for such applications. The present work describes the structural properties and the hydrous behavior of an Mg-saturated smectite (i.e. montmorillonite: SWy-2) when it was submitted to a continuous variation of environmental surroundings condition (specifically RH%).

2 Materials and Methods

2.1 Starting Sample and Ionic Exchange

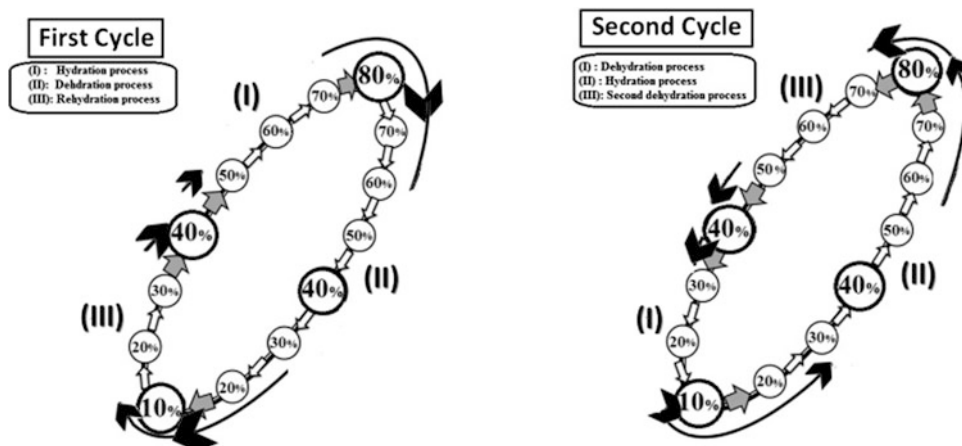
A standard dioctahedral smectite SWy-2 originated from bentonites of Wyoming (USA) is selected for the present study. The structural formula is given by [7]. A pre-treatment of the host materials was carried out in order to prepare a Na-rich montmorillonite suspension. To achieve this aim, a classical exchange process protocol was performed [8]. The same ionic exchange procedure was followed to prepare Mg-rich montmorillonite suspension using $MgCl_2$ solution (1 M) and the final obtained clay suspension was labeled SWy-2-Mg. Two oriented slides [9] were prepared for the obtained samples (SWy-2-Mg) to be analyzed by XRD technique.

2.2 “in Situ” XRD Analysis

The “in situ” XRD analysis is performed under controlled atmosphere upon two overturn hydration-dehydration cycles (Fig. 1). These cycles were created by varying gradually the

M. Ammar · W. Oueslati (✉) · A. Ben Haj Amara
UR13ES46 Physique Des Matériaux Lamellaires et
Nano-Matériaux Hybrides (PMLNMH), Faculté Des Sciences de
Bizerte, Université de Carthage, 7021 Zarzouna, Tunisia
e-mail: walidoueslati@gmail.com

Fig. 1 A sequence variation of the RH% during different hydration-dehydration cycles



RH% and then reversing the sequence with a 10% step. For that, an Anton Paar TTK450 chamber coupled to a D8 Advance Brüker installation equipped with an Ansyco RH-plus 2250 humidity control device were used.

The XRD profile modeling approach is used in order to propose theoretical structural models estimating respectively the gradual evolution of the interlayer water amount versus the hydration sequences. A detailed description of the fitting strategy is detailed in [10, 11].

3 Results

3.1 First Hydration-Dehydration-Hydration Cycle

The qualitative XRD investigation shows a gradual evolution of the d_{001} basal spacing values as a function of RH. Figure 2 shows a clear hysteresis between $40 \leq \text{RH}\% \leq 10$. For this RH range, the structure was dominated by a mixed hydration behavior between 1 and 2 W. By contrast, the variation of the d_{001} spacing between 80 and 40% RH and back follows the same trend which can be interpreted in terms of hydrous stability of the interlayer spaces. Results derived from XRD profile analysis proves that the studied complex (SWy-2-Mg) evolves, all over the cycle, with mixed hydration behavior. Indeed, all proposed models were described by a Mixed Layer Structure (MLS) composed by diverse hydration states contributions (0, 1, 2 and 3 W) at different RH values. Heterogeneous hydration behavior can be explained by sequential transitions between different hydration states induced by the continuous RH% variation. The evolution of different relative layer type (e.g. 0, 1, 2 and 3 W) abundances versus RH shows a continuous diffusion of H_2O molecules in the interlayer spaces during the hydration process leading a progressive and continuous 1 W \rightarrow 2 W and 2 W \rightarrow 3 W transition.

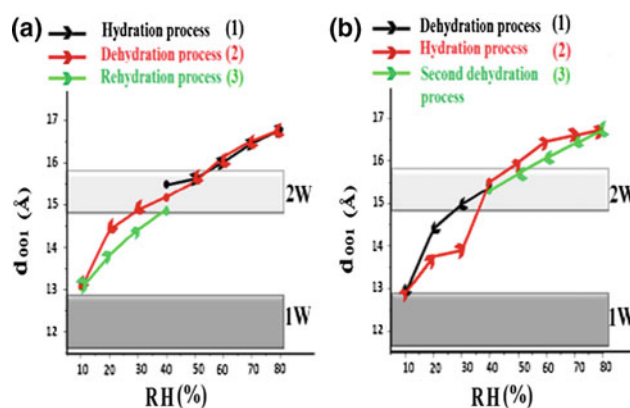


Fig. 2 Evolution of the given d_{001} spacing values according to RH% values during the first and the second cycle

3.2 Second Dehydration-Hydration-Dehydration Cycle

The evolution of the d_{001} as a function of the RH along the second cycle was characterized by the appearance of a clear hysteresis at the RH range extending between 40 and 10% (Fig. 2). A slow increase of the interlayer spacing was noted by inversion of the RH sequence. Over this RH domain the d_{001} were attributed to an interstratified 2 W-1 W hydration state. Between 40 and 20% RH, a slow 2 W \rightarrow 1 W transition is observed where the XRD profile is reproduced by MLS containing a major contribution of the 2 W layer types. A notable increase of the 1 W layers abundance was detected toward the lowest RH condition (i.e. 10%). At this RH rate, the MLS used to fit experimental XRD patterns was composed by 70% of monohydrated states and 30% of the bi-hydrated ones randomly distributed. The continuous variation of the RH values along both cycles brings automatically a sequential transition between different hydration states in the interlayer spaces of the SWy-2-Mg complex, which logically leads a continuous change on the interlayer

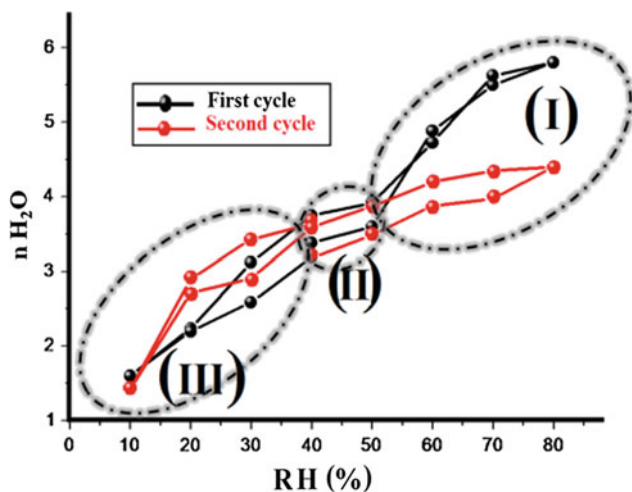


Fig. 3 Evolution of the interlayer water contents as function of the RH% along the first and the second cycles

water abundances and distribution. In Fig. 3, a comparison between the evolution of the interlayer water molecule versus RH, along the first and the second cycle is reported. A dissimilar progression of n_{H_2O} was perceived in three principal RH sections depending on the interlayer water amounts retained by the structure versus hydration sequence.

4 Conclusions

This work describes, using XRD profile modeling approach, the detailed hydration behavior of Mg rich-montmorillonite in response to an environmental solicitation. The main results obtained show that: (i) The hydration behavior of the studied sample strongly depended on the sequence of the RH variation over different cycles (ii) The proposed theoretical

models describing the evolution of the structural properties suggests the coexistence of more than one MLS indicating the hydration heterogeneity whatever the RH% sequence (iii) The montmorillonite's interlayer water content growth depends on the nature of the bivalent exchangeable cations.

References

- Vengris, T.: Nickel, copper and zinc removal from waste water by modified clay sorbent. *Appl. Clay Sci.* **18**, 183–190 (2001)
- Anderson, R.L.: Clay swelling-A challenge in the oilfield. *Earth Sci. Rev.* **98**, 201–216 (2010)
- Gu, X.: Modeling the adsorption of Cd(II), Cu(II), Ni(II), Pb(II) and Zn(II) onto montmorillonite. *Geochim. Cosmochim. Acta* **74**, 5718–5728 (2010)
- Xu, Y.: Remediation of heavy metal-polluted agricultural soils using clay minerals: a review. *Pedosphere* **27**(2), 193–204 (2017)
- Tachi, Y.: Diffusion and sorption of Cs^+ , Na^+ , I^- and HTO in compacted sodium montmorillonite as a function of porewater salinity: Integrated sorption and diffusion model. *Geochim. Cosmochim. Acta* **132**, 75–93 (2014)
- Huber, F.: Radionuclide desorption kinetics on synthetic Zn/Ni-labeled montmorillonite nanoparticles. *Geochim. Cosmochim. Acta* **148**, 426–441 (2014)
- Mermut, A.R.: Baseline studies of the clay minerals society source clays: chemical analyses of major elements. *Clays and Clay Miner* **49**(5), 381–386 (2001)
- Tessier, D.: Etude expérimentale de l'organisation des matériaux argileux. [these], Université de Paris VII, Publication INRA Versailles, Paris, France (1984)
- Cuadros, J.: Experimental kinetic study of the smectite-to-illite transformation. *Geochim. Cosmochim. Acta* **60**, 439–453 (1996)
- Ferrage, E.: New insights on the distribution of interlayer water in bi-hydrated smectite from X-ray diffraction profile modeling of 00 *l* reflections. *Chem. Mater.* **17**, 3499–3512 (2005)
- Oueslati, W.: XRD investigations of hydrated homoionic montmorillonite saturated by several heavy metal cations. *Desalination* **271**, 139–149 (2011)

Potassium Fixation in Beidellite Through Wetting and Drying

Hachemi Zaidi, Abdellah Bakhti, and Mohamed Larid

Abstract

The present study is conducted in a bid to highlight the variation noticeable in the potassium (K) exchange capacity for a K-beidellite, as a function of the number of wetting and drying (WD) cycles. The reached findings proved to reveal that the amount of fixed K^+ appears to be noticeably related to both of the number of WD cycles and the negative charges arising from the substitution occurring in the octahedral sheets.

Keywords

Potassium • Exchange • Beidellite • Wetting-drying

1 Introduction

Smectites display an irreversible liability to fix K, particularly under the effect of drying [1, 2]. Most of the relating studies prove to be predominantly focused on treating the fixation of K in montmorillonites with dominant octahedral charge deficit [1–3]. It would be useful, however, to examine whether other swelling clay minerals, characterized with different layer charge location and very common in soils, such as beidellites [4], could evolve in the same way when K intervenes to saturate their cation exchange capacity (CEC). Accordingly, we undertake to study the exchange properties of K-beidellite, with mixed charge location, as submitted to alternate WD cycles.

2 Materials and Methods

The raw clay used was provided by the National Company of Non Ferrous Mining Products and Useful Substances (Algeria). It was purified by sedimentation. The less than $2 \mu\text{m}$ fraction was agitated for 4 h in a chloride solution of the selected cation to saturate its CEC. The samples of clay thus obtained (Na-Bed, K-Bed and Ca-Bed) were then stored in water suspension.

The treatment of samples by a WD cycle followed the procedure reported in a previous works [1]. 1 g of clay sample was suspended in 50 ml of distilled water and oven dried at 60°C for 12 h.

The X-ray diffraction analyses were performed at ambient conditions (average temperature around 18°C and relative humidity about 53%), via a Bruker D8 Advance diffractometer.

The chemical composition was determined by means of X ray fluorescence spectrometry with a Thermo Scientific device.

CEC was measured through the conductometric method [5].

3 Results

3.1 Physicochemical Characterization of the Fine Fraction (Na-Bed)

The detailed mineralogical characterization of clay minerals was obtained by displacing the main line corresponding to the (001) plane, under the action of specified treatments [6] (Figs. 1 and 2). The Na-Bed sample proves to display a basal spacing d_{001} similar to that associated with Na-smectites or Na-vermiculite, to one layer of water ($d_{001} = 12.44 \text{ \AA}$) (Fig. 1a). Noteworthy, however, is that the Na-Bed sample, as treated with glycerol, appears to reveal a basal spacing d_{001} characteristic of smectites, with a swelling range

H. Zaidi · A. Bakhti (✉) · M. Larid
Laboratory of Biodiversity and Conservation of Water and Soil,
University of Mostaganem, BP 992 RP, 27000 Mostaganem,
Algeria
e-mail: bakhti02@yahoo.fr

Fig. 1 XRD patterns of air-dried oriented aggregates (<2 μm fraction) of: **a** Na-Bed and **b** glycerolated Na-Bed

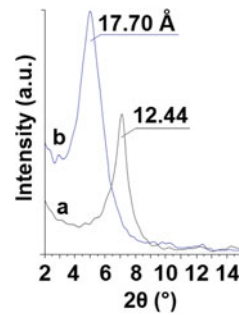
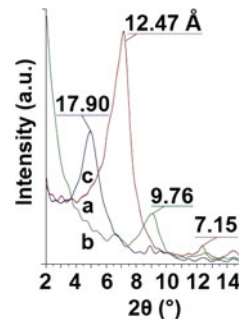


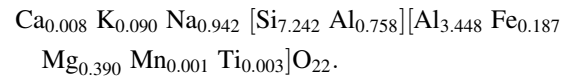
Fig. 2 XRD patterns of Na-Bed: **a** after Li^+ saturation, **b** followed by heating at 300 °C for 24 h, **c** and glycerolated



varying between 17.7 and 18.0 Å (Fig. 1b), contrary to the vermiculites, which prove to swell with a range of 14.3 Å following the same test. Hence, it proves to stand as a smectite. The glycerol Li-saturated sample, as heated overnight at 300 °C, resulted in a basal spacing of 17.90 Å, highlighting that the fine fraction Na-Bed is not of a montmorillonite type. The fine fraction Na-Bed is mainly composed of a dioctahedral smectite (beidellite or nontronite), with a low trioctahedral character (Fig. 3).

Moreover, the 7.15 and 3.55 Å characteristic lines of kaolinite, and those of illite at 10.03 and 3.33 Å [3, 6] also appear to demonstrate a low intensity.

The structural formula established for the dehydrated Na-Bed, on the basis of its chemical composition (Table 1), in conformity with the Mauguin method [6], turns out to be:



Based on Table 1 reported results, it appears clear that the studied clay fraction proves to exhibit Fe and Mg contents that are much lower than those associated with the Fe- and Mg-smectites, nontronites and saponites respectively [6]. Thus, the fine fraction Na-Bed turns out to be a mixed beidellite with dominant tetrahedral charge (70%). It contains small kaolinite and illite quantities.

3.2 Evolution of Exchange Properties

The initial state of the studied clay materials is the same as that persisting before the initial drying, i.e., following the CEC saturation, relevant to the fraction below 2 μm , of the raw clay by Ca, Na or K. The measured CEC values are 100, 98 and 93 mEq/100 g for Ca-Bed, Na-Bed and K-Bed minerals, respectively. The experimental results relevant to the CEC evolution in the Na-Bed, Ca-Bed and K-Bed samples, with the number of WD cycles (Fig. 4), primarily indicate that the WD cycles prove to have no effect on CEC variation of minerals Na-Bed and Ca-Bed. As for the K-Bed sample, the CEC appears to decrease rapidly, but following 40 WD cycles, a constant minimum quantity of K exchangeable (71.4 mEq/100 g) is reached. This behavior has also been observed by other authors who studied the K-montmorillonites as submitted to a series of WD cycles [1, 3]. These authors have predominantly considered the K retention to be associated with a superposition order modification of the elementary layers appearing during WD cycles. Under the effect of dehydration, the layers get closer and their proportion turns out to superimpose. This state corresponds to a stacking, case in which the hexagonal cavities of two adjacent layers are facing each other. The initial turbostratic structure proves to evolve into a well-ordered one. The structural rearrangement helps reduce the interlayer distance and, thereof, increases the interaction energy, resulting in the most possible stable situation as that of illites. This situation will prevent water accessibility to a part of the interlayer spaces. As a result, a proportion of K^+ turns out to be no longer exchangeable. On comparing this achieved result to that released in respect of the K-montmorillonite Wyoming [1], where the quantity of K exchangeable appeared to attain a value inferior to 33 mEq/100 g after 100 WD cycles, one could well note that the retention of K proves to be stronger for the Wyoming specimen than that relating to the K-Bed. This difference in behavior between the Wyoming montmorillonite and our

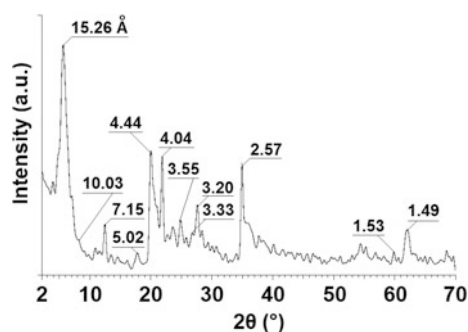
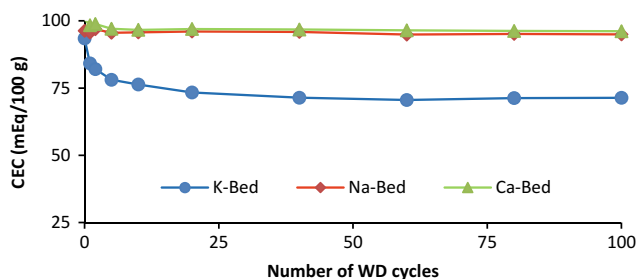


Fig. 3 Powder XRD pattern of the raw clay

Table 1 Chemical composition (oxide wt%) of dehydrated Na-Bed

SiO ₂	Al ₂ O ₃	Fe ₂ O ₃	MgO	CaO	K ₂ O	Na ₂ O	MnO	TiO ₂	P ₂ O ₅
60.90	30.00	2.09	2.20	0.06	0.60	4.09	0.02	0.03	0.02

**Fig. 4** CEC variation as a function of the number of cycles WD

investigated sample may be related to the heterogeneity noticeable in the charges' distribution among our examined mineral sheets, a common phenomenon recurring in smectite minerals [7, 8].

This heterogeneity is partly attributed to the presence of different types of layers to microstructural scale within of the same crystal. Some of these layers are characterized with a purely tetrahedral charge, while others with a purely octahedral charge, and all possibilities can be expected to exist between these two extreme cases [7, 8]. Yet, they may exhibit a different behavior towards WD cycles. This suggests that the effect of WD cycles favours rotations and slips of the octahedral load sheets, as existing in mixed beidellites. Concerning the tetrahedral sheets, however, the proximity of the tetrahedral charge to the interlayer space turns out to yield a strong interaction with the compensating cations. This situation implies the persistence of a remarkable cohesion associated with the structure. It is, therefore, possible to consider that these layers are not concerned with the structural reorganization, as their contained K remains exchangeable. The calculation of the non-exchangeable K⁺ relating percentage must also account for the absorbed K⁺, usually considered as exchangeable. As for the smectites, the CEC, as emanating from the adsorbed cations, is estimated to be about 10% of the total CEC [7]. Following 40 WD cycles, one could well note that a proportion of 26% of interlayer K⁺ (84 mEq/100 g) remains fixed on the mineral K-Bed. This fixed K⁺ proportion, close to the octahedral original charge, proves to display an acceptable agreement

with the previously set hypothesis, as advanced to provide a satisfactory explanation of the irreversible fixation of K⁺ by the studied clay.

4 Conclusions

A sequence of 100 wetting and drying cycles has been performed on a K-beidellite, with mixed charge deficit. The reached findings proved to highlight that the diffusion of K⁺ into the interlayer spaces turns out to be accompanied with a reduction of the CEC. The proportion of retained K⁺ is closely related to the octahedral charge deficit.

References

- Mamy, J., Gaultier, J.P.: Comparative study of the evolution of bionics K-Ca montmorillonites of Camp-Berteaux and Wyoming under the effect of humectation and desiccation cycles. *Clay Miner.* **14**(3), 181–192 (1979)
- Inoue, A.: Potassium fixation by clay minerals during hydrothermal treatment. *Clays Clay Miner.* **31**(2), 81–91 (1983)
- Miklos, D., Cichel, B.: Development of interstratification in K and NH₄-smectite from Jelsovy Potok (Slovakia) treated by wetting and drying. *Clay Miner.* **28**(3), 435–443 (1993)
- Hetzel, F., Harvey, E.D.: Some colloidal properties of beidellite: comparison with low and high charge montmorillonites. *Clays Clay Miner.* **41**(4), 453–460 (1993)
- Chiu, Y.C., Huang, L.N., Uang, C.M., Huang, J.F.: Determination of cation exchange capacity of clay minerals by potentiometric titration using divalent cation electrodes. *Colloids Surf.* **46**(2), 327–337 (1990)
- Caillère, S., Henin, S., Rautureau, M.: *Clay mineralogy*, 2nd edn. Masson, Paris (1982)
- Ben Hadj-Amara, A., Besson, G., Tchoubar, C.: Structural characteristics of a dioctahedral smectite as a function of order-disorder in the electric charge-distribution. 1. Study of *00 l* reflections. *Clay Miner.* **22**, 305–318 (1987)
- Ferrage, E., Lanson, B., Michot, L.J., Robert, J.L.: Hydration properties and interlayer organization of water and ions in synthetic Na-smectite with tetrahedral layer charge. Part 1: results from X-ray diffraction profile modeling. *J. Phys. Chem. C* **114**(10), 4515–4526 (2010)

Geochemistry of Hydrothermal Chlorite in the OB48 Borehole (Nefza, Northern Tunisia)

Randa Ben Abdallah, Mounir Medhioub, and Jean Marc Baele

Abstract

The Oued Belif 48 borehole samples have been analyzed in order to reveal the mineralogical composition of the Triassic successions and their alteration outcomes, namely, chlorite, phlogopite and talc. Clay minerals from Oued Belif borehole were studied via XRD, SEM, TEM, CL and AEM. In this work, we are interested in the petrographic, mineralogical and geochemical characterization of these materials to understand, firstly, how they are set up and, secondly, the thermal impact of the intrusive acid magmatism affecting them. Chemical composition of chlorite, as determined through electron microprobe, underline the chlorites' magnesian character as persisting in the OB48 borehole. The evaporitic and carbonate mineralization associated with these phyllosilicates were also studied due to their predominance in the OB 48 borehole.

Keywords

Chlorite • Phlogopite • Petrography • Mineralogy • Chemical composition • Hydrothermal alteration • Metamorphism

1 Introduction

Clay minerals are widely distributed over the Earth's surface as the outcomes of different processes, such as hydrothermal alteration and chemical weathering of rocks, as resulting

R. B. Abdallah (✉)
Department of Geology, Faculty of Bizerte,
University of Carthage, Tunis, Tunisia
e-mail: randa.benabdallah@gmail.com

M. Medhioub
Department of Geology, Faculty of Sciences,
University of Sfax, Sfax, Tunisia

J. M. Baele
Polytechnic Faculty, Fundamental and Applied Geology,
University of Mons, Mons, Belgium

from rock-water-gas interaction. The diagenetic formation of chlorite, by the effect of a reaction involving the breakdown of dolomite, has already been described by Muffler and Doe [13] and White [17], in regard of the Pliocene and Quaternary siltstones and sandstones of the Salton Sea geothermal field, California. In this respect, Mehdi et al. [11] determined the burial degree of evaporitic Triassic samples, as drawn from the OB48 borehole, by means of the “illite crystallinity” index of Kubler and Jaboyedoff [9], and through the evolution of the other phyllosilicates, essentially, chlorite, talc and illite/chlorite as well as illite/smectite mixed-layers. The illite crystallinity value (IC), as measured through the ethylene-glycol solvated oriented mounts of the Oued Belif 48 samples, appears to oscillate globally between 1 and 2.5 characterizing the Epizonal zone with a range of 300–400 °C temperatures.

The aim of this paper is to apply the relating mineralogical and geochemical characterization to understand the formation conditions of chlorite deposit, while integrating them within the orogenic context.

2 Geological Setting

The Belif Oued structural framework consists mainly in its location in the north of Tunisia close to the Tamra iron mine, north of the Nefza city (Fig. 1). It is bordered on the south by the reliefs of Jebel Ed Diss, and on the north by the reliefs formed by Numidian sandstones [16]. It is a vast structure of elliptical shape, oriented ENE-WSW. Inside this structure, there persist metamorphic rocks, represented by skarns and sericitoschists [3, 14]; evaporites (sandstone, gypsum and carnageules) attributed to Trias [4, 7, 14, 16] and identified mio-plio-quadernary deposits. The OB 48 borehole crosses 318 m of the Triassic attributed succession. The macroscopic examination helps to underline the evaporitic character of materials (prevalently sulphates), along with the importance of the polygenic facies [5]. From bottom to top, the following terms are identified [2]:

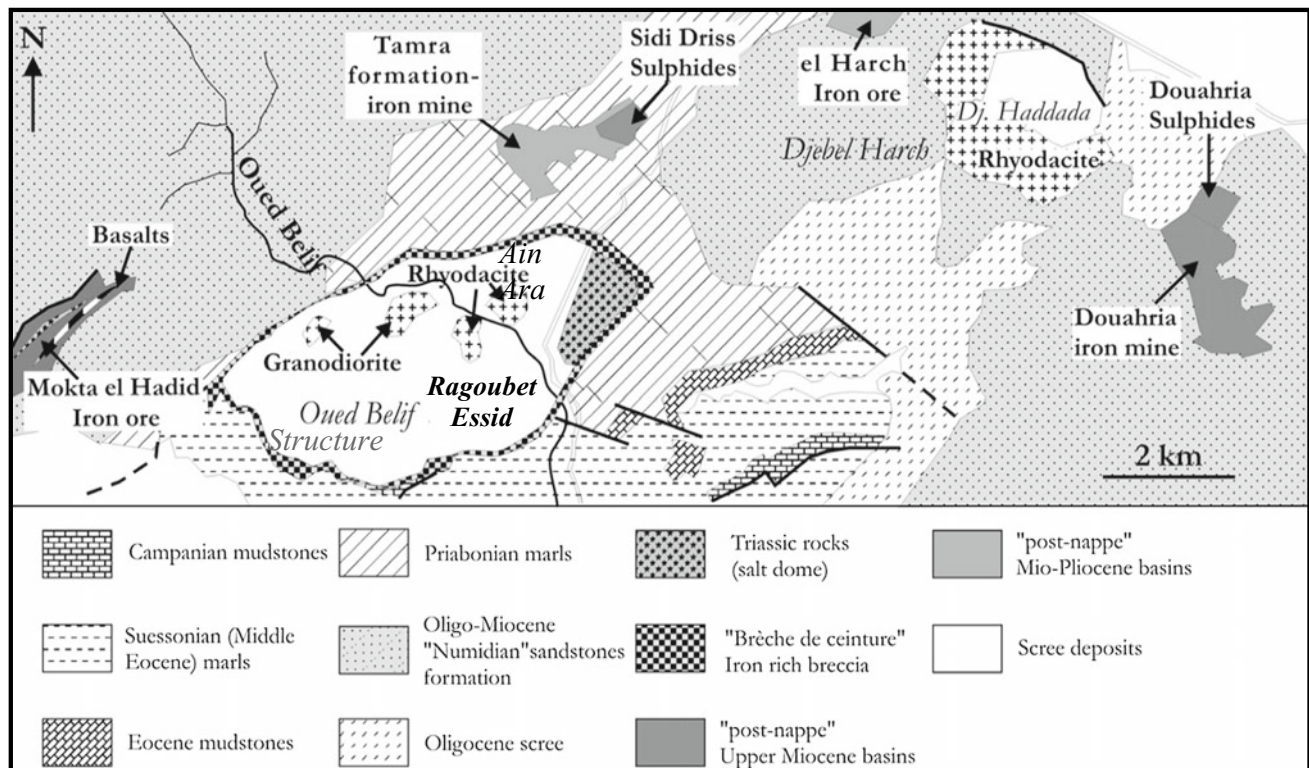


Fig. 1 Geological map of the studied area (as modified, after Gottis and Sainfeld [6])

- a carbonated unit called skarn;
- a polygenic breccia, mostly greenish, and rich in pyrite;
- massive anhydrite layers, very rich in pyrite;
- a saccharoïd unit, intercalated with dolomitic elements rich in pyrite;
- a grey clayey unit, containing hardened and very feruginous elements;
- a beige-yellow to yellowish clayey unit, and
- a very clayey red soil.

3 Materials and Methods

Overall, some 98 samples were collected from the OB48 borehole. Clay minerals were studied via XRD, SEM, TEM, CL and AEM. The petrographic analysis was carried out by means of an optical microscope type Zeiss equipped with an Olympus digital Camera (3.3 mega pixel). The minerals morphology and chemical composition was performed by means of MEB (JEOL JSM-7500 F Field Emission Scanning Electron Microscope coupled to EDS analysis) and TEM (JOEL JEM-100 C X II). The mineralogical compositions of the bulk and clay fractions were determined using a Siemens Cristaloflex 810 (radiation Cu K α , 40 kV, 30 mA). The traditional oriented-aggregate clay determination

methodology [12] has been applied, including treatment with ethylene-glycol and heating to 550 °C. The relevant chemical analysis was administered by means of X-ray fluorescence (XRF) via a Philips PW XRF spectrometer. The electronic microprobe used is of a type of CAMECA SX50 model. The operating conditions were 15 kV and 20 nA.

4 Results and Discussion

The microscopic observation of polished thin sections enabled the identification of a variety of mineral phases (phyllosilicates, sulphates and carbonates). Phyllosilicates are also widely represented in the survey studied. The Phlogopites and chlorites stand as the two major predominant types, appearing in the form of a particular assemblage corresponding to phlogopite-chlorite intergrowths (Fig. 2a). These two mineral phases also reveal the persistence of other habitus in pure phases. Phlogopite occurs either in small lamellae, in acicular minerals (Fig. 2b), or in tuft. Chlorite is also expressed in automorphic sections with pleochroism in green (Fig. 2c). It also exists in rosettes replacing dolomite rhombohedra (Fig. 2d). The XRD analysis of the total rock and the oriented aggregate slides have also helped to specify the clay minerals' composition: illite, smectite and talc. The latter can be considered, in this context, to stand as an

Fig. 2 Photomicrographs showing materials intersected by OB48 borehole (polarized light analyzed), **a** phlogopite-chlorite intergrowths; **b** phlogopite in small lamellae; **c** chlorite growing in a gypsum matrix; **d** chlorite replacing porphyroblastic dolomite

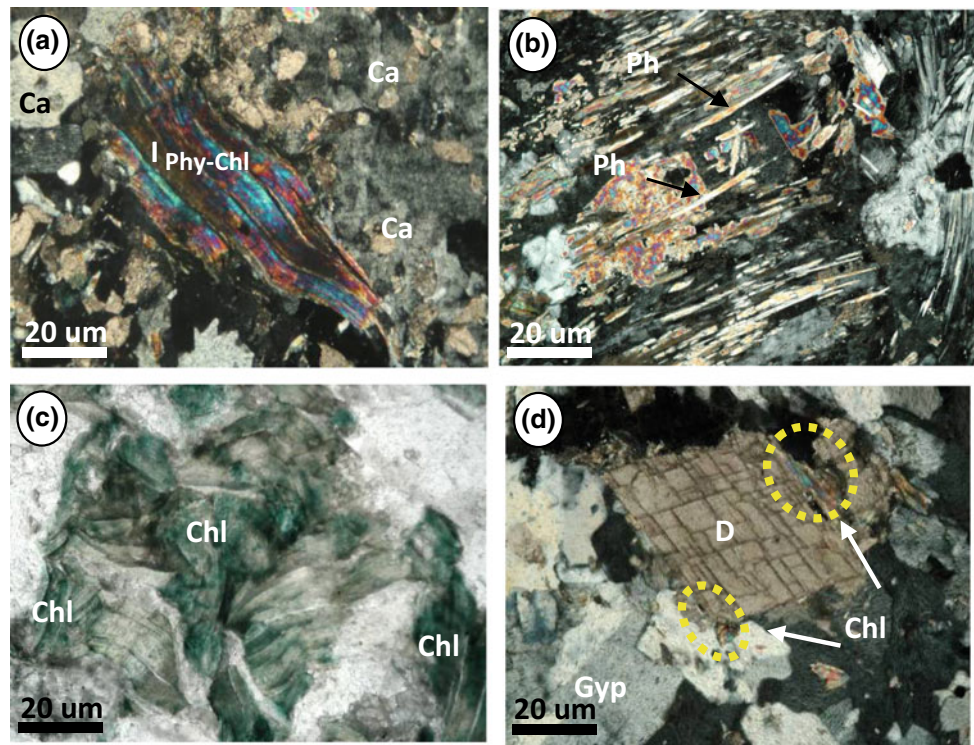
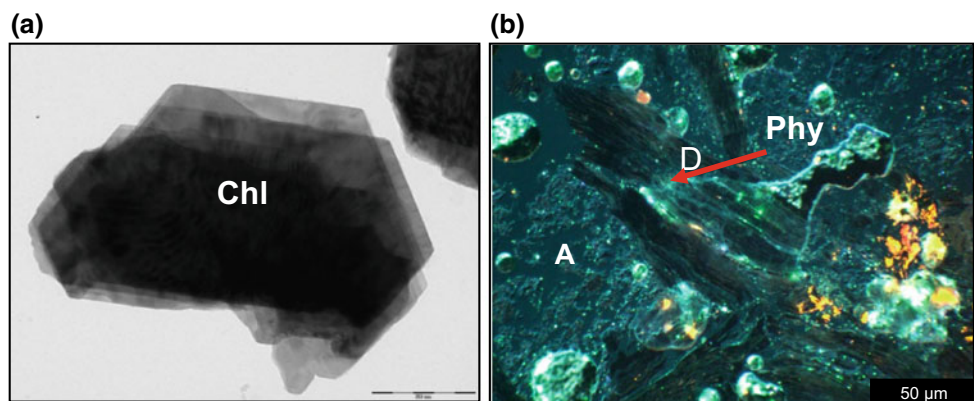


Fig. 3 **a** TEM textural image of the OB48-33 sample, showing pseudo-hexagonal shapes of chlorites; **b** CL image showing chlorite substituting anhydrite crystal



indicator of a metamorphic environment. The observation also allowed to recognize pyrite and pyrrothite. The latter is considered to be an iron sulphide that is generally persistent in magmatic, metamorphic or sedimentary rocks affected by hydrothermal activity. The pyrrothite-pyrite combination can be used as a geothermometer, indicating a set-up temperature of the order of 316 °C [1, 8, 10, 15].

TEM observation show pseudo-hexagonal shapes of chlorites, with generally rounded borders (Fig. 3a). The CL related observation revealed well the phyllosilicates progressively replacing carbonates (Fig. 3b). The electron microprobe chemical analyses are depicted on Table 1. The atomic concentrations of Si range are: a.p.f.u.atoms. The structural formulas relating results prove to underline

the chlorites' magnesian character associated with the OB48 borehole.

5 Conclusion

Chlorite, phlogopite and talc appear to stand as the predominantly common clay minerals in evaporitic Triassic series of the OB48 borehole samples, North of Tunisia. They are authigenic minerals in type, formed during burial diagenesis/metamorphism at temperatures of $\rightarrow 300$ °C. Whole-rock mineralogical and chemical analyses proved to reveal that chlorite authigenesis occurred by the effect of carbonate substitutions, very recurrent in Triassic rocks and

Table 1 Chemical analyses (oxide wt%) of chlorite predominant in the OB48 borehole samples

Oxide	1	2	3	4	5	6	7	8	9	10	11	12
SiO ₂	30.866	33.882	34.505	32.633	34.274	30.994	34.182	31.617	41.737	38.131	31.326	39.104
Al ₂ O ₃	16.215	15.724	16.568	16.984	16.616	18.575	13.404	14.875	13.904	14.052	14.864	13.725
SrO	0.111	0.128	0.118	0.11	0.134	0.089	0.13	0.098	0.15	0.149	0.076	0.142
MgO	21.344	20.562	22.789	22.883	22.117	21.721	11.162	21.233	24.122	24.423	20.391	26.305
K ₂ O	0.154	0.26	0.139	0.176	1.633	0.141	0.283	0.481	0.744	0.476	0.027	2.013
CaO	0.364	0.61	0.739	0.554	0.558	0.551	0.659	0.565	2.775	2.088	0.634	0.793
Cl	0.067	0.092	0.037	0.017	0.033	0.056	0.019	0.078	0.083	0.114	0.092	0.195
P ₂ O ₅	0.005	0.005	0	0	0.025	0.021	0.009	0.002	0.046	0.016	0.039	0.014
FeO	17.549	13.294	10.454	12.494	12.011	13.782	26.406	17.446	2.503	6.059	20.077	2.628
MnO	0	0	0	0	0.019	0	0	0.014	0	0.023	0	0
TiO ₂	0	0.073	0.175	0.113	0.359	0.305	0.017	0.619	0.622	0.621	0.294	0.786
BaO	0	0	0	0	0.056	0	0.076	0	0	0	0.012	0.008
Na ₂ O	0.155	0.221	0.129	0.182	0.15	0.144	0.168	0.146	0.609	0.516	0.135	0.112
F	0.412	0.432	0.655	0.614	0.575	0.364	0.337	0.433	0.31	0.366	0.413	0.256
O = F	-0.173	-0.181	-0.275	-0.258	-0.242	-0.153	-0.141	-0.182	-0.131	-0.154	-0.173	-0.107
Cl = F	-0.015	-0.021	-0.008	-0.003	-0.007	-0.012	-0.004	-0.017	-0.018	-0.025	-0.021	-0.044
Total	87.053	85.075	86.023	86.497	88.311	86.577	86.705	87.407	87.455	86.854	88.185	85.929

traces through the diversity of habitus and the various salt evolution stages. Talc evidence, although punctual and confirmed by means of X-ray diffraction, does actually validate the already advanced presumptions, highlighting that fairly intense metamorphic conditions have been reached.

References

- Cathelineau, M., Nieva, D.: A chlorite solid solution geothermometer. The Los Azufres (Mexico) geothermal system. *Contrib. Mineral. Petrol.* **91**, 235–244 (1985)
- Chafar, R.: Programme de reconnaissance par sondages mécaniques; Ragoubet Es Seid. Rapport d'exécution des sondages mise au point (rapport inédit O.N.M) (1997)
- Crampon, N.: Métamorphisme hydrothermal en faciès salin et pénésalin sur l'ensemble salifère de l'extrême-nord tunisien. *Contrib. Minéral. Petrol.* **39**, 117–140 (1973)
- Dermech, M.: Le complexe de l'oued Bélif-Sidi Driss (Tunisie septentrionale) Hydrothermalisme et métallogénie, 336p. Thèse, Université Paris VII. (1990)
- Ghazghazi, H.: Pétrographie-minéralogie des évaporites du Trias et effets thermiques du magmatisme acide néogène (oued Bélif-Tunisie septentrionale). *Mém. Mastère. Géol. Appl. Fac. Sc. Bizerte*, 107p. Univ. 7 Novembre- Carthage (2004)
- Gottis, Ch., Sainfeld, P.: Les gîtes métallifères tunisiens. XIXème Congrès Géologique International. Monographies régionales, 2e séries: Tunisie – no 2,104 p (1952)
- Halloul, N.: Géologie, pétrologie et géochimie du bimagmatisme néogène de la Tunisie septentrionale (Nefza et Mogods). Implications pétrogénétique et interprétation géodynamique, 207 p. Thèse, Blaise Pascal University, Clermont-Ferrand (1989)
- Hemadi, H.: Les silicates et carbonates authigènes des diapirs du nord de la Tunisie: signification chimique et thermique, 182p. Thèse, University of Paris-Sud, Orsay (1987)
- Kubler, B., Jaboyedoff, M.: Illite crystallinity. *C R Acad. Sci. Paris, Sci. Terre planètes* **331**, 75–89 (2000)
- Kulke, H.: Sédimentation, diagenèse et métamorphisme léger dans un milieu sursalé: exemple du Trias maghrébin. *Sci. Terre, Nancy* **XXIII**(2), 39–74 (1979)
- Medhi, D.: Burial history determination of the Triassic succession of Central and Northern Tunisia using clay minerals. *Arab. J. Geosci.* **6**, 4347 (2012)
- Moore, D.M., Reynolds, R.C.: X-ray Diffraction and the Identification and Analysis of Clay Minerals, 378 pp. Oxford University Press, Oxford (1997)
- Muffler, L.P.J., Doe, B.: J. *Sediment. Petrol.* **38**, 384–99 (1968)
- Negra, L.: Pétrologie, minéralogie et géochimie des minéralisations et des roches encaissantes des bassins associés aux structures tectoniques et magmatiques de l'Oued Bélif et du Jebel Haddada (nord des Nefza, Tunisie septentrionale), 223p. Thèse. University of Paris-Sud, Orsay (1987)
- Perthuisot, V.: Dynamique et pétrogenèse extrusions triasiques en Tunisie septentrionale. *Presse. Ecole Normale Sup. Paris*, 312p (1978)
- Rouvier, H.: Géologie de l'extrême nord tunisien. Tectonique et paléogéographie superposées à l'extrémité orientale de la chaîne maghrébine. *Thèse Doct. D'Etat-Paris VI*. 703p (1977)
- White, D.E.: *Bull. Geol. Soc. Am.* **80**, 157–182 (1969)

Elaboration and Characterization of New Ceramic Ultrafiltration Membranes from Natural Clay: Application of Treatment of Textile Wastewater

Saida Bousbih, Emna Errais, Raja Ben Amar, Joelle Duplay, Malika Trabelsi-Ayadi, and Fadila Darragi

Abstract

A new filtration membrane was developed based on Tunisian natural clay. The choice of Tunisian clay as raw material in this work rests mainly on the related cost reduction and abundance characteristics, as the clay materials display noticeable ceramic pastes of a high plasticity and liable to exhibit an effective shaping ability. The raw material was milled and sieved at 250 μm , then mixed with water and organic additives to obtain a homogeneous paste. A ceramic porous tube was then prepared by extrusion and sintering at a temperature of 950 $^{\circ}\text{C}$. Interesting properties of resistance to corrosion and extreme pH solutions as well as mechanical endurance were displayed. The deposition of a coating layer inside the tube was then achieved by means of “slip-casting” method, using 40 μm clay powder, water and polyvinyl alcohol solution (PVA). After thermal treatment at 800 $^{\circ}\text{C}$, the membrane proved to be characterized with the water-permeability determination feature. The attained value of 256 L/h m^2 bar appears to reveal that the prepared membrane proves to belong to the Ultrafiltration domain. The relevant liability to be applied to the treatment of industrial textile wastewater turns out

to display an interesting retention liability of pollutants, in terms of COD (Chemical Organic Demand), of 80% and turbidity of (>99%). A total color retention disposition was also achieved at a pressure above five bars.

Keywords

Membranes • Support • Separation • Filtration Clay

1 Introduction

Membranes are used in many application domains thanks to the various advantages they provide, mainly, low energy consumption, efficiency, and easy implementation [1, 2]. More particularly, membrane processes have displayed a cost-effective solution for water recovery in the textile industry, as applied in various production processes. They are, therefore, increasingly used since they stand as a major registered treatment method useful for recuperating textile wastewater [7]. Among the membranes, ceramic membranes exhibit high chemical and thermal stability, long life, pressure resistance and good mechanical strength in respect of organic membranes [3–6]. These inorganic membranes are usually made of Alumina, Silica, Zircon and Titanium [7, 8]. Considering a sustainable approach, however, the use of cheaper raw materials turns out to be highly recommended for the production of low-cost ceramic membranes [9, 10]. In this regard, recent research dealing with the fabrication of membranes has been focused on the utilization of less expensive materials such as apatite powder, raw Algerian clay [11], carbon [12], Tunisian clay [13], dolomite, kaolin [14–16], and phosphate [17].

The objective of this study is to describe and characterize the development of innovative ceramic membranes based on Tunisian natural clay materials in great abundance. The proposed ultrafiltration (UF) membrane was evaluated through an application in the treatment of textile wastewater.

S. Bousbih (✉) · M. Trabelsi-Ayadi · F. Darragi
Laboratoire des applications de la Chimie aux ressources et substances naturelles et à l’environnement (LACRESNE), Faculté des sciences de Bizerte, Université de Carthage, Bizerte, Tunisie
e-mail: bousbih_saida@yahoo.fr

E. Errais
Laboratoire Physique des Matériaux Lamellaires et Nanomatériaux Hybrides, Faculté des sciences de Bizerte, Université de Carthage, Bizerte, Tunisie

R. Ben Amar
Laboratoire Sciences des Matériaux et Environnement, Faculté des Sciences de Sfax, Université de Sfax, Sfax, Tunisie

J. Duplay
Laboratoire d’hydrologie et de géochimie de Strasbourg, Strasbourg, France

2 Materials and Methods

2.1 Characterization of the Clay Powder

The clay powder was harvested in the Wadi Melah clay formation area (North of Tunisia), of Miocene Serravalian-Tortonian age. It was characterized by means of different techniques. Their mineralogical composition was determined by means of XRD analysis. The mineralogical analyses of the total fraction of samples proved to reveal that Wadi Melah associated clay contains 30% kaolinite, 30% illite, 25% chlorite, and 15% Interstratified illite/smectite. The non-clayey minerals enclose, mainly, quartz, calcite and trace amounts of gypsum and feldspar (Fig. 1). The chemical composition of the clayey material, as expressed in weight percentages of oxides, reveals that it is essentially formed of large amounts of silica and alumina and a lower proportion of iron oxide. As for the clay powder of Tabarka (in the North–West of Tunisia), it was characterized using different techniques, mainly, mineralogical analyses of the samples' total fraction, which prove to indicate that the Tabarka based clay consists, essentially, of kaolinite (61%) and illite (39%). The non-clayey minerals fraction involves mainly quartz material, while the chemical composition reveals that the

clay powder predominantly contains a high amount of silica, along with lower proportions of alumina.

2.2 Elaboration of the Clay Support

The process used to make a tubular support using the Wadi Melah clay is described below. Empirically, the optimal formulation of the ceramic paste is prepared. The plastic paste was prepared from the <250 μm fraction of Wadi Melah clay powder, mixed with organic additives and water. A plasticizer and a binder are required to prepare paste with rheological properties allowing for shaping by extrusion. The composition adopted for the preparation of the paste involves 84% (w/w) of sifted clay, 4% (w/w) Amijel, 8% (w/w) starch and 4% (w/w) Methocel.

2.3 Preparation of the Clay Ultrafiltration Layer

The active UF layer of natural Tabarka clay was made by the slip casting method (superpose on a support 140 mm long, with an internal diameter of 6 mm). The optimal composition of Barbotine was: 2 g Tabarka Clay of 40 μm size

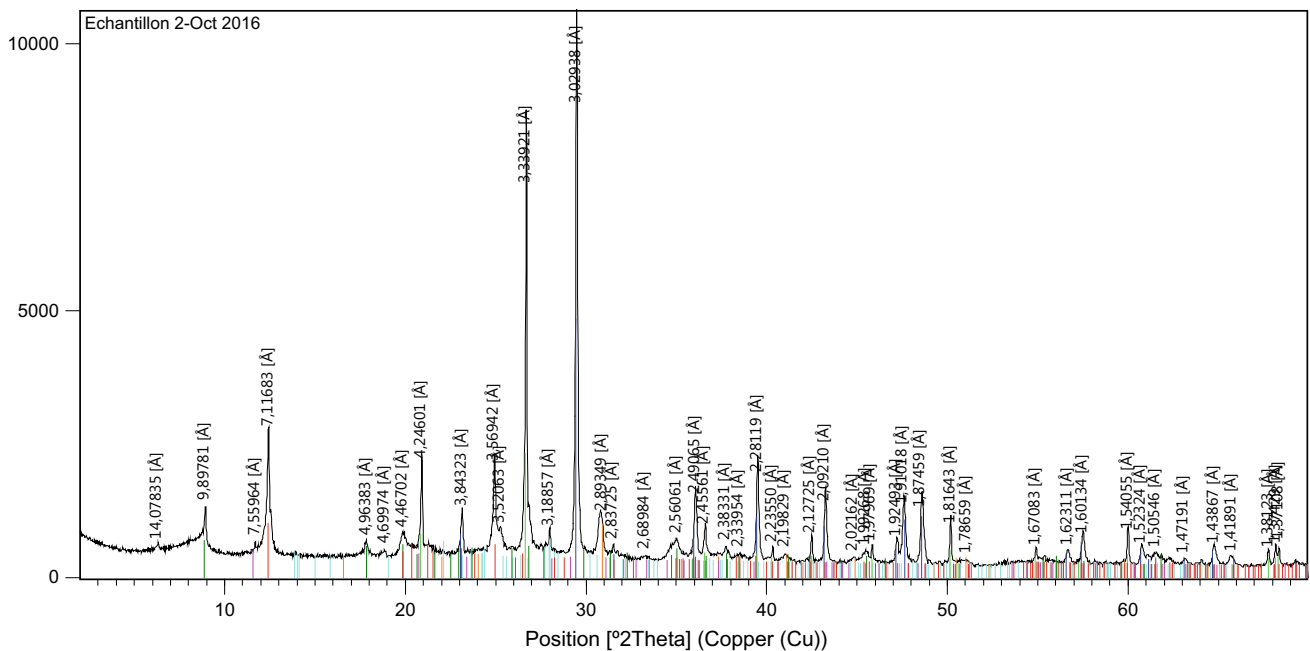


Fig. 1 X-Ray diffraction pattern of the Wadi Melah bulk clay

particles; 30 g APV (of polyvinyl alcohol) and 68 g water. The membrane sintering temperature was 800 °C.

3 Results and Discussion

3.1 Characterization of the Support

- (a) **Mechanical resistance.** The evolution of the value of the constraint modulus to the rupture (σ) in three-point bending according to the sintering temperature. This test reveals an elastic strain (linearity) and joins the observations noted on the porous texture of the material. In fact, densification causes an increase in the maximum stress before rupture and a gain of the stiffness of the material. The charred media at 950 °C have a very good mechanical resistance close to 16.8 MPa.
- (b) **Corrosion resistance.** The sintered support at 950 °C was subjected to corrosion resistance tests. The support was soaked at 80 °C in baths solution of NaOH (pH = 12) and of nitric acid (pH = 3). The control of weight loss was for 3 days. The mass loss did not

exceed 1% in both media. This shows that the clay-based support is resistant in both basic medium and acidic medium.

3.2 Characterization of the Membrane

The flux stabilization is almost observed after 10–20 min. The obtained permeability is 256.08 L/h m²bar (Fig. 2).

4 Application of Ultrafiltration for Textile Effluent Treatment

The results obtained for the filtration of textile effluent by the ultrafiltration membrane are transparent in Table 1. We can see that the COD retention rate (Chemical Organic Demand) was about 80% and was characterized by a decrease of turbidity (>99%). For a pressure of 5 bars, almost total retention of color was obtained (about 98%) (Fig. 3).

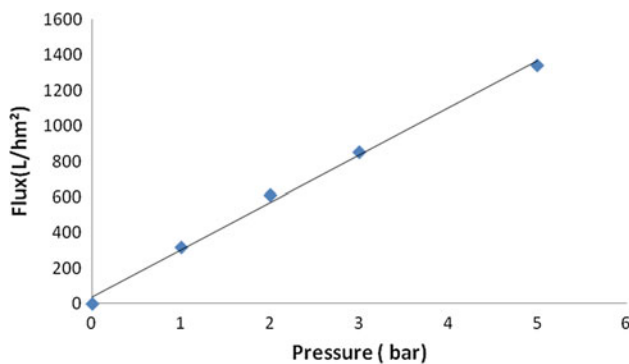


Fig. 2 Variation of permeate flux with time

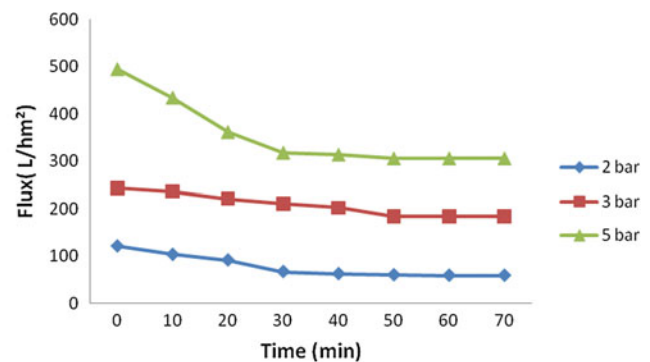
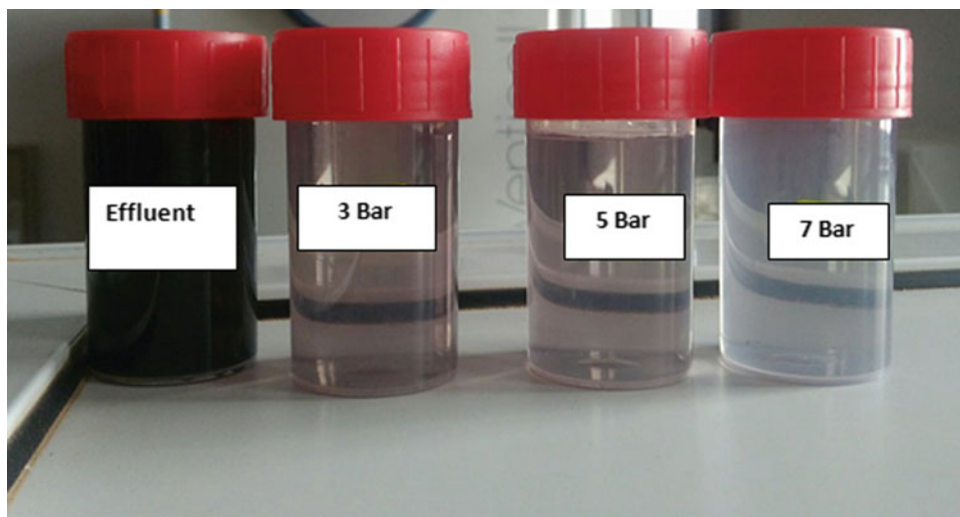


Table 1 Characteristics of raw effluent and treated effluent

Sample	pH	Salinity (g/ml)	Conductivity (MS/cm)	Turbidity (NTU)	COD	Color (590 nm)
Effluent	12.68	4.2	4.4	651	2235	2.254
3 bar	12.53	3.2	3.2	1.96	497.5	0.099
5 bar	10.92	3.1	2.4	1.80	447.5	0.087
7 bar	10.93	3.1	3.7	1.90	458.2	0.044

Fig. 3 Photo of the textile wastewater effluent before and after ultrafiltration



5 Conclusions

For this work, it has been proved that low cost UF membranes developed by a slip casting process on tubular microporous clay substrates can find an application of ultrafiltration, such as the treatment of textile effluents. The membrane obtained at a sintering temperature of 800 °C from natural clay showed a good adhesion between the filter layer and the support, and a significant efficiency in the treatment of textile effluents (a total retention of color was also achieved at a pressure above 5 bars and COD reduction).

References

- Cui, Z., Peng, W., Fan, Y., Xing, W., Xu, N.: Ceramic membrane filtration as seawater RO pre-treatment: influencing factors on the ceramic membrane flux and quality. *Desal. Wat. Treat.* **51**, 2575–2583 (2013)
- Kujawa, J., Kujawski, W., Koter, S., Jarzynka, K., Rosicka, A., Larbo, A.: Membrane distillation properties of TiO₂ ceramic membranes modified by perfluoroalkylsilanes. *Desal. Wat. Treat.* **51**, 1352–1361 (2013)
- Lee, S.H., Chung, K.C., Shin, M.C., Dong, J.I., Lee, H.S., Auh, K. H.: Preparation of ceramic membrane and application to the cross flow microfiltration of soluble waste oil. *Mater. Lott.* **52**, 66–71 (2002)
- Ding, X., Fan, Y., Xu, N.: A new route for the fabrication of TiO₂ ultrafiltration membranes with suspension derived from a wet chemical synthesis. *J. Membr. Sci.* **270**, 179–186 (2006)
- Larbot, A.: Fundamentals on inorganic membranes: present and new developments. *Pol. J. Chem. Technol.* **6**, 8–13 (2003)
- Cot, L., Ayrat, A., Durand, J., Guizard, C., Hovnanian, N., Julbe, A., Larbot, A.: Inorganic membranes and solid state sciences. *Solid State Sci.* **2**, 313–334 (2000)
- Yeung, K.L., Sebastian, J.M., Varma, A.: *J. Membr. Sci.* **131**, 9 (1997)
- Ahmad, A.L., Sani, N.A.A., Zein, S.H.S.: *Ceram. Int.* **37**, 2981 (2011)
- Anbri, Y., Tijani, N., Coronas, J., Mateo, E., Menéndez, M., Bentama, J.: *Desal.* **221**, 419 (2008)
- Tahri, N., Jedidi, I., Cerneaux, S., Cretin, M., Ben Amar, R.: Development of an asymmetric carbon microfiltration membrane: application to the treatment of industrial textile wastewater. *Sep. Purif. Technol.* **118**, 179–187 (2013)
- Masmoudi, M., Larbot, A., El Feki, H., Ben Amar, R.: Elaboration and characterisation of apatite based mineral supports for microfiltration and ultrafiltration membranes. *Ceram. Int.* **33**(3), p337 (2007)
- Rakib, S., Sghyar, M., Rafiq, M., Larbot, A., Cot, L.: Elaboration et caractérisation d'une ceramique macroporeuse à base d'arène granitique. *Ann. Chim. Sci. Mat.* **25**, 567–576 (2000)
- Bouzzara, F., Harabi, R., Achour, S., Larbot, A.: Porous ceramic supports for membranes prepared from kaolin and dolomite mixtures. *J. Eur. Ceram. Soc.* **26**(9), 1663 (2006)
- Abidi, N., Duplay, J., Elmchaouri, A., Jada, A., Trabelsi-ayadi, M.: Textile dye adsorption onto raw clay: influence of clay surface properties and dyeing additives. *J. Colloid Sci. Biotechnol.* **3**, 98–110 (2014)
- Khemakhem, S., Ben Amar, R., Ben Hassen, R., Larbot, A., Ben Salah, A., Cot, L.: Production of tubular ceramic membranes for microfiltration and ultrafiltration. *Indust. Ceramics* **24**(3), 117–120 (2004)
- Messaoudi, L., Larbot, A., Rafiq, M., Cot, L.: Mise au point d'une membrane de microfiltration sur supports tubulaires à base d'argile marocaine. *Ind. Ceram. Ver.* **12**(910), 831–835 (1995)
- Khemakhem, M., Khemakhem, S., Ayedi, S., Ben Amar, R.: Study of ceramic ultra-filtration membrane support based on phosphate industry sub-product: application for the cuttlefish conditioning effluents treatment. *Ceram. Int.* **37**, 3617–3625 (2011)

Characterization at High Temperature of the Porcelanite Mineral Phases from the Gafsa-Metlaoui Basin and Valuation in the Ceramic Domain

Rahma Bourawi, Ali Tlili, Jalila Essid, Raja Saidi, and Nabil Fattah

Abstract

In a bid to test the potential use of the porcelanites of the Gafsa-Metlaoui basin in the ceramic manufacturing domain, three porcelanites were collected from three different areas: the Kef el Ghiss, Oued Thelja and Kef Eddour. These porcelanites were treated at 800, 1000 and 1200 °C for three to six hours. The aim has been to understand their relating phase transformations at high-temperature, by simple calcination and activated calcination with an alkaline flux (Na₂CO₃). The treated and raw samples were analyzed through various techniques (XRD, X-ray Fluorescence). All samples were discovered to be opal C/T-rich. The Oued Thelja and Kef Eddour samples appear to be carbonate-rich, while the Kef el Ghiss's sample turns out to be rather clayey and contain trace amounts of quartz, francolite and feldspars. Following calcination, all samples have appeared to lose a large part of their mineralogical constituents (clay minerals, calcite, dolomite, quartz, francolite, hematite and feldspars), while the opal C/T proved to transform into cristobalite and tridymite. Thus, the activated calcination, within the ranges of 1000–1200 °C, of the samples of Oued Thelja and Kef Eddour proved to yield cristobalite and tridymite. The same mineral phases were obtained with enstatite and/or diopside, following a simple

1200 °C calcination process. The administered ceramic tests appear to reveal that the Kef Eddour and Kef el Ghiss associated samples are not suitably fit for ceramic applications. As for the Oued Thelja relevant sample, it proves to display satisfactory properties (in terms of shrinkage, porosity and loss on ignition), and could therefore be valued in ceramics manufacture through applying it in formulas of up to 20% in range, in conformity with the following formula: 20% Opal C/T + 12% Tabarka clay + 30% feldspars + 38% clay from Ukraine.

Keywords

Porcelanite • Calcination • Opal CT • Cristobalite • Mineralogy • Ceramic

R. Bourawi (✉) · A. Tlili · J. Essid · R. Saidi
Laboratory of GEOGLOB, Department of Earth Sciences, Faculty of Sciences, Sfax University, 3029 Sfax, Tunisia
e-mail: bourawirahma@gmail.com

A. Tlili
e-mail: alitlili@yahoo.fr

J. Essid
e-mail: jalila.essid@yahoo.fr

R. Saidi
e-mail: Saidi_raja@yahoo.fr

N. Fattah
Gafsa Phosphates Company, The Metlaoui Research Center, 2130 Metlaoui, Tunisia
e-mail: nabil.fattah@cpq.com.tn

1 Introduction

In Tunisia, the most recently conducted works dealing with the Gafsa-Metlaoui basin based siliceous rocks prove to indicate well that they correspond to the porcelanites' group [1, 2]. They appear to consist mainly of opal C/T, and belong to the Chouabine formation of the Ypresian series of the Gafsa-Metlaoui basin. These porcelanites have been subjected to extensive mineralogical characterization. Still, the high-temperature associated mineral transformations appear to require rather thorough studies to test the porcelanite potential application in the ceramic manufacturing. In this context, the porcelanites-rich carbonates have been tested in liquid sulfur filtration [3] and ceramic [4].

2 Materials and Methods

Three samples of the Chouabine formation were collected from the siliceous intercalations which occurs between VI and VII phosphatic layers belonging to the three sections:

Kef Eddour, Oued Thelja and Kef El Ghiss. These samples were treated at 800, 1000 and 1200 °C for 3 and 6 h by simple calcination and activated calcination by adding an alkaline flux (Na_2CO_3). Treated and untreated samples were analyzed by XRD and fluorescence X. For the ceramic tests three components were used in the formulas: Tabarka clay, feldspars and Ukraine clay.

3 Results

3.1 The Raw Samples

All raw samples were found to be opal C/T-rich. The Oued Thelja and Kef Eddour samples are carbonate-rich, contain phyllosilicates, trace amount of quartz and francolite. While the Kef el Ghiss sample is more clayey and contains a small amount of quartz, francolite and feldspars.

Chemical analysis shows that these porcelanites are SiO_2 rich, exceeding 72 wt%, while Al_2O_3 , Fe_2O_3 , MgO , are present and vary with the proportion of clay minerals (Table 1).

3.2 The Treated Samples

After calcinations, the color of all samples changed from whitish to yellowish for carbonate-rich porcelanites and to reddish for clay-rich porcelanites due to iron oxide content. The characterization by XRD shows that after calcination, all samples have lost a large part of their mineralogical constituents (clay minerals from 800 °C; calcite, dolomite, quartz, francolite, hematite and feldspars at high temperatures) and the Opal CT transforms to cristobalite and tridymite (Fig. 1). Enstatite and/or diopside appears respectively in the Oued Thelja and Kef Eddour samples after simple and activated calcination.

3.3 Ceramic Tests

The first test consists in evaluating the porcelanites through the manufacture of pellets consisting of 100% of each sample. Table 2 shows the properties of the three samples calcined in three types of oven (single firing, double firing

and stoneware). For the two samples Kef Eddour and Oued Thelja, the results were acceptable and they can be then introduced in ceramic formulas. For the Kef el Ghiss sample, the obtained results were not convincing, due to bad properties after calcination [high shrinkage (5%)], low resistance to thermal shock and admitted cracks which subsequently prevented the measurement of its porosity. Thus, the sample of Kef el Ghiss was not further considered (Table 2). The second tests consists of introducing porcelanite sample as a mixture with other components whose properties are previously known. Beginning by introducing 12% of each sample, the tests show that the Kef Eddour sample cannot be used in the ceramic field because it requires a significant amount of water that exceeds 50%, which is economically unprofitable. Instead, the sample of Oued Thelja shows satisfactory properties (shrinkage, porosity and loss on ignition) (Table 3; Fig. 2) and can therefore be valued in ceramics until 20% according to the following formula: 20% Opal C/T + 12% Tabarka clay + 30% feldspars + 38% clay from Ukraine.

4 Discussion

After calcination, the Kef Eddour sample display the highest weight loss due to its high carbonate content and organic matter. The water losses are recorded rather during the activated calcination than during the simple calcination.

All calcined sample have lost a large part of their mineralogical constituents (clay minerals, calcite, dolomite, quartz, francolite, hematite and feldspars), while the opal C/T is transformed to cristobalite and tridymite after heating above 1000 °C. Therefore, the activated calcination of the samples of Oued Thelja and Kef Eddour, from 1000 °C, yields cristobalite. However, the appearance of cristobalite in the Kef el Ghiss sample occurred only around 1200 °C. After simple calcination, this result was obtained only at 1200 °C for all samples. It can be concluded therefore that the addition of the alkaline flux (Na_2CO_3) favours the transformation of opal CT to cristobalite.

For the ceramic tests, the results show that the Kef Eddour and the Kef el Ghiss samples are not suitable for ceramics. The former gives an excessive water consumption, exceeding 50%, which may be related to its high carbonate content. The latter shows large shrinkage and poor

Table 1 Chemical analysis of raw porcelanites (as weight percentages, wt%)

	SiO_2	Al_2O_3	MgO	CaO	Fe_2O_3	TiO_2	K_2O	P_2O_5	SO_3	LOI	Total
Kef el Ghiss	80.1	5.37	2.64	1.57	2.37	0.27	0.33	0.67	0.13	10	103.45
Oued Thelja	77	2.75	2.55	4.52	0.9	0.11	0.27	0.85	0.79	11.4	101.14
Kef Eddour	72.7	3.6	2.57	7	1.09	0.15	0.35	1.21	0.67	12.95	102.29

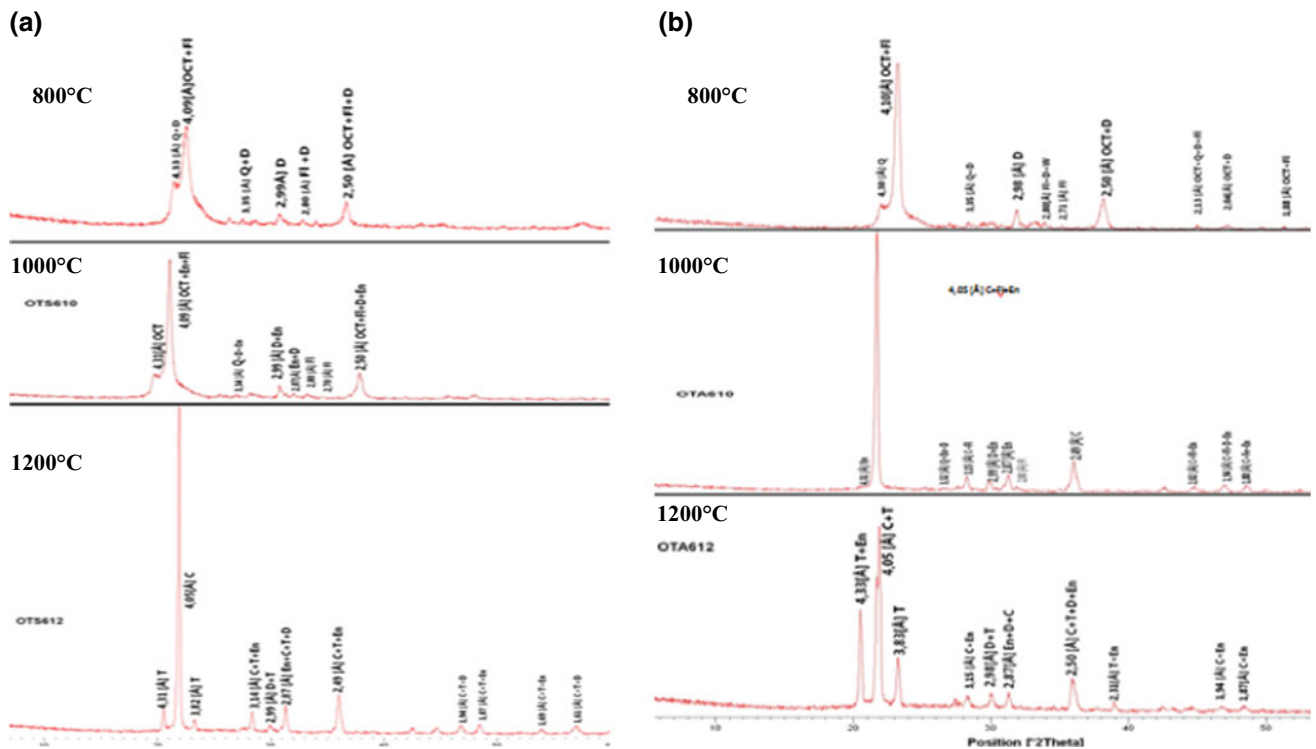


Fig. 1 X-ray diffraction patterns of the Oued Thelja sample treated by simple calcination **a** and activated calcination **b** for 6 h at different temperatures (800, 1000 and 1200 °C)

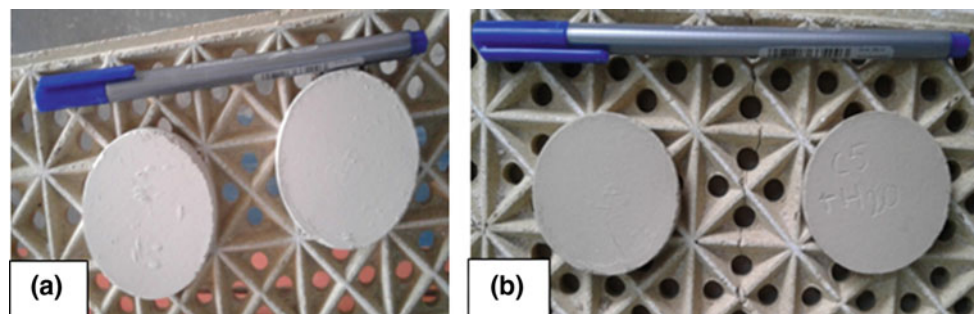
Table 2 Properties of ceramic using 100% porcelanite of each sample

	Single firing			Double firing			Stoneware		
	Weight loss	Shrinkage	Porosity	Weight loss	Shrinkage	Porosity	Weight loss	Shrinkage	Porosity
Kef Eddour	8.91	2.56	45.6	11.17	1.95	59.9	12.02	3.96	43.61
Oued Thelja	6.67	2.18	41	6.91	1.84	43.67	9.86	3.67	41.41
Kef el Ghiss	10.33	5	–	9.68	4	–	10	5	–

Table 3 Properties of ceramic using 12 and 20% porcelanite of Oued Thelja (OT) and Kef Eddour (KE)

	Weight loss	Shrinkage	Porosity	Color
Test with 12% KE	4.25	11.78	0.38	Beige
Test with 12% OT	4.7	10.6	3.4	Beige
Test with 20% OT	5.07	12.77	0.75	Beige

Fig. 2 Ceramics prepared with the porcelanite sample of Oued Thelja



properties, which can be related to the significant phyllosilicates content, which can induces welling. By contrast, the sample of Oued Thelja shows satisfactory properties (in terms of shrinkage, porosity and loss on ignition) and can therefore be valued in ceramics until 20% according to the following formula: 20% Opal C/T + 12% Tabarka clay + 30% feldspars + 38% clay from Ukraine.

5 Conclusions

The studied porcelanite samples are rich in SiO₂ and opal C/T. The Kef el Ghiss sample is the richest in SiO₂ and contains significant amount of clay, whereas the Kef Eddour sample is more carbonate-rich than the Oued Thelja sample. The calcination of porcelanite at high temperature transforms opal C/T into cristobalite and tridymite. Valuation of these porcelanites shows only that the sample of Oued Thelja can be used in ceramics manufacture until 20% according to the

following formula: 20% Opal C/T + 12% Tabarka clay + 30% feldspars + 38% clay from Ukraine.

References

1. Tlili, A., Saidi, R., Fourati, A., Ammar, N., Jamoussi, F.: Mineralogical study and properties of natural and flux calcined porcelanite from Gafsa-Metlaoui basin compared to diatomaceous filtration aids. *Appl. Clay Sci.* **55**, 62–63, 47–57 (2012)
2. Saidi, R., Felhi, M., Tlili, A., Khilil, L., Fourati, A., Kammoun, L., et Jamoussi, F.: Depositional environment and stability of the porcelanite within the Ypresian phosphatic series of the Gafsa-Metlaoui basin, southwestern Tunisia. *Arab. J. Geosci.* (2014)
3. Saidi, R.: Etude géochimique et minéralogique des niveaux de porcelanite du bassin de Gafsa-Metlaoui: Perspectives de valorisation dans la filtration industrielle, 284p. Thèse de Doctorat, Université de Sfax. FSS (2015)
4. Massoudi, K.: Les porcelanites du bassin de Gafsa: caractérisation des phases à haute température et perspective de valorisation en céramique. Mém. Master Univ. Sfax, FSS (2016)

Mineralogy and Geochemistry of Supergene Alteration of Neogene Hawaiites of Moktaa el Hadid (Nefza, Northern Tunisia)

Sonia Lazaar, Randa Ben Abdallah, Marilyne Soubrand, Emmanuel Joussein, and Mounir Medhioub

Abstract

This work is conducted to study the mineralogical, petrographic and geochemical aspects of the basic volcanic Neogene rocks (hawaiites) as persistent in the Nefza region (northern Tunisia), and their alteration outcomes. The outcrops, as studied in the area, are those belonging to Moktaa El Hadid. These rocks appear to display argilization associated with weathering and significant hydrothermal circulation [1]. Among the magnetic minerals, titanomagnetites are the most abundant and represent the major spinel in basalts.

Keywords

Basic hawaiites • Alteration • Clay products • Mineralogy • Geochemistry

1 Introduction

Outcrops of Tertiary basaltic rocks, in abundance in many areas of Northern Tunisia (Guelb Saad Moun; Mogods; Moktaa El Hadid; Nefza etc.), prove to be predominantly covered with fertile soils, intensively used for paint or ceramic. Among the magnetic minerals, illmenite, titanomagnetites and magnetites are the most abundant and represent the major spinel in basalts.

S. Lazaar (✉) · M. Medhioub
Laboratory of Spectroscopic Characterization and Optics of Materials (LaCSOM), University of Sfax, Sfax, Tunisia
e-mail: sonyelazaar@gmail.com

M. Medhioub
e-mail: mounirmedhioub@yahoo.fr

R. B. Abdallah
Department of Geology, Faculty of Bizerte,
University of Carthage, Carthage, Tunisia

S. Lazaar · M. Soubrand · E. Joussein
Laboratoire PEREINE, University of Limoges,
EA 7500 Limoges, Cedex, France

The titanomagnetites form a complete solid-solution series, but intermediate compositions can only be preserved as single-phase minerals once very rapidly cooled [2]. This high-temperature oxidation is also called deuteric alteration. Hence, the iddingsite outcomes, as resulting from an alteration of this type, represent partial or total pseudo-morph of olivine [3].

The aim of this paper is to characterize the alteration processes associated with iron titanium oxides, which occur in the rock either in an early in the form of deuteric alteration, or at a later stage, i.e., during argilization.

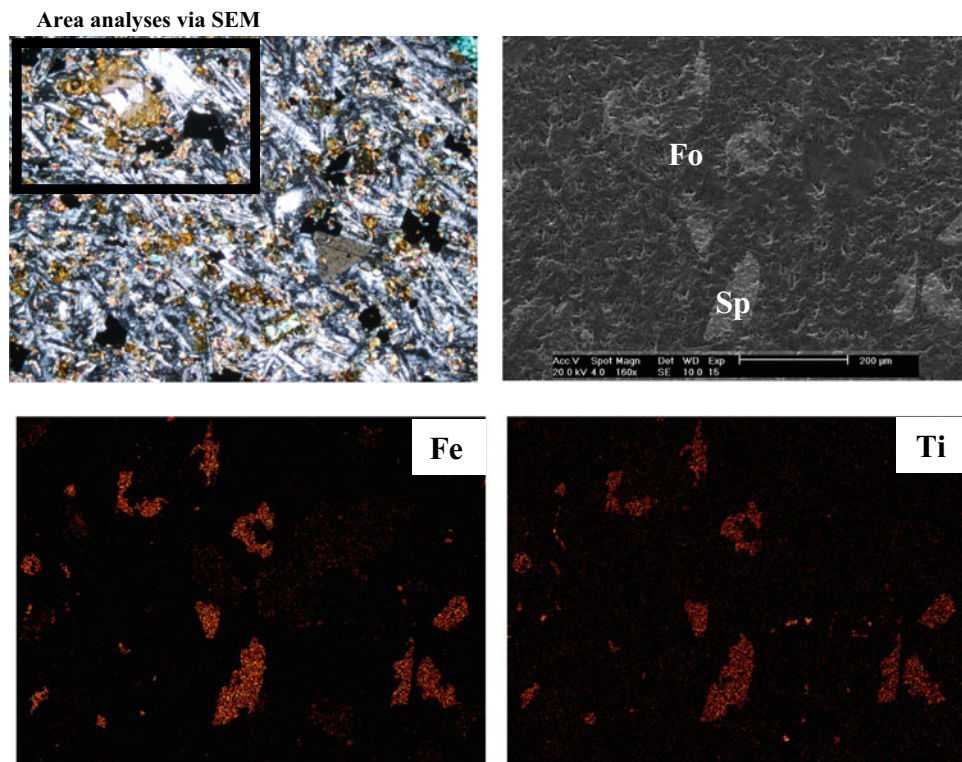
2 Materials and Methods

The petrographic study of thin sections was supplemented by occasional chemical analysis with SEM, coupled with an EDS analysis system relevant to the distinction of primary minerals and their alteration products. Acquisitions and analyses of the SEM images were applied to quantify the basalt percentages related to the different mineral phases. All samples were prepared for clay mineral analyses via X-ray diffraction (XRD) and transmission infrared spectroscopy.

3 Results and Discussion

Observations by light microscopy and SEM appear to reveal that the hawaiites prove to display a microlitic structure, microlitic porphyry and, often, a fluidal texture (orientation plagioclase microlites provides information on the lava flow). Plagioclase phenocrysts have labrador compositions (An 68), with some microcrystals of calcium clinopyroxene, including titaniferous augites (Ti rich) and magnesium-rich olivine (Fo78 Fa22), along with inclusions of titanomagnetite, subhexagonal globular crown of iddingsite (Fig. 1). The matrix or the mesostasis consists of brown and black oxides in presence of the glassy phase (isotropic), along with microlites of very abundant plagioclase. Some samples

Fig. 1 Photos in optic microscopy of iddingsitized forsterite (Fo) and titanomagnetite (Sp) of bedrock before and after SEM analyzes. Elemental distribution maps (Fe, Ti) as drawn via SEM



appear to exhibit a certain alteration degree in minerals, such as olivine, plagioclase and the glassy phase. The evolutions of basalt minerals are progressive. Detailed SEM analyses of the various altered basalts show well that glass is the first phase to deteriorate [4] in poorly crystalline product, followed by olivine and iddingsite [5] and plagioclase in halloysite. Pyroxene and ilmenite are the last to deteriorate.

4 Area Analyses via SEM

The mineralogical determinations were carried out by means of X-ray diffraction. Relevant analyses were carried out on clay fractions ($<2 \mu\text{m}$) (Fig. 2). The traditional clay determination methodology of oriented aggregates, including treatment with ethylene glycol and heating to $550 \text{ }^\circ\text{C}$, were adopted [6]. Showing essentially: Sm: smectites, k: kaolin, Mag: magnetite, Plg: plagioclase and O: olivine.

Analyses of MEH 2-10 sample by means of infrared spectroscopy, with a spectral range extending from 500 to 4000 cm^{-1} , prove to reveal two bands at (3620 cm^{-1}) and (3693 cm^{-1}), likely to be associated with inner and outer

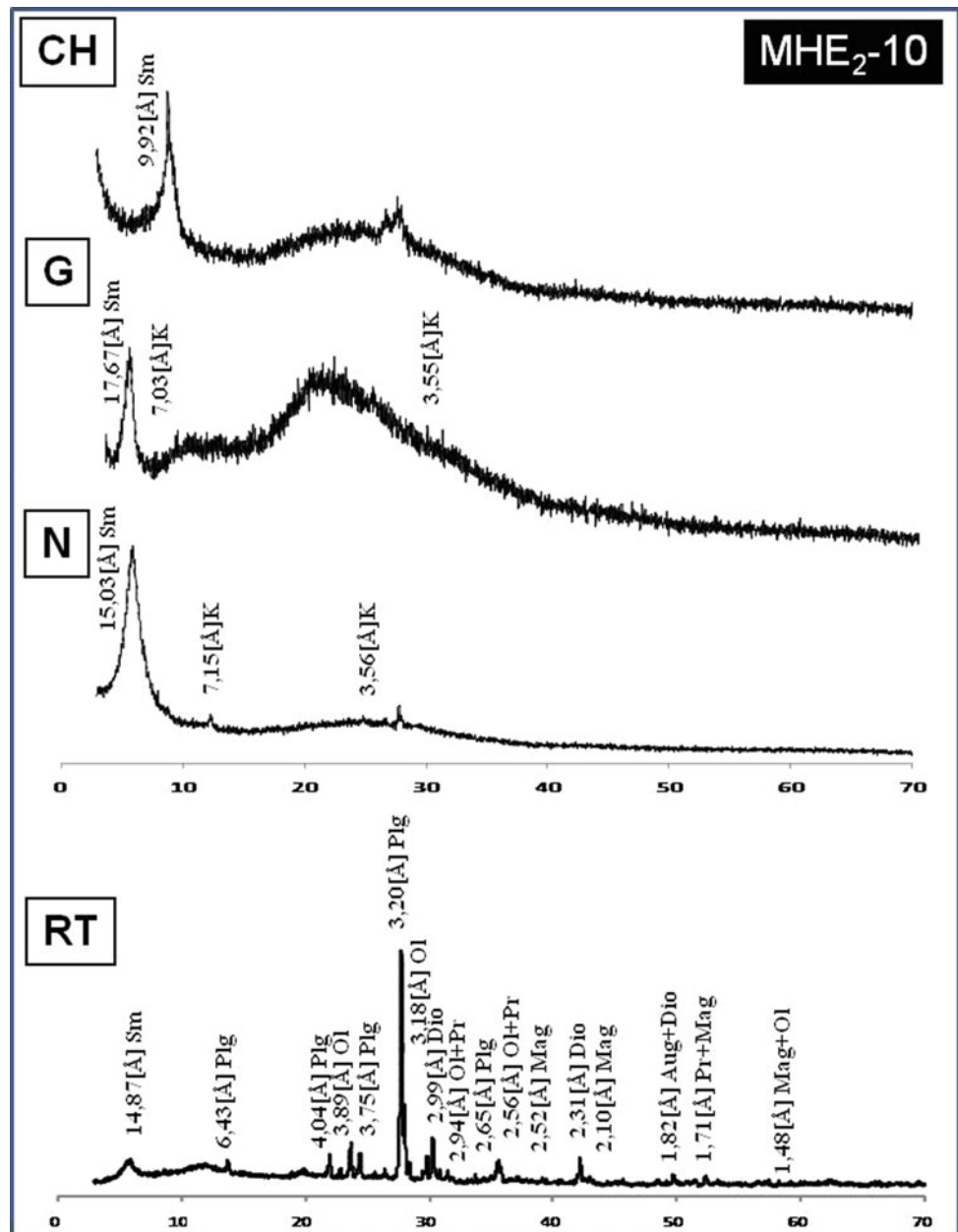
stretching vibrations of kaolinite, showing bands 3360 and 1000 cm^{-1} , characteristics of smectites. The 3620 cm^{-1} band is also characteristic of the OH-stretching vibration of smectite. The presence of the band at 910 cm^{-1} corresponds to the deformation vibrations associated with the Al–OH–Al groups in halloysite. The spectrum proves to display halloysite relating characteristic bands of the ranges of 3693 , 3620 , 1040 and 910 cm^{-1} [7, 8], and smectites associated bands of the ranges of 3360 and 1000 cm^{-1} .

5 Conclusions

Magnetic properties are complementarily used with mineralogy to characterize the alteration of iron titanium oxides as occurring in basaltic rocks.

The evolution of the basalt alteration minerals turns out to be gradual and selective. Secondary products involve, mainly, clay minerals (smectite, halloysite and kaolinite) and titaniferous minerals, titanomagnetite. The magnetites and titanomagnetites of the basaltic rocks are respectively converted to maghemites and titanomaghemites in soils.

Fig. 2 Diffractogram of sample MEH₂-10, RT: total rock, and of fractions <2 μm, with: N: normal clay; G: glycol clay and CH: clay heated to 550° C, showing essentially: Sm: smectites; k: kaolin; Mag: magnetite; Plg: plagioclase and O: olivine



References

1. Meddeb, N.: Potentialités géothermiques de la Tunisie septentrionale. Université de Tunis, Thèse de spécialité (1993)
2. Lindsley, D.H.: Experimental studies of oxide minerals. *Rev. Miner.* **25**, 69–106 (1991)
3. Soubrand-Colin, M., Bril, H., Neel, C., Courtin-Nomade, A., Martin, F.: Weathering of basaltic rocks from the French Massif Central: origin and fate of Ni, Cr, Zn, Cu. *Can. Mineral.* **43**(3), 1103–1118 (2005)
4. Gislason, S.R., Euster, H.P.: Meteoric water-basalt interactions. II: A field study in N.E. Iceland. *Geochimica Cosmochim. Acta* **51**, 2841–2855 (1987)
5. Baker, I., Haggerty, S.E.: The alteration of olivine in basaltic and associated lavas. Part II: intermediate and low temperature alteration. *Contrib. Miner. Petrol.* **16**, 258–273 (1967)
6. Brown, G.: *The X-ray Identification and Crystal Structures of Clay Minerals*. Mineral Society, London (1961)
7. Farmer, V.C.: *The Infra-red spectra of minerals*. Mineral. Soc. Monogr. **4**, 539 pp
8. Joussein, E., Kruyts, N., Righi, D., Petit, S., Delvaux, B.: Specific retention of radiocesium in volcanic ash soils devoid of micaceous clay minerals. *Soils Sci. Soc. Am. J.* **68**(1), 313–319 (2004)

Structural Properties of Phosphate-Washing Waste Based Geopolymeric Mortars

Rawia Dabbebi, José Barroso de Aguiar, and Samir Baklouti

Abstract

The phosphate ore extraction activities often generate serious environmental problems, particularly those engendered by the phosphate washing waste. The waste was characterized by X ray fluorescence. The powder was calcined at 700 °C. The calcined and uncalcined samples were then investigated by means of X-ray powder diffraction (XRD). The calcined PWW was activated with sodium hydroxide and sodium silicate to produce geopolymeric materials. The reached results prove to reveal that the present phases in the powder appeared to have a remarkable effect on the result of compressive strength.

Keywords

Phosphate-washing waste • Calcination • Sodium hydroxide • Sodium silicate • Geopolymeric mortar

1 Introduction

Phosphate ore stands as the principal mineral product in Tunisia. This ore is extracted by the Gafsa Phosphate Company (CPG), based in the Tunisian southwest. This ore

R. Dabbebi (✉) · S. Baklouti
Laboratory of Industrial Chemistry, University of Sfax, 3038 Sfax,
Tunisia
e-mail: dabbebirawia@gmail.com

S. Baklouti
e-mail: Baklouti.samir@gmail.com

R. Dabbebi · J. B. de Aguiar
C-TAC Research Centre, University of Minho, 4800-058
Guimarães, Portugal
e-mail: aguiar@civil.uminho.pt

is composed of fluorapatite, silica, carbonate, gypsum, organic and aluminosilicates materials [1, 2]. The CPG uses the washing and flotation techniques as means whereby the aluminosilicate, silica and carbonate could be eliminated, and a high percentage (~80%) of phosphate ore recovered for commercial use. This process creates a large volume of waste, engendering a real environmental problem.

This waste named phosphate washing waste (PWW), contains quartz, carbonate, aluminosilicate and fluorapatite in respect of the phosphate ore relating mineralogical composition of [3, 4]. Based on the relevant literature, such waste can be explored in different fields as lightweight [5], Ceramic [6], Membrane [7, 8]. The composition of the PWW can be also adequate for the synthesis of other products, particularly, alkali activated materials (geopolymeric mortars).

2 Materials and Methods

The phosphate washing waste, as used in this study, is collected from the Metlawi storage pond (Lavrie IV). It was filtered and dried at 105 °C, for 24 h, to remove the water, then crushed and sieved to the grain size of less than 100 µm. The obtained powder was calcinated at 700 °C for 2 h in a muffle furnace at a heating rate of 10 °C/min.

The powder was, then, characterized via X-ray fluorescence, and the samples via X ray diffraction (XRD), with Cu K α radiation $\lambda = 1.54060 \text{ \AA}$ at 40 kV and 40 Ma. The sample was then scanned from 5° to 60°, at a speed of 0.02 s⁻¹.

The powder was activated using alkaline solutions based on a sodium hydroxide NaOH solution 10 M, and a sodium silicate solution Na₂SiO₃. The (Na₂SiO₃/NaOH) ratio is of the order of 1.

The obtained samples of geopolymers mortar were covered and left in the laboratory at ambient temperature, to be characterized at 7 and 28 days.

3 Results

3.1 Chemical Composition

The data figuring on Table 1 display the chemical composition of the PWW, revealing that the silica, calcium, aluminum and phosphorus persist in major quantities, while the other elements are present in trace amount.

3.2 XRD Characterization

Figure 1 depicts the X-ray diffractograms of the PWW at 25 and 700 °C. The pattern of PWW at 25 °C shows the persistence of carbonates, essentially as a calcite, at 3 Å. It displayed peaks at 8.76 Å, indicating the presence of natural zeolite heulandites as a main aluminosilicate mineral. The PWW also contains a fibrous clay palygorskite, displayed at a peak of 10.09 Å, a small amount of quartz with a peak of 3.41 Å, and gypsum with a peak of 2.8 Å.

The patterns reveal crystalline and amorphous phases, which are important for the powder calcined at 700 °C. It displays that the fluorapatite mineral still appears after calcinations. The curves also indicate that the calcite, palygorskite, and heulandite phases were progressively decreased. This decrease in the calcite phase is related to the decarbonation. For the heulandites, the decrease was related to the temperature effect on the decomposition of the heulandites structure [9]. In addition, reflections of new phase emerge, mainly, C₂S.

4 Discussion

Figure 2 reports the geopolymer XRD as based on the powder calcined at 700 °C (G⁷⁰⁰) at 7 and 28 days. The patterns represent a crystalline and amorphous phases. The comparison established between the XRD calcined PWW results at 700 °C with those of the hardened samples, reveals that the crystalline phases, originally existing at 700 °C as the Heulandites, palygorskite and anhydrite proved to disappear. Traces of calcite can be detected in the

geopolymeric mortars, which could well be the result of either the samples' carbonation, or the quantities persistent in the calcined sample. The patterns appear to reveal that the fluorapatite was unaltered by the alkali solution. In the patterns, the peaks of quartz appear more intensely than those relevant to the calcined materials. This is mainly due to some sand particles used as aggregate, which could not be totally eliminated during the XRD samples' preparation. Furthermore, the crystalline sodium compounds did not appear in the XRD patterns; it could be assumed that the sodium was included in the amorphous geopolymers phase. This G⁷⁰⁰ associated performance can be approved by the SEM image, as appearing in Fig. 3, highlighting that the mortar was noticeably heterogeneous with a compact structure.

The compressive strength, depicted in Fig. 4, indicates that the geopolymer phases persistent in G⁷⁰⁰, as resulting from the aluminosilicates phases related destruction, stem from the heulandites and the palygorskite. The evolution of the compressive strength has its interpretation in the amorphous phases and the C₂S predominant in the powder calcined at 700 °C. According to Sanchez et al. [10], the C₂S prevalent in the alkali medium proves to have a positive effect on the mechanical strength. The reached compressive strength value is of the range of ~11 MPa, satisfying the BS 6073 relating requirements, which entails a value ≥ 7 MPa of compressive strength for the masonry brick application [11].

5 Conclusions

The most obvious finding emanating from the conduction of such a study is that the calcination, as associated with the phosphate washing waste, proved to have a noticeable effect on the phases persistent in the powders.

During the G⁷⁰⁰ curing time, for 7 and 28 days at ambient temperature, the compressive strength appeared to evolve, due mainly to the presence of the aluminosilicate phases.

The microscopic observation revealed well that the G⁷⁰⁰ turns out to display a noticeable heterogeneous and dense structure.

Table 1 The PWW chemical composition

Oxides	SiO ₂	CaO	P ₂ O ₅	Al ₂ O ₃	Na ₂ O	K ₂ O	MgO	SO ₃	Fe ₂ O ₃	F ₂ O	LOI
%	42	26.5	10	9.77	1.12	0.673	3.09	3.39	2.31	0.96	17

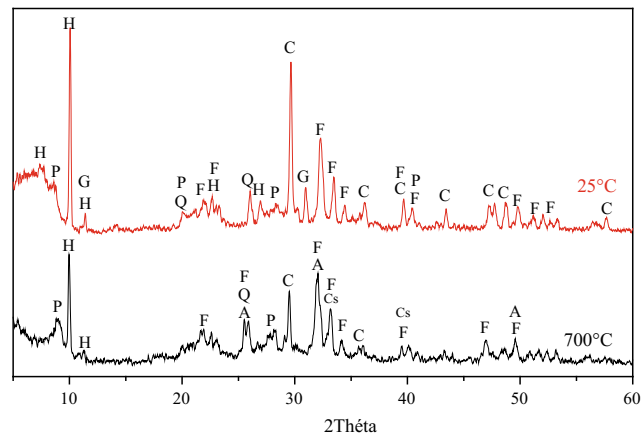


Fig. 1 X ray diffractograms of the PWW uncalcined and calcined 700 °C. C: Calcite, H: Heulandites, G: Gypsum, Q: Quartz, F: Fluorapatite, P: Palygorskite A: Anhydrite, Cs: C_2S

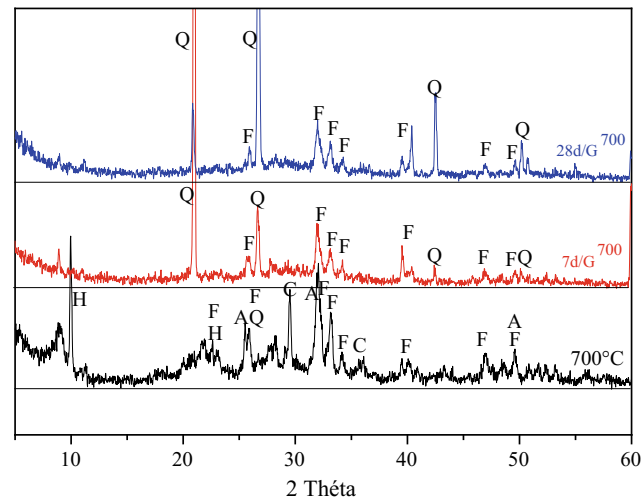
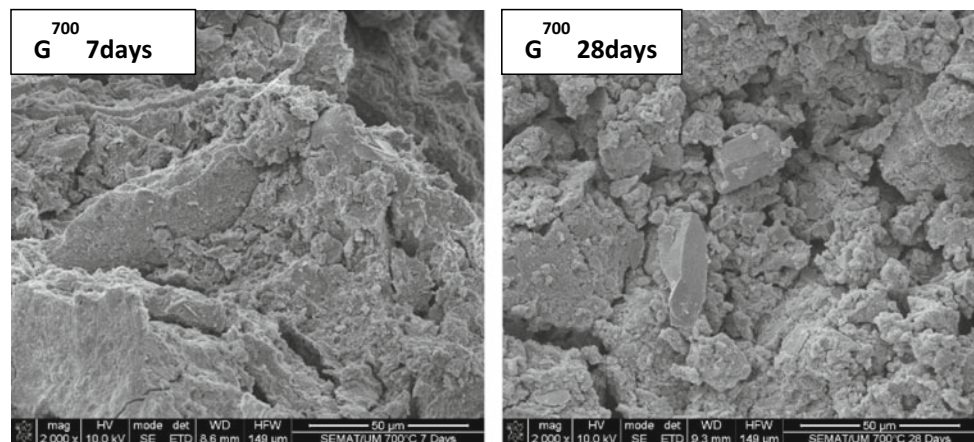


Fig. 2 X ray diffractograms of the PWW calcined 700 °C and G^{700}

Fig. 3 SEM of G^{700} at 7 and 28 days



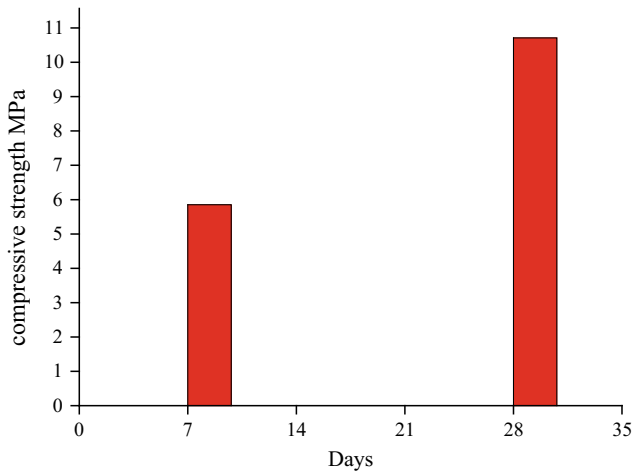


Fig. 4 Compressive strength of the G700

Based on the BS 6073 requirements, the compressive strength reached results make the product fit for masonry applications.

References

- Gallala, W., Saïdi, M., el Hajji, S., Zayani, K., Gaied, M.E., Montacer, M.: Characterization and valorization of Tozeur-Nefta phosphate ore deposit (Southwestern Tunisia). *Procedia Eng.* **138**, 8–18 (2016)
- Boughzala, K., Fattah, N., Bouzouita, K., Hassine, H.B.: Etude minéralogique et chimique du phosphate naturel d'Oum El Khecheb (Gafsa, Tunisie). *Rev sci matériaux, Lab LARHYSS* **6**, 11–29 (2015)
- Daik, R., Lajnef, M., Amor, S., Ezzaouia, H.: Effect of the temperature and the porosity of the gettering process on the removal of heavy metals from Tunisian phosphate rock. *Results Phys* **7**, 4189–4194 (2017)
- Elgharbi, S., Horchani-Naifer, K., Ferid, M.: Investigation of the structural and mineralogical changes of Tunisian phosphorite during calcinations. *J. Therm. Anal. Calorim.* **119**, 265–271 (2015)
- Loutou, M., Hajjaji, M., Mansori, M., Favotto, C., Hakkou, R.: Phosphate sludge: thermal transformation and use as lightweight aggregate material. *J. Environ. Manage.* **130**, 354–360 (2013)
- Yang, Y., Wei, Z., Chen, Y.-L., Li, Y., Li, X.: Utilizing phosphate mine tailings to produce ceramisite. *Constr. Build. Mater.* **155**, 1081–1090 (2017)
- Khemakhem, M., Khemakhem, S., Ayedi, S., Cretin, M., Amar, R. B.: Development of an asymmetric ultrafiltration membrane based on phosphates industry sub-products. *Ceram. Int.* **41**, 10343–10348 (2015)
- Khemakhem, M., Khemakhem, S., Ayedi, S., Amar, R.B.: Study of ceramic ultrafiltration membrane support based on phosphate industry subproduct: application for the cuttlefish conditioning effluents treatment. *Ceram. Int.* **37**, 3617–3625 (2011)
- Ostrooumov, M., Cappelletti, P., de'Gennaro, R.: Mineralogical study of zeolite from New Mexican deposits (Cuitzeo area, Michoacan, Mexico). *Appl. Clay Sci.* **55**, 27–35 (2012)
- Sánchez-Herrero, M.J., Fernández-Jiménez, A., Palomo, Á., Klein, L.: Alkaline hydration of C2S and C3S. *J. Am. Ceram. Soc.* **99**, 604–611 (2016)
- Abdullah, M.M.A., Ibrahim, W.M.W., Tahir, M.F.M.: 12—The properties and durability of fly ash-based geopolymeric masonry bricks. In: *Eco-efficient Masonry Bricks and Blocks*, pp. 273–287. Woodhead Publishing, Oxford (2015)

The Montagut Fault System: Geometry and Fluid Flow Analysis (Southern Pyrennes, Spain)

Luis Fernando Martinez Casas, Anna Travé, David Cruset, and Daniel Muñoz-López

Abstract

The Montagut fault system stands as part of the Sant Corneli and Boixols anticline, located in the frontal part of the Boixols thrust belt of the southern Pyrenees, as developed during the Alpine compression. Structural in-field data, as associated with petrographic and cathodoluminescence study, has yielded recognition of three different generations of calcite cement relating to different fluid-flow deformation stages. During the layer-parallel shortening, as related to the early folding stage, fluids proved to circulate through strike-slip and normal faults precipitating in the form of cement Cc1 and CC2. During the fold growth stage, calcite cement three was precipitated filling micro-vein coeval to the generation of stylolite, and could likely well represent the active deformation episode.

Keywords

Anticline • Calcite cement • Fluid flow • Vein • Pyrenees

1 Introduction

Fluid-rock interactions as occurring in faults and joints prove to play an important role in sediments during diagenetic changes and metamorphism, resulting in the formation of ore deposits, the migration and trapping of hydrocarbons [1–3].

In addition, these fluids' distribution can be strongly controlled by the existence of faults and joints, which act as seals or routes to the fluid migration, directly influencing the architecture and the petrophysical features of the fault rocks.

L. F. Martinez Casas (✉) · A. Travé · D. Cruset
D. Muñoz-López
Departament de Mineralogia, Petrologia i Geologia Aplicada,
Universitat de Barcelona (UB), Martí i Franquès s/n, 08028
Barcelona, Spain
e-mail: luisfer1927@gmail.com

2 Geological Setting and Methodology

The Montagut fault system lies between Sant Corneli and Boixols anticline and occupies the frontal position of the Boixols thrust belt of the southern Pyrenees (Fig. 1a). It is resulting from a continental collision occurring between the Iberian and European plates, as generated from Late Cretaceous to Miocene [4, 5].

The geological mapping of the fault system and host rocks were performed in three selected well-exposed outcrops (Fig. 1b). For each case, acquired in situ structural data were carried out in a bid to identify fault kinematics and the possible associated deformations and diagenetic characteristics. In addition, the samples were carefully oriented in the field, through marking dip and strike of a planar surface of the specimen on that surface. Finally, host rocks and fracture cements were systematically sampled for petrographic and geochemical study purposes.

Analyses of 34 thin sections concerning the host and fault rocks were administered by means of microscopic observations and Cathodoluminescence for the different cements to be distinguished. Additionally, a detailed thin-section mapping was performed to gather effective information concerning the predominant crosscutting relationships, diagenetic process and sedimentary components.

3 Results

3.1 Structural Data in Field

The Montagut Fault is well exposed towards the northern sector of the Sant Corneli anticline at outcrop A (main fault) and Vilanoveta at outcrop B (Fig. 1b). It is a normal fault trending NNW–SSE and dipping between 50 and 70 toward the SE, with a sub-vertical displacement (Fig. 1a), while they become subparallel to the Sant Corneli anticline axis around the outcrop C nearby area (Fig. 1b).

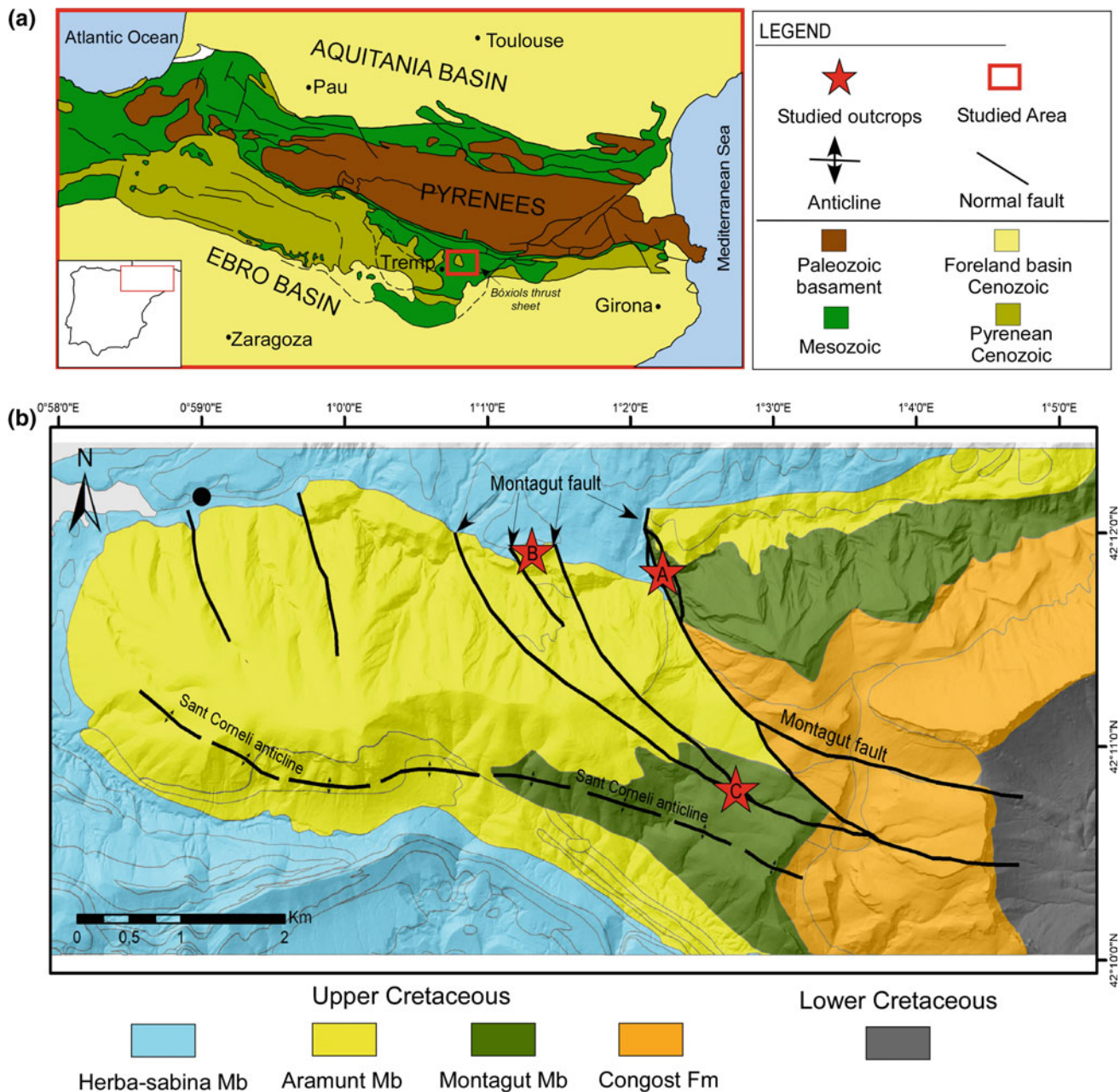


Fig. 1 Geological setting of the studied Area. **a** Structural map of the South Pyrenean thrust belt highlighting the studied area's site (red box). Modified from Muñoz (2002). **b** Geological map highlighting the outcrops' locations

The kinematic indicators on fault planes as slickenside and S-C structure appear to highlight a strike-slip trend superimposed by a dip-slip sense, changing to the extensional reactivation of prior strike-slip trend of the faults.

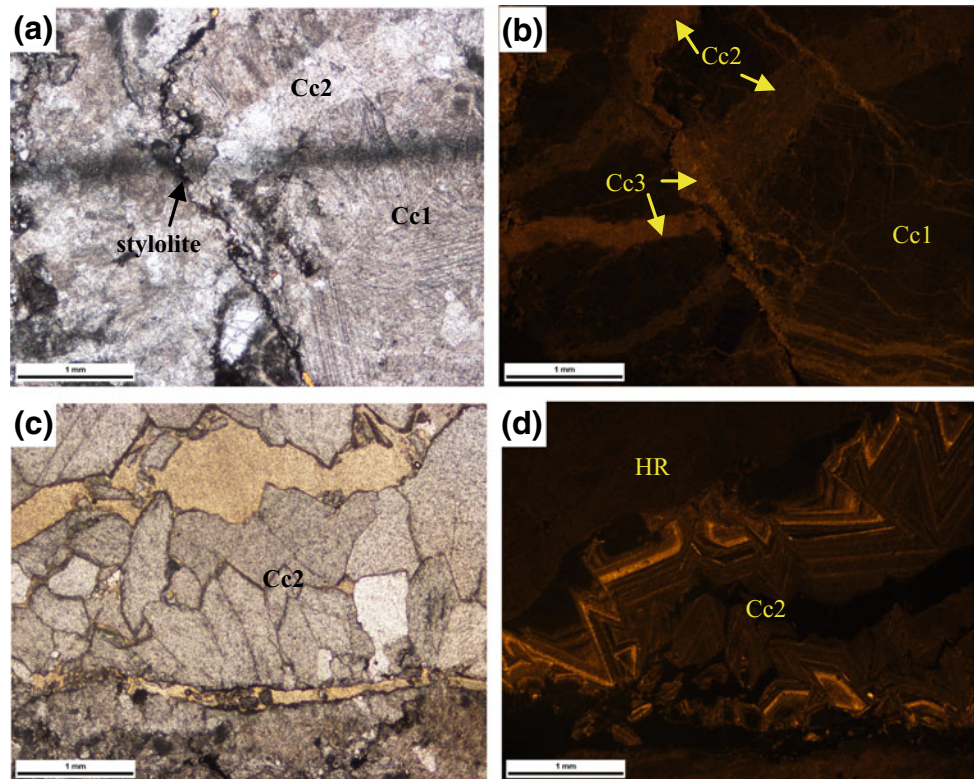
3.2 Petrology

Three different generations of calcite cement have been distinguished (Fig. 2). The first generation (Cc1), marked in dark

brown to dull-orange luminescence, reveals different textures, such as elongated crystals of twinned calcite, as observed in the shear bands parallel to the main planes, highlighting a synkinematic growth and change laterally to blocky twinned sparite.

Under Cathodoluminescence, calcite cement two (Cc2) is depicted in a dull to orange zoning. Calcite cement two (Cc2) present bladed to blocky texture, with sizes ranging between 1 mm and 2 mm (Fig. 2d), it has been observed as filling extensional veins perpendicular to the striated shear veins (Cc1).

Fig. 2 Microphotographs under optical (OP) and cathodoluminescence (CL) of the main calcite cements, the scale bar is 1 mm. **a–b** Plane light and CL images showing cross-cutting relationship between Cc1 (dark-brown luminiscent), Cc2 (more luminiscent), and Cc3 (bright-orange) cements and stylolite. **c–d** Plane light and CL images showing bladed and blocky Cc2 with zonation



The third generation of calcite cement (Cc3) was generated filling micro-veins parallel to the main plain coeval to the generation of stylolite, and represents the active deformation.

4 Discussion

Based on in situ data observation, crosscutting relationship in petrographic and cathodoluminescence analysis, the preliminary results prove to reveal that calcite cement one (Cc1) and calcite cement two (Cc2) represent the first stage (E1) associated with the deformation of the Montagut fault. Such finding could well be attributed to the development of folding taking place during the early compression stage, possibly due to layer parallel shortening, or during another type of sediment burial phases [6].

In effect, as suggested through the present study, the first-stage associated precipitation might well have taken place prior to the anticline growth stage and during the layer-parallel shortening phase. The Cc3, as precipitated in micro-veins (E2), is associated with the extensional reactivation of joints or veins during active folding.

5 Conclusions

Structural data and in situ kinematic indicators appear to reveal a strike-slip trend overprinted with a dip-slip trend, standing as an extensional reactivation of earlier strike-slip movements. The petrographic and cathodoluminescence data relating to calcite cements, as filling different microfracture, highlight the persistence of two migrating fluids, yielding two cementation stages: Cc1 and Cc2, closely associated with the layer-parallel shortening, along with Cc3, highly related to the anticline development. The study of the fractures in field was implemented together with the petrographic and geochemical analyses (in progress) of the fracture-filling cement phases, in a bid to identify the type of fluids that were precipitated.

References

1. Evans, M.A., Fischer, M.P.: On the distribution of fluids in folds: a review of controlling factors and processes. *J. Struct. Geol.* **44**, 2–24 (2012)

2. Lacombe, O., Swennen, R., Caracausi, A.: Fluid–rock–tectonics interactions in basins and orogens. *Mar. Petrol. Geol.* **55**, 332 (2014)
3. Oliver, J.: Fluids expelled tectonically from orogenic belts: their role in hydrocarbon migration and other geologic phenomena. *Geology* **14**, 99–102 (1986)
4. Muñoz, J.A.: The pyrenees. In: Gibbons, W., Moreno, T. (eds.) *The Geology of Spain*, pp. 370–385. Geol. Soc, London (2002)
5. Verges, J., Millan, H., Roca, E., Muñoz, J.A., Marzo, M., Cires, J., Den Bezemer, T., Zoetmeijer, R., Cloetingh, S.: Eastern Pyrenees and related foreland basins: pre-, syn- and post-collisional crustal scale cross-section. *Mar. Petrol. Geol.* **12**, 893–915 (1995)
6. Tavani, S., Storti, F., Lacombe, O., Corradetti, A., Muñoz, J., Mazzoli, S.: A review of deformation pattern templates in foreland basin systems and fold-and-thrust belts: implications for the state of stress in the frontal regions of thrust wedges. *Earth Sci. Rev.* **141**, 82–104 (2015)

From Rock-Buffered to Open Fluid System During Emplacement of the Lower Pedraforca Thrust Sheet (South Pyrenees)

David Cruset, Jaume Vergés, Irene Cantarero, and Anna Travé

Abstract

The evolution of fluid flow during the emplacement of the Lower Pedraforca thrust sheet has been inferred from fracture data, petrography and geochemistry of calcite cements. The reached results reveal that during the earlier compression stages, fluids migrating along the fractures were in equilibrium with their adjacent host rocks. Inversely, external fluids, displaying disequilibrium with their adjacent host rock migrated along fractures during the later emplacement stages of the thrust sheet. Similar evolution has been observed in other areas of the Pyrenees and other orogens worldwide.

Keywords

South pyrenean fold and thrust belt • Fluids • Fractures

1 Introduction

The cements precipitated in fractures record the composition and evolution of fluids during the tectonic history of fold and thrust belts [1].

In this work we define the evolution of fluids during the development of the Lower Pedraforca thrust sheet (South Pyrenees) integrating structural, petrographic and geochemical data. The results are compared with previous works done in the Southern Pyrenees (Jaca, Vallfugona and

L'Escala thrusts, Ainsa Basin and Puig-reig anticline) and other orogens worldwide (Bighorn Basin and North Oman and Canadian Rocky Mountains) [2].

2 Geological Setting

The south Pyrenean fold and thrust belt (SPFTB) consists of a southward directed thrust system, emplaced from Late Cretaceous to Oligocene, predominantly detached above Triassic and Eocene evaporites [3].

The Lower Pedraforca thrust sheet (LPTS), is an imbricated thrust system emplaced during the Lutetian (Middle Eocene) [4]. It consists of an allochthonous klippe detached above Eocene sediments, and involves Lower Triassic evaporites, Lower Jurassic limestones and dolostones, Upper Cretaceous limestones (Areny Fm.), Paleocene continental deposits (Garumnian) and Eocene syn-orogenic sediments deposited in the thrust front [3].

3 Methodology

Field work consisted of fracture data acquisition (dip directions and dips) and sampling of calcite cements precipitated in fractures and host rocks for petrographic and geochemical studies. Fracture data were plotted in stereograms and restored with respect to host rock bedding. Petrographic observations of 26 polished thin sections were made by means of optical and cathodoluminescence microscopy for the purpose of determining the different calcite cements and their crosscutting relationships. The geochemical characterization of fluids consists of carbon- and oxygen-isotope analysis of fracture-filling cements and their adjacent carbonate host rocks.

D. Cruset (✉) · I. Cantarero · A. Travé
Departament de Mineralogia, Petrologia i Geologia Aplicada,
Facultat de Ciències de la Terra, Universitat de Barcelona (UB),
Martí i Franquès s/n, 08028 Barcelona, Spain
e-mail: d.cruset@ub.edu

J. Vergés
Institut de Ciències de la Terra Jaume Almera, ICTJA-CSIC, Lluís
Solé i Sabarís s/n, 08028 Barcelona, Spain

4 Fractures and Cements

Up to seven fracture sets have been identified across the studied area. The F1 and F2 fractures comprise N-S and E-W bed-perpendicular veins, respectively. F2 is abutting F1, indicating a later formation time. The F3 fractures consist of bed-parallel slip surfaces, while F4 consists of conjugated NW-SE and NE-SW bed-perpendicular veins abutting F1 and F2. As for F5, it consists of conjugated NNE-SSW and NW-SE veins associated with major thrusts cross-cutting bedding at high angle. Concerning F6 and F7, they include small and major south-verging thrusts and strike-slip faults cross-cutting bedding at high angle, respectively.

The petrographic study undertaken on the LPTS fracture fillings have allowed to identify six types of calcite cements. Cc1 consists of non-luminescent microsparite precipitated in the intergranular and moldic porosity of the Areny Fm. Cc2 consists of non-luminescent sparite precipitated in vug porosity affecting the Garumnian. Cc3 consists of orange luminescent sparite crystals, blocky or elongated parallel to fracture walls, precipitated in F1, F2 and F3 fractures and vug porosity postdating Cc1 and Cc2. Cc4 consists of dull to orange luminescent sparite precipitated in F1, F2 and F4 affecting Eocene syn-orogenic sediments. Cc5 consists of zoned non-luminescent to dull orange cement precipitated in F1, F2 and F4 fractures postdating the previous cements. Cc6 consists of dull-brown sparite precipitated in F4, F5, F6 and F7 postdating Cc5.

Marine carbonates from the Areny Fm. have $\delta^{13}\text{C}$ ranging between +1.5 and +1.7‰ VPDB, and $\delta^{18}\text{O}$ ranging between -4.5 and -3.2‰ VPDB. Garumnian palustrine limestones have $\delta^{13}\text{C}$ comprised between -17.5 and -3.7‰ VPDB and $\delta^{18}\text{O}$ between -8.2 and -4.8‰ VPDB (Fig. 1a). The Cc1 has a $\delta^{13}\text{C}$ of +1.5‰ VPDB and $\delta^{18}\text{O}$ of -5.2‰ VPDB. Cc2 has a $\delta^{13}\text{C}$ of -10.1‰ VPDB and $\delta^{18}\text{O}$ of -6‰ VPDB. For Cc3, the $\delta^{13}\text{C}$ ranges between -10.8 and -0.4‰ VPDB and the $\delta^{18}\text{O}$ between -5.5 and -3.9‰ VPDB. Cc4 has $\delta^{13}\text{C}$ values between -5.9 and -3.7‰ VPDB and $\delta^{18}\text{O}$ between -5.9 and -2.6‰ VPDB. Cc5 has $\delta^{13}\text{C}$ values between +0.8 and +1.6‰ VPDB and $\delta^{18}\text{O}$ ranging between -5.7 and -4.4‰ VPDB. As for Cc6, the $\delta^{13}\text{C}$ range between -15.2 and +1.8‰ VPDB and the $\delta^{18}\text{O}$ between -9.2 and -6.1‰ VPDB.

5 Discussion

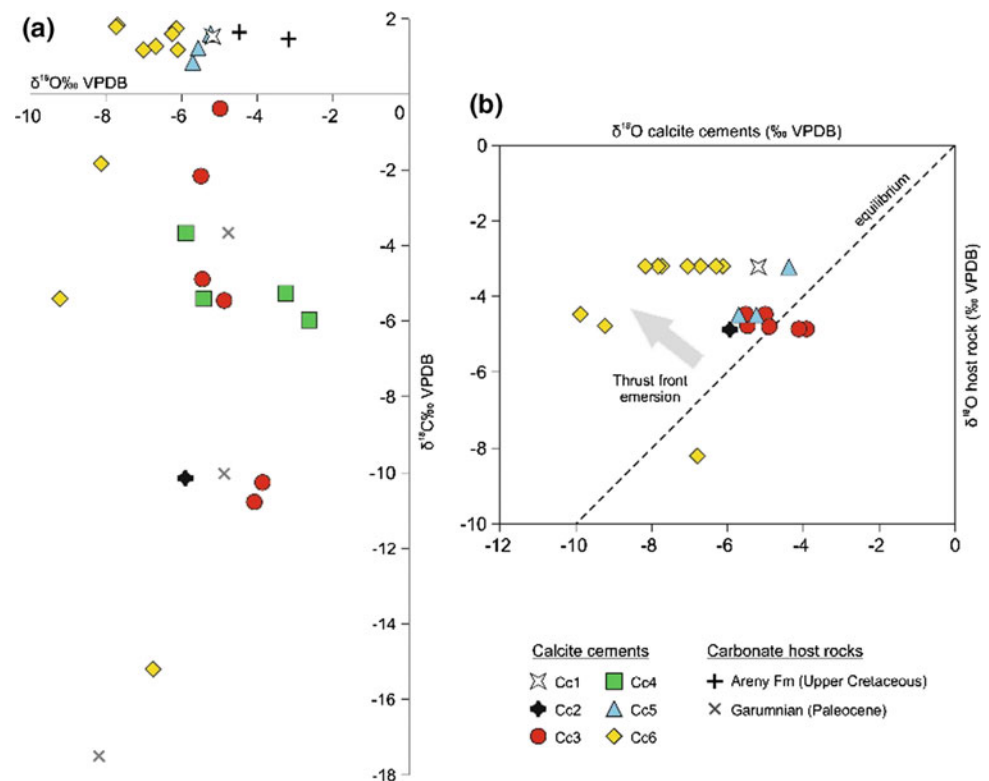
Crosscutting relationships between the LPTS associated fractures and bedding indicates that F1 to F4 were formed during the first compression stages, whereas F5 to F7 formed during the last deformation stages, once strata were already folded [5].

The $\delta^{13}\text{C}$ associated with the entirety of calcite cements appear to display noticeable similarities with their host rocks, indicating the persistence of a rock-buffered system. Similarly, the $\delta^{18}\text{O}$ values relating to Cc1, Cc2, Cc3 and Cc5 are also in equilibrium with their host rocks (Fig. 1b), indicating the predominance of a rock-buffered fluid system during calcite precipitation in the early vug porosity and also during formation of F1 to F4. Inversely, the $\delta^{18}\text{O}$ associated with the calcite cement Cc6 is more depleted in respect of its adjacent carbonate host rocks, indicating the opening of the system to exotic fluids as F4 to F7 formed (Fig. 1b). This trend has already been reported to prevail in other SPFTB relating areas, mainly, the Jaca, Vallfogona and L'Escala thrusts, Ainsa Basin and Puig-reig anticline [2, 6, 7]. Similarly, it also occurs in other regions worldwide, mainly, in the Bighorn Basin, North Oman and Canadian Rocky Mountains [2, 8, 9], where it has been interpreted as the input of upward migrating hot and saline fluids mixed, at depth, with progressively more abundant meteoric waters, probably linked to the emersion of the structure.

6 Conclusions

During the early compression of the LPTS, fluids in equilibrium with their adjacent host rock appear to have migrated along the N-S and E-W bed-perpendicular veins and bed-parallel slip surfaces. The precipitation of $\delta^{18}\text{O}$ -depleted calcite cements, as perceived in the faults formed during the late compression stages, prove to indicate the input of external fluids into the system. This evolution in fluid behavior, also observed in other areas of the SPFTB and worldwide, is interpreted as the input of hot and saline fluids mixed at depth with progressively more abundant meteoric waters during the structure emersion.

Fig. 1 **a** $\delta^{18}\text{O}$ versus $\delta^{13}\text{C}$ cross-plot of calcite cements and host rocks and **b** $\delta^{18}\text{O}_{\text{calcite cement}}$ versus $\delta^{18}\text{O}_{\text{host rock}}$ cross-plot from the LPTS calcite cements



Acknowledgements The isotopes were carried out at CCiTUB of the Universitat de Barcelona. This research was funded by the projects CGL2015-66335-C2-1-R and 2017SGR-824.

References

- Roure, F., Andriessen, P., Callot, J.P., Faure, J.L., Ferket, H., Gonzales, E., Guilhaumou, N., Lacombe, O., Malandain, J., Sassi, W., Schneider, F., Swennen, R., Vilasi, N.: The use of paleo-thermo-barometers and coupled thermal, fluid flow and pore-fluid pressure modelling for hydrocarbon and reservoir prediction in fold and thrust belts. In: Goffey, G.P., Craig, J., Needham, T., Scott, R. (eds.) *Hydrocarbons in Contractional Belts*, pp. 87–114. Geological Society, Special Publications, London (2010)
- Cruset, D., Cantarero, I., Vergés, J., John, C.M., Muñoz-López, D., Travé, A.: Changes in fluid regime in syn-orogenic sediments during the growth of the south Pyrenean fold and thrust belt. *Global Planet. Change* (2017). <https://doi.org/10.1016/j.gloplacha.2017.11.001>
- Vergés, J.: *Estudi geològic del vessant sud del Pirineu oriental i central. Evolució 947 cinemàtica en 3D*. Ph.D. thesis, Universitat de Barcelona, 203 pp (1993)
- Burbank, D.W., Vergés, J., Muñoz, J.A., Bentham, P.: Coeval hinward- and forward-imbricating thrusting in the south-central Pyrenees, Spain: timing and rates of shortening and deposition. *Geol. Soc. Am. Bull.* **104**, 3–17 (1992)
- Casini, G., Gillespie, P.A., Vergés, J., Romaine, I., Fernández, N., Casciello, E., Saura, E., Mehl, C., Homke, S., Embry, J.-C., Aghajari, L., Hunt, D.W.: Sub-seismic fractures in Foreland fold and thrust belts: insight from the Lurestan Province, Zagros Mountains. *Iran. Petrol. Geosci.* **17**, 263–282 (2011)
- Lacroix, B., Travé, A., Buatier, M., Labaume, P., Vennemann, T., Dubois, M.: Syntectonic fluid-flow along thrust faults: example of the South-Pyrenean fold-and-thrust belt. *Mar. Pet. Geol.* **49**, 84–98 (2014)
- Travé, A., Labaume, P., Calvet, F., Soler, A.: Sediment dewatering and pore fluid migration along thrust faults in a foreland basin inferred from isotopic and elemental geochemical analyses (Eocene Southern-Pyrenees, Spain). *Tectonophysics* **282**, 375–398 (1997)
- Beaudoin, N., Bellahsen, N., Lacombe, O., Emmanuel, L., Pironon, J.: Crustal-scale fluid flow during the tectonic evolution of the Bighorn Basin (Wyoming, USA). *Basin Res.* **26**(3), 403–435 (2014)
- Breesch, L., Swennen, R., Vincent, B.: Fluid flow reconstruction in hanging and footwall carbonates: compartmentalization by Cenozoic reverse faulting in the Northern Oman Mountains (UAE). *Mar. Pet. Geol.* **26**, 113–128 (2009)

Evolution of the Fluid System During the Formation of the Fault-Related Bóixols Anticline (Southern Pyrenees)

Nicholas Nardini, Daniel Muñoz-López, David Cruset, Irene Cantarero, Juan Diego Martín-Martín, and Anna Travé

Abstract

Structural, petrological and geochemical data allow us to constrain the fluid flow system at the frontal part of the Bóixols thrust sheet, Southern Pyrenees, focusing on the fluid origin, pathways and regimes. Throughout the evolution process of the fault-related Bóixols anticline, different fracture sets have been developed and mineralized with at least four generation of calcite cements. Such developments testify that such structures allowed the migration and interaction of four types of fluids during the early contraction, the syn folding stage and the latest folding stages.

Keywords

Bóixols anticline • Fluid migration • Fractures • Southern pyrenees

1 Introduction

The fracture pattern originated during the evolution of fold-and-thrust belts controls the migration of fluids, including hydrocarbons [1]. The study of outcrop analogues allows to constrain the subsurface fracture network and the geological history of an area [2]. Petrology and geochemistry of vein-filling minerals and host rocks provide information on the fluid origin, regime, timing and degree of fluid-rock interaction [3].

In this respect, the Southern Pyrenees are an outstanding field analogue for the study of fluid migration, as the relationship between thrusting and syntectonic sediments is well observed [4]. Formed by continental collision between the

Iberian and European plates, the Pyrenees consist of an asymmetrical and double-verging orogenic system generated from Late Cretaceous to Miocene [5]. Concerning the present study, the focus of interest is laid on studying the Bóixols anticline, a south-verging structure developed in relation to the Bóixols thrust sheet in the southern Pyrenees [6]. We combined structural field data with petrological and geochemical studies of cements filling fractures in order to assess the fracture network developed during the evolution of the anticline and observe the fluid regime associated changes through time.

The stratigraphic record analyzed in this work includes Jurassic limestones, Lower Cretaceous marls (Lluçà Fm.), Upper Cretaceous limestones (Santa Fé Fm.) and Paleocene synorogenic continental sediments from the Garumnian facies.

2 Methodology

Forty polished thin-sections were analyzed with an optical and a cathodoluminescence microscopy. Cements and host rocks were sampled for carbon and oxygen isotope analyses using an automated Kiel Carbonate Device attached to a Thermal Ionization Mass Spectrometer Thermo Electron (Finnigan) MAT-252.

3 Fracture Sets and Related Calcite Cements

Five fracture sets (F1 to F5) and four generations of calcite cements (Cc1 to Cc4) have been identified.

F1 is the Bóixols thrust. One calcite cement (Cc1) precipitated in related veins and consists of calcite fibers and blocky crystals with a dark orange luminescence. F2 is formed of E-W bed-perpendicular empty joints affecting the Santa Fé Fm. F3 consists of a conjugate set of NW-SE and NE-SW faults in the Lluçà Fm, showing both strike- and dip-slip motions. They are filled by Cc1 (described above)

N. Nardini · D. Muñoz-López (✉) · D. Cruset · I. Cantarero
J. D. Martín-Martín · A. Travé
Departament de Mineralogia, Petrologia i Geologia Aplicada,
Facultat de Ciències de la Terra, Universitat de Barcelona (UB),
Martí i Franquès s/n, 08028 Barcelona, Spain
e-mail: munoz-lopez@ub.edu

Table 1 Carbon and oxygen isotopic values of host rocks and cements

Samples		$\delta^{18}\text{O}$ (‰ VPDB)	$\delta^{13}\text{C}$ (‰ VPDB)
Host rocks	Jurassic	-8.7 to -6.2	+0.7 to +1.7
	Lluçà Fm.	-5.1 to -3	+1.6 to +2.5
	Santa Fé Fm.	-6.6	-2.1
	Garumnian	-7.7 to -6.6	-13.1 to -11
Calcite cements	Cc1	-13.2 to -10.4	+0.4 to +1.7
	Cc2	-9.2 to -6.6	+1 to +2.7
	Cc3	-8.3 to -7.8	-10.4 to -8.3
	Cc4	-14.3 to -9.9	-12.5 to -4.1

and Cc2, represented by nearly black luminescent blocky crystals. F4 represents NW-SE striking veins affecting the Garumnian sequence. They are filled with Cc3 and Cc4. Cc3 consists of unequal blocky crystals with orange to bright yellow luminescence. Cc4 is characterized with blocky crystals bearing a dull to bright orange luminescence. F5 involves right- and left-lateral faults striking NW-SE and NE-SW and cemented by Cc4.

The isotopic values of host rocks and calcite cements are depicted on Table 1.

4 Discussion

The results presented above are consistent with at least four deformation stages (T1–T4), occurring during the Bóixols anticline evolution process.

During the early contraction (T1) stage, the emplacement of the Bóixols thrust (F1) resulted in the development of F2, represented by E-W joints affecting the Santa Fé Fm. and F3, defined by NW-SE and NE-SW conjugate faults affecting the Lluçà Fm. Similar fractures were attributed to a pre-to-early folding stage occurring in the western sector of the Bóixols anticline [7]. The calcite cement Cc1 precipitated along the Bóixols thrust and F3. The $\delta^{18}\text{O}$ depletion of Cc1 with respect to its adjacent host rocks (Fig. 1) points out to a hot external fluid migrating through these fractures.

The presence of two generations of striae sets in F3 indicates that these fractures were reactivated during the main folding stage (T2), allowing for the migration of a second fluid that precipitated as Cc2. The latter's enrichment in $\delta^{18}\text{O}$ values, in respect of Cc1 (Fig. 1), suggests a lower precipitation temperature or a more saline fluid flowing from the underlying Triassic evaporites [8]. The similar carbon

isotopic composition between the calcite cements Cc1 and Cc2 and the adjacent host rocks appears to reveal a rock-buffered system with high fluid-rock interaction.

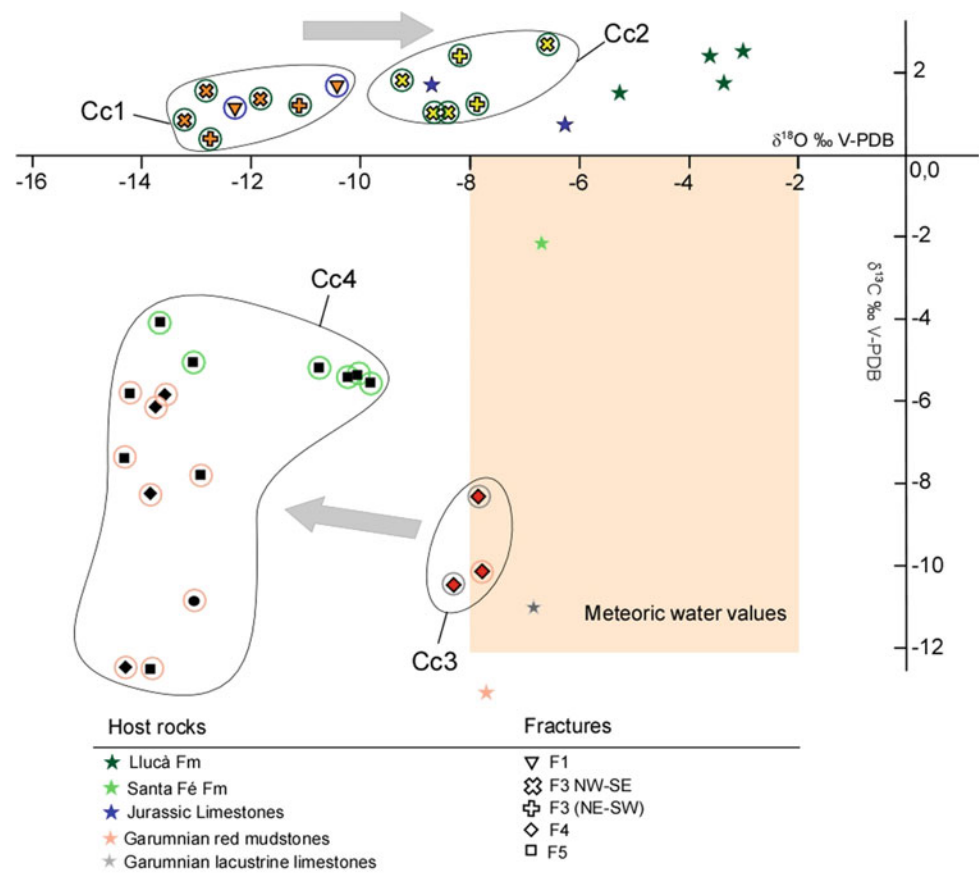
Once the Bóixols anticline had reached its maximum amplification, it was fossilized by the continental Garumnian facies and the fractures F4 (T3) and F5 (T4) were formed. During T3, local meteoric fluids in equilibrium with its adjacent host rock precipitated as calcite cement Cc3. Then, during T4, hot external fluids mixed with meteoric waters and precipitated as Cc4, as evidenced by the depletion in $\delta^{18}\text{O}$ of Cc4 with respect to Cc3 (Fig. 1). The isotopic disequilibrium between Cc4 and its adjacent host rock, coincides with a more open paleohydrogeological system, as reported in other areas of the Pyrenees [9].

5 Conclusions

During the Bóixols anticline evolution, five different fracture sets were recognized affecting the folded sequence. The analysis of these fractures and the geochemistry of their related infilling reflects the evolution of the structure and the relationships between folding and fluid migration. Fractures developed during the early contraction and main folding stages allowed the migration of two external fluids that precipitated as Cc1 and Cc2, respectively. On comparing the carbon isotopic composition characterizing these cements and their host rocks, it is observed the persistence of a rock-buffered system.

Conversely, during the latest folding stages, Cc3 precipitated from local meteoric waters migrating along F4, and Cc4 precipitated in F5 from hot ascending fluids mixed at depth with meteoric waters in a more open paleohydrogeological system.

Fig. 1 $\delta^{18}\text{O}$ versus $\delta^{13}\text{C}$ cross-plot of calcite cements and related host rocks. The colored box indicates meteoric water limestones



References

- Evans, M.A., Fischer, M.P.: On the distribution of fluids in folds: a review of controlling factors and processes. *J. Struct. Geol.* **44**, 2–24 (2012)
- Gomez-Rivas, E., Bons, P.D., Koehn, D., Urai, J.L., Arndt, M., Virgo, S., Laurich, B., Zeeb, C., Stark, L., Blum, P.: The Jabal Akhdar Dome in the Oman Mountains: evolution of a dynamic fracture system. *Am. J. Sci.* **314**, 1104–1139 (2014)
- Travé, A., Labaume, P., Vergés, J.: Fluid systems in Foreland Fold and thrust belts: an overview from the Southern Pyrenees. In: Lacombe, O., Lavé, J., Roure, F., Vergés, J. (eds.), *Thrust Belts and Foreland Basins from Fold Kinematics to Hydrocarbon Systems*, pp. 93–115. Springer (2007)
- Vergés, J., Marzo, M., Muñoz, J.A.: Growth Strata in foreland settings. *Sed. Geol.* **146**, 1–9 (2002)
- Muñoz, J.A.: Evolution of a continental collision belt: ECORS-Pyrenees crustal balanced cross-section. In: McClay, K. R. (eds.), *Thrust Tectonics*, pp. 235–246. Chapman & Hall, London (1992)
- Vergés, J., Muñoz, J.A.: Thrust sequences in the southern central Pyrenees. *Bull. Soc. géol. Fr.* **6**, 265–271 (1990)
- Tavani, S., Mencos, J., Bausà, J., Muñoz, J.A.: The fracture pattern of the Sant Corneli Bóixols oblique inversion anticline (Spanish Pyrenees). *J. Struct. Geol.* **33**, 1662–1680 (2011)
- Cruset, D., Cantarero, I., Vergés, J., John, C.M., Muñoz-López, D., Travé, A.: Changes in fluid regime in syn-orogenic sediments during the growth of the south Pyrenean fold and thrust belt. *Glob. Planet. Change* (2017)
- Travé, A., Labaume, P., Calvet, F., Soler, A.: Sediment dewatering and pore fluid migration along thrust faults in a foreland basin inferred from isotopic and elemental geochemical analyses (Eocene southern Pyrenees, Spain). *Tectonophysics* **282**, 375–398 (1997)



Controls on Convective Fluid Flow Systems Resulting in the Formation of Massive Diagenetic Alterations

Enrique Gomez-Rivas, Juan Diego Martín-Martín, Paul D. Bons, Albert Griera, Shuqing Yao, Maria-Gema Llorens, and Anna Travé

Abstract

This contribution presents a series of heat and fluid flow numerical simulations to evaluate the main controls on the activation of convective fluid flow systems that cause massive diagenetic alterations in carbonate basins. The models are based on the Aptian-Albian Benicàssim outcrop analogue, in which large bodies of hydrothermal dolostone replace shallow-marine platform limestones. The results indicate that a convective fluid flow system could only be active if a series of conditions were met. These include a relatively high geothermal gradient, a nearly hydrostatic fluid pressure gradient and high-permeability faults. Moreover, the presence of strong permeability differences among the different limestone units, together with a top seal, favors the formation of stratabound alteration geometries. These factors are in agreement with geological observations and data of the case study.

Keywords

Hydrothermal • Diagenesis • Fluid flow
Thermal convection • Fluid-rock interaction

1 Introduction

Massive diagenetic alterations are commonly observed in many carbonate basins in a variety of tectonic settings. A typical example of such alterations lies in the formation of large-scale bodies of hydrothermal dolostones that replace limestones [1]. In such systems, Mg-rich fluids warmer than the host rocks circulate in the basin and produce a replacement reaction, changing the rock's mineralogy and, in most cases, its texture. Such fluids are transported from below along faults, fracture networks and high-permeability beds. A variety of fluid flow systems with different driving forces can be claimed to explain the formation of massive high-temperature diagenetic alterations [2]. These include topography-driven fluid flow, expulsion of interstitial fluids due to burial or tectonic stress, release of overpressured fluids from underlying units, or thermal convection systems, among others [3]. Thermal convection associated with temperature differences in the basin is typically claimed to stand as a driving force for the diagenetic flow systems that deliver large fluid volumes at high temperatures to reaction zones. Most of the existing case studies focus on characterizing the diagenetic processes, the resulting products and analyzing the fingerprints of fluids to propose conceptual models fit for monitoring the flow system responsible for the rock reaction. However, in most cases the hydrodynamic plausibility of such systems is not actually validated, sometimes resulting in unrealistic models. In this contribution, we evaluate the key controls on fluid flow in a convective system driven by temperature differences in a post-rift basin, based on the well-studied Benicàssim outcrop analogue (Maestrat Basin, E Spain). Accordingly, a series of fluid and heat flow numerical simulations were applied to evaluate the geological conditions under which such systems could be active and deliver the required fluid volumes at the appropriate temperature to account for the dolostone volume, geometry and stratabound distribution.

E. Gomez-Rivas (✉) · J. D. Martín-Martín · A. Travé
Departament de Mineralogia, Petrologia i Geologia Aplicada,
Facultat de Ciències de la Terra, Universitat de Barcelona (UB),
Martí i Franquès s/n, 08028 Barcelona, Spain
e-mail: e.gomez-rivas@ub.edu

E. Gomez-Rivas · S. Yao
School of Geosciences, King's College, University of Aberdeen,
Aberdeen, AB24 3UE, UK

P. D. Bons
Department of Geosciences, University of Tübingen, Wilhelmstr.
56, 72074 Tübingen, Germany

A. Griera · M.-G. Llorens
Departament de Geologia, Universitat Autònoma de Barcelona,
08193 Bellaterra, Barcelona, Spain

© Springer Nature Switzerland AG 2019

D. M. Doronzo et al. (eds.), *Petrogenesis and Exploration of the Earth's Interior*,
Advances in Science, Technology & Innovation, https://doi.org/10.1007/978-3-030-01575-6_54

223

2 Geological Setting and Methods

The Benicàssim half graben was formed in the Maestrat Basin during rifting in the Early Cretaceous. In this area, a very thick pile (>1600 m) of shallow-marine syn-rift ramp sediments accumulated during the Aptian and Albian [4]. The Benicàssim area is dominated by two large-scale synrift fault systems that controlled sedimentation in the area. Limestones were partly dolomitized during the Late Cretaceous post-rift cycle, resulting in a variety of replacement geometries, ranging from large-scale dolostone patches around the fault zones to stratabound geobodies that extend over long distances away from the faults, which acted as feeding points for warm fluids [5]. These dolostones have been interpreted to have been formed due to the circulation of warm (90–180 °C) seawater-derived brines that exchanged with underlying basin and basement rocks. They also host Mississippi Valley Type (MVT) ore deposits. Mass balance calculations indicate that a thermal convection system that mobilized fluids at the basin scale could have provided enough fluid volume to account for the Benicàssim dolostone [3]. The fluid that produced MVTs, however, is restricted to fault zones.

The commercial software Tough2 [6] has been utilized to carry out a series of heat and fluid flow simulations. The models are based on field and petrographic data. We systematically varied: (i) the geothermal gradient, (ii) fluid pressure gradient, (iii) fault zone permeability, (iv) the existence of a top sealing unit and (v) the relative permeability of host rock layers.

3 Results, Discussion and Conclusions

The simulation results indicate that thermal convection in the study area could only have been active if certain conditions were met at the same time. These include: (i) a geothermal gradient of at least 30 °C/Km or higher, (ii) a nearly hydrostatic fluid pressure gradient, and (iii) high permeability of fault zones. Moreover, a contrasting permeability of two orders of magnitude between reacting and non-reacting layers, and a low-permeability unit at the top of the carbonate succession acting as a seal for warm fluids appear to favor their channeling through high-permeability beds, resulting in a stratabound replacement geometry. These conditions turn out to be in agreement with the geological data drawn from the Benicàssim case study during the Late Cretaceous, when dolomitization took place. The limited damage of the host limestones, as associated with syn- and post-rift stages, indicates that the fluid pressure gradient would have been close to hydrostatic. Additionally, a relatively high geothermal gradient, occurring during the rifting period, would have continued

even after the end of extension. The preferential dolomitization of grainy facies indicates that strong permeability differences between limestone beds were also likely, including the effect of pre-dolomitization chemical compaction and calcite and dolomite cementation [5–9]. The simulations indicate that relatively high velocities of warm fluids (above 150 °C) could have been achieved in specific layers coinciding with those replaced by stratabound dolostones. The fluid volume required to account for the size of dolostones would have required mobilizing fluids at a scale significantly larger than that of the Benicàssim area. It is, therefore, likely that the convective fluid flow system involved part of the Maestrat Basin. This conforms with the presence of similar hydrothermal dolostones elsewhere in the basin [10].

References

1. Davies, G.R., Smith Jr., L.B.: Structurally controlled hydrothermal dolomite reservoir facies: an overview. *AAPG Bull.* **90**, 1641–1690 (2006)
2. Whitaker, F.F., Smart, P.L., Jones, G.D.: Dolomitization: from conceptual to numerical models. *Geol. Soc. Lond. Spec. Publ.* **235**, 99–139 (2004)
3. Gomez-Rivas, E., Corbella, M., Martín-Martín, J.D., Stafford, S. L., Teixell, A., Bons, P.D., Griera, A., Cardellach, E.: Reactivity of dolomitizing fluids and Mg source evaluation of fault-controlled dolomitization at the Benicàssim outcrop analogue (Maestrat Basin, E Spain). *Mar. Pet. Geol.* **55**, 26–42 (2014)
4. Martín-Martín, J.D., Gomez-Rivas, E., Bover-Arnal, T., Travé, A., Salas, R., Moreno-Bedmar, J.A., Tomás, S., Corbella, M., Teixell, A., Vergés, J., Stafford, S.L.: The Upper Aptian to Lower Albian syn-rift carbonate succession of the southern Maestrat Basin (Spain): facies architecture and fault-controlled stratabound dolostones. *Cretac. Res.* **41**, 217–236 (2013)
5. Yao, S., Gomez-Rivas, E., Martín-Martín, J.D., Gómez-Gras, D., Travé, A., Griera, A., Howell, J.: Controls on fault-associated dolomitization geometries in a sequence stratigraphic framework. *Sedimentology* (in review) (2018)
6. Pruess, K.: TOUGH2: a general numerical simulator for multi-phase fluid and heat flow. Technical Report LBL-29400, Lawrence Berkeley Laboratory, USA (1991)
7. Martín-Martín, J.D., Travé, A., Gomez-Rivas, E., Salas, R., Sizun, J.-P., Vergés, J., Corbella, M., Stafford, S.L., Alfonso, P.: Fault-controlled and stratabound dolostones in the Late Aptian-earliest Albian Benassal Formation (Maestrat Basin, E Spain): petrology and geochemistry constrains. *Mar. Pet. Geol.* **65**, 83–102 (2015)
8. Gomez-Rivas, E., Martín-Martín, J.D., Bons, P.D., Koehn, D.: Can stylolite networks control the geometry of hydrothermal alterations? *Geotectonic Res.* **97**, 34–36 (2015)
9. Martín-Martín, J.D., Gomez-Rivas, E., Gómez-Gras, D., Travé, A., Ameneiro, R., Koehn, D., Bons, P.D.: Activation of stylolites as conduits for overpressured fluid flow in dolomitized platform carbonates. *Geol. Soc. Lond. Spec. Publ.* 459 (2018)
10. Grandia, F.: Origen, evolució i edat dels fluids associats a les mineralitzacions de Zn-Pb en carbonats cretàtics de la Conca del Maestrat (Castelló-Teruel). Ph.D. thesis, Universitat Autònoma de Barcelona (2001)

Biogenic Methane Production from Various Coal Rank and Its Controlling Factors Using Ruminant Waste as a Microorganism-Consortium Source

Ahmad Helman Hamdani, Ellin Harlia, and Winantris Sanusi

Abstract

The rumen contents of ruminant livestock waste, such as beef cattle, as a consortium source of microorganisms, were jointly used with three different coal ranks (lignite, sub-bituminous and bituminous) in an experiment of biogenic methane production from various coal ranks. Maceral composition, coal rank and volatile fatty acid were the parameters measured. The methane production rates proved to be higher in the lignite than in the sub-bituminous and bituminous coal ranks. Therefore, the maceral composition, coal rank and volatile fatty acid (especially acetate acid) were controlled in the final methane production stage.

Keywords

Coal bed methane • Biogenic • Maceral • Vitrinite reflectance • Acetate acid

1 Introduction

In Indonesia, approximately 80.72% of the total electricity generated in 2015 was produced based on fossil fuels (coal, oil and natural gas) [1]. These constitute the leading energy sources used today. Fossil fuels are formed when organic materials, such as plants or animals, decay underground close to an underground heat source. The major advantage of fossil fuels lies in their high efficiency. Nevertheless, recent findings about their environmental impacts have raised several new concerns. With the growing concerns for the

environment and sustainability related issues, the government is persistently enticing the enhancement of renewable alternative energy sources. In this respect, the coal bed methane (CBM) resource appears to represent one of the most effective energy sources among others.

In this regard, Fallagreen et al., along with a number of other scholars [2–5], document that the low-rank coal (lignite) based methane yields turn out to be higher than those produced by the other coal ranks. Noteworthy, however, is that other research studies prove to highlight that the bituminous coals appear to produce greater methane amounts than do the lignites [6]. Actually, intense research has been conducted to investigate the relationship binding the various coal ranks and the methane formation process. Yet, the coal rank nature and methane production relationship remain unclear. Indeed, a critical gap persists as to the extent of coal adaptability, and the kinds of coal fit for enhanced methanogenesis. In effect, there is no clear information specifying the coal based natural gas production and the appropriate coal type suitable for an enhanced biogenic natural gas production. Hence, the purpose of the present study lies in exploring the relationship binding the biogenic natural gas production at the different coal-rank levels (lignite, sub bituminous and bituminous) and the relevant controlling factors.

2 Materials and Methods

Three coal samples of various ranks were collected from different basins sited on the Kalimantan Island, Indonesia, namely, lignite (Berau Basin), sub bituminous (Berau Basin) and High Volatile Bituminous (Wain Basin). Four livestock sample types (beef cattle feces, dairy cattle feces, buffalo feces and rumen) for inoculum were collected from a dairy farm located in Jatinangor, West Java. Culture was enriched in such mineral mediums as Ogimoto and Imai [7] and on agar slants, using coal as substrate and a Hungate tube. Used

A. H. Hamdani (✉) · W. Sanusi
Faculty of Geology, Universitas Padjadjaran, Jatinangor,
Indonesia
e-mail: ahmad.helman@unpad.ac.id

E. Harlia
Faculty of Animal Husbandry, Universitas Padjadjaran, Jl. Raya
Bandung-Sumedang KM 21, Jatinangor, West Java 45363,
Indonesia

10^{-7} diluted rumen content of feed stock waste was applied as a source of microorganisms' consortium

Gas production was observed at day 2 and day 5, following the incubation process. The CH_4 sample analysis was implemented using Gas Chromatography (GC) with Flame Ionization Detector (FID). Coal maceral composition was identified by means of a Leica MPV type of microscope, with both white incident light and fluorescence modes (magnification 500X). The VFA (volatile fatty acid) was measured including acetic, propionic, iso-butyric, butyric, iso-valeric, and valeric acid.

3 Results

3.1 Methane Production

The CBM production was observed over several intervals: on day 2, on day 5, on day 10 and on day 14, based on the Ogimoto and Imai methods [7]. Figure 1 depicts the net microbial methane production, as observed from the hungate tube. The highest range of methane yield was obtained on day 15, with respect to the entirety of the three coal types. Still, the methane production proves to reach its highest level with regard to the lignite coal type (10,100 ppm), in respect of the other coal ranges, i.e., the sub-bituminous coal (2400 ppm), and the bituminous coal (1850 ppm).

3.2 Coal Petrography

The coal-organic petrography analysis proves to reveal that coals are discovered to be exceedingly rich in vitrinite (Table 1).

Figure 2 displays the variability noticeable in maceral composition. The vitrinite contents (vol.%) appear to range from 75.2 to 82.1% (a.r.), the liptinite contents from 6.3 to

12.9%, while the inertinite contents turn out to be low with respect to the entirety of samples (max. 2.5%). The lignite and bituminous coals prove to score the highest vitrinite contents, while lignite appears to record the highest liptinite proportion.

3.3 Volatile Fatty Acids (VFA)

The volatile fatty acid concentrations (VFAs relevant to the three coal ranges) are depicted in Fig. 3.

4 Discussion

There are special relationships binding the maceral composition, coal rank (Ro) and Volatile fatty acid, especially acetate acid, and the methane yield. In the scope of this study, it has been discovered that the highest methane yield turns out to prevail in the lignite coal range. Indeed, it is actually related to the high vitrinite maceral content, low Ro value and high acetate acid content. The vitrinite proves to display a higher microporosity rate, as compared to other macerals, enabling it to provide a surface area liable to a large gas storage capacity, as the amounts of heteroatoms predominant in vitrinite make microbes more easily degraded into gases. Actually, a low Ro value should lead to a greater bioavailability and would, therefrom, result in higher amounts of methane than of coal rank. The vitrinite reflectance (Ro) proves to display a negative correlation with the methane yield ($r = -0.8$), implying that a lower Ro rank (low Ro) should be reflected in a higher production of final methane yield. The acetate acids prove to have a remarkable effect on the community composition and the biogenic methane associated potential. The presence of high acetate acid helps favorize the formation of an appropriate environment fit for the development of microbial methanogens of the types *Bacteroidales* and *Pelobacter*. The Acetate acid proves to display a positive correlation ($r = 0.9$) with the final methane yield. The overall result turns out to indicate that both of the coal rank and acetate stand as strong factors that help in controlling the final methane-production yield.

5 Conclusions

Based on the study reached findings, it was discovered that the low-rank coals, particularly the lignite, prove to yield higher end-product inputs than the high-rank coals (bituminous coal). This is mainly due to the availability of greater acetate-acid amounts persistent in the low-rank coal, in addition to the high bioavailability rates available.

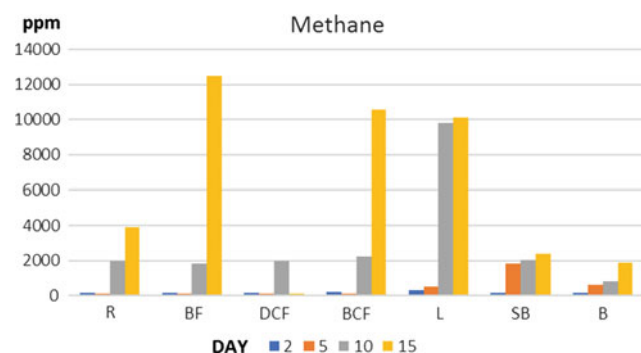
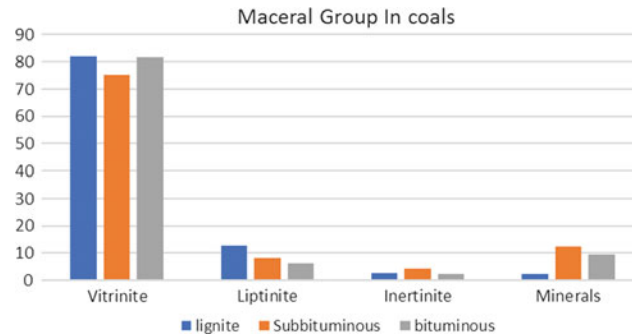
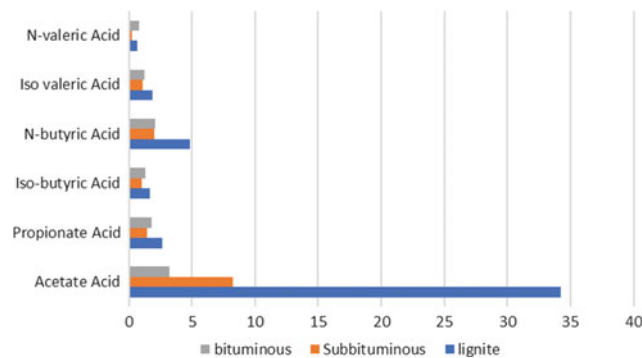


Fig. 1 Methane yields relevant to the different coal ranges and feed stock combinations. The histogram is plotted on observation period bases: on days 2, 5, 10 and 16

Table 1 Petrographic characteristics of the coal samples

Maceral group	Lignite (%)	Subbituminous (%)	Bituminous (%)
Vitrinite	82.1	75.2	81.8
Liptinite	12.9	10.1	6.3
Inertinite	2.7	2.2	2.5
Minerals	2.3	12.4	9.4
Vitrinite reflectance (%)	0.35	0.45	0.6

**Fig. 2** Maceral composition of coals as used in enrichment culture substrate**Fig. 3** Volatile fatty acid concentrations in coals

References

- Indonesian National Energy Council: Outlook Energy Indonesia (2016)
- Fallgren, P.H., Zeng, C., Ren, Z., Lu, A., Ren, S., Jin, S.: Feasibility of microbial production of new natural gas from non-gas-producing lignite. *Int. J. Coal Geol.* **115**, 79–84 (2013)
- Strapoć, D., Mastalerz, M., Dawson, K., Macalady, J., Callaghan, A.V., Wawrik, B., Turich, C., Ashby, M.: Biogeochemistry of microbial coal-bed methane. *Annu. Rev. Earth Planet. Sci.* **39**, 617–656 (2011)
- Kurnani, T.B.A., Harlia, E., Hidayati, Y.A., Marlina, E.T., Sugiarto, A.N., Rahmah, K.N., Joni, I.M.: Biogas production from various coal types using beef cattle rumen's liquid as a source of microorganisms consortium. In: The 1st International Conference and Exhibition on Powder Technology Indonesia (ICePTi), 4 pp (2017)
- Harlia, E., Hamdani, H., Kurnani, W.T.B.A., Hidayati, Y.A., Marlina, E.T., Rahmah, K.N., Arief, H., Ridwan, R., Joni, I.M.: The impact of anaerobic microorganisms activities in ruminant waste and coal. In: The 1st International Conference and Exhibition on Powder Technology Indonesia (ICePTi), 4 pp (2017)
- Fallgren, P.H., Jin, S., Zeng, C., Ren, Z., Lu, A., Colberg, P.J.S.: Comparison of coal rank for enhanced biogenic natural gas production. *Int. J. Coal Geol.* **115**, 92–96 (2013)
- Ogimoto, K., Imai, S.: Atlas of Rumen Microbiology. Japan Scientific Societies Press, Tokyo (1981)

Part V

Geological Research Applied to Mineral Deposits

Sn-W Mineralization Associated with the DJILOUET Complex, Eastern Hoggar (Algeria)

Fatiha Oulebsir, Mokrane Kesraoui, and Dalila Nemmour-Zekiri

Abstract

The Djilouet complex forms a cupola made up of leucocratic granites associated with Sn-W mineralization. It could represent the Hoggar's easternmost rare-metal granite (GMR). It is located in the Djanet terrane, 12 km NE of the town of the same name in the far east of the Tuareg shield in Algeria. The geology of the area is characterized with the presence of a magmatic complex evolving from quartz-diorites to leucocratic granites. The latter intrudes into the Upper Proterozoic terrigenous sedimentary rocks of the Djanet series. Djilouet is located in a tectonically weakened sublatitudinal area, known as the Tamrit area of major accidents affecting the basement, and considered as the region's main structural control. These extend, further north, affecting the Paleozoic cover. The granite cupola covers an area of 0.56 km², with a zoned concentric structure, typical of the Hoggar post-orogenic granites. It is made up of leucocratic granites with progressive mutual transitions. The latter enclose fine-grained garnet bearing granite contains, in addition to almandine-spessartite garnet, other accessory minerals, observed in SEM, such as rutile, apatite, xenotime, zircon, monazite and uranothorite. The Djilouet W-Sn mineralization is located in a network of quartz-greisen veins and veinlets subparallel to each other, but sometimes forming a real stockwork. The ore is mainly made up of wolframite and, to a lesser extent, cassiterite. The iso-content contours of tin and tungsten, as produced from a sampling covering the whole cupola, overlap very little. They would indicate that these metals have different origins and come from different levels,

where the parent magmas have crystallized. The Chemical analysis of these granites' major elements reveals that they are clearly peraluminous and of calc-alkaline affinity, highly potassic and strongly fractionated. In discriminant diagrams, they project into the post-orogenic domain, with a tendency towards the anorogenic domain. As for the facies that outcrop in the Djilouet cupola, they cannot be qualified as rare metal granite as a whole. Petrographically, a great similarity proves to persist with the post-orogenic granites of the Tamanrasset area. Nevertheless, its mineralization could be related to a more recent event (probably Hercynian), and has a source that evolved rare metal granite, not observed at surface level.

Keywords

The djilouet complex • Leucocratic granites • Sn-W mineralization • Almandine-spessartite garnet • Mineralization could be related to a more recent event hercynian

1 Introduction

The Djilouet complex forms a cupola made up of leucocratic granites associated with Sn-W mineralization. It could well stand as a representation of the Hoggar's easternmost rare-metal granite (GMR). It is located in the Djanet terrane, 12 km NE of the town bearing the same name, is sited in the far east of the Algerian Tuareg shield. The related characteristics indicate well that it is deposited, sub-horizontally, on a bottom base, suggesting the persistence of a stable cratonic area. The late panafrikan phase is marked by the emplacement of large porphyroid batholiths of the Djanet granite type, at around 570 Ma [1], controlled by mega-shear zones, causing a delithic linear delamination.

The area's geology is characterized with the presence of a magmatic complex evolving from quartz-diorites to

F. Oulebsir (✉) · M. Kesraoui
Laboratory of Metallogeny and Magmatism of Algeria.
FSTGAT/USTHB/BP 32 El Alia, 16111 Algiers, Algeria
e-mail: fatiha.oulesir@gmail.com; foulesir@yahoo.fr

D. Nemmour-Zekiri
Laboratory of Geodynamics, Geology of the Engineer and Planetology, FSTGAT/USTHB/, Algiers, Algeria

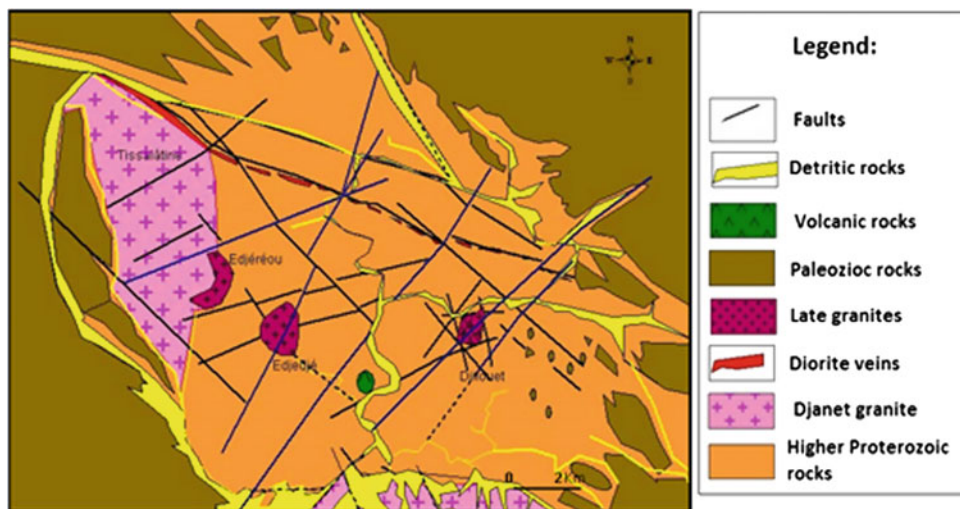
leucocratic granites. The latter intrudes into the Upper Proterozoic terrigenous sedimentary rocks of the Djanet series. Djilouet is located in a tectonically weakened sub-latitudinal area, known as the Tamrit area, of major accidents affecting the basement and considered as the main structural control of the region (Fig. 1). The complex intersects, at its southwestern limit, a ductile mylonitic corridor that is linked to the pan-African event [2]. It is affected, in turn, with a NW-SE and NE-SW fault system, which determines the appearance of diamond-shaped blocks. The NE-SW faults served as a drain for mineralization in the eastern part of the cupola. These tend to extend further north, affecting the Paleozoic cover.

2 Description of the Djilouet Massif

The granite cupola covers an area of 0.56 km² (Fig. 2). It has a zoned concentric structure, typical of the Hoggar post-orogenic granites. It is made up of leucocratic granites with progressive mutual transitions.

The greatest part is occupied with a coarse biotite granite. It is a two micas granite, with zircon as accessory mineral and oxides included in muscovite, while fluorite is secondary. The central part is formed of a coarse-grained muscovite granite, while the North-Eastern part and the cupola's periphery is a fine-grained granite bearing garnet. The granite contains, in addition to the almandine-spessartite garnet, other accessory minerals, observed in SEM, such as rutile, apatite, xenotime, zircon, monazite and uranothorite. The marginal part, east of the intrusion, is composed of fine gray-spotted granite with rounded smoked quartz. Aplite veins, of 5–10 cm in thickness, intersect the cupola. They stand as small-scattered outcroppings with a radial orientation.

Fig. 1 Structural scheme of the Djilouet area for aerial photography (70 FG 32 III-IV/800 n° 194) [2])



3 Mineralogy

The Djilouet W-Sn mineralization is located in a network of quartz-greisen veins and veinlets subparallel to each other, but sometimes forming a real stockwork. These veins and veinlets are oriented NE (10°–40°) with a subvertical dip (70°–85°). The ore is mainly made up of wolframite and, to a lesser extent, of cassiterite. It is located in the quartz veins with greisenised wall rocks of decimetric thickness (10–15 cm). The wolframite, as analyzed via the X-ray powder method, yields ferrous compositions, often forming black crystals with metallic luster of ferberite. Cassiterite occurs in the form of stocky crystals, with a zoned structure and a color ranging from light yellow to dark brown.

4 Distribution of Mineralization in the Djilouet Cupola

The iso-content contours of tin and tungsten, as testified through a sampling covering the whole cupola, prove to overlap very little. They would indicate that these metals are of different sources and originate from different levels where the parent magmas have crystallized (Fig. 3).

5 Geochemistry of Granites

The Chemical analysis of these granites' major elements reveals that they are poor in Fe₂O₃, CaO and MgO, and rich in SiO₂, Al₂O₃, K₂O and Na₂O. They, in Maniar and Piccoli [4] diagrams, are clearly peraluminous (Fig. 4) and of calc-alkaline affinity, highly potassic and strongly fractionated. In discriminant diagrams, they prove to project into the post-orogenic domain, with a tendency towards the

Fig. 2 Geological map of the Djilouet cupola [2]

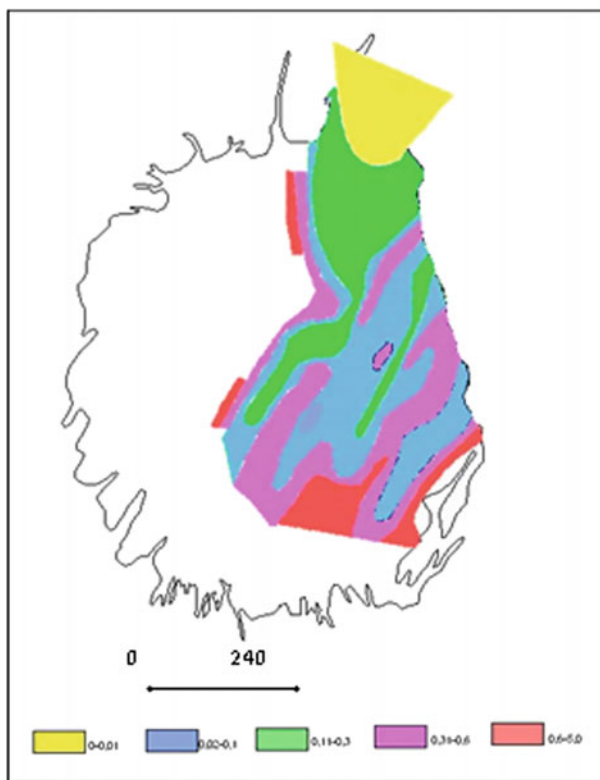
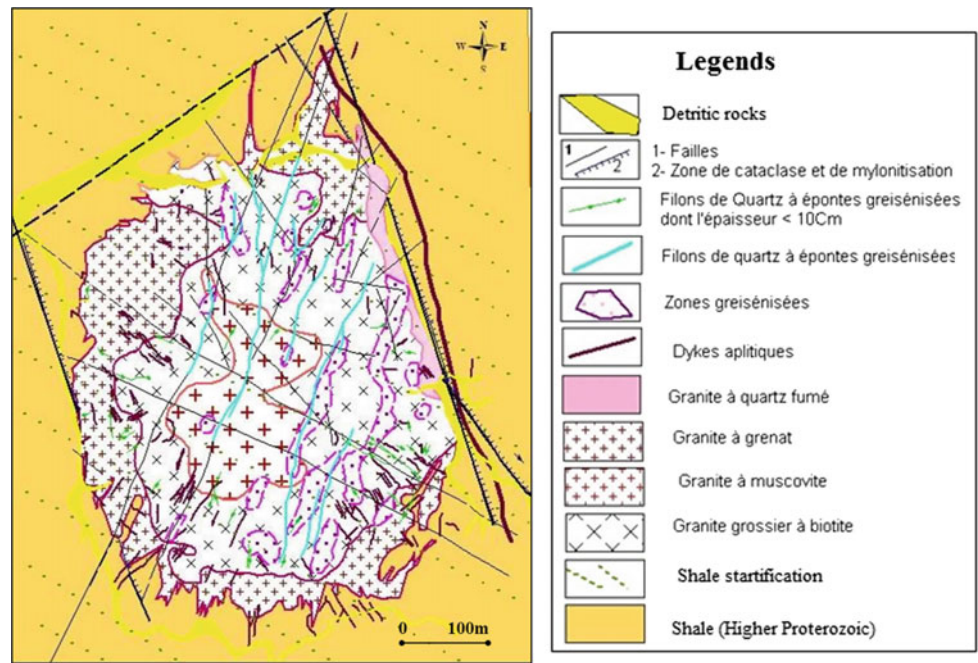


Fig. 3 Map of the Sn/WO₃ ratio distribution in stockwork [2, 3]

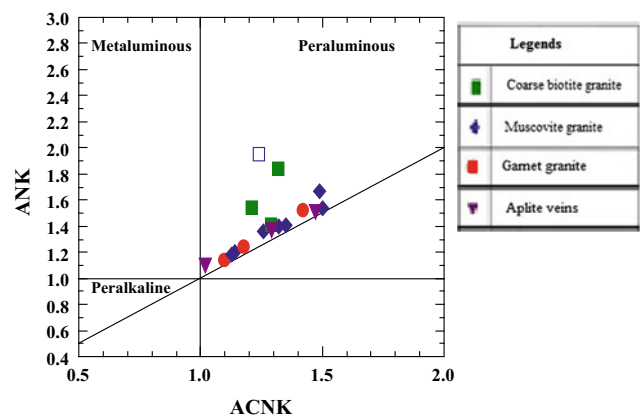


Fig. 4 A/NK versus A/CNK diagram (Maniar and Piccoli [4]) showing the peraluminous character of the rocks of the Djilouet cupola [2]

anorogenic domain (Fig. 5). Considering the facies outcropping the Djilouet cupola, the latter cannot be qualified to represent rare metal granites, in general. Petrographically, a great similarity with the post-orogenic granites of the Tamanrasset area prevails. Nevertheless, its mineralization could be related to a more recent event (probably Hercynian), and have a source evolving into rare metal granite, not observable on the surface level.

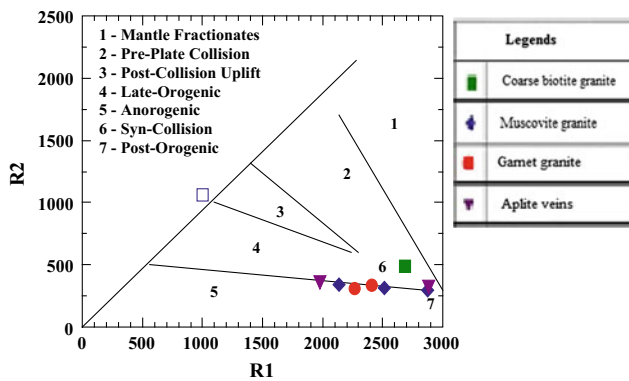


Fig. 5 Djilouet cupola project in R1-R2 diagram of geotectonic discrimination [5] of Batchelor and Bowden (1985) [2]

6 Conclusions

The Djilouet cupola proves to be highly linked to the most eastern Sn-W deposit of the Hoggar. It has the shape of an intrusive cupola in the upper Proterozoic schist formations. At its southwestern limit, the massif intersects with a ductile mylonitic corridor closely linked to the pan-African event.

Mineralization follows the direction of the faults that continue to affect the Paleozoic cover. Hence, it turns out to be closely related to a Hercynian post-pan-African event.

The granites, outcropping and forming the cupola, do not appear to display the characteristics of granite with rare metals, even though they prove to be evolved enough. The most differentiated type of granite is garnet granite, characterized with a strong almandine component and a low proportion of spessartite. The granite attached accessory minerals are, proportionately, hafniferous zircon, Ce-monazite, xenotime, uranothorite and rutile.

The Sn and W lying minerals are found in veins and veins, with Greisenized cliffs forming “stockwork” in places. Cassiterite is bipyramid with a characteristic color zoning. Wolframite is more often composed of ferberite.

The curves of tin and tungsten isotherms are superimposed only to a very little extent. Tungsten is concentrated towards the north of the cupola, while tin is lying towards the south. Hence, these metals might well have different origins.

The granites, making up the dome are clearly peraluminous. They are of calco-alkaline affinity, highly potassic and strongly fractionated, therefore, clearly post-orogenic.

The characters of Djilouet predominating granites are not sufficiently available to make them rare-metal granites. The granite, at the origin of the mineralization, would be more in depth, intrusive in the previous facies. It would certainly be of a later age. Nevertheless, its mineralization could be related to a more recent event (may be Hercynian), and may well have its source evolving into rare metal granite, not noticeable at surface level.

References

1. Fezaa, N.: Géochronologie et géochimie du magmatisme panafricain de Djanet et de son encaissant métasédimentaire (Hoggar oriental, Algérie). Conséquences Géodynamiques. Thèse doctorat, USTHB, Alger, 254p (2010)
2. Oulebsir, F.: Pétrographie, géochimie et minéralisations à Sn-W associées du massif de Djilouet (Djanet, Hoggar Oriental). Mémoire de Magister, USTHB, Alger, 110 p (2009)
3. Oulebsir, F., Kesraoui, M.: Etude préliminaire des minéralisations à W - Sn associées à la coupole granitique de Djilouet (Djanet, Hoggar Oriental). XIIème Sémin. N. S.T. Oran, pp. 67–68 (2006)
4. Maniar, P.D., Piccoli, P.M.: Tectonic discrimination of granitoids. Geol. Soc. Amer. Bull. **101**, 635–643 (1989)
5. Batchelor, R.A., Bowden, P.: Petrogenetic interpretation of granitoid rocks series using a multicaticonic parameters. Chem. Geol. **48**, 43–55 (1985)

Mineralogic Data and Geochemical Characteristics of the Berrahal Banded Iron Formations (Edough Massif, NE of Algeria)

Bachir Henni

Abstract

The aim of this work is to characterize Berrahal magnetite \pm hematite deposits, which are located in the southern area of the Edough massif. The ore bodies appear in the form of iron lenticular stratiform layers with a calcitic or calc-silicate global composition, and are hosted in kyanite-staurolite-garnet schists. The main minerals of the ore bodies are magnetite, hematite, siderite, quartz, calcite, fayalite, hedenbergite and garnet (almandine). Three types of facies can be distinguished on petrographic and geochemical observations: The first facies designated Mc corresponds to a carbonate ore. This ore is characterized by a carbonate gangue with alternating layers of calcite and calcite + magnetite. Siderite is sporadically present. Quartz is also present. The second facies, Ms, is a silicate ore characterized by a fayalite and hedenbergite gangue. Amphibole occurs as ferroedenitic to hastingsitic hornblende, while garnet is present as almandine. The third facies, denoted Mi, is considered as intermediate facies because of its lower silica content compared to that of Ms. The gangue consists of olivine and calcite, with some intercalated calcitic bands. Calcite and fayalite are at equilibrium. The early minerals are affected by Mn+2 metamorphism expressed by a N130-140 lineation on the surface of ore bodies, and a concordant foliation with hosting micaschists. The geochemical data show that the deposits of Berrahal correspond to a mixing in variable proportions, of a chemical iron-calcic pole with a pelitic detrital pole or volcano-sedimentary origin (mixing of iron-calcic pole with a volcano-sedimentary pole). The ore bodies are located at several sites and petro-geochemical similarities of Berrahal banded iron formations suggest that regional extent of mineralization is inherited from protolithes of sedimentary or

volcano-sedimentary nature, which were subsequently transformed by regional isochemical metamorphism.

Keywords

Berrahal • Edough Massif • BIF • Magnetite • Metamorphism • Metasedimentary

1 Introduction

The Edough, the most oriental crystalline massif of the Algerian coast belongs to the Alpine peri-Mediterranean range (Fig. 1); it is famous for the presence of ancient iron deposits (magnetite \pm hematite).

The iron formations of the Edough massif are located, mainly, in several sites extending from East to West, about forty kilometers, from Bou Hamra through Béliéliéta, Berrahal to Bou Maïza (Fig. 2). In this work, we provide several mineralogical and geochemical precisions of Berrahal banded iron formations.

The analysis of major and trace elements will allow us to determine the nature of the geological formations related to mineralizations before the metamorphism. This will lead us to discuss the geochemical results in diagrams and characterize the mineralization to make an approach on the geochemical nature of Berrahal iron mineralizations protolithes.

2 Materials and Methods

For a better approach to study the Berrahal iron formations, it seems appropriate to begin with geological and geochemical characteristics in order to know nature of protoliths and to deduce a genetic model of mineralization. The metamorphic formations of the Berrahal area are characterized by a gneissic series surmounted by a micaschist complex [4]. The ore bodies appear as iron lenticular stratiform layers with a calcitic or calc-silicate global composition, and are hosted in

B. Henni (✉)
Sciences Department, High School of Teaching, Ecole Normale Supérieure (ENS- Kouba), BP 92, Alger, Algeria
e-mail: henni@ens-kouba.dz

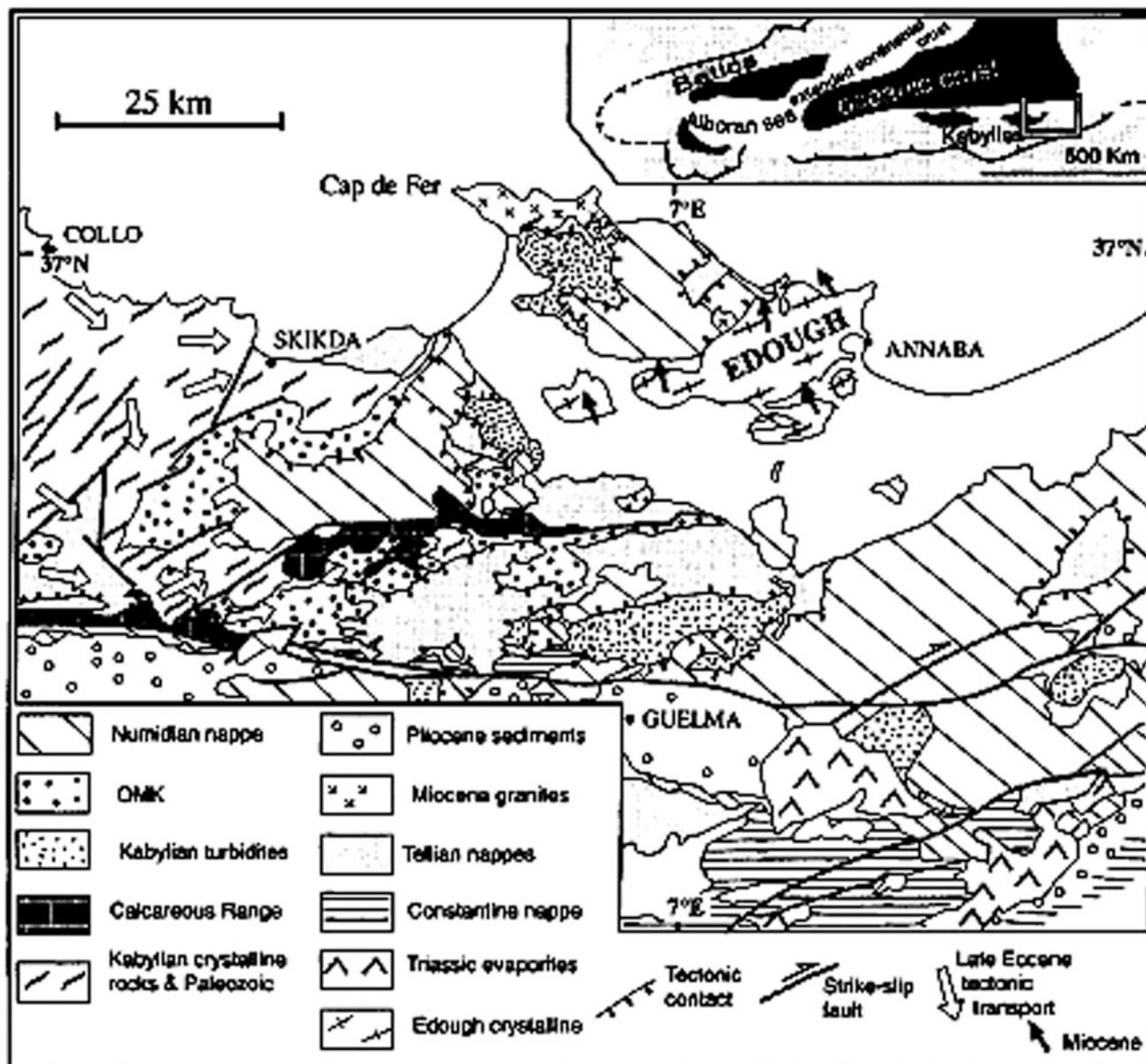


Fig. 1 Location of the Edough Massif (after [1])

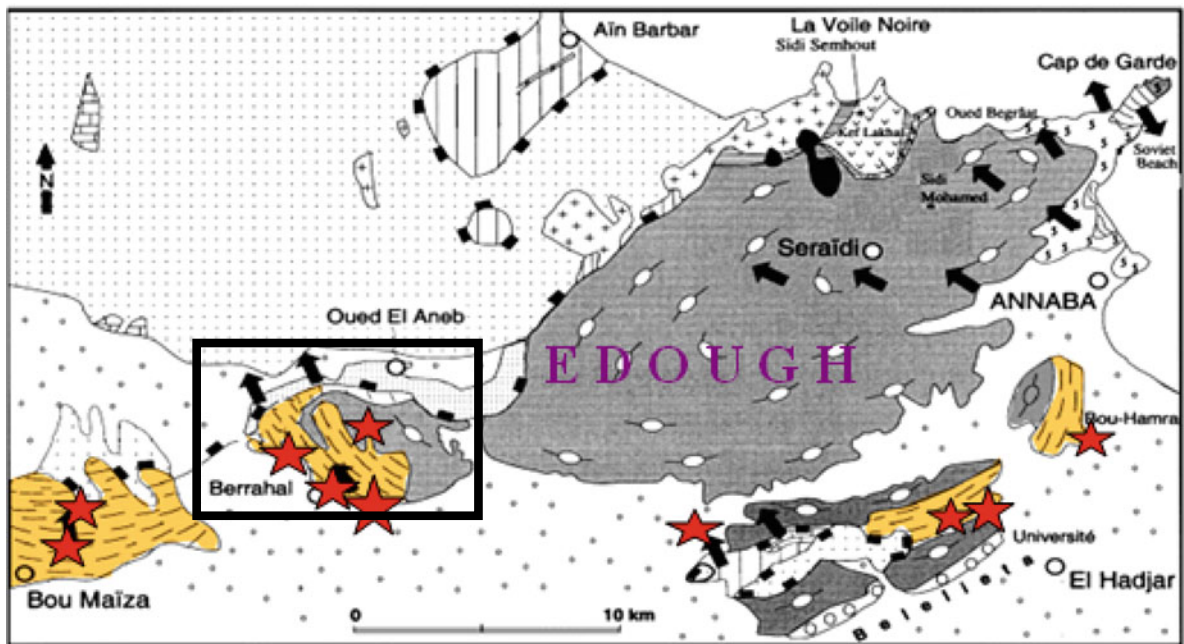
kyanite-staurolite-garnet micaschists. The main minerals of the ore bodies are magnetite, hematite, siderite, quartz, calcite, fayalite, hedenbergite and garnet (almandine) [6]. The early minerals composing the mineralized bodies are affected by Mn+2 metamorphism expressed by a N130-140 lineation and a concordant foliation with hosting micaschists [3] indicating non-coaxial deformation with NW vergence attesting the same type of Edough ductile shear zones [1].

The analysis of the major and trace elements of the Berrahal samples were performed by X-ray fluorescence (XRF) and by plasma excitation source emission spectrometry (ICP-AES) at the "Ecole Nationale Supérieure des Mines de Saint Etienne – France".

3 Results

Three types of facies [4, 7] can be distinguished on petrographic and geochemical observations (Fig. 3):

"The first facies denoted "Mc" corresponds to a carbonate ore. This ore is characterized by a carbonate gangue with alternating layers of calcite and calcite + magnetite (Fig. 4). Siderite is sporadically present and quartz is also present. The second facies, denoted "Ms", is a silicate ore characterized by a silicate gangue consisting of fayalite and hedenbergite (Fig. 5). Amphibole occurs as ferroedenitic to hastingsitic hornblende, while garnet is present as



 Iron ores

Fig. 2 Location of the Berrahal and Edough iron formations

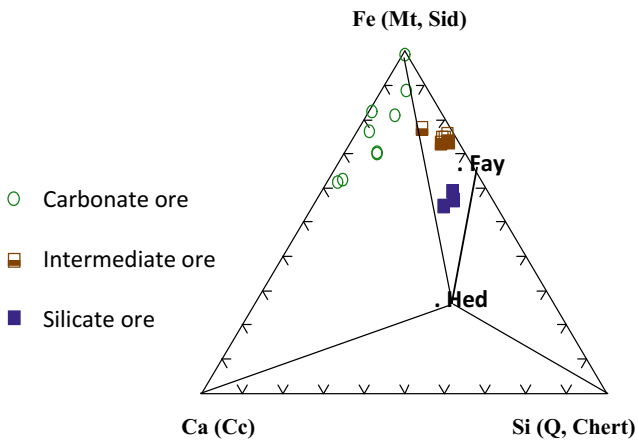


Fig. 3 The facies of the ores in the Ca/Fe/Si ternary diagram (wt%) from Berrahal. Sid: Siderite, Mt: Magnetite, Fay: Fayalite, Hed: Hedenbergite, Q: Quartz, Cc: Calcite

almandine. The third facies, denoted “Mi”, is considered as intermediate facies because of its lower silica content compared to that of Ms. The gangue consists of olivine, with intercalated calcitic bands. Calcite and fayalite are at equilibrium” (Fig. 6) [7].

The total rock chemical analyzes (Fig. 7) of the various samples analyzed show significant levels of major and traces elements from one sample to another.



Fig. 4 Metamorphic bands of carbonate ore (alternation of iron oxides (dark) bands and carbonates (light) bands)

4 Discussion

The analyzes show very high contents of iron in all samples. The abundance of silica (especially in silicate ore samples) is generally accompanied by a decrease in the iron content. CaO are also variable from one facies to another. However, there is a correlation between iron and CaO levels. This correlation



Fig. 5 Silicate ore from Berrahal iron formations. El Mour Ouan'ya mine. Hed: Hedenbergite; Fay: Fayalite. Thin section, crossed nicols view

Fig. 6 Intermediate ore from Berrahal iron formations. Cc: Calcite; Mt: Magnetite; Fa: Fayalite. Thin section, crossed nicols view

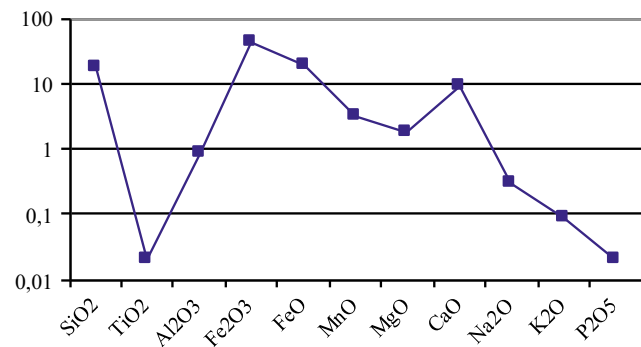
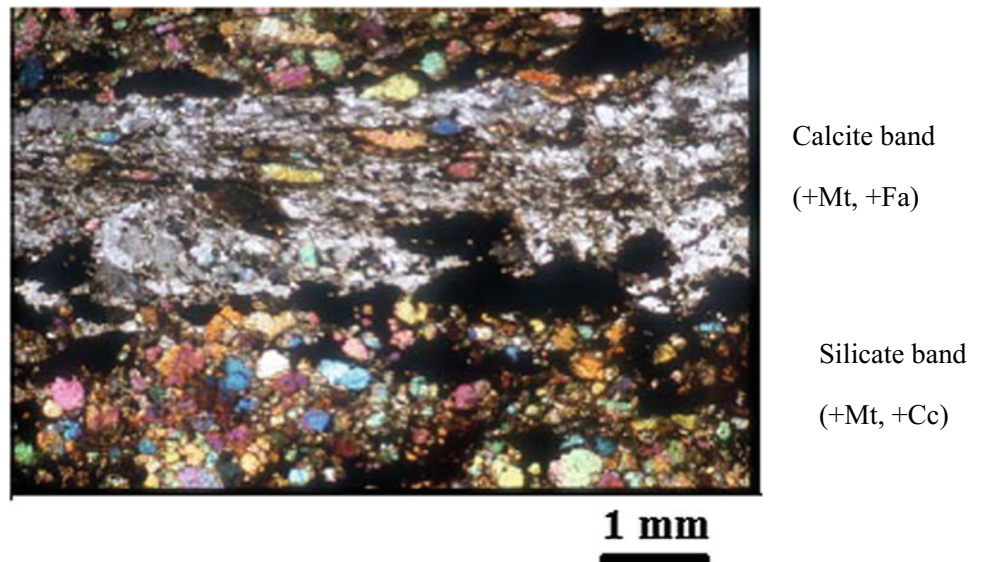


Fig. 7 Graphical sketch of average geochemical trends (wt%) of Berrahal, banded iron formations

does not always follow a precise rule because of the variations in the proportions of the carbonated gangue of ore.

Alumina contents are generally low; only rocks containing almandine garnet (based on microprobe analyzes) show significant levels of alumina (up to 3.83%). In the Al₂O₃/TiO₂ diagram, we observe a good correlation between these two elements, which have the reputation of being inert during metamorphic transformation and hydrothermal alterations processes ($r = 0.96$ with an Al₂O₃/TiO₂ ratio of the various samples fairly constant in both carbonate and silicate facies, suggesting that these constituents are carried by a more or less abundant detrital fraction of shales in iron formations protolithes.

The good correlation between Alumina and TiO_2 is well known in shales [2], which can be explained by a substitution of TiO_2 in the clay and varies according to the type of clay. The good correlation between Al_2O_3 and TiO_2 at the different studied sites indicates that the iron ore bodies of the Berrahal iron formations are of metasedimentary origin and can correspond to a mixture according to variable proportions between a carbonato-ferriferous pole \pm siliceous of chemical origin and a detritic pelitic pole or a carbonato-ferriferous pole and a volcano-sedimentary pole since the $\text{Al}_2\text{O}_3/\text{TiO}_2$ ratios can be the same.

Vanadium shows good correlations with Al_2O_3 ($r = 0.91$), TiO_2 ($r = 0.95$) and K_2O ($r = 0.94$).

Fe_2O_3 (+ FeO), CaO and SiO_2 are the three main critical constituents that have been based on the classification of iron formations in three main facies: carbonate, intermediate and silicate ores (Fig. 3).

The facies Ms and Mi are relatively rich in silica and the quartz appears in very fine intermeshed and interstitial crystals between the silicate minerals, whereas in the carbonate facies Mc, it appears in crystals scattered among the crystals of calcite and magnetite or sometimes constituting bands relatively rich in finely crystallized quartz and interspersed with calcite-magnetite bands (\pm siderite). The study of thin sections shows that it has the appearance of detrital origin sometimes constituting true quartzitic bands or show the appearance of chert finely recrystallized (in silicate facies essentially).

5 Conclusion

The geological study and the interpretation of the major and trace elements analyzes show that the Berrahal mineralized bodies are of metasedimentary origin (volcano-sedimentary). The regional uniformity in the geochemical characters and the characterization of the detrital fraction (from inter-element correlations) show the metasedimentary origin

of the mineralized bodies. "The location of the ore bodies of Berrahal banded iron formations at several sites and their petrographic and geochemical similarities suggest that regional extent of mineralization is inherited from protoliths of sedimentary or volcano-sedimentary nature, which were subsequently transformed by regional isochemical metamorphism" [5, 6]. Regional metamorphism has contributed to the departure of some elements such as volatiles and to a reconcentration of other elements such as iron by decarbonation [7]. The metasedimentary origin of the mineralization as well as its uniformity and continuity suggests a high probability of revealing new hidden deposits.

References

1. Caby, R., Hammor, D., Delor, C.: Miocene exhumation of lower crust in the Edough metamorphic core complex, West Mediterranean orogen, Eastern Algeria. *Tectonophysics* **342**, 239–273 (2001)
2. Goldschmidt, V.: *Geochemistry*. Clarendon Press, 759 p (1954)
3. Henni, B., Guy, B., Aïssa, D.E., Garcia, D.: Les gisements et indices de magnétite de la région de Berrahal (massif de l'Edough, NE algérien). *Environnement géologique et données pétrographiques*. Bulletin du Service Géologique de l'Algérie **13**(1), 33–48 (2002)
4. Henni, B.: Les formations ferrifères du massif de l'Edough (Annaba, NE algérien). Etude géologique, géochimique et approche thermodynamique. Thèse Doctorat d'Etat, Université des Sciences et de la Technologie Houari Boumédiène (USTHB), Alger, 224 p (2006)
5. Henni, B., Aïssa, D.E.: Géologie et géochimie des formations ferrifères de l'Edough (Annaba, NE algérien). *Bulletin du Service Géologique National* **18**(3), 297–314 (2007)
6. Henni, B., Guy, B.: Stabilité de l'association fayalite + calcite dans les formations ferrifères métamorphisées; l'exemple des minéralisations en magnétite du massif de l'Edough (N-E algérien). <hal-00523266>, 24 p (2007)
7. Henni, B., Guy, B.: Stability of the association fayalite + calcite within metamorphosed banded iron formations: the case of the magnetite ores of Edough massif (N-E Algeria). *Comptes Rendus Géoscience* **344**(6–7), 349–356 (2012). (Elsevier Masson)



Contribution to the Study of Bauxites' Formation in the Fongo-Tongo (Western Cameroon) Sites

Franck Wilfried Nguimatsia Dongmo, Rose Fouateu Yongue, Anthony Temidayo Bolarinwa, Ralain Bryan Ngatcha, Christopher Fuanya, and Marc Anselme Kamga

Abstract

The present study is aimed at identifying and characterizing the morphological, mineralogical, and geochemical features of Fongo-Tongo bauxite (western Cameroon). Fongo-Tongo is part of the Bamilélé plateau sited in the Western Cameroon highland, on which lateritic bauxites are developed. The study was implemented using XRD; ICP-AES and ICP-MS techniques. The XRD identified minerals include mainly gibbsite and goethite. The geochemical data prove to reveal the persistence of high alumina (Al_2O_3) content, ranging from 37.4 to 57.5 wt%, with relatively low Fe_2O_3 (<29.5 wt%), TiO_2 (<7.5 wt%) and SiO_2 (0.48–3.21 wt%). Trace and REE concentrations of Zr (504–2310), Nb (104–350), Sr (0.7–345), V (8–667), Ce (24.9–239), La (2.4–144) and Nd (3.1–126) ppm of the analysed samples appear to vary from low to high. Additionally, the highest Zr concentration turns out to depict the enrichment of such immobile elements as the Al, Ti, Zr and Nb during the bauxitization process. In effect, the Fongo-Tongo lateritic bauxite is discovered to be high in alumina content while displaying low impurities, which makes it metallogenetically important as a major source of raw material for the aluminium industry.

Keywords

Western Cameroon • Fongo-Tongo • Bauxites • Mineralogy • Geochemistry

1 Introduction

Bauxite stands as a basic primary raw material used in heavy industries. Indeed, the increasingly growing demand for high-grade bauxite for the development and production of quality refractory materials has actually fostered the exploration of new deposits. According to the bedrock lithology, bauxite deposits can be classified into two major categories: karstic bauxites, that help overly carbonate rocks regardless of karstification degree, and lateritic bauxites, which overly help almosilicate rocks [1]. To note, Karst-type deposits originate from a wide range of materials, depending on the source area [1], while Lateritic bauxite is generally formed by means of in-situ lateritization. Hence, the major factors that interfere in determining the extent and grades of bauxite ranges turn out to be the parent rock composition, climate, topography, drainage, groundwater chemistry and movement, location of the water table, microbial activity, along with the duration of weathering processes [2, 3]. In addition, the lateritic bauxites attached features are usually directly related to the underlying source rocks associated textures and compositions [2]. It is worth noting, in this respect, that Lateritic bauxite stands as the major resource of bauxite type available in Cameroon [4–7]. Noteworthy, also, is that although the Fongo-Tongo bauxite constitutes the largest western Highlands' deposit, it appears to be less investigated in respect of the other resources. Hence, a detailed knowledge of the geological and geomorphological settings, mineralogy as well as the geochemistry of the Fongo-Tongo lateritic bauxite occurrences seems imposed. Actually, the present work's major objective lies in investigating the Fongo-Tongo bauxite associated mineralogical and geochemical facies, in a bid to identify the ores' precursor by means of the major and trace elements' distribution, along with the deposits relating comprehensive geological, mineralogical and geochemical characterization.

F. W. N. Dongmo (✉) · A. T. Bolarinwa · R. B. Ngatcha
Department of Geology, Pan African University, Life and Earth
Sciences Institute (PAULESI), University of Ibadan, Ibadan,
Nigeria
e-mail: fngumatsia-dongmo0116@stu.ui.edu.ng

F. W. N. Dongmo · R. F. Yongue · C. Fuanya · M. A. Kamga
Department of Earth Sciences, University of Yaounde 1, Yaounde,
Cameroon

© Springer Nature Switzerland AG 2019

D. M. Doronzo et al. (eds.), *Petrogenesis and Exploration of the Earth's Interior*,
Advances in Science, Technology & Innovation, https://doi.org/10.1007/978-3-030-01575-6_58

2 Materials and Methods

The major as well as the trace components of the rare earth elements (REE) relevant to the lateritic bauxite samples were analyzed at the ALS Chemex laboratories (South Africa). The major elements were determined via an atomic emission source (ICP-AES), while the trace elements were analysed by means of inductively coupled plasma mass spectrometry (ICP-MS). As for the X-ray diffraction (XRD) analyses, they were performed using the SCINTAG XDS 2000 diffractometer belonging to the Department of Geology, University of Liege, Belgium. The instrumental settings are 40 kV, 35 mA and Co-K α radiation.

3 The Reached Results

The analyzed samples' mineralogical composition, as extracted from the Fongo-Tongo bauxite, include gibbsite and goethite with traces of quartz, anatase, maghemite, kaolinite and hematite. Variations in the major, trace and rare-earth elements are depicted in Fig. 1a–c, respectively.

4 Discussion

The Fongo-Tongo associated bauxite proves to display a significant concentration of zirconium (504–2310 ppm), likely to be associated with the presence of zircon in granitic rock.

Besides, this particular bauxite appears to reveal a significant concentration of trace elements, notably Sr, Ba and LREE; La, Ce, Pr and Nd relative to HREE. The geochemical data suggest that Zr, Y, Nb, Mo, V, Sc, Sr, and Ba could be enriched during the bauxitization process; the LREE enrichment could well be related to the differences perceived in the alteration minerals' stability. Lanthanum, Ce and Pr accumulation can also be well associated to the prevalent physico-chemical conditions [9]. Analysis of the ternary diagram in accordance to [10], prove to indicate that the investigated Fongo-Tongo bauxitic materials turn out to be derived from an environment characterized with strong lateritization (Fig. 2). Their position in the diagram as undertaken in [11] proves to reveal that they correspond to the bauxites class (Fig. 3). The analyzed bauxites, as figuring on Table 1 after [12], highlight well that they could have diverse industrial applications thanks to their particular chemical composition.

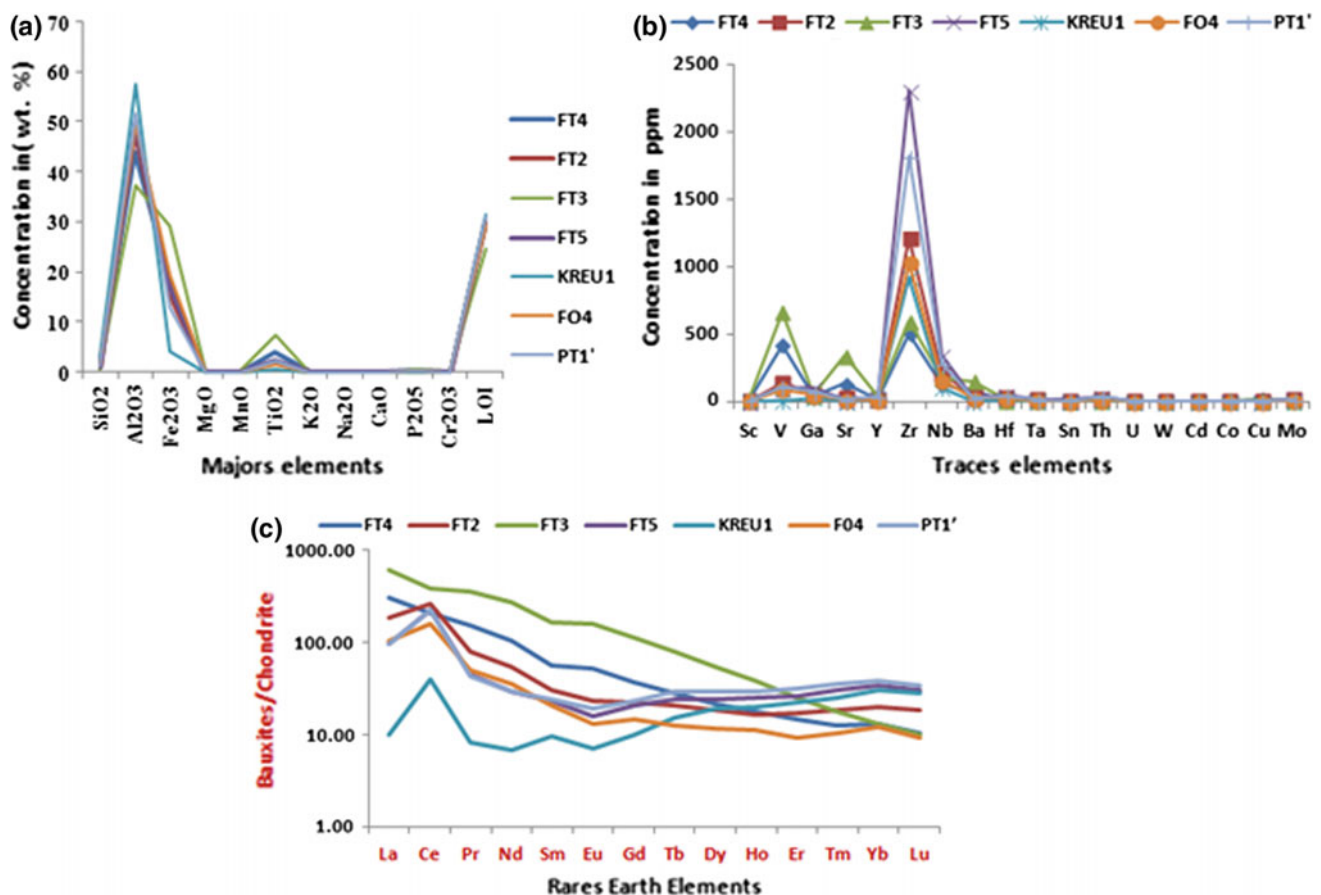


Fig. 1 a, b The major and trace elements related variation, concerning the Fongo-Tongo lateritic bauxite. c Chondrites normalized rare-earth composition of the Fongo-Tongo lateritic bauxites (after [8])

Fig. 2 Fongo-Tongo bauxitic samples on the $\text{SiO}_2\text{-Fe}_2\text{O}_3\text{-Al}_2\text{O}_3$ ternary diagram (after [9])

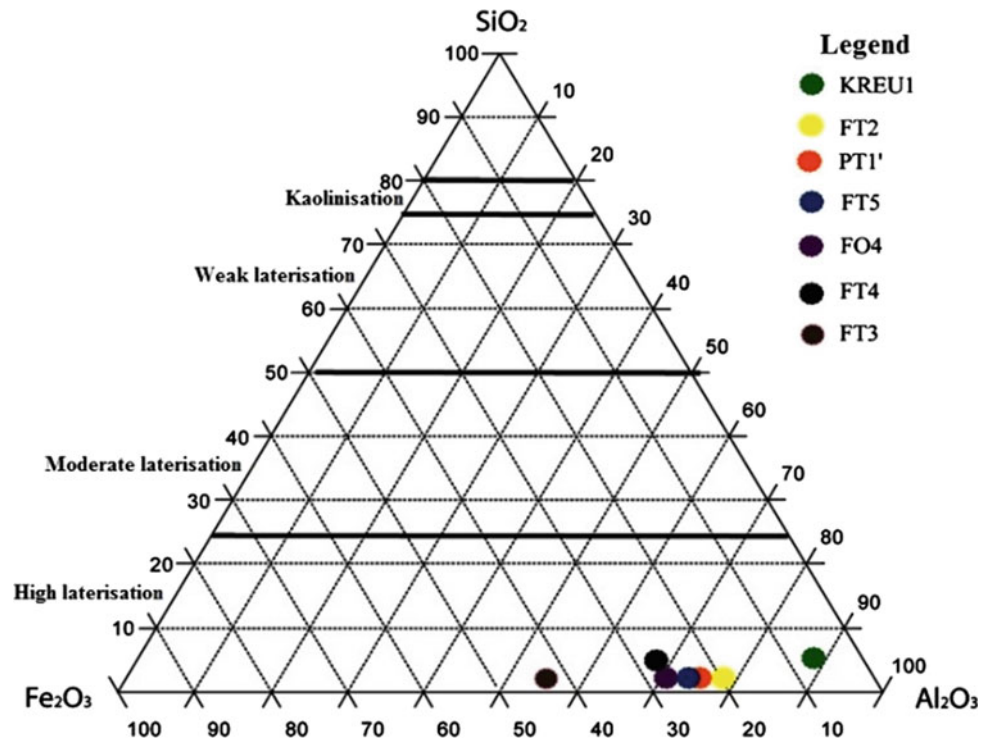


Fig. 3 Fongo-Tongo bauxitic samples on the $\text{SiO}_2\text{-Fe}_2\text{O}_3\text{-Al}_2\text{O}_3$ ternary diagram (after [10])

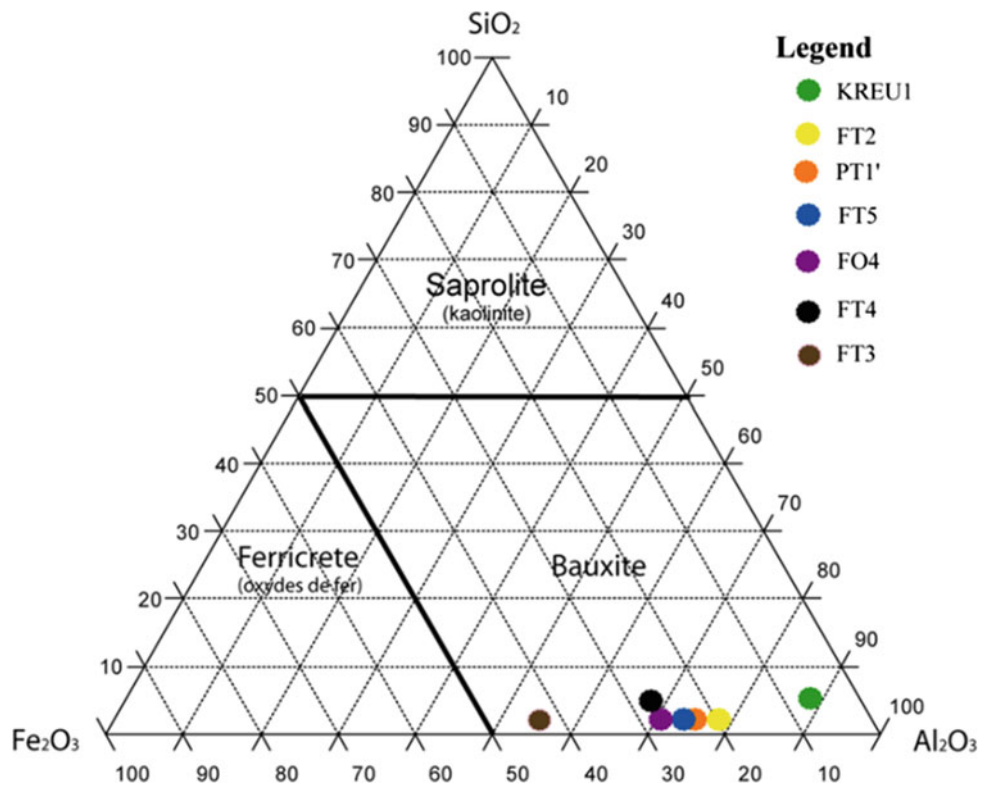


Table 1 Classification of bauxites according to their respective uses

Designation		Bauxite used in the production of aluminum and alloys	Bauxite used in the elaboration of abrasive materials	Bauxite use in the elaboration of refractory	Bauxite use in the production of chemical products/compounds	Bauxite use in cement composition
Major oxides %	Al ₂ O ₃	50–55	80–88	Min: 84.5	55–60	45–55
	SiO ₂	0–15	Max: 5	7.5	Max: 5–18	Max: 6
	Fe ₂ O ₃	5–30	2–5	Max: 2.5	Max: 2	20–30
	TiO ₂	0–6	2–4	Max: 4	0–6	3
Corresponding bauxite		FT5 FO4 PT1'			KREU1	FT4 FT2

5 Conclusions

The Fongo-Tongo area involves three major geomorphic domains occurring in a step-wise manner, lying at an average altitude of 1500–1650 m, corresponding to the bauxite availability zone. The Lateritic bauxite outcrops lie in the form of slabs and discontinuous blocks. The lateritic bauxites vary from massive, vesicular, cellular and conglomeratic to nodular. They are indurated materials of various colors, including red, brick-red to reddish brown, brown, pink, yellow and ochers. While some of them have armor spots and purple frames, others are mottled greenish. They consist mainly of gibbsite, subordinate goethite, with traces of quartz, anatase, hematite, maghemite and kaolinite.

They are characterized with high alumina contents ranging from 37.4 to 57.5 wt%. Other oxide traces Fe₂O₃ (<29.5 wt%), TiO₂ (<7.5 wt%) and SiO₂ (0.48 to 3.21 wt%), appear to be very low. The bauxite is also characterized with significant levels of trace and rare-earth elements, including Zr (504–2310), Nb (104–350), Sr (0.7–345), V (8–667), Y (24.9–239), La (2.4–144) and Nd (3.1–126) ppm. In effect, the geochemical data of the Kreu site lateritic bauxite, as figuring on (Table 1), located west of Fongo-Tongo, proves to display the highest rate of alumina content (57.5%), with low concentration of impurities, such as, SiO₂ (3.21), Fe₂O₃ (3.97) wt% and Zr (923), Nb (104), Sr (0.7), V (8.0), Ce (24.9) La (2.4) and Nd (3.1) ppm.

The Fongo-Tongo lateritic bauxite appears to be rather suitable as raw material fit for application in heavy industries. Noteworthy, however, is that further research is required to investigate the bauxite deposits' quantification as well as the designing of the environmentally fit sustainable exploitation methods.

References

- Bardossy, G.: Karst Bauxites. Bauxite Deposits on Carbonate Rocks. Elsevier, Amsterdam, Oxford, New York, 441p (1982)
- Bardossy, G.Y., Aleva, G.J.J.: Lateritic Bauxites: Developments in Economic Geology, vol. 27, p. 624. Elsevier Scientific Publication, Amsterdam (1990)
- Price, G.D., Valdes, P.J., Sellwood, B.W.: Prediction of modern bauxite occurrence: implications for climate reconstruction. *Palaeogeogr. Palaeoclimatol. Palaeoecol.* **131**, 1–13 (1997). [https://doi.org/10.1016/S0031-0182\(96\)00145-9](https://doi.org/10.1016/S0031-0182(96)00145-9)
- Eno Belinga, S.M.: L'altération des roches basaltiques et le processus de bauxitisation dans l'Adamaoua (Cameroun). Thèse Doc. Etat, Univ. Paris VI, 571p (1972)
- Nyobe, J.B.: A Geological and Geochemical Study of the Fongo Tongo and Areal Related Bauxite Deposits, Western Highlands, Republic of Cameroon. Doc. Ph.D., Lehigh Univ., 352p (1987)
- Laplaine, L.: Indice minéraux et ressources du Cameroun. Direction des Mines et de la Géologie Bulletin **5**, 9–182 (1969)
- Momo, N.M., Tematio, P., Yemefack, M.: Multi-scale organization of the Doumbouo-Fokoué bauxites ore deposits (West Cameroon): implication to the landscape lowering. *Open J. Geol.* **2**, 14–24 (2012). <https://doi.org/10.4236/ojg.2012.21002>
- Mc Donnough, W.F., Sun, S.S.: The composition of the Earth. *Chem. Geol.* **120**, 223–253 (1995). [https://doi.org/10.1016/0009-2541\(94\)00140-4](https://doi.org/10.1016/0009-2541(94)00140-4)
- Meen, J.K.: Negative Ce anomalies in Archean amphibolites and Laramide granitoids, southwestern Montana, USA. *Chem. Geol.* **81**(3), 191–207 (1990). [https://doi.org/10.1016/0009-2541\(90\)90115-N](https://doi.org/10.1016/0009-2541(90)90115-N)
- Schellmann, W.: A new definition of laterite. *Memoirs of the Geological Survey of India. J. Afr. Earth Sci.* **120**, 1–7 (1986)
- Mutakyahwa, M.K.D., Ikingura, J.R., Mruma, A.H.: Geology and geochemistry of bauxite deposits in Lushoto District, Usambara Mountains, Tanzania. *J. Afr. Earth Sci.* **36**, 357–369 (2003). [https://doi.org/10.1016/S0899-5362\(03\)00042-3](https://doi.org/10.1016/S0899-5362(03)00042-3)
- Rusel, A., et al. Bauxite and alumina. A guide to non-metallurgical uses and markets. Industrial mineral information limited, park house, park terrace, surrey KT47HY.UK ISBN: 1900663619 (1999)

Mapping Geochemical Anomalies Through Principal Components Analysis in BIF Mines: An Approach Referring to the Bonito Mine, Northeastern Brazil

Helano Fonteles, Henrique Pereira, Carla Rocha, and César Veríssimo

Abstract

Given the subtle complexity associated with the geochemical composition of iron ore deposits, a full understanding of their behavior appears to entail a well-structured geochemical database. In this context, the Principal Components Analysis (PCA) approach has been applied to map geochemical anomalies throughout an exhaustive database concerning the banded iron formation (BIF) deposit of the Bonito Mine, as sited in Rio Grande do Norte State in Northeastern Brazil. The BIF deposit is related to the Serra dos Quintos Formation, Seridó Group, considered as a Neoproterozoic metasedimentary sequence, deposited and metamorphosed during the Brasiliano-Pan African orogeny. The ore typology scheme comprises hematitic itabirites, magnetitic itabirites, martitic itabirites and amphibolitic itabirites. The PCA drawn data appear to reveal that two first principal components prove to explain almost 73% of the cloud information and, as expected, the Fe_2O_3 and SiO_2 contents turn out to have the highest factorial loads on PC1. In addition, the geochemical anomalies, as projected on the factorial plane, appear to reveal some relevant information regarding the geological processes occurring during the iron ore formation. The qualitative correlation between Mn and P- Al_2O_3 contents indicate that an important sedimentary input have taken place, culminating in the development of the Bonito Mine BIF deposit.

Keywords

PCA • BIF • Bonito mine • Iron oxide ore

H. Fonteles (✉) · C. Veríssimo
Universidade Federal do Ceará, Avenida Mister Hull, S/N. Bloco 913, Fortaleza, CE 60455-760, Brazil
e-mail: helano.fonteles@alu.ufc.br

H. Pereira · C. Rocha
Universidade de Lisboa, Avenida Rovisco Pais, 1, 1049-001
Lisbon, Portugal

1 Introduction

The Bonito Mine is located in Jucurutu, Rio Grande do Norte State, Northeastern Brazil. Geologically, it is linked to the Serra dos Quintos Formation, Seridó Group, made up mainly of schists, gneisses, marbles, ferruginous quartzites and banded iron formations (BIFs), from which the geochemical database is predominantly derived. Most studies highlight that the sedimentation and metamorphic processes pertain to the Neoproterozoic age [1].

The present paper is intended to present the preliminary results achieved following a comprehensive study dealing with the iron-ore typology model of the Bonito Mine. The BIFs represent the most important geological features characterizing the Serra dos Quintos Formation as they enclose hematitic itabirites (HI), magnetitic itabirites (MgI), amphibolitic itabirites (AmI) and martitic itabirites (MI). The Principal Components Analysis (PCA) procedures have been opted for as a reliable method whereby some underlying geological relations among variables and samples could be disclosed. In presence of anomalous values, the PCA outcomes could well help in revealing relevant information likely to help identify unclear geochemical relationships.

2 Methods and Materials

The Principal Component Analysis (PCA) is one of the most used multivariate statistical methods that stands as an exploratory tool useful for application with large dataset contexts. In the present context, the major purpose lying behind implementation of the PCA framework consists in reducing the databases associated dimensionality, while providing an intelligible graphical display of the data points, as provided by their relating factorial coordinates, drawn from diagonalization of the correlation matrix. Besides, the PCA displays the remarkable advantage of promoting a quick assessment of the outlying data points [2].

The investigated dataset involves 1.384 samples related to five variables (Fe_2O_3 , SiO_2 , Al_2O_3 , P and Mn), available in eighty four drilled holes. The entire set has been treated in order to obtain the relevant principal components and to depict all the relating geochemical data. It is actually this particular application which has enabled us to examine the geological relationships persistent among the samples associated variables.

3 Results

The basic descriptive statistics are depicted on Table 1. As can be noted, the high C.V. values may well indicate high data variability. An exploratory linear regression analysis has been performed to examine the correlations persisting between variables. Noteworthy, however, is that weak correlations have been obtained, with the exception of the $\text{SiO}_2 \times \text{Fe}_2\text{O}_3$ linear regression fit, which proves to yield a Pearson's coefficient rate of $r^2 = 0.6669$.

An analysis of Table 2 highlights well that two axes appear to suffice, at first sight, to interpret the geochemical data set. In fact, the plane PC1-PC2 (appearing in Fig. 1a) proves to retain almost 73% of the cloud based information, while the entirety of variables have been 'reasonably' interpreted, just on the basis of their projection onto this plane, as shown in Fig. 1a.

All variables were interpreted in statistical terms in plane PC1-PC2, under the presumption that a linear correlation coefficient higher than 0.5 proves to be 'significant'. It is worth noting, however, that 'significance' can only be dealt with in a multivariate Gaussian context, which is not obviously the case for the Bonito Mine attached input data. However, once the multivariate gaussianity does not appear to be strictly feasible and liable to assessments, the 0.50 boundary should prove to be acceptable, even for Mn. The same rule also applies to the interpretation of other variables at the factorial plane (Fig. 1a).

4 Discussion

It is worth noting that a continuum of samples projecting along the PC 1 plane appears to persist. Indeed, the smaller is the sample coordinate in PC 1, the greater is its SiO_2 content; conversely, however, the higher its coordinate in PC 1, the greater its Fe_2O_3 content (Fig. 1b). This is a geochemical portrait of the exact meaning of the banded iron formation or *itabirite* (namely in this work), once the rock is defined by the alternating bands of silicatic minerals (mainly quartz) and iron oxide ore. Regarding the PC 2 relating samples, one could well maintain that there is an arbitrary upper limit for Mn influence (the farther from the origin, along PC 2 is, the stronger that influence will turn out to be; conversely, there may be an arbitrary lower limit for the $\text{Al}_2\text{O}_3 + \text{P}$ influence, the farther from the origin, along PC 2 is, the stronger the influence will be). The box #2 (as split into two sub-boxes) contains samples with P- Al_2O_3 anomalies. In the box #2a, samples with high Al_2O_3 grades are positioned and the same can be observed in the box #2b for the P grades.

The box #1 encompasses the richer Mn-content. The raw geochemical values are higher than the average content (see Table 1, for reference). In terms of PC-reading perception, the samples lying farther from PC 2 (along the PC 1) will be displayed as poorer Mn values. The geochemical cycles of manganese and iron are well-known for long time [3]. These elements have similar geochemical behaviors due to their chemical properties (ionic radii, ionic charges, etc.). However, in the deposition environments where pH-Eh conditions play an important role, manganese tends to follow a distinct path away from iron on the sedimentary processes [3, 4]. Thus, Fig. 1b clearly displays many samples in a proper field on factorial plane.

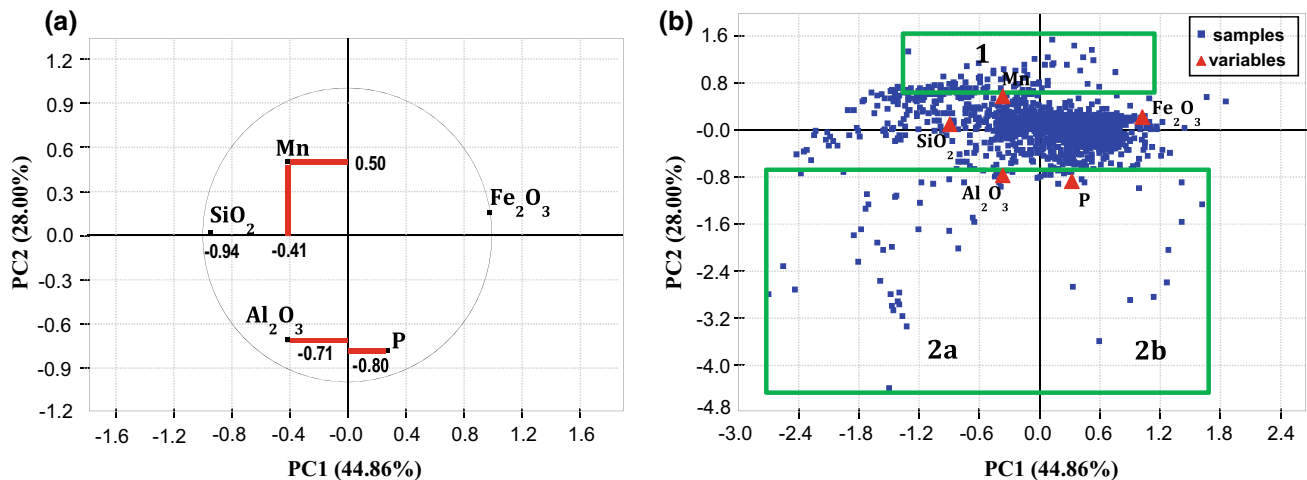
Aluminum oxide grades are essentially attached to terrigenous input to the basin as this variable have a close factorial relation to SiO_2 grades. The anomalies were interpreted as possible punctual events due to an increase of the

Table 1 Summary of the exploratory statistics (%wt.)

Variable	Mean	Median	Min.	1st Quant.	3rd Quant.	Max.	Std. Dev.	C.V. (%)
Fe_2O_3	41.68	43.18	4.81	38.01	46.90	70.01	8.54	20.48
SiO_2	56.83	55.68	28.11	52.28	60.17	90.23	7.77	13.67
Al_2O_3	1.134	0.505	0.010	0.250	0.905	18.230	2.26	199.60
P	0.041	0.040	0.007	0.030	0.050	0.252	0.02	55.82
Mn	0.309	0.210	0.010	0.130	0.360	2.030	0.29	95.20

Table 2 Eigenvalues and accumulated explained cloud information (in italics)

Principal component	PC1	PC2	PC3	PC4
Eigenvalue	2.243 (<i>44.86%</i>)	1.400 (<i>72.86%</i>)	0.803 (<i>88.93%</i>)	0.553 (<i>100%</i>)

**Fig. 1** Projections of variables and samples onto planes PC1-PC2. The ANDAD statistical software allows, on the ground of a graphical scaling procedure, to project samples and variables onto the same plot

pelitic sedimentation into the basin as a product of the weathering of felsic rocks. On the other hand, phosphorus grades bring some new information about the iron oxide ores. This element has a dual geochemical character being both siderophile and lithophile [4] and as it can be seen in Fig. 2 the highest P values are related to iron richer BIFs samples, such as the hematitic itabirites. This could be explained taking into account the possibility that phosphate radicals could be brought by colloidal iron hydroxides due to their linkage to the surface of this compound [5].

5 Conclusions

Considering the results discussion, one could well conclude that, despite the fact that the multiGaussian distribution model does not necessarily appear to fit predominantly for the research data presented in this work, the PCA has proved to display a noticeable efficiency in evaluating the exhaustive dataset, and mapping the geochemical anomalies. Once the main correlation ($\text{Fe}_2\text{O}_3 \times \text{SiO}_2$) was determined on the factorial plane, the other variables were interpreted to stand as auxiliary sources of relevant information.

The joint Al_2O_3 -Mn plot analysis may represent an important terrigenous input to the basin. The phosphorus

content proves to have a strict relationship with the Fe-rich BIFs origin. Notwithstanding, the lack of additional mineralogical data does not allow us to identify what is the primary source of phosphorus contents. Nevertheless, the mapped anomalies can be considered as a starting point for a rather accurate investigation of what the real sources could be.

Acknowledgements Helano Fonteles: CAPES Ph.D. funding grant n. 8887.116689/2016-00. Carla Rocha: FCT Ph.D. funding grant n. SFRH/BD/105622/2015.

References

- Nascimento, R.S.C., Sial, A.N., Pimentel, M.M.: Chemostratigraphy of medium-grade marbles of the late Neoproterozoic Seridó Group, Seridó Fold Belt, Northeastern Brazil. *Gondwana Res.* **7**(3), 731–744 (2004)
- Wold, S.: Principal components analysis. *Chem. Intellig. Lab. Sys.* **2**, 37–52 (1987)
- Krauskopf, K.B.: Separation of manganese from iron in sedimentary processes. *Geochim. Cosmochim. Acta* **12**, 61–84 (1957)
- Rankama, K., Sahama, T.G.: *Geochemistry*. In: 4th Impression. The University Chicago Press, Chicago (1960)
- Alberède, F.: *Geochemistry: An Introduction*. Cambridge University Press, Cambridge (2009)

The Mineral Exploration of the Iron Ores in the Eastern Aswan, by Using Geophysical Techniques

Mahmoud Mekkawi, Sultan Arafa, Ayman Ismail, and Mohamed Abbas

Abstract

The magnetite and hematite mines are located in the Eastern Desert of the Abu Subera area, some 35 km far from the Aswan city, commonly recognized as a volcano-tectonic area. It constitutes one of the largest arc sedimentary rock units lying in the Precambrian sequence. It was strongly affected with multiple deformation stages, resulting in the appearance of folding and faulting. The ironstone deposits predominant in the area are of a bedded-oolitic type, and occur in the form of two bands, inter-bedded with ferruginous sandstone and clay-capping Precambrian rocks, of a thickness varying from 0.5 to 3.5 m. The magnetic measurements are condensing along the six mines where the iron ore bodies are centered. Seven geoelectrical profiles were measured by means of a dipole-dipole configuration of electrode spacing 5, 10 and 15 m of lengths, ranging from 160 to 240 m. The reached results appear to indicate that the ore deposits prove to refer to low resistive zones, of high chargeability with moderate to high magnetic anomalies.

Keywords

East Aswan iron ores • Alter mineralized zone
Magnetic and electrical methods

1 Introduction

The iron-ore deposit reserves, lying in the eastern Aswan area, were estimated to range between 120 and 135 million tons, with average iron contents of 46.8% [1]. The iron-bearing minerals of the Aswan deposits are mainly hematite, chamosite, goethite, in addition to the persistence

M. Mekkawi (✉) · S. Arafa · A. Ismail · M. Abbas
National Research Institute of Astronomy and Geophysics
(NRIAG), Cairo, Egypt
e-mail: mekkawi05@yahoo.com

of other constituents like pyrite and siderite [4]. They are distributed in the north eastern, eastern and western zones of the Aswan Lake [5]. The area is covered with Quaternary deposits represented by sandstone and Nile mud, along with Miocene sediments manifested in graben-fill sandstone and conglomerates. Nubian sandstone of upper Cretaceous is overlain across Pre-Cambrian crystalline rocks. The East-Aswan sedimentary iron ores occur in Upper Cretaceous (**Senonian**) sediments, and are characterized with the oolitic hematites of Abu-Aggag Fm., Timsah Fm. and Umm Baramil Fm [3].

2 Geophysical Methods

Relevant magnetic and electrical surveys were carried out in profiles crossing the Abu-Subeira Wadi. The magnetic measurements were collected by means of two magnetic magnetometers, one of them was used as a base station, to record the diurnal daily variations, and the other as a mobile magnetometer. The total number of reached profiles was 70, covering the entire study area. For the shallow and deep structures of the Abu-Subeira Wadi to be thoroughly investigated, a number of magnetic and electrical techniques were used for qualitative and quantitative interpretation purposes.

The magnetic survey covers the six major mines, already opened by the Nasser Metallurgic Company (Fig. 1). Eleven geoelectrical profiles were measured by means of dipole-dipole configuration of an electrode spacing 5, 10 and 15 m, of length ranges varying between 160 and 240 m. The measurements were carried out through the implementation of the electrical resistivity (**ER**) and induced polarization (**IP**) methods. The electrical cross-sections seem to reflect well the conductive mineralization zones.

The relevant land magnetic survey, of the area under review, is about $(1000 * 3000 \text{ m}) \approx 3.0 \text{ km}^2$. The total number of magnetic stations amounted up to **2750**, and the average station distribution was of the range of 915 stations per km^2 , approximately. The stations' separation intervals

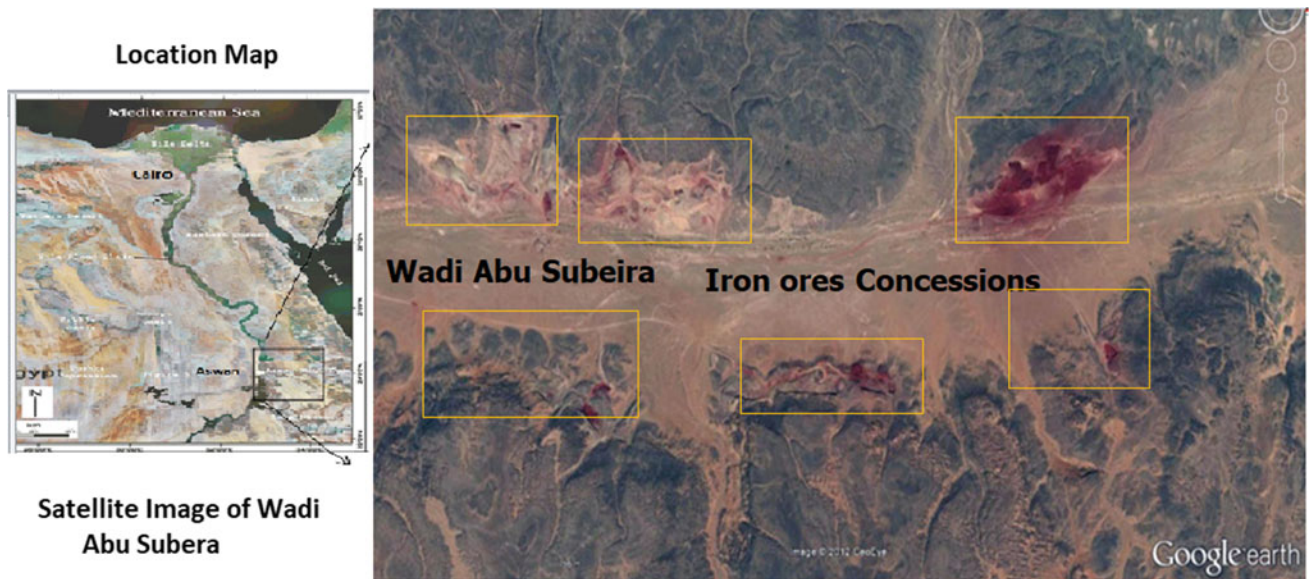


Fig. 1 Location map of Egypt (left) showing the location of the study area. (Right) A satellite image of the Wadi Abu-Subeira area and the iron-ore concessions [2]

proved to range between 15 and 20 m, according to the area related topography. The profiles separating distance intervals varied according to mountain elevation rates, ranging, predominantly, between 20 and 40 m. The total magnetic intensity map of the Abu Subeira Wadi is depicted in Fig. 2. The station position and elevation at the measurement time were recorded through a handheld **GPS** system. The data were subsequently corrected, for the base station to remove the diurnal variations noticeable in the Earth's magnetic field.

3 Results

To estimate the depth of magnetic sources and the fractures' basement zone, the Euler deconvolution method (Reid 1990) was applied to the magnetic data. The structure indexes of 0, 0.5 and 1.0 were tested and the Euler solutions' drawn results were reported in Fig. 3, using structure index 1.0 for faults and dykes. The magnetic sources associated depths were of the ranges of 15–70 for the shallow structures (mineralization zone), and 120–280 m for the deep structures and basement complex.

Electrical profiles were carried out perpendicular to the strike of wadi Abu-Subeira along with six iron-ore

concessions, already opened by the Nasser Metallurgic Company. Resistivity and induced polarization techniques were carefully implemented for the low resistive zone and high chargeability to be maintained, as the soil and ground appear to display high resistivity values. The eleven electrical profiles relevant locations were represented by P1, P2, P3, ..., P11, as illustrated in Fig. 2.

4 Conclusions

The area is characterized with the prevalence of high magnetic anomaly marking the southern and northern parts, and extending both eastwards and westwards, referring to the iron-ore bodies. The depths associated with the mineralized zones reaches 15–70 m for the shallow structures, and 120–180 m with respect to the deep structures (Fig. 3) concerning the study area. The electrical interpretation reached results prove to indicate that the deposits turn out to display low resistivity values, and relatively high chargeability values (Fig. 4). The ore deposits turn out to be represented with lenses ranging from few meters to more than 30 m. The minerals relating distributions as predominant in the Wadi Abu-Subeira area prove to be controlled by the major faults and subsurface structures, in which the mineralization zones

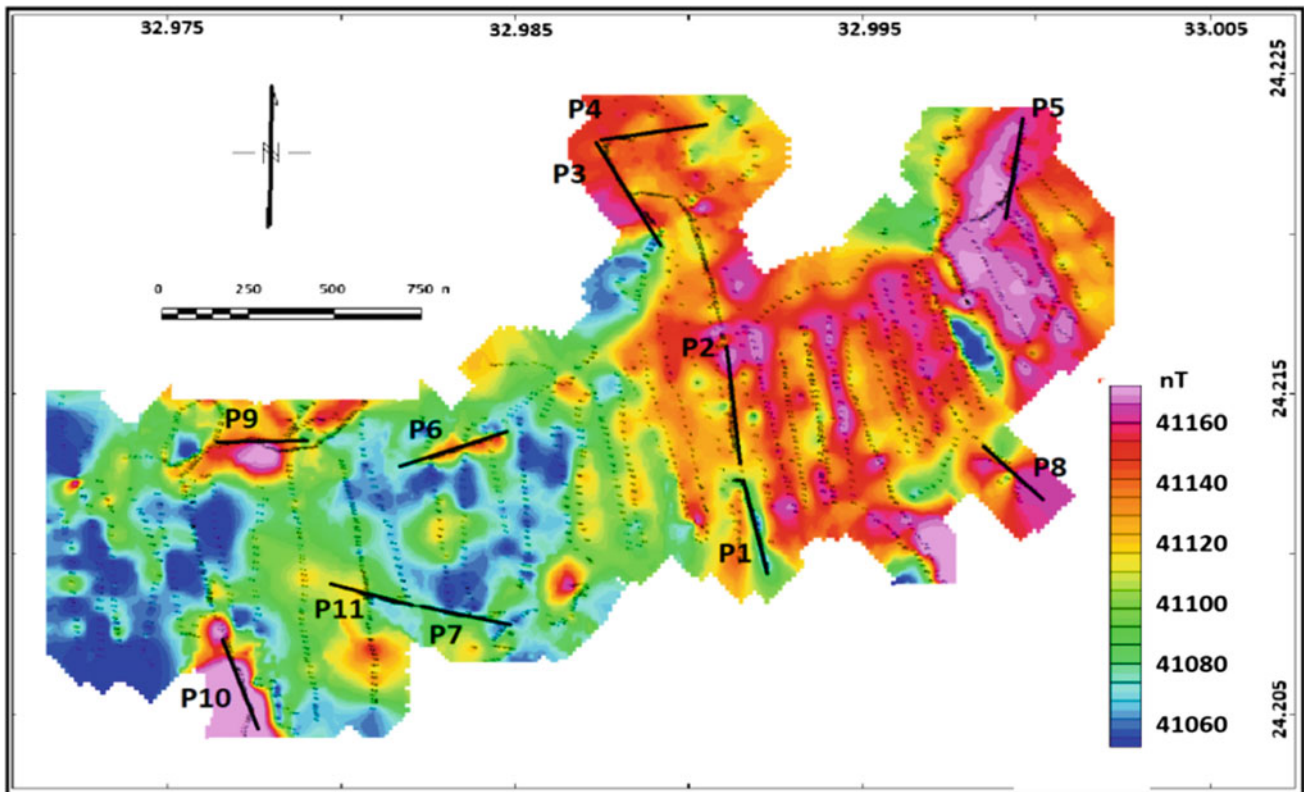


Fig. 2 The total magnetic intensity map of the Wadi Abu-Subeira area. **Black lines** designate the electrical profiles (resistivity & induced polarization)

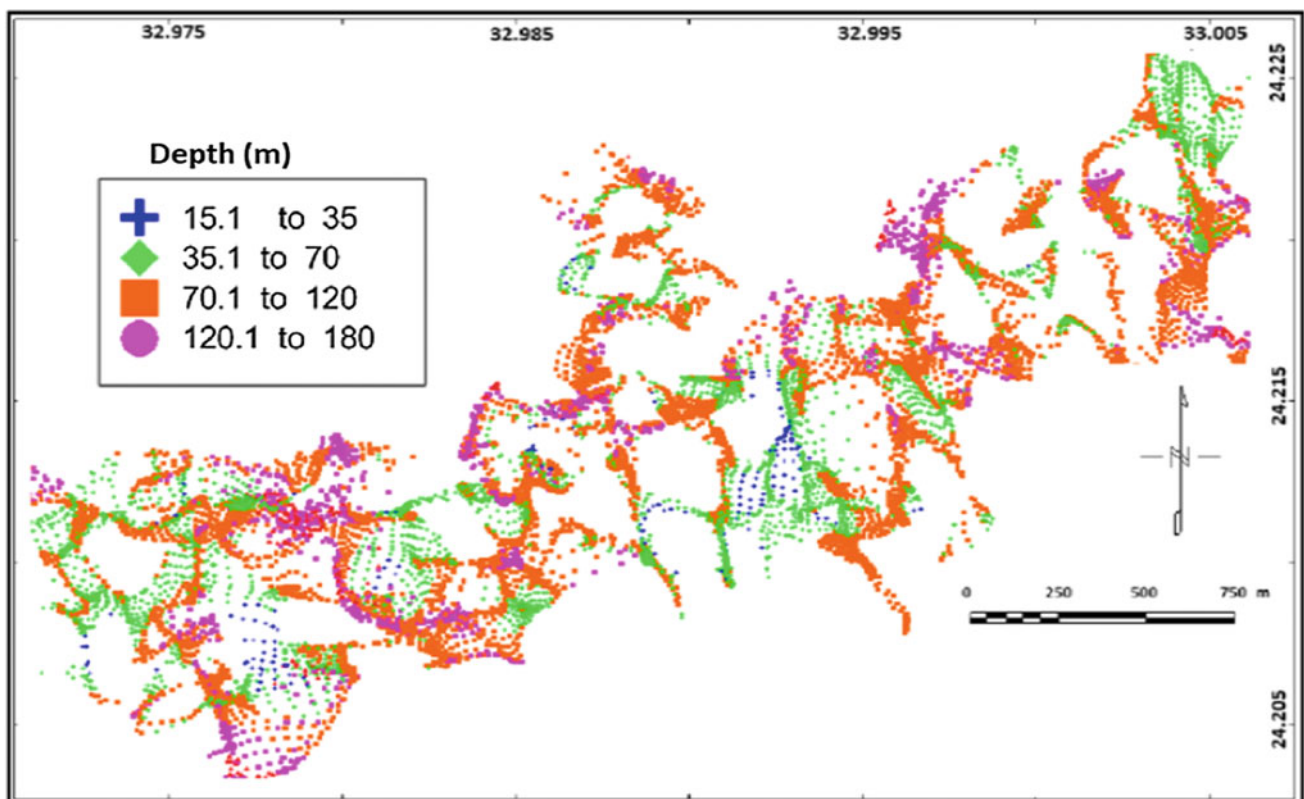


Fig. 3 The 3D-Eular deconvolution solution relevant to the Wadi Abu-Subeira area

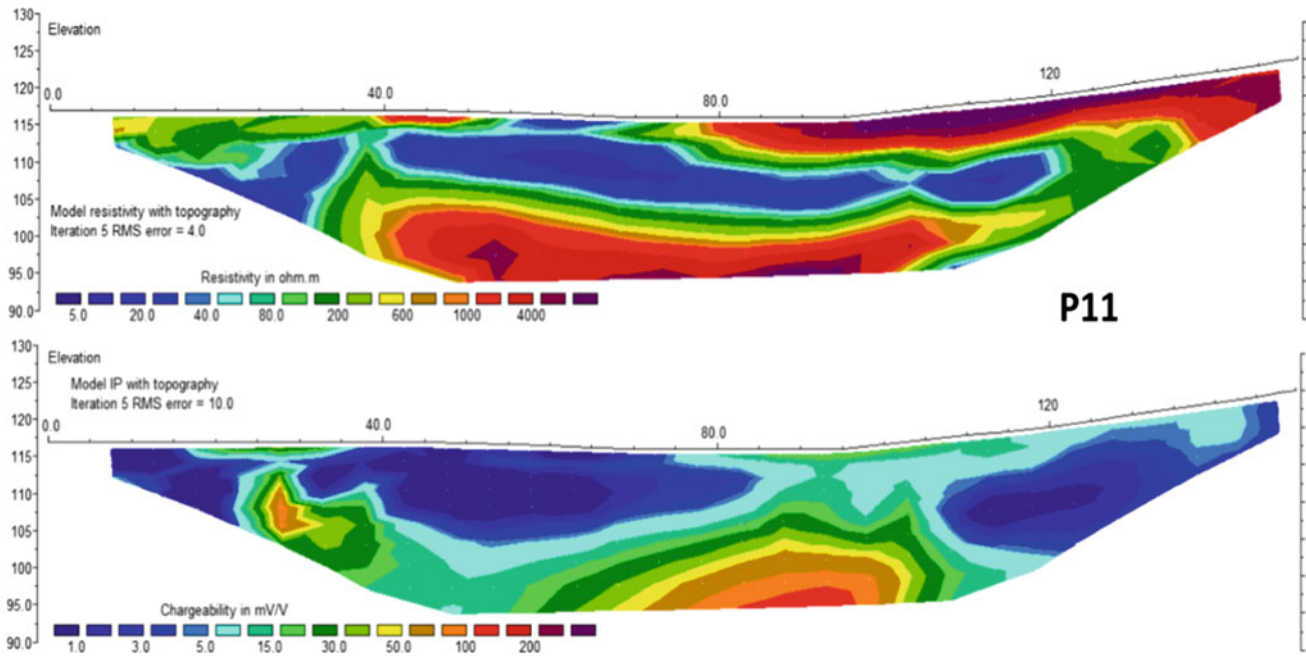


Fig. 4 Example of electrical interpretation of cross-section (P11). The Resistivity (**upper**) and chargeability (**lower**) using dipole-dipole configurations

were introduced by hydrothermal solutions migrating along these faults. As a potential study, we consider extending the same concept, and apply it to the Allaqi area, in joint combination with the magnetic, electrical resistivity and induced polarization techniques, to investigate not only the iron deposits, but also the copper and gold-ore reserves.

Acknowledgements Acknowledgement Special thanks is due to STDF (Science Technology Development Fund) for financial support economic mineral exploration of East Aswan project (ID: 25288) and providing the chance to carry out different geophysical tools. At Aswan Canter of Earthquakes, Prof. Haggag Hamed and his colleagues, gave me all support and encouragement during field work. Also many thanks to Prof. Hatem Odah, Gad El-Qady, Ahmed Saleh, Ahmed Baker, Dr. Ahmed El-Qutb, Dr. Ayman Ismail and Mr. Mohamed Kamal (NRIAG-Helwan) for helping me during research work.

References

1. Attia, M.: Topography, geology and iron-ore deposits of this district east of Aswan, Cairo: Les Editions Universitaires d’Egypt, xii, 262 p. Earth Sciences Library (Branner) (1955)
2. Google Earth. Online. Satellite image of Abu Subeira area (2011)
3. Lansbery, L.: Geological and Geomorphological Evolution of the Egyptian Nile Between Aswan and Kom Ombo: A Remote Sensing and field Study Approach. MSc thesis. Missouri University of Science and Technology, Rolla, MO, p. 83 (2011)
4. Mücke, A.: Environmental conditions in the late Cretaceous African Tethys: conclusions from a microscopic-micro-chemical study of ooidal ironstones from Egypt, Sudan and Nigeria. *J. Afr. Earth Sci.* **30**, 25–46 (2000)
5. Salem, S., El-Gammal, N.: Iron ore prospection East Aswan, Egypt, using remote sensing techniques. *Egypt. J. Remote Sens. Space Sci.* **18**(2), 195–206 (2013)

Unique PGE-Cu-Ni Oktyabr'skoe Deposit (Noril'sk Area, Siberia, Russia): New Data on Its Structure and Mineralization

Nadezhda Krivolutskaya, Maria Nesterenko, Bronislav Gongalsky, Dmitry Korshunov, Yana Bychkova, and Natalia Svirskaya

Abstract

The present work involves a study of the internal structure, rock and ore compositions of the Oktyabr'skoe deposit. Two massive orebodies, C-3 and C-4, located in the north and south of the deposit central part are related to gabbro-dolerites subdivided by the Devonian sediments in space. Despite the closely similar structure and composition of the intrusive rocks, the disseminated and massive ores prove to display different chemical and mineralogical compositions. The C-3 orebody consists mostly of tetragonal chalcopyrite and pyrrhothite, while the C-4 orebody appears to enclose sulfur-poor chalcopyrite group minerals, namely, talnakhite, putronite etc. The C-4 orebody turns out to be rich in Cu and PGE in respect of the C-3 one. This ore-associated mineralogical diversity appears to result from differing fs_2 taking place during the sulfide melts relating crystallization. It is also suggested that the orebodies, as originating from different portions of magmas, culminated in the formation of two intrusive branches.

Keywords

Noril'sk deposits • Platinum group elements • Nickel • Ore

1 Introduction

The PGE-Cu-Ni Oktyabr'skoe deposit occupies an outstanding position among the other magmatic deposits worldwide, owing mainly to its critically important economic value and unusual geological structure. It is located within the Siberian trap province. Massive sulfide ores (50 m thick) enriched in Ni and PGE are related to the thin (150 m) basic-ultrabasic Kharaelakh intrusion, which displays an irregular shape on plan in respect of the Talnakh and Noril'sk elongated intrusions. The origin of this deposit has made subject of intense discussions and debates for several decades [1–4]. Our recently obtained data concerning the deposit relating structure and mineralization has led us to conclude that the Kharaelakh intrusion proves to involve several intrusive bodies containing a wide range mineralization. This finding highlights an evidence of a rather complicated history of deposit formation with respect to the earlier suggested data provided.

2 Materials and Methods

We have undertaken to study the silicate rocks and sulfide ores, as penetrated by 12 boreholes drilled by OOO “Norilskgeologia” in 2015–2016 years in the central part of the deposit. These boreholes were dug into two orebodies, C-3 and C-4, located to the north and south of the intrusion's central part, subdivided by a block of Devonian sediments. The cores of the two boreholes (RT-30 and RT-107) were comprehensively studied. The internal structure of the intrusion was logged and sampled. The major elements in rocks were analyzed by means of XRF at IGEM RAS, while the rare elements were determined via ICP-MS sited at the Lomonosov Moscow State University. The composition of rock-formations and ore minerals have been examined by means of a Cameca SX 100 electron microprobe, as made available at the Vernadsky Institute.

N. Krivolutskaya (✉) · N. Svirskaya
Vernadsky Institute of Geochemistry and Analytical Chemistry,
Russian Academy of Science, Kosygin st., 19,
119991 Moscow, Russia
e-mail: nakriv@mail.ru

M. Nesterenko · D. Korshunov · Y. Bychkova
Lomonosov Moscow State University, Leninskie Gory 1,
119991 Moscow, Russia

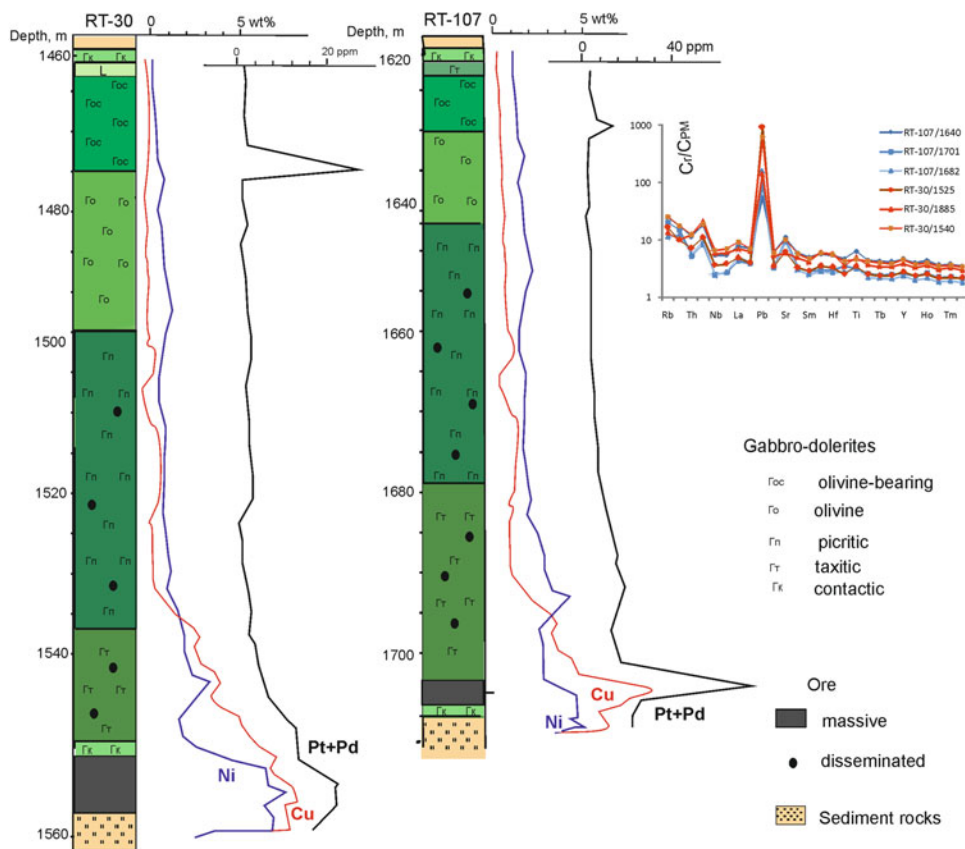
B. Gongalsky
Institute Geology of Ore Deposits, Petrography, Mineralogy and
Geochemistry, Russian Academy of Science, Staromonetny per.,
35, 119017 Moscow, Russia

3 Results

3.1 Intrusive Rocks

The intrusive rocks, as studied from the boreholes RT-30 and RT-107, are depicted in Fig. 1. Several horizons are discovered to persist inside the intrusive bodies, represented by gabbro-dolerites (from the bottom to top): contactic ($\Gamma\kappa$), taxitic ($\Gamma\tau$), picritic ($\Gamma\pi$), olivine ($\Gamma\omicron$), olivine-bearing ($\Gamma\omicron c$) and olivine-free, upper taxitic and leucogabbro (L). Overall, the intrusions' internal structure appear to be similar, except for the thickness of some horizons (mainly the taxitic). The main ore-forming minerals are: olivine FO_{82-56} , Cpx ($Mg\#86-66$), Pl (An_{82-44}), chromite, orthopyroxene. The amount of olivine and forsterite mol% proves to increase to the bottom of the intrusion. The composition of rocks' varieties (major and rare elements) are similar with respect to both boreholes, ranging from picritic gabbro-dolerites (26 wt % MgO) to leucogabbro (6 wt % MgO). The rare elements' distribution patterns in rocks are similar with regard to both cores.

Fig. 1 Structure of the intrusive bodies as penetrated by boreholes RT-30 (with massive orebody C-3) and RT-107 (orebody C-4) (a) and spider-diagrams for rocks (b)



3.2 Sulfide Ores

Two types of sulfide ores were recognized: disseminated in picritic and taxitic gabbro-dolerites and massive ore persisting in sedimentary rocks (borehole RT-30, 20 m thick) and in gabbro-dolerites (RT-107, 4 m in thick). As for the massive orebodies' chemical composition, they prove to differ (Fig. 1). The C-3 body (RT-30) is characterized with the prevailing $Cu/Ni = 1.2$ and ordinary PGE contents (12–20 ppm), while the C-4 body (RT-107) turns out to be rich in Cu, $Cu/Ni \geq 5$ and contains high platinum metal contents (up to 80 ppm). Beside the Cu-Ni ores, the intrusive rocks appear to contain low-sulfide mineralization in the upper parts of the sections (see metals peaks in Fig. 1), which stands as a typical feature characterizing high PGE concentrations and low Cu and Ni contents.

The sulfide ores' differing chemical composition is reflected in their mineral contents. The C-3 orebody and related disseminated ore prove to contain tetragonal chalcopyrite and pyrrhotite in equal proportions, while the C-4 orebody consists mainly of chalcopyrite group minerals—

talnakhite, putoranite, Ni-putoranite—and other Cu mineral species with sulfur deficit in the structure. Rare minerals for the Oktyabr'skoe deposit Cu minerals, such as bornite, chalcocite et ctr. persist in these ores as well. The C-4 orebody encloses a wide range of rare minerals, especially Pt-Pd phases (sperrylite, froodite et ctr.). This mineralogical type of ore is similar to the composition of the central part of the main orebody of the Kharaelakh intrusion (Kh-O), located to the west of the C-4 orebody. Meanwhile, the composition of the peripheral part of the main orebody appears to correlates with the composition of the C-3 orebody.

4 Discussion

The Oktyabr'skoe deposit proves to display a complicated structure and a wide range of massive orebodies. Our attained data prove to highlight a similarity characterizing the intrusive rocks and a difference concerning ore compositions characterizing two parts of the deposit. This finding suggests well that there exist two different intrusive bodies formed by two portions of silicate melt. The temporal relationships binding these bodies are unknown, due mainly to the absence of visual geological boundaries. These magma portions could well be simultaneously emplaced in the Devonian rocks from the Noril'sk-Kharaelakh fault and intrude to the west in subparallel ways. They prove to have carried away different sulfide melts: Cu-Ni and Cu-rich that have crystallized under various conditions (T , f_{S_2}). The mineralogical similarities characterizing the disseminated and massive ores provide evidence as to the accumulation of the last ones in situ, without their moving along the intrusions bottoms. Thus, the morphology of the Oktyabr'skoe deposit can be determined by a combination of several elongated intrusive branches similar to the Talnakh and

Noril'sk ones. Together, they form a triangular intrusion on the plane. Presumably, the main orebody (Kh-O) could well be made up of several parts of silicate and sulfide melts.

5 Conclusions

Our study has been conducted to demonstrate the essential differences persisting in the ore composition (orebodies C-3 and C-4) of similar silicate rocks, likely to testify the existence of two independent intrusive branches within the Kharaelakh intrusion structure. It provides evidence highlighting that the sulfides have been transported into the modern chamber by two portions of magmas, which have crystallized under different conditions (T , f_{O_2} , f_{S_2}) and formed two orebodies.

Acknowledgements The authors thanks the geologists of Norilskgeologia Ltd. V. Rad'ko, Yu. Burmistrov, V. Sitnikov for their helpful collaboration with boreholes sampling. This study was supported by RFBR (project No 18-05-70094).

References

1. Dodin, D.A., Batuev, B.N.: Geology and petrology of the Talhakh differentiated intrusions and their metamorphic aureole. In: Urvantsev, N.N. (ed.) *Petrology and Ore Resource Potential of the Talnakh and Noril'sk Differentiated Intrusions*, pp. 31–100. Nedra, Leningrad (in Russian) (1971)
2. Dyuzhikov, O.A., Distler, V.V., Strunin, B.M., et al.: Geology and metallogeny of sulfide deposits of Noril'sk region USSR. *Econ Geol. Monogr 1. Ontario. Spec. Volume* (1992)
3. Likhachev, A.P.: Ore-bearing intrusions of the Noril'sk Region. In: *Proceeding of the Sudbury–Noril'sk Symposium, Spec. vol. 5*, pp. 185–201. Ontario Geol. Surv. (1994)
4. Naldrett, A.J., Fedorenko, V.A., Asif, M., et al.: Controls on the composition of Ni-Cu sulfide deposits as illustrated by those at Noril'sk, Siberia. *Econ. Geol.* **91**, 751–773 (1996)

Micro-Geochemical Research in Mineral Exploration, Case Study of the Massive Sulfides of the Bathurst Mining Camp, Canada

Azam Soltani Dehnavi

Abstract

Geochemical exploration approaches using micro-chemical techniques are being developed in order to better enhance the understanding of mineral-chemical variations of alteration zones, as well as the effective strategies related to high depth drilling. Herein, is a summary presentation of vectoring tools as developed by Laser Ablation Inductively Coupled Plasma Mass spectrometry (LA-ICP-MS), useful for measuring fluid-mobile elements within indicator minerals of alteration haloes, as sited around the massive sulfide deposits of the Bathurst Mining Camp, Canada. Three vectoring tools, namely, white mica, applicable in proximal and distal zones, chlorite, as an effective proximal tool, and pyrite, applicable in both distal and proximal zones, are presented. The fluid-mobile dispersion patterns noticeable within chlorite, white mica, and pyrite, at the deposit scale, prove to display increasing trend with proximity to ore bodies. These approaches can be potentially applied to other VMS deposits and mineralization modes as complementary techniques.

Keywords

Chlorite • LA-ICP-MS • Micro-chemical vectoring tool • Pyrite • Volcanogenic massive sulfide deposits • White mica

1 Introduction

Mineral reserves are steadily declining, particularly in historically considered prospective regions, as traditional exploration methods have discovered most of the deposits that are either exposed or shallowly buried. Endeavoring to

make new discoveries, particularly high depth mineralization, necessitates developing novel tools, enhancing our knowledge, applying techniques in unconventional approaches, data integration, and effective communication. Geochemical approaches have been significantly improved mainly due to technological advances. Noticeable among these techniques are the micro-analytical approaches, such as the LA-ICP-MS method, subject of intense research, both in theory and application [1]. The current study related contribution consists in applying the LA-ICP-MS to measure fluid-mobile elements' suite (As, Bi, Cd, Hg, In, Ga, Ge, Sb, Se, Sn, Te, and Tl), within indicator minerals of alteration zones of volcanogenic massive sulfide (VMS) deposits, relevant to the Bathurst Mining Camp, Canada, as a novel introduction of potential micro-chemical vectoring tools for VMS exploration purposes [2].

2 Methodology and Sampling

2.1 LA-ICP-MS Systematics in Quantification of Fluid-Mobile Elements

The LA-ICP-MS technique is used for quantitative measurement of fluid-mobile elements (As, Bi, Cd, Hg, In, Ga, Ge, Sb, Se, Sn, Te, and Tl) in phyllosilicate and sulfide phases. The LA-ICP-MS associated advantages include the capability to measure a wide elemental range with good-spatial resolution sampling (<50 μm) and low detection limits (ppb level), as compared to other micro-analytical techniques, such as the EPMA. The detail of methodologies can be find in [2].

2.2 Sampling

Representative samples of the major deposits of the Bathurst Mining Camp (Brunswick No. 12 and No. 6, Heath Steele B zone, Halfmile Lake Deep zone, Key Anacon East zone,

A. Soltani Dehnavi (✉)
Department of Earth Sciences, University of New Brunswick,
Fredericton, NB E3B 5A3, Canada
e-mail: azam.soltani@unb.ca

Louvicourt, Armstrong A, and Restigouche) were selected for this study. Selection of indicator minerals was done based on the occurrence of ubiquitous minerals in the alteration zones enveloping the known VMS deposits. A generalized model [3] includes four hydrothermal alteration zones (I to IV) in the footwall (Fig. 1a, Table 1). Mineralogy of the hydrothermal alteration summarized in Fig. 1b–e for footwall zone of the Heath Steele B zone. Approaching the ore bodies, pyrite is much more abundant. Chlorite abundance increases towards the proximal zone, whereas white mica is increasingly more widespread towards the distal zones. In some deposits, continued post-ore hydrothermal activity led to extensive III and IV alteration types into the hanging wall for up to several tens of meters.

3 Results

3.1 Fluid-Mobile Element Budget of Phyllosilicates and Sulfides

Figure 2 depicts binary plots of some fluid-mobile elements as perceived in the examined phases of Restigouche deposit. Distribution of fluid-mobile elements is a mineral-specific characteristic, most likely due to structural substitution.

In the host rocks, white mica appears to contain most of the Tl, Sn, Hg, In, and Ba, while pyrite and pyrrhotite stand as the primary host for Bi, As, Sb, Se, Cd, Pb, Ni, Cu, and Co. Chlorite is enriched in Zn relative to pyrite and pyrrhotite in the host rocks (Fig. 3).

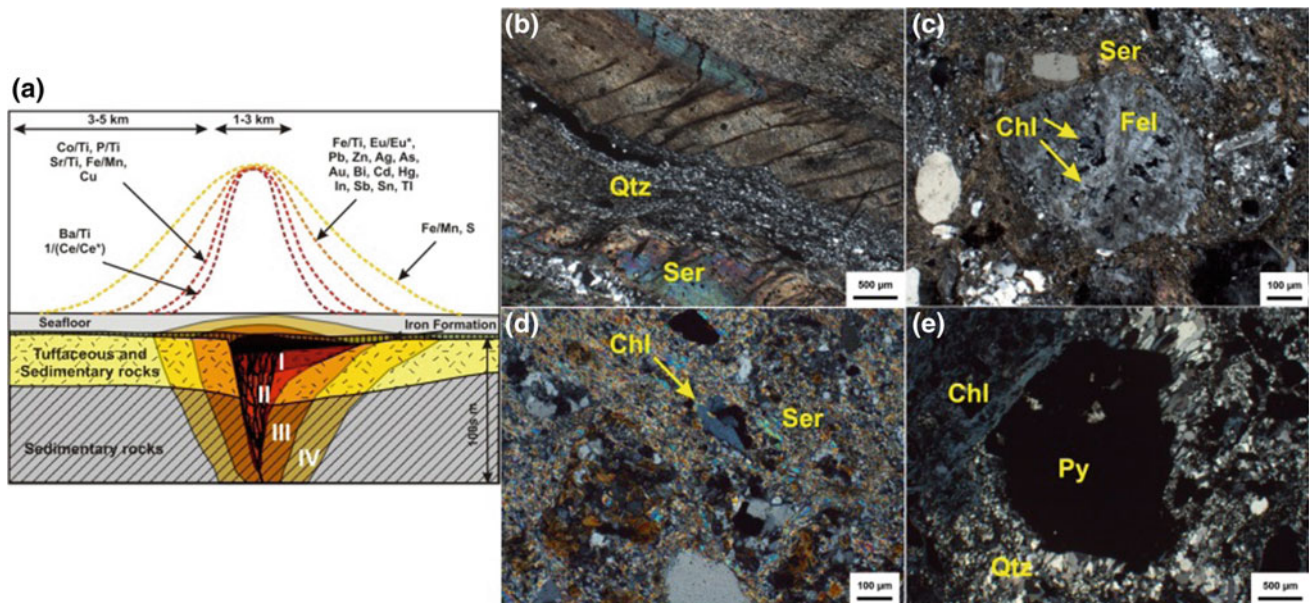


Fig. 1 a Schematic diagram illustrating the lateral extent of chemical haloes, forming different hydrothermal alteration zones surrounding the massive sulfide deposits, case of the Brunswick No. 12 deposit, BMC

(modified from [3]). The images b–e display the photomicrographs of footwall zone of Heath Steele B zone, from b to e from distal to proximal zone to ore horizon

Table 1 Summary of mineralogy of the alteration zones of Brunswick No. 12 deposit, BMC [3]

Zone I (silica alteration zone)	Fine-grained milky quartz (40–90%), Fe-rich chlorite (3–15%), carbonate (5–12%) and variable sericite (10–12%), and sulfides (5–25%)
Zone II (potassic alteration zone)	K-feldspar (5–25%), Fe-rich chlorite (3–10%), sericite (10–55%), minor quartz (10–15%), and sulfides (5–10%)
Zone III (Na-Mg alteration zone)	Sericite (30–60%), Fe-Mg-chlorite (15–60%), albite (5–20%), and subordinate sulfides (0–15%)
Zone IV	Albite (30–70%) and Mg-rich chlorite (40–50%)

Fig. 2 Binary plot of Tl versus **a** Sb and **b** Sn for phyllosilicates and sulfides of Restigouche and sulfides of Restigouche deposit, BMC

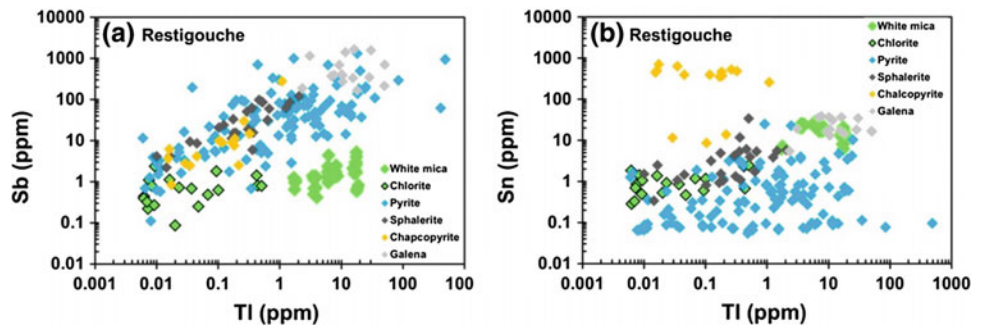
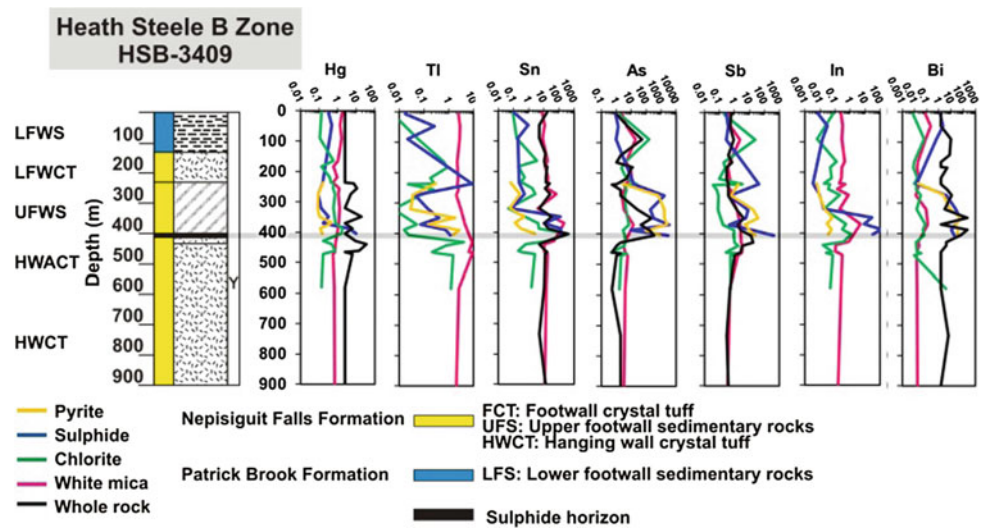


Fig. 3 LA-ICP-MS integrated geochemical data profiles illustrating representative mean elemental concentrations (in ppm) of sulfide minerals (blue line), pyrite (orange line), chlorite (green line), and white mica (pink line) (also, the black line represents the whole-rock data), plotted with respect to stratigraphic profile of Heath Steele B Zone deposit along drill hole HSB 3409 [4]



4 Discussion

Systematic spatial variation in the fluid-mobile element concentrations among phyllosilicates (white mica and chlorite), as well as sulfides (pyrite and pyrrhotite) in the footwalls and hanging walls of VMS deposits constitutes the basis of a micro-chemical vectoring tool proposed in this study. The multiple mineral vectoring tools presented in this context appear to reveal increasing pattern of fluid-mobile elements with proximity to the ore bodies. The Sn and In, as well as Zn and Mn contents of chlorite are potential indicators for the persistence of ore bodies. In the distal zones (along, below or above strike), the sulfide horizon (several hundred meters from the ore), subtle increases in Tl, Sb, Sn, and Hg within white mica is probably related to the presence of sulfide at depth. Proportion of pyrite incrementally increases towards the ore horizons. Besides, the increasing patterns of Tl, Sn, Sb, In, and Bi advocate the dispersion patterns noticeable in chlorite and white mica.

5 Conclusions

The sign of fluid-mobile elements within phyllosilicates and sulfides of alteration haloes as related to recognized VMS deposits of the BMC provide valuable vectoring tools. It constitutes a pilot study that helps in revealing valuable geochemical information locked in the indicator minerals. Such micro-chemical vectoring tools can potentially serve as complementary methods to other geochemical and geophysical exploration techniques in prospecting buried VMS mineralization and other mineralization modes.

References

1. Cook, N.J., Ciobanu, C.L., George, L., Zhu, Z., Wade, B., Ehrig, K.: Trace element analysis of minerals in magmatic-hydrothermal ores by laser ablation inductively-coupled plasma mass spectrometry: approaches and opportunities. *Minerals* **6**, 111 (2016)

2. Soltani Dehnavi, A.: Volatile-Element Signature of Volcanogenic Massive sulfide Deposits in the Bathurst Mining Camp, New Brunswick, Canada, 615 p. Ph.D. thesis, The University of New Brunswick, Fredericton (2017)
3. Lentz, D.R., Goodfellow, W.D.: Character, distribution, and origin of zoned hydrothermal alteration features at the Brunswick No. 12 massive sulfide deposit, Bathurst Mining Camp, New Brunswick. In: Abbott, S.A. (ed.) Current Research, New Brunswick Department of Natural Resources and Energy, Minerals Resources, Information Circular 94-1, pp. 94–119 (1994)
4. Lentz, D.R., Hall, D.C., Hoy, L.D.: Chemostratigraphic, alteration, and oxygen isotopic trends in a profile through the stratigraphic sequence hosting the Heath Steele B zone massive sulfide deposit, New Brunswick. *Can. Mineral.* **35**, 841–874 (1997)



Gold Metallogeny of the Egyptian South Eastern Desert

Basem Zoheir, Ashraf Emam, Nehal Soliman, and Astrid Holzheid

Abstract

The South Eastern Desert, is the northern part of the Nubian Shield, characterized by abundant ophiolites, extensive high strain zones, and a multilayered structural architecture. Gold mineralisation is related to discrete occurrences of mesothermal quartz \pm carbonate veins (< 100 m-long), cutting dismembered ophiolites and schistose metasedimentary-metavolcanic rocks. Though generally controlled by shear/fault zones, the mineralized quartz veins display a spatial association with granitoid-gabbroid intrusions exhibiting signs of forceful emplacement into the country rocks. In the areas where no intrusions are exposed, rhyolite and dacite dykes or granophyre sills appear to cut the structural trend in the host rocks and control the mineralized quartz veins. K-metasomatism is conspicuously associated with gold lodes, despite the variability of the host lithologies. Most of the mineralization is related to visible free-milling gold/electrum inclusions persistent in arsenopyrite or along pyrite fractures and grain boundaries, with subordinate invisible gold in As-pyrite. The mineralogy, fluid inclusions and stable isotope characteristics of several deposits in the region prove to reveal similar mineralization styles, ore fluids and isotope signatures, suggesting inherent similarities in the deposition process, fluid source and likely in the gold introduction related timing.

Overheating by thrusting and concomitant calc-alkaline magmatism, along with metamorphic dehydration and devolatilization promoted the circulation of hydrothermal fluids in a metallogenically fertile, mafic crust and deposited gold in accretionary and transpressional structures.

Keywords

Gold metallogeny • Structural control • Genetic aspects • South eastern desert • Egypt

1 Introduction

The structural architecture of the SED comprises three main high strain systems [1, 2]. The WNW-ESE, Allaqi-Heiani fold-and-thrust belt (AHS; \sim 250 km-long, 40 km-wide) is part of the major Allaqi-Heiani-Onib-Sol Hamed Suture, which was formed at ca. 730–700 Ma [3] by progressive folding, thrusting, refolding, and transpressional/transensional shearing during the N-S terrane accretionary regime. A post-accretion, E-W shortening regime led to the formation of the N-S Hamisana shear zone (HSZ; 660–550 Ma) [4] that deformed the pattern and dislocated the strike of the accretion-related structures. In the calc-alkaline emplacement, volcanic arc granitoid intrusions was coeval with the early folding in an intra-arc environment. Subsequent to the east-west compression, non-coaxial convergence and northward escape tectonics manifested in the NW-SE Wadi Hodein-Rahaba shear zone (HRSZ). The latter is considered as the most conspicuous sinistral shear/fault zone in the Eastern Desert, likely developed synchronous with the activity of the NW-SE Najd fault system in the Arabian Shield (655–540 Ma [5]).

In the SED, nearly 30 gold occurrences appear to be confined to the shear zones, commonly where early and late structures prove to overlap (see Fig. 1). Gold mining in this district was intermittently active over the last 3600 years, but

B. Zoheir (✉)

Department of Geology, Faculty of Science, Benha University, Benha, 13518, Egypt
e-mail: basem.zoheir@gmail.com

B. Zoheir · A. Holzheid

Institute of Geosciences, University of Kiel, Ludewig-Meyn Str. 10, 24118 Kiel, Germany

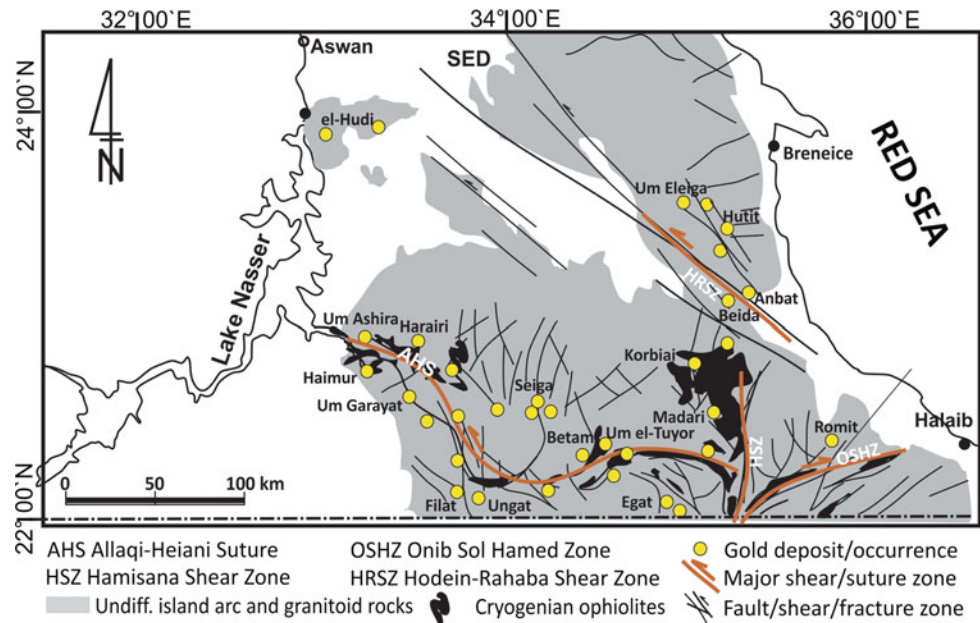
A. Emam

Geology Department, Faculty of Science, Aswan University, Aswan, 81528, Egypt

N. Soliman

National Authority for Remote Sensing & Space Sciences, Cairo, 1564, Egypt

Fig. 1 Simplified geomap of the major deformation systems in the South Eastern Desert



mostly abandoned since the early 20th century. The area is now witnessing a rush in small-scale mining by local people and new non-professional miners, and steps are taken to attract international companies. Hence, the actual need for incorporating new explicit structural models into an ample geological understanding to optimize exploration, development and production.

2 Methods

A review of published and new field observations, petrographic studies, microchemical and isotope data is attempted to reveal the structural control and genesis of auriferous quartz veins lying in the South Eastern Desert. The application of image processing techniques on satellite imagery data helped in featuring the setting of Au mineralization relevant to the regional geological and structural evolution.

3 Gold Mineralization Style and Controls

3.1 The Hodein-Rahaba Shear Zone

The gold-bearing quartz veins lying across the Wadi Hodein-Rahaba shear corridor are confined to steeply dipping, sinistral strike-slip faults and shear zones, stretching near contacts between ophiolitic and island arc rocks, i.e., Wadi El-Beida, and Wadi Khashab [6, 7]. Attenuation and wrapping of the host shear zones around rigid metabasalt/metagabbro masses (e.g., Beida and Hutit mines) resulted in pinch and swell structures, which served as loci for quartz

and quartz-carbonate veins. A continuous deformation following vein formation is distinguished from the undulatory shear fabrics and through the variable degrees of quartz recrystallization and granulation. In the tuffaceous and agglomerate host rocks, heterogeneous strain resulted in the formation of distortion and dilation zones. In the Anbat mine, gold-bearing quartz veins prove to cut a wide (~ 200 m) transpressional contact zone between carbonized serpentinite and highly deformed metavolcaniclastic rock, where the latter appear to be cut by aplite dikes and granitic porphyries.

Extensive zones of sericite, iron oxide and clay mineral alteration in the area delimit NNW-SSE high-order shears of the major Wadi Khashab fault in the deformed metatuffs and agglomerates, where granophyre dikes and quartz pockets are abundant.

3.2 The Hamisana Shear Zone

Asymmetric isoclinal, mostly tight, folds intersect cleavages and wedged quartz pods and lenses in addition to high angle reverse ductile-brittle faults, lying everywhere, especially where old gold-mining works are located, and stand as a strong evidence for structural control of gold in the Hamisana structure. Variable deformation of gold-bearing quartz veins, as stretching along the shear zones, may well testify their formation during a long-lived terrane convergence regime.

The geology, mineralogy and geochemistry of mineralized veins in the Romite, Korbai and Madari gold deposits emphasize their orogenic style and reveal their spatial and

temporal relationships with the NNE- and NNW-trending shear zones. Gold deposits occur in the marginal zones of high-topography terranes, commonly related to complex structures. The isotope data of the Romit and Korbai deposits highlight overlap with metamorphic or mixed metamorphic and meteoric fluids [8, 9].

3.3 The Allaqi-Heiani Belt

Gold mineralization in the Allaqi Heiani belt is related to ductile-brittle shear zones lying in the ophiolitic or island arc terranes. These shear zones cut either carbonaceous ophiolites/pelitic metasedimentary, or volcanoclastic rocks with or without granitic dikes (e.g., the Um El-Tuyor, Betam, Seiga, Shashoba, and Haimur deposits). Gold-bearing quartz veins lying along the main structural trend of the AHS are observed in the metagabbro-diorite complex terranes, where kaolinite and carbonate alterations are witnessed.

In the metavolcanic/volcanoclastic terranes, where the gossan alterations and magnetic anomalies highlight well the persistence of buried massive sulfide ores, gold turns out to be either commonly enriched in the iron-oxide cap zone, or associated with listvenite bodies lying next to folded ophiolites.

4 Discussion and Conclusions

Gold mineralization persisting in the SED is clearly of orogenic style, most likely deposited from carbonic-rich metamorphic fluids. The carbon and oxygen isotope data of hydrothermal carbonate, as persistent in quartz veins, suggest the availability of mixed metamorphic and mantle-derived fluids (Fig. 2). As most of the mineralized structures are discovered to be of high-order accretionary and post-accretionary fabrics, it is assumed that overheating subsequent to the termination of collision and crustal

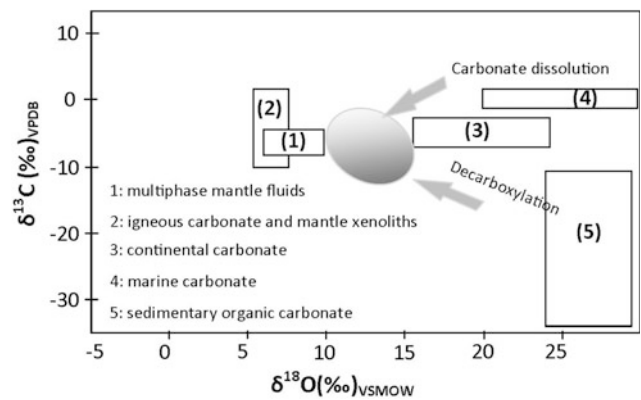


Fig. 2 $\delta^{13}\text{C}$ ‰ versus $\delta^{18}\text{O}$ diagram for hydrothermal carbonate from Romit, Um Garayat, Qurbiai, Eleiga, and Betam deposits in SED (grey ellipsoid). For field references see [10]

thickening led to the fluids infilling extension fractures forming auriferous quartz veins.

Potentially structural analyses, mineralogical and isotopic studies would help noticeably in identifying new target areas and increasing the estimated resources. The greenschist facies shear zones, with variable orientations and lithological contacts, lying close to the major seals, should be assigned the highest priorities. Such an undertaking should entail a new industry-supported reconnaissance and assay program.

References

1. Greiling, et al.: *Geol. Rundsch.* **83**(3), 484–501 (1994)
2. Abdelsalam, et al.: *Precamb. Res.* **124**, 87–104 (2003)
3. Ali, et al.: *Gondwana Res.* **18**, 583–595 (2010)
4. Stern et al.: *J. Geol. Soc., London* **146**, 1017–1029 (1989)
5. Stern, R.: *Tectonics* **4**, 497–511 (1985)
6. Zoheir, B.: *J. Geochem. Explor.* **111**, 23–38 (2011)
7. Zoheir, B.: *J. Geochem. Explor.* **114**, 82–97 (2012)
8. Zoheir, B.: *Geosci. Front.* **3**(5), 571–585 (2012)
9. Zoheir et al.: *Mineralium Deposita* (2018). <https://doi.org/10.1007/s00126-018-0807-3>
10. Niu, J.: *Ore Geol. Rev.* (2017). <https://doi.org/10.1016/j.oregeorev.2017.10.016>

Geology, Petrography, and Mineral Chemistry of the Zn Pb-Cu-Sulfide Deposits of the Filfila Massif (East Algeria)

Touati Lyes, Kolli Omar, and Boutaleb Abdelhak

Abstract

The Filfila Massif consists of four stacked tectonic units, which are superimposed on a metamorphic basement. The Filfila metasomatic-type polymetallic deposit of the Northeast crosscut the tectonic units of the Filfila and the proximal granites. The deposits consists of lead and zinc mineralization associated with iron oxides, hydroxide and accessory minerals. To highlight the mineralogical, petrographical and geochemical characteristics of the deposit, several methods have been combined: Microscopic observation, XRD diffractometry, XRF spectrometry, scanning electron microscopy with energy-dispersive X-ray spectrometry (SEMEDS) and fluid inclusion microthermometry. Field observations and Analyses indicate that the orebody in Filfila displays a complex geometry. The shows are located in the limits of the thrust sheet structure within the metamorphic basement that plunges eastward at about 20°–30°. The veins range between 60 m and 1000 m lengths and from 10 cm up to 3 m in the thickness. The strikes follow the same directional trend (E-W) as the Filfila granites, and are steeply dipping 60°–80°. Ore minerals include quartz, fluorite, barite, galena, sphalerite, copper sulfides, sulfosalts and oxides. The deposit turns out to be closely associated with to the Miocen post-orogenic Filfila granite.

Keywords

Lead and zinc deposit • Miocene • Filfila • Granite • Fluid inclusions

1 Introduction

The Filfila zinc and lead polymetallic deposit is situated in the eastern part of the filfila mountain, northeast Algeria, distant about 350 km from the capital city and 20 km east of the Skikda city. The central point of the deposit is located in the following geographic coordinates: 36°54'30.76"N and 7°8'10.29"E. The deposits are of great economic importance and have protracted history. The site was mined as early as 50 B.C. by the romans, then, from 1882 to 1942 under the French occupation. In 1969. The ore resources were estimated by the Algerian mining company to amount to 87,000 tons, with grades of 3.4% Pb, 12.30% Zn, 0.37% Cu and 8.1 g/t Ag.

In geological terms, the Filfila Massif corresponds to an east-west elongate granitic body, located in the eastern part of the Lesser Kabylia Massifs. This region of lesser Kabilian zone is characterized with a southward-directed overthrusting of the Kabylia basement rocks onto the Tellian areas, caused by the alpine orogeny as occurring during the Miocene. The Filfila massif is represented by the stacking of four tectonic units described, from bottom to top, as follows (Perrin 1969; [1, 2]): a para-autochthonous unit, a metamorphic unit and its Tertiary cover, a shale—sandstone unit and an upper Numidian sandstone unit. The last unit is intruded by Miocen granite.

The main objective of this paper is to characterize the site relating lead and zinc mineralization. More particularly, the following aspects will be reviewed. In a first place, a systematic description of geology and mineralization will be presented. In a second place, the bulk chemical composition of the ore, properties and evolution of ore formation fluids will be determined by means of microthermometry. Finally, a clear constraint on the genesis of the deposit and a possible mineralization model are provided.

T. Lyes (✉) · K. Omar · B. Abdelhak
Laboratoire de Metallogenie et Magmatisme de l'Algérie, Earth
Science Department, FSTGAT - USTHB, B.P. 32 El Alia 16.111,
Algiers, Algeria
e-mail: lyes.touati2@gmail.com

2 Materiel and Methods

More than 150 hand specimens representing the polymetallic zinc and lead ores and different host-rock types were collected from the outcrops of the Oued Meçadjet and Oued Saboune vein-type deposits. The most representative samples in terms of mineralogical association and structure were selected to prepare polished thin sections, polished sections for petrographic observations, Scanning Electron Microscopy with Energy Dispersive Spectroscopy. After cleaning the altered surfaces and the secondary veins, the selected ore samples were finely crushed using an agate mortar for chemical and mineralogical analysis.

Samples for fluids inclusion were collected from quartz-fluorite-sulfide veins and tailing. Unfortunately, fluid inclusions in quartz associated to the hydrothermal event appear to be too small to be used in this study. After petrographic observation, five (05) representative double-polished thin sections were selected for microthermometric measurements. The sample selections were administered at the Department of Geology (LMMA, USTHB), and the microthermometric measurements were accomplished at the economic geology laboratory of the kyushu university, using the Linkam heating-freezing stages of a NIKON microscope. The precision of temperature measurements on the homogenization temperatures (T_h) and halite dissolution temperatures (T_s) were conducted in the heating/freezing stage at ± 2 °C within the 150–400 °C interval.

3 Results

3.1 Mineralogy, Petrography and Paragenesis

Petrographical and mineralogical observations on thin sections, polished sections and SEMEDS appear to display three assemblages, gangue minerals, three-ore mineral stages and alteration assemblage.

The ore-hosting rocks include the metamorphic basement and partially the para-autochthonous cover. It consists mainly of Filfila schist rocks and limestones which are observed in the eastern part of the study area, in association with satin-schists and greyish-schists and finely crystalline hornfels.

Polymetallic mineralization occurs mainly within several generations of quartz followed by sulfides. In both zones, the Oued Saboune and Oued Meçadjet veins, the mineral deposition sequence reveals three successive stages, (i.e., stages I, II and III).

Overall, sphalerite is the dominant mineral, occurring in the form of dissemination or massive aggregates, is always associated with quartz and fluorite as gangue minerals.

In general, sphalerite is intergrown with chalcopyrite, arsenopyrite, quartz ad fluorite in the massive aggregates, whereas the fine-grained sphalerite is more commonly associated with galena in the banded ore. The Galena is associated with the sulphides formed earlier and the specular hematite persists in the form of needles cemented by quartz or pyrite, while the arsenopyrite is present as idiomorphic crystals in inclusion in sphalerite and chalcopyrite. Titanium oxides and bismuth were detected only by SEM-EDS as trace elements as an inclusion in hematite and pyrite.

3.2 Fluids Inclusions

Abundant fluid inclusions have been observed in hydrothermal minerals. The number of fluid inclusions as investigated in the fluorite crystals can reach up to 1000 in every square millimeter. Based on the definition of Bodnar [3], the individual, isolated inclusions and random groups of inclusions in fluorite crystals are assumed to stand as primary in origin, while those aligned along micro-fractures or intersecting several grains have been designated as secondary. All the observed inclusions are two-phase inclusions in type, with liquid content associated with a gas bubble, with sizes generally less than 35 μm . The vapor-liquid ratios, visually estimate, vary from 10 to 20% by volume and do not display any significant variations.

The freezing temperatures of the fluid inclusions range between -52.5 and -59.1 °C. The temperature of first melting, when recognized, is always between -20 and -18 °C, suggesting low concentrations. The ice-melting temperatures range between -0.3 and -14.8 °C with a mode of -13.6 °C. The data obtained by means of microthermometric measurement, relevant to 68 single fluid inclusions on fluorite crystal, are depicted in the plot Fig. 1.

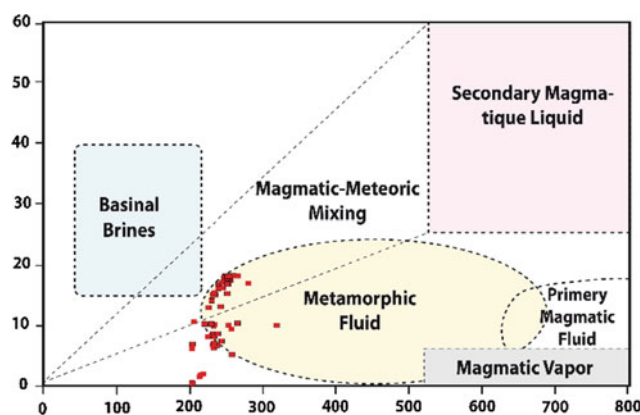


Fig. 1 Plot of homogenization temperature versus salinity for fluid inclusions from the Filfila polymetallic deposit (from Beane 1983)

4 Discussion

Petrography and paragenesis: Although the three polymetallic-mineralization stages prove to exhibit similar mineral assemblages, they are distinguishable by macroscopic and microscopic textures and transverse relationships. Stage i: the “pre-ore stage” is the earliest stage; the mineral paragenesis consists mainly of quartz, hematite, pyrite and rarely sphalerite. Stage ii: the “ore stage” or epithermal polymetallic mineralization, which consists mainly of a sulfide association with a second generation of quartz related to abundant sphalerite, hematite, pyrite, chalcopyrite, galena, chlorite and fluorite. Stage iii: the “supergene stage”, it is the last stage of mineralization. All minerals contain limonite as secondary replacements, which was formed during the weathering of supergene and weathering. They appear in the form of irregular proliferations of iron oxide.

Fluid inclusions: The homogenization temperatures were comprised within the interval of 230–260 °C, with a median of 245 °C. The salinity of fluid in the main ore stage is calculated in terms of the R.J. BODNAR equation [3]. It is ranged between 0.53 and 18.47 wt% NaCl eq with a median of 14.3 wt% NaCl eq. abnormally low and high values, represent 5% of the studied statistical population. Those abnormal measures are probably related to the nicking-down or bowling phenomena.

5 Conclusions

In sum, the tectonic position appears to demonstrate that the mineralization is post Lutetian, as it proves to cross the tectonic units of filfila, clearly post-dating the thrust tectonics

of the Lutetian [4]. The veins display a strong structural control, as manifested in the subvertical fractures oriented N-E, which follow the same trend as the Filfila granites.

The deposit also exhibits a polyphased metallogenic event, manifested in the three mineralization phases. The formation of this epigenetic mineralization is associated with a medium and high-temperature fluids, and probably deposited from the melting of magmatic-meteoritic mixing brines and metamorphic fluids.

References

1. Lemoy, C.: Stratigraphie des Unités Allochtones: Structures et Métamorphisme du Massif. Thèse 3ème Cycle, Univ., Nancy (1969)
2. Ouabadi, A.: Pétrologie, géochimie et origine des granitoïdes peralumineux à cordiérite (Cap Bougaroun, Beni Toufout et Filfila), Algérie Nord-Orientale. Thèse, Univ. USTHB (1994)
3. Bodnar, R.J.: Introduction to aqueous fluid systems. In: Samson, I., Anderson, A., Marshall, D. (eds.) Fluid Inclusions: Analysis and Interpretation. Mineral Assoc, Canada, Short Course. vol. 32, pp. 81–99 (2003)
4. Raoult, J.F.: Géologie du centre de la chaîne numidique (Nord du Constantinois, Algérie). Mem. Soc. Géol., France, 53/121 (1974)
5. Chaa, H., Boutaleb, A.: Mineralogical and geochemical characteristics of the Zaccar Fe-(Ba-Pb-Zn-Cu) deposit in Ain Defla, Algeria (Northwestern Algeria). Arab. J. Geosci. (2016)

Reef Cenomanian Carbonate Hosted Fluorite Ore Deposits at Jebel Mokta, Northeastern Tunisia

Bejaoui Jaloul

Abstract

The Cenomanian limestone-hosted Fluorite deposit of Jebel Mokta is located in the north east of Tunisia, 35 km SE the capital city Tunis. This deposit occurs in the form of open-space fillings and veins hosted in the upper Cenomanian reef limestone. In the present paper, field work, petrography and microthermometric studies of fluid inclusions were implemented to characterize the relevant fluid mineralization aspects. The relating data proved to indicate that primary fluid inclusions persistent in the fluorite appear to display homogenization temperatures ranging between 124 °C and 135 °C. The fluid inclusions salinities ranging from 15 wt% NaCl equiv to 18 wt% NaCl equiv. The homogenization temperatures of primary fluid inclusions in calcite turn out to range between 9 and 5% NaCl equiv and 13 wt% NaCl equiv. Such features could well stand as a microthermometric evidence for the mixing of two fluids with different temperatures and different salinities. Mineralization is spatially and, possibly, genetically related to the NE-SW and E-W-trending fractures, which acted as conducts and/or depositional sites for the circulating hydrothermal fluids. The fluorite deposit is considered to have be formed from basinal fluids, and has been compared to Mississippi Valley-type.

Keywords

Jebel mokta • Cenomanian • Fluid inclusions • Mississippi Valley-type • Tunisia

1 Introduction

In Tunisia, the fluorite deposits are well known as a province hosted by Jurassic limestone [1–3]. Differently, however, the Jebel Mokta fluorite deposits, located in the northeast of Tunisia, (Fig. 1), prove to display deposits that were hosted by upper Cenomanian reef limestone, as initially described by Sainfeld et al. [4]. The sedimentary section is made up of carbonates and shale rocks, ranging in age from the Lower Cretaceous to the Eocene age. Rudist and corals predominantly constitute the main limestone facies. With a thickness of about 15 m, the Cenomanian reef limestone reflects that shallow-water carbonates were deposited during the moderate period.

The deformed Cretaceous sequences of Jebel Mokta prove to be affected with abundant N-S to E-W faults. Mineralization occurs in the form of karst, veins and massive ore bodies persistent in the Cenomanian reef limestone, and are composed of fluorite and minor celestite minerals.

2 Materials and Methods

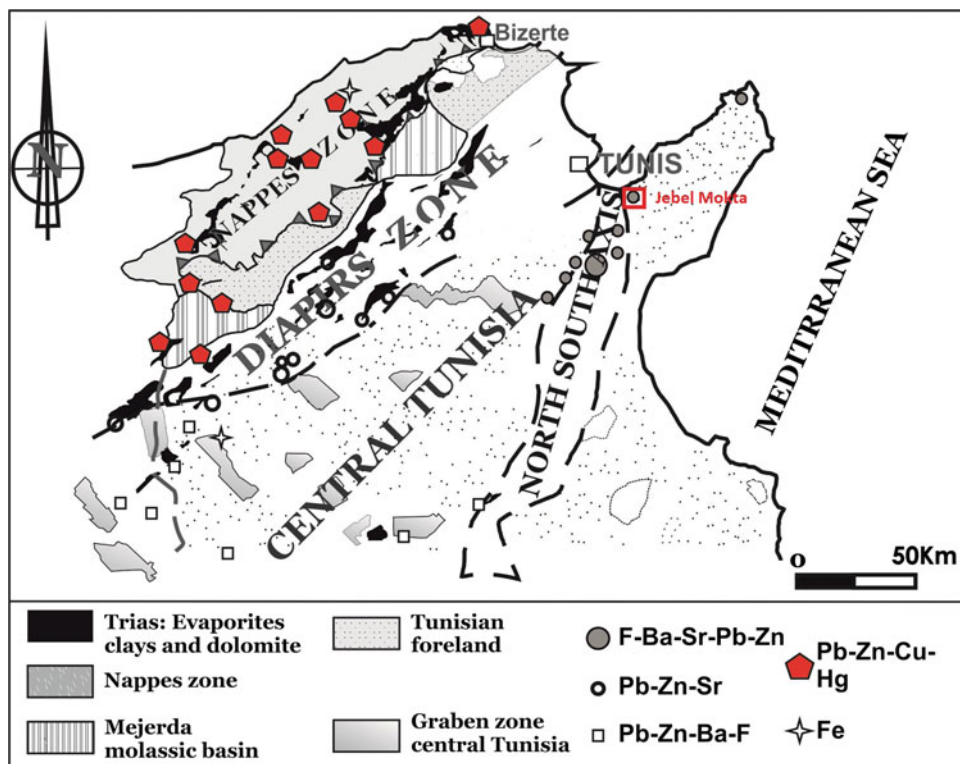
Fluorite and calcite samples of karst and vein materials were prepared for fluid-inclusion investigations, implemented by means of microthermometry and fluorescence microscopy. Microthermometric characterization of fluid inclusions was performed on 250 µm thick doubly polished. Fluid inclusion, ice melting and homogenization temperatures were measured on a Linkam MDS-600 heating-freezing stage.

3 Petrography and Fluid-Inclusion Microthermometry Results

The fluorite deposit is hosted by Cenomanian reef limestone, karst and veins. Mineralization consists mainly of epigenetic fluorite with minor celestite and calcite. The ore bodies occur

B. Jaloul (✉)
UR-MDTN National Center of Nuclear Sciences and
Technologies, Sidi Thabet, Tunisia
e-mail: bjaloui_geo@yahoo.fr

Fig. 1 Location of the study area and the Pb-Zn deposits, on the Structural units of Central-North Tunisia and related Pb-Zn ore deposits [2]



in the form of massive to discordant lenses, filling caves and fractures in limestone.

The data relating to the primary fluid inclusions' petrography turn out to be biphasic (L + V) at room temperature, with sizes ranging between 10 μm and 300 μm that occur either grouped or isolated, displaying smooth to irregular shapes (Fig. 2a). They are liquid-rich, with a small vapor bubble filling 5–10% of the inclusion volume.

The microthermometric measurements, as derived from the fluorite-hosted fluid inclusions, are illustrated in (Fig. 2b). All primary inclusions were homogenized to the liquid phase at temperatures ranging from 124 $^{\circ}\text{C}$ to 135 $^{\circ}\text{C}$. The salinity rates appear to range from 15 wt% NaCl equiv to 18 wt% NaCl equiv, with a mean of 16 wt% NaCl equiv.

The calcite (gangue mineral) primary fluid inclusions were homogenized to the liquid phase at temperature ranging from 65 $^{\circ}\text{C}$ to 100 $^{\circ}\text{C}$, and salinities varying from 9.5 wt% NaCl equiv to 13 wt% NaCl equiv (Fig. 2b).

The administered petrography proved to reveal the persistence of several Hydrocarbon Fluid Inclusions (HCFI), with sizes close to 100 μm .

The fluid-inclusion assemblages selected for conducting the study are primary (Fig. 2c). Fluorite HCFI are spatially separated by approximately 100 micron.

The Raman spectrometry and fluorescence of hydrocarbon fluid inclusions appear to confirm that the green-blue-white inclusion assemblage proves to contain much lighter oil (Fig. 2d).

4 Discussion

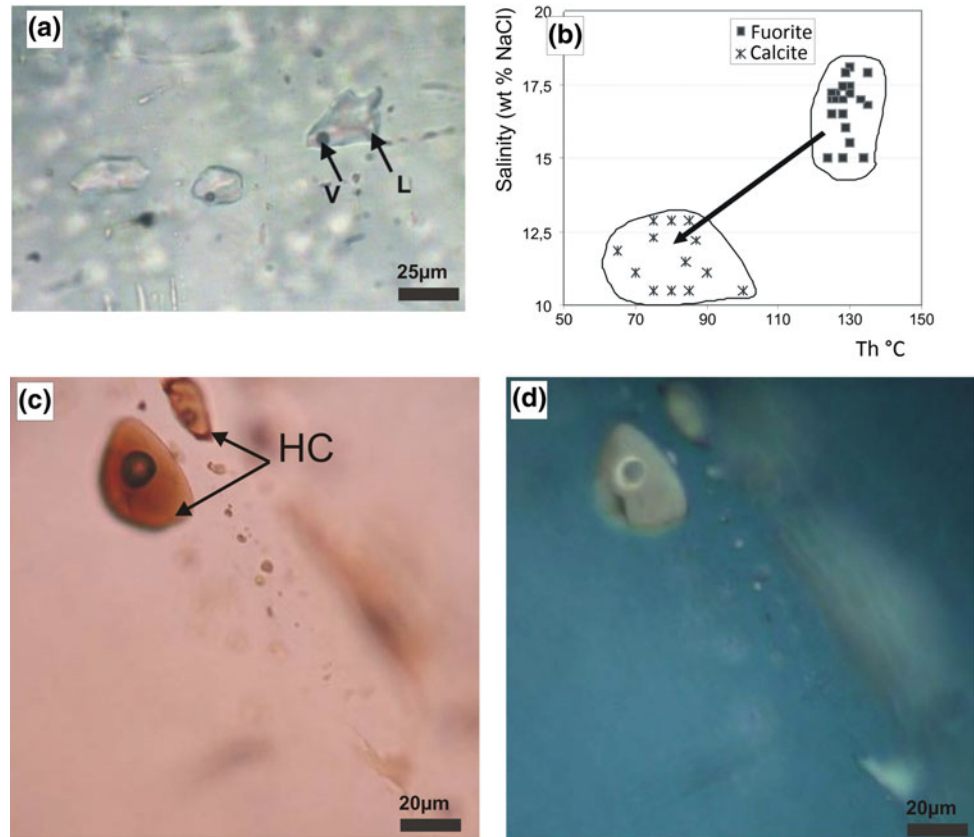
The reached microthermometric data appear to suggest that brines, as involved in the fluorite deposition, were characterized with high temperature and high salinity rates. The joint mixing of two fluids proves to yield fluids of high temperatures and salinities, as depicted in the salinity-homogenization temperature diagram (Fig. 2b). The hydrothermal fluids are characterised with the presence of divalent cations other than Na^+ in the hydrothermal system, such as Ca^{2+} and Mg^{2+} . The observed results prove to highlight that, as a major mechanism for cavity formation and mineral precipitation is the mixing of two hydrothermal fluids of different chemistry saturated in carbonates.

5 Conclusions

The fluorite mineralization, as taking place at Jebel Mokta deposit, is hosted by Cenomanian karst and veins. Mineralization appears to consist of hypogene fluorite, celestite and calcite. The ore bodies occur as massive and discordant lenses in caves and fractures. The reached microthermometric data prove to suggest that brines, as involved in the fluorite deposit, were characterized with the predominance of high temperature and high salinity. The mixing of two fluids led to the formation of fluids of high temperatures and

Fig. 2 Photomicrographs of the fluid inclusion types from fluorite ore (room temperature).

a Biphasic (L + V) fluid inclusions in fluorite. **b** Plots of homogenization temperatures (Th) versus salinity (wt% NaCl equiv). **c** Photomicrographs of Hydrocarbon fluid inclusions. **d** Fluorescent image of fluid inclusion



salinities. The hydrothermal fluids are characterized with the presence of divalent cations other than Na^+ in the hydrothermal system, such as Ca^{2+} and Mg^{2+} . The geological and fluid-inclusions results proved to highlight that the fluorite deposit is considered to be formed from basinal fluids, and has been compared to the Mississippi Valley-type.

References

1. Bejaoui, J.: Géologie, Minéralogie, Eléments en traces Inclusions Fluides, Isotopes et Modélisation Génétique des Gisements à Pb-Zn et ou F, Ba de la Tunisie centro-septentrionale (Fedj Hassène, El Hamra, Ajered, El Kohol, Mecella, El Mokta et M'Tak). Thèse doct., Univ. Tunis II, 260 pp (2012)
2. Bejaoui, J., Bouhleb, S., Barca, D.: Geology, mineralogy and fluid inclusions investigation of the fluorite deposit at Jebel Kohol, Northeastern Tunisia. *Periodico di Mineralogia* 01, **82**(2), 217–237 (2013)
3. Bouhleb, S., Fortuné, J.P., Guilhaumou, N., Touray, J.C.: Les minéralisations stratiformes à F-Ba de Hammam Zriba du Jebel Guebli (Tunisie nord-orientale): l'apport des études d'inclusions fluides à la modélisation génétiques. *Miner. Deposita* **23**, 166–173 (1988)
4. Sainfeld, P.: Les gîtes Plombo-Zincifères de Tunisie. *Annales des Mines et Géologie de Tunis* n°9 285p, et un Atlas de 60 planches (1952)

Geomagnetic Assessment of the Igbeti Marble Deposit (Nigeria)

Saminu Olatunji and Warith Adebisi

Abstract

The Magnetic Intensity data of aeromagnetic survey, as conducted by Nigerian Geological Survey Agency, were acquired from sheets 200 and 201 for qualitative and quantitative interpretation purposes. The area is bounded by latitudes 8.5°N–9.0°N and longitudes 3.5°E–4.5°E covering an area of about 6150.50 km². The data were reduced off the regional field to obtain the residual field. Upward continuation and analytical signal were employed for qualitative interpretations. In addition to Euler and Werner Deconvolutions, spectral depth analyses were carried out to estimate the depth to causative geologic structures and basement of the target marble deposit. The residual field contour shows an intensity ranging from –63.05 to 52.65 nT, indicating series of magnetic highs and lows. The obtained positive residual anomalies could stand as responses to the outcrops common in the area, while the negative field could be associated with the presence of granitoids and felsic volcanic rocks or major fault zones. The reached result prove to reveal minimum and maximum depths of 1.07 and 3.79 km, suggesting an expected thickness extent of the deposit. Further Depth estimate around the current mining appears to range from 2.0 to 2.2 km.

Keywords

Magnetics • Upward continuation • Residual • Spectral analysis

1 Introduction

The magnetic method has proved to be successfully applied to investigate in areas in regard of such purposes as oil exploration, to determine the depth to basement [1], in mineral exploration, for magnetic minerals prospecting ends [2], in gold exploration, to determine gold-bearing structures [3], and, overall, in general structural mapping related studie [1]. In this respect, Theopjile et al. [4] have used aeromagnetic data to locate buried faults lying in Southeastern Cameroon. It has also been used for geothermal exploration purposes, and in the investigation of unexposed granite plutons [5] as well as the subsurface continuity of a rock unit [6]. Besides, it is often integrated with sensing techniques to map out lineaments [7].

The magnetic field, whose amplitude has already been measured, is a vector sum of the following components: the earth's main magnetic field, as originating from dynamo action of conductive fluids in the earth's deep interior [8], induced field caused by magnetic induction in magnetically susceptible earth materials as polarized by the main field [9], field caused by remanent magnetism of the earth's material [9], field caused by solar activities, atmospheric and cultural influences [2]. However, it is the induced and remanent fields that are of particular interest to a regolith geoscientist, as these fields' magnitudes are directly related to the magnetic susceptibility, spatial distribution and concentration of local crustal materials. Fortunately, a good number of minerals occur abundantly in nature to make a significant contribution to the induced and remanent fields.

The study area, Igbeti (Fig. 1), is a town located in Olorunsogo Local Government Area, in the Northern part of the Oyo State. The area lies between the coordinates 8.5°N–9.0°N and 3.5°E–4.5°E. The aim of this research is to estimate the depth extent of marble reserve in Igbeti, lying between the coordinates 8.5°N–9.0°N and 3.5°E–4.5°E, on a section of the basement complex of Nigeria geology, by processing Total Magnetic Intensity (TMI) data, as acquired from the aeromagnetic sheets 200 and 201.

S. Olatunji · W. Adebisi (✉)
University of Ilorin, Ilorin, Nigeria
e-mail: adebisiadewale5@gmail.com



Fig. 1 Inset of the Oyo State within Nigeria, showing the study area

2 Materials and Methods

Some marble mining pits sited at Igbeti were visited, and location coordinates at the sites were taken prior to the data acquisition. The purpose is to identify the surface area limit of the data to be extracted from the digitized data sheets 200 and 201, as obtained from the NGSA. The main data source relevant to this work is the aeromagnetic data relating to a specifically set section of the Oyo State (sheets 200 and 201).

The digitized data, as drawn from NGSA are in x, y, z worksheet format. The x values represent the distance of a point from the origin, pointing to the easting (longitude), the y values represent the distance of the point from the origin in the northing direction (latitude), while the z values represent the total magnetic field intensity at a point. The Total Magnetic Field Intensity (TMI) was stripped off 33,000 nT by the NGSA. Hence, a 33,000 nT was added to each value of the TMI to obtain the actual TMI, as measured during the survey. Thereafter, the data were sorted to check for spurious values, likely to result from possible magnetic storms.

The research area was sub-divided into eight square blocks for spectral depth determination ends. Each of the blocks represents a square grid of residual field points, corresponding to a quarter degree by quarter degree

$(\frac{1}{4})^0 X (\frac{1}{4})^0$ map. Each of these blocks covered a total area of about 756.25 km², as depicted on Table 1.

3 Results and Discussion

3.1 Residual Anomaly Map

The residual field contour is shown in Fig. 2.

Basically, the magnetic data, as observed from geophysical surveys comprise the sum of all magnetic fields produced by all underground sources. Hence, the compound or composite map produced on the basis of such data proves to contain two main signal sources stemming from the causative bodies, which are different in order of sizes and generally super-imposed. Super-imposed on the regional field, but frequently camouflaged by them, are the smaller, local disturbances which are secondary in size but primary in importance. These are actually the residual anomalies [9]. Therefore, the residual field contour shows an intensity ranging from -63.05 to 52.65 nT. The positive residual anomalies are considered to emanate from the outcrops common in the area, while the negative field could be associated with the presence of granitoids, felsic volcanic rocks and, possibly, major fault zones. This is likely to constitute the basis for the marble mineralization persistent in the area.

3.2 Depth-to-Basement Anomaly

Spectral depths were obtained by plotting graphs of logarithms of spectral energies against frequency for various blocks. The spectral plots appear to display clear linear segments due to deeper, intermediate and shallower sources. With respect to the present work's focus of interest, the deep source gradient stands as the most interesting segment. Based on the segments associated gradients, the average depths to the causative bodies were determined through the equation: $z = h = -\frac{m}{4\pi}$ where m designates the gradient and z gives the mean depth of the causative body. The depth-to-basement variation, as obtained via spectral analysis, is displayed on Table 2.

The contour of the depth-to-basement relevant to the study area (Fig. 3) indicates well that, generally, the magnetic basement lying beneath the study area turns out to be shallow. The deepest magnetic depth is of 3.79 km, observed to lie around the SW and SE corner of the area,

Table 1 Table showing block division for spectral analysis

Spectral block	Longitude, °E		Latitude, °N	
	Minimum (x ₁)	Maximum (x ₂)	Minimum (y ₁)	Maximum (y ₂)
Block 1	3.50	3.75	8.75	9.00
Block 2	3.75	4.00	8.75	9.00
Block 3	4.00	4.25	8.75	9.00
Block 4	4.25	4.50	8.75	9.00
Block 5	3.50	3.75	8.50	8.75
Block 6	3.75	4.00	8.50	8.75
Block 7	4.00	4.25	8.50	8.75
Block 8	4.25	4.50	8.50	8.75

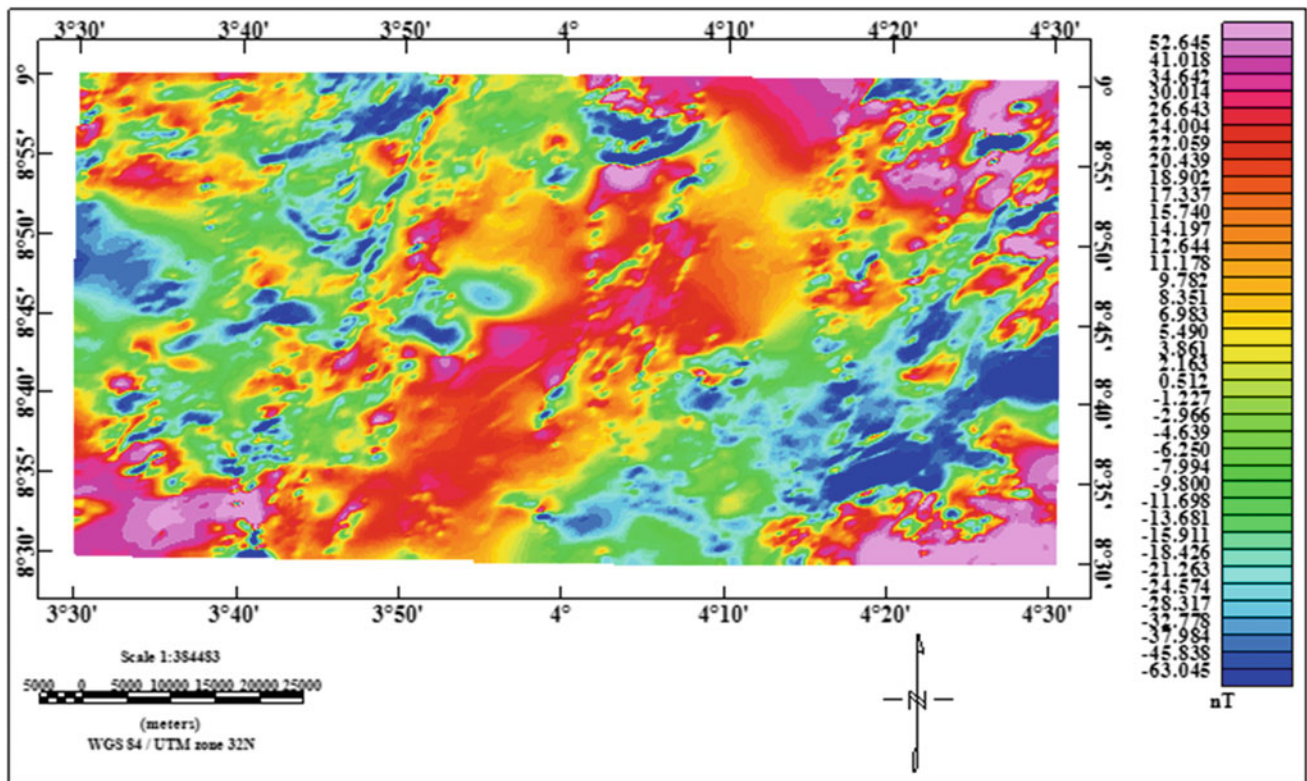


Fig. 2 Residual anomalies of the study area

Table 2 Block division with depth estimate

Spectral block	Longitude °E		Latitude °N		h (km)
	Minimum (x ₁)	Maximum (x ₂)	Minimum (y ₁)	Maximum (y ₂)	
Block 1	3.50	3.75	8.75	9.00	1.49
Block 2	3.75	4.00	8.75	9.00	1.57
Block 3	4.00	4.25	8.75	9.00	1.96
Block 4	4.25	4.50	8.75	9.00	1.07
Block 5	3.50	3.75	8.50	8.75	3.32
Block 6	3.75	4.00	8.50	8.75	1.40
Block 7	4.00	4.25	8.50	8.75	2.32
Block 8	4.25	4.50	8.50	8.75	3.79

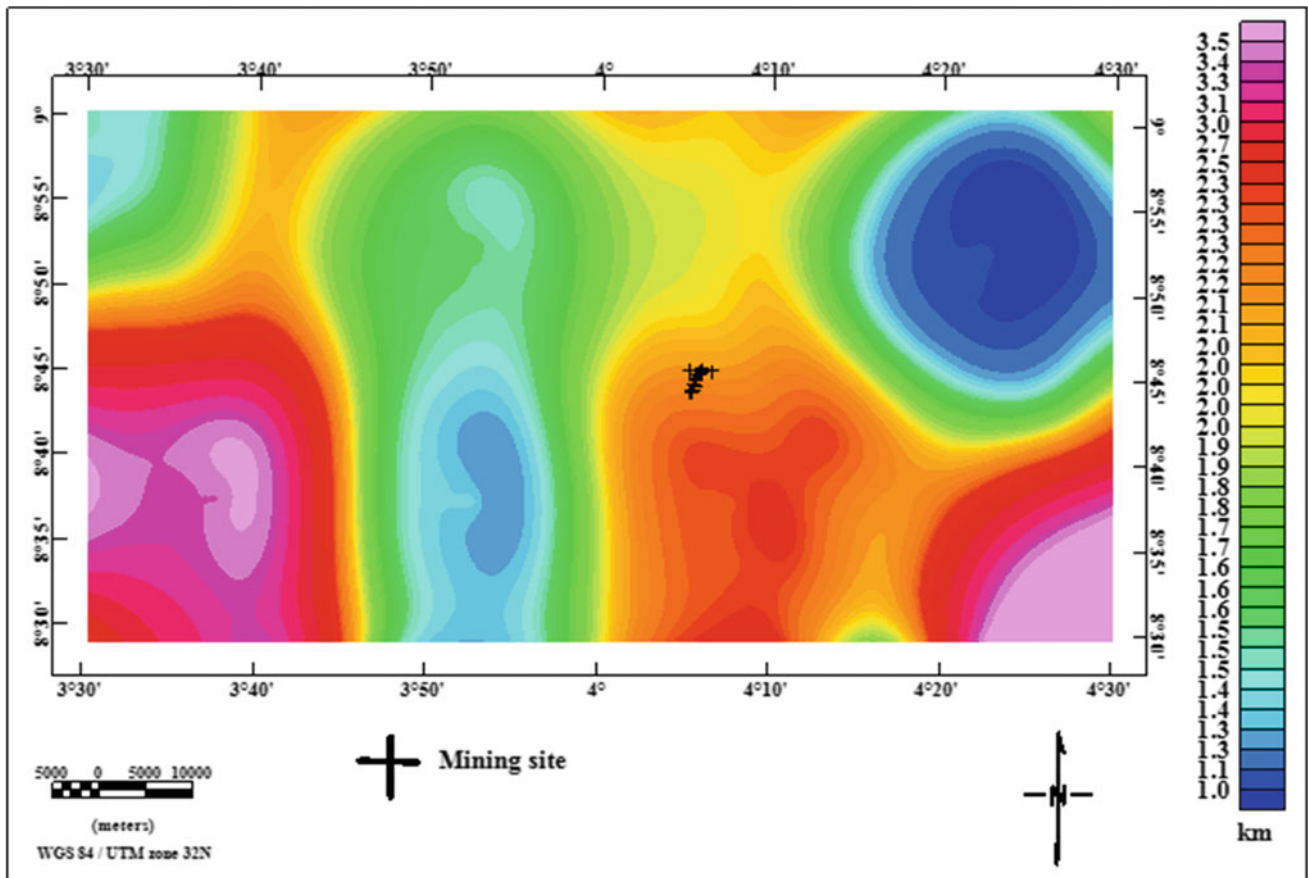


Fig. 3 Basement depth anomaly of the study area

while the shallowest depth (1.07 km) lies around the NE corner of the study area. A depth range of about 2.0–2.2 km is observed around the mining site zone of the study area.

4 Conclusions

The prominent granitic outcrops, common in the area, appears to have a significant influence on the magnetics field responses obtained. Moreover, though the present mining locations are not too poorly sited, a better mine location could still be achieved in the southern part of the area, owing mainly to the availability of greater depth and occurrence of fault zone, as highlighted through the achieved results.

References

- Hassan, H.H., Robert, A.C., John, W.P.: Mapping Depth to Basement Using 2D Werner Inversion of High Resolution Aeromagnetic (HRAM) Data. Search and Discovery Article N41595 (2015)
- Salau, S.L., Danbatta, U.A., Agunleti, Y.S.: The interpretation of aeromagnetic and satellite imagery for structures in coincident with gold mineralization in Anka Schist Belt, Northwestern Nigeria. *J. Geol. Geophys.* (2016)
- Telford, W.M., Geldart, L.P., Sheriff, R.E., Keys, D.A.: *Applied Geophysics*, 2nd edn, p. 860. Cambridge University Press, Cambridge (1990)
- Theopjile, N., Feumone, A.N., Eiezer, M., Fairhead, J.D.: Aeromagnetic data interpretation to locate buried faults in South East Cameroon. *Geophysical* **48**(1–2), 48–63 (2012)
- Raimi, J., Dewu, B.B.M., Sule, P.: Existence of a possible subsurface ring complex in Northeastern Part of the Nigerian Younger Granite Province: a contribution from aeromagnetic and remote sensing data. *Saudi Soc. Geosci.* (2014)
- Abubakar, Y.I.: An integrated technique in delineating structures: a case study of the Kushaka Schist Belt Northwestern Nigeria. *J. Appl. Sci. Technol.* **2**(5), 164–173 (2012)
- Merril, R.T., McEthing, M.W., McFadden, P.L.: *The Magnetic Field of the Earth: Paleomagnetism, the Core and the Deep Mantle*, p. 531. Academic Press, San Diego (1996)
- Doell, R., Cox, A.: Magnetization of Rocks. *Min. Geophys.* **2**, 446–4561 (Society for Exploration Geophysics) (1967)
- Bonde, D.S., Udensi, E.E., Rai, J.K.: Spectral depth analysis of Sokoto Basin. *IOSR J. Appl. Phys.* **6**(1), 15–21 (2014)

Mineralogical and Sulfur Isotopes in Ghar Roubane Barite Lead–Zinc Deposit, (Western Algeria)

Nacera Hadj Mohamed, Abdelhak Boutaleb, Maria Boni, and Djamel Eddine Aissa

Abstract

The Ghar Roubane barite lead–zinc deposit lies in the metallogenic province of Western Algeria. This mineralization site occurs in the form of barite veins, taking place within the Paleozoic schists and granites and fracture-filling in Liassic limestones. The Paleozoic basement shows barite veins of several hundred meters in length, orientated from N50° to N75°, and dip mainly between 60° and 90°, with a thickness range comprised between 0.1 and 2 m. Barite pink, white to transparent in color. The barite veins are hosted in Liassic limestones with rare sulphides, related to fractures of NS and EW directions. The thermometric investigations performed on barite extracts from the granites indicate that homogenization temperatures (Th) for primary fluid inclusions appear to range from 130 to 140 °C. As for the barite extracts from schists and limestones, they display Th ranges ranging between 110 and 120 °C. Mean salinities are 15% equivalent NaCl for fluid inclusions in granite based barite, and 21% equivalent NaCl regarding the cover based barite. The interpretation of these data with respect to their relating geologic context favors a mixing process between basinal (prevailing) and basement fluids. The $\delta^{34}\text{S}$ values relevant to the barite minerals prove to reveal a noticeable variation ranging from 21.3 to 29.4‰. The sulfur isotopic compositions suggest that the ore-based formations turn out to be derived from different sources that may well include seawater along with magmatic fluid mixtures.

Keywords

Barite veins • Pb–Zn mineralization • Fluid inclusions • Sulfur isotopes

1 Introduction

The Ghar Roubane polymetallic mineral area is located in the North Western part of the Tellian Chain, along the Algeria–Morocco border. Barite veins and accessory Cu–Pb–Zn are trending NE to EW. They crosscut both the basement rocks and the Jurassic carbonate cover. Only some descriptions have so far been achieved, and nothing is known about the fluids, isotope geochemistry and genesis related conditions.

In this paper, two kinds of barite veins are investigated (those hosted in the Paleozoic basement and the Liassic cover relating ones). The aim is twofold: determining their genesis conditions, and recognizing whether they pertain to same metallogenic stage or to two distinct phases.

1.1 Geological Setting

The Mounts of Ghar Roubane constitute an elongated belt (30 km long and 6 km wide). They display a predominant WSW–ENE orientation limited to the North by the Maghnia Plain, to the South by the Oran High Plains, to the East by the Tlemcen Mountains, and to the West by the Oujda Mountains. This region is affected with major sinistral strike-slip faults, involving a displacement to the North of the different units [4]. As studied by Lucas [6], and Elmi [3, 5] the geology of Ghar Roubane can be divided into two main units, each characterized with a predominant lithology and type of mineralization: the Paleozoic basement and the Jurassic cover.

The Basement Complex includes Silurian to early Carboniferous sedimentary rocks, folded during Hercynian

N. Hadj Mohamed (✉) · A. Boutaleb · D. E. Aissa
Metallogeny and Magmatism Laboratory of Algeria,
FSTGAT - USTHB, BP 32 El Alia, 16111 Bab Ezzouar, Algeria
e-mail: nacerahadj@gmail.com

M. Boni
Department of Earth Sciences, Environment and Resources,
University of Naples, Naples, Italy

orogeny and affected by a contact metamorphism (hornfels). The cover comprises Triassic and Liassic rocks, resting unconformably on the Paleozoic basement.

2 Methodology

More than 70 samples were collected from the Ghar Roubane deposit. They were selected for petrographical, geochemical and fluid-inclusion microthermometrical studies.

The petrographic studies, involving thin and polished sections, were performed in the microscopy laboratory of the Houari Boumediene University. The fluid-inclusion microthermometric studies were administered on double polished wafers through application of standard techniques, as described by Shepherd et al. [8]. The measured parameters included the last ice-melting temperature (T_m) and the homogenisation temperature (T_h) (Table 1). The relevant salinities were calculated via the computer program of Chi and Ni [1]. The measurements were performed on a Linkam THMS 600 combined heating/freezing stage at the Cergy Pontoise University. The relating sulfur isotope analyses were performed on barite samples, at the Glasgow University.

3 Mineralization

Barite mineralization occurs along faults and fractures in the form of veins in the granites, schistes and limestones.

The veins related strike and dip are N50° and 60°–85°SE, respectively. Most of these veins appear to be simple extensional fractures, though massive and disseminated vein textures are observed in certain places.

The undertaken petrographic analysis proves to reveal that the deposit attached mineralogy turns out to be relatively simple. It consists of barite, as the main mineral, along with quartz, calcite and small amounts of Fe-oxide.

Barite proves to form euhedral to subhedral crystals, while calcite turns out to form the second common mineral occurring in the form of patches, tension gashes or tiny veins

in limestones. Iron oxides are also discovered to persist as small grains.

Ore minerals in veins are mainly pyrite sphalerite and galena. Pyrite occurs as cubic forms; chalcopryrite, generally occurs as disseminated grains in pyrite or forms massive lumps with galena. Galena is abundant and occurs as single grains in barite; it contains inclusions of chalcopryrite. Sphalerite is green or red and fine to coarse-grained (0.01–3 mm) with anhedral texture.

4 Geochemistry

4.1 The Fluid Inclusions' Microthermometry Analysis

The fluid-inclusion microthermometric analysis was conducted on representative barite samples as extracted from the Paleozoic basement, barite, sphalerite and calcite samples from lower Liassic limestones. Due to the excellent barite cleavage, care was taken so that only fluid inclusions, which could distal to fractures, were to be selected. Primary and pseudo-secondary inclusions were of simple two-phase liquid-vapor types, with no daughter mineral or separated CO₂ phase at room temperature. The vapor makes up less than 15 vol.%. The inclusions, generally lensoid, proved to vary from 5 to 400 microns in diameter.

The eutectic temperatures were -51 ± 2 °C, indicating that the solutes persisting in the mineralizing brines were largely dominated by CaCl₂ [2].

Barite from the Hercynian granite yielded homogenization temperatures ranging between 135 and 164 °C, and ice-melting temperatures comprised between -20 and -10 °C, along with salinity rates ranging between 18 and 15.6 wt% NaCl equiv.

As for the cover based sphalerite and calcite, they proved to display homogenization temperatures ranging between 100 and 130 °C, and ice-melting temperatures ranging between -23 and -15 °C, corresponding to salinities of the rates of 21 and 23 wt% NaCl equiv.

Table 1 Microthermometric data relating to the studied area water-rich inclusions

Sample (localities)	Host rocks	Th	Thh	Tm	Te	Salinities
Barite (Beni Snouss)	Hercynian granite	150	-32	-20	-52	21.03
Barite (Beni Abir)	Paleozoic schists	130	-21	-23	-43	21.03
Barite (Beni Bahdel)	Jurassic limestone	140	-30	-18	-52	19.98
Calcite (B. Bahdel)	Jurassic limestone	105	-28	-18	-52	20.10
Sphalerite (B. Bahdel)	Jurassic limestone	100	-30	-19	-52	20.58

Th: Homogenization temperature, Thh: hydrohalite temperature, Tm: ice melting temperature, Te: eutectic temperature

Table 2 $\delta^{34}\text{S}$ data related to the Ghar Roubane barite deposit

Area	Host rocks	Paragenesis	$\delta^{34}\text{S}$ (CDT) ‰
Mallal	Granite	Pink barite-tour	21.3
Mallal	Granite	Barite-quartz	22.8
Tairat	Granite	White barite	24.4
Bouabdous	Granite	White barite-ga-py	22.8
Beni Abir	Schist	White barite-galena	29.1
Beni Abir	Schist	Transparent barite	28.4
Beni Bahdel	Limestone	White barite-galena	27.1

4.2 Sulfur Isotopes

Possible sources of sulfur that may include sulfate-bearing evaporate connate seawater, diagenetic sulfides, sulfur-bearing organic material, or H_2S reservoir gas [7]. The sulfur isotopic data relevant to the barite samples figure on Table 2.

The $\delta^{34}\text{S}$ associated with the Ghar Roubane based barite samples was analyzed in a bid to interpret the origin of the deposit. The $\delta^{34}\text{S}$ values appear to vary from 22.8 to 29.4‰. Most of these values are discovered to exceed those associated with modern seawater sulfate ($\delta^{34}\text{S} = 20.3\text{‰}$).

Based on the host rocks, two groups can be distinguished: the 1st group: 21.3 and 24.4‰: mixture with magmatic fluid, and the 2nd group: 27.1 to 29.1‰: far higher than modern sea water (21, 24‰): Mesozoic seawater (Basinal fluid).

5 Conclusion

The Ghar Roubane barite deposit might well stand as an epigenetic vein occurrence, with open-space filling veins. It occurs in the form of massive and replacement ores stretching across faults and fractures of Paleozoic granite and Liassic limestone host rocks. The Ghar Roubane deposit displays a simple mineralogical paragenesis, with barite standing as the main mineral, along with smaller amounts of calcite, quartz and opaque minerals (consisting of iron oxide, pyrite, chalcopyrite and covellite).

On the basis of geological and geochemical data, as drawn from the Ghar Roubane barites, one could well

conclude that the Ghar Roubane barite was deposited from hydrothermal fluids that may include seawater along with magmatic fluid mixtures. Additionally, the achieved results prove to suggest that the fluids passing through the host rocks turn out to be influenced with such hostings.

References

- Chi, G., Ni, P.: Equation for calculation of $\text{NaCl}/(\text{NaCl}+\text{CaCl}_2)$ ratios and salinities from hydrohalite-melting and ice-melting temperatures in the $\text{H}_2\text{O}-\text{NaCl}-\text{CaCl}_2$ system. *Acta Petrologica Sinica* **23**, 33–37 (2007)
- Crawford, M.L.: Phase equilibria in aqueous fluid inclusions. In: Hollister, L.S., Crawford, M.L. (eds) *Short Course in Fluid Inclusions: Applications to Petrology*. Mineral. Assoc. Canada, vol. 6, pp. 75–100 (1981)
- Elmi, S.: La sédimentation carbonatée en bordure du horst de Rhar Roubane (Algérie occidentale) pendant le Carixien. *Bulletin de la Société Géologique de France* **2**, 355–365 (1977)
- Elmi, S.: L'évolution des monts de Rhar Roubane (Algérie occidentale) au début du Jurassique. *Livre Jubilaire Gabriel Lucas. Mémoire de l'Université de Dijon* **7**, 401–412 (1983)
- Elmi, S.: L'histoire des monts de Rhar Roubane (Algérie occidentale) ou l'œuvre de Gabriel Lucas à l'épreuve du temps. *Mémoires de la Société Géologique de France* **169**, 17–24 (1996)
- Lucas, G.: Bordure des Hautes Plaines dans l'Algérie occidentale. *XIXème Congrès géologique international, Alger. Monographies régionales d'Algérie (1)* **21**, 1–139 (1952)
- Leach, D.L., Taylor, R.D., Fey, D.L., Diehl, S.F., Saltus, R.W.: A deposit model for Mississippi Valley-Type lead-zinc ores, chap. A of *Mineral deposit models for resource assessment*: U.S. geological survey scientific investigations report, pp. 5070–5213 (2010)
- Shepherd, T.J., Rankin, A.H., Alderton, D.H.: *A Practical Guide to Fluid Inclusion Studies*. Blackie, Glasgow (London), p. 239 (1985)

Cr-Ni-PGE Mineralization and Serpentinization of Peridotites in Beni Bousera Massif (Internal Rif, Morocco)

Zaineb Hajjar, Fernando Gervilla, and Amina Wafik

Abstract

The Beni Bousera ultramafic massif outcrops at the base of the internal zones of the Alpine Rif belt of northern Morocco. It is characterized with the presence of two types of magmatic ores (i) chromite and Ni arsenides, associated with orthopyroxene and cordierite (Cr-Ni ores), and (ii) Fe-Ni-Cu sulfide mineralization, containing variable amounts of graphite and chromite associated with phlogopite, clinopyroxene and plagioclase (S-G ores). The Cr-Ni and S-G ores endured High-T alterations related to injection of leucogranite dykes, producing Ni and Co rich in chromite from Cr-Ni ores; and low-T alteration, due mainly to serpentinization/weathering process. The latter resulted in the serpentinization phenomenon of peridotites, followed by carbonation, along with the leaching of the Ni-arsenides and sulfides, giving rise to Ni-rich silicates in the Cr-Ni ores, and Fe-rich silicates in the S-G ores.

Keywords

Cr-Ni ores • S-G ores • Serpentinization • Beni bousera

Seiland subfacies of the spinel lherzolite facies at the bottom. This evolution took place along with the infiltration of small volumes of asthenospheric melts [1], which, in turn, reacted with the host producing Si-, Al-, Ti-, Fe- volatiles (CO₂, CH₄, and H₂O), S-, chalcophile elements, and As-rich melts [2]. The fractionation of these melts and their mixing with As-rich, crustal-derived felsic ones produced noble metal (platinum-group elements and gold)—rich chromite-Ni arsenide ores (Cr-Ni ores). The formation of Cr-Ni ores was followed by the segregation of PGE-poor sulfide melts, which constituted the parental melts of sulfide-graphite ores (S-G ores) [2, 3]. Acid dykes (cordierite leucogranite and pegmatites) were injected subsequently to the intra-crustal emplacement of peridotite, in the NE contact [4].

Despite the several studies dealing with the Beni Bousera massif related peridotite and magmatic mineralization, only the recently-conducted present work seems to be interested in the study of the serpentinization phenomenon and its effect on magmatic mineralization. The present paper is designed to highlight the main characters of the serpentinization processes, along with the mineral assemblages formed during the multiphase alteration events affecting magmatic ores in the Beni Bousera massif (Fig. 1).

1 Introduction

The Beni Bousera ultramafic massif (Morocco) corresponds to a portion of sub-continental lithospheric mantle, exhumed into the crust in the internal domain of the Alpine Rif Cordillera. Across the uplift, these mantle peridotites became deformed and recrystallized, giving rise to a petrographic zoning: from the mylonites and Ariegite subfacies of the spinel lherzolite facies, at the top of the massif, to the

2 Materials and Methods

Twenty samples were collected from the Beni Bousera ore deposits for petrographic observations. They were studied via a SUPRA40VP scanning electron microscope using SE, STEM and EDX detectors. Besides, an electron-probe microanalysis (EPMA) has also been performed with a CAMEBAX SX100 instrument, sited at the Centro de Instrumentación Científicas (CIC) of the University of Granada. The relevant operating conditions are described in [3]. Twenty-four sections from serpentinite rocks were analyzed via Raman spectroscopy to characterize the associated serpentine minerals. The Raman spectra were recorded at the French Lille 1 University (Génie Civil and

Z. Hajjar (✉) · A. Wafik
Cadi Ayyad University, Marrakech, Morocco
e-mail: zaineb.hajjar@edu.uca.ma

F. Gervilla
Universidad de Granada, Granada, Spain

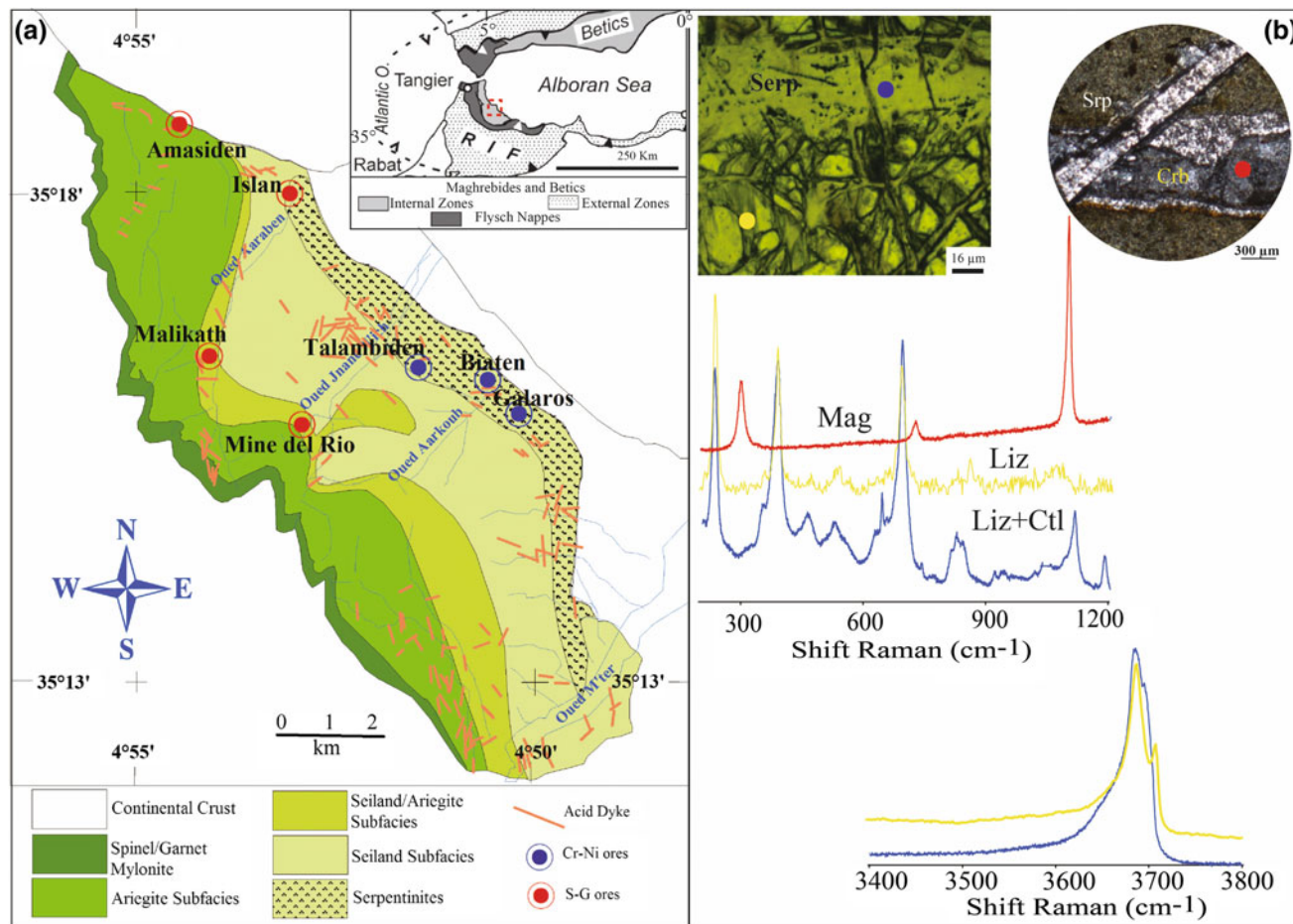


Fig. 1 a Geological map of the Beni Bousera massif [3], b Raman spectra, as acquired from lizardite (Liz), lizardite + chrysotile (Liz + Ctl) and magnesite in low frequency ($200\text{--}1200\text{ cm}^{-1}$) and OH stretching ($3600\text{--}3800\text{ cm}^{-1}$) ranges, with corresponding microphotographs

Géo- Environment Laboratory), by means of a LabRam HR800 Jobin-Yvon- microspectrometer. Details of the analytical procedures are described in [5].

3 Results

The injection of acid dykes (cordierite leucogranite and pegmatites) yielded mineralogical changes in Cr-Ni ores, like the transformation of orthopyroxene into phlogopite and nickeline into maucherite [3], along with an enrichment of NiO and CoO in chromite ([3]; Fig. 2a).

The peridotite relating serpentinization is manifested by the formation of mesh and hourglass textures in the highly serpentinized peridotites, as well as brecciated textures in the least serpentinized peridotites. The Raman spectra appear to

reveal that the serpentine minerals, as sited in the above textured rocks, prove to correspond to lizardite, while the veins or as fracture-filling ones appear to be formed by the assemblage lizardite + chrysotile [5]; Fig. 1b. Magnesite precipitation was formed by the CO_2 -rich hydrothermal fluids filling fractures, which prove to affect the serpentinized peridotites remarkably (Fig. 1b). Hence, the carbonation process turns out to take place following the peridotites' serpentinization phenomenon [6].

In turn, the Cr-Ni and S-G ores did not seem to escape this low alteration stage. In the Cr-Ni, the ores' serpentinization process is manifested by the formation of Ni-serpentine intergrowth, with chlorite/vermiculite being associated with chromite (Fig. 2b, c). The Ni-arsenides appear to be totally leached out. In S-G ores, the alteration proves to depend highly on the silicate/sulfide ratio. In silicate-dominated ores,

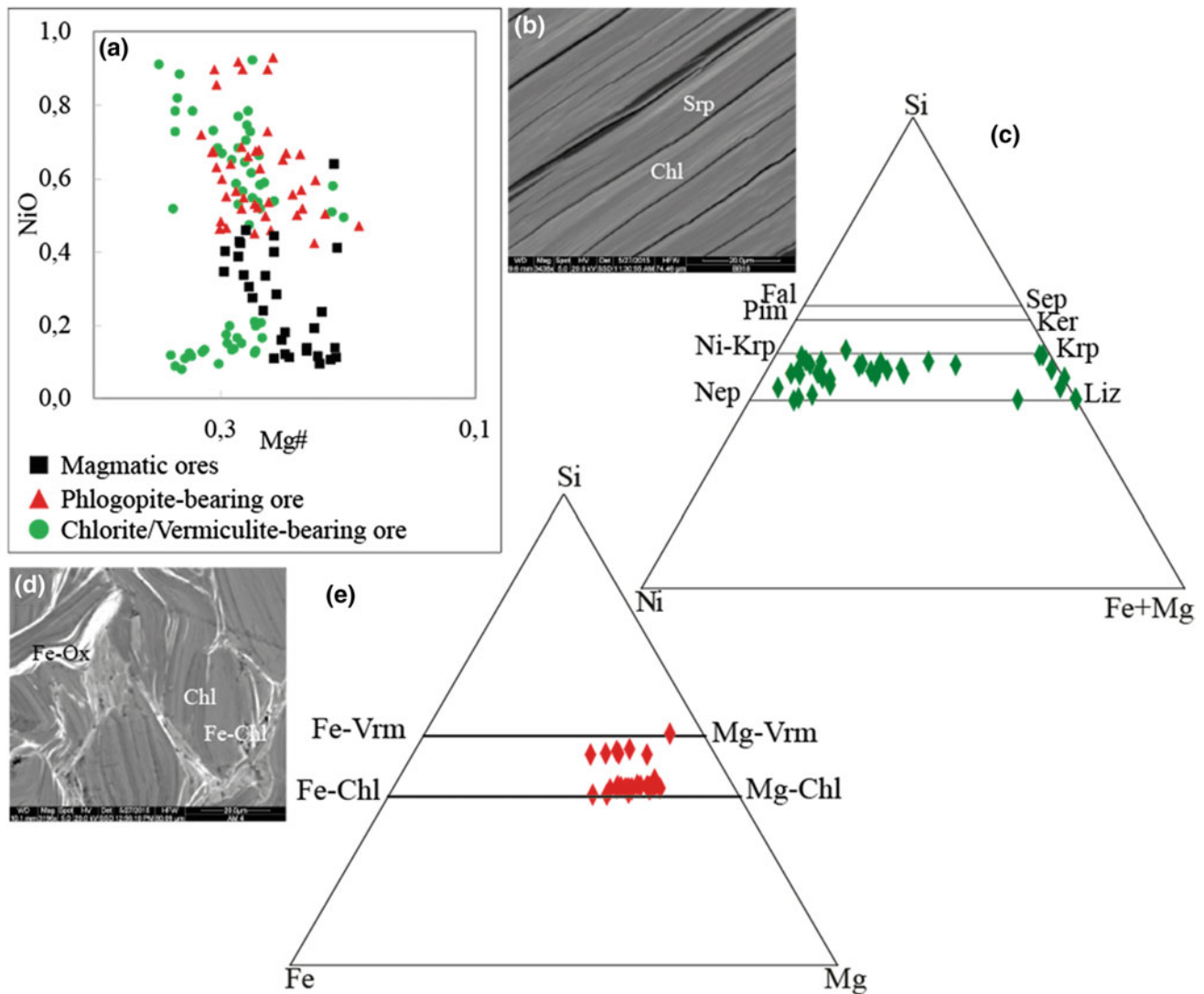


Fig. 2 a Compositional variations of chromite grains from Cr-Ni ores, in NiO versus Mg# diagram. b interstratifications of chlorite and Ni-serpentine. c composition of serpentine in the Si-Ni-(Fe + Mg)

diagram [3]. d interstratification of Mg-rich chlorite (dark) with Fe-rich chlorite (light), e composition of chlorite/vermiculite from S-G ores in S-Fe-Mg diagram [3]

alteration appears to produce re-equilibrium of sulfides at low temperatures in a zeolite \pm pectolite \pm chlorite assemblage, as formed after plagioclase and clinopyroxene. Alteration of sulfide-rich ores produces sulfide leaching, giving rise to iron oxides and hydroxides associated with Fe-rich vermiculite ([3]; Fig. 2d, e).

4 Conclusions

Two magmatic ores (Cr-Ni and S-G ores) have been distinguished to persist in the Beni Bousera massif. They appear to be formed from residual magmatic liquids, as generated by fractionation of small-volume melts. A high-temperature alteration stage, respectively marked by

the replacement of nickeline with maucherite, and orthopyroxene by phlogopite, accompanied with the amalgamation of gold grains in maucherite or along the boundaries separating the nickeline and maucherite, is highlighted. The beginning of arsenide lixiviation increased the availability of Ni and Co in the altering fluids, promoting their diffusion into chromite grains. The S-G ores did not appear to preserve such an alteration stage. A low-temperature alteration stage, expressed by serpentinization/weathering processes, proved to affect the peridotite, Cr-Ni ores and S-G ores. Peridotites became serpentinized, especially in presence of the above-referred NE contact, and along the mylonitized highlighting the NE contact of peridotite with crustal rocks. In the Cr-Ni ores, nickeline was leached out enhancing the increase of Ni availability, to form Ni-rich serpentine

intergrowth with chlorite and vermiculite. Chromite proves to retain its previous composition, as the chemical diffusion in chromite was inhibited at low-temperature. In regard of the S-G ores, the result of alteration proves to depend highly on the silicates/sulfides ratio.

References

1. Frets, E.C., et al.: The Beni Bousera peridotite (Rif belt, Morocco): an oblique-slip low-angle shear zone thinning the subcontinental mantle lithosphere. *J. Petrol.* **55**(2), 283–313 (2014)
2. González-Jiménez, J.M., et al.: Zircon recycling and crystallization during formation of chromite- and Ni-arsenide ores in the subcontinental lithospheric mantle (Serranía de Ronda, Spain). *Ore Geol. Rev.* **90**(March), 193–209 (2017)
3. Hajjar, Z., Gervilla, F., Essaifi, A., Wafik, A.: Mineralogical and geochemical features of the alteration processes of magmatic ores in the Beni Bousera ultramafic massif (north Morocco), *J. Afr. Earth Sci.* **132** (2017)
4. Elbaghdadi, M.: Les filons acides dans le massif ultrabasique des Beni Bousera (Rif interne, Maroc) : Caractérisation pétrographique, géochimique et âge de mise en place (Rb-Sr) (1993)
5. Hajjar, Z., Wafik, A., Constantin, M., Bhlisse, M.: Process of serpentinization in the ultramafic massif of Beni Bousera (internal Rif, Morocco). *Arab. J. Geosci.*, **9**(6) (2016)
6. Hajjar, Z., Wafik, A., Constantin, M.: Magnesite Veins from Ultramafic Massif of Beni Bousera (Internal Rif, Morocco). *J. Tethys* **3**(2), 152–162 (2015)

The Use of Rare Earth Elements Patterns in the Exploration of Massive Sulphide Ores, Ariab Area, Red Sea Hills, NE Sudan

Samia Ibrahim, Elshiek Mohammed, and Murad Ali

Abstract

The Rare Earth Elements study relevant to the Ariab massive sulphides has illustrated the persistence of a positive Europium (Eu) anomaly conserved when massive sulphides appear to be subjected to greenschist grade of metamorphism and supergene weathering. The positive Eu anomaly, as detected in the Ariab gossans, are considered as a product of supergene weathering of massive sulphides, displaying a similar positive Europium anomaly. Positive Europium anomalies, as detected in the hydrothermally altered schists and gossans, can be used as a guide for massive sulphide-ore discoveries. Such an ossanization process has led to a complete consumption of ore metals Cu and Zn from the gossan, which makes the conservation of the positive Eu anomaly stand as a good sign of massive sulphide gossan. In hydrothermally altered schists, this positive anomaly is also a sign of the influence of an intense hydrothermal metal-bearing sulphide system. A clear correlation between Eu_d and Pb has been established in the massive sulphide ores. The observed REE patterns of the Ariab mineral district rocks have their explanation in an input of hydrothermal solutions noticeable in the chemical sedimentation site. The characterizing REE pattern and consistent stratigraphic positioning of the chemical sediment zones have led to a sequence of events detected within the hydrothermal system. It started with the alteration of volcanic glass and ferromagnesian minerals, resulting in the release of Cu and Fe into the solution forming the Cu-rich sulphide.

Then, the alteration of feldspar with very concentrated brine proved to enrich the solution in Pb, Zn, Ba, and heavy REE, forming silica barite. Finally, the continuous removal of Fe from the volcanic rocks without any noticeable alteration in the large amount of the solid phases proves to result in the formation of an iron cape.

Keywords

Rare earth elements • Massive sulphides • Ariab area • Europium (Eu)

1 Introduction

REE fractionation during precipitation can generate small to moderate anomalies in magnitudes, observable in many units of the samples. If a solution is already enriched in Eu, the process will certainly enhance the initial anomaly in the precipitate, while the source of observed anomalies lies probably in the solutions themselves enrichment in Eu, prior to the precipitation of chemical sediments ([4, 8]).

Positive Europium (Eu) anomalies are common in volcanogenic massive sulphide deposits and the associated exhalite material and Gossans, as noticeable in the Paleoproterozoic Flin Flon-Snow Lake District (Trans-Hudson Orogen) of Manitoba [5]. Concerning the present study, similar positive Eu anomalies are discovered to persist in the Neoproterozoic VMS and associated gossans pertaining to the Ariab Mineral District. The positive Eu signatures appear to extend well beyond the limit of the recognized sulphide ores. In addition, the REE patterns related to the rocks belonging to the stratigraphically underlying alteration zones and barren sulphides are distinctively different from patterns advocated for exhalite-bearing material and iron sulphide [6]. Such differences noticeable in REE contents can be utilized for the VMS deposits understanding and exploration purposes. Similarly, the Eu anomaly along with the relative amounts of light and heavy REE (reflected by its La/Lu or

S. Ibrahim (✉)

Department of Geology, Faculty of Science, University of Khartoum, Khartoum, Sudan
e-mail: samiaibrahim125@gmail.com

E. Mohammed

Ministry of Minerals, Geological Research Authority of the Sudan & al Neelain University Faculty of Petroleum and Minerals, Khartoum, Sudan

M. Ali

Department of Geology, University of Taiz, Taiz, Yemen

La/Yb ratio), as perceived in the alteration zones, gossans, and massive sulphide deposits can be used to provide information relevant to the REE behavior of during the metamorphism, hydrothermal alteration and supergene weathering stages.

The purpose of this study is to apply the REE pattern associated variances in the exploration of massive sulphide deposits. Similarly, these patterns are applied to determine the presence of off-hole metal-bearing sulphide zones and distinguish the poor metal deposits, related to economic hydrothermal activity, from the barren sulphide facies iron formation. Similarly, the presence of ore-equivalent strata in some volcanic rocks will also be determined.

2 Geochemical Analytical Methods

A total of 90 rock samples, extracted from the Ariab mineral district, have been analyzed for major trace and rare earth elements (REE) monitoring ends. These rock samples include host rocks (least altered + altered), and ore samples (silica barite, gossans, massive sulphides). REE were analyzed by means of ICP-MS, and the relevant data were normalized through chondrite values [13]. The CRM standards were run concurrently for the analytical results to be checked.

The Eu anomaly related magnitude is reflected either with respect to the associated Eu_d values, which according to [5] turn out to be:

$Eu_d = (Eu_n / 1/2 Sm_n + 1/2 Gd_n) - 1 * 100$, (where n designates the chondrite-normalized value), or with respect to Taylor and McLennan [17] Eu/Eu^* such as:

$Eu/Eu^* = Eu_N / \sqrt{[(Sm_N) \cdot Gd_N]}$, to the measured REE concentrations and REE ratios of LRRE and HRRE.

3 Results

3.1 REE Patterns of Sulphide Ores

Overall, the massive solid sulphides (i.e., rocks with more than 90% sulphide minerals) of the Ariab deposits have typically revealed enriched LREE and a positive Eu_d , but also displayed low HREE concentrations (except for Yb). Inversely, however, the ores nearing massive to disseminated sulphide (i.e., 50–90% sulphides) have displayed HREE contents that are well above the detection limits, along with LREE chondrite-normalized values that are equal to or higher than those associated with Yb and Lu. Massive sulphide ores (solid sulphides) and disseminated ores (near solid sulphides) belonging to Oderuk, Adasidakh, Adaiamet and

Hadal Awateb also appear to display positive Eu anomalies and Eu_d values, ranging from 76 to 265 and from 4.7 to 49.5, respectively. They also represent an overall proportion of 50–265% increase of Eu_d in addition to low La/Lu and La/Yb ratios (high Yb), and a negative Ce anomaly.

The REE patterns with positive Eu anomalies are illustrated in Figs. 1, 2 and 3. Similar chondrite normalized REE patterns were also obtained with respect to layered sulphides pertaining to the Brunswick deposit in Canada [8], the layered and breccia matrix sulphides relating to the Halfmile Lake VMS deposit [1] as well as the ores associated with the Broken Hill sediment hosted deposits, Australia [11].

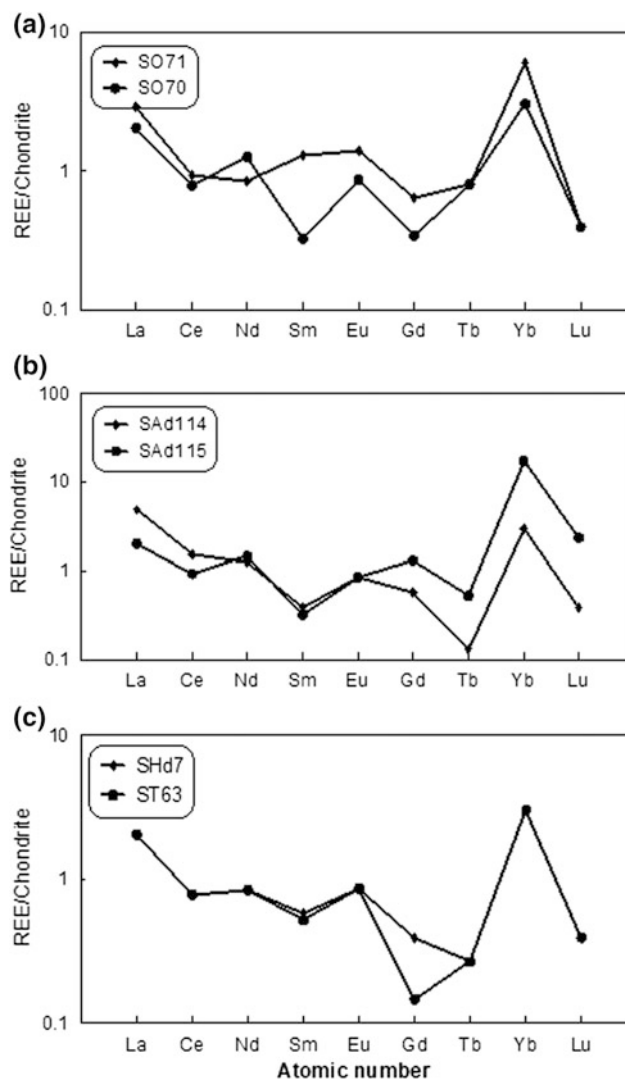


Fig. 1 REE patterns of Oderuk (a), Adasidakh (b), and Hadal Awateb (c) solid massive sulphide (base metal rich massive pyrite) samples with positive Eu anomalies

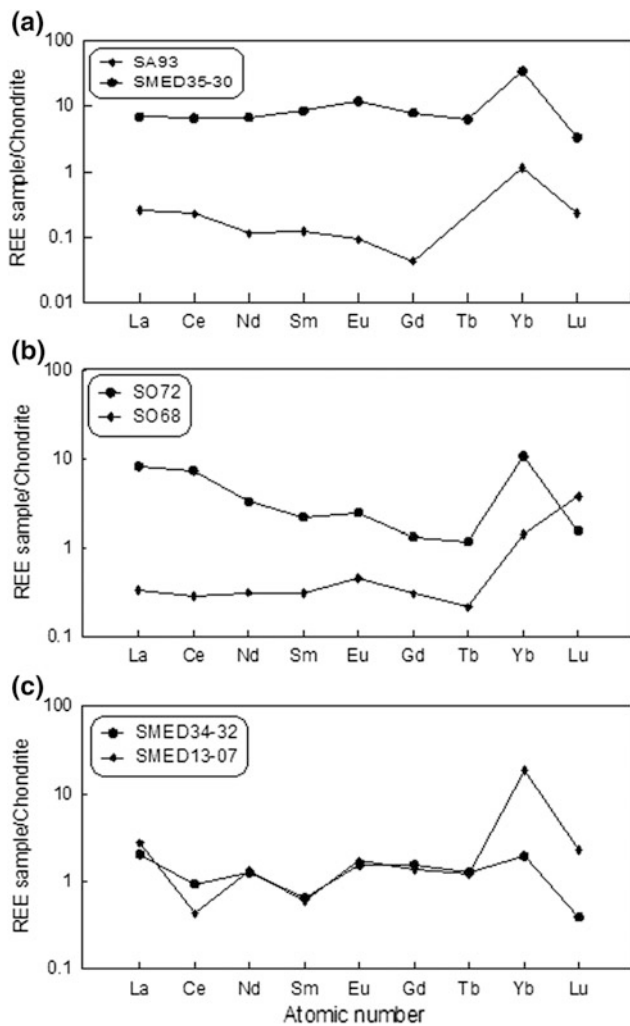


Fig. 2 REE patterns of Adaiamet (a), Oderuk (b) and Medadip1 (c) near solid massive sulphides (metal-rich disseminated massive pyrite samples) showing positive Eu anomalies

3.2 REE Patterns of Gossans and Chert

The Ariab gossans prove to comprise iron oxides (iron cap) and silica barite. Most of these gossans remarkably have similar REE profiles as compared to the other metal-rich sulphides (Fig. 3), and to the massive sulphides related to modern hydrothermal systems. The preservation of REE profiles and positive Eu anomalies during gossanization is well documented with regard to the massive sulphide of the Bathurst Mining Camp in New Brunswick, Canada [18].

Iron formation (iron cap) samples reflect +ve Eu anomalies (Eu_d values), REE patterns (Fig. 3a) like metal-rich massive pyrite samples (Fig. 2) and hydrothermally altered schists, Eu_d values for Ariab gossans range between -24.25 and 199.8 . It is difficult to separate the effects of location or mineralogy but within one

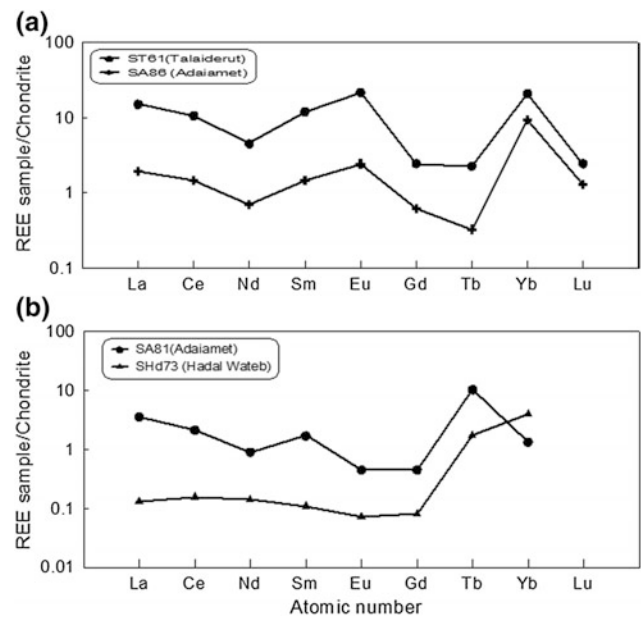


Fig. 3 a REE patterns of iron-oxides (iron cap) rock samples show +ve Eu anomalies b REE patterns of cherts rock samples showing flat Eu anomalies

iron-formation closer to a sulphide body it usually shows higher Eu_d values and elevated La/Lu ratios as well.

4 Discussion

From the exploration perspective, applying the trace-element geochemistry available evidences do not appear to provide strong indications of where the REE may start to display a mobile behavior, as the fossil hydrothermal system is blindly approached. Still, the evidence does provide a number of indications as to how such a mobility may be recognized at the periphery of a fossil halo. Divalent Eu is clearly the most susceptible among the REE to the effects of hydrothermal alteration [10].

Campbell et al. [3] infer that the degree of REE mobility may be related to the deposit size, but did not undertake a mass-balance analysis. Maclean [12] reviews several REE studies and highlights that, from a mass balance perspective, both enrichment and depletion occur in the stockwork zone of VMS deposits. Michard [14] investigates the REE contents of actively venting hydrothermal fluids, including those associated with submarine fluid venting, and generally found very low concentrations of LREE and much lower relative contents of HREE; supporting the minimal mobility of REE in general. Usually the divalent Eu ([16]) proves to be more mobile than the trivalent REE and is readily leached during feldspar breakdown reactions. In theory, REE are not mobile under typical seawater

hydrothermal conditions [15] although at lower pH (3) and temperatures greater than 350 °C, LREE are noticeably soluble as trivalent chloride complexes, which would be consistent with the earlier cited REE patterns of seafloor vent fluids [14].

The relatively higher Eu contents in hydrothermally altered schists of Ariab Mining District recognized in this study indicates that considerable leaching has occurred, enhancing the negative Eu/Eu^* and/or Eu_d in the footwall volcanic rocks of the area. Moreover, the positive Eu anomalies detected in the Ariab massive sulphide deposits are preserved, as the massive sulphide body have undergone greenschist metamorphism and the subsequent supergene weathering. Besides, the gossans with large positive Eu anomalies are likely to be the products of supergene weathering of massive sulphide exhibiting a corresponding positive Eu anomaly. Therefore, the positive Eu anomalies in hydrothermally altered schists and gossans can be applied as a guide to massive sulphide mineralization in the Ariab area. The gossanization process can lead to an almost complete loss of some metals (especially Cu and Zn) from the gossan, so the preservation of the positive Eu anomaly represents a good indicator of either a massive sulphide gossan or the influence of an intense hydrothermal metal-bearing system, as is the case with hydrothermally altered schists [8, 9, 11]. The study establishes a clear correlation between Eu_d and Pb (although it represents a minor component in the massive sulphide compared to Cu and Zn) for the Ariab massive sulphide deposits. Bakheit [2] attributes the lower Pb content to the absence of continental basement below the rock assemblage or generation of Ariab sulphides from more primitive magma.

The magnitude of the Eu_d values in sulphide-rich samples is related to the total sulphide content of each sample, but it appears to be more a function of the persistent types of sulphide minerals, i.e., the metal content of the sample [5]. In general, a positive correlation persists between the Eu anomaly (Eu_d value) and the concentration of some sulphide minerals. This is clearly detected with regard to Pb more than to Cu, Zn, or Ba. Zn is enriched in the massive sulphide relative to the schists but the leaching of highly mobile Zn during supergene weathering proves to reduce the amount of Zn in the gossan down to concentration, similar to the schists relating ones [7].

5 Conclusion

The use of the REE patterns of the massive sulphide deposits, gossans, alteration zones and country rocks give a useful information, which may play avital rule as tool for exploration of volcanogenic massive sulphide deposits in the Ariab

Mining District NE Sudan, and elsewhere. The results of this study illustrated that positive Eu anomalies are preserved in Ariab massive sulphide when the sulphides undergo greenschist grade metamorphism and supergene weathering. The Gossans with positive Eu anomalies must be the products of supergene weathering of massive sulphides having a similar positive Eu anomaly as the sulphides.

References

1. Adair, R.N.: Stratigraphy, structure, and geochemistry of the Halfmile Lake massive-sulphide deposit, New Brunswick. *J. Explor. Min. Geol.* **1**, 151–166 (1992)
2. Bakheit, A.K.: Geochemical and tectonic control of sulphide-gold mineralization in Ariab mineral district, Red Sea Hills, Sudan. Ph. D. thesis: Techn. Univ. Berlin, 157p (1991)
3. Campbell, I.H., Lencher, C.M., Coast, P., Franklin, J.M., Gorton, M.P., Thurston, P.C.: Rare earth mobility in alteration pipes below massive sulfide Cu-Zn sulfide deposits. *J. Chem. Geol.* **45**, 181–202 (1984)
4. Cullers, R.L., Medaris, L.G., Haskin, L.A.: Experimental studies of the distribution of rare earth as trace elements among silicate minerals and liquids and water. *J. Geochim. Cosmochim. Acta* **37**, 1499–1512 (1973)
5. Gale, G. H., Fedikow, M. A. F.: The application of rare earth element analyses in the exploration for volcanogenic massive sulphide type deposits in Manitoba; In: Report of Activities, 1999, Manitoba Industry, Trade and Mines, Geological Services, p. 9 (1999)
6. Galley, A.G.: Target vectoring using litho-geochemistry: application to the exploration for volcanic-hosted massive sulfide deposits. *CIM Bull.* **88**(990), 15–27 (1995)
7. Ghavami-Riabi, R., Theart, H.F.J.: Geochemical and mineralogical characteristic of the VHMS alteration pipe, major elements variations and peraluminous ratio, in high grade metamorphosed rocks. *J. Min. Environ.* **1**(2), 29–36 (2010)
8. Graf, J.L.: Rare earth elements as hydrothermal tracers during the formation of massive sulfide deposits in volcanic rocks. *J. Econ. Geol.* **72**, 527–548 (1977)
9. Hart, T., Gibson, H., Leshner, C.: Trace element geochemistry and petrogenesis of felsic volcanic rocks associated with volcanogenic massive Cu-Zn-Pb sulphide deposits. *Econ. Geol.* **99**(5), 1003–1013 (2004)
10. Lentz, D.R.: Trace-element systematics of felsic volcanic rocks associated with massive deposits in the Bathurst mining camp: Petrogenetic, tectonic, and chemostratigraphic implications for VMS Exploration: Geological association of Canada Short course notes, vol. 12, pp. 359–402 (1996)
11. Lottermoser, B.G.: Rare earth element study of exhalites within the Willyama Supergroup, broken hill Block, Australia. *J. Miner. Deposita* **25**, 92–99 (1989)
12. Maclean, W.H.: Rare earth element mobility at constant inter-REE ratios in the alteration zone at the Phelps Dodge massive sulphide deposit, Matagami, Quebec. *J. Mineralium Deposita* **23**, 231–238 (1988)
13. McDonough, W.F., Sun, S., Ringwood, A.E., Jagoutz, E., Hofmann, A.W.K.: Rb and Cs in the earth and the evolution of the earth's mantle. *J. Geochim. Cosmochim. Acta*, Ross Taylor Symposium volume (1991)

14. Michard, A.: Rare earth element systematics in hydrothermal fluids. *J. Geochim. Cosmochim. Acta* **53**, 745–750 (1989)
15. Scott A., Anthony E.: The aqueous geochemistry of the rare-earth elements and yttrium 4. Monazite solubility and REE mobility in exhalative massive sulphide-depositing environments. *J. Chem. Geol.* 47–60 (1994)
16. Sverjensky, D.A.: Europium redox equilibrium in aqueous solutions. *J. Earth Planet. Sci. Lett.* **67**, 70–78 (1984)
17. Taylor, S.R., McLennan, S.M.: *The continental crust: its composition and evolution*, Blackwell Scientific Publications, Boston, Massachusetts. 312 pp (1985)
18. Volesky, J.C., Leybourne, M.I., Boyle, D.R.: Mobility of rare earth elements during weathering of massive sulphide deposits, Bathurst Mining Camp, New Brunswick, Canada. *GAC Abstr. Programs* **23** (7), 8 (2000)

Classification of Composite Pegmatite via Staining and Digital Image Processing in the Bulfat Complex, Qala Deza, NE (Iraq)

Shareef Th. Al-Hamed, Khalid J. Aswad, and Nabaz R. Aziz

Abstract

The pegmatites associated classification aspects are usually considered with caution, due mainly to the relating coarse-grained texture enclosing interlocking grains often greater than 2.5 cm in size. In addition to the large size of the constituent mineral crystals, the Bulfat pegmatites clearly reflect a composite nature. Consequently, classifying these rocks by means of thin section and chemical classification processes turns out to be invalid. For such a seemingly insurmountable problem to be effectively surmounted, we consider implementing special classification criteria, which rests on a rather practical approach, whereby the Bulfat pegmatite peculiar mineralogy could be efficiently determined. Hence, for the mineral contents to be accurately quantified, the classification area must be noticeably greater than the thin section. Accordingly, the advanced calculation mode analysis has been implemented on two selected samples of polished slab area. The proposed computational process outcome appears to suggest that the slab area need be larger than 15 cm², as a lower limit, for the pegmatite rocks' classification procedure to be achieved. To overcome the difficulty associated with the studied samples relating coarse-grained sizes and chemical composites, we consider classifying the rocks in conformity with the classical classification schemes (i.e., by means of mineralogy content), using selective staining of K-feldspar and plagioclase on the examined rock slabs. Accordingly, the K-feldspar minerals are stained in yellow color by means of Sodium Cobaltinitrite (Na₃Co(NO₂)₆), while the plagioclase feldspar is stained red by means of Amaranth (C₂₀H₁₁N₂Na₃O₁₀S₃). The images concerning the polished rock slabs and the stained

surfaces, as captured via a digital camera, have to be transformed into a different image mode using the ENVI software. An image processing analysis has been undertaken for the mineral proportions to be automatically evaluated and the appropriate nomenclature to be retrieved. Thus, the digital image processing is applied on polished slabs for the purpose of calculating and recalculating the color index M', quartz, alkali-feldspar, and for the plagioclase proportions to be suitably plotted in a QAPF type of diagram. Moreover, and for the purpose of distinguishing between the Dioritic type of pegmatite and the Gabbroic pegmatite, the staining method, as associated with image processing technique, has been applied to the composite pegmatite rocks, while an aid extinction angle has been computed with regard to the plagioclase for the Plagioclase relating Anorthite content to be recognized. The image analyses as implemented on the stained polished slab of the Bulfat composite pegmatites appears to reveal well that the contrasting components' contact with varying mineral constituents prove to mingle down to a small scale in single intrusion. Still, such finding appears to entail further dissection due mainly to the fact that the persistence of composite-pegmatite bodies with a small-scale contrasting composition might well have its explanation in the liquid associated immiscibility.

Keywords

Bulfat complex • Composite pegmatite • Classification Staining • Image processing

1 Introduction

The pegmatite bodies and associated plutonic rocks stand as part of the igneous complexes associated with the Bulfat block, sited in Qala Deza, NE Iraq (Jassim et al. 1982) (Fig. 1). Field investigations of the accessible areas at

S. Th. Al-Hamed (✉) · K. J. Aswad
Mosul University, Mosul, Iraq
e-mail: shareefalhamed@yahoo.com

N. R. Aziz
Sulaymania University, Sulaymania, Iraq

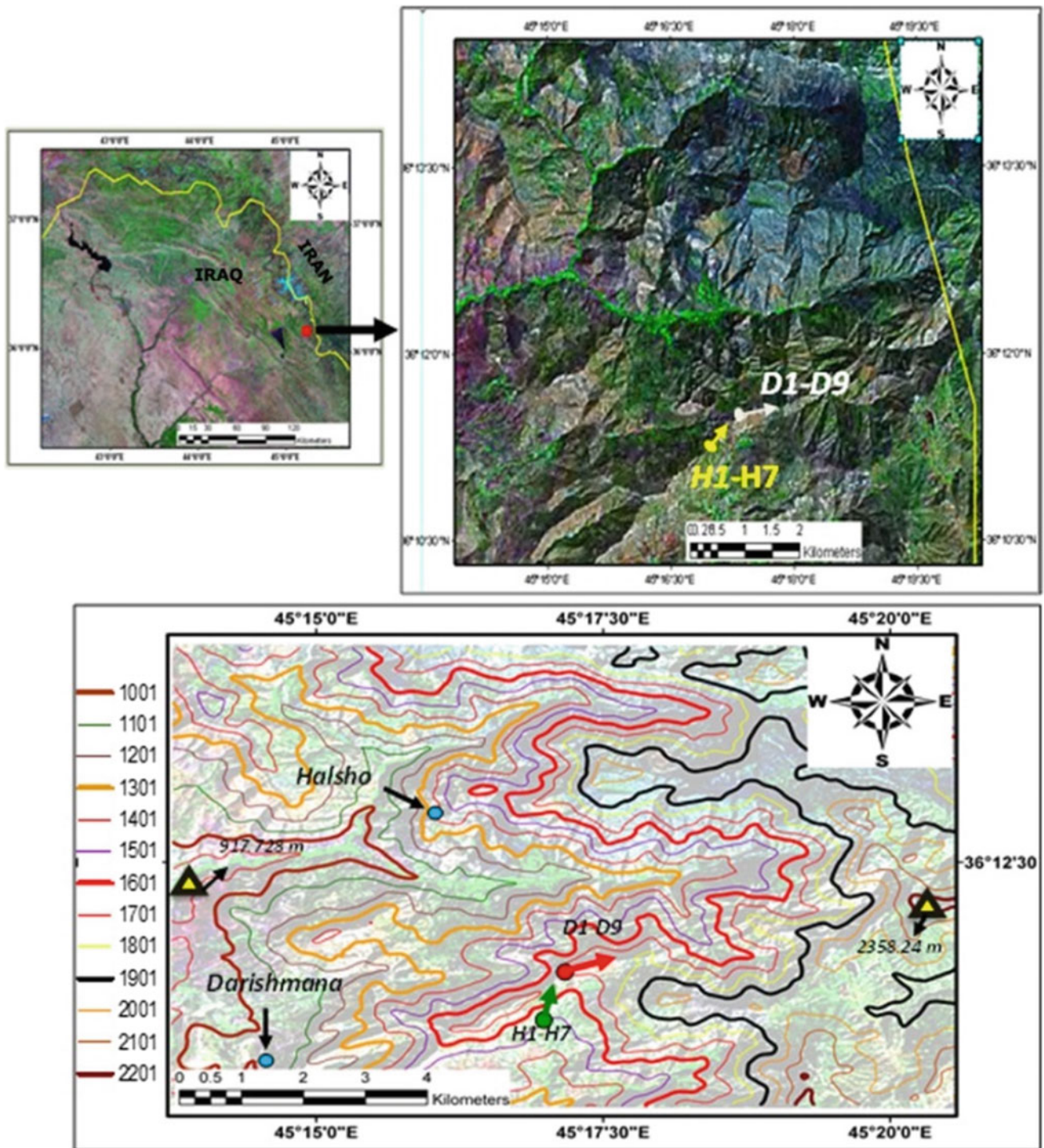


Fig. 1 Location and topographic map of the studied area showing the selected samples' traverses and distributions

Darishmana appear to reveal that these pegmatite bodies have intruded the Albian-Cenomanian metasedimentary sequences (Gemo-Qandil Formation), which experienced a medium-grade regional metamorphism, as overprinted by a high-grade contact metamorphism during Paleogene (Jassim et al. 1982).

The Iraqi Bulfat Complex (100 km² in size) outcrops in Jabal Bulfat near Qala Diza (Fig. 2). It is an incomplete ophiolite sequence that comprises a volcano-sedimentary unit, originally referred to as the Bulfat Group (Jassim et al. 1982), and presently as the Gimo and Sirginil Group (Jassim et al. 1982). The intrusive complex comprises gabbro-diorite

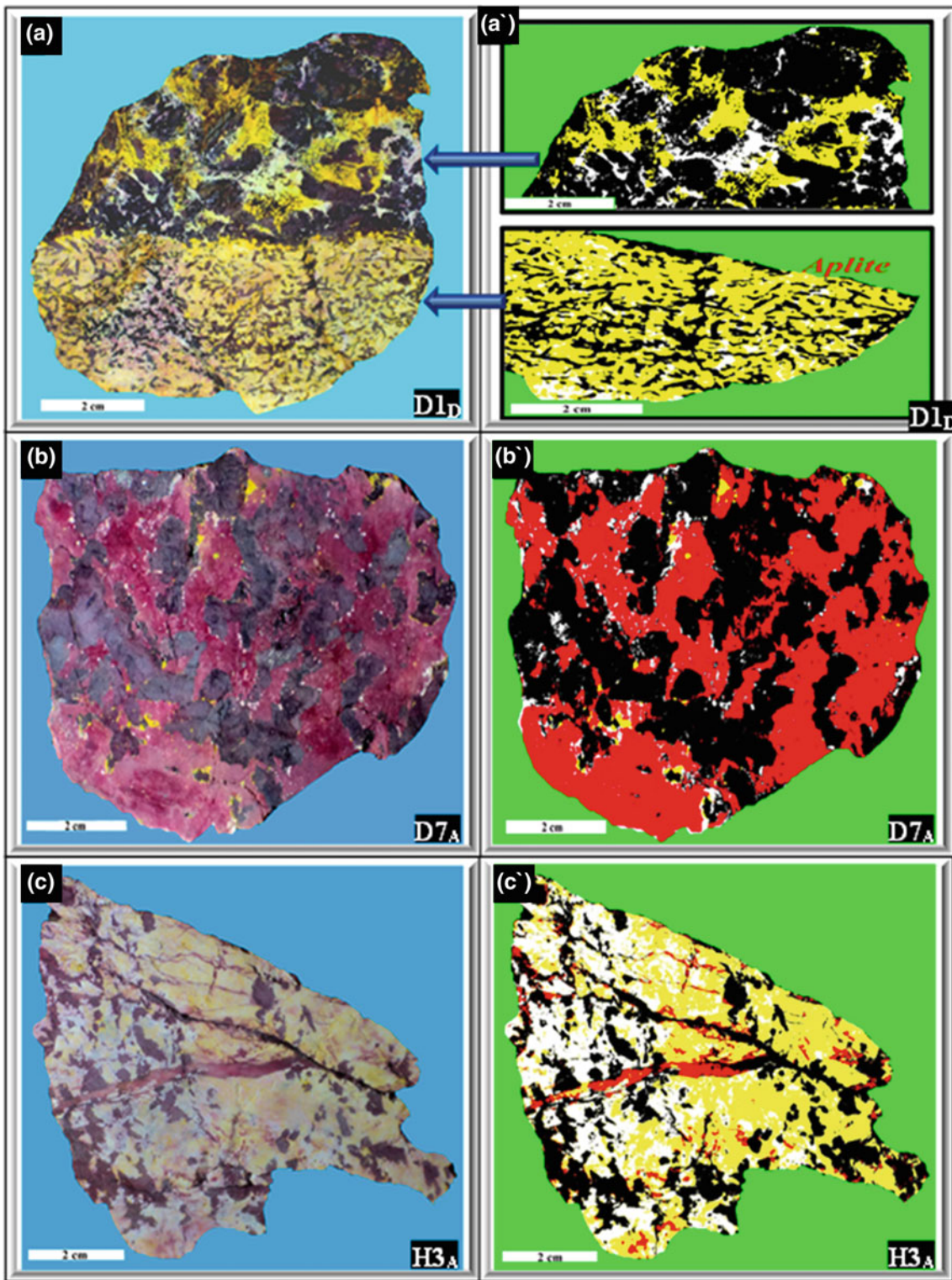


Fig. 2 Digital image processing of the stained slabs. A, B and C the stained slabs; A', B' and C' the same slabs following application of the digital image processing

Table 1 Classification and nomenclature of pegmatite, specifying recalculation of the color index (M' %), Alkali-feldspar (A' %), and plagioclase (P' %)

Samples	M' %	Alkali Feldspar %	Plagioclase %	Total Feldspars = 100		Rock name
				A' %	P' %	
D1 _A	17	59.8	23.2	72	28	Syenitic pegmatite
D1 _B	35	44	21	67.7	32.3	Syenitic pegmatite
D1 _C	23	60.1	16.9	78	22	Syenitic pegmatite
D1 _D	(1) Aplite 37.7	(1) 56	(1) 6.3	(1) 89.9	(1) 10.1	(1) Syenitic Aplite
	(2) Pegmatite 67	(2) 20.5	(2) 12.5	(2) 62.2	(2) 37.8	(2) Melano-monzonitic Pegmatite
	Avg = 52.35	Avg = 38.25	Avg = 9.4	Avg = 76.05	Avg = 23.95	Avg = Melano-syenitic Pegmatite
D2 _A	52	0	48	0	100	Gabbroic pegmatite
D2 _B	60	0	40	0	100	Gabbroic pegmatite
D3 _A	57	0.6	42.4	1.5	98.5	Gabbroic pegmatite
D4 _B	20	31.4	48.6	39.2	60.8	Monzonitic pegmatite
D5 _B	50	3.8	46.2	7.5	92.5	Gabbroic pegmatite
D5 _C	51	4.4	44.6	9	91	Gabbroic pegmatite
D6 _A	61.5	0	38.5	0	100	Gabbroic pegmatite
D7 _A	58.3	0.8	40.9	1.8	98.2	Melano-dioritic pegmatite
D7 _B	61.8	0	38.2	0	100	Melano-dioritic pegmatite
D7 _C	51	0	49	0	100	Melano-dioritic pegmatite
D8 _A	53	0	47	0	100	Gabbroic pegmatite
D8 _B	62.5	0.6	36.9	1.7	98.3	Gabbroic pegmatite
D9 _A	(1) Mafic part 54	(1) 17.9	(1) 28.1	(1) 39	(1) 61	(1) Melano-monzonitic Pegmatite
	(2) Felsic part 27	(2) 6.4	(2) 66.6	(2) 8.8	(2) 91.2	(2) Dioritic Pegmatite
	Avg = 40.5	Avg = 12.15	Avg = 47.35	Avg = 23.9	Avg = 76.1	Avg = Monzodioritic Pegmatite
H1	11	75.6	13.4	85	15	Syenitic pegmatite
H2	12	61.6	26.4	70	30	Syenitic pegmatite
H3 _A	34	21.8	44.2	33	67	Monzodioritic pegmatite
H3 _B	(1) Mafic part 44.7	(1) 19.4	(1) 35.9	(1) 35.1	(1) 64.9	(1) Monzodioritic Pegmatite
	(2) Felsic part 26.9	(2) 5.5	(2) 67.6	(2) 7.5	(2) 92.5	(2) Dioritic Pegmatite
	Avg = 35.8	Avg = 12.45	Avg = 51.75	Avg = 21.3	Avg = 78.7	Avg = Monzodioritic Pegmatite
H4	65	0.8	34.2	2.3	97.7	Gabbroic pegmatite
H5	19	55.2	25.8	68.2	31.8	Syenitic pegmatite
H7	22	60.1	17.9	77	23	Syenitic pegmatite

Abbreviations

$$M' \% = 100 \times [M/(M + A+P)]$$

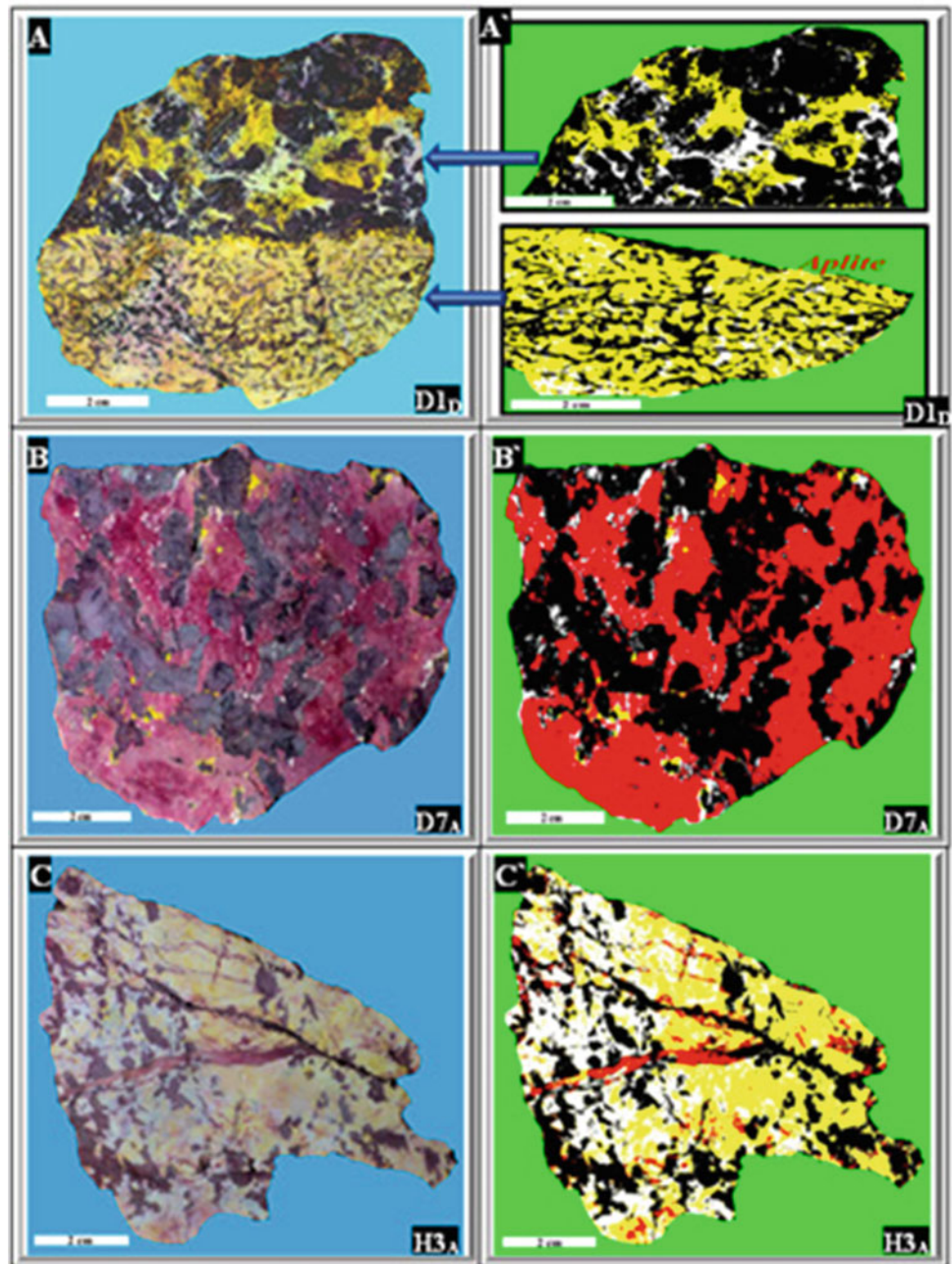
$$A' \% = 100 \times [A/(A + P)]$$

$$P' \% = 100 \times [P/(A + P)]$$

$$A' + P' = 100$$

M Mafic minerals, *A* Alkali-feldspar, and *P* Plagioclase

Fig. 3 A, B and C the stained slabs; A', B' and C' the same slabs which applied it the digital image processing to calculate the ratio of alkali-feldspar, plagioclase, and quartz



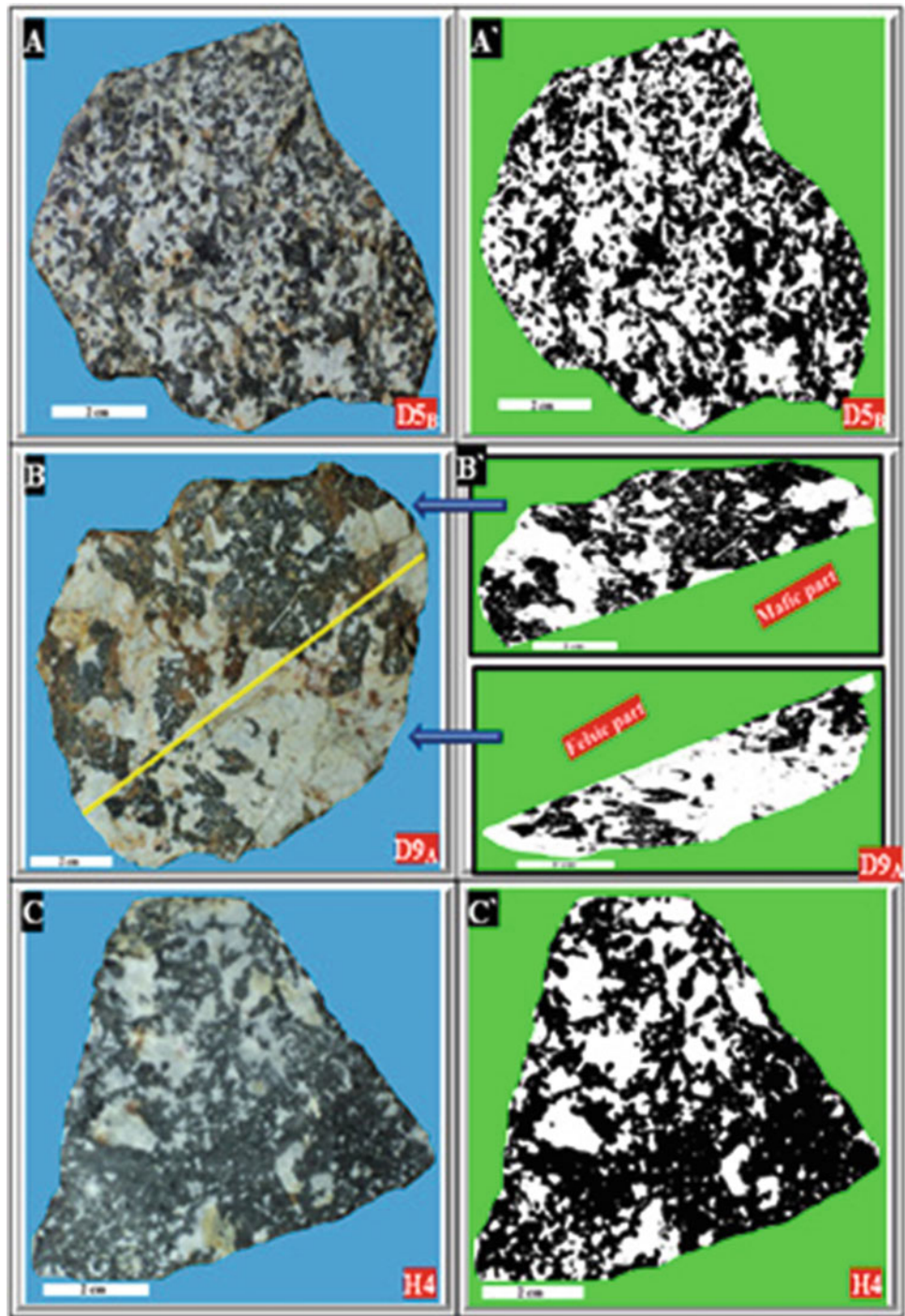
intrusions, along with late-stage differentiated syenite and nepheline syenite.

2 Materials and Methods

The staining process has been implemented according to the following steps, as modified by Al-Hamed (2013).

1. In a well-ventilated hood, hydrofluoric acid is poured into a vessel to about 1/4 in. to the top.
2. The polished surface is dipped into the hydrofluoric Acid for approximately two minutes.
3. The polished surface is dipped in distilled water for 10 s, while moving the polished face under the water surface or gently dipping the slab in water and out of the water repeatedly for approximately 10 s.
4. The same surface is dipped into an amaranth solution for approximately 2–5 s.
5. The polished surface is dipped in a second vessel of distilled water for 10 s to rinse off the amaranth, as it is the case in step 2 above.

Fig. 4 A, B and C original samples; A', B' and C' the same slabs which applied it the digital image processing to calculate the color index



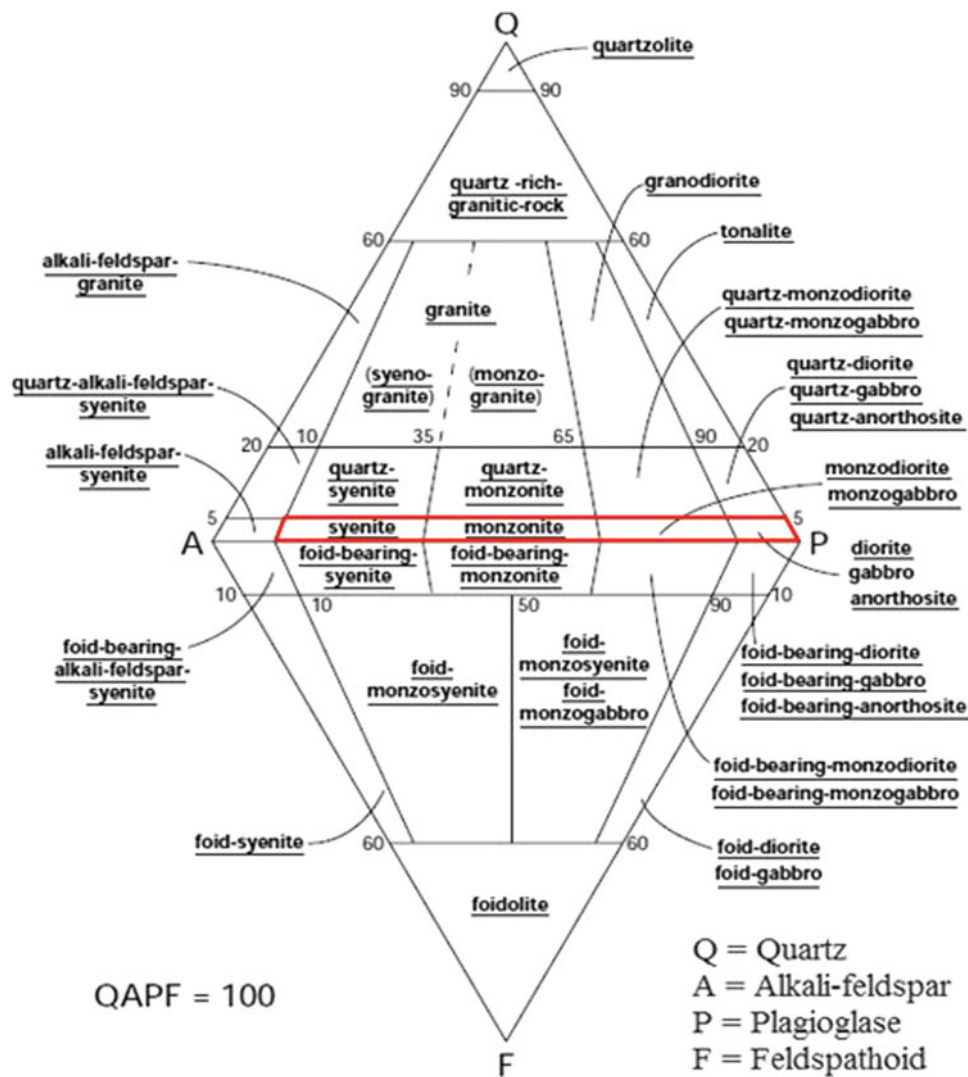


Fig. 5 Classification and nomenclature of the coarse-grained crystalline rocks (as based on Streckeisen 1976)

6. The slab is kept in a tilted position to be dried from excess amaranth by means of a blow dryer, while being very careful not to blow off any of the red colored stains already formed on the plagioclase.
7. The same slab surface is dipped into a sodium cobaltinitrite solution for approximately 1.5 min.
8. The same surface is dipped in a third vessel of distilled water for 10 s, as is the case in step 2 above.
9. The slab should be dried off, as in step 5, and the obtained K-feldspar should bear a yellow color stain.
10. The stained slabs should be placed, face up, on a towel paper and let dry under a heat lamp for several minutes or left to dry overnight. The staining process is now completed. At this level, every plagioclase should bear a red color and each K-feldspar should be yellow stained. To note, quartz and most of the ferromagnesian

minerals should remain unstained, preserving their original color.

3 Results and Discussion

As a very coarse-grained intrusive igneous rock, pegmatite englobes interlocking grains usually larger than 2.5 cm in size, in addition to the composite character it bears. Hence, any attempt to classify these rocks by means of thin section and chemical classification appears to be unscientific, as such methods are discovered to be non-representative of bulk minerals.

To overcome the difficulty related to the coarse-grained sizes and chemically composite nature of the studied

samples, the rocks are classified in conformity with the classical classification schemes (i.e., based on their mineralogical content), by implementing the selective K-feldspar and plagioclase staining techniques on the selected rock slabs.

Initially, the objective lying behind implementation of such a method consists in enabling the classification of pegmatite by allowing to get rid of two major problems associated with the grains' size and mineral type determination (Albite distribution between Alkali-feldspar and Plagioclase). Such a method proves to be remarkably effective from the researcher's perspective, through application of selective K-feldspar and plagioclase staining on the sample rock slabs. Accordingly, the K-feldspar minerals turn out to be yellow-color stained owing to the Sodium Cobalt nitrite ($\text{Na}_3\text{Co}(\text{NO}_2)_6$) effect, while the plagioclase feldspar is discovered to be red stained under the effect of Amaranth ($\text{C}_{20}\text{H}_{11}\text{N}_2\text{Na}_3\text{O}_{10}\text{S}_3$). Images of the polished rock slabs and stained surfaces, as captured via a digital camera, have to be transformed into a different new image by means of ENVI software. Applied on the stained samples (Fig. 3) as well as on the non-stained ones (Fig. 4), this method is opted for in a bid to achieve a rather effective classification of the pegmatite rocks. In addition, the digital image processing

technique has also been implemented on the original samples prior to the staining step for the purpose of determining the appropriate color index (M'), and classifying every rock type depending on the Alkali-feldspar, Plagioclase mode analyses (Table 1).

Depending on Fig. 5 the area of the thin section should be larger than 15 cm so that the mineral classification of pegmatites is successful and this figure simplify inefficiency thin section (Made in the university workshop) to representation all mineral of pegmatite.

References

- Jassim, S. Z., Buda, G., Neuzilova, M., Suk, M.: Metamorphic development of the Iraqi Zagros ophiolitic zone, vol. 16, pp. 21–40. Academia publishing House of the Czechoslovak Academy of Science, Krystalinikum (1982)
- Al-Hamed, S. Th.: Mineralogy and petrogenesis of pegmatite in Bulfat complex, Qala Deza, NE-Iraq, p. 175. M.Sc. thesis, University of Mosul, College of Sciences, Iraq (In Arabic with English abstract) (2013)
- Streckeisen, A.: To each plutonic rock its proper name. *Earth Sci. Rev.* **12**:1–33 (1976)